A THESIS

entitled

GEOCHEMICAL INVESTIGATIONS ON SEDIMENTS FROM THE EASTERN PACIFIC

submitted for the

DEGREE OF DOCTOR OF PHILOSOPHY

in the

FACULTY OF SCIENCE OF THE UNIVERSITY OF LONDON

by

SOTERIOS PETROU VARNAVAS

Applied Geochemistry Research Group,

Department of Geology,

Royal School of Mines,

Imperial College of Science and Technology,

London.

October, 1979

" Ἔζεε δέ χθών πᾶσα καί Ὠκεανοῖο ῥέεθρα πόντός τ' ἀτρύγετος".

ΗΣΙΟΔΟΣ - ΘΕΟΓΟΝΙΑ

"All the land seethed, and Ocean's streams and the endless sea."

HESIOD - THEOGONY

ABSTRACT

Bulk and partition chemical analyses of sediment cores collected from an East Pacific Rise fracture zone at $9^{o}S$, the Galapagos spreading center and the Bauer Deep have been used to determine metal distribution patterns in these sediments.

In the F.Z. area two hydrothermal centers have been located which are responsible for the metal-enrichment in the sediments. Comparison of the chemical composition of sediments collected from the basins with that of sediments obtained from the elevated areas showed metalliferous sediment ponding within the deep basins. The geochemical partition data of the surface and buried sediments have shown remarkable differences between the two. It has been found that the acid-reducible Fe, Mn, Ni, Cu and Zn decrease with depth of burial, while there is a parallel increase in the proportion of these metals in the HCl-soluble fraction. Moreover, there is a gradual increase of the hydroxylamine HCl-insoluble residue with depth in the sediments, which suggests a corresponding increase in the proportion of more resistant phases. Thus, some post-depositional transformation of phases has occurred. It has also been shown that due to the dissolution of $CaCO_3$ in deeper waters a shift of Fe, Mn and Cu from the carbonate phase into the Fe-Mn oxide phase may occur with increasing depth of water.

In the Galapagos bydrothermal center there has been a fractionation between Mn and Fe in the sediments, the Mn being deposited at tbe top of the sediment column, in the form of Mn oxide crusts, while Fe forms distinct horizons of Fe-rich nontronites. The Fe-rich sediments precipitated directly from hydrothermal solutions and they are depleted in trace metals.

In the Bauer Deep sediments the geochemical behaviour of elements is dependent upon the water depth. The geochemical partition data have demonstrated diagenetic transformation of Fe-Mn oxides to Fe-rich smectites which is promoted with increasing water depth and which is directly linked to the dissolution of $CaCO_3$ and biogenic Si.

ACKNOWLEDGEMENTS

The research described in this thesis was carried out in the Applied Geochsmistry Research Group, Department of Geology, Imperial College of Science and Technology.

I wish first to express my gratitude to my supervisor, Dr. D.S. Cronan, who introduced me to the subject of deep sea sedimentation and for his inspiring guidance, valuable criticisms and helpful discussions during the research and the writing of this thesis.

The majority of the samples were collected by Dr. D.S. Cronan aboard the English research vessel RRS Shackleton, the Master and crew of which I would like to thank. Furthermore, I wish to thank the chief scientists, Dr. R. Hekinian and Dr. B.R. Rosendahl, and the other participants of Deep Sea Drilling Project, Leg 54, especially Dr. S. Humphries, for collecting a set of samples which I have also studied. The receipt of samples from the Scripps Institute of Oceanography, California (U.S.A.) is also gratefully acknowledged.

Special thanks are due to Professor A.G. Panagos of the University of Patras, Greece, who suggested that I study Marine Geochemistry at Imperial College and who helped me implement his suggestion. His personal interest, helpful suggestions and constant encouragement are greatly appreciated.

I am also grateful to Professor G. Christodoulou of the same University for useful discussions regarding sea bottom topography.

My thanks also go to the following persons at Imperial College:

- Professor J.S. Webb for making the analytical facilities of the Applied Geochemistry Research Group available;

- Dr. M. Thomson for advice regarding analytical techniques;

- Dr. S.A. Moorby for useful discussions;

- Mr. R. Curtis for assistance with the X-ray diffraction studies;

- Mr. B. Thompson for providing a bathymetric map;

- All the academic staff and my fellow students in the Applied Geochemistry Research Group who remained friendly throughout this project;

- All the technical staff for help with the analytical work.

Also thanks to Mrs S. Murdock for typing the final manuscript.

I gratefully acknowledge the receipt of a three-year leave of absence from the University of Patras and a research studentship from the State Scholarships Foundation of Greece for the preparation of this thesis.

Finally, I would like to thank my wife, Danae, for her encouragement, support and understanding. Although our household was interrupted constantly during my thesis work, she never complained.

TABLE OF CONTENTS

LIST OF TABLES

LIST OF FIGURES

1.18 Distribution of Al in surface sediments from the East Pacific Rise fracture zone at 9°S.

1.19 Distribution of SiO_2 in surface sediments from the East Pacific Rise fracture zone at 9°S.

1.20 Scatter plot showing the positive correlation between Fe and SiO_2. Concentrations are corrected to a calcium carbonate-free basis.

2.1-2.50 Lithological and Chemical Description of the Cores:

2.1 Core SH 1525 ($CaCO_3$, Mn, Fe, Ni, Co and Pb).
2.2 Core SH 1525 (Zn, Cu, Ba, Al and SiO_2).

2.3 Core SH 1526 ($CaCO_3$, Mn, Fe, Ni, Co and Pb).
2.4 Core SH 1526 (Zn, Cu, Ba, Al and SiO_2).

2.5 Core SH 1528 ($CaCO_3$, Mn, Fe, Ni, Co and Pb).
2.6 Core SH 1528 (Zn, Cu, Ba, Al and SiO_2).

2.7 Core SH 1529 ($CaCO_3$, Mn, Fe, Ni, Co and Pb).
2.8 Core SH 1529 (Zn, Cu, Ba, Al and SiO_2).

2.9 Core SH 1530 ($CaCO_3$, Mn, Fe, Ni and Co).
2.10 Core SH 1530 (Pb, Zn, Cu, Ba and Al).

2.11 Core SH 1531 ($CaCO_3$, Mn, Fe, Ni, Co and Pb).
2.12 Core SH 1531 (Zn, Cu, Ba, Al and SiO_2).

2.13 Core SH 1532 ($CaCO_3$, Mn, Fe, Ni, Co and Pb).
2.14 Core SH 1532 (Zn, Cu, Ba, Al and SiO_2).

2.15 Core SH 1533 ($CaCO_3$, Mn, Fe, Ni and Co).
2.16 Core SH 1533 (Pb, Zn, Cu, Ba and Al).

2.17 Core SH 1534 ($CaCO_3$, Mn, Fe, Ni, Co and Pb).
2.18 Core SH 1534 (Zn, Cu, Ba, Al and SiO_2).

2.19 Core SH ;535 ($CaCO_3$, Mn, Fe, Ni and Co).
2.20 Cpre SH 1535 (Pb, Zn, Cu, Ba and Al).

2.21 Core SH 1536 ($CaCO_3$, Mn, Fe, Ni, Co and Pb).
2.22 Core SH 1536 (Zn, Cu, Al and Ba).

2.23 Core SH 1537 ($CaCO_3$, Mn, Fe and Ni),
2.24 Core SH 1537 (Zn, Cu, Al, Ba and SiO_2).

2.25 Core SH 1538 ($CaCO_3$, Mn, Fe, Ni, Co and Pb).
2.26 Core SH 1538 (Zn, Cu, Ba, Al and SiO_2).

2.27 Core SH 1539 ($CaCO_3$, Mn, Fe and Ni).
2.28 Core SH 1539 (Zn, Cu, Ba, Al and SiO_2).

2.29 Core SH 1540 ($CaCO_3$, Mn, Fe and Ni).
2.30 Core SH 1540 (Zn, Cu, Ba, Al and SiO_2).

2.31 Core SH 1541 ($CaCO_3$, Mn, Fe, Ni, Co and Pb).
2.32 Core SH 1541 (Zn, Cu, Al and Ba).

2.33 Core SH 1543 ($CaCO_3$, Mn, Fe, Ni and Co).
2.34 Core SH 1543 (Pb, Zn, Cu, Ba and Al).

2.35 Core SH 1544 ($CaCO_3$, Mn, Fe, Ni and Co).
2.36 Core SH 1544 (Pb, Zn, Cu, Ba and Al).

2.37 Core SH 1545 ($CaCO_3$, Mn, Fe, Ni, Co and Pb).
2.38 Core SH 1545 (Zn, Cu, Ba and Al).

2.39 Core SH 1546 ($CaCO_3$, Mn, Fe, Ni, Co and Pb).
2.40 Core SH 1546 (Zn, Cu, Ba, Al and SiO_2).

2.41 Core SH 1547 ($CaCO_3$, Mn, Fe, Ni, Co and Pb).
2.42 Core SH 1547 (Zn, Cu, Ba, Al and SiO_2).

2.43 Core SH 1548 ($CaCO_3$, Mn, Fe, Ni, Co and Pb).
2.44 Core SH 1548 (Zn, Cu, Al and Ba).

2.45 Core SH 1550 ($CaCO_3$, Mn, Fe, Ni and Co).
2.46 Core SH 1550 (Pb, Zn, Cu, Ba and Al).

2.47 Core SH 1551 ($CaCO_3$, Mn, Fe, Ni, Co and Pb).
2.48 Core SH 1551 (Zn, Cu, Ba and Al).

2.49 Core SH 1552 ($CaCO_3$, Mn, Fe, Ni, Co and Pb).
2.50 Core SH 1552 (Zn, Cu, Ba, Al and SiO_2).

2.51 The distribution of the acetic acid-soluble Fe in fracture zone sediment cores expressed as a percentage of the total Fe concentration.

2.52 The distribution of the acetic acid-soluble Fe in fracture zone sediment cores expressed as a percentage of the total Fe concentration.

2.53 The distribution of the hydroxylamine HCl-soluble Fe in fracture zone sediment cores expressed as a percentage of the total Fe concentration.

2.54 The distribution of the hydroxylamine HCl-soluble Fe in fracture zone sediment cores expressed as a percentage of the total Fe concentration.

2.55 The distribution of the HCl-soluble Fe in fracture zone sediment cores expressed as a percentage of the total Fe concentration.

2.56 The distribution of the HCl-soluble Fe in fracture zone sediment cores expressed as a percentage of the total Fe concentration.

2.57 The distribution of the acetic acid-soluble Mn in fracture zone sediment cores expressed as a percentage of the total Mn concentration.

2.58 The distribution of the acetic-acid soluble Mn in fracture zone sediment cores expressed as a percentage of the total Mn concentration.

2.59 The distribution of the hydroxylamine HCl-soluble Mn in fracture zone sediment cores expressed as a percentage of the total Mn concentration.

2.60 The distribution of the hydroxylamine HCl-soluble Mn in fracture zone sediment cores expressed as a percentage of the total Mn concentration.

2.61 The distribution of the HCl-soluble Mn in fracture zone sediment cores expressed as a percentage of the total Mn concentration.

2.62 The distribution of the HCl-soluble Mn in fracture zone sediment cores expressed as a percentage of the total Mn concentration.

2.63 The distribution of the hydroxylamine HCl-soluble Ni in fracture zone sediment cores expressed as a percentage of the total Ni concentration.

2.64 The distribution of the hydroxylamine HCl-soluble Ni in fracture zone sediment cores expressed as a percentage of the total Ni concentration.

2.65 The distribution of the hydroxylamine HCl-soluble Ni in fracture zone sediment cores expressed as a percentage of the total Ni concentration.

2.66 The distribution of the HCl-soluble Ni in fracture zone sediment cores expressed as a percentage of the total Ni concentration.

2.67 The distribution of the HCl-soluble Ni in fracture zone sediment cores expressed as a percentage of the total Ni concentration.

2.68 The distribution of the HCl-soluble Ni in fracture zone sediment cores expressed as a percentage of the total Ni concentration.

2.69 The distribution of the acetic acid-soluble Zn in fracture zone sediment cores expressed as a percentage of the total Zn concentration.

2.70 The distribution of the acetic acid-soluble Zn in fracture zone sediment cores expressed as a percentage of the total Zn concentration.

2.71 The distribution of the hydroxylamine HCl-soluble Zn in fracture zone sediment cores expressed as a percentage of the total Zn concentration.

2.72 The distribution of the hydroxylamine HCl-soluble Zn in fracture zone sediment cores expressed as a percentage of the total Zn concentration.

2.73 The distribution of the HCl-soluble Zn in fracture zone sediment cores expressed as a percentage of the total Zn concentration.

2.74 The distribution of the HCl-soluble Zn in fracture zone sediment cores expressed as a percentage of the total Zn concentration.

2.75 The distribution of the HCl-soluble Zn in fracture zone sediment cores expressed as a percentage of the total Zn concentration.

2.76 The distribution of the acetic acid-soluble Cu in fracture zone sediment cores expressed as a percentage of the total Cu concentration.

2.77 The distribution of the acetic acid-soluble Cu in fracture zone sediment cores expressed as a percentage of the total Cu concentration.

2.78 The distribution of the hydroxylamine HCl-soluble Cu in fracture zone sediment cores expressed as a percentage of the total Cu concentration.

2.79 The distribution of the hydroxylamine HCl-soluble Cu in fracture zone sediment cores expressed as a percentage of the total Cu concentration.

2.80 The distribution of the HCl-soluble Cu in fracture zone sediment cores expressed as a percentage of the total Cu concentration.

2.81 The distribution of the HCl-soluble Cu in fracture zone sediment cores expressed as a percentage of the total Cu concentration.

2.82 The distribution of the HCl-soluble Cu in fracture zone sediment cores expressed as a percentage of the total Cu concentration.

2.83 The distribution of the hydroxylamine HCl-insoluble residue in fracture zone sediment cores.

2.84 The distribution of the hydroxylamine HCl-insoluble residue in fracture zone sediment cores.

2.85 The distribution of the hydroxylamine HCl-insoluble residue in fracture zone sediment cores.

2.86 Scatter plot showing the negative correlation between the acetic acid-soluble Mn (expressed as a percentage of the total Mn concentration) in the surface sediments, and the water depth.

2.87 Scatter plot showing the positive correlation between the hydroxylamine HCl-soluble Mn (expressed as a percentage of the total Mn concentration) in the surface sediments, and the water depth.

2.88 Scatter plot showing the negative correlation between the acetic acid-soluble Fe (expressed as a percentage of the total Fe concentration) in the surface sediments, and the water depth.

2.89 Scatter plot showing the positive correlation between the hydroxylamine HCl-soluble Fe (expressed as a percentage of the total Fe concentration) in the surface sediments, and the water depth.

2.90 Scatter plot showing the positive correlation between the hydroxylamine HCl-soluble Ni (expressed as a percentage of the total Ni concentration) in the surface sediments, and the water depth.

2.91 Scatter plot showing the negative correlation between the HCl-soluble Ni (expressed as a percentage of the total Ni concentration) in the surface sediments, and the water depth.

2.92 Scatter plot showing the positive correlation between the hydroxylamine HCl-soluble Zn (expressed as a percentage of the total Zn concentration) in the surface sediments, and the water depth.

2.93 Scatter plot showing the negative correlation between the HCl-soluble Cu (expressed as a percentage of the total Cu concentration) in the surface sediments, and the water depth.

2.94 Scatter plot showing the positive correlation between the HCl-soluble Cu (expressed as a percentage of the total Cu concentration) in the surface sediments, and the water depth.

2.95 Scatter plot showing the negative correlation between the acetic acid-soluble Cu (expressed as a percentage of the total Cu concentration) in the surface sediments, and the water depth.

2.96 Scatter plot showing the positive correlation between the hydroxylamine HCl-soluble Cu (expressed as a percentage of the total Cu concentration) in the surface sediments, and the water depth.

2.97 Scatter plot showing the negative correlation between the $CaCO_3$ content in the surface sediments and the water depth.

3.1 General bathymetric map of the Eastern Pacific Ocean showing the DSDP Site 424 (Leg 54) from the Galapagos spreading center.

3.2 Lithologic columns for the holes drilled in the Galapagos spreading center area (adapted from Hekinian et al, 1978).

3.3 Distribution of Pb, Mn and Fe in Hole 424. Concentrations are corrected to a calcium carbonate-free basis.

3.4 Distribution of Ni, Zn, Cu and Co in Hole 424. Concentrations are corrected to a calcium carbonate-free basis.

3.5 (a) Scatter plot of SiO_2 content versus Fe. Concentrations are corrected to a calcium carbonate-free basis.

(b) Scatter plot of SiO_2 content, corrected to a calcium carbonate-free basis, versus hydroxylamine HCl-soluble Fe expressed as a percentage of the total Fe concentration.

3.6 Distribution of the hydroxylamine HCl and the HCl-soluble Mn in Hole 424 expressed as a percentage of the total Mn concentration.

3.7 Distribution of the acetic acid-soluble Mn in Hole 424 expressed as a percentage of the total Mn concentration.

3.8 Distribution of the hydroxylamine HCl- and the HCl-soluble Ni in Hole 424 expressed as a percentage of the total Ni concentration.

3.9 Distribution of the hydroxylamine HCl- and the HCl-soluble Zn in Hole 424 expressed as a percentage of the total Zn concentration.

3.10 Distribution of the hydroxylamine HCl-soluble Al and that remaining in the HCl-insoluble residue in Hole 424 expressed as a percentage of the total Al concentration.

3.11 Scatter plot of SiO_2 content, corrected to a calcium carbonate-free basis, versus HCl-soluble Fe expressed as a percentage of the total Fe concentration.

3.12 Ternary diagram of Fe-Mn-Si.

4.1 Map showing the location of cores studied.

4.2 Core SH 1557. Lithological and chemical description ($CaCO_3$, Mn, Fe, Ni and Co).

4.3 Core SH 1557. Lithological and chemical description (Pb, Zn, Cu, Al and SiO_2).

4.21 Distribution of the hydroxylamine HCl-soluble Zn in Bauer Deep sediment cores expressed as a percentage of the total Zn concentration.

4.22 Distribution of the HCl-soluble Zn in Bauer Deep sediment cores expressed as a percentage of the total Zn concentration.

4.23 Distribution of the acetic acid-soluble Cu in Bauer Deep sediment cores expressed as a percentage of the total Cu concentration.

4.24 Distribution of the hydroxylamine HCl-soluble Cu in Bauer Deep sediment cores expressed as a percentage of the total Cu concentration.

4.25 Distribution of the HCl-soluble Cu in Bauer Deep sediment cores expressed as a percentage of the total Cu concentration.

4.26 Distribution of the acetic acid-soluble Al in Bauer Deep sediment cores expressed as a percentage of the total Al concentration.

4.27 Distribution of the hydroxylamine HCl-soluble Al in Bauer Deep sediment cores expressed as a percentage of the total Al concentration.

4.28 Distribution of the HCl-soluble Al in Bauer Deep sediment cores expressed as a percentage of the total Al concentration.

4.29 Distribution of the acetic acid-insoluble residue in Bauer Deep sediment cores.

4.30 Distribution of the hydroxylamine HCl-insoluble residue in Bauer Deep sediment cores.

4.31 Distribution of the HCl-insoluble residue in Bauer Deep sediment cores.

4.32 Scatter plot showing the negative correlation between Fe and SiO_2 in Bauer Deep sediments. Concentrations are corrected to a calcium carbonate-free basis.

4.33 Scatter plot showing the positive correlation between the hydroxylamine HCl-soluble Fe (expressed as a percentage of the total Fe concentration) and the SiO_2 content (C.F.B.) in Bauer Deep sediments.

4.34 Scatter plot showing the negative correlation between the HCl-soluble Fe (expressed as a percentage of the total Fe concentration) and the SiO_2 content (C.F.B.) in Bauer Deep sediments.

4.35 Scatter plot showing the decrease of $CaCO_3$ content with water depth in Bauer Deep surface sediments.

4.36 Scatter plot showing the negative correlation between the carbonate-free concentrations of Co in Bauer Deep surface sediments and the water depth.

4.37 Scatter plot showing the positive correlation between the carbonate-free concentrations of Mn in Bauer Deep surface sediments and the water depth.

4.38 Scatter plot showing the positive correlation between the carbonate-free concentrations of Fe in Bauer Deep surface sediments and the water depth.

4.39 a. Scatter plot showing the negative correlation between the acid-reducible Fe (expressed as a percentage of the total amount present) in the surface sediments, and the water depth.

b. Scatter plot showing the positive correlation between the HCl-soluble Fe (expressed as a percentage of the total amount present) in the surface sediments, and the water depth.

4.40 Scatter plot showing the negative correlation between the hydroxylamine HCl-soluble Ni (expressed as a percentage of the total Ni concentration) in Bauer Deep surface sediments, and the water depth.

4.41 Scatter plot showing the positive correlation between the HCl-soluble Ni (expressed as a percentage of the total Ni concentration) in Bauer Deep surface sediments, and the water depth.

4.42 Scatter plot showing the negative correlation between the hydroxylamine HCl-soluble Zn (expressed as a percentage of the total Zn concentration) in Bauer Deep surface sediments, and the water depth.

4.43 Scatter plot showing the positive correlation between the HCl-soluble Zn (expressed as a percentage of the total Zn concentration) in Bauer Deep surface sediments, and the water depth.

4.44 a. Scatter plot showing the positive correlation between the hydroxylamine HCl-insoluble residue and the water depth in Bauer Deep surface sediments.

b. Scatter plot showing the positive correlation between the acetic acid-insoluble residue and the water depth in the same sediments.

4.45 Scatter plot showing the decrease of the HCl-insoluble residue in Bauer Deep surface sediments with water depth.

LIST OF PLATES

INTRODUCTION

The first report of an anomalous chemical composition for what are now termed marine metalliferous sediments was by Boström and Peterson (1966). Since then, a large number of papers have been published on metalliferous sediments and this has been greatly facilitated by the Deep Sea Drilling Project (Boström and Peterson, 1969; Boström et al, 1969; Fisher and Boström, 1969; Horowitz, 1970; Chester and Messiha Hanna, 1970; Bender et al, 1971; Veeh and Boström, 1971; Dasch et al, 1971; Cronan, 1972; Cronan et al, 1972; Bruty et al, 1972; Aston et al, 1972a, b; Piper, 1973; Cronan and Garret, 1973; Dymond et al, 1973; Cronan, 1974; Smith and Cronan, 1975; Cronan, 1976a, b; Heath and Dymond, 1977; Bonatti et al, 1979).

Deep sea sediments that are anomalously enriched in transition metals and other elements relative to normal pelagic clays are found near active oceanic ridges (Boström and Peterson, 1966, 1969), in the Bauer Deep a basin between the East Pacific Rise and the Galapagos Rise between 5 and 20°S (Dasch et al, 1971; Bischoff and Sayles, 1972; Sayles and Bischoff, 1973; Sayles et al, 1975), and as basal deposits recovered by the Deep Sea Drilling Project (D.S.D.P.) directly above young oceanic crust. The occurrence of these deposits together with similar deposits on land in Cyprus shows that the process of their formation is not just a recent phenomenon. The basal metal-rich sediments appear to have a widespread distribution, having been reported from the Pacific by von der Borch and Rex (1970), von der Borch et al (1971), Cronan et al (1972), Dymond et al (1973) and Cronan (1976a); from the Atlantic by Boström et al (1972a), and Horowitz and Cronan (1976), and from the Indian Ocean by Cronan et al (1974), Fleet and Kempe (1974), Marchig and Vallier (1974), Pimm (1974)

and Warner and Gieskes (1974). It was suggested that the basal metal-rich sediments represent the ancient analogues of those forming at the ridge crests at the present time and which have been moved to their present position by processes of sea floor spreading (von der Borch and Rex, 1970; Cook, 1971; Boström et al, 1972a; Cronan, 1974; Horowitz and Cronan, 1976).

In general, mid-ocean ridge metalliferous sediments are poor in Al, Ti, Si and Mo and enriched in Fe, Mn, Ba, Mg, Ni, As, Cr, Cu, V, Ag, Tl, Zn, Pb, Hg, Cd, U and B, when compared to normal pelagic sediments (Boström and Peterson, 1966, 1969; Boström et al, 1969; Horowitz, 1970; Cronan, 1972).

For a long time there has been considerable argument over the sources of the constituents in ridge crest and basal metalliferous sediments. Their association with active volcanism near oceanic spreading centers led to the suggestion that these sediments formed by precipitation of metals from deep-seated hydrothermal exhalations. Boström and Peterson (1966, 1969) suggested that such metals were derived from the lower crust or upper mantle. Corliss (1971) suggested that metal-bearing solutions may be produced by the leaching of newly extruded basalt. He found that the interiors of basalts from the Mid-Atlantic Ridge were depleted in Fe, Mn and other elements relative to the flow margins. More recently, Seyfried and Bischoff (1977), in an experimental study, presented evidence that sea water reacts with basaltic glass leaching heavy metals which it can maintain in solution. Other theories not involving volcanic activity have also been proposed to account for the origin of at least some of the constituents of the sediments, such as: biogenic origin (von der

Borch et al, 1971), deposition under reducing conditions (Turekian and Bertine, 1971), submarine weathering of basalts (Bertine, 1974), authigenic precipitation from sea water (Cronan, 1974). It is now recognised that a single element can be supplied to the sediments by more than one process (Cronan, 1976a; Heath and Dymond, 1977). However, it is considered that the formation of these sediments is mainly a result of hydrothermal activity associated with the generation of new ocean floor.

The chemical composition of active-ridge sediments shows considerable variations from one ocean to another. Boström et al (1969) found that Fe and Mn levels in these sediments are greatest in the Pacific, intermediate in the Indian Ocean and lowest in the Atlantic. Cronan (1972) reported higher concentrations of Hg and As in Atlantic sediments than in Pacific ones. Such compositional variations may reflect the variations of rates of terrigenous sedimentation causing dilution of the authigenic constituents (Cronan, 1974), the Atlantic Ocean having the highest detrital sedimentation rate, the Pacific Ocean the lowest, and the Indian Ocean an intermediate rate (Ku et al, 1968). They may also reflect the variations in spreading rates or the basalt chemistry on the various ocean ridges (Cronan, 1974).

In order to study the nature and the chemical character of metalliferous sediments from the south-east Pacific in the present work, three sets of sediment samples, each taken from a rather different environment, have been investigated in detail. The first set is a group of surface and buried sediments taken by gravity corers from an East Pacific Rise fracture zone at $9^{o}S$; the second set is a

group of sediments collected by the Deep Sea Drilling Project, Leg 54 from the Galapagos spreading center; and the third set is a group of surface and buried sediments obtained by gravity corers from the Bauer Deep.

All sediment samples have been analysed using bulk and partition geochemical techniques in an effort to determine their nature, mode of formation, and the process of their metal enrichments. For this purpose the level of metal enrichment in each area has been determined and the metal distribution in the sediments measured, Furthermore, the role of environmental conditions (water depth, biogenic $CaCO_3$ content, biogenic SiO_2 content, bottom topography, water currents) in the distribution of metals among the various components of the sediments has been evaluated.

Comparative study of the partitioning of elements between different phases in the surface and buried sediments can help to identify post-depositional transformations of phases and transfer of elements from one phase to another.

The East Pacific Rise fracture zone sediments were collected from a variety of water depths above and below the lysocline with this aim in mind. The partition geochemical data for these sediments provide information about the role of calcium carbonate dissolution in supplying metals to other phases.

The great distance of the Bauer Deep metalliferous sediments (more than 500 km) from an active spreading center and their distinct compositional features, which are different from those of the metalliferous sediments found on the East Pacific Rise (Dymond et al, 1973), make their origin uncertain. The bulk and partition geochemical data presented in this thesis for Bauer Deep sediments do not support a single mechanism origin for these sediments.

SECTION 1

GEOCHEMISTRY OF SURFACE SEDIMENTS FROM AN EAST PACIFIC RISE FRACTURE ZONE AT 9°S

1.1 INTRODUCTION

Bostrom and Peterson (1966, 1969) were the first to recognise the association of hydrothermal activity with the East Pacific Rise. They demonstrated that sediments from areas of high heat flow contained greater amounts of metals when compared to those obtained from areas of moderate or low heat flow. Hydrothermal exhalations were considered to be responsible for the metal enrichment in the East Pacific Rise sediments. Subsequently Horowitz (1970) studied the distribution of Pb, Ag, Sn, Tl and Zn in sediments from the three main active oceanic ridges. On the basis of high concentrations of Pb, Tl and Zn in East Pacific Rise sediments he suggested that the East Pacific Rise is the most active ridge. Determinations of the accumulation rates of Mn in sediments from East Pacific Rise (Bender et al, 1971) showed that this element accumulates about thirty times faster than in average pelagic sediments. It was suggested that at least some of the elements present in the East Pacific Rise sediments have a local hydrothermal source. However, the volcanic origin of Mn was considered to be suspect due to the fact that only a small decrease in Mn content was found in the holocrystalline basalts which cooled in the presence of sea water. It was also shown that U, Sr and REE were derived from sea water.

Piper (1973) compared the elemental composition of tholeiitic basalt with that of sediments from the crest of the East Pacific Rise and he found that As, B, Ag, Tl, Mn, Cd, Pb and Cu were the most enriched elements in the sediments compared to the basalt. Based on the order of metal enrichment, the author suggested that these elements were extracted from newly-upwelled basalt by sea water which invaded

along cracks of the rock and ascended in the form of hydrothermal solutions. In a later work, Piper and Graef (1974) studied the distribution of REE and gold in surface sediments across the East Pacific Rise at 39^{o}S. They confirmed the seawater source of REE while they found an anomalously high Au concentration for the crestal sediments. It was concluded that Au, like Fe, had a hydrothermal origin. However, the similarity of Au concentrations in the sediments from the flanks with those of marine basalt suggested its partial association with lithogenic material.

Rydell et al (1974) determined the distribution of uranium and thorium in East Pacific Rise crest sediments, and they found very unusual values. Uranium was enriched, while ^{232}Th was depleted in these sediments. Post-depositional injections of solutions, similar in composition to carbonate emanations (rich in U and depleted in ^{232}Th) were considered to be responsible for this distribution pattern. It was observed that, despite the fact that the sediments were obtained from a site well above the calcium carbonate compensation depth (CCD), the foram tests present in the sediments were corroded. This corrosion was considered to be a result of post-depositional injections of hydrothermal solutions in the sediments.

In a comparative geochemical and mineralogical study of metalliferous sediments from East Pacific Rise, the Bauer Deep and the Deep Sea Drilling Project (DSDP), Dymond et al (1973) suggested their common origin. They concluded that the only hypothesis which could explain the chemistry and the geologic setting of these sediments was that involving precipitation of metals from hydrothermal emanations.

McMurtry (1975) studied the distribution of Mn, Fe, Cu, Ni, Co and Cr in surface sediments across the Nazca Plate at 12°S. He found that the average composition of sediments obtained from the East Pacific Rise was markedly different from that reported by Bostrom and Peterson (1969), Piper (1973) and Dymond et al (1973). The most remarkable difference lay in the concentrations of Fe and Mn, which were similar to their average values in normal pelagic sediments. The values of Cu, Ni, Co and Cr were found to be higher when compared to those reported by the above authors.

More recently, Heath and Dymond (1977), using a normative method, determined the proportional contribution of hydrothermal, detrital and hydrogenous supply of elements in East Pacific Rise sediments at 10°S. They demonstrated that most of Fe, Mn, Zn, Ba, Ni, Si and Al were of hydrothermal origin.

The work on surface sediments from the East Pacific Rise at 9°S (see Figure 1.1) was initiated in order:

(i) to study the possibility of metalliferous sediment ponding within basins in the East Pacific Rise fracture zone at 9°S, and

(ii) to determine the distribution of metals in sediments away from the crest ridge.

For this purpose, surface sediment samples at increasing distance from the intersection of the fracture zone with the crest of the Rise, and from the whole depth range encountered in the fracture zone, have been investigated. The results of this work are compared with those from the Mid-Atlantic Ridge and other mid-ocean ridges in order to see if environmental differences between these areas, and particularly the possibility of partially restricted conditions occurring in the fracture zone, are reflected in the geochemical behaviour of the elements studied.

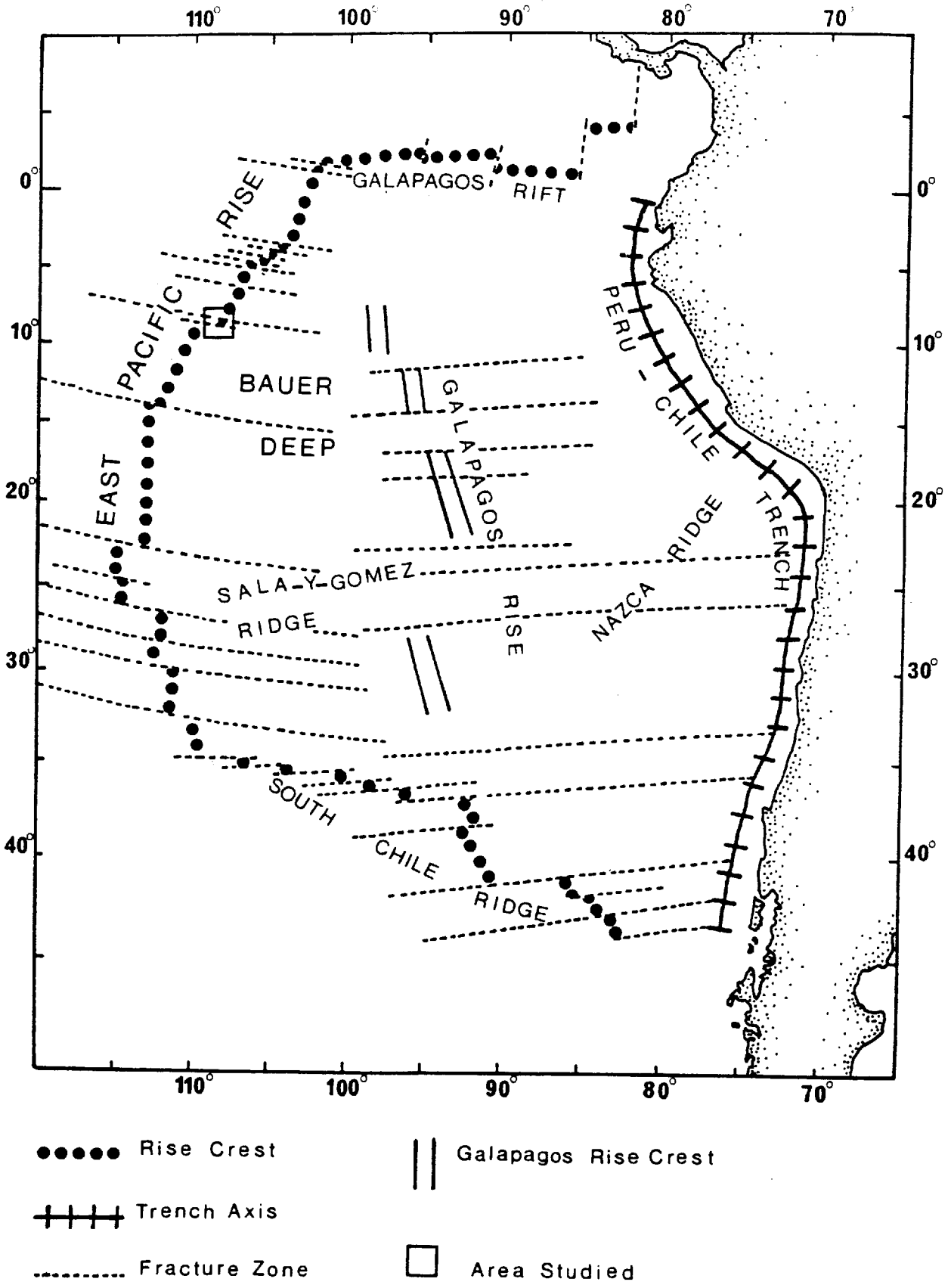

Figure 1.1: Location map showing the area studied and major tectonic features on the Nazca Plate.

1.2 GEOLOGY AND BATHYMETRY OF THE 9°S FRACTURE ZONE

The 9°S fracture zone offsets the East Pacific Rise axis 200 km right laterally from 109.8°W south of the fracture zone to 108°W to the north. According to Rea (1975), the blocks of this fracture zone were formed by jumps in spreading activity from the Galapagos Rise. The part of the East Pacific Rise south of the 9°S fracture zone formed 8 m.y.a. and that to the north about 6.4 m.y.a. Thus, for a period of approximately 1.5 m.y. the new East Pacific Rise was connected with the old Galapagos Rise by a 900 km long active transform fault which was what is now the 9°S fracture zone. The structure of this fracture zone changed relatively recently. A shift in the spreading rates or their directions occurred 1.0 to 1.2 m.y.a. which caused changes in the stresses in the lithosphere near the East Pacific Rise axis and which resulted in deeper faulting. These alterations were reflected in the structure of the 9°S fracture zone, which at that time was a simple step offset. It started to widen and became a 100 km wide feature with discontinuous ridges and troughs. Its topography is more complex 80 km west of its southern bound block and 100 km east of its northern bound block (Rea, 1975).

The bottom topography of the part of the fracture zone studied here is generally rough, the water depth ranging from 2400 m to 3800 m. The most striking feature of this topography is the presence of a large number of narrow basins and hills (see Figure 1.2). It is noted that the basins containing the stations SH 1529, SH 1530, SH 1531 and SH 1546 have an ellipsoidal shape, the long axis of which falls on the same line. Their relative position, one after the other, produces a continuous chain of long narrow basins resembling

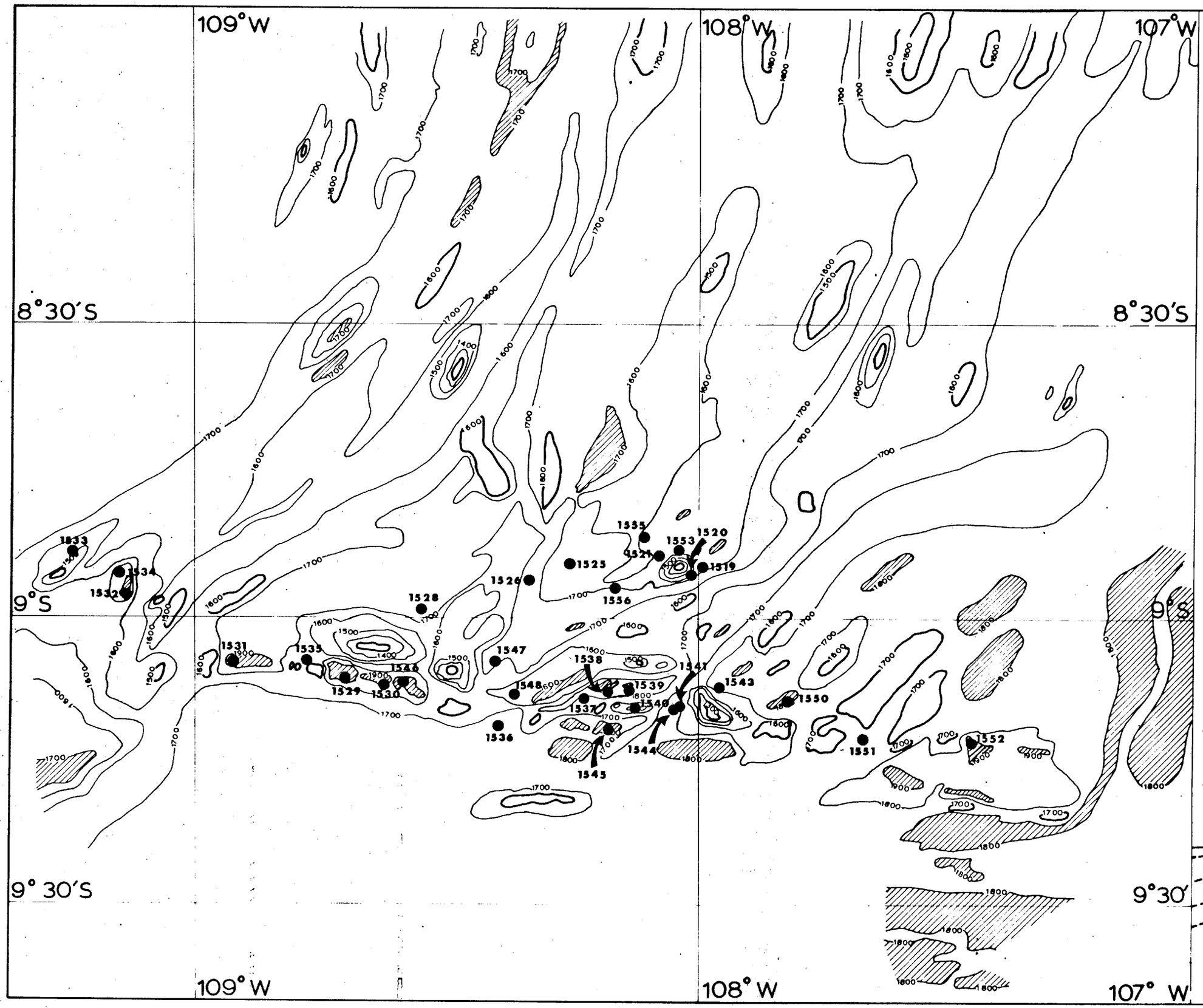

FIG. 1.2 BATHYMETRIC MAP OF THE EAST PACIFIC RISE FRACTURE ZONE AT 9° S SHOWING THE SAMPLE LOCATIONS

a long furrow with an E-W direction. The above depressions are surrounded by a number of hills, some of which are also of ellipsoidal shape, the long axis of which is parallel to the long axis of the basins. It is of interest to note that the direction of most of the elongated basins and hills present east of 108°W and west of 109°W is not parallel to the direction of those present between 108°W and 109°W. In the eastern part of the fracture zone (at about 107°W) two elongated and relatively wide basins occur. One of them has a N-S direction, while the direction of the other one changes from N-S to E-W.

North of the fracture zone the water depth becomes considerably shallower and the isobaths have a NE-SW direction, in contrast to the NW-SE direction dominant in the fracture zone. It is noteworthy that this direction is nearly perpendicular to the long axis of the fracture zone basins and also parallel to the direction of the East Pacific Rise axis at this latitude. At 108°2.3'W, 8°53.94'S, a large sea mount occurs which rises 750 m above the surrounding area.

On the basis of Ocean Bottom Seismographs (OBS) the crest of the Rise at about 9°S is located between 108°10'W and 108°20'W (Francis and Lilwall, personal communication, 1979). This is consistent with the topography of this area, which shows an elevated and elongated feature of NE-SW direction. Based on the direction of the isobaths and on the position of the East Pacific Rise crest, it may be suggested that the East Pacific Rise-fracture zone intersection should occur near the station SH 1547.

1.3 CHEMICAL COMPOSITION OF THE SEDIMENTS IN THE EAST PACIFIC RISE 9°S FRACTURE ZONE

All surface sediments from the area studied have been analysed in bulk by atomic absorption spectroscopy according to the procedures described in Appendix B. The results are given on a carbonate-free basis (C.F.B.) in Table 1.1.

The surface sediments are divided into four major groups according to their geographic location: Group A includes sediments from the crest of the Rise, Group B consists of non-crest sediments, Group C includes all sediments from the elevated areas of the fracture zone, and Group D represents sediments from the basins in the fracture zone floor. The average chemical composition of all surface sediments and that of each group are given in Table 1.2, along with the composition of other sediments for comparison.

The sediments from all groups are enriched in Mn, Fe, Ni, Cu, Pb and Zn relative to the average background values of pelagic sediments and hence could be characterized as metalliferous. Comparison of the crest sediments (Group A) with the sediments of the other groups (B, C and D) indicates that they contain higher amounts of Fe, Mn, Ni, Zn and Cu than the other sediments. In contrast, the concentrations of Co in the sediments from Group A are lower compared with the other groups. Except for Pb and Ba, the metal enrichment in the sediments from the fracture zone basins is greater than those taken from the elevated areas (see Table 1.1). Figures 1.3, 1.4, 1.5, 1.6 and 1.7 indicate that there is a positive correlation between the carbonate-free concentrations of Mn, Fe, Zn, Cu and Ni and the depth of water.

Table 1.1: Chemical composition of surface fracture zone sediments,

	Station No.	$CaCO_3$ %	Ca %	Mn %	Fe %	Ni ppm	Co ppm	Pb ppm	Zn ppm	Cu ppm	Al %	Ba %	SiO_2 %
GROUP A	SH 1525	72.82	29.77	4.49	13.54	533	107	132	331	728	0.40	0.84	20.31
	SH 1537	84.18	34.58	3.22	13.15	341			278	601	0.76	1.07	20.29
	SH 1547	81.64	33.23	3.54	13.73	321	44	87	321	632	0.93	0.87	24.07
	Average	79.55	32.53	3.75	13.47	398	76	110	310	654	0.70	0.93	21.56
GROUP B	SH 1521	83.96	34.14	2.74	12.41	262	162	175	293	611	1.75	0.94	28.87
	SH 1526	78.20	31.88	3.03	11.65	248	41	78	284	564	0.69	0.69	21.74
	SH 1528	76.37	31.16	2.20	10.28	212	55	97	216	423	3.72	0.47	31.15
	SH 1553	80.20	32.67	2.02	9.55	182	71	126	232	439	1.92	1.52	24.44
	SH 1555	77.89	31.76	2.53	11.17	226	86	86	253	525	1.22	0.63	23.20
	SH 1556	72.36	29.58	1.99	10.42	213	83	76	232	459	2.21	0.51	28.69
	Average	78.16	31.87	2.42	10.19	224	83	106	252	504	1.92	0.79	26.35
GROUP C	SH 1533	82.39	33.53	3.18	9.99	290	34	114	267	494	0.68	1.59	25.16
	SH 1535	81.78	33.29	2.09	8.84	263	126	154	209	406	1.48	0.77	20.53
	SH 1536	83.43	33.94	2.60	9.60	199	115	133	266	513	0.72	1.99	15.33
	SH 1540	81.68	33.25	2.51	9.77	251			218	480	0.66	1.47	18.01
	SH 1541	84.91	34.52	2.39	8.15	232	73	166	225	411	0.66	1.72	20.41
	SH 1543	86.59	35.18	1.94	7.38	231	149	209	224	410	0.67	0.97	14.39
	SH 1548	85.60	34.79	2.08	7.92	257	118	132	215	368	1.04	1.04	17.99
	SH 1551	85.54	34.77	1.66	5.60	263	76	118	173	325	0.55	1.45	13.83
	Average	83.99	34.16	2.31	8.41	248	99	147	225	426	0.81	1.38	18.21

Table 1.1: Continued

Station No.		$CaCO_3$ %	Ca %	Mn %	Fe %	Ni ppm	Co ppm	Pb ppm	Zn ppm	Cu ppm	Al %	Ba %	SiO_2 %
GROUP D	SH 1529	71.98	29.44	3.21	12.10	282	39	71	264	575	1.14	0.79	18.31
	SH 1530	78.62	32.05	3.04	11.65	267	37	75	257	543	0.84	0.84	18.76
	SH 1531	67.08	27.51	2.98	11.54	228	94	106	255	529	2.10	1.06	27.73
	SH 1532	70.60	28.89	3.71	13.27	269	102	116	299	616	1.50	0.75	21.87
	SH 1534	75.29	30.74	3.04	11.45	320	40	77	259	514	1.05	0.69	17.08
	SH 1538	76.68	31.28	2.06	8.32	163	26	99	274	566	0.51	1.29	15.69
	SH 1539	81.76	33.28	2.91	10.91	280			258	543	0.77	1.21	18.09
	SH 1544	86.03	34.96	2.65	9.31	265	115	107	258	494	0.72	1.07	19.90
	SH 1545	81.01	32.98	2.53	9.16	253	121	153	232	458	0.63	1.00	18.85
	SH 1546	78.86	32.14	2.70	10.17	222	128	90	241	497	0.80	0.66	18.50
	SH 1550	87.74	35.63	2.53	8.32	277	147	212	245	465	0.65	1.14	20.23
	Average	77.79	31.72	2.85	10.56	257	85	103	258	527	0.97	0.95	19.55

Group A: Sediments from the crest of the Rise.

Group B: Non-crest sediments.

Group C: Sediments from the elevated areas.

Group D: Sediments from the basins in the fracture zone floor.

All data except Ca are corrected to a calcium carbonate-free basis.

Table 1.2: Composition of sediments from the Pacific, Atlantic and Indian Oceans.

	Ca %	Fe %	Mn %	Ni ppm	Co ppm	Pb ppm	Zn ppm	Cu ppm	Al %	Ba %	Si %
1	32.53	13.47	3.75	398	76	110	310	654	0.70	0.93	10.08
2	31.87	10.91	2.42	224	83	106	252	504	1.92	0.79	12.32
3	34.16	8.41	2.31	248	99	147	225	426	0.81	1.38	8.51
4	31.72	10.56	2.85	257	85	103	258	527	0.97	0.95	9.14
5	32.57	10.84	2.83	282	86	117	261	528	1.10	1.01	10.01
6		18.00	6.00	430	105	152	380	730	0.50		
7		9.62	0.54	214		349	228	399	5.30		
8		10.30	0.12	39		63	140	92	5.88		
9	34.36	4.31	0.77	178	118	92	161	319	2.38	0.67	9.14
10	26.88	6.86	0.40	481	68	71	168	306	8.12	0.37	16.05
11		5.07	0.48	211	101	68		323			

1) This study: all crest sediments.

2) This study: all non-crest sediments.

3) This study: all sediments from the elevated areas.

4) This study: all sediments from the basins.

5) This study: all fracture zone sediments.

6) Boström and Peterson (1969), Horowitz (1970): East Pacific Rise sediments.

7) Horowitz (1974): Mid-Atlantic Ridge, 45°N, Median Valley sediments.

8) Horowitz (1974): Reykjanes Ridge sediments.

9) Horder (1979): Central Indian Ocean Ridge crestal sediments.

10) Horder (1979): Central Indian Ocean Ridge fracture zone sediments.

11) Cronan (1969): Pacific surface pelagic sediments.

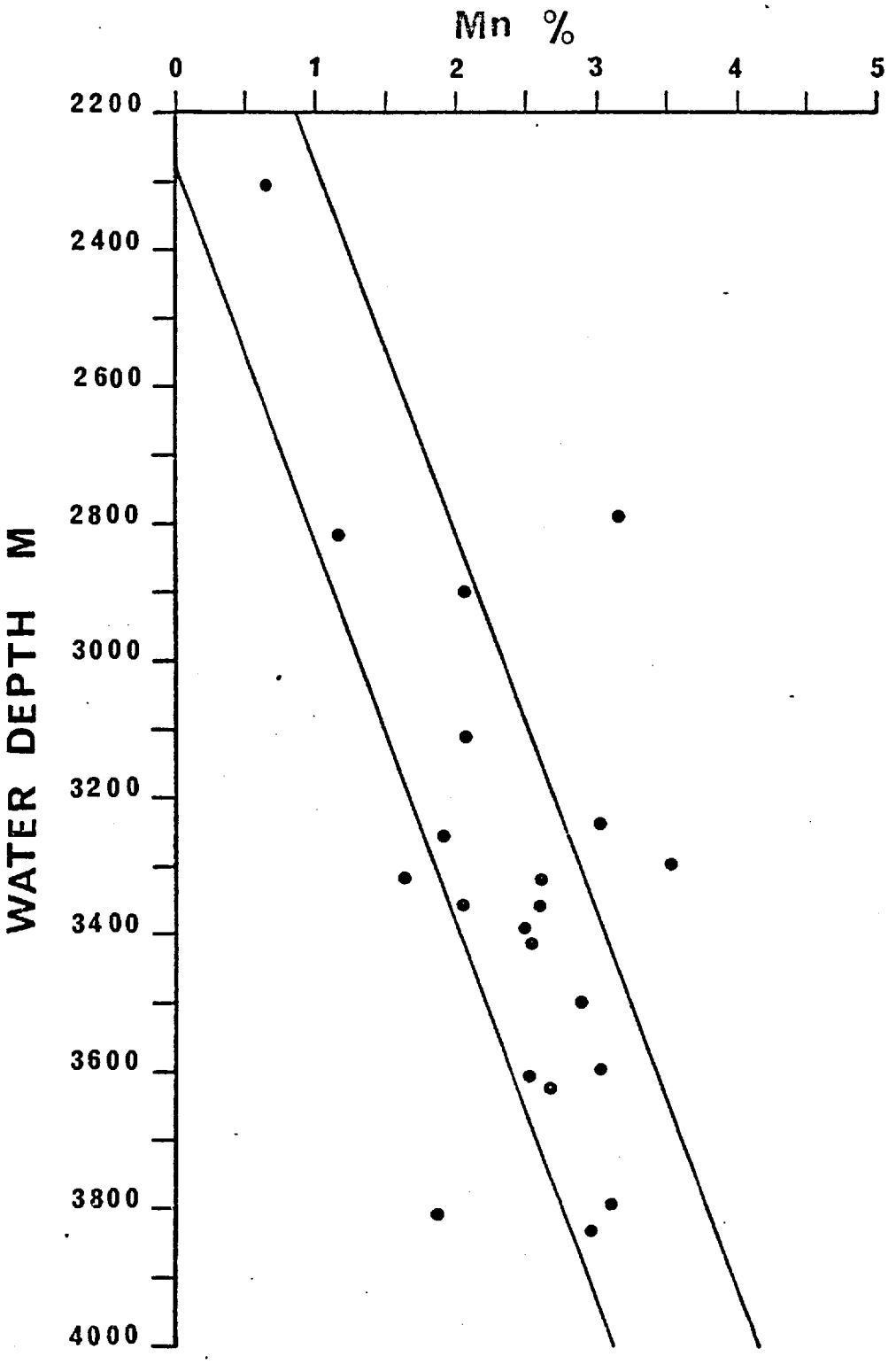

Figure 1.3: Scatter plot showing the positive correlation between the carbonate-free concentrations of Mn in the surface sediments and the water depth.

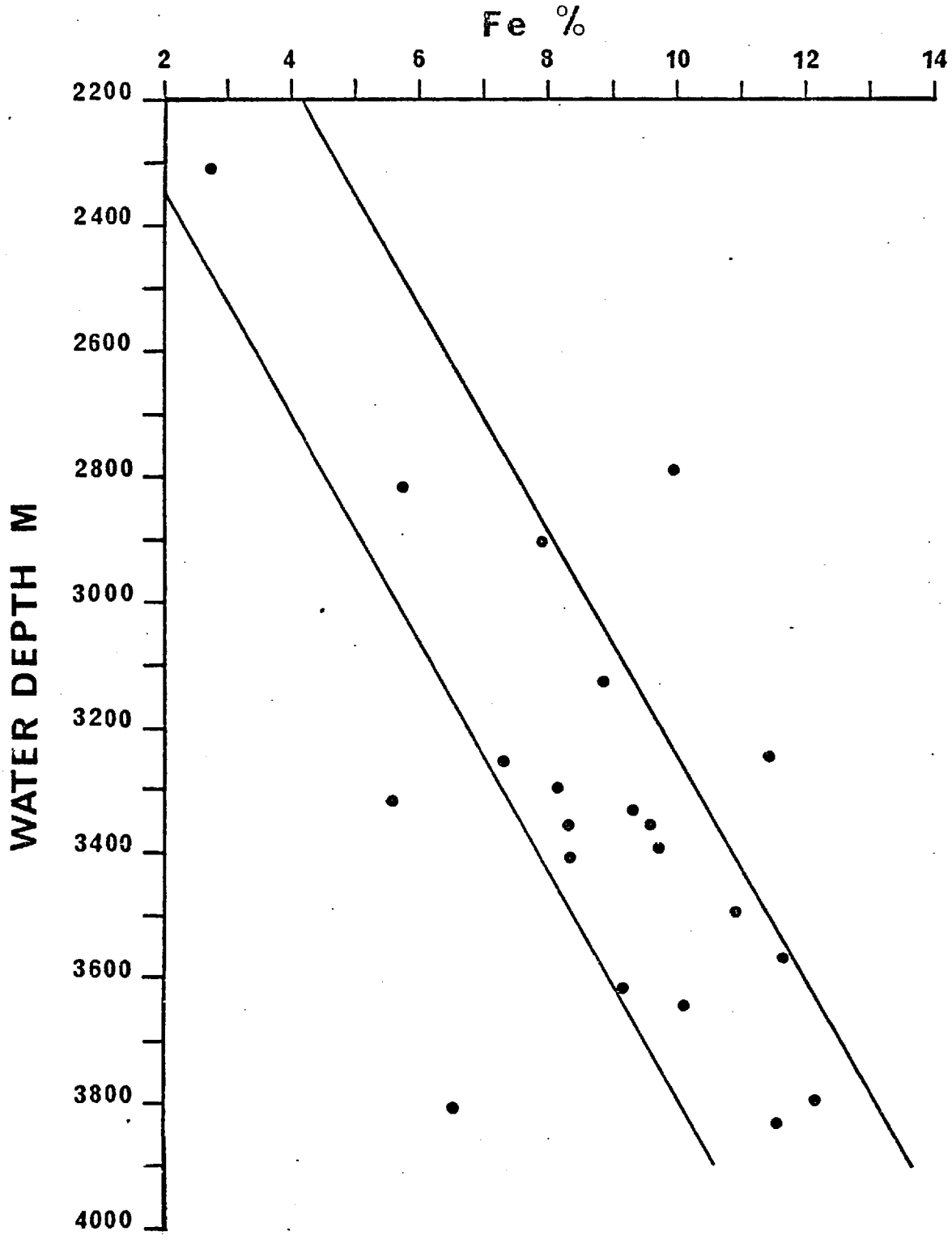

Figure 1.4: Scatter plot showing the positive correlation between the carbonate-free concentrations of Fe in the surface sediments and the water depth.

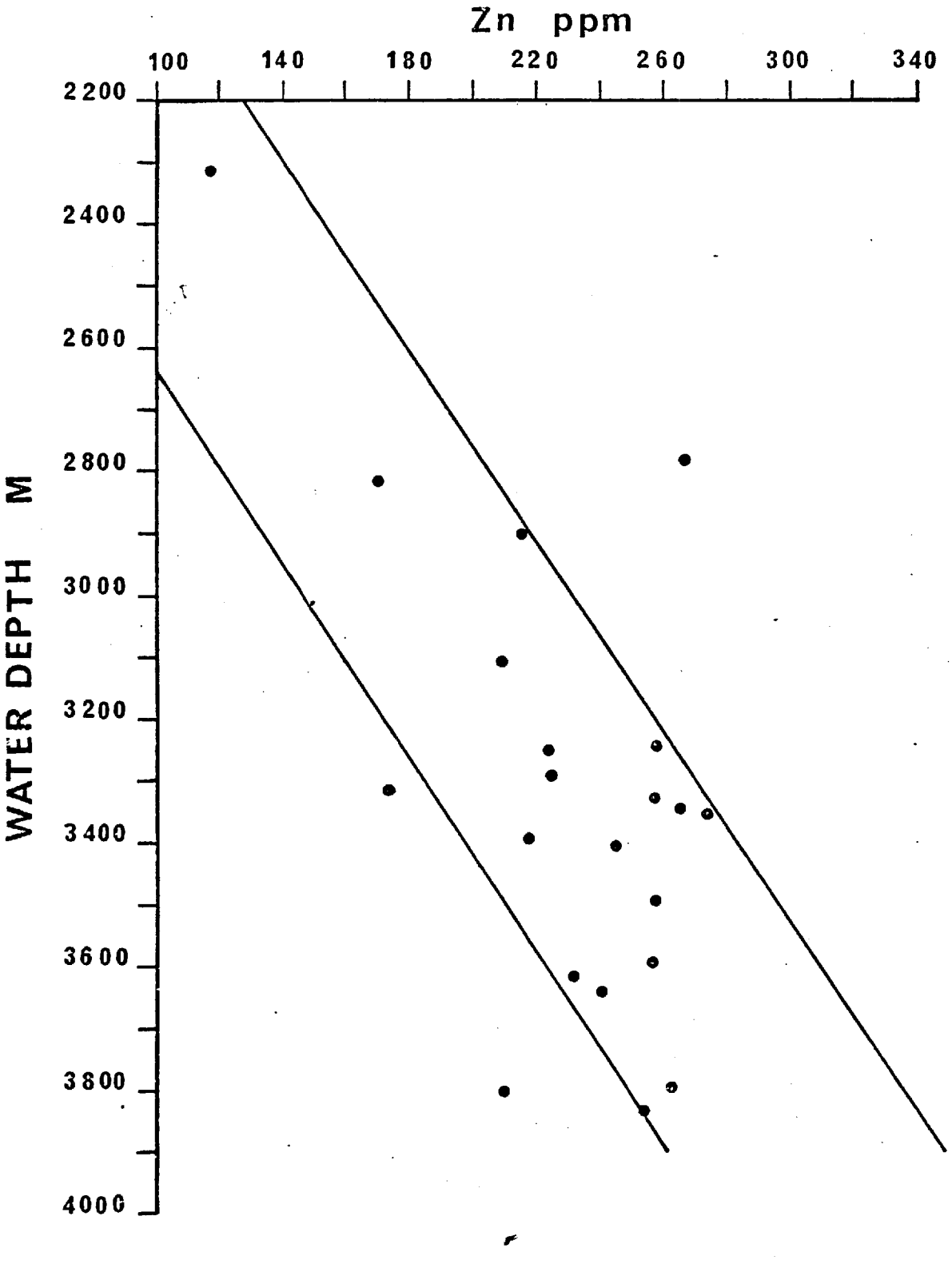

Figure 1.5: Scatter plot showing the positive correlation between the carbonate-free concentrations of Zn in the surface sediments and the water depth.

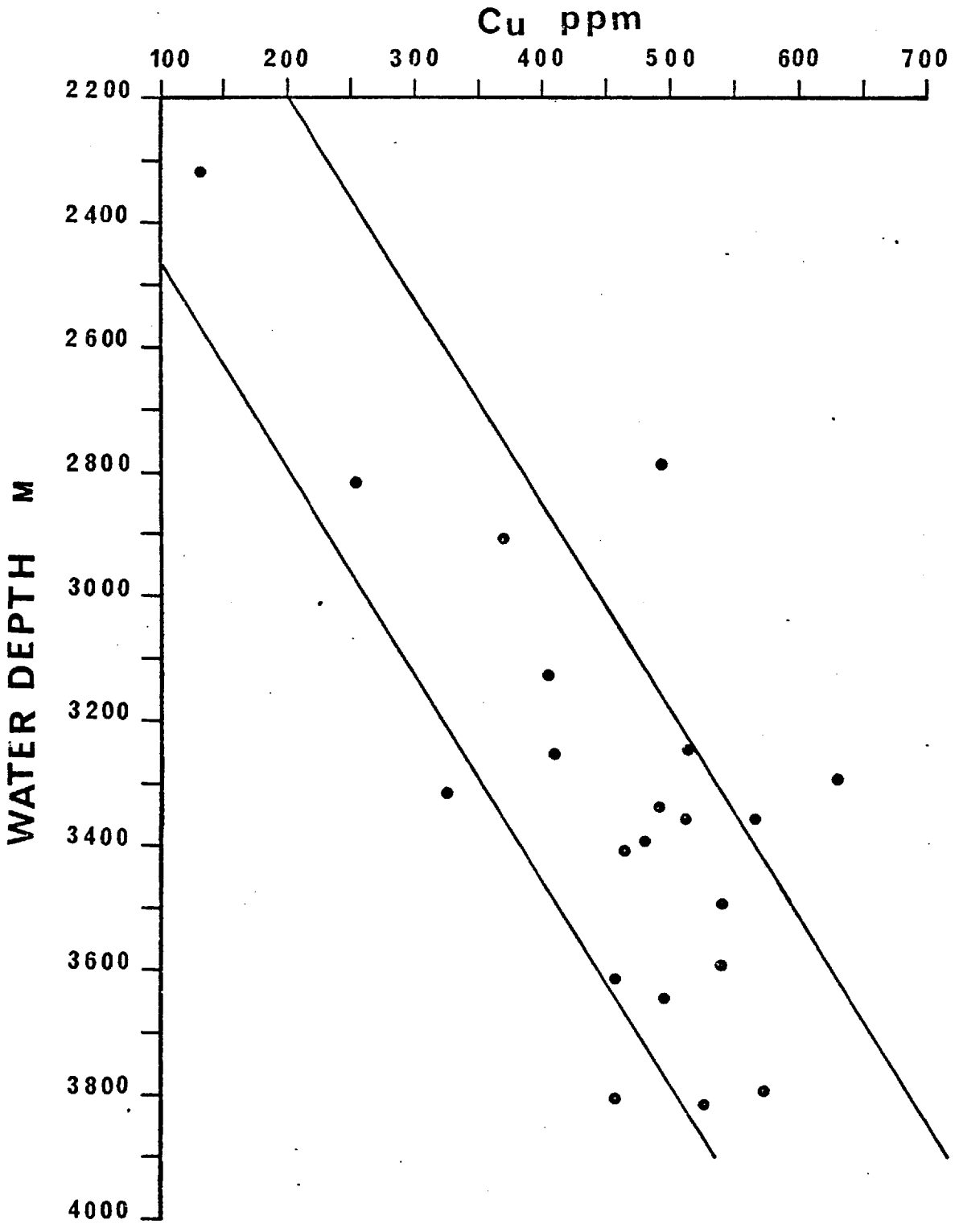

Figure 1.6: Scatter plot showing the positive correlation between the carbonate-free concentrations of Cu in the surface sediments and the water depth.

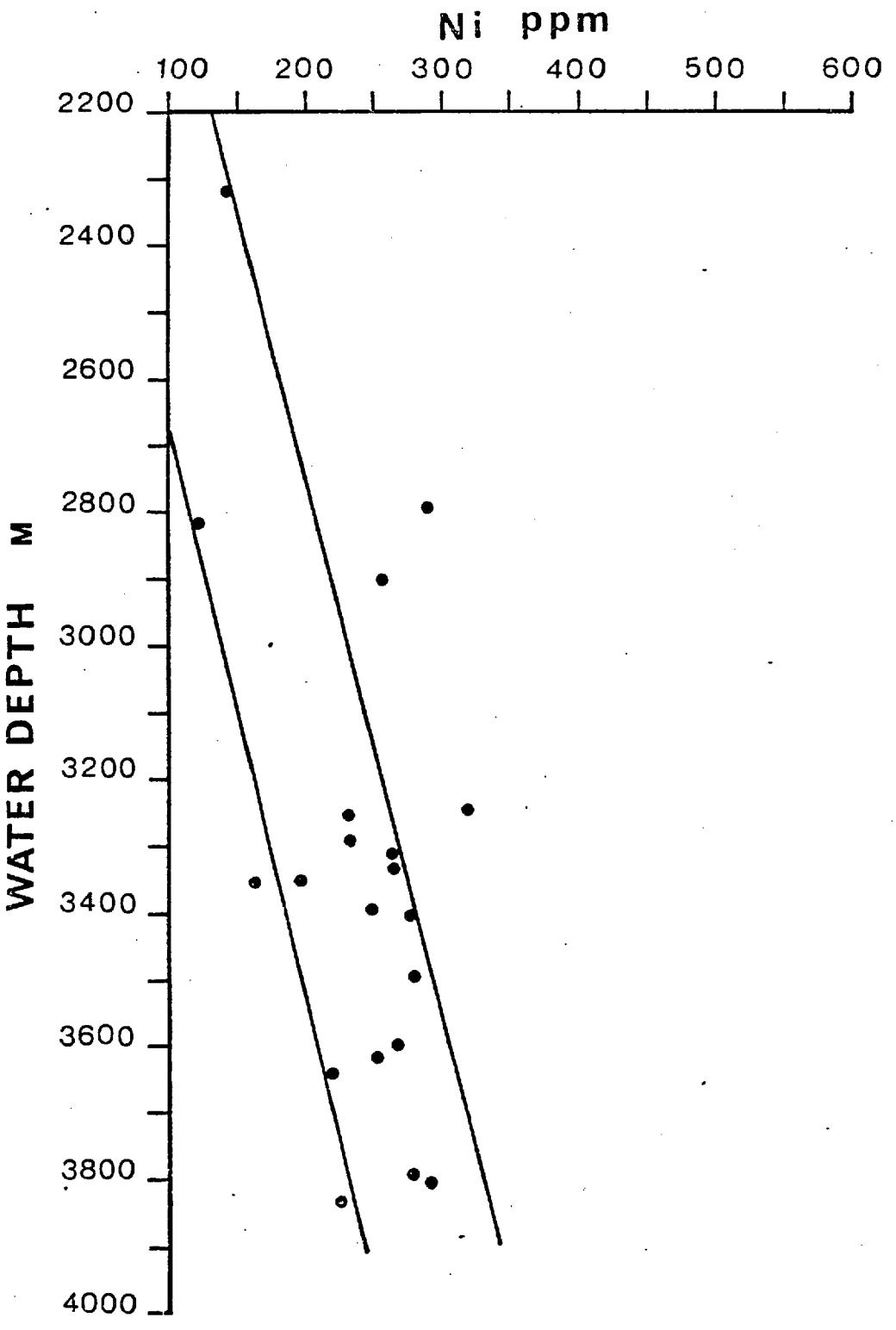

Figure 1.7: Scatter plot showing the positive correlation between the carbonate-free concentrations of Ni in the surface sediments and the water depth.

Comparison of the average chemical composition of Group A with that of Group b reported by Boström and Peterson (1969) for the crest of East Pacific Rise indicates that the crest sediments at $9^{o}S$ contain lower amounts of Fe, Mn, Ni, Co, Pb, Zn and Cu. By contrast, the concentrations of Fe, Mn, Ni, Zn and Cu in the East Pacific Rise fracture zone sediments are higher relative to the average concentration of these metals in sediments from the Mid-Atlantic Ridge. However, the concentrations of Pb are lower in the former than in the latter sediments (Horowitz, 1974). Similarly, the East Pacific Rise fracture zone sediments contain higher amounts of Fe, Mn, Co, Pb, Zn, Cu and Ba and lower amounts of Ni compared with Indian Ocean fracture zone sediments (Horder, 1979) (see Table 1.2).

1.4 HORIZONTAL CHEMICAL VARIATIONS THROUGHOUT THE SURVEY AREA

To examine possible relationships between the concentrations of elements and the depth of water, the elemental concentrations for each station have been plotted on bathymetric maps (see Figures 1.8 to 1.14 and 1.16 to 1.19).

1.4.1 Calcium Carbonate (see Figure 1.8)

The distribution of $CaCO_3$ in marine sediments is generally a reflection of depth of water. The highest content of $CaCO_3$ is found in sediments on the sea mount area, which is well above the lysocline. A zone exists between $107^{\circ}25'W$ and $108^{\circ}W$ where the content of $CaCO_3$ is uniformly high ($>85\%$) (stations SH 1519, SH 1543, SH 1550, SH 1551, SH 1552). Between $108^{\circ}W$ and $108^{\circ}25'W$ the concentration of $CaCO_3$ is lower (80-85%) (stations SH 1541, SH 1539, SH 1540, SH 1545, SH 1547, SH 1537, SH 1536), but relatively high when compared with its content in the other sediments. It is observed that sediments with high concentrations of Fe and other metals have generally low concentrations of $CaCO_3$ (stations SH 1525, SH 1526, SH 1556, SH 1555, SH 1532, SH 1534, SH 1529, SH 1530). Despite the fact that the depth of water at station SH 1525 is remarkably shallower than at stations SH 1529 and SH 1530, the content of $CaCO_3$ is lower at the former than at the latter stations.

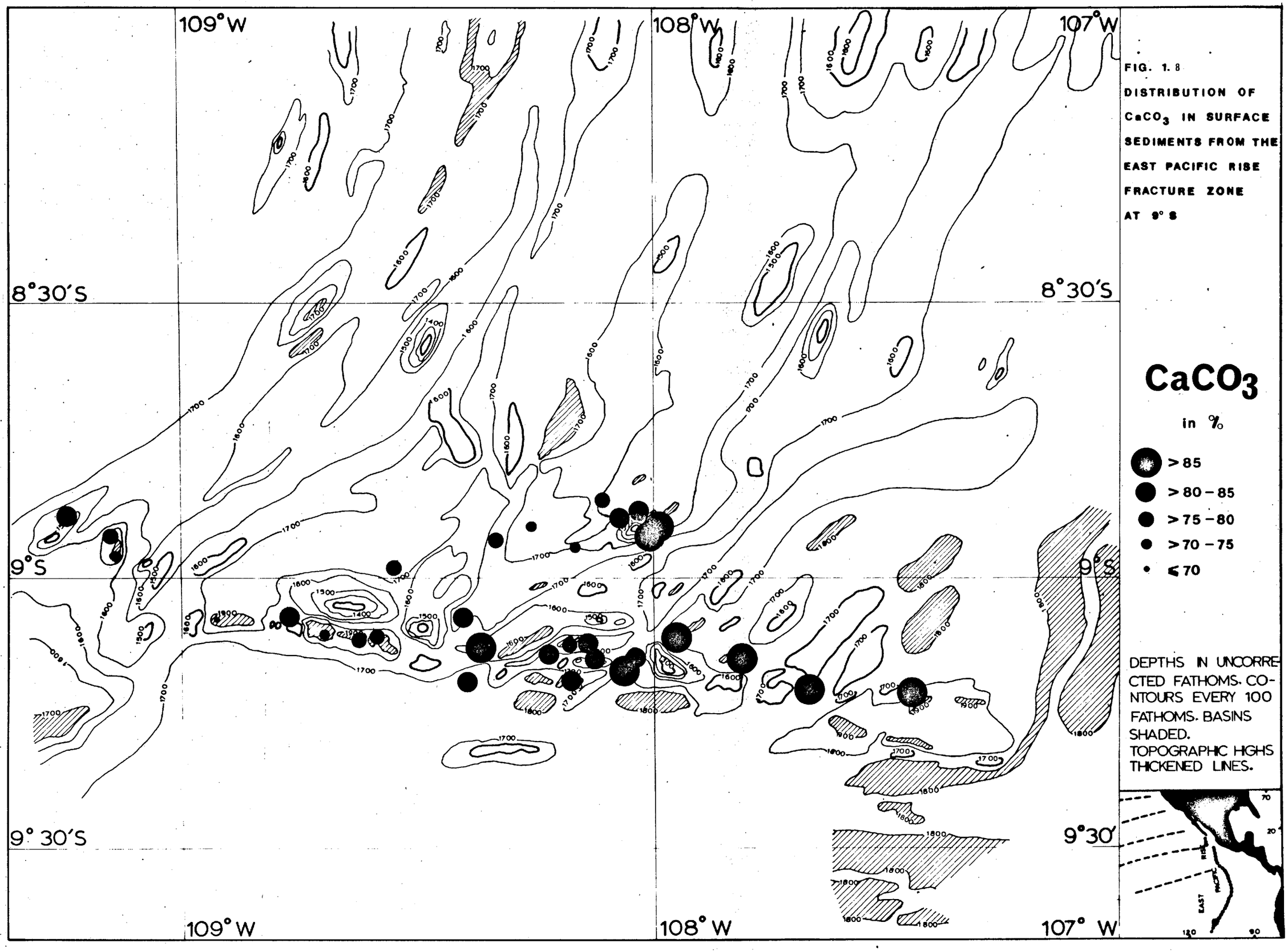

FIG. 1.8
DISTRIBUTION OF $CaCO_3$ IN SURFACE SEDIMENTS FROM THE EAST PACIFIC RISE FRACTURE ZONE AT 9° S

1.4.2 Iron (see Figure 1.9)

The concentrations of Fe vary throughout the survey area from 2.74% up to 13.54%. Its distribution in the surface sediments supports its local hydrothermal origin. The highest concentration of Fe is shown at the station SH 1547 (13.73%) while sediments from SH 1525, SH 1537 and SH 1532 also have high concentrations of Fe (>13%). Around the stations SH 1525 and SH 1547 there is an enrichment with lower concentrations of Fe (10-13%) (SH 1539, SH 1556, SH 1521, SH 1555, SH 1526, SH 1528, SH 1546, SH 1530, SH 1529). South of the station SH 1539 a third zone occurs where the concentrations of Fe range between 7 and 10%. It includes the following stations: SH 1536, SH 1545, SH 1538, SH 1540, SH 1544, SH 1543, SH 1550, SH 1548 and SH 1541. Despite the limited number of samples available from the western part of the area (SH 1532, SH 1533, SH 1534, SH 1531, SH 1535) it can be seen that Fe around the station SH 1532 displays a similar distribution. The sediments at the stations SH 1551, SH 1552, SH 1519 and SH 1520 are not enriched in Fe; their values are similar to those of normal pelagic sediments.

1.4.3 Manganese (see Figure 1.10)

Although the general distribution of Mn is similar to that of Fe, Mn has a more widespread dispersion. The highest concentration of Mn is shown in sediments from station SH 1525 and not from SH 1547, as in the case of Fe. However, sediments around the stations SH 1532 and SH 1547, where Fe shows its highest concentrations, are remarkably enriched in Mn.

FIG. 1-9

DISTRIBUTION OF Fe IN SURFACE SEDIMENTS FROM THE EAST PACIFIC RISE FRACTURE ZONE AT 9° S

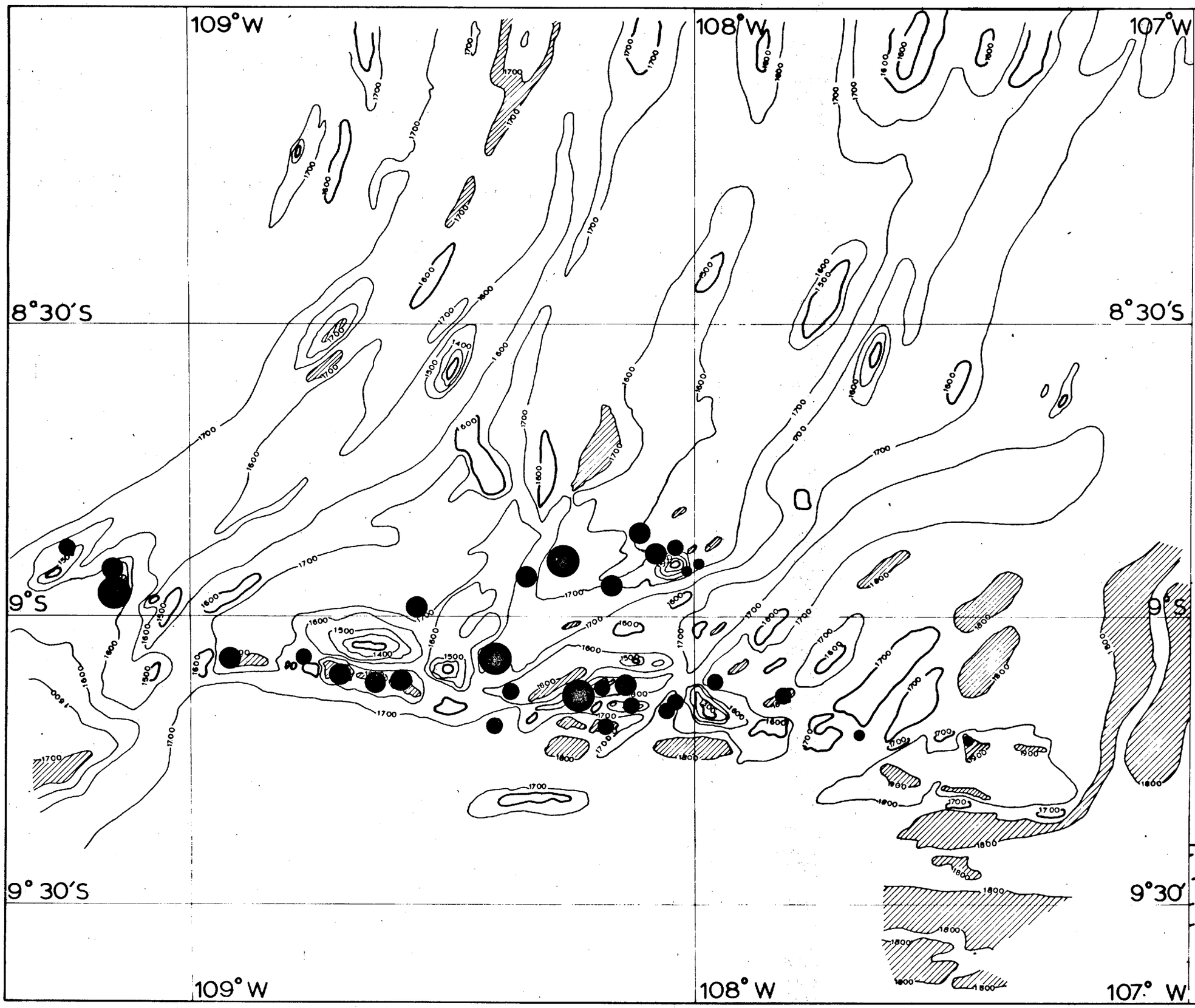

109°W

108°W

107°W

8°30'S

9°S

9°30'S

109° W

108° W

107° W

9°30'

FIG. 1.10
DISTRIBUTION OF Mn IN SURFACE SEDIMENTS FROM THE EAST PACIFIC RISE FRACTURE ZONE AT 9° S

Mn

CFB in %

- > 4
- > 3 - 4
- > 2 - 3
- ≤ 2

DEPTHS IN UNCORRECTED FATHOMS. CONTOURS EVERY 100 FATHOMS. BASINS SHADED. TOPOGRAPHIC HIGHS THICKENED LINES.

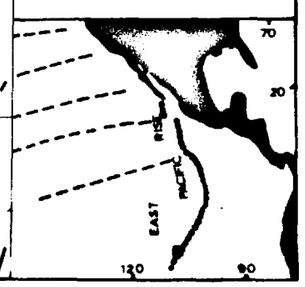

Two main areas of enrichment can be recognised in the distribution of Mn in the eastern part of the survey area: the first is defined by the stations SH 1525, SH 1547, SH 1526, SH 1537 and includes sediments whose Mn content is higher than 3%. The second area extends around the first, being fairly wide and including the following stations: SH 1528, SH 1546, SH 1536, SH 1548, SH 1545, SH 1540, SH 1539, SH 1538, SH 1544, SH 1541, SH 1556, SH 1521 and SH 1555. The concentrations of Mn in these sediments range between 2 and 3%. East of this area is a third zone where the sediments are slightly enriched in Mn ($< 2\%$). Stations SH 1519, SH 1520, SH 1543, SH 1551 and SH 1552 fall within this zone. It is of interest to note that although the concentrations of Mn drop gradually towards the eastern part of the area and at about $108^{o}W$ its values are well below 2%, the sediments in the basin containing station SH 1550 show an abrupt increase in the concentration of Mn ($\sim$ 2.5%).

In the western part of the area (stations SH 1532, SH 1533, SH 1534 and SH 1531) the sediments are enriched in Mn by a factor similar to that of the central zone of the eastern area. In contrast to the case of Fe, the concentrations of which drop fairly rapidly east and west of station SH 1532, the concentrations of Mn remain high in a more extensive zone ($\geqslant 3\%$). It is also noticeable that the concentrations of Mn in the sediments from stations SH 1529 and SH 1530 are relatively high, being similar to those of SH 1532 and SH 1525.

1.4.4 Nickel (see Figure 1.11)

The distribution of Ni in the surface sediments resembles that of Mn rather than that of Fe. The highest concentration of Ni is found in the sediments from station SH 1525, while stations SH 1537 and SH 1547 also show relatively high levels of Ni. Around SH 1525 the values of Ni drop off very sharply (stations SH 1526, SH 1555, SH 1556 and SH 1528) but they increase again in a fairly wide zone around station SH 1537 (stations SH 1548, SH 1545, SH 1544, SH 1540 and SH 1539). At about 108°W the concentrations of Ni reach very low values, being comparable to those of normal pelagic sediments. However, there is a tendency for the concentrations of Ni to increase markedly towards stations SH 1551 and SH 1552, where they reach values similar to those found at station SH 1539.

In the western part of the area, the highest concentration of Ni is shown at SH 1533, in contrast to the case of Fe and Mn, the greatest enrichment of which is found at SH 1532. However, there is a decrease of the concentrations of Ni east and west of SH 1533. Despite the fact that stations SH 1529, SH 1530 and SH 1535 are surrounded by sediments which show no enrichment in Ni relative to the average background values in normal pelagic sediments, the concentrations of Ni at these stations are fairly high.

1.4.5 Copper, Zinc (see Figures 1.12 and 1.13)

Copper and zinc display similar distributions. Stations SH 1525 and SH 1547 define a center where these metals show their highest concentrations. A well-defined enrichment, especially in the

109°W

108°W

107°W

8°30'S

9°S

9°30'S

109° W

108° W

107° W

9°30'

FIG. 1.11
DISTRIBUTION OF NI IN SURFACE SEDIMENTS FROM THE EAST PACIFIC RISE FRACTURE ZONE AT 9° S

Ni

CFB ppm

- > 500
- > 300-500
- > 250-300
- > 200-250
- < 200

DEPTHS IN UNCORRECTED FATHOMS CONTOURS EVERY 100 FATHOMS. BASINS SHADED. TOPOGRAPHIC HIGHS THICKENED LINES.

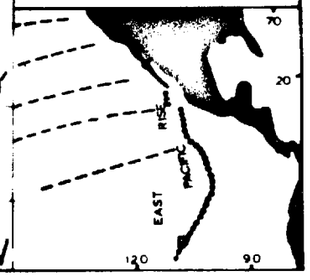

109°W

108°W

107°W

8°30'S

9°S

9°30'S

109° W

108° W

107° W

9°30'

FIG. 1.12
DISTRIBUTION OF Cu IN SURFACE SEDIMENTS FROM THE EAST PACIFIC RISE FRACTURE ZONE AT 9° S

Cu

CFB ppm

- > 700
- > 600-700
- > 500-600
- > 400-500
- < 400

DEPTHS IN UNCORRECTED FATHOMS. CONTOURS EVERY 100 FATHOMS. BASINS SHADED. TOPOGRAPHIC HIGHS THICKENED LINES.

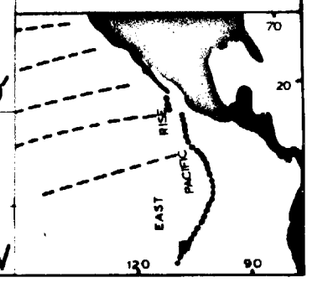

109°W

108°W

107°W

8°30'S

9°S

9°30'S

109° W

108° W

107° W

FIG. 1.13

DISTRIBUTION OF Zn IN SURFACE SEDIMENTS FROM THE EAST PACIFIC RISE FRACTURE ZONE AT 9° S

Zn

CFB ppm

- ≥ 300
- > 250-300
- > 200-250
- ≤ 200

DEPTHS IN UNCORRECTED FATHOMS. CONTOURS EVERY 100 FATHOMS. BASINS SHADED. TOPOGRAPHIC HIGHS THICKENED LINES.

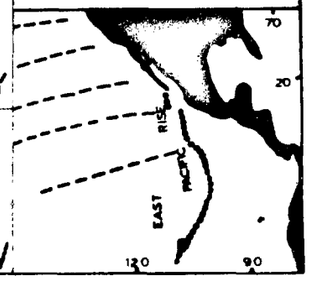

case of Zn, with lower concentrations of Zn and Cu, occurs around this center. The concentrations of Cu and Zn tend to decrease east and west of this area so that a third zone with lower concentrations is recognised. Cu and Zn, like the other metals mentioned, have high values at SH 1532 and decrease east and west of this station. As in the case of Fe, Mn and Ni, the concentrations of Cu and Zn at SH 1529 and SH 1530 are markedly high when compared with the surrounding sediments. It is noted that Cu and Zn at station SH 1551 drop to values similar to those of normal pelagic sediments. However, at SH 1552 they display a marked enrichment in contrast to the case of Fe, the values of which remain similar to those of normal pelagic sediments.

1.4.6 Lead (see Figure 1.14)

The distribution of Pb in the surface sediments is completely different from that of the other metals. In general, the sediments which are enriched in Fe, Mn, Ni, Cu and Zn are poor or only slightly enriched in Pb. The stations SH 1555, SH 1556, SH 1526, SH 1547, SH 1528, SH 1546, SH 1530, SH 1529 and SH 1538 define an extensive zone, the sediments in which are characterized by low concentrations of Pb (< 100 ppm). Away from this zone the concentrations of Pb tend to increase, but the most remarkable enrichment of this metal is shown towards the eastern part of the area (between $107^{o}45'$ and $108^{o}W$). In the sea mount area and at the stations SH 1545 and SH 1541, the Pb levels are between 150 ppm and 200 ppm, while at the stations SH 1543 and SH 1550 this element reaches values higher than 200 ppm. It is interesting to note that these two stations fall within the zone with

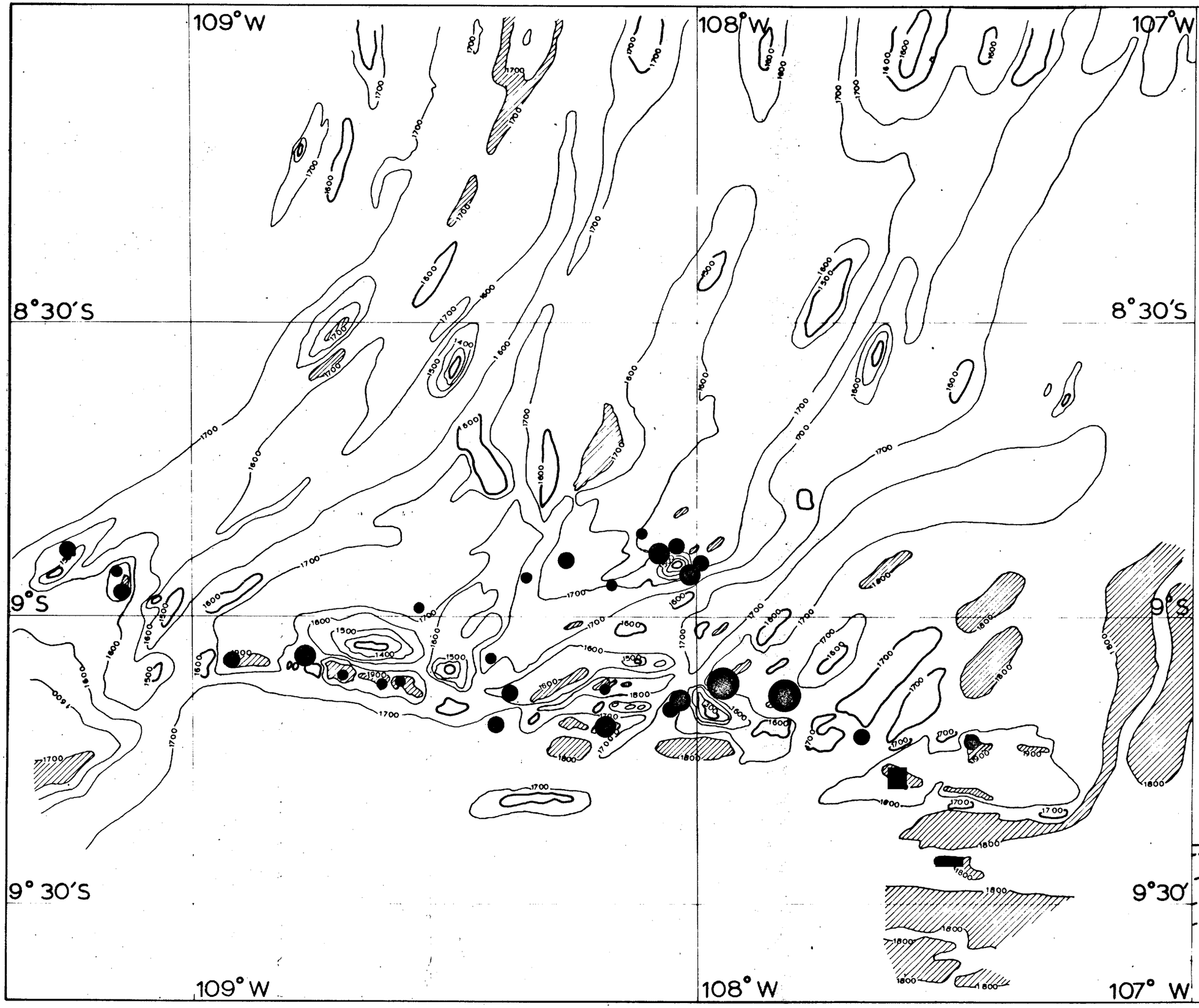

FIG. 1.14
DISTRIBUTION OF Pb IN SURFACE SEDIMENTS FROM THE EAST PACIFIC RISE FRACTURE ZONE AT 9° S

the highest content of $CaCO_3$. Moreover, the sediments of the large central zone which is characterized by the lowest concentrations of Pb also contain the lowest amount of $CaCO_3$. Therefore, it is concluded that Pb follows $CaCO_3$ in its distribution in the fracture zone sediments. Figure 1.15 shows a positive correlation between Pb and $CaCO_3$.

Lead, unlike the other metals (Fe, Mn, Ni, Cu, Zn) shows no enrichment in the sediments from stations SH 1529 and SH 1530. By contrast, a marked enrichment of Pb is found in the sediments from station SH 1552.

1.4.7 Cobalt (see Figure 1.16)

The distribution of Co, like that of Pb, is generally similar to the distribution of $CaCO_3$, thus showing its association with biogenic material. Low values of Co occur in the eastern part of the area (stations SH 1533, SH 1534), in the basins containing the stations SH 1529 and SH 1530 and at stations SH 1526, SH 1538 and SH 1547, containing relatively low amounts of $CaCO_3$. Cobalt is markedly enriched at station SH 1521. The presence of a large amount of volcanic ash in the sediments from this station may suggest an origin of Co by inclusion of volcanic detritus.

1.4.8 Barium (see Figure 1.17)

The distribution of Ba, like that of Pb, is different from that of the other metals. The sediments from the area between $108^{o}10'W$ and $108^{o}20'W$, which contain the highest amount of Fe, Mn, Ni,

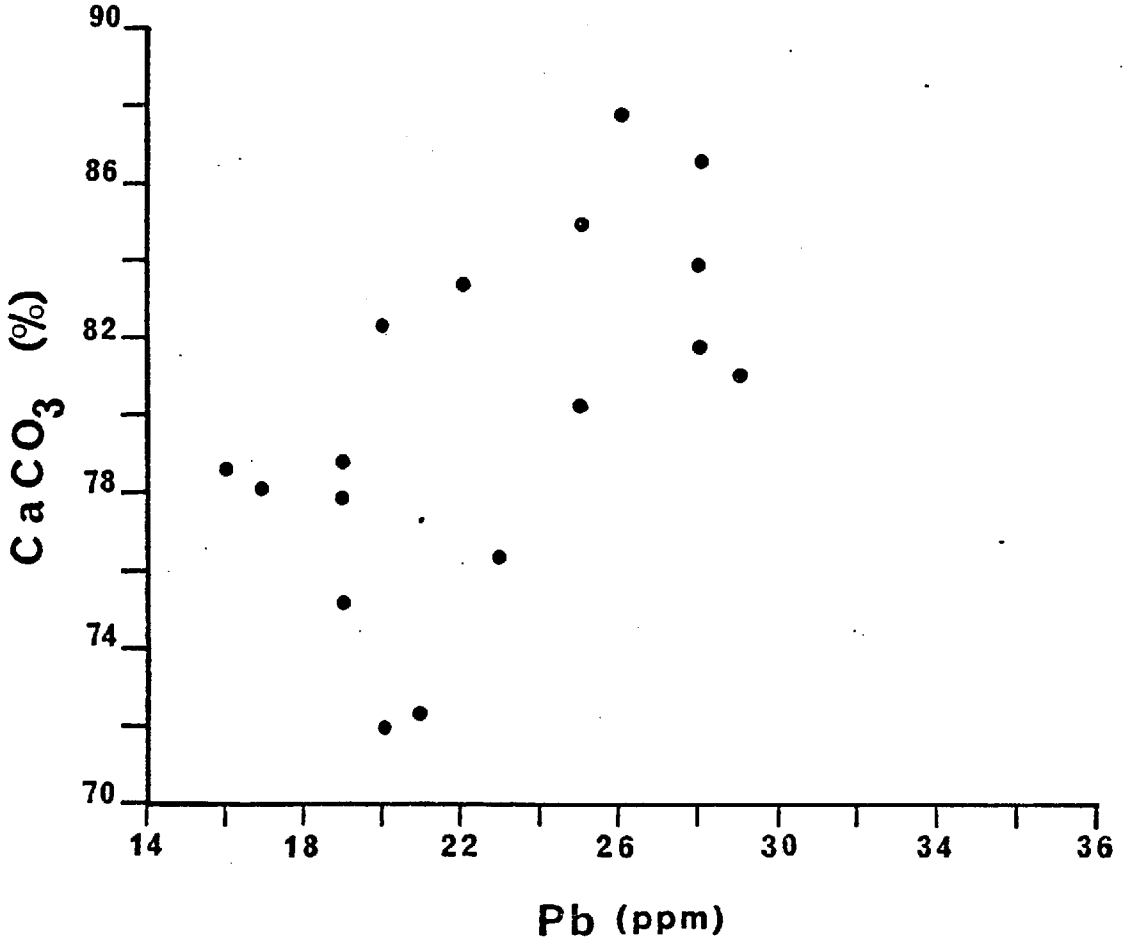

Figure 1.15: Scatter plot showing the positive correlation between $CaCO_3$ and Pb.

FIG. 1.16
DISTRIBUTION OF Co IN SURFACE SEDIMENTS FROM THE EAST PACIFIC RISE FRACTURE ZONE AT 9° S

Co

CFB ppm

- >150
- >100-150
- > 50-100
- ≤ 50

DEPTHS IN UNCORRECTED FATHOMS. CONTOURS EVERY 100 FATHOMS. BASINS SHADED. TOPOGRAPHIC HIGHS THICKENED LINES.

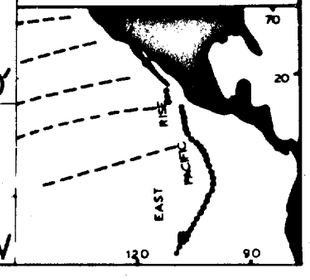

109°W

108°W

107°W

8°30'S

9°S

9°30'S

109° W

108° W

107° W

FIG. 1.17
DISTRIBUTION OF Ba IN SURFACE SEDIMENTS FROM THE EAST PACIFIC RISE FRACTURE ZONE AT 9° S

Ba

CFB in %

- > 1.5
- > 1.0 - 1.5
- > 0.5 - 1.0
- < 0.5

DEPTHS IN UNCORRECTED FATHOMS CONTOURS EVERY 100 FATHOMS. BASINS SHADED. TOPOGRAPHIC HIGHS THICKENED LINES.

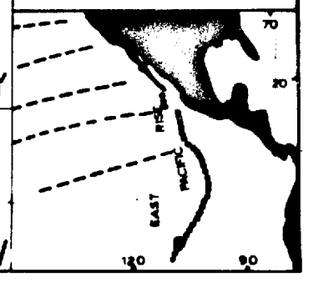

Cu and Zn are poor in Ba. By contrast, the sediments from stations SH 1536, SH 1533, SH 1552 and SH 1553, which are characterized by low concentrations of Fe, Mn, Ni, Cu and Zn are relatively enriched in Ba. It is noteworthy that these sediments are highly enriched in $CaCO_3$, thus suggesting an association of Ba with biogenic material, in a similar way to Pb and Co.

1.4.9 Aluminium (see Figure 1.18)

The distribution of Al in the surface sediments does not display any distinct zones of enrichment, as was found for most of the other metals determined. Except for the sea mount area, in the sediments of which Al reaches relatively high levels, the amount of this element present in the surface sediments is uniformly low in the region studied. In the greatest part of the survey area the concentrations of Al show little variation, ranging between 0.5 and 1.0%. Generally there is a marked depletion of Al in the sediments characterized by high or moderate enrichment of other metals. However, the concentration of Al at SH 1532 is markedly higher than at SH 1525, SH 1547, SH 1537 despite the fact that the other metal concentrations are similar at all these stations. Similarly, the sediments from SH 1529 contain a relatively high amount of Al when compared with the Al content of stations SH 1525 and SH 1537. Sporadic enrichments of Al also occur elsewhere throughout the area (see Figure 1.18).

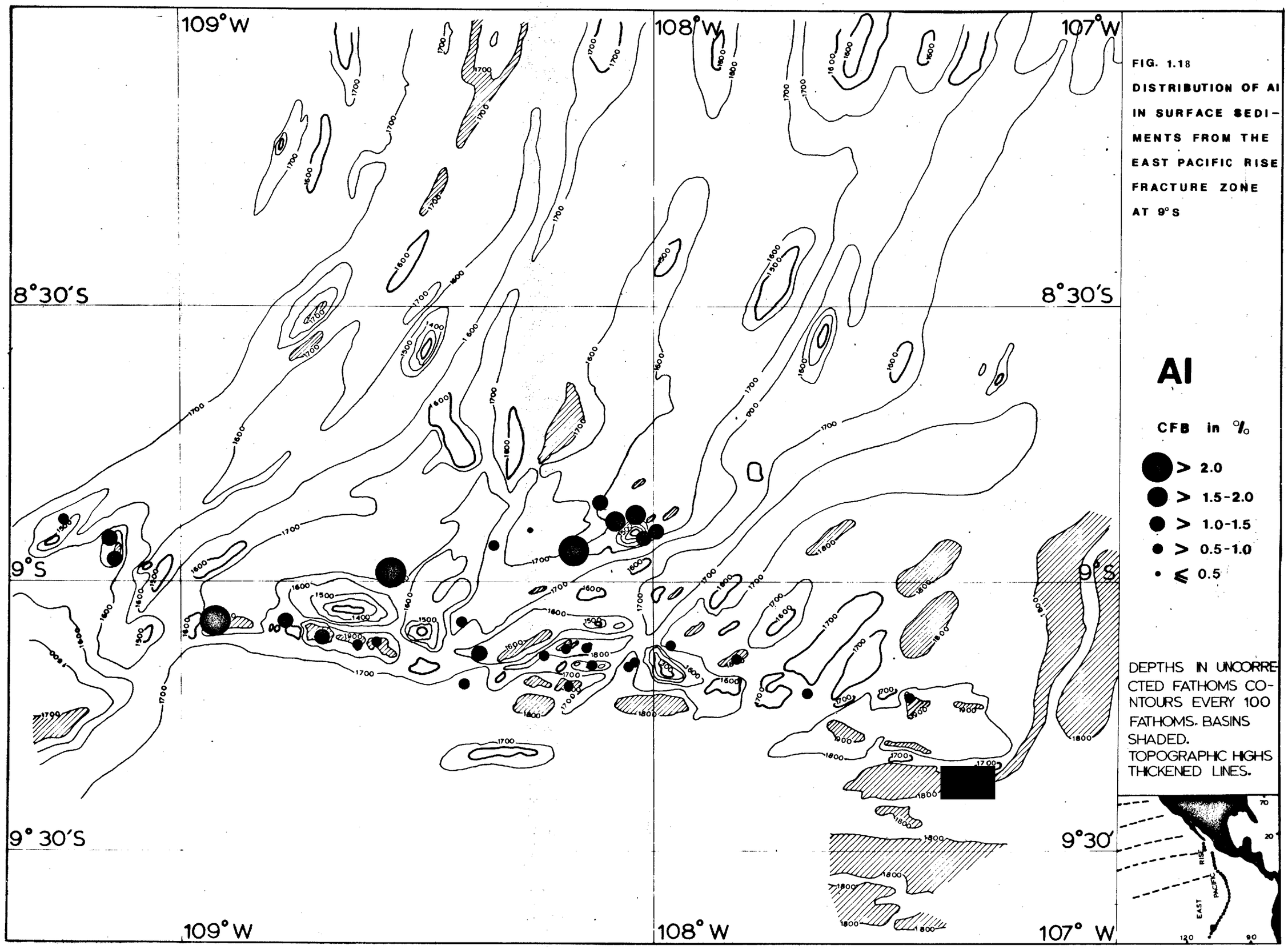

FIG. 1.18
DISTRIBUTION OF AI IN SURFACE SEDIMENTS FROM THE EAST PACIFIC RISE FRACTURE ZONE AT 9°S

1.4.10 Silica (see Figure 1.19)

Silica, like Al, shows its highest concentrations ($> 25\%$) around the sea mount area; and also on a line defined by the stations: SH 1521, SH 1526, SH 1528 and SH 1531. Sediments from stations SH 1525, SH 1537, SH 1547 and SH 1532, which are highly enriched in Fe, Mn, Ni, Cu and Zn, also contain a considerable amount of SiO_2 (20-25%). In the fracture zone sediments between 108°W and 108°45'W there is a long narrow zone with low concentrations of SiO_2 (15-20%).

It is noticeable that the concentrations of SiO_2 in the sediments from SH 1529 and SH 1530 do not fall in the same range as those of SH 1525, SH 1537 and SH 1547, as in the case for the metals.

Figure 1.20 shows a strong positive correlation between SiO_2 and Fe.

1.5 DISCUSSION

The geochemical data obtained in this study are of interest in that they present evidence of metalliferous sediment formation on the East Pacific Rise and its ponding within deep basins in a fracture zone floor. This process is evinced in the following ways:

1) The degree of metal enrichment in sediments from the fracture zone basins is greater than in those collected from the elevated areas (see Table 1.1).

2) There is a positive correlation between the carbonate-free concentrations of Mn, Fe, Ni, Zn and Cu and the depth of

109°W

108°W

107°W

8°30'S

9°S

9°30'S

109° W

108° W

107° W

FIG. 1.19

DISTRIBUTION OF SiO_2 IN SURFACE SEDIMENTS FROM THE EAST PACIFIC RISE FRACTURE ZONE AT 9° S

SiO_2

CFB in %

- > 25
- > 20 - 25
- > 15 - 20
- < 15

DEPTHS IN UNCORRECTED FATHOMS CONTOURS EVERY 100 FATHOMS. BASINS SHADED. TOPOGRAPHIC HIGHS THICKENED LINES.

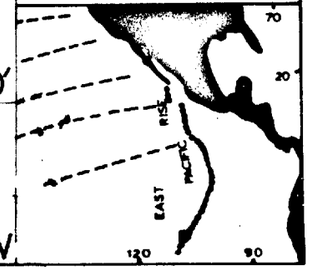

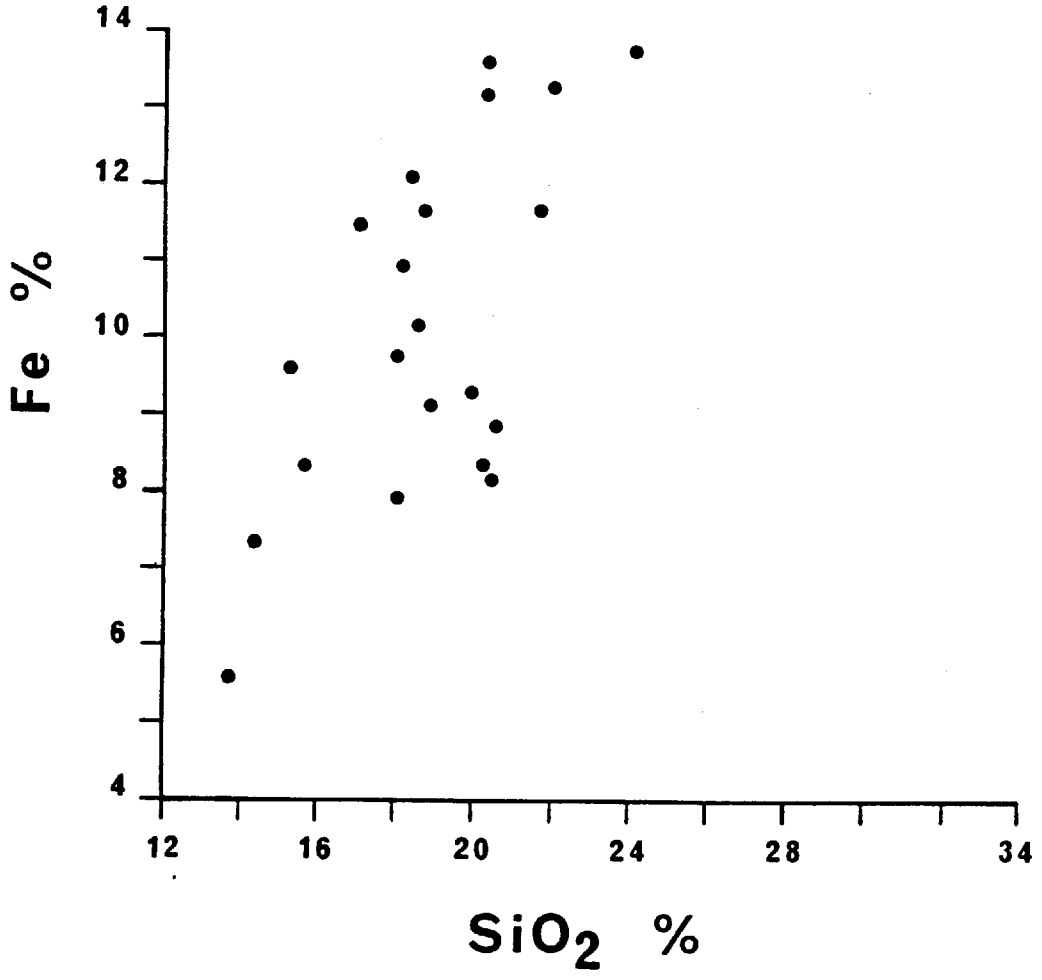

Figure 1.20: Scatter plot showing the positive correlation between Fe and SiO_2. Concentrations are corrected to a calcium carbonate-free basis.

water (see Figures 1.3, 1.4, 1.5, 1.6 and 1.7).

The geochemical distribution patterns found for Fe, Mn, Ni, Zn and Cu in the fracture zone surface sediments are similar to those reported by Boström and Peterson (1969) and Horowitz (1970) for other East Pacific Rise sediments. Similar geochemical distributions have also been reported for the Mid-Atlantic Ridge and the Central Indian Ocean Ridge by Boström et al (1969) and Horowitz (1970).

It is suggested that the localised area showing high concentrations of Fe, Mn, Ni, Cu and Zn at 108°15'W (see Figures 1.9, 1.10, 1.11, 1.12 and 1.13) is a reflection of volcanic activity. Hence, the area between 108°10'W and 108°20'W probably contains the main hydrothermal center. This is consistent with the geophysical data according to which the crest of the Rise was located within this area (Francis and Lillwall, personal communication, 1979). Furthermore, the designation of the area between 108°10'W and 108°20'W as a hydrothermal center is consistent with the bathymetry of the survey area, which indicates that the region with the highest concentrations of metals is an elevated area.

The stations SH 1525 and SH 1547 fall within the crest area as defined, and the concentrations of metals decrease away from these stations. It is, therefore, concluded that SH 1525 and SH 1547 define the approximate position of hydrothermal vents which are responsible for the metal enrichment in most of the present sediments. It is also observed that the level of metal enrichment at station SH 1532 is similar to that of SH 1525 and SH 1547. Since station SH 1532 is located at the floor of a deep basin, the high metal enrichment here could either be attributed to metalliferous sediment ponding, or to a local hydrothermal vent.

A hydrothermal supply of Si to the sea floor is well-established by direct sampling and analysis of hydrothermal fluids from the Galapagos spreading center (Corliss et al, unpub. ms.). In the fracture zone sediments, except for a few stations where there is an anomalously high concentration of Si due to the presence of disseminated volcanic ash (SH 1521, SH 1536, SH 1528), the distribution of Si resembles that of Fe. Moreover, there is a strong positive correlation between these two elements (see Figure 1.20). It is, therefore, suggested that a high proportion of Si in the fracture zone sediments is of hydrothermal origin. The fact that the concentration of Si, like that of Fe, at station SH 1532, is of the same level as that of SH 1525 and SH 1547, suggests a second hydrothermal vent, or system of vents, near this station. This is also supported by the decrease of the concentrations of metals away from this station.

It can be seen from the topography of the fracture zone (see Figure 1.2) that the basins containing stations SH 1529, SH 1530, SH 1531 and SH 1546 have an ellipsoidal shape, the long axis of which falls on the same line. Their relative position, one after the other, produces a continuous chain of long narrow basins resembling a long furrow, which is nearly perpendicular to the axis of the Rise. This furrow should be followed by water currents if eastward flow of abyssal waters across the East Pacific Rise occurs (Lonsdale, 1976). In this case metal-bearing waters and fine-grained metalliferous material from the vents present at SH 1532 could be transported eastward, having the possibility of being trapped in the basins containing stations SH 1529, SH 1530 and SH 1546, which are surrounded by hills. This process could explain the greater metal enrichment

in sediments from SH 1529 and SH 1530 when compared to the surrounding sediments. Although the values of Fe and Mn at SH 1529 and SH 1530 are similar to those of the crest sediments at SH 1525 and SH 1547, Si is depleted in these sediments. This rules out the presence of local hydrothermal vents in the basins containing SH 1529 and SH 1530. It is, therefore, concluded that metalliferous sediment ponding is the most probable process responsible for the greater metal enrichment in these basins.

Despite the likely common hydrothermal origin of metals in the fracture zone sediments, there are differences in their geochemical dispersion patterns. For example, although the general distribution pattern of Mn is similar to that of Fe, Figure 1.10 shows that Mn has a more widespread distribution of high values. The concentrations of Mn at SH 1533 and SH 1534 are of the same level as those of SH 1532, whereas there is a decrease in the concentration of Fe towards SH 1534 and SH 1533. This is probably due to the relatively high mobility of Mn in the marine environment compared with Fe (Seyfried and Bischoff, 1977).

The concentrations of Pb, Co and Ba, unlike the other metals (Fe, Mn, Ni, Zn and Cu), are higher in the sediments from the elevated areas than in those from the fracture zone basins. This is due to the tendency of these elements to be enriched in carbonate sediments. Similarly, the higher concentrations of Pb and Ba in the East Pacific Rise fracture zone sediments, when compared to the Indian Ocean fracture zone sediments (see Table 1.2), may be a result of the higher content of $CaCO_3$ in the former than in the latter sediments. Generally,

Pb exhibits a completely different distribution pattern in the fracture zone sediments than the other metals. It follows $CaCO_3$ in its distribution, which suggests the association of Pb with biogenic remains. This is also supported by the positive correlation between Pb and $CaCO_3$ (see Figure 1.15). Since most of the $CaCO_3$ is in the form of calcite in foraminifera tests, it is suggested that at least some of the Pb is concentrated in them. The distribution of Pb in the present sediments differs strikingly fron that reported by Boström and Peterson (1966) for East Pacific Rise sediments. It was shown that at $14^{o}S$ Pb followed the distribution of Fe, Mn, Ni and Cu, showing its highest peak at the crest of the Rise, while at $6^{o}N$ it did not show any peaks at all across the Rise. Since Pb, in the present sediments, is depleted at the crest of the Rise and displays its highest concentration away from it, its geochemical behaviour is similar to that reported by Horowitz (1970) for RISEPAC samples. The highest peak of Pb in these sediments was found in the non-crest area. A minimum in the concentration of Pb in ridge crest sediments was also reported by Horowitz (1974) for the Reykjanes Ridge.

The higher concentrations of Al and SiO_2 in sediments of group B than in group A is due to the presence of considerable amounts of volcanic ash in these sediments. Distinct volcanic ash layers were found, suggesting evidence of volcanic eruptions in this area. The distribution of Al along the fracture zone shows that its concentrations are very low within the rise crest fracture zone intersection area (see Figure 1.18). This is in full agreement with Boström et al (1969) who demonstrated that metalliferous sediments from active volcanic ridges have very low Al concentrations. However, large amounts of

detrital material derived from the alteration of basalts, located on the sea mount, dilute the surrounding sediments and are responsible for the anomalously high concentrations of Al at some stations (SH 1521, SH 1556, SH 1528).

It is noticeable that at SH 1525 and SH 1532, where the discharge of hydrothermal exhalations are thought to occur, the sediments contain very low amounts of $CaCO_3$ (see Figure 1.8). This is probably due to the rapid deposition of colloidal Fe and Mn hydroxides which leads to a local suppression of the $CaCO_3$ concentrations. By contrast, there is an increase of the $CaCO_3$ content away from these stations (between 108°W and 107°30'W).

1.6 CONCLUSIONS

1) The fracture zone sediments (average all surface sediments) are enriched in Mn, Fe, Ni, Pb, Zn and Cu relative to normal Pacific sediments. The degree of enrichment is, however, not as great as that reported for other sections of the East Pacific Rise.

2) Of the enriched metals Mn, Fe, Ni, Zn and Cu follow each other in their horizontal distribution, having their highest concentrations at the crest of the Rise, whilst Pb exhibits a completely different distribution pattern. It is depleted at the crest of the Rise and displays its highest concentration in the non-crest area. Moreover, Pb follows $CaCO_3$ in its horizontal distribution, suggesting a strong association with organic remains.

3) The enrichment of Fe, Mn, Ni, Zn and Cu is greater in the deeper than in the shallower areas. This conclusion is based on comparison of chemical averages for the material obtained from the deep basins and on that collected from the elevated areas. It can also be seen in the geochemical maps which are drawn on the bathymetry.

4) Careful examination of the distribution of metals in relation to the topography indicates that the basins with the stations SH 1529 and SH 1530 are the most probable basins where colloidal hydrothermal material, being transported from the hydrothermal vents close to SH 1532, is being trapped and concentrated.

5) In general, the geochemical distribution patterns of Fe, Mn, Ni, Zn and Cu in the survey area support a local hydrothermal origin for these metals.

6) The general dispersion patterns of Mn and Ni are similar to that of Fe; however, these two elements display a more widespread distribution than Fe.

7) Two hydrothermal centers have been located in the study area; one at the crest of the Rise, in the vicinity of stations SH 1525 and SH 1547, and the other at SH 1532.

8) There is a high positive correlation between Fe and Si. The distribution pattern of Si supports its hydrothermal origin. It can be used as an indicator in determining whether the hydrothermal material is of strictly local origin or is transported from elsewhere.

9) The fast deposition of colloidal Fe and Mn hydroxides at the two hydrothermal centers results in suppression of the $CaCO_3$ concentrations. The highest contents of $CaCO_3$ are found away from the crest.

SECTION 2

COMPARATIVE GEOCHEMICAL STUDY OF SURFACE AND BURIED SEDIMENTS FROM AN EAST PACIFIC RISE FRACTURE ZONE AT $9^{o}S$

2.1 INTRODUCTION

For a long time the distribution of major and trace elements in marine sediments has been determined by the total chemical analysis of the sediments. However, it has been realized recently that the overall distribution of the elements is not able to provide information about the form in which the various elements are incorporated into the deposits, and thus some selective analysis is necessary.

Goldberg and Arrhenius (1958), working on a series of Pacific pelagic sediments, used separation processes to study their partition geochemistry. These processes were based on: (i) settling velocity, (ii) differences in density, and (iii) magnetic properties of the sediments. For the first procedure they used 0.01N ammonia as a suspension liquid and repeated settling and decantation for the separation of the size fractions above 1 μ, while a CEPA continuous flow supercentrifuge was used for the separation of fractions smaller than 1 μ. For the second process they used tetrabromoethene as a heavy liquid, and for the magnetic separation a Franz Isodynamic separator. All these separation techniques, as well as the isolation of mineral grains, microfossils, or other sediment components under the microscope for the purpose of subjecting them to chemical analysis, involve many difficulties, are time-consuming, and do not apply to all categories of marine sediments.

In recent years chemical separation of sediment components has attracted the attention of a number of investigators. The term 'partition geochemistry', becoming more widespread in the literature of marine sediments, may be defined as the distribution of major and

trace elements among the various components of the sediments which have been chemically separated. This is of importance because it leads to a better understanding of the paths by which the elements reach their present positions in the sediments.

However, the interpretation of partition geochemical data is not simple, since most of the elements have more than one source. Furthermore, a large number of factors control their geochemical behaviour in the marine environment before and during their incorporation into the various components of the sediments.

In this work partition geochemistry is used for the investigation of surface and buried sediments from the East Pacific Rise fracture zone at 9^{o}S. The lithological and overall chemical description of the sediment cores examined are also presented here for a better understanding of the partition geochemistry.

2.2 LITHOLOGICAL AND CHEMICAL DESCRIPTION OF THE CORES

Figures 2.1-2.50 illustrate the lithological and overall chemical description of the cores. For the lithological description the Olausson's classification system was followed, which is described in detail in Appendix A. The Munsell colour system was also used. The number code showing the colour of the sediment is on the right of the core log (see Table A1).

In the chemical logs the data for Mn, Fe, Ni, Co, Pb, Zn, Cu, Ba, Al and SiO_2 are presented on a carbonate-free basis (C.F.B.).

The following signs were used in the lithological description of the cores:

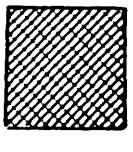

Foraminiferal chalk ooze

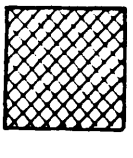

Foraminiferal marl ooze

Figure 2.1:

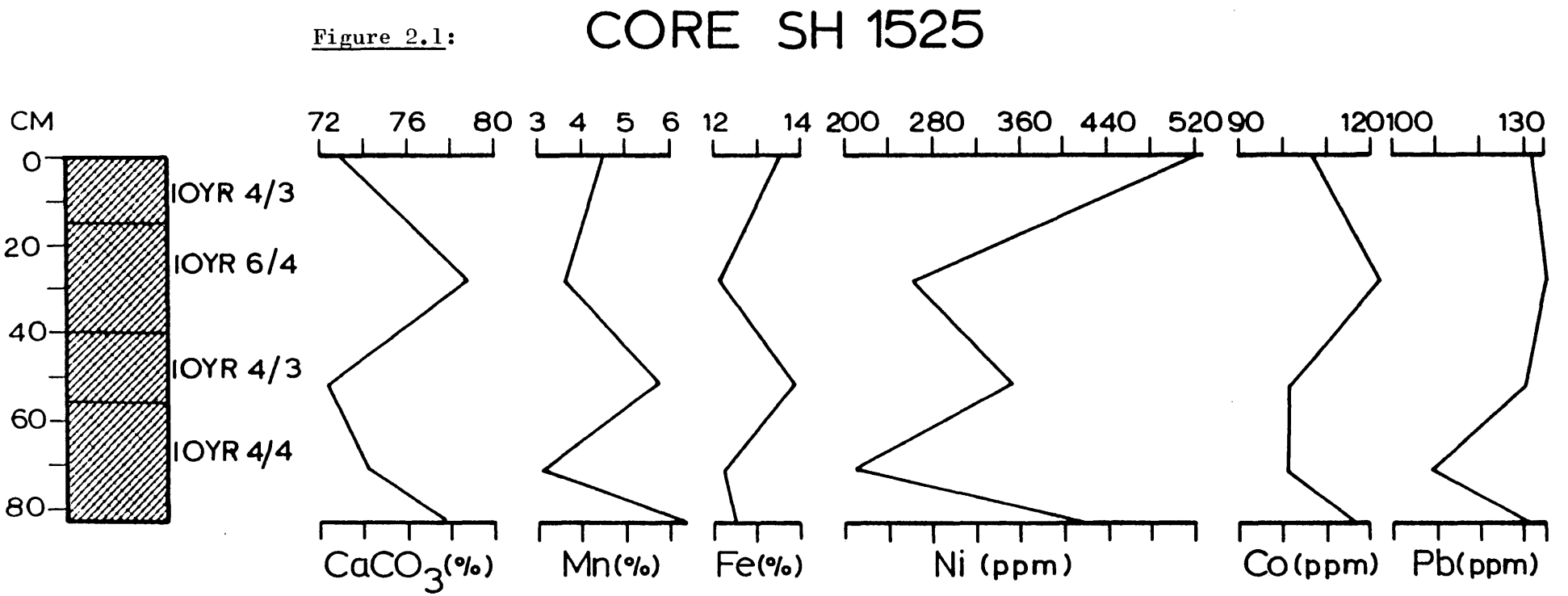
CORE SH 1525
CM
0
20
40
60
80
10YR 4/3
10YR 6/4
10YR 4/3
10YR 4/4
72 76 80
CaCO3(%)
3 4 5 6
Mn(%)
12 14
Fe(%)
200 280 360 440 520
Ni (ppm)
90 120
Co(ppm)
100 130
Pb(ppm)

Figure 2.2:

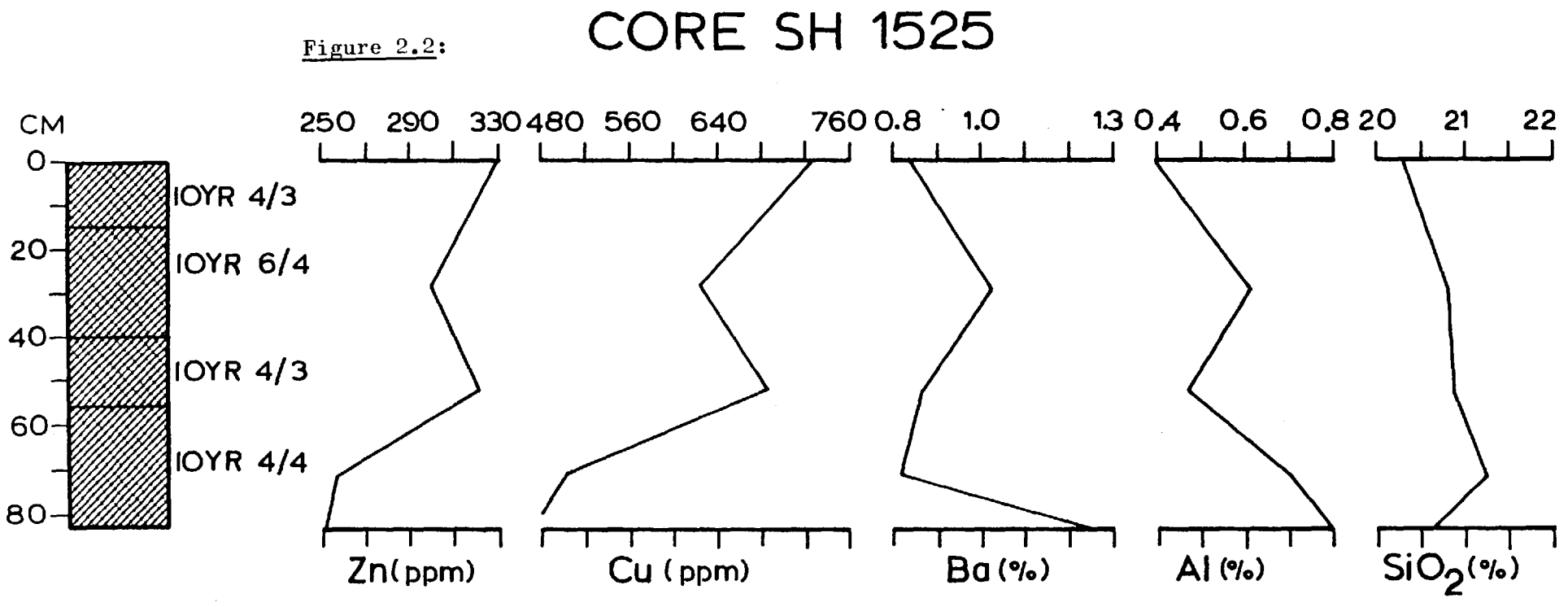
CORE SH 1525
CM
0
20
40
60
80
10YR 4/3
10YR 6/4
10YR 4/3
10YR 4/4
250 290 330
480 560 640 760
0.8 1.0 1.3
0.4 0.6 0.8
20 21 22
Zn(ppm)
Cu (ppm)
Ba (%)
Al (%)
SiO2 (%)

Figure 2.3:

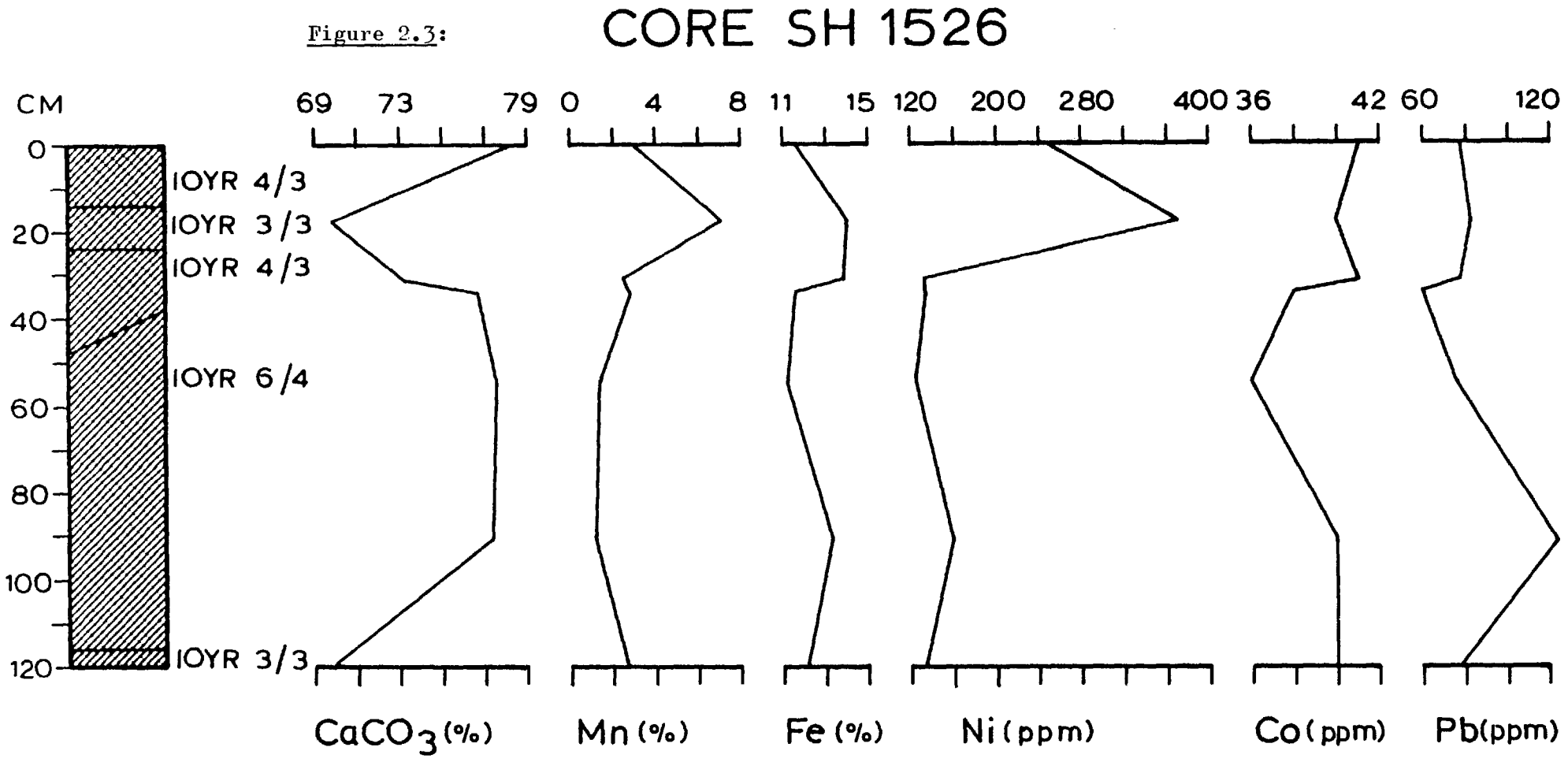
CORE SH 1526
CM
0
20
40
60
80
100
120
10YR 4/3
10YR 3/3
10YR 4/3
10YR 6/4
10YR 3/3
69 73 79
0 4 8
11 15
120 200 280 400
36 42
60 120
CaCO3 (%)
Mn (%)
Fe (%)
Ni (ppm)
Co (ppm)
Pb (ppm)

Figure 2.4:

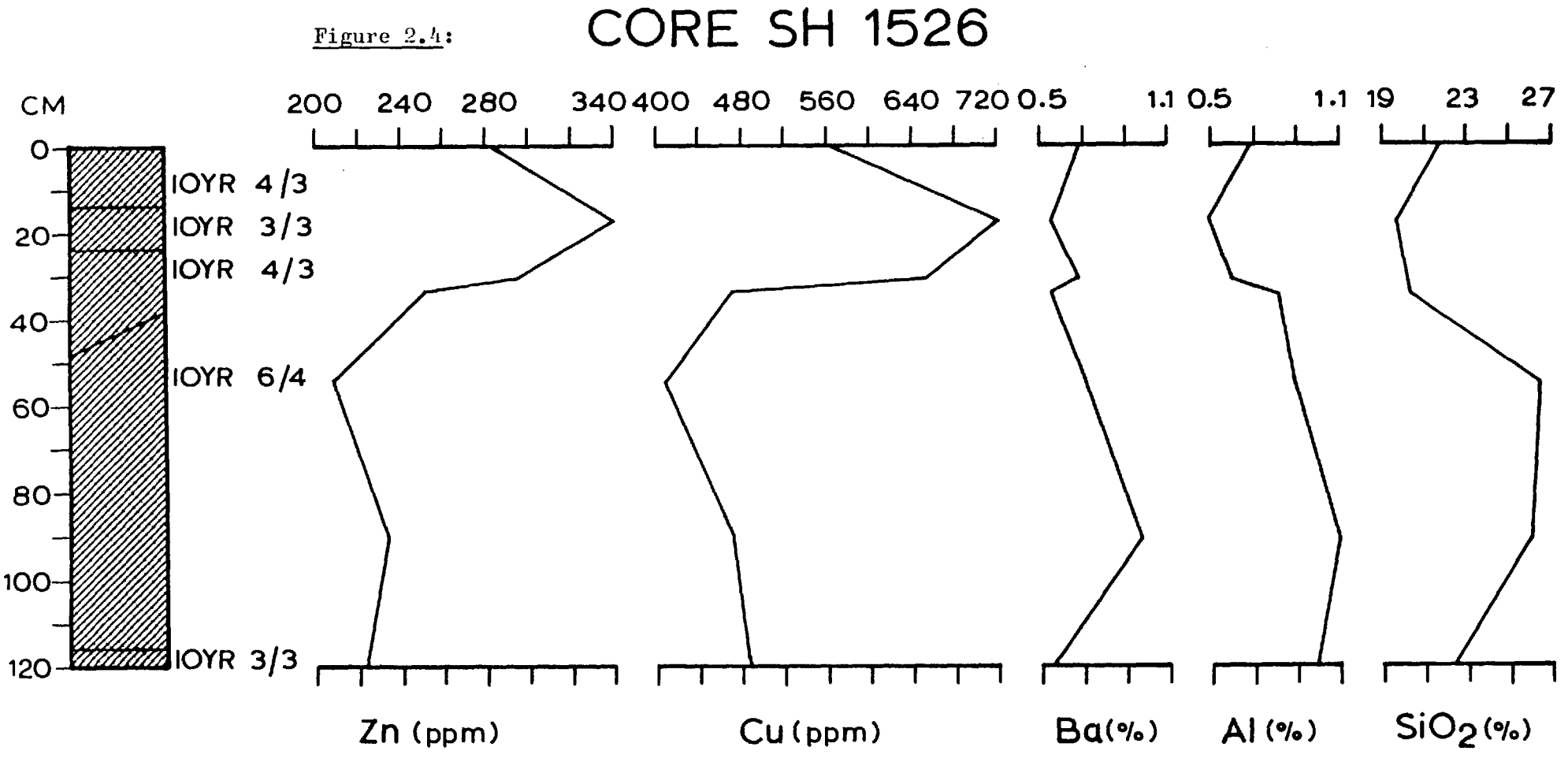
CORE SH 1526
CM
0
20
40
60
80
100
120
10YR 4/3
10YR 3/3
10YR 4/3
10YR 6/4
10YR 3/3
200 240 280 340
400 480 560 640 720
0.5 1.1
0.5 1.1
19 23 27
Zn (ppm)
Cu (ppm)
Ba(%)
Al (%)
SiO2 (%)

Figure 2.5:

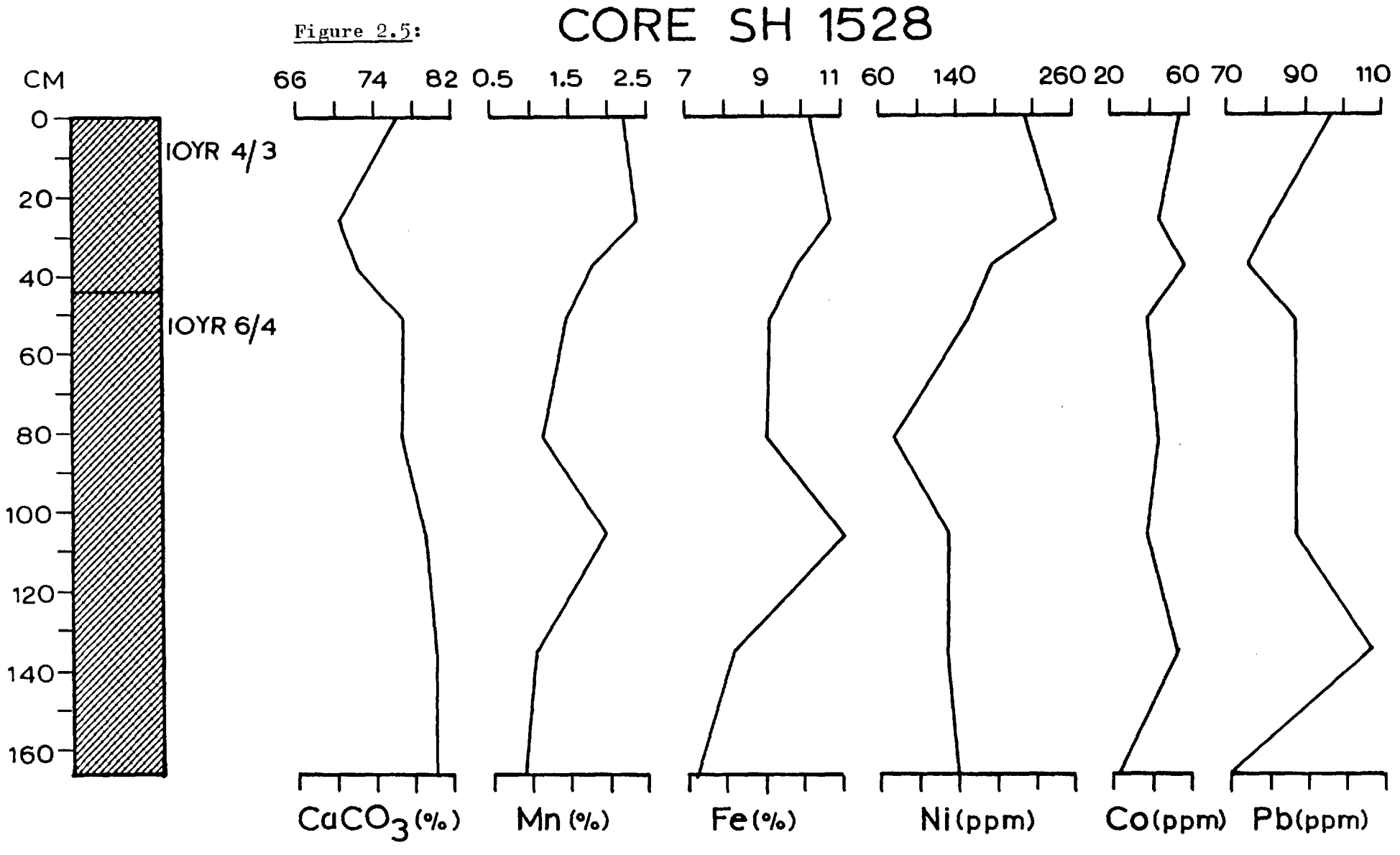
CORE SH 1528
CM
0
20
40
60
80
100
120
140
160
10YR 4/3
10YR 6/4
66 74 82
0.5 1.5 2.5
7 9 11
60 140 260
20 60
70 90 110
CaCO3 (%)
Mn (%)
Fe (%)
Ni (ppm)
Co (ppm)
Pb (ppm)

Figure 2.6:

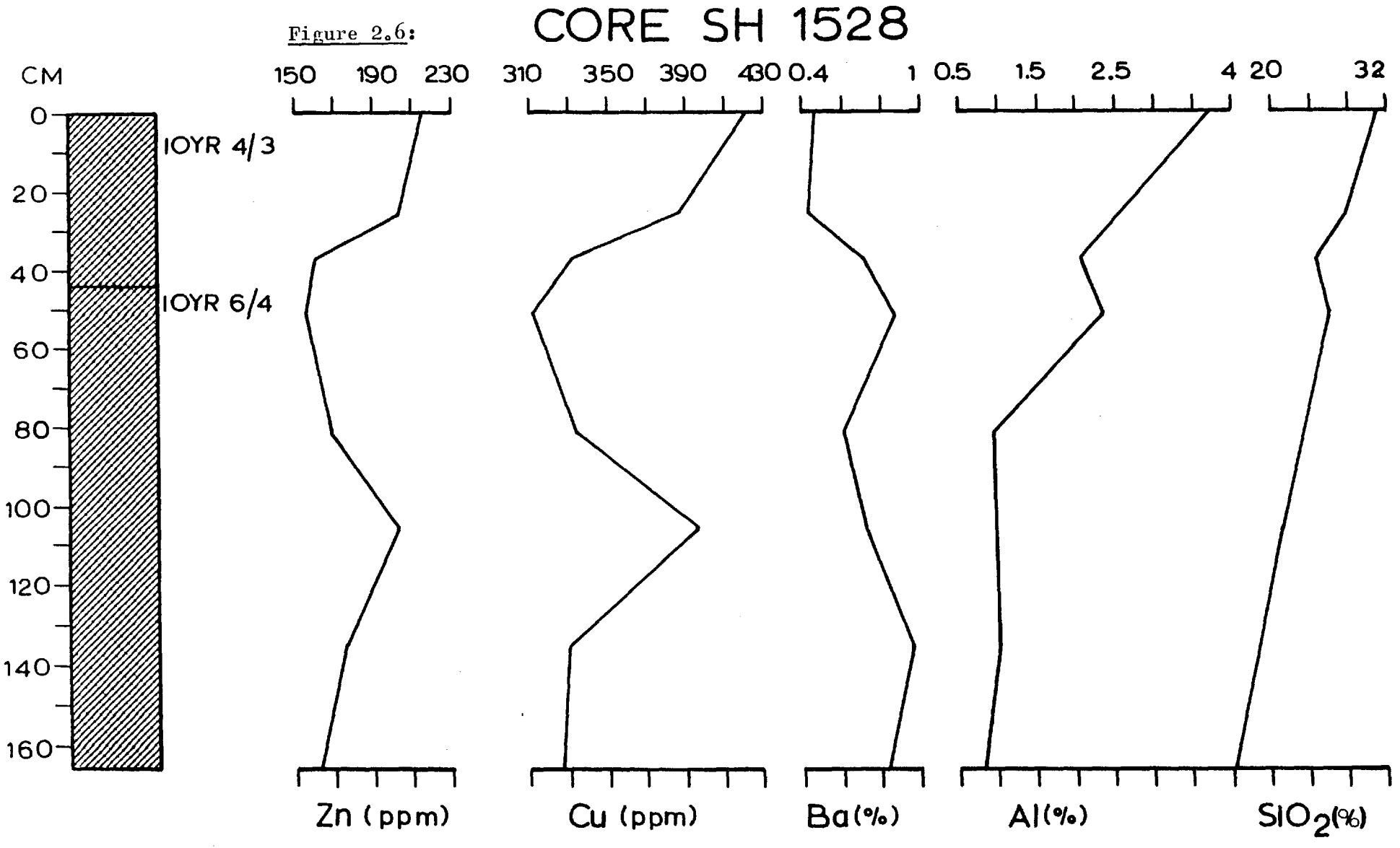
CORE SH 1528
CM
0
20
40
60
80
100
120
140
160
10YR 4/3
10YR 6/4
150
190
230
Zn (ppm)
310
350
390
430
Cu (ppm)
0.4
1
Ba(%)
0.5
1.5
2.5
4
Al(%)
20
32
SiO2(%)

Figure 2.7:

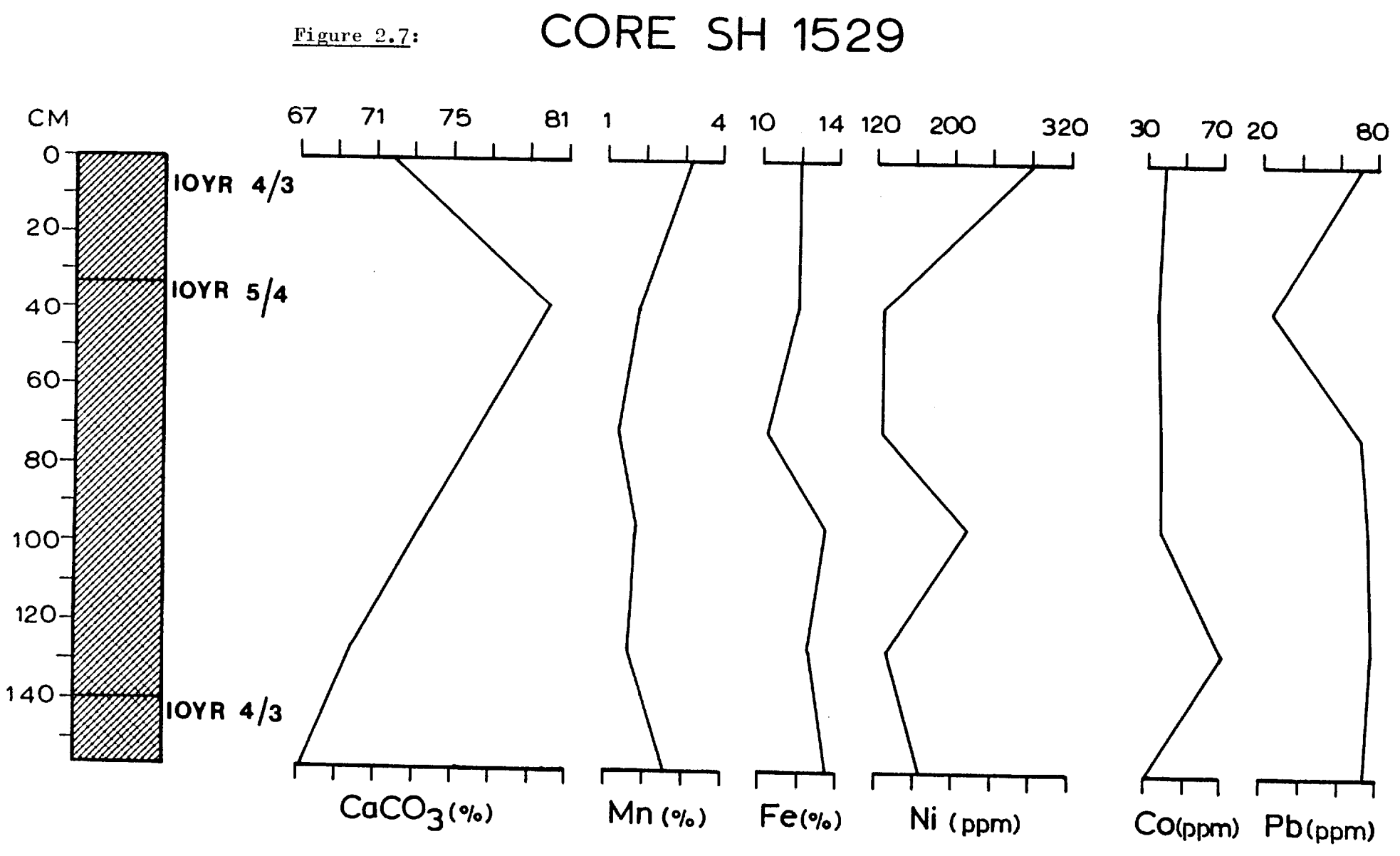
CORE SH 1529
CM
0
20
40
60
80
100
120
140
10YR 4/3
10YR 5/4
10YR 4/3
67 71 75 81
CaCO3 (%)
1 4
Mn (%)
10 14
Fe(%)
120 200 320
Ni (ppm)
30 70
Co(ppm)
20 80
Pb(ppm)

Figure 2.8:

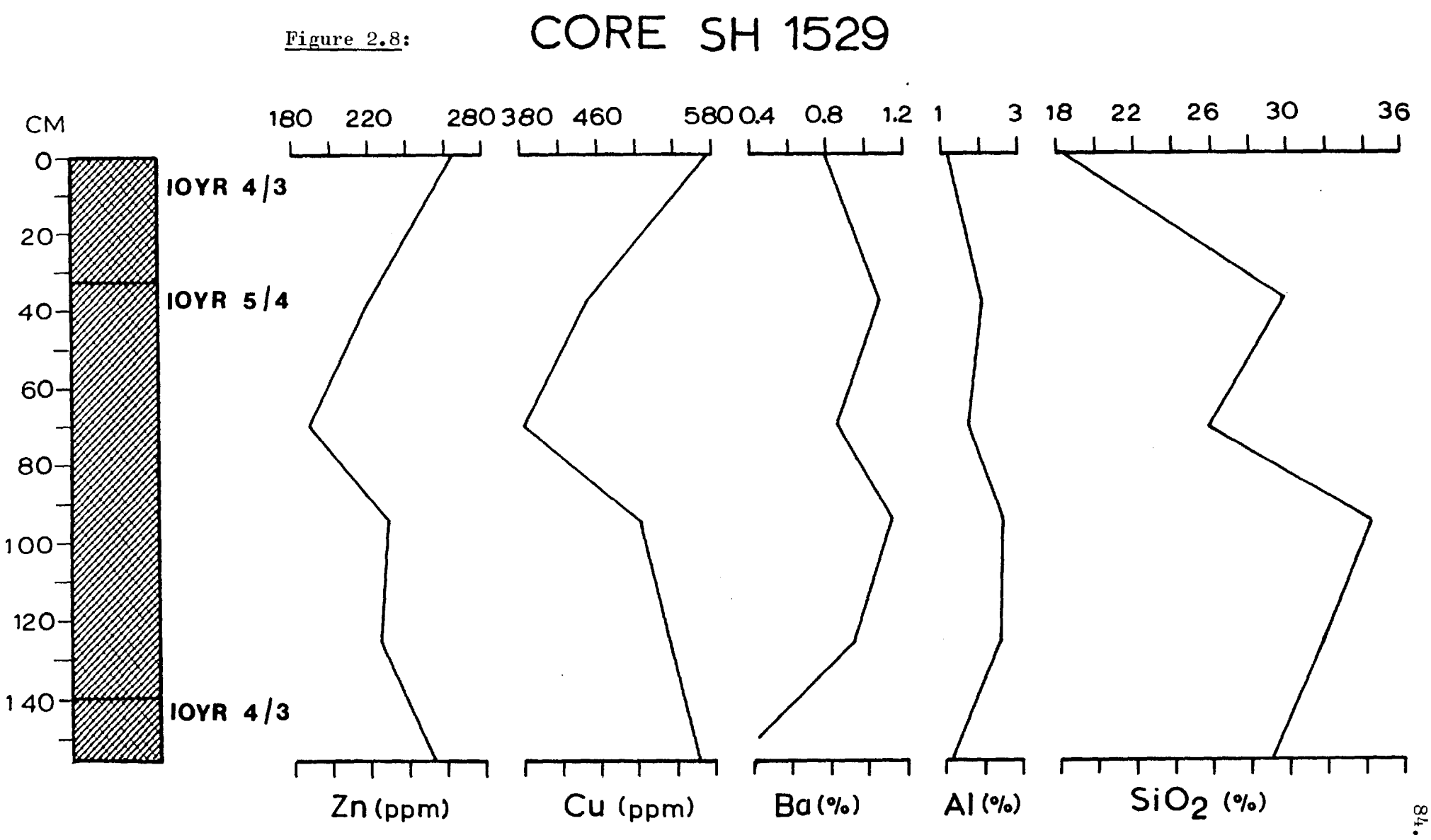
CORE SH 1529
CM
0
20
40
60
80
100
120
140
10YR 4/3
10YR 5/4
10YR 4/3
180 220 280
380 460 580
0.4 0.8 1.2
1 3
18 22 26 30 36
Zn (ppm)
Cu (ppm)
Ba (%)
Al (%)
SiO2 (%)

Figure 2.9:

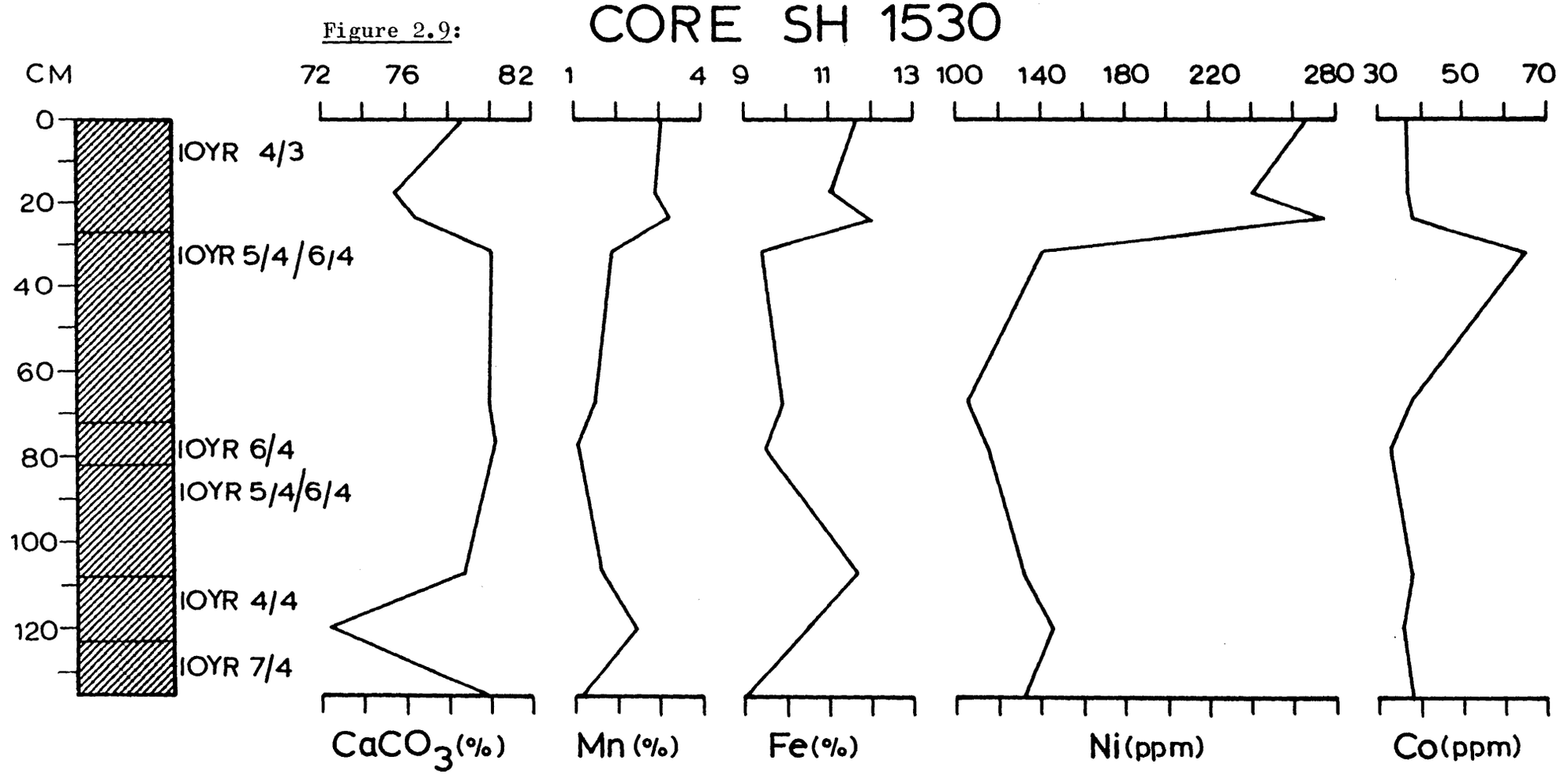
CORE SH 1530
CM
0
20
40
60
80
100
120
10YR 4/3
10YR 5/4/6/4
10YR 6/4
10YR 5/4/6/4
10YR 4/4
10YR 7/4
72 76 82
CaCO3(%)
1 4
Mn (%)
9 11 13
Fe(%)
100 140 180 220 280
Ni(ppm)
30 50 70
Co(ppm)

Figure 2.10:

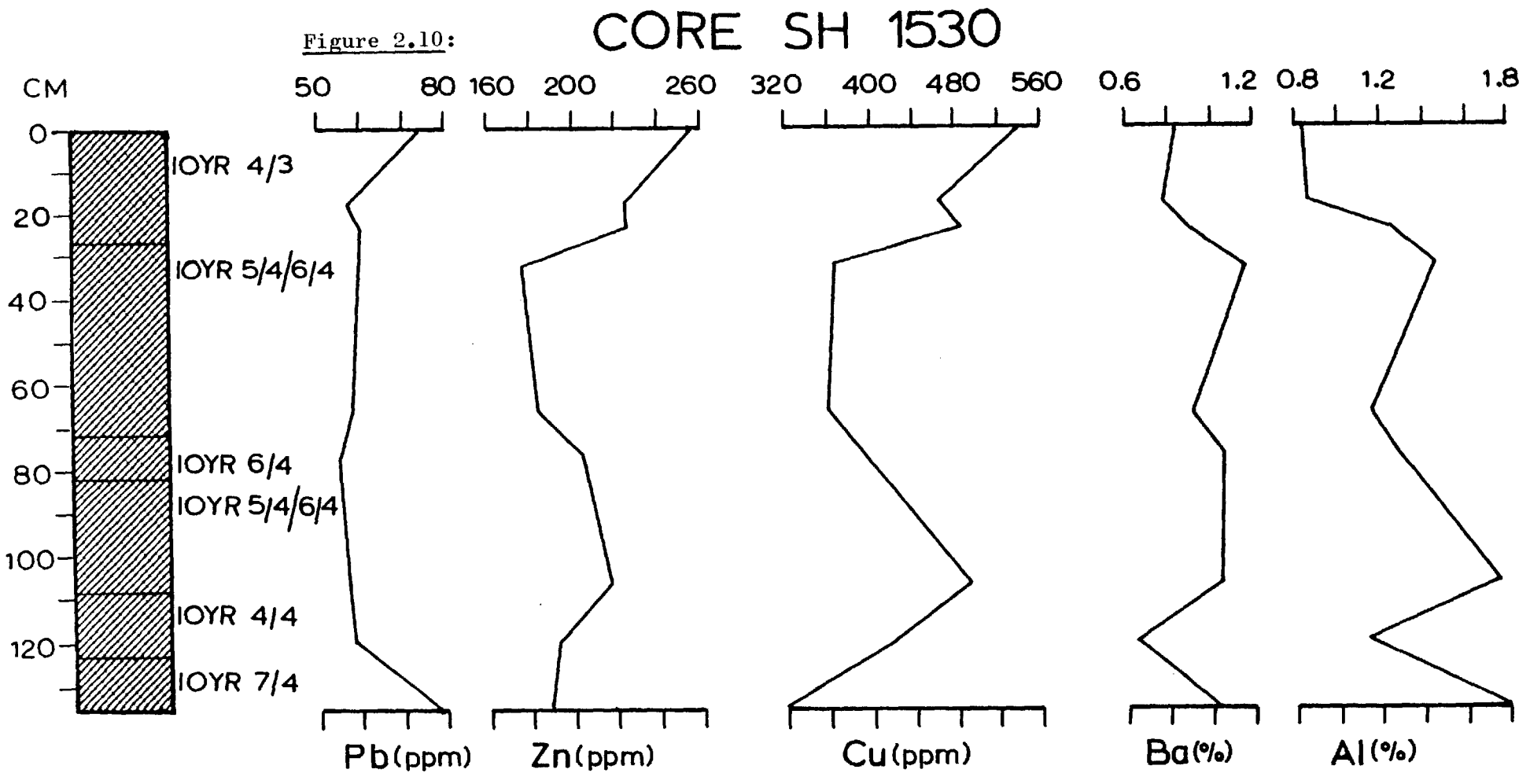
CORE SH 1530
CM
0
20
40
60
80
100
120
10YR 4/3
10YR 5/4/6/4
10YR 6/4
10YR 5/4/6/4
10YR 4/4
10YR 7/4
50
80
160
200
260
320
400
480
560
0.6
1.2
0.8
1.2
1.8
Pb (ppm)
Zn (ppm)
Cu (ppm)
Ba (%)
Al (%)

Figure 2.11:

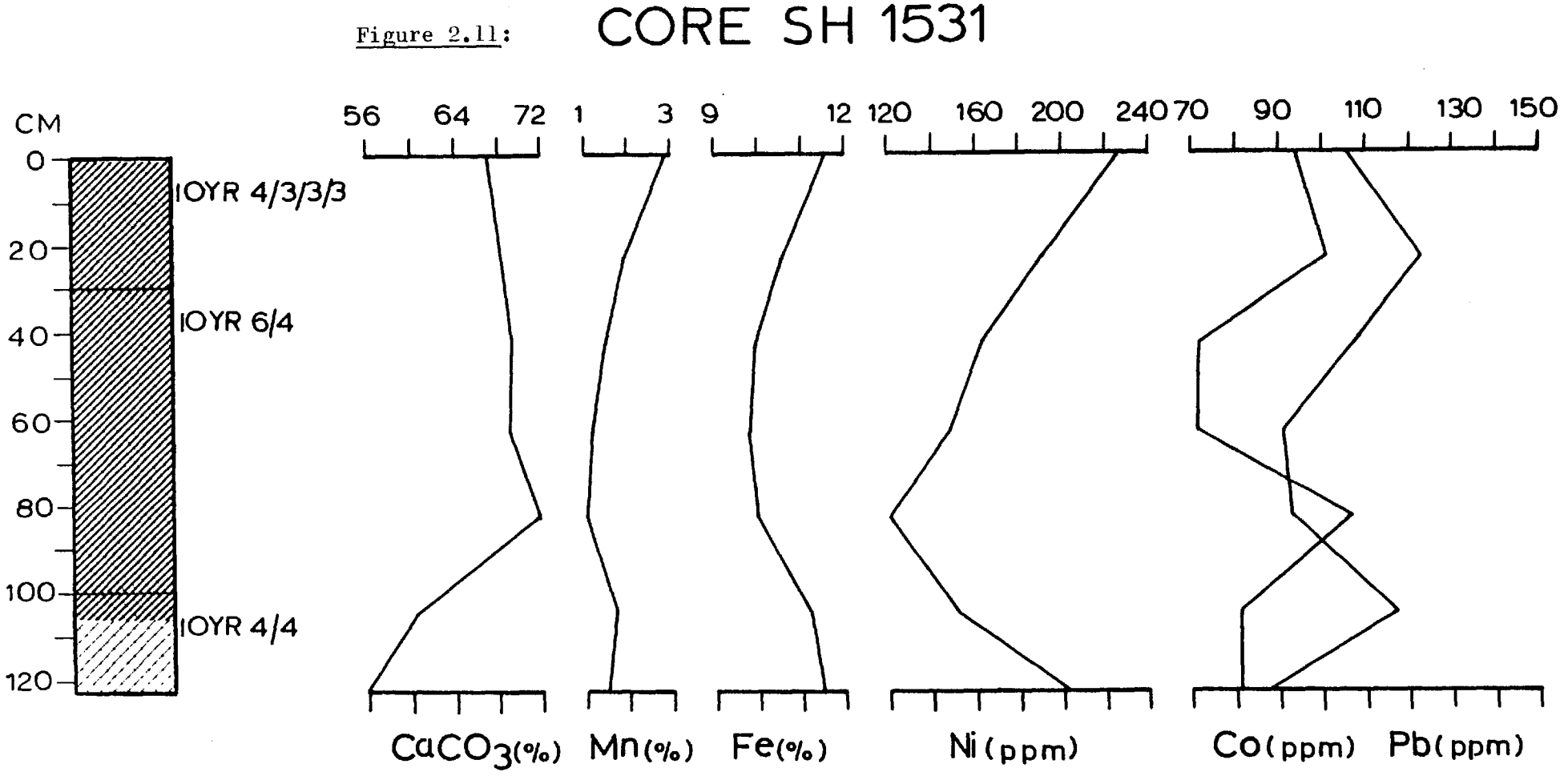
CORE SH 1531
CM
0
20
40
60
80
100
120
10YR 4/3/3/3
10YR 6/4
10YR 4/4
56
64
72
1
3
9
12
120
160
200
240
70
90
110
130
150
CaCO3(%)
Mn(%)
Fe(%)
Ni(ppm)
Co(ppm)
Pb(ppm)

Figure 2.12:

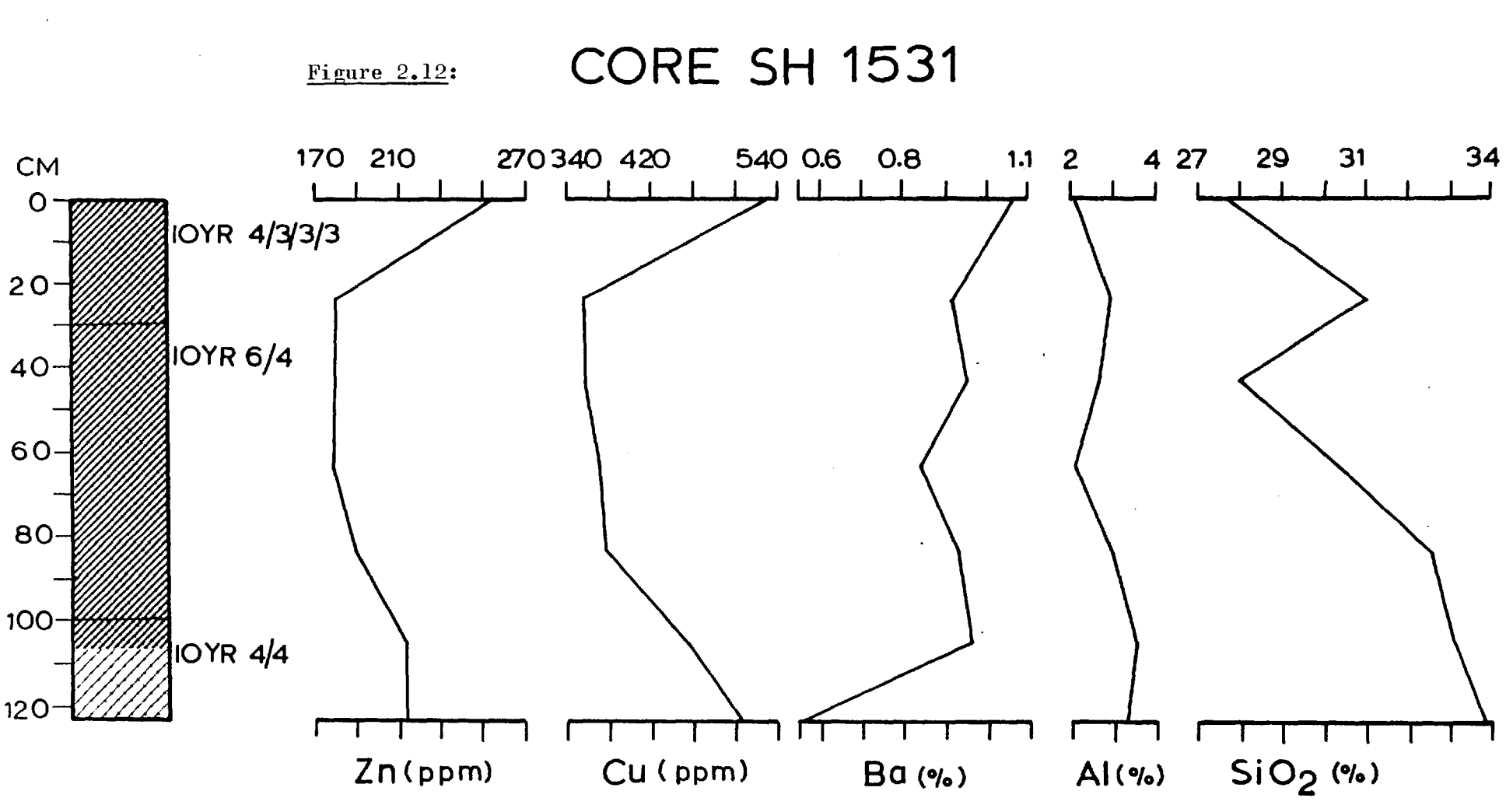
CORE SH 1531
CM
0
20
40
60
80
100
120
10YR 4/3/3/3
10YR 6/4
10YR 4/4
170 210 270
340 420 540
0.6 0.8 1.1
2 4
27 29 31 34
Zn (ppm)
Cu (ppm)
Ba (%)
Al (%)
SiO2 (%)

Figure 2.13:

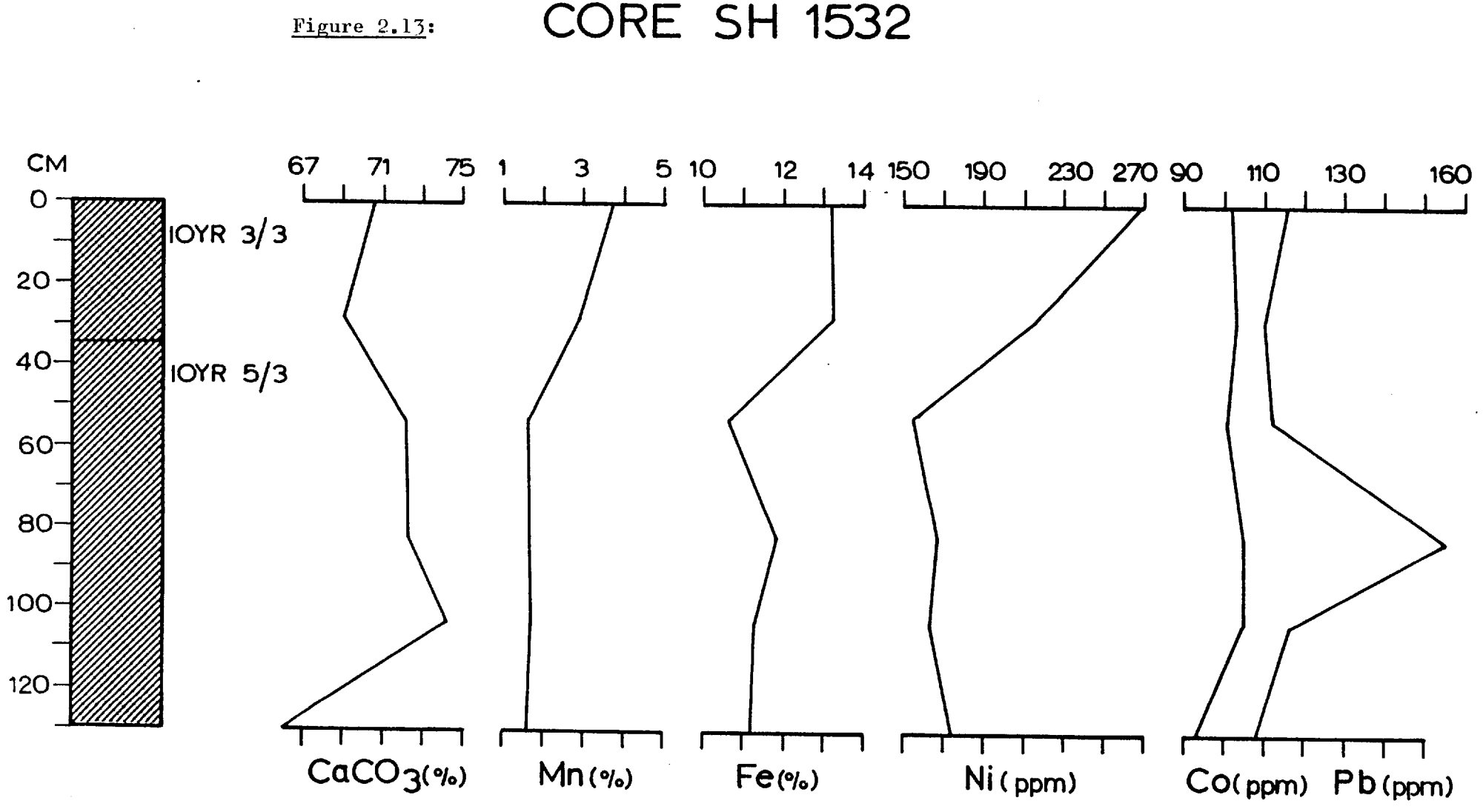
CORE SH 1532
CM
0
20
40
60
80
100
120
10YR 3/3
10YR 5/3
67 71 75
CaCO3(%)
1 3 5
Mn(%)
10 12 14
Fe(%)
150 190 230 270
Ni(ppm)
90 110 130 160
Co(ppm)
Pb(ppm)

Figure 2.14:

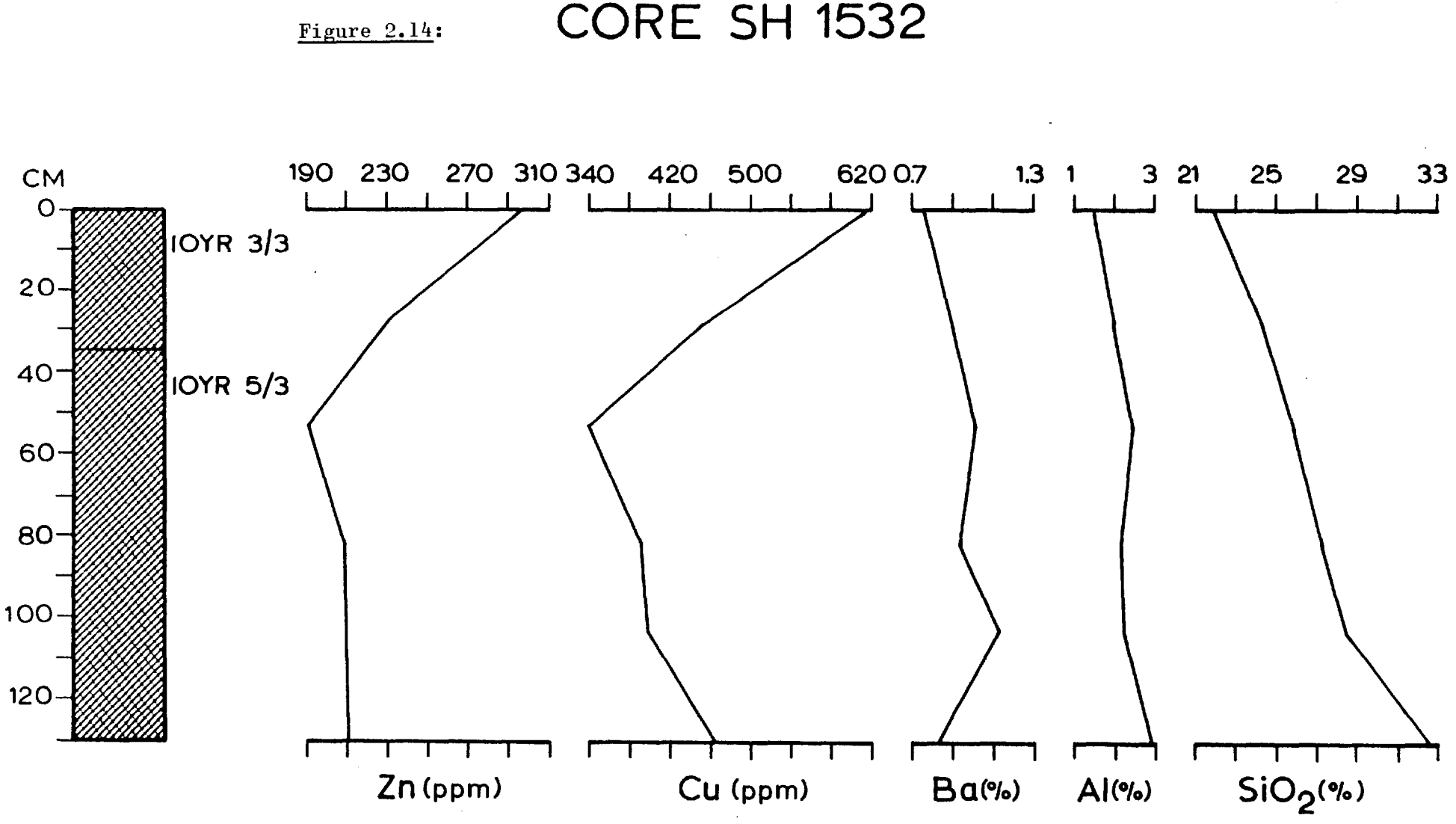
CORE SH 1532
CM
0
20
40
60
80
100
120
10YR 3/3
10YR 5/3
190 230 270 310
Zn (ppm)
340 420 500 620
Cu (ppm)
0.7 1.3
Ba(%)
1 3
Al(%)
21 25 29 33
SiO2(%)

Figure 2.15:

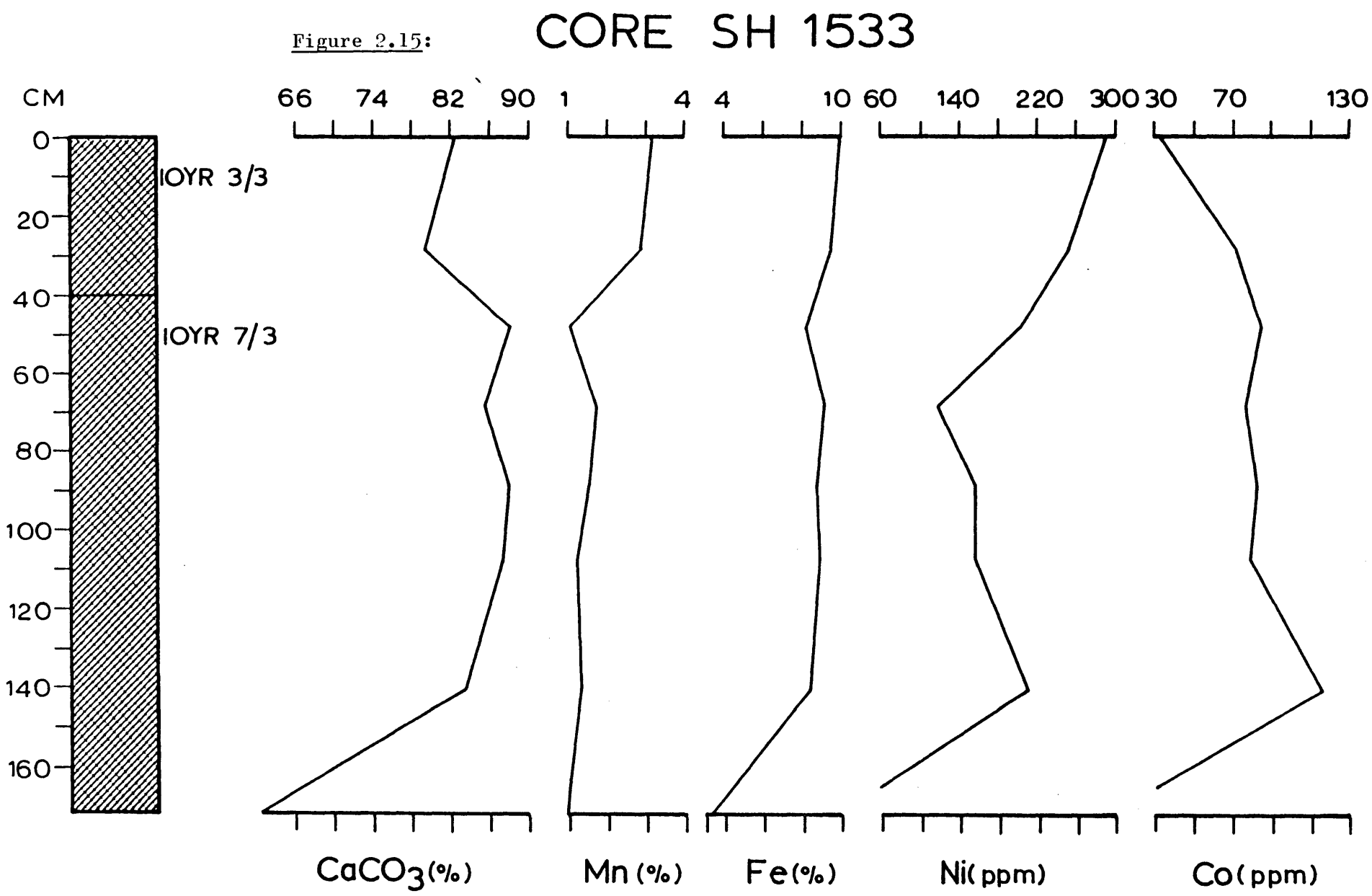
CORE SH 1533
CM
0
20
40
60
80
100
120
140
160
10YR 3/3
10YR 7/3
66 74 82 90
1 4
4 10
60 140 220 300
30 70 130
CaCO3(%)
Mn (%)
Fe(%)
Ni(ppm)
Co(ppm)

Figure 2.16:

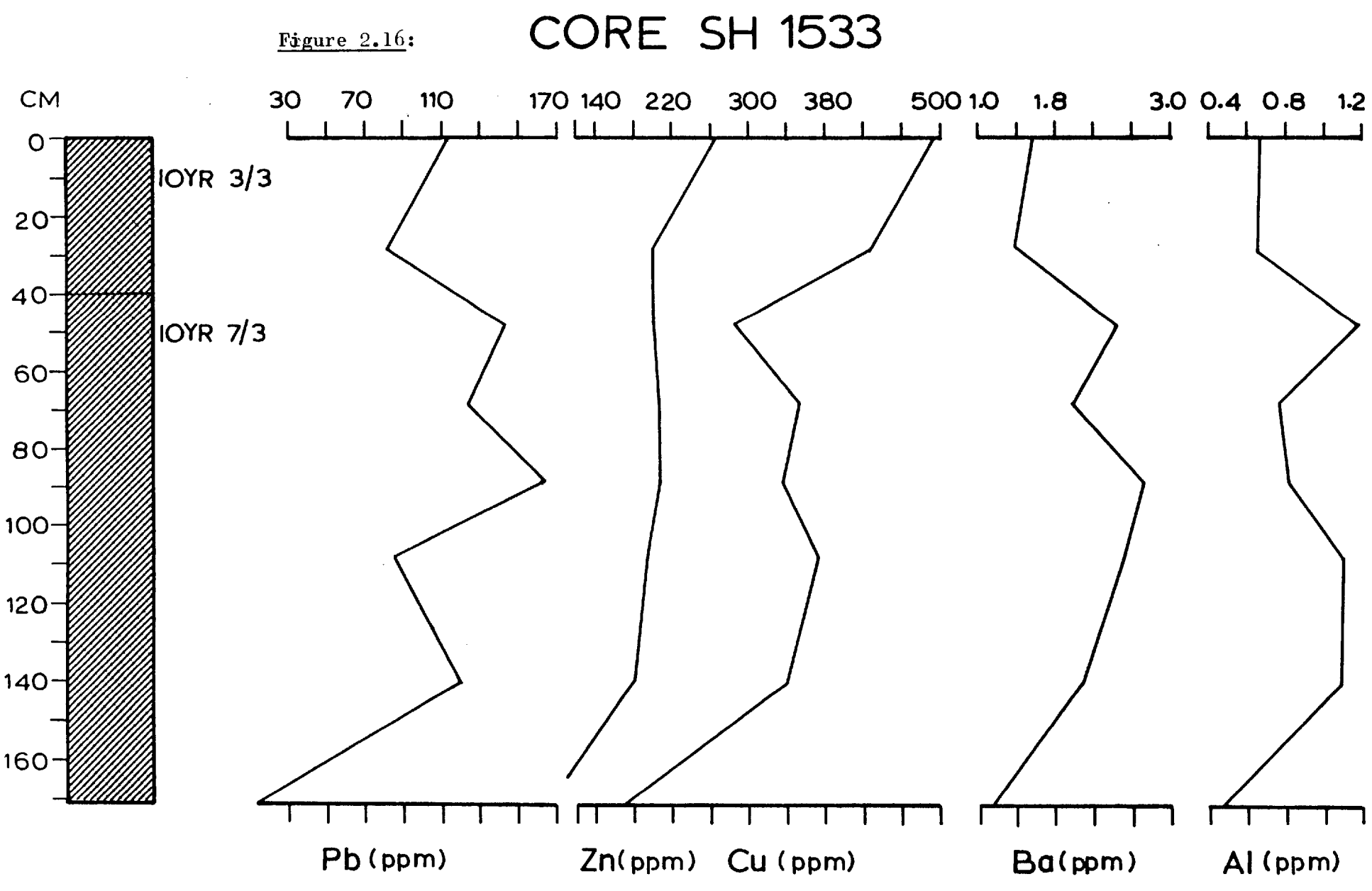
CORE SH 1533
CM
0
20
40
60
80
100
120
140
160
10YR 3/3
10YR 7/3
30 70 110 170
Pb (ppm)
140 220 300 380 500
Zn (ppm)
Cu (ppm)
1.0 1.8 3.0
Ba (ppm)
0.4 0.8 1.2
Al (ppm)

Figure 2.17:

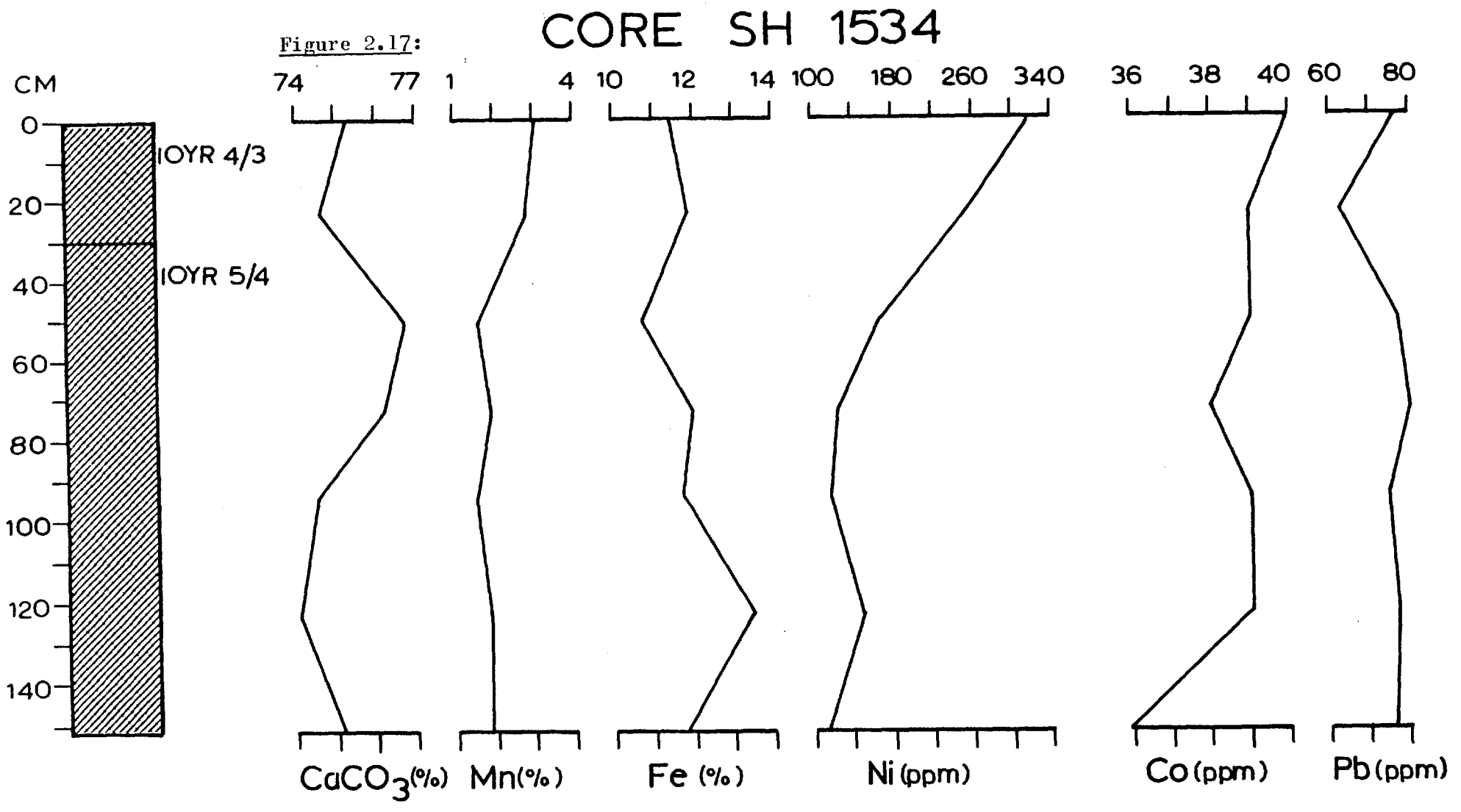
CORE SH 1534
CM
0
20
40
60
80
100
120
140
10YR 4/3
10YR 5/4
74
77
1
4
10
12
14
100
180
260
340
36
38
40
60
80
CaCO3(%)
Mn(%)
Fe (%)
Ni (ppm)
Co (ppm)
Pb (ppm)

Figure 2.18:

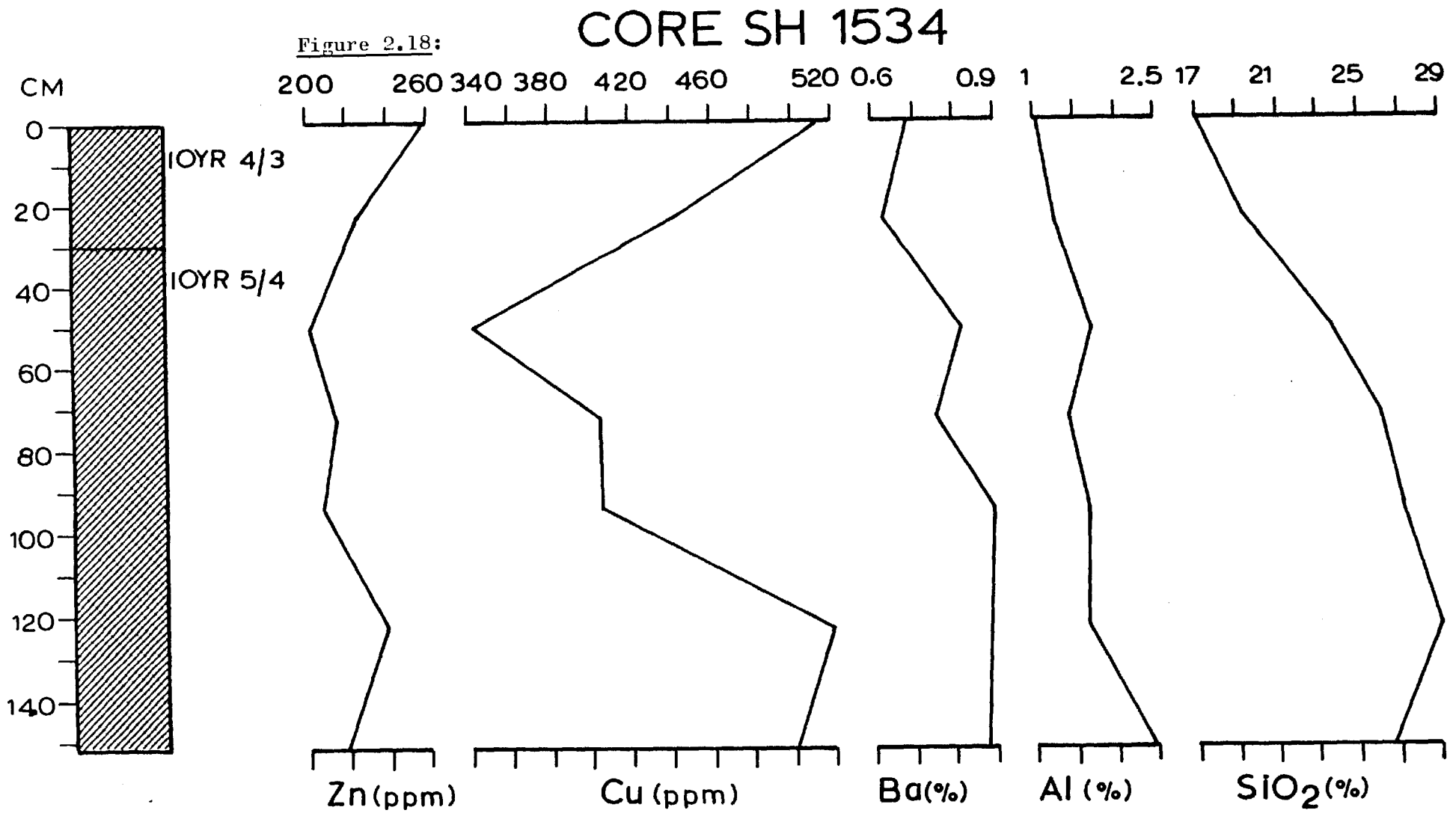
CORE SH 1534
CM
0
20
40
60
80
100
120
140
10YR 4/3
10YR 5/4
200
260
340
380
420
460
520
0.6
0.9
1
2.5
17
21
25
29
Zn (ppm)
Cu (ppm)
Ba(%)
Al (%)
SiO2 (%)

Figure 2.19:

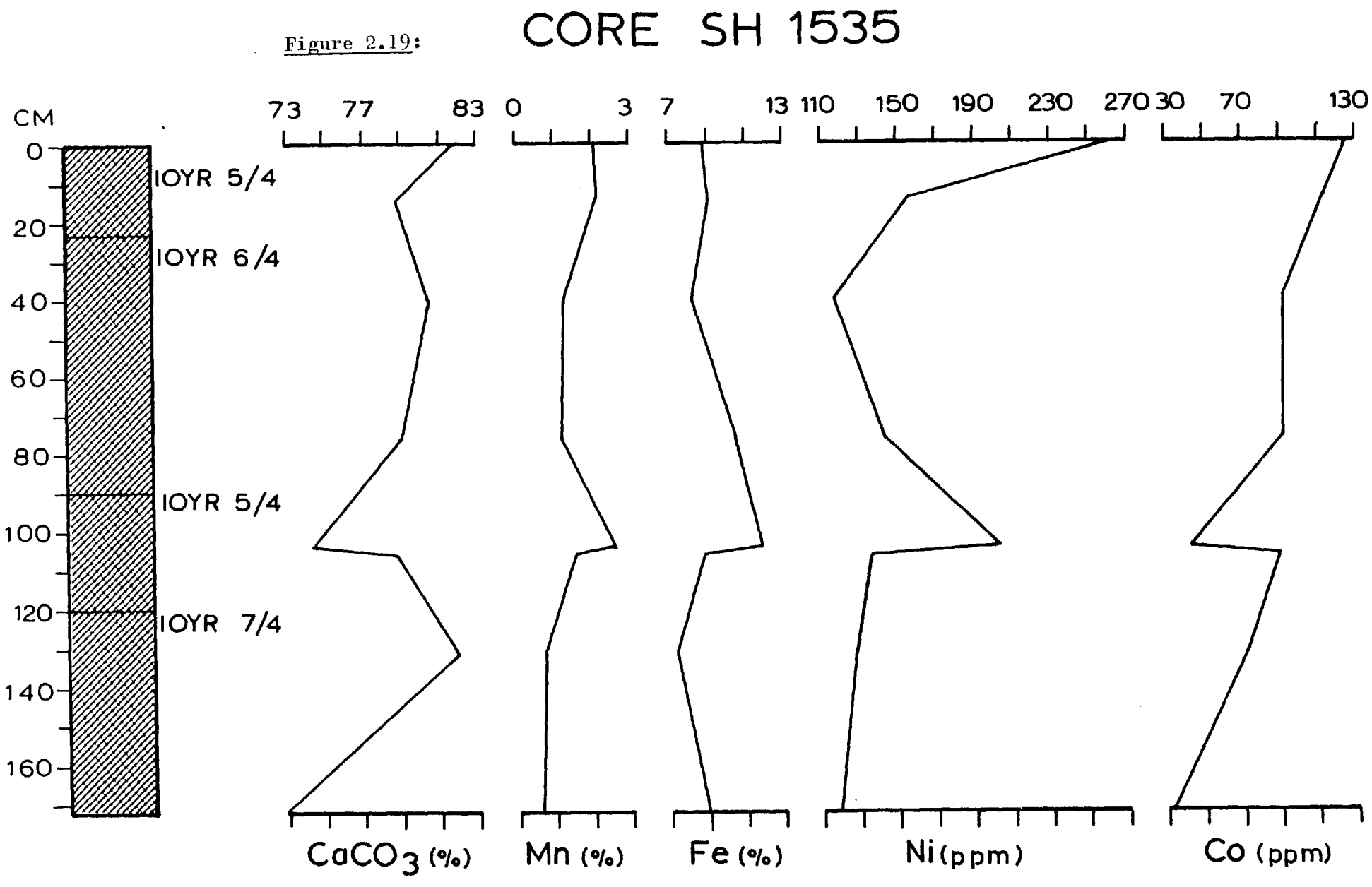
CORE SH 1535
CM
0
20
40
60
80
100
120
140
160
10YR 5/4
10YR 6/4
10YR 5/4
10YR 7/4
73 77 83
0 3
7 13
110 150 190 230 270
30 70 130
CaCO3 (%)
Mn (%)
Fe (%)
Ni (ppm)
Co (ppm)

Figure 2.20:

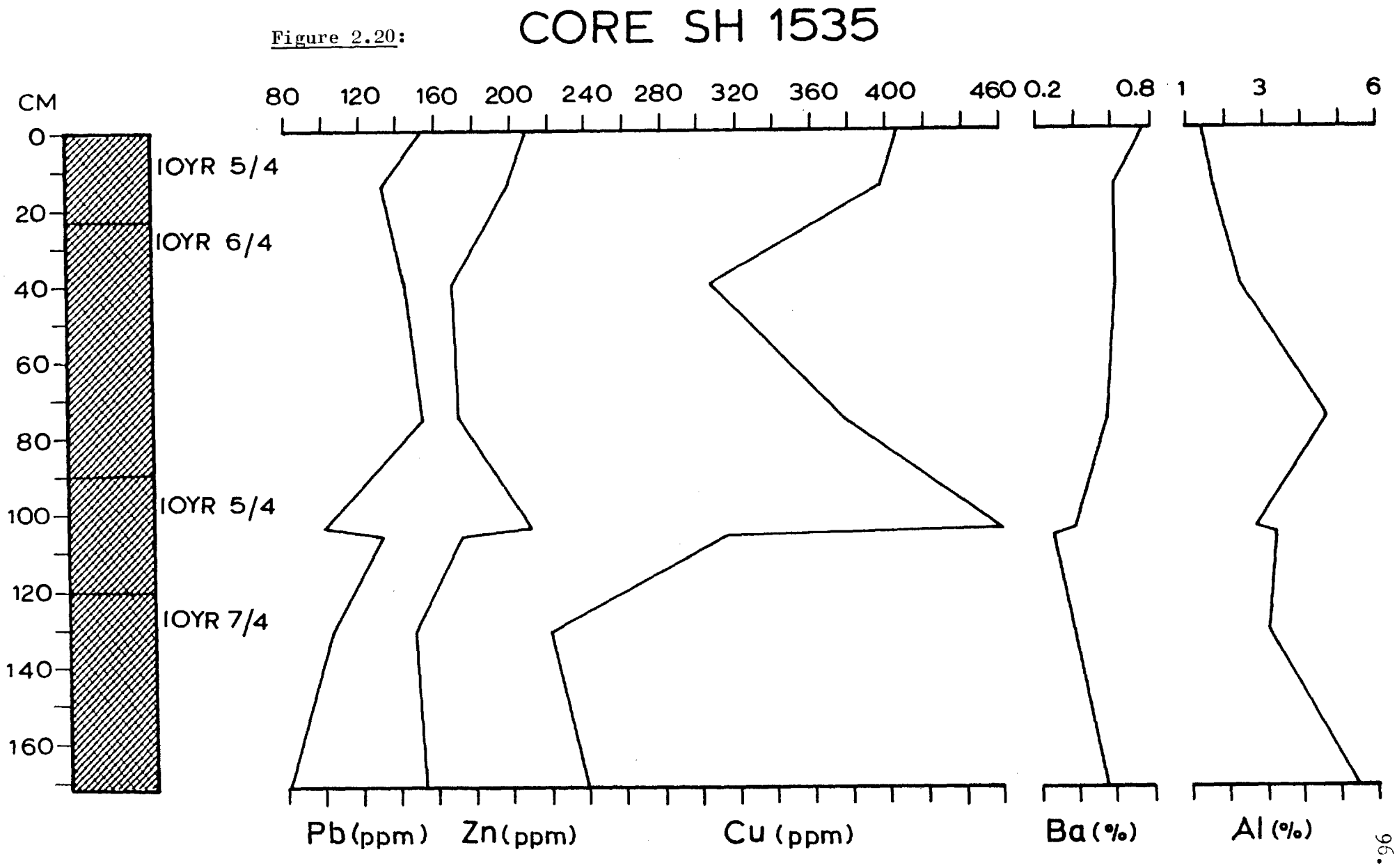
CORE SH 1535
CM
0
20
40
60
80
100
120
140
160
10YR 5/4
10YR 6/4
10YR 5/4
10YR 7/4
80 120 160 200 240 280 320 360 400 460
0.2 0.8
1 3 6
Pb (ppm)
Zn (ppm)
Cu (ppm)
Ba (%)
Al (%)

Figure 2.21:

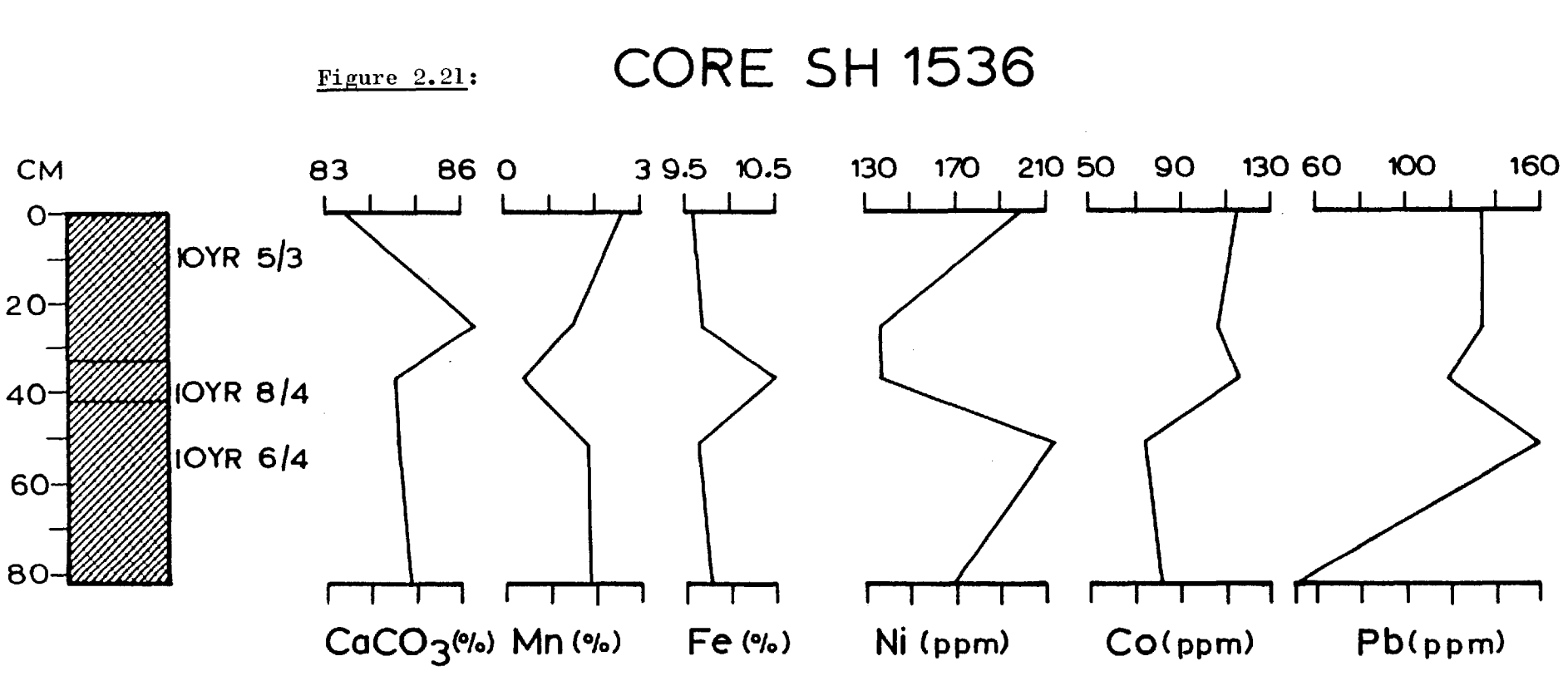
CORE SH 1536
CM
0
20
40
60
80
10YR 5/3
10YR 8/4
10YR 6/4
83
86
0
3
9.5
10.5
130
170
210
50
90
130
60
100
160
CaCO3(%)
Mn (%)
Fe (%)
Ni (ppm)
Co(ppm)
Pb(ppm)

Figure 2.22:

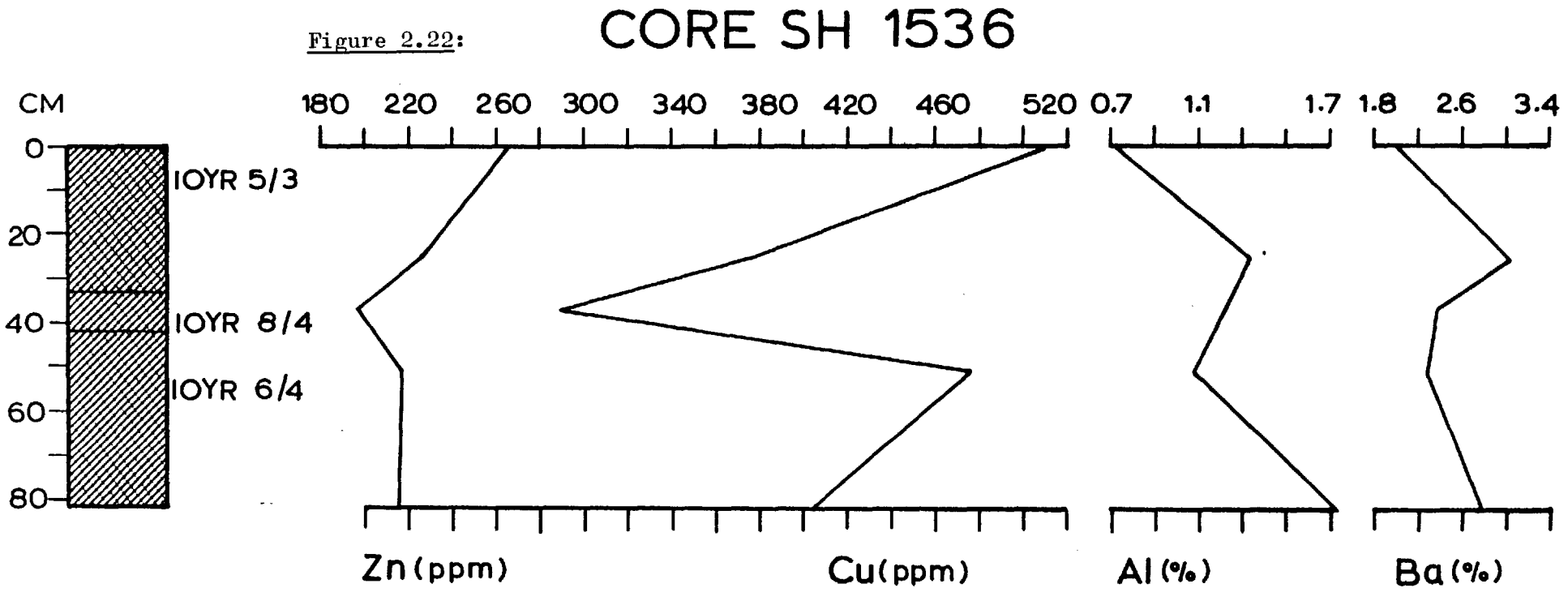
CORE SH 1536
CM
0
20
40
60
80
10YR 5/3
10YR 8/4
10YR 6/4
180 220 260 300 340 380 420 460 520
Zn (ppm)
Cu (ppm)
0.7 1.1 1.7
Al (%)
1.8 2.6 3.4
Ba (%)

Figure 2.23: CORE SH 1537

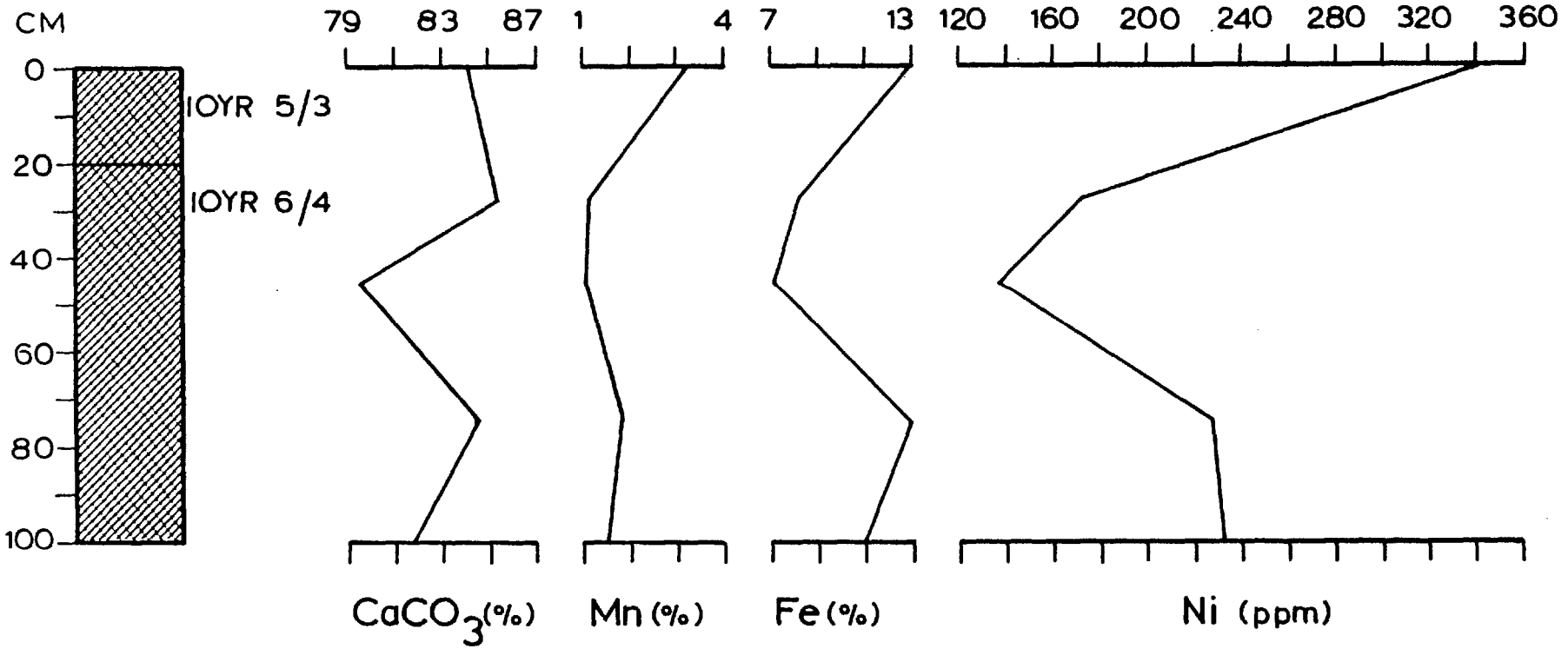

Figure 2.24:

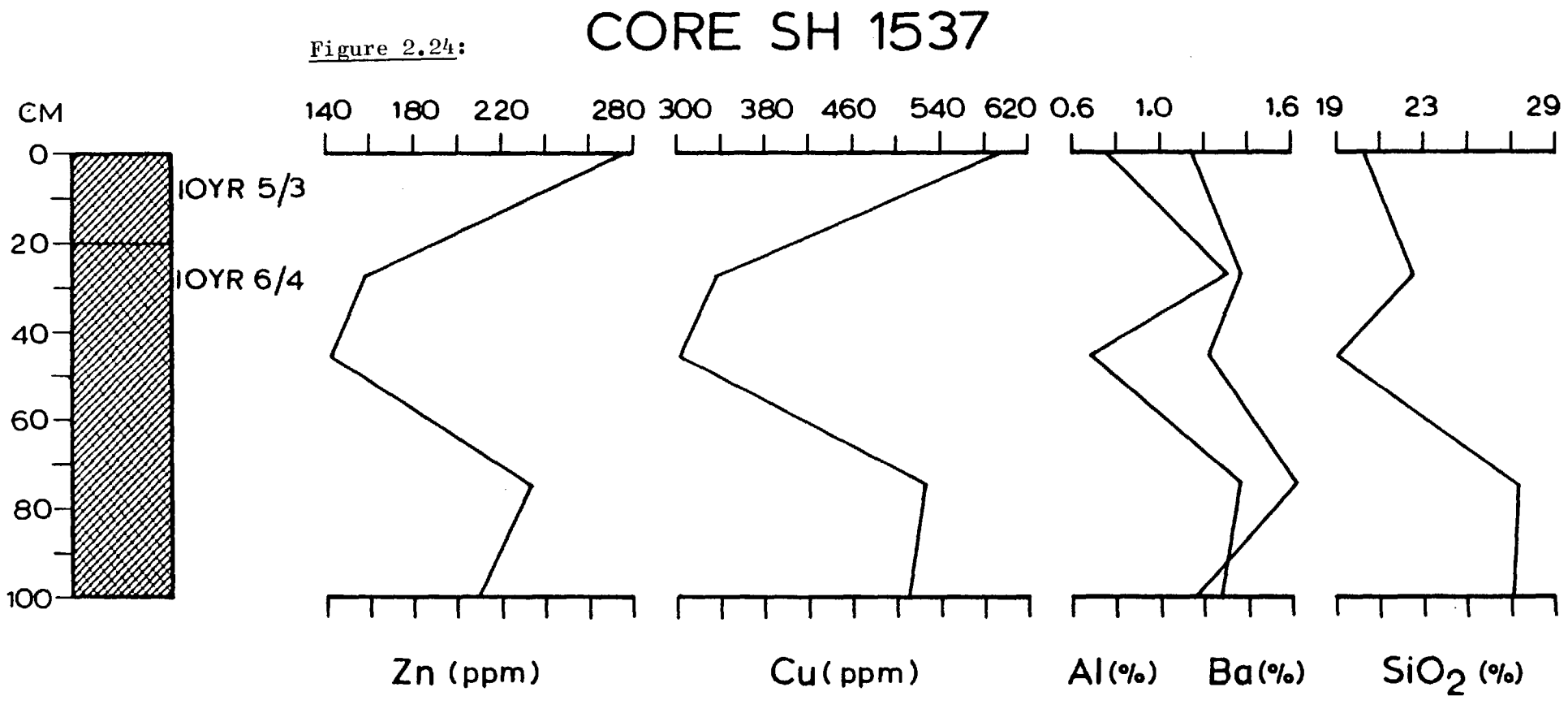
CORE SH 1537
CM
0
20
40
60
80
100
10YR 5/3
10YR 6/4
140 180 220 280
300 380 460 540 620
0.6 1.0 1.6
19 23 29
Zn (ppm)
Cu (ppm)
Al (%)
Ba (%)
SiO2 (%)

Figure 2.25:

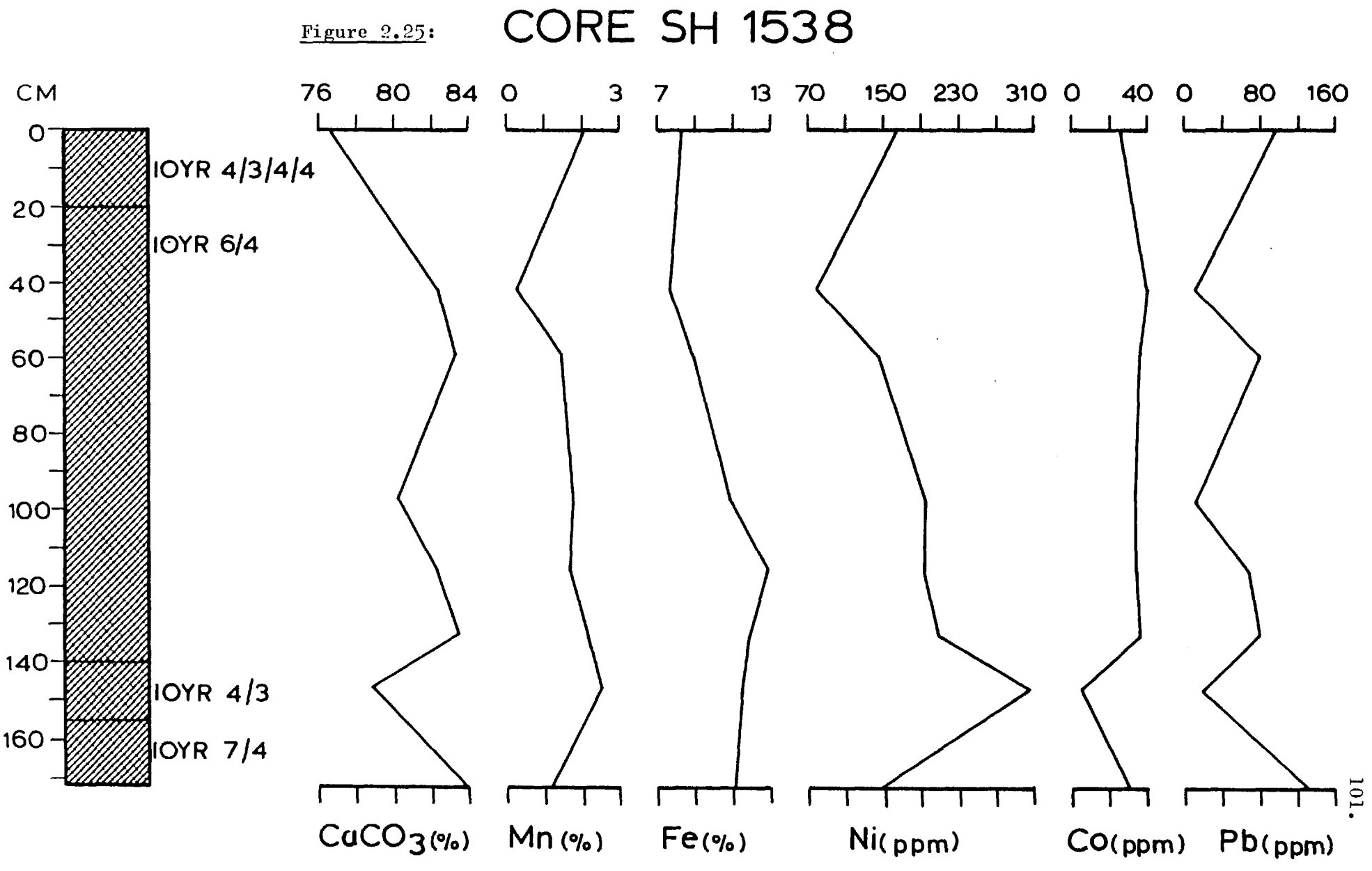
CORE SH 1538
CM
0
20
40
60
80
100
120
140
160
10YR 4/3/4/4
10YR 6/4
10YR 4/3
10YR 7/4
76 80 84
CaCO3 (%)
0 3
Mn (%)
7 13
Fe (%)
70 150 230 310
Ni (ppm)
0 40
Co (ppm)
0 80 160
Pb (ppm)

Figure 2.26:

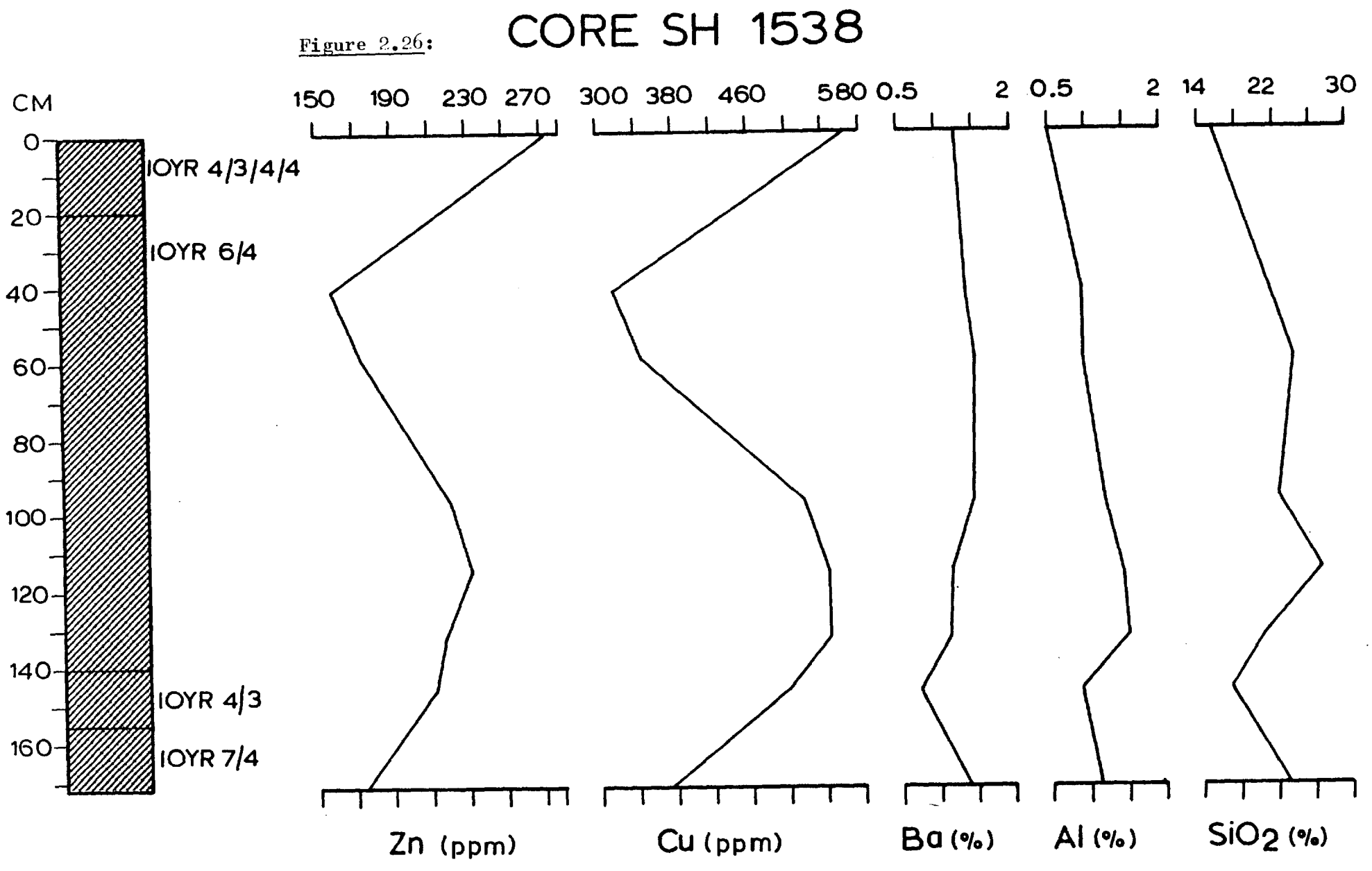
CORE SH 1538
CM
0
20
40
60
80
100
120
140
160
10YR 4/3/4/4
10YR 6/4
10YR 4/3
10YR 7/4
150 190 230 270
Zn (ppm)
300 380 460 580
Cu (ppm)
0.5 2
Ba (%)
0.5 2
Al (%)
14 22 30
SiO2 (%)

Figure 2.27:

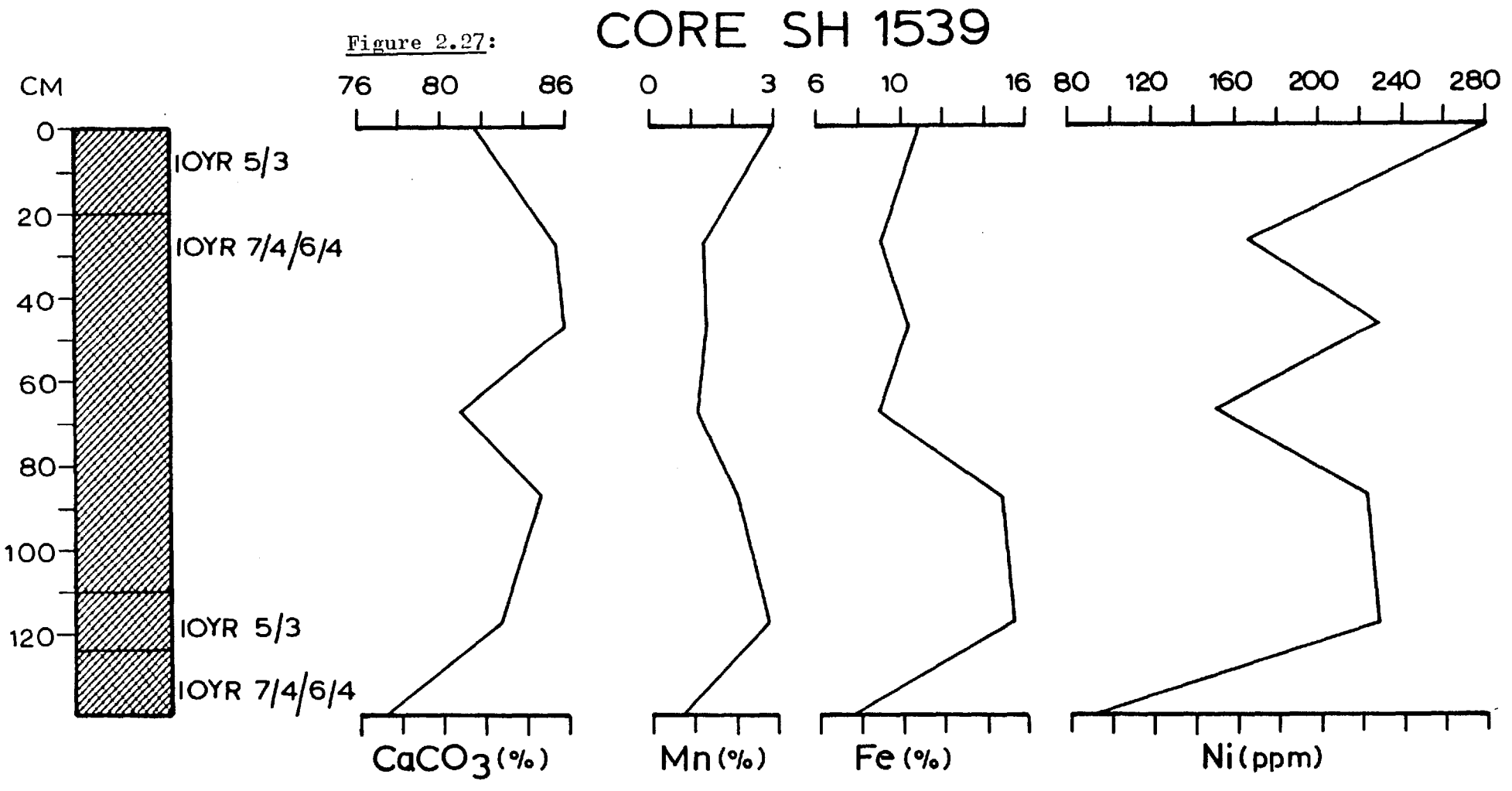
CORE SH 1539
CM
0
20
40
60
80
100
120
10YR 5/3
10YR 7/4/6/4
10YR 5/3
10YR 7/4/6/4
76
80
86
CaCO3 (%)
0
3
Mn (%)
6
10
16
Fe (%)
80
120
160
200
240
280
Ni (ppm)

Figure 2.28:

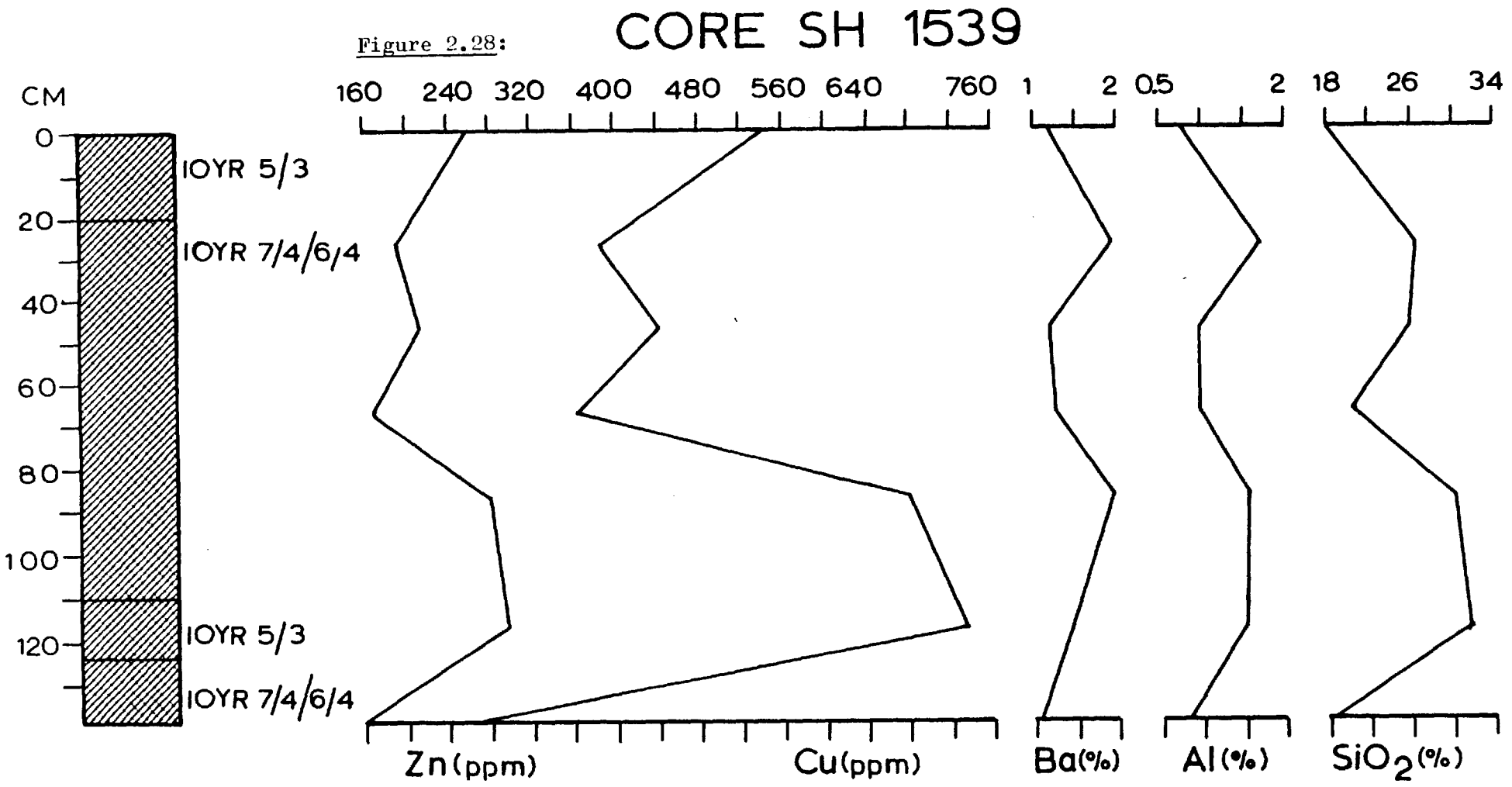
CORE SH 1539
CM
0
20
40
60
80
100
120
10YR 5/3
10YR 7/4/6/4
10YR 5/3
10YR 7/4/6/4
160 240 320 400 480 560 640 760
Zn(ppm)
Cu(ppm)
1 2
Ba(%)
0.5 2
Al(%)
18 26 34
SiO2(%)

Figure 2.29:

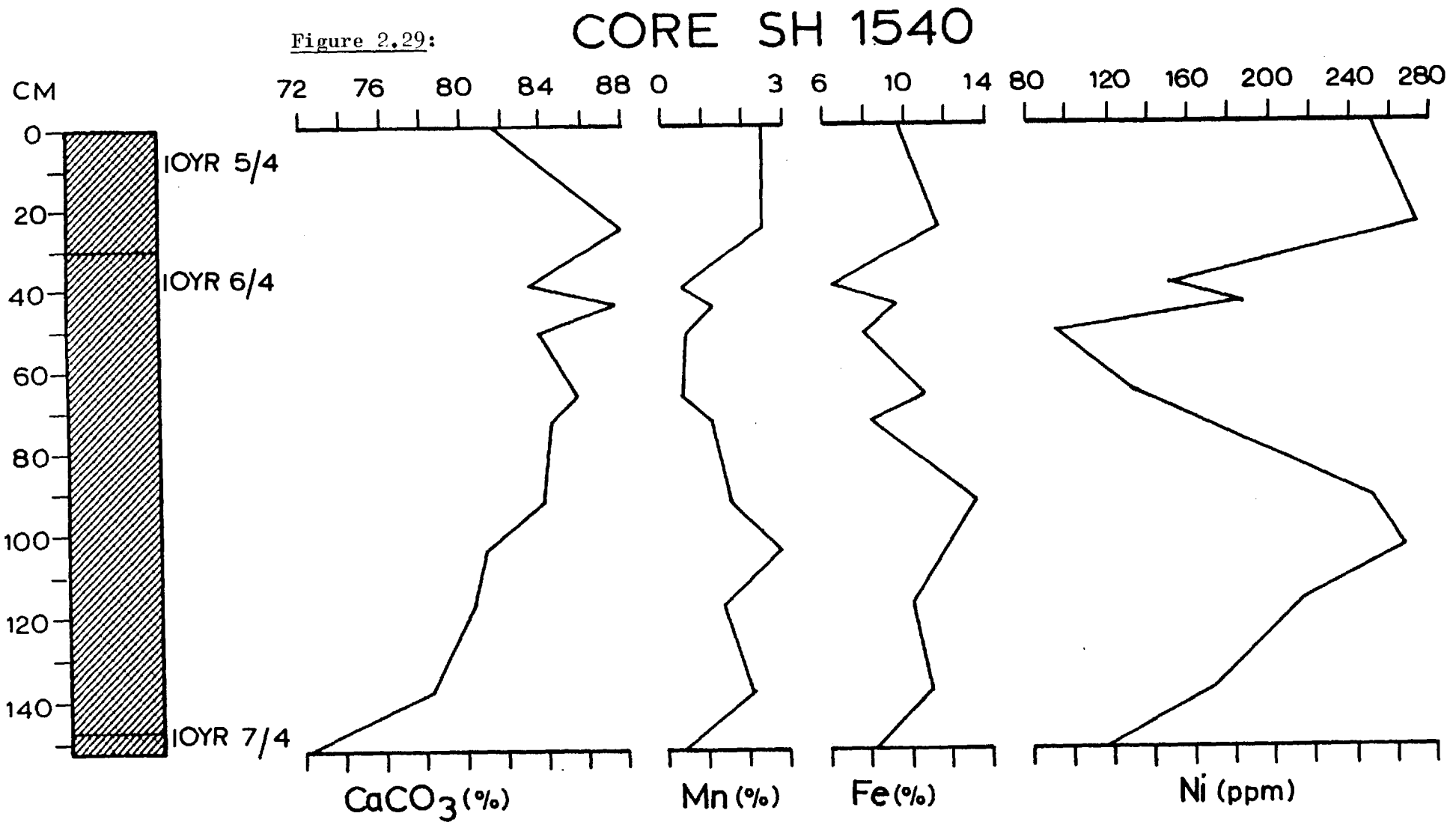
CORE SH 1540
CM
0
20
40
60
80
100
120
140
10YR 5/4
10YR 6/4
10YR 7/4
72 76 80 84 88
CaCO3 (%)
0 3
Mn (%)
6 10 14
Fe (%)
80 120 160 200 240 280
Ni (ppm)

Figure 2.30:

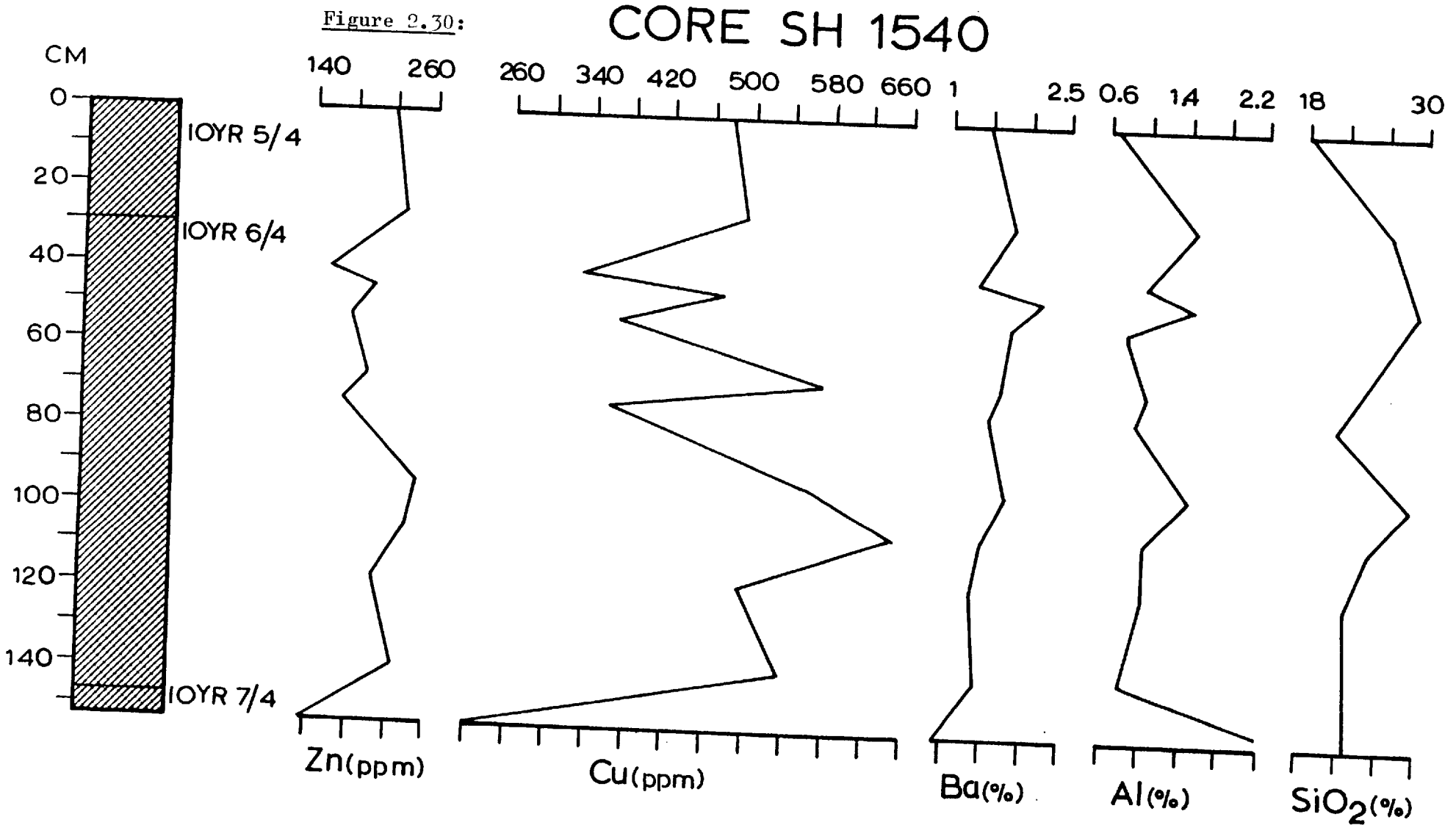
CORE SH 1540
CM
0
20
40
60
80
100
120
140
10YR 5/4
10YR 6/4
10YR 7/4
140
260
Zn(ppm)
260
340
420
500
580
660
Cu(ppm)
1
2.5
Ba(%)
0.6
1.4
2.2
Al(%)
18
30
SiO2(%)

Figure 2.31:

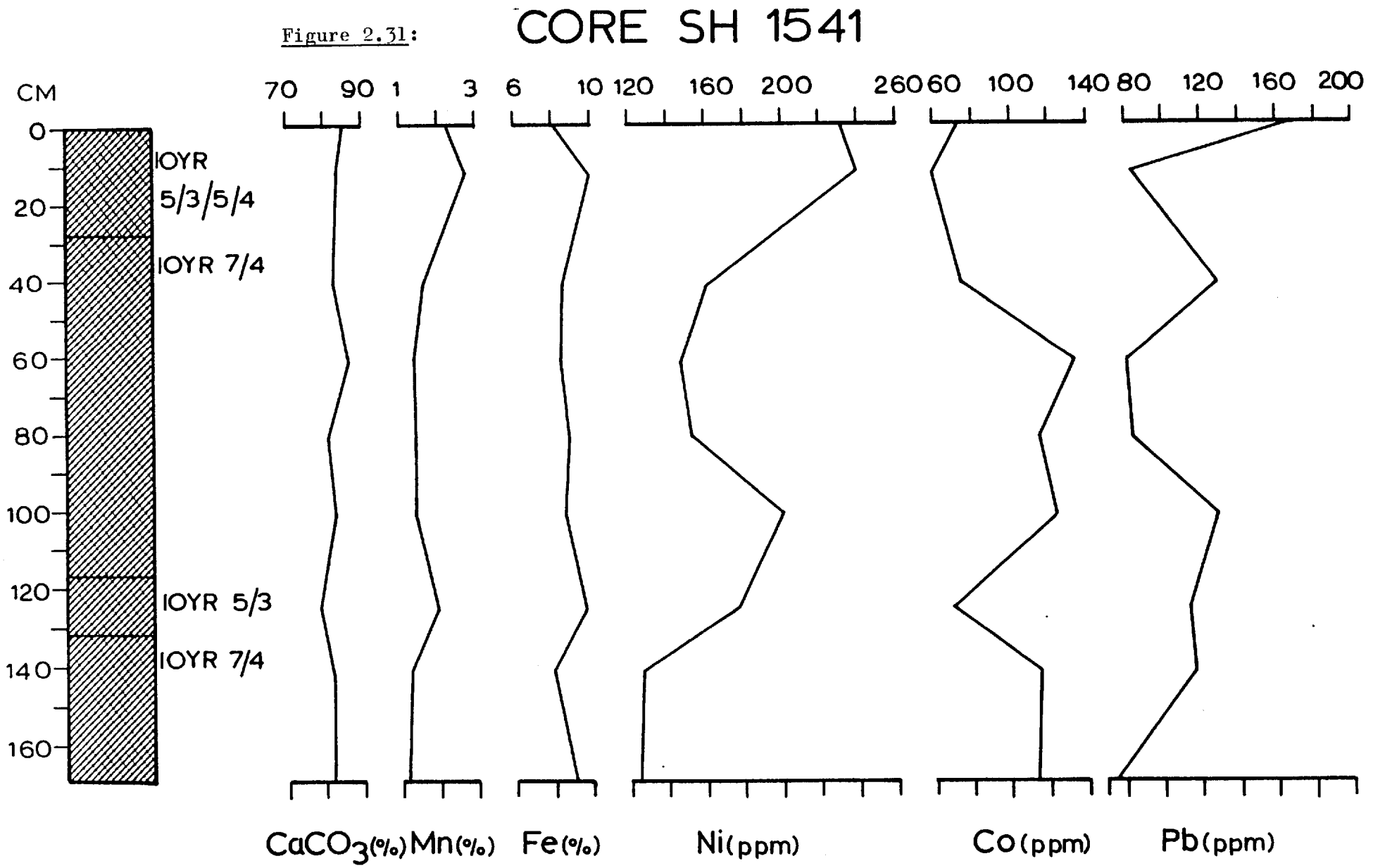
CORE SH 1541
CM
0
20
40
60
80
100
120
140
160
10YR 5/3/5/4
10YR 7/4
10YR 5/3
10YR 7/4
70 90
1 3
6 10
120 160 200 260
60 100 140
80 120 160 200
CaCO3(%)
Mn(%)
Fe(%)
Ni(ppm)
Co(ppm)
Pb(ppm)

Figure 2.32:

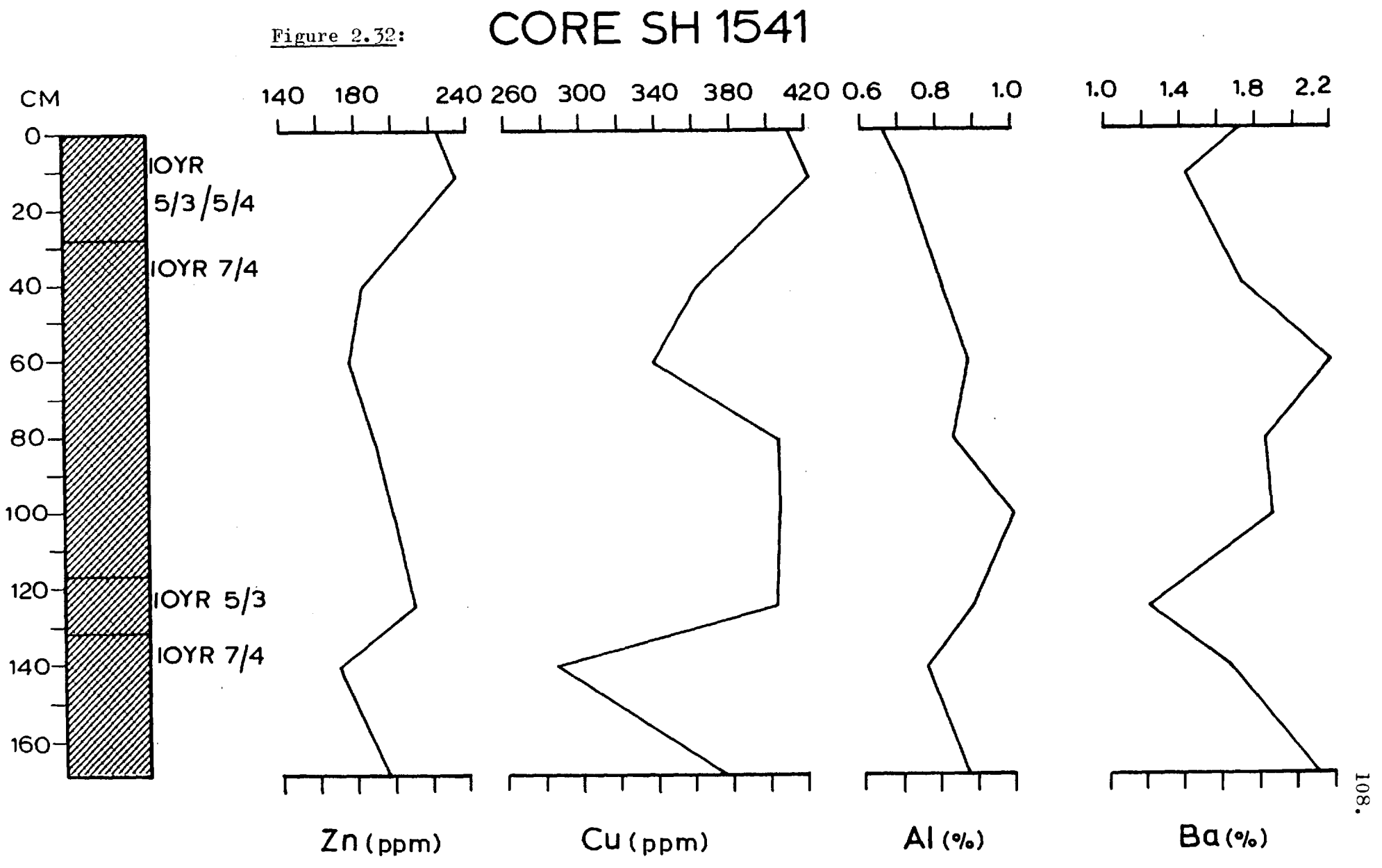
CORE SH 1541
CM
0
20
40
60
80
100
120
140
160
10YR 5/3/5/4
10YR 7/4
10YR 5/3
10YR 7/4
140 180 240
260 300 340 380 420
0.6 0.8 1.0
1.0 1.4 1.8 2.2
Zn (ppm)
Cu (ppm)
Al (%)
Ba (%)

Figure 2.33:

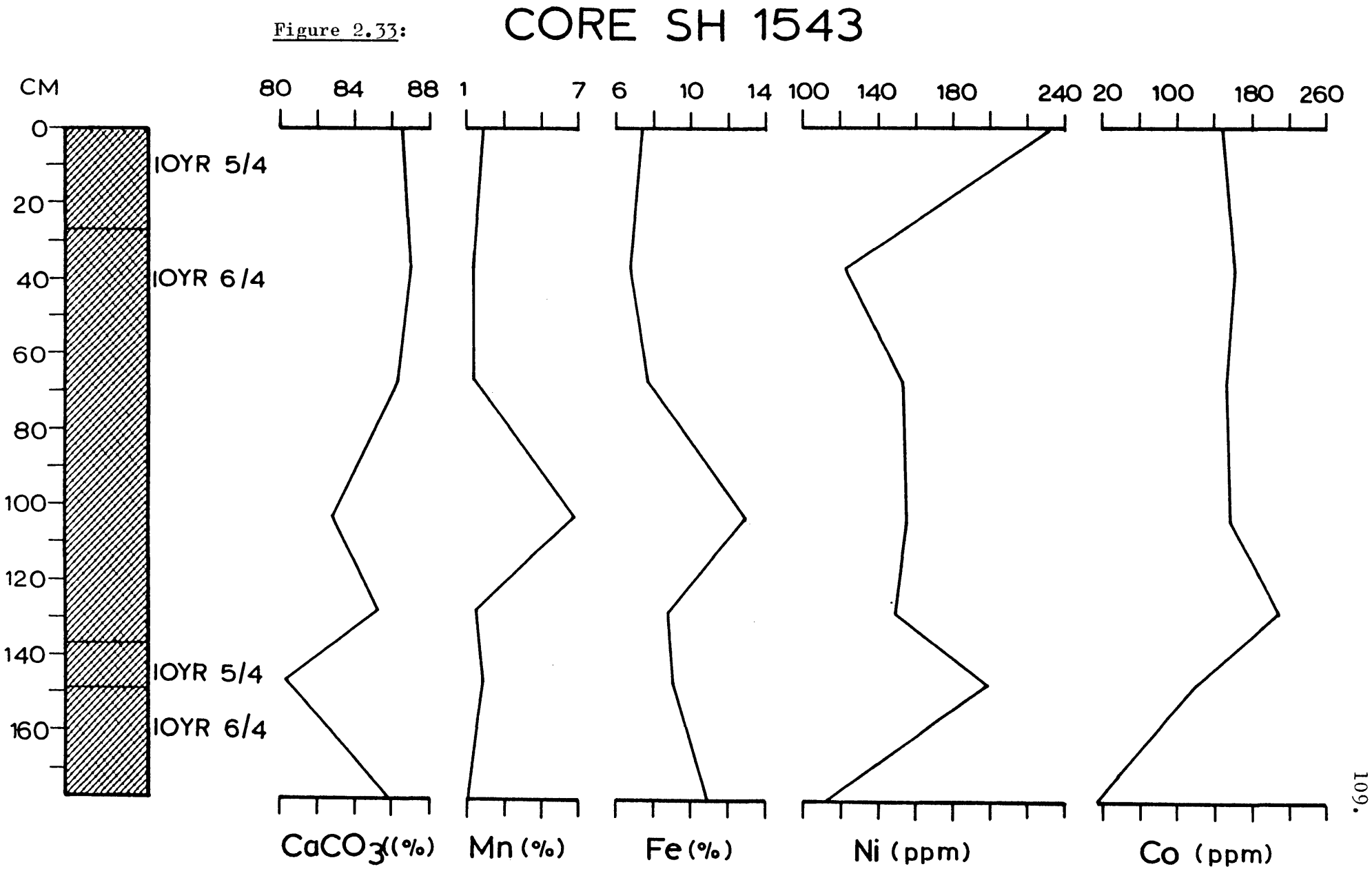
CORE SH 1543
CM
0
20
40
60
80
100
120
140
160
10YR 5/4
10YR 6/4
10YR 5/4
10YR 6/4
80 84 88
1 7
6 10 14
100 140 180 240
20 100 180 260
CaCO3 (%)
Mn (%)
Fe (%)
Ni (ppm)
Co (ppm)

Figure 2.34:

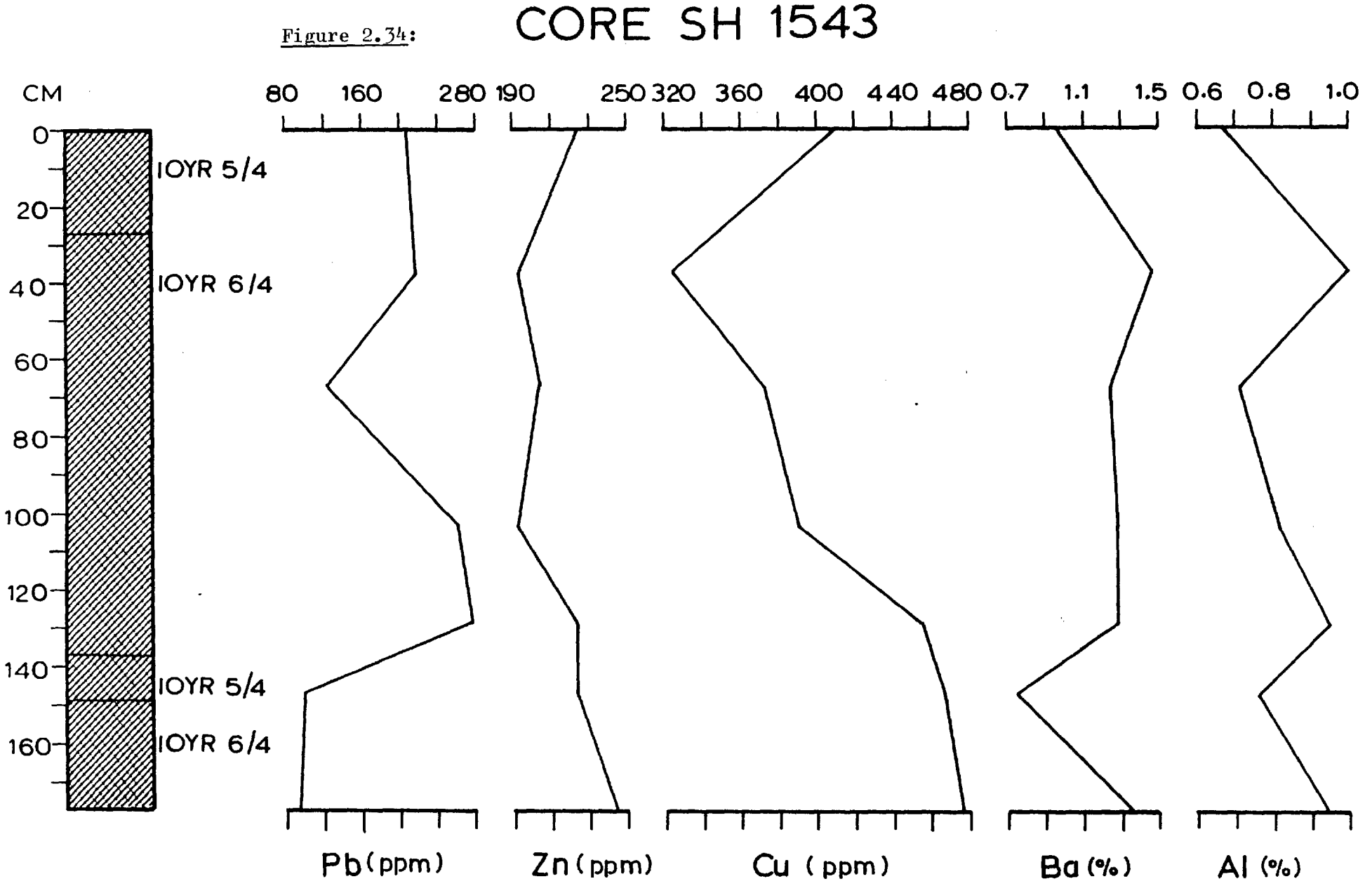
CORE SH 1543
CM
0
20
40
60
80
100
120
140
160
10YR 5/4
10YR 6/4
10YR 5/4
10YR 6/4
80 160 280
Pb (ppm)
190 250
Zn (ppm)
320 360 400 440 480
Cu (ppm)
0.7 1.1 1.5
Ba (%)
0.6 0.8 1.0
Al (%)

Figure 2.35:

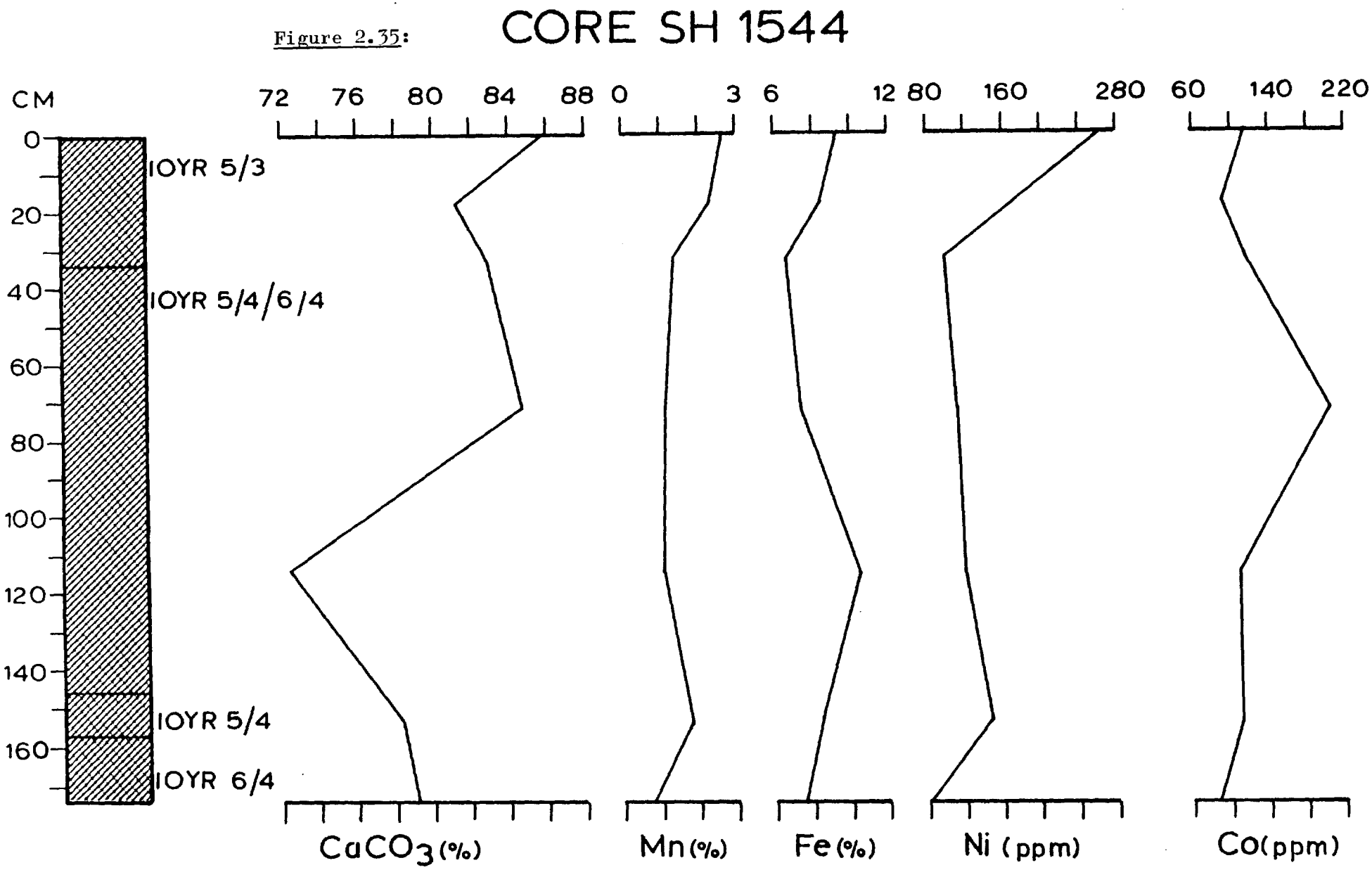
CORE SH 1544
CM
0
20
40
60
80
100
120
140
160
10YR 5/3
10YR 5/4/6/4
10YR 5/4
10YR 6/4
72 76 80 84 88
CaCO3 (%)
0 3
Mn (%)
6 12
Fe (%)
80 160 280
Ni (ppm)
60 140 220
Co(ppm)

Figure 2.36:

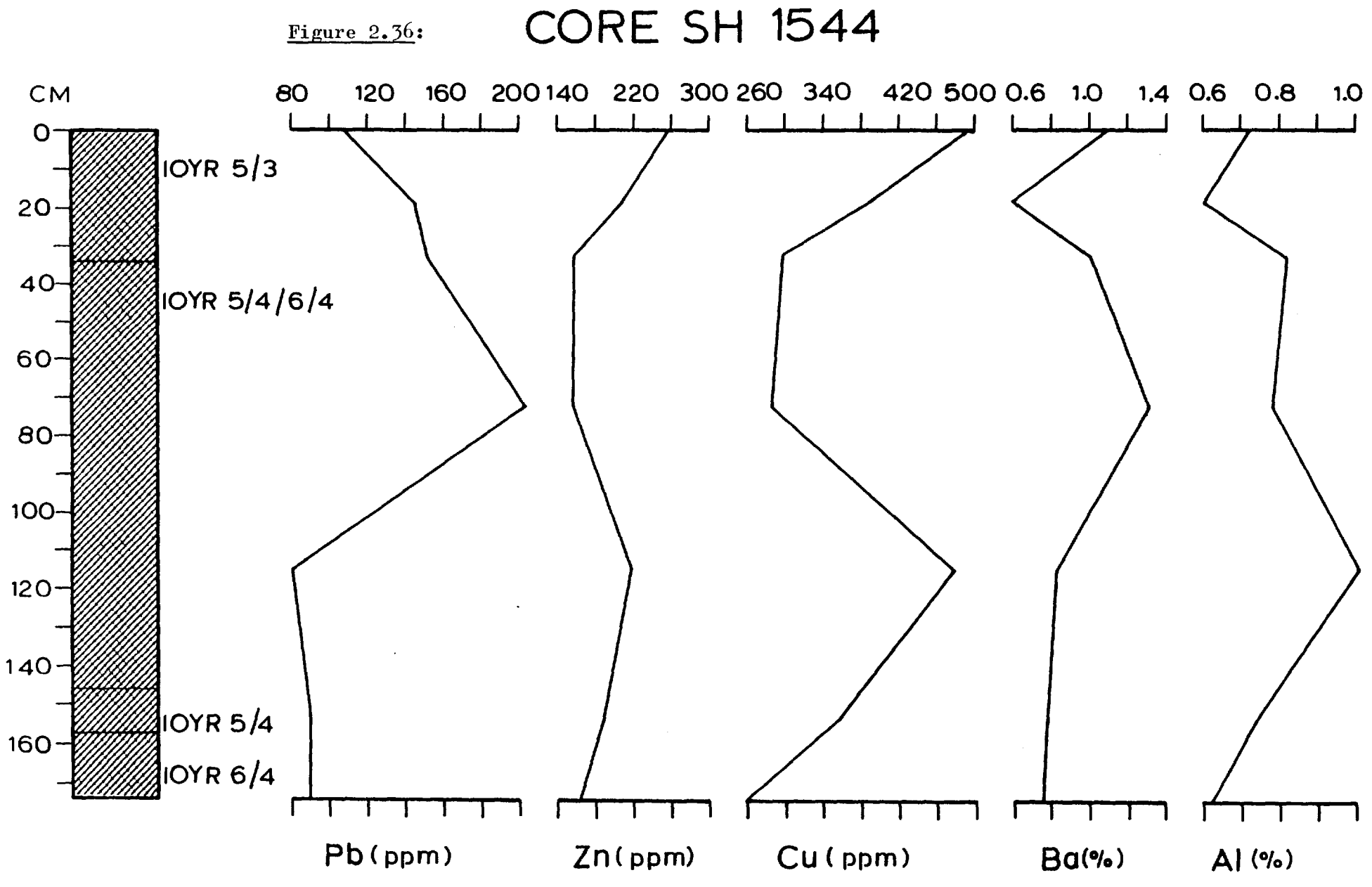
CORE SH 1544
CM
0
20
40
60
80
100
120
140
160
10YR 5/3
10YR 5/4/6/4
10YR 5/4
10YR 6/4
80 120 160 200
140 220 300
260 340 420 500
0.6 1.0 1.4
0.6 0.8 1.0
Pb (ppm)
Zn (ppm)
Cu (ppm)
Ba(%)
Al (%)

Figure 2.37:

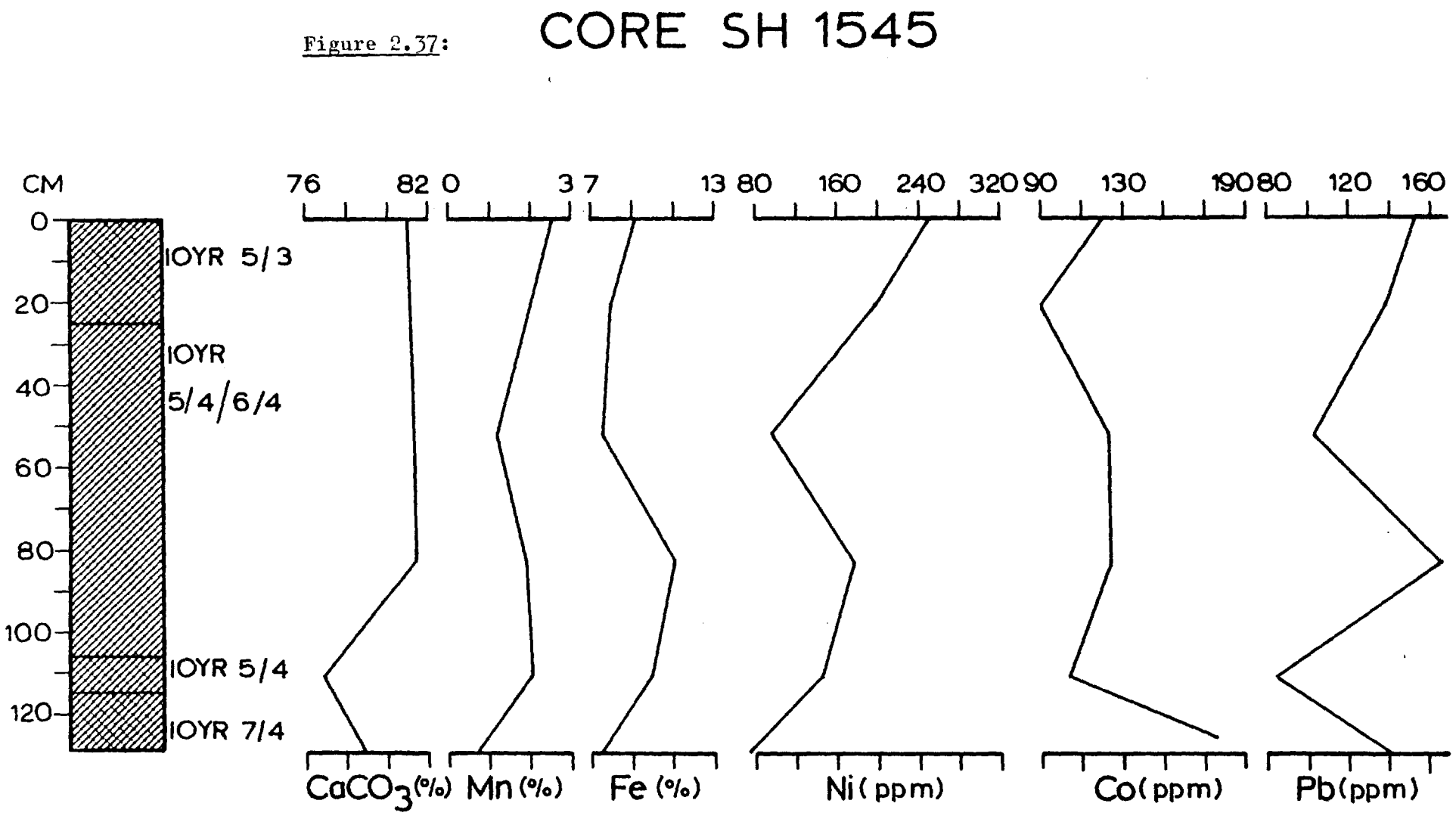
CORE SH 1545
CM
0
20
40
60
80
100
120
10YR 5/3
10YR
5/4/6/4
10YR 5/4
10YR 7/4
76
82
0
3
7
13
80
160
240
320
90
130
190
80
120
160
CaCO3(%)
Mn(%)
Fe(%)
Ni(ppm)
Co(ppm)
Pb(ppm)

Figure 2.38:

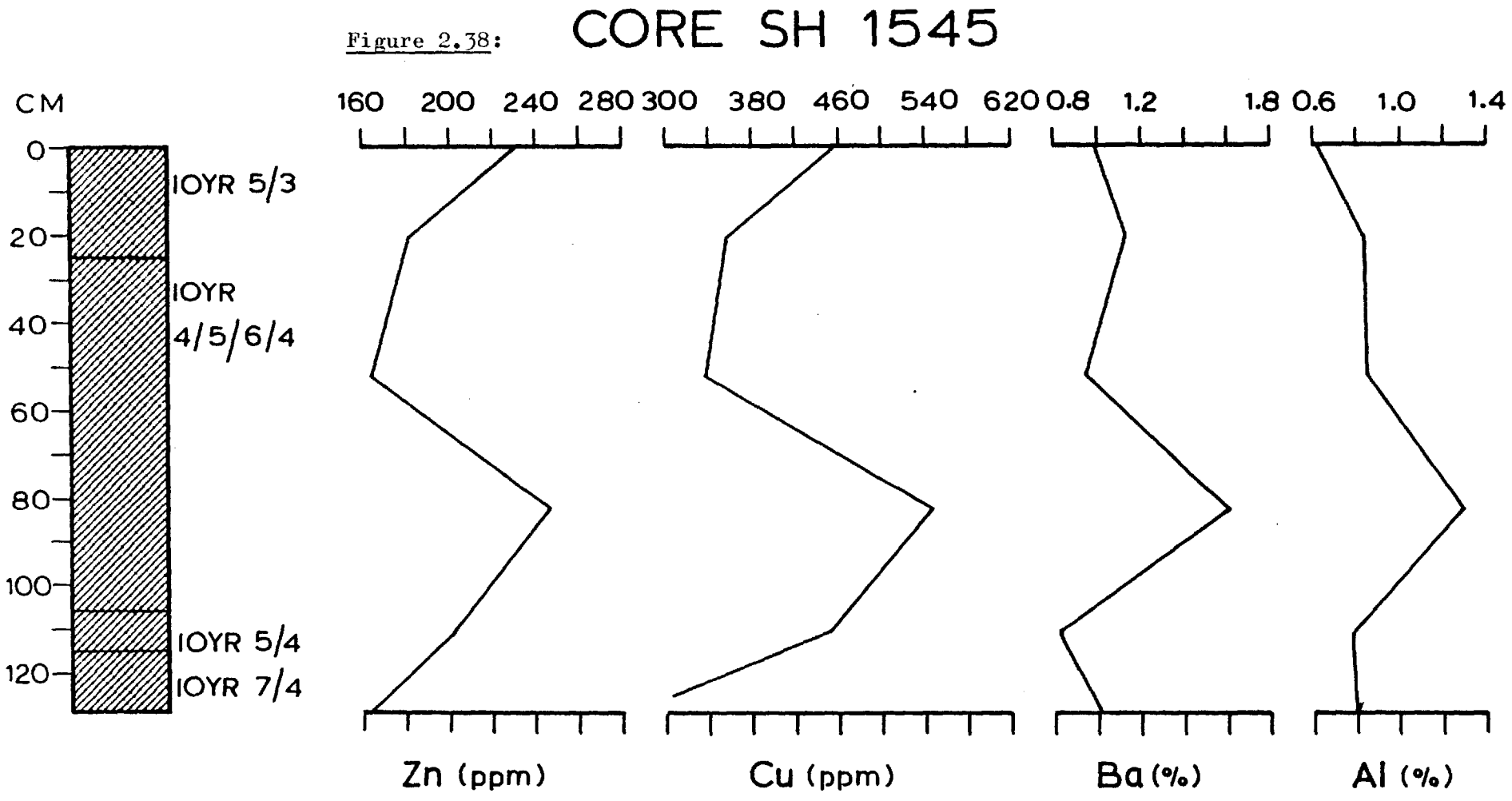
CORE SH 1545
CM
0
20
40
60
80
100
120
10YR 5/3
10YR
4/5/6/4
10YR 5/4
10YR 7/4
160 200 240 280
Zn (ppm)
300 380 460 540 620
Cu (ppm)
0.8 1.2 1.8
Ba (%)
0.6 1.0 1.4
Al (%)

Figure 2.39:

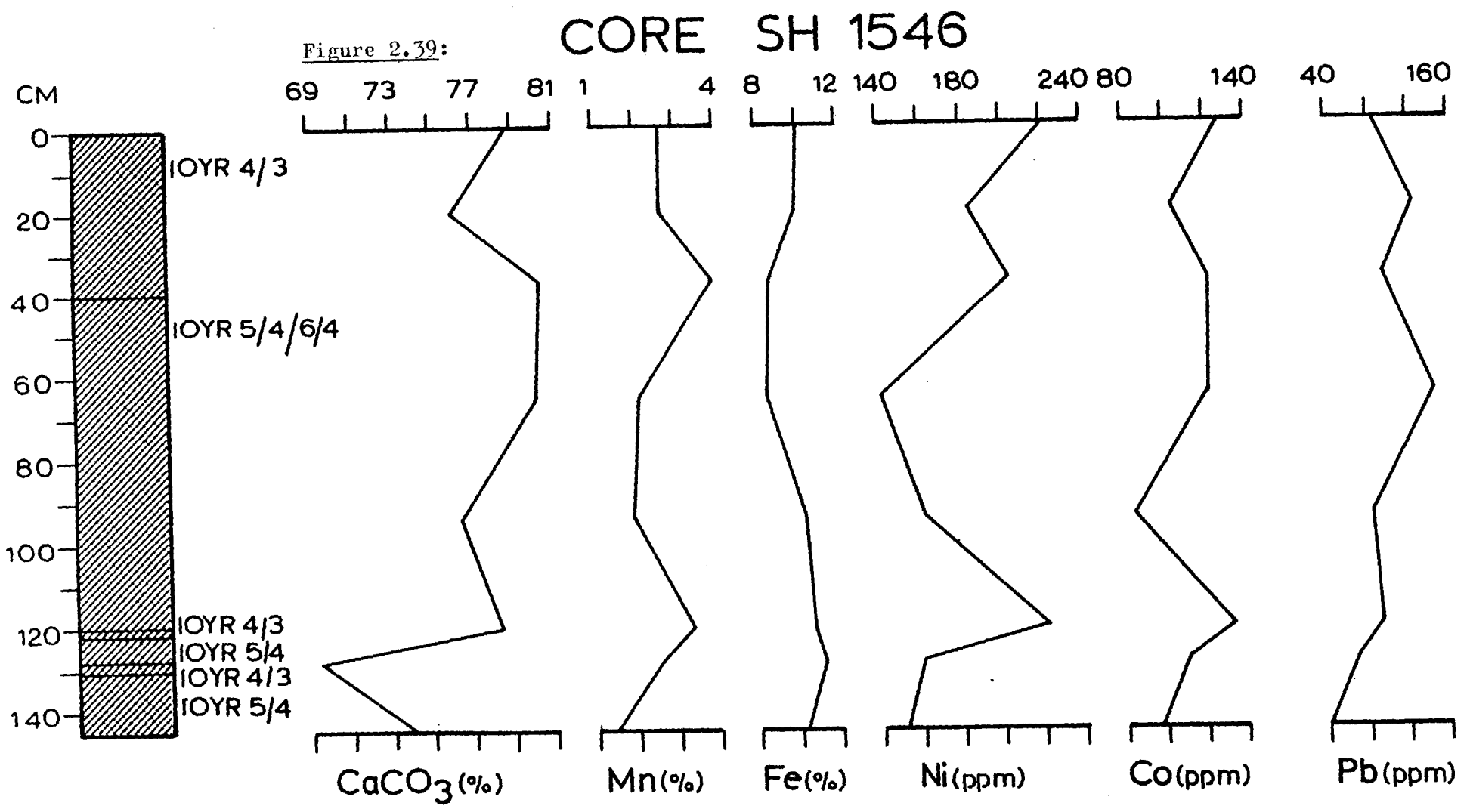
CORE SH 1546
CM
0
20
40
60
80
100
120
140
10YR 4/3
10YR 5/4/6/4
10YR 4/3
10YR 5/4
10YR 4/3
10YR 5/4
69 73 77 81
CaCO3 (%)
1 4
Mn (%)
8 12
Fe (%)
140 180 240
Ni (ppm)
80 140
Co (ppm)
40 160
Pb (ppm)

Figure 2.40:

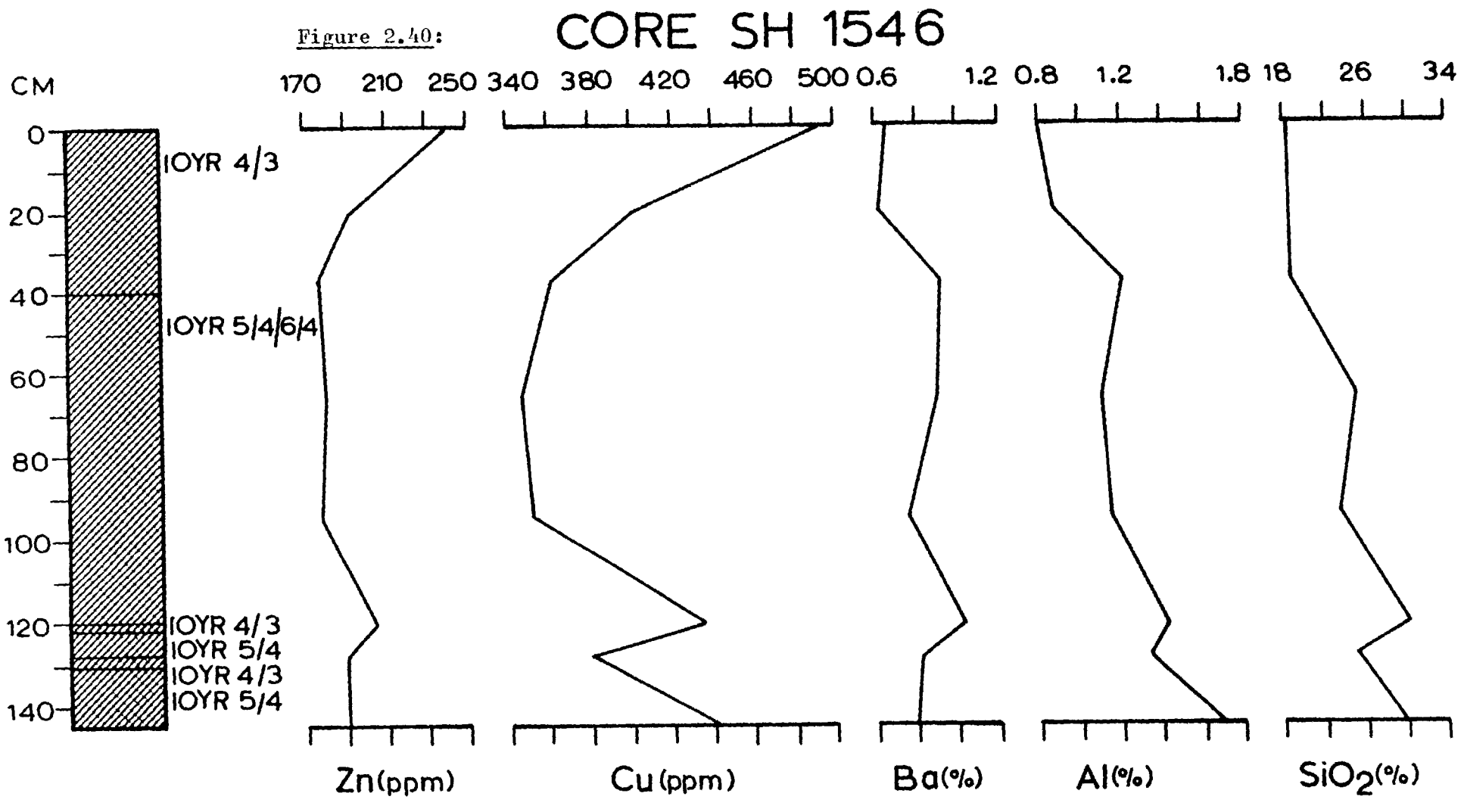
CORE SH 1546
CM
0
20
40
60
80
100
120
140
10YR 4/3
10YR 5/4/6/4
10YR 4/3
10YR 5/4
10YR 4/3
10YR 5/4
170 210 250
340 380 420 460 500
0.6 1.2
0.8 1.2 1.8
18 26 34
Zn(ppm)
Cu(ppm)
Ba(%)
Al(%)
SiO2(%)

Figure 2.41:

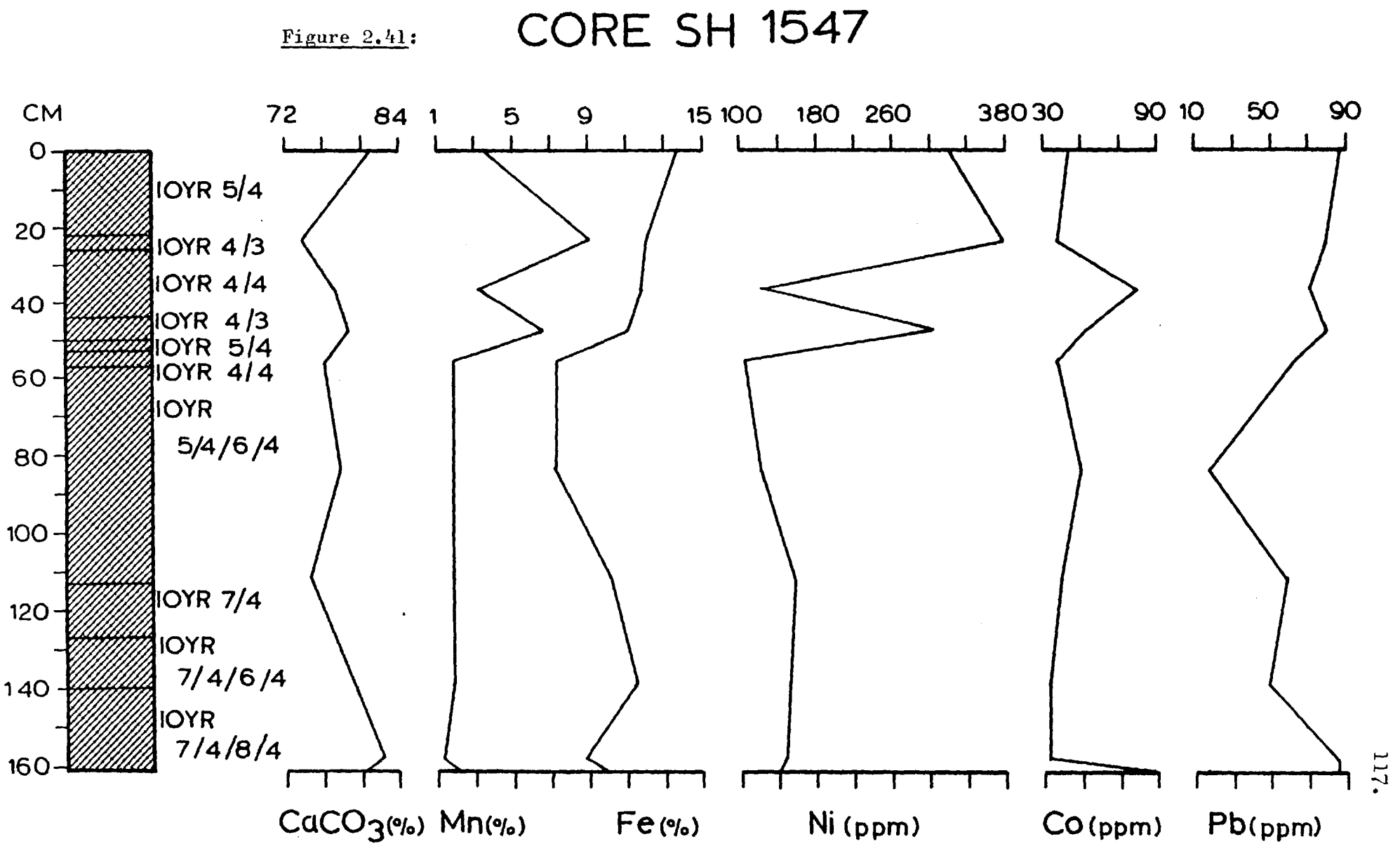
CORE SH 1547
CM
0
20
40
60
80
100
120
140
160
10YR 5/4
10YR 4/3
10YR 4/4
10YR 4/3
10YR 5/4
10YR 4/4
10YR 5/4/6/4
10YR 7/4
10YR 7/4/6/4
10YR 7/4/8/4
72
84
CaCO3(%)
1
5
9
15
Mn(%)
Fe(%)
100
180
260
380
Ni (ppm)
30
90
Co (ppm)
10
50
90
Pb(ppm)

Figure 2.42:

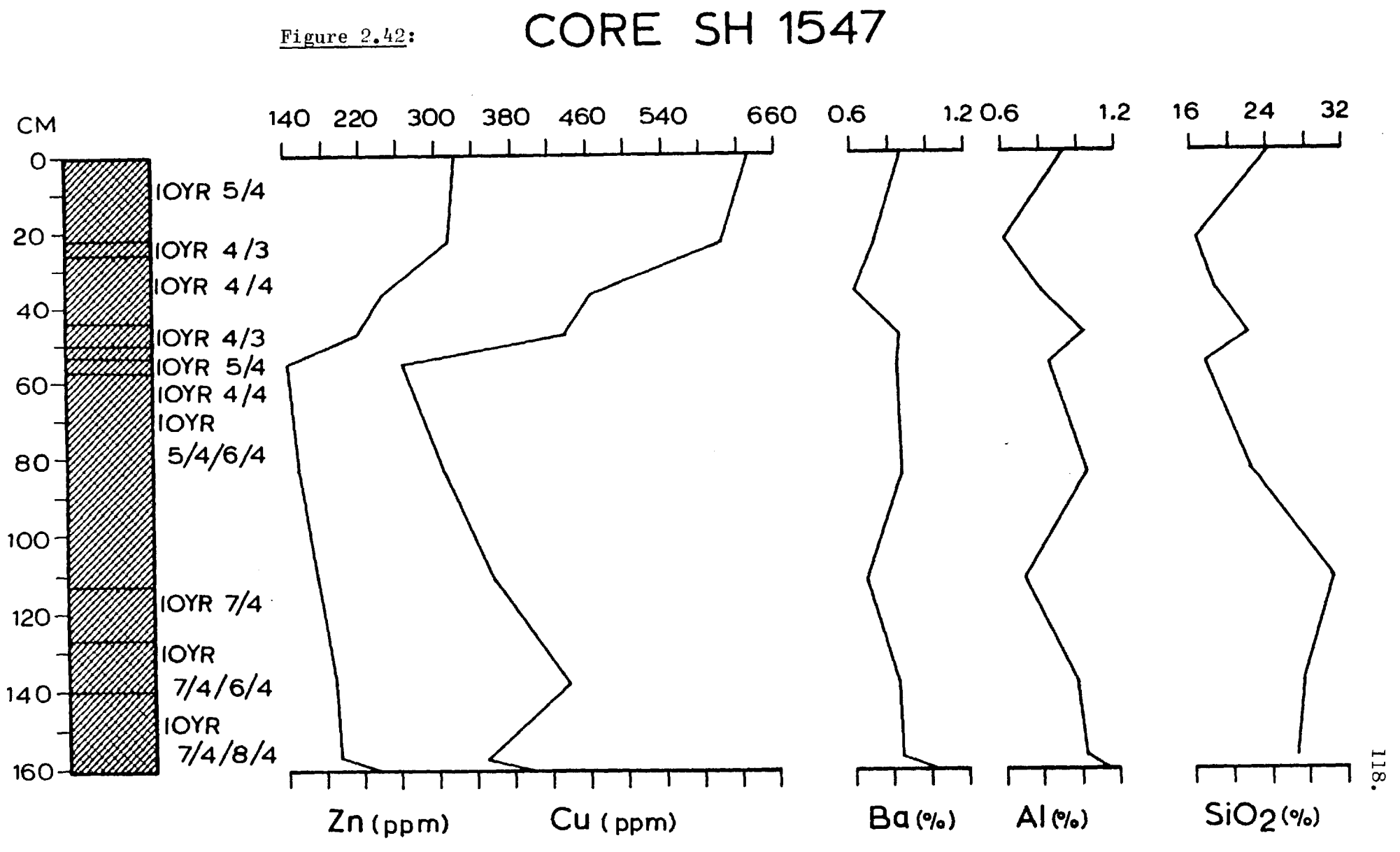
CORE SH 1547
CM
0
20
40
60
80
100
120
140
160
10YR 5/4
10YR 4/3
10YR 4/4
10YR 4/3
10YR 5/4
10YR 4/4
10YR 5/4/6/4
10YR 7/4
10YR 7/4/6/4
10YR 7/4/8/4
140 220 300 380 460 540 660
Zn (ppm)
Cu (ppm)
0.6 1.2
Ba (%)
0.6 1.2
Al (%)
16 24 32
SiO2 (%)

Figure 2.43:

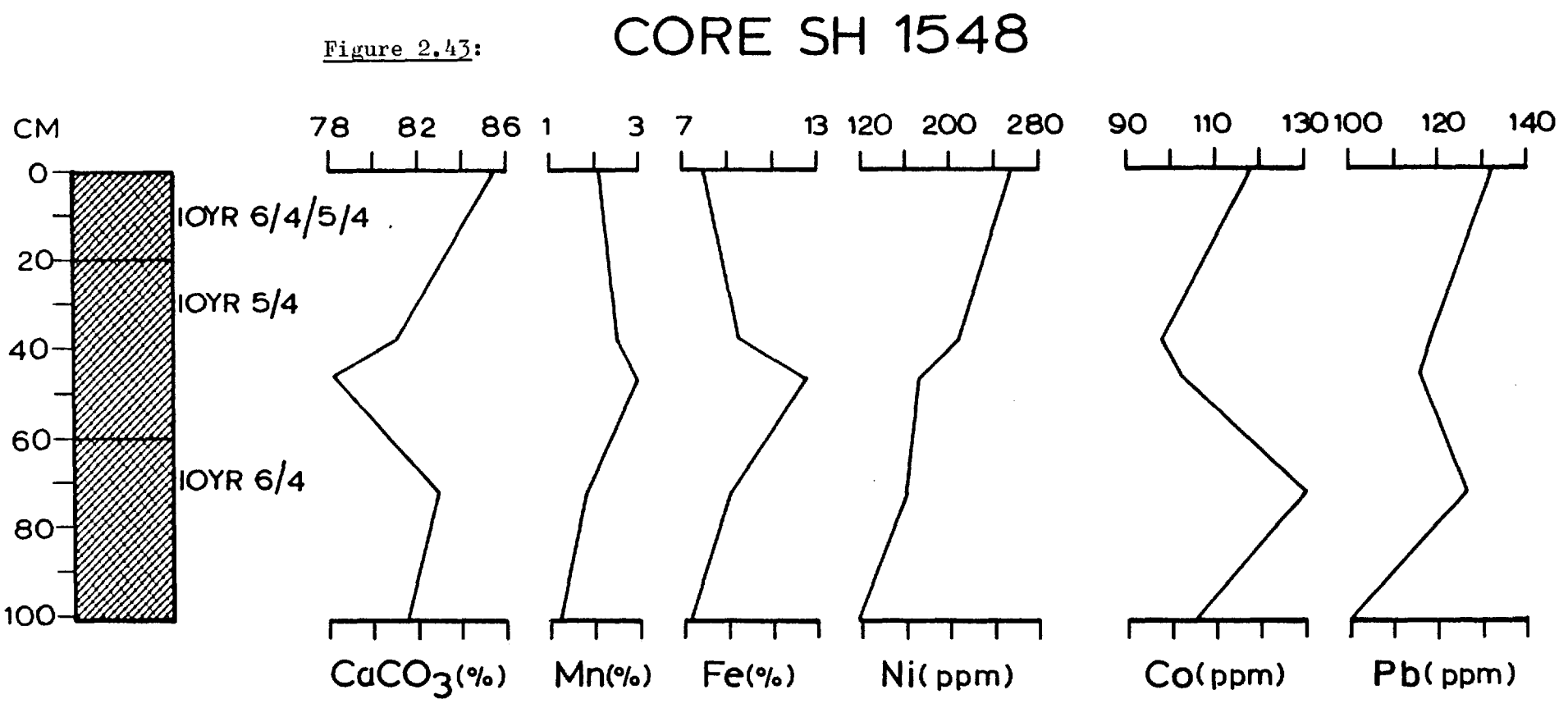
CORE SH 1548
CM
0
20
40
60
80
100
10YR 6/4/5/4
10YR 5/4
10YR 6/4
78 82 86
1 3
7 13
120 200 280
90 110 130
100 120 140
CaCO3(%)
Mn(%)
Fe(%)
Ni(ppm)
Co(ppm)
Pb(ppm)

Figure 2.44:

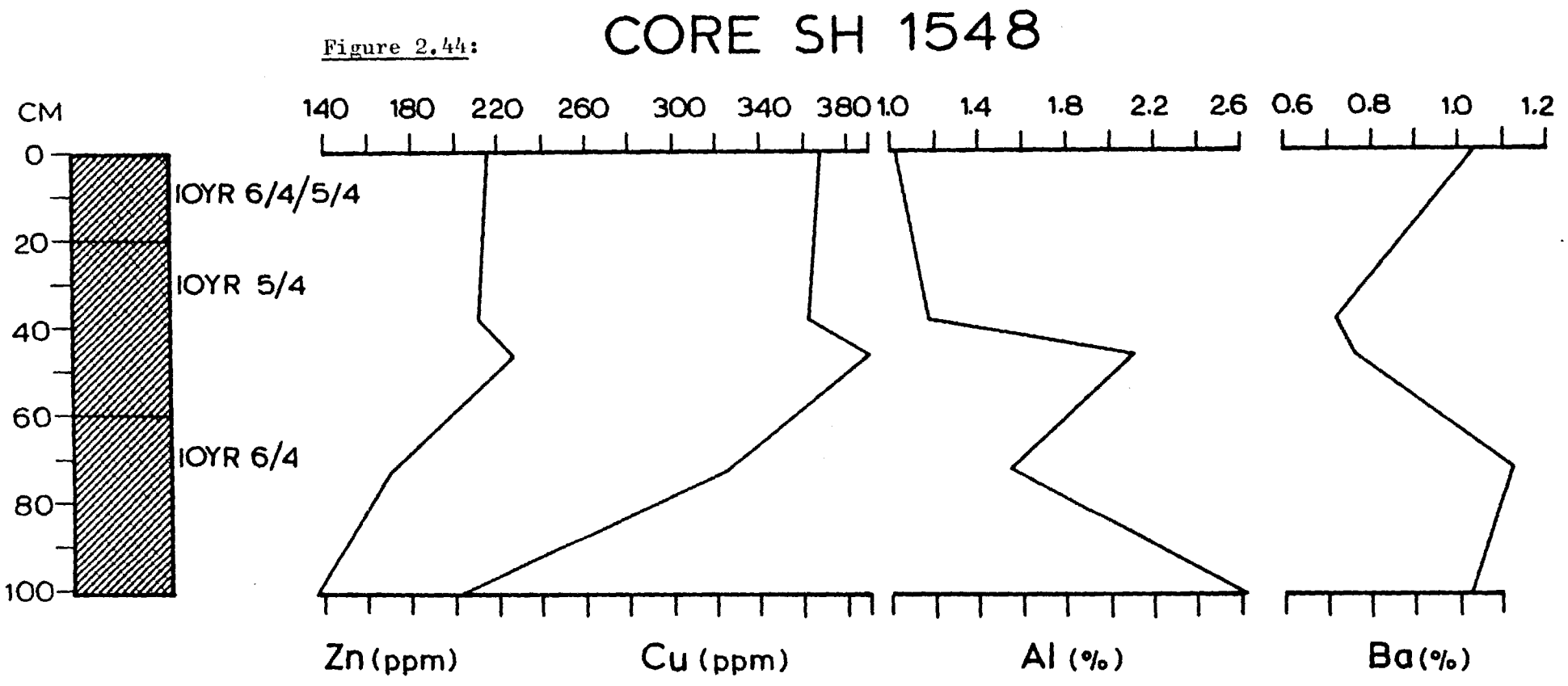
CORE SH 1548
CM
0
20
40
60
80
100
10YR 6/4/5/4
10YR 5/4
10YR 6/4
140 180 220 260 300 340 380
1.0 1.4 1.8 2.2 2.6
0.6 0.8 1.0 1.2
Zn (ppm)
Cu (ppm)
Al (%)
Ba (%)

Figure 2.45:

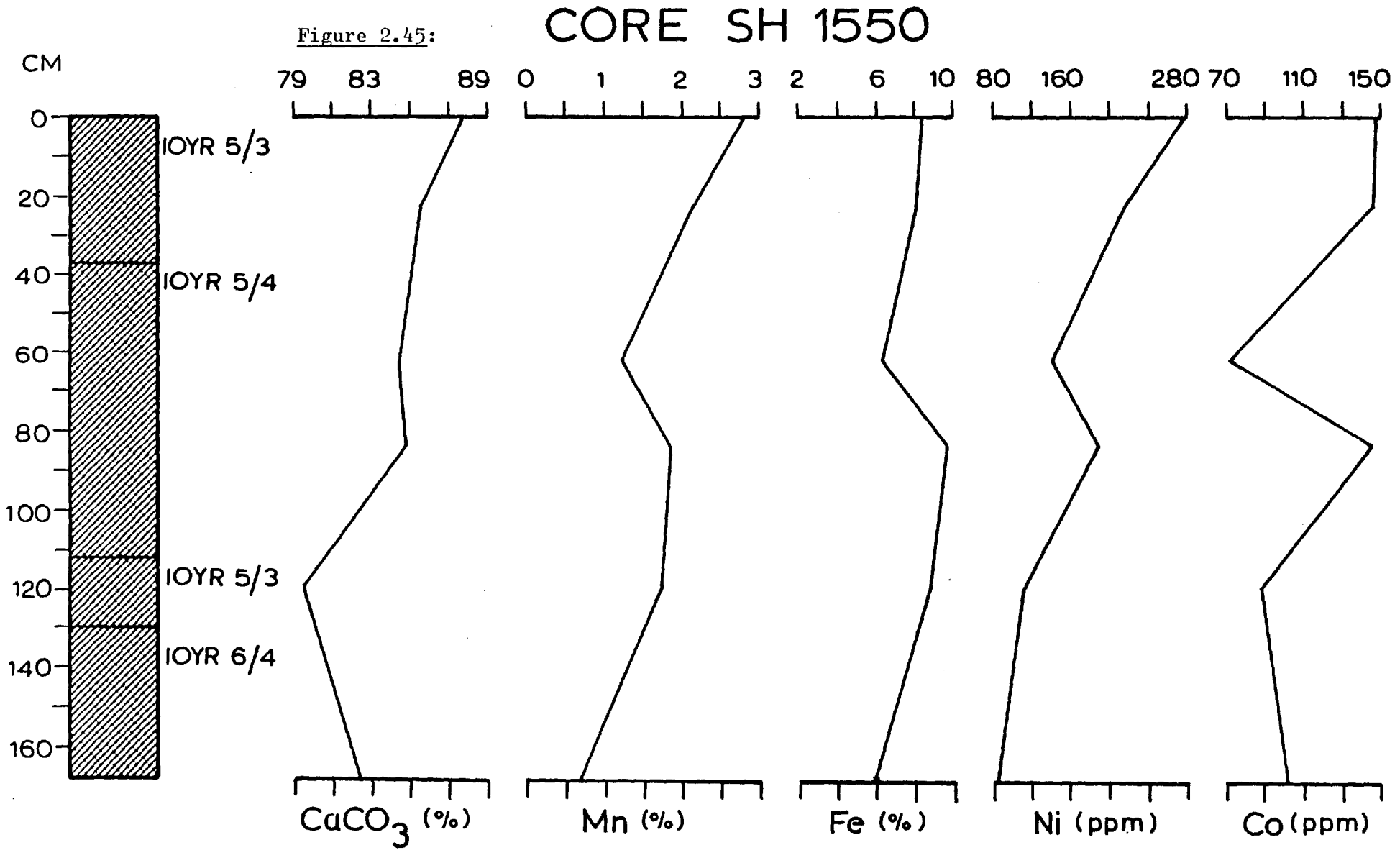
CORE SH 1550
CM
0
20
40
60
80
100
120
140
160
10YR 5/3
10YR 5/4
10YR 5/3
10YR 6/4
79 83 89
CaCO3 (%)
0 1 2 3
Mn (%)
2 6 10
Fe (%)
80 160 280
Ni (ppm)
70 110 150
Co (ppm)

Figure 2.46:

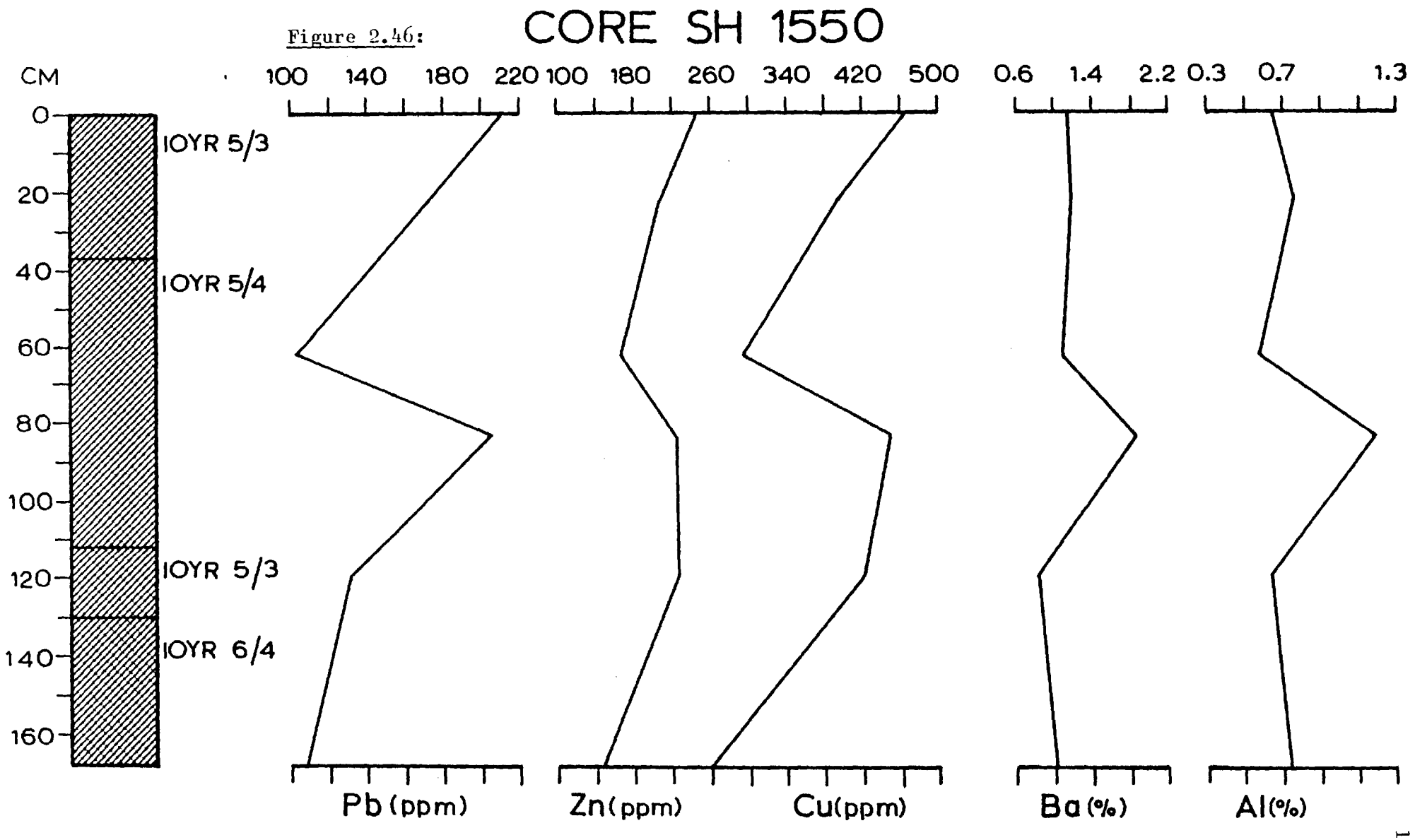
CORE SH 1550
CM
0
20
40
60
80
100
120
140
160
10YR 5/3
10YR 5/4
10YR 5/3
10YR 6/4
100 140 180 220
Pb (ppm)
100 180 260 340 420 500
Zn (ppm)
Cu (ppm)
0.6 1.4 2.2
Ba (%)
0.3 0.7 1.3
Al (%)

Figure 2.47:

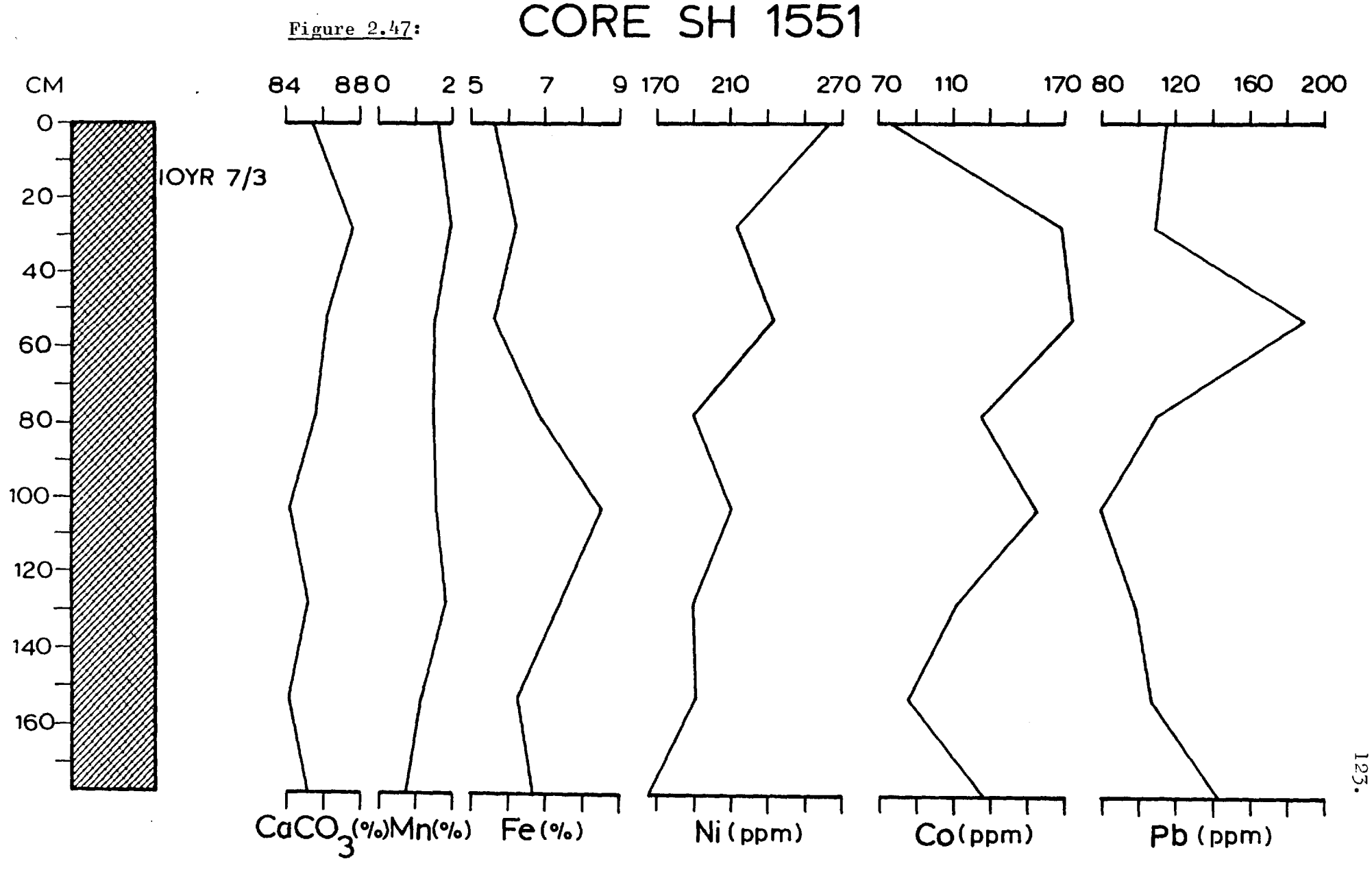
CORE SH 1551
CM
0
20
40
60
80
100
120
140
160
10YR 7/3
84
88
0
2
5
7
9
170
210
270
70
110
170
80
120
160
200
CaCO3(%)
Mn(%)
Fe(%)
Ni(ppm)
Co(ppm)
Pb(ppm)

Figure 2.48:

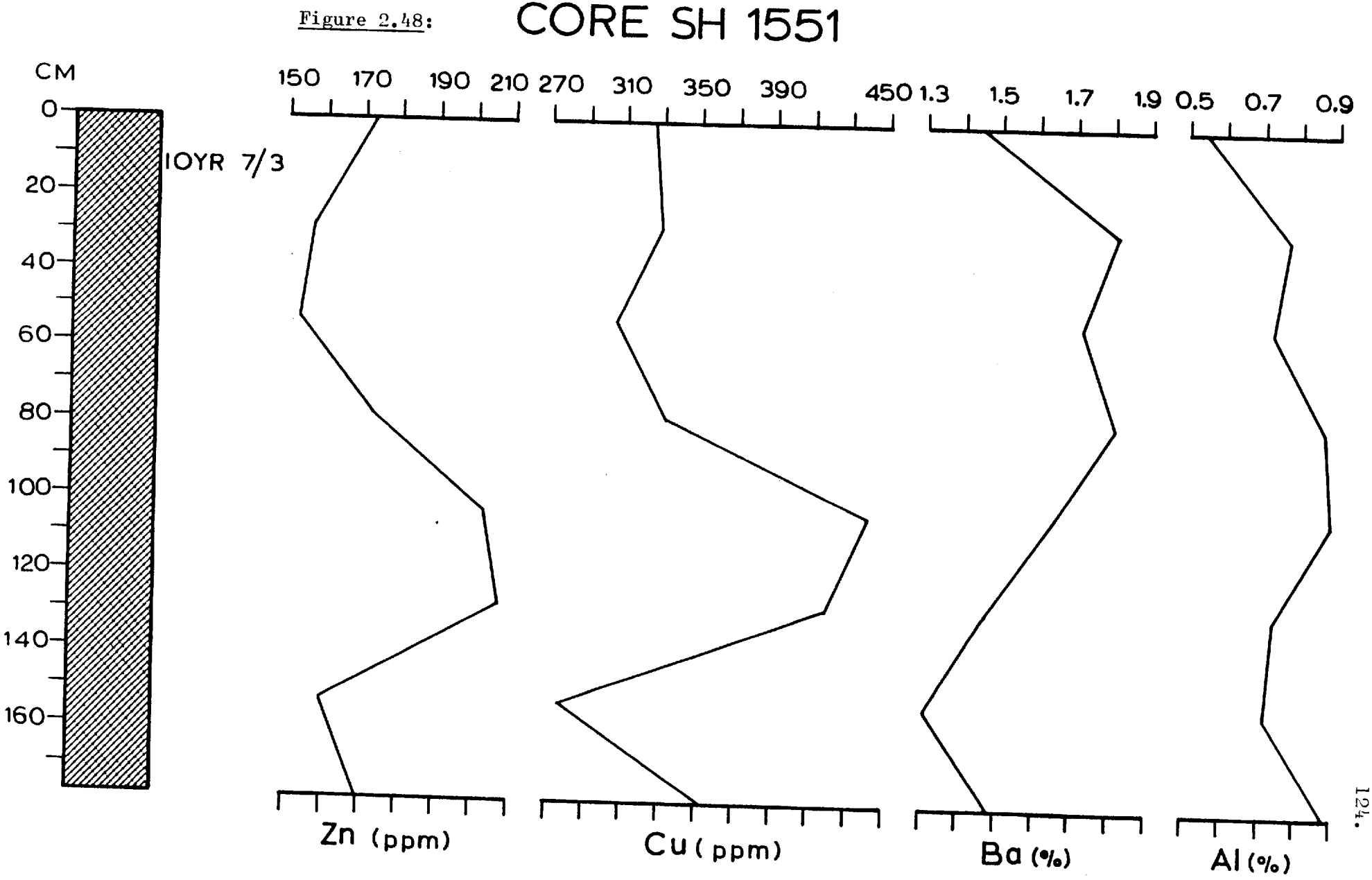
CORE SH 1551
CM
0
20
40
60
80
100
120
140
160
10YR 7/3
150 170 190 210
270 310 350 390 450
1.3 1.5 1.7 1.9
0.5 0.7 0.9
Zn (ppm)
Cu (ppm)
Ba (%)
Al (%)

Figure 2.49:

CORE SH 1552

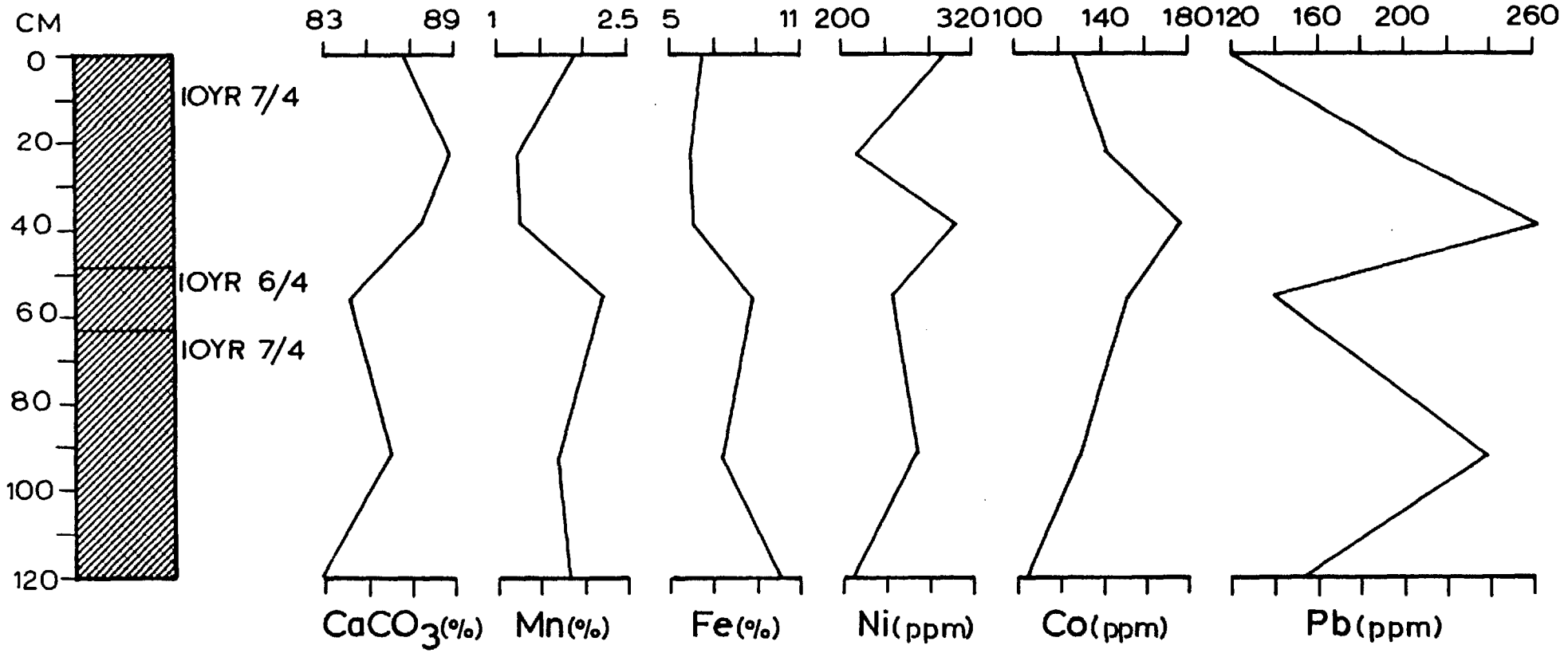

Figure 2.50:

CORE SH 1552

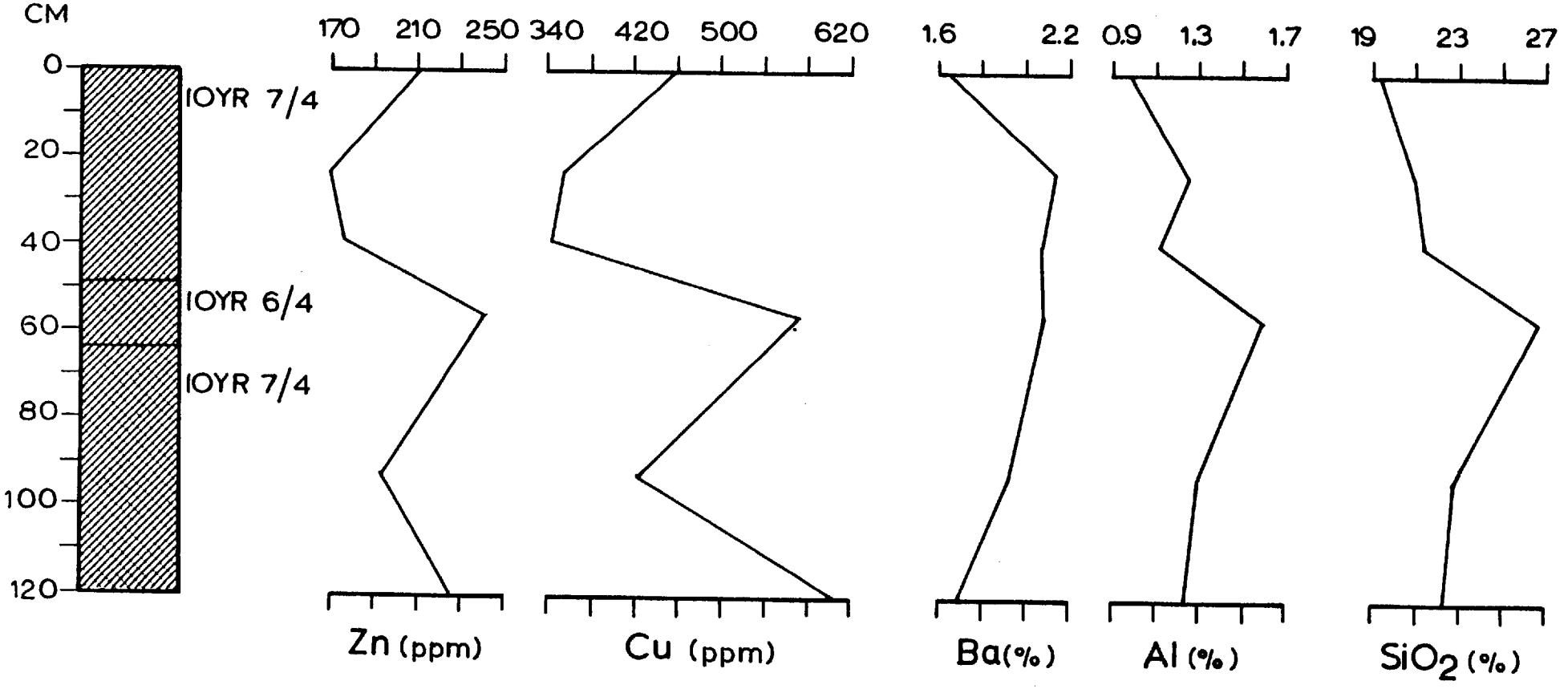

2.3 COMPONENTS OF MARINE SEDIMENTS

A knowledge of the components of deep-sea sediments facilitates the interpretation of partition geochemistry. Several attempts have been made to classify the constituents of marine sediments. Goldberg (1954) introduced the terms lithogenous, hydrogenous, biogenous, cosmogenous and atmogenous in regard to their sphere of origin. Lithogenous material was defined as that arising from land erosion, submarine volcanoes, or from underwater weathering where the products of weathering remain chemically unaltered during their residence in sea water. The hydrogenous components are formed in the hydrosphere by simple precipitation or other inorganic reactions, biological process being excluded. The biogenous components are formed from the biological remains of various organisms, consisting of their hard inorganic parts, such as siliceous or calcareous shells and their soft tissues. The cosmogenous part is produced in outer space and reaches the oceans in the form of rain of extra-terrestrial particles. The relative proportion of these categories of components and the amount of the different minerals present in each one determine the elemental variations in the sediments. Therefore, the separation and relative proportion of each component must be determined during the performance of partition geochemical analyses.

Although Goldberg's classification scheme provides the base on which partition geochemical data can be interpreted, Chester and Hughes (1967) divided the hydrogenous material further into two sub-groups: i) the primary hydrogenous material which was formed directly by precipitation from sea water, and ii) the secondary hydrogenous material which was produced by submarine alteration of pre-existing minerals.

Elderfield (1976) argued against the classification system given by Chester and Hughes (1970) for hydrogenous material, since it is difficult to apply to all marine sediments. For instance, some primary marine materials (e.g. phosphates) are not always formed in the absence of pre-existing minerals. Despite this argument Elderfield (1976) accepted the above classification system as a useful one and he proposed an analogous but more detailed scheme. He classified the hydrogenous material into: i) halmyrolysates which were produced from the reaction between sea water and sediment components (usually silicates), and ii) precipitates which were formed from the direct removal of elements from sea water without any active participation of pre-existing sediments. All the chemical and physico-chemical processes resulting from reactions between sediment components and sea water after the in situ weathering were called halmyrolysis. Such chemical and physico-chemical processes are very common in areas where the fresh water of rivers is mixed with the sea water. These processes cause alteration of the minerals suspended in the rivers before they reach their final site of deposition. Similar processes also occur subsequent to the weathering and transportation of marine volcanic assemblages or any other particulates in the marine environment.

Although the sequence: weathering $\longrightarrow$ halmyrolysis $\longrightarrow$ diagenesis is well defined in Elderfield's classification scheme, the boundaries between weathering and halmyrolysis and halmyrolysis and diagenesis are not very clear. Since the diagenesis of the upper layers of the sediment column is partly controlled by the overlying sea water, an overlap between the last stage of halmyrolysis and the very early stage of diagenesis could occur.

2.4 PREVIOUS GEOCHEMICAL PARTITION STUDIES

Selective chemical separation is based on the principle that different chemicals or different concentrations of chemicals will dissolve certain constituents of marine sediments.

Hirst and Nicholls (1958) described a chemical method, involving the use of 25% acetic acid, for the separation of the detrital and non-detrital fraction of limestones. This acid dissolved the carbonates but did not destroy the clay mineral lattice. The undissolved residue was filtered and the metals were then precipitated from the filtrate by adding a combination of organic reagents. The results of this procedure were compared with those after using HCl of the same strength instead of acetic acid. It was found that the fraction soluble in HCl was greater than the acetic acid-soluble fraction. The difference was attributed to the dissolution of some clay minerals.

The experimental work carried out by Goldberg and Arrhenius (1958), using EDTA as an extractant, showed that this reagent attacks various minerals at different rates. The minerals investigated by these workers, arranged in order of increasing rate of dissolution, are as follows: biotite, titanite, goethite, magnetite, rutile, hematite, lepidocrocite, nontronite, and augite. Calcite dissolved more rapidly than the last member of this series, but no quantitative measurements were made for this mineral. Ferromanganese oxide minerals and microcrystalline apatite were also dissolved very rapidly and this was attributed to the small particle size of these minerals. To study the distribution of Mg, Sr, B, Cu and V in Pacific pelagic clays Goldberg and Arrhenius (1958) attacked various size fractions of the

sediments with EDTA. The most prevalent minerals in the fraction $> 32\,\mu$ were apatite, phillipsite and MnO_2, in the fraction 10-32 μ phillipsite, apatite and MnO_2, in the fraction 3-10 μ amorphous Fe-oxides, silicates, clay minerals, phillipsite, apatite and MnO_2, and in the fraction 1-3 μ amorphous Fe-oxides, silicates, clay minerals, phillipsite and MnO_2. It was observed by the above workers that the amount of insoluble Mn, B, Cu and V increased with increasing content of clay minerals, indicating that most of the insoluble portion of these elements was located in the clay minerals. In contrast, the soluble fraction of the same elements was thought to be sorbed or held in the lattice structure of apatite, phillipsite, and ferromanganese oxide minerals.

Chester and Hughes (1966) applied the technique described by Goldberg and Arrhenius (1958) to study the partition of Mn, Ni and Fe among the components of a North Pacific pelagic clay core. They found that about 88% of the total Mn was soluble in EDTA. The large number of small dark particles present in these sediments were soluble in EDTA and therefore were identified as manganese micro-nodules. It was suggested by these authors that most of the Mn soluble in EDTA must occur in the form of these micro-nodules. The lack of Mn in the EDTA-soluble portion of the $< 2\,\mu$ fraction of the sediments indicated that no Mn was adsorbed on the surface of clay minerals. However, a small portion of Mn was probably held in the lattice structure of clay minerals. About 56% of the total Ni was soluble in EDTA and associated with the Mn in the manganese micro-nodules. This would suggest that Ni was removed from the sea water by the same reactions which removed Mn, e.g. direct scavenging of Ni from sea water by hydrous Mn oxide (Goldberg, 1954), co-precipitation with Fe and Mn (Laevastu and

Mellis, 1955), and sorption of dissolved Ni onto colloidal Mn dioxide particles (Landergren, 1964). Since no Ni was found in the EDTA-soluble portion of the $<2\mu$ fraction of the sediments, the Ni not associated with manganese micro-nodules ($\sim$ 44%) was attributed to the lattice structures of the clay minerals and not to adsorption onto their mineral surfaces, or to ion-exchange reactions. A very small amount of Fe ($\sim$ 5%) was found to be soluble in EDTA, indicating the different origin and the different processes of incorporation of this element into the sediments (Chester and Hughes, 1966).

More recently, Chester and Hughes (1967) carried out chemical investigations to establish a chemical method for the separation of ferromanganese minerals, carbonate minerals and adsorbed trace elements from deep-sea sediments. Their method involves leaching of the sediments firstly with 25% acetic acid, and secondly with a combined acid-reducing agent solution (a mixture of acetic acid and hydroxyl-amine HCl solution). The results of these two selective chemical attacks showed that the elements associated with carbonate minerals (excluding dolomites) and those adsorbed onto mineral surfaces were liberated in the acetic acid solution, whereas most of the total Mn ($\sim$ 78%) and a small amount of Fe (only 4%) were soluble in the acid-reducing agent solution. Because Ni and V had been reported previously in the literature to have different marine geochemical behaviour (Goldberg and Arrhenius, 1958; Chester and Hughes, 1966) they were chosen by Chester and Hughes (1967) for the examination of the effect of the acid-reducing agent solution on the trace elements. Their results showed that 52% of the total Ni and 15% of the total V had been taken in the solution, after the leaching of the sediments.

These results were in good agreement with those given in previous studies. For instance, Goldberg and Arrhenius (1958) demonstrated that V was mainly of lithogenous origin in a series of Pacific pelagic sediments, whereas Ni was found by Chester and Hughes (1966) to be of hydrogenous origin in a North Pacific deep-sea clay core.

Cronan (1976a) modified Chester and Hughes' (1967) method of selective chemical partition by using 50% HCl as an additional leach after the hydroxylamine HCl attack which dissolved everything remaining in the sediments (including Fe-oxide minerals), except the more resistant silicates and aluminosilicates.

To summarise: (1) Carbonate minerals and sorbed ions on mineral surfaces in deep-sea sediments are soluble in 25% acetic acid solution. (2) Ferromanganese oxide minerals, together with the above phases, are digested in the acetic acid-hydroxylamine HCl solution (acid-reducing agent solution). (3) 50% HCl solution can dissolve Fe-oxide minerals and every other phase except the more resistant silicates and aluminosilicates. There is not much difference between the results taken from the total chemical analysis of deep-sea sediment samples from areas with low detrital input and those taken after the leaching of the same samples with 50% HCl solution.

Since the above three selective chemical attacks have been established by the authors mentioned above, they have been used successfully by several investigators in the study of the distribution of major and trace elements between phases in recent and ancient deep-sea sediments.

Chester and Hughes (1969) applied their chemical technique (Chester and Hughes, 1967) to study the partition geochemistry of a North Pacific pelagic clay core. The fraction of the sediment which was leached by the acid-reducing agent solution was termed the total hydrogenous fraction, whilst the residue left after the acid-reducing agent attack was termed the lithogenous fraction. Carbonate minerals, biogenous material, montmorillonite and zeolites were virtually absent from these sediments. Because the 25% acetic acid solution dissolved only 5% of the Fe and 6% of the Mn associated with ferro-manganese nodules, the part of the sediment soluble in this solution was termed the non-nodular-hydrogenous fraction. The difference between the total hydrogenous fraction and the non-nodular hydrogenous fraction gave the nodular hydrogenous fraction of the sediment. The chemical composition of the litho genous fraction was estimated by the subtraction of the metal concentrations found in the total hydrogenous fraction from those found in the total sediment.

The lithogenous part of the sediment was considered to be land-derived material consisting of clay minerals stripped of their adsorbed trace elements, and quartz. The partition geochemistry of the North Pacific pelagic clay core showed that only 3 or 4% of the total Fe was of hydrogenous origin. A change also in the distribution of the hydrogenous Fe between the nodular and the non-nodular fraction was found down the length of the core. In the upper part of the core 50% of the hydrogenous Fe was associated with micro-nodules whereas in the lower part of the core between 70% and 90% of the hydrogenous Fe was associated with nodules. Most of the total Mn (between 80% and 90%) was of hydrogenous origin. Between 85% and 95% of the hydrogenous Mn was associated with the nodular hydrogenous

fraction. A change in the distribution of the total and the hydrogenous Mn was observed down the length of the core. The total Mn in the upper part of the core was less than the total Mn in the lower part. The same change was found also for the hydrogenous Mn in the two sections of the core.

The following differences were observed between the vertical distribution of the hydrogenous Fe and Mn: 1) The total hydrogenous Fe was constant down the core, whereas there was a decrease in the hydrogenous Mn in the upper sediments relative to that in the lower sediments. 2) A change in the partition of the nodular hydrogenous Fe occurred in the lower core section; by contrast, the hydrogenous Mn associated with micronodules was constant throughout the core.

Chester and Messiha Hanna (1970) working on Atlantic sediments demonstrated that the concentrations of Ni, Co, Ga, Cr, V, Mn and Sr in the lithogenous fraction of the Atlantic deep-sea sediments were similar to those of the total samples of near-shore sediments, and they classified various elements according to their lithogenous character. This character decreased in the order: $Fe > V > Cr > Ba > Ni > Cu > Co=Ga > Mn > Sr$. On the basis of their average lithogenous contribution to the total sediment these elements were divided into four groups:

I. More than 80% of the total elements was contributed by the lithogenous fraction.

II. Between 60 and 80% of the total element content was in the form of lithogenous material.

III. Between 20 and 60% of the total elements were held in the lithogenous fraction.

IV. Less than 20% of the total element content was contributed by lithogenous material.

Of the investigated elements, Fe was in the first group, while V, Cr and Ba were included in the second group. The elements Ni, Cu, Co and Ga, which fell in the third group, showed geographical variations in their lithogenous contribution with a decrease in distance from the continents. The only element included in the fourth group was Sr, because it was chiefly associated with calcium carbonate of biological origin.

Cronan (1976a) studied the partition of Fe, Mn, Ni, Co, Cu, Zn, Pb, Ca, Mg, Na, K, Al and Ba between four chemically separated fractions in basal metalliferous sediments from the eastern Pacific. He found that most of the total Fe was concentrated in the HCl-soluble fraction, whereas most of the Mn was associated with the fraction soluble in the hydroxylamine HCl solution. The different geochemical behaviour of Fe and Mn in the basal metalliferous sediments led to the conclusion that these two elements had been derived from two independent sources. Fe was considered to be of hydrothermal origin, whilst Mn could have been incorporated into the sediments from sea water during the authigenic formation of ferromanganese micro-nocules and coatings consisted of ferromanganese minerals such as todorokite, birnessite, psilomelane, and others. This could be the answer to Boström's et al (1972) argument against the hydrothermal leaching of basalt as a source of Mn, showing that more basalt is required to supply the Mn

present in the sediments than is needed to supply the Fe. The "excess" Mn might be removed from sea water, probably by the catalytic action of Fe-oxides. The geochemical behaviour of Fe in its partition between phases was explained by Cronan (1976a) in terms of the mineralogy of the sediments. Dymond and others (1973) demonstrated that authigenic Fe-rich montmorillonite, goethite, and Mn-hydroxides are the dominant minerals present in metalliferous sediments from the eastern Pacific. It is known that goethite is soluble in the HCl solution but not in the hydroxylamine HCl reagent. In the same way Fe of the Fe-rich montmorillonite can be extracted by the HCl. In the eastern Pacific basal metalliferous sediments almost all Ni, Co, and to a lesser extent Pb, were removed by the acid-reducing reagent, indicating their association with the ferromanganese oxide minerals of the sediments. By contrast, most of the total Cu and Zn were associated with the Fe-minerals in the HCl-soluble fraction.

The geochemical partition studies carried out by Horowitz and Cronan (1976) on basal sediments from the North Atlantic Ocean showed similar results to those given by Chester and Messiha-Hanna (1970) for the northern Mid-Atlantic Ridge surface sediments. They were also similar to those reported by Horowitz (1974) for surface sediments from Reykjanes Ridge and by Cronan (1976a) for eastern Pacific basal metalliferous sediments. About 57% of the total Mn was found in the acid-reducible phase, whilst about 91% of the total Fe was in the HCl-soluble fraction and the residue. It was found that the percentage of the sample being dissolved in the acid-reducing agent solution was smaller for the Atlantic basal sediments than for the East Pacific Rise samples. Since land-derived lithogenous

material is soluble in HCl but not in the hydroxylamine HCl solution, this difference was explained as the result of greater detrital input in the North Atlantic than in the Pacific. Horowitz and Cronan (1976) noted some relatively high concentrations of Mn in the acetic acid-soluble fraction for certain basal and non-basal sediment samples. The relatively low content of carbonates in these sediments excluded the possibility of the association of Mn with carbonates. It was more likely to be adsorbed onto the surface of clay minerals which were the major components of the sediments.

Overall comparisons of the geochemical partitioning data of basal metalliferous sediments, non-basal sediments, surface metalliferous sediments and normal pelagic sediments have indicated that a similarity exists in the partitioning of the elements between the various constituents of the sediments (Chester and Highes, 1969; Cronan, 1976a; Horowitz and Cronan, 1976). They generally do not contain markedly different phases, but the same phases in different proportions.

2.5 GEOCHEMICAL PARTITIONING DATA

In the investigation of the distribution of Fe, Mn, Ni, Co, Pb, Zn, Cu and Al among the components of the fracture zone sediments from the East Pacific Rise at $9^{o}S$, partition analysis has been carried out on 24 surface samples from all the stations. In addition, 70 analyses were performed on buried samples from 14 cores covering the whole range of water depth within the study area. Tables 2.1, 2.2 and 2.3 show the average partitioning of elements in each core, in all the surface and in all the buried sediments, respectively. Details concerning the selective chemical attacks performed for the partition analysis are included in Appendix C.

2.5.1 Iron

Iron in the surface sediments is more concentrated, on average, in the acid-reducible fraction ($\sim$ 43%) than in any of the other fractions, which suggests a substantial association with ferro-manganese oxide minerals in these sediments. However, a large proportion of Fe ($\sim$ 40%) is present in the HCl-soluble fraction, whilst in the acetic acid solution about 14% of the total Fe is dissolved. Very low concentrations of Fe ($\sim$ 3%) have been detected in the HCl-insoluble residue, and in many samples no Fe at all occurs in the residue. The low concentrations, or the complete absence of Fe from the insoluble residue, reflect the small amount or the absence of Fe from the detrital material.

The proportion of Fe which is liberated into the acetic acid solution decreased systematically with increasing depth from the

Table 2.1: Average partition of elements between different phases of fracture zone sediments from the East Pacific Rise at 9°S. (The data are averages of the analyses of buried sediment samples. They are expressed as percentages of the total amount present.)

Station Number		Mn	Fe	Ni	Co	Pb	Zn	Cu	Al
SH 1525									
	HAc	4.1	8.9	5.7	0	4.0	24	35	16
	A/R	91	44	34	1.9	0	30	36	21
(4 samples)	HCl	2.7	46	59	98	87	45	25	42
	Res	1.7	0.4	1.4	0	8.7	0.4	4.6	21
SH 1526									
	HAc	4.5	4.0	0	0	15	9.7	21	13
	A/R	93	33	24	22	0	27	37	19
(4 samples)	HCl	2.4	61	72	78	83	63	42	47
	Res	0	2.2	4.1	0	1.8	0	0	21
SH 1528									
	HAc	2.1	8.4	7.4	0	30	26	32	5.3
	A/R	88	32	57	0	11	15	33	5.9
(3 samples)	HCl	10	55	26	100	54	59	35	75
	Res	0	4.2	9.6	0	4.4	0	0	14
SH 1529									
	HAc	2.3	3.3	0	0	0	13	20	6.7
	A/R	81	33	70	0	91	29	35	11
(5 samples)	HCl	17	59	29	90	9.5	56	45	58
	Res	0	5.3	1.1	9.5	0	1.4	0	25
SH 1531									
	HAc	2.9	5.2	1.0	0	0	12	20	4.3
	A/R	76	28	44	3.5	28	20	27	5.5
(6 samples)	HCl	14	62	45	75	50	68	52	62
	Res	3.8	4.7	10	21	22	0	0.2	29

Table 2.1: Continued.

Station Number		Mn	Fe	Ni	Co	Pb	Zn	Cu	Al
SH 1532									
	HAc	1.9	4.6	0	0	4.3	9.4	22	6.3
	A/R	88	31	21	0	0	28	35	8.1
(5 samples)	HCl	5.7	60	68	99	86	61	41	50
	Res	4.1	3.8	7.1	0.6	9.8	0.7	1.3	36
SH 1534									
	HAc	2.3	4.2	0	0	0	15	22	9.4
	A/R	80	30	70	0	87	34	29	8.3
(5 samples)	HCl	18	64	30	100	13	49	48	55
	Res	0	2.3	0	0	0	1.9	0	27
SH 1537									
	HAc	4.3	5.6	0			31	27	17
	A/R	83	27	51			7.4	25	11
(4 samples)	HCl	13	65	41			62	47	57
	Res	0	2.4	8.4			0	1.4	15
SH 1538									
	HAc	4.2	5	0			15	27	15
	A/R	86	29	51			25	27	10
(3 samples)	HCl	9.7	63	36			60	44	60
	Res	0	2.4	13			0	1.1	16
SH 1539									
	HAc	4.3	4.6	0			18	25	15
	A/R	83	29	50			21	31	15
(6 samples)	HCl	11	62	45			60	44	54
	Res	1.1	3.5	5.1			0.5	0.3	16

Table 2.1: Continued.

Station Number		Mn	Fe	Ni	Co	Pb	Zn	Cu	Al
SH 1540									
	HAc	4.2	4.8	3.0			17	26	14
	A/R	83	30	41			19	29	14
(6 samples)	HCl	13	62	41			65	45	51
	Res	0	2.6	14			0	0.8	21
SH 1546									
	HAc	7.6	3.6	0	0	5.7	15	24	9.5
	A/R	75	33	44	0	55	22	33	10
(6 samples)	HCl	17	60	54	64	36	62	43	61
	Res	0.2	3.2	2.1	36	3.5	0.8	0	20
SH 1547									
	HAc	19	4.8	0.2	0		31	30	13
	A/R	69	42	49	4.8		19	31	13
(8 samples)	HCl	12	53	49	84		49	38	51
	Res	0	0.8	1.7	11		0.6	0	23
SH 1552									
	HAc	4.7	3.7	0	0	0	26	28	12
	A/R	76	41	63	0	76	17	36	15
(5 samples)	HCl	20	55	35	41	14	56	36	47
	Res	0	0.5	2.1	59	11	1.1	0	26

HAc: Acetic acid leach.
A/R: Acid-reducing agent leach only (i.e. A/R agent leach - HAc leach).
HCl: Hydrochloric acid leach only (i.e. HCl leach - A/R agent leach).
Res: HCl-insoluble residue (Bulk-HCl leach).

Table 2.2: Average partition of elements between different phases of surface sediments from the East Pacific Rise fracture zone at 9°S. (All data are expressed as percentages of the total amount present. Number of samples analysed = 24.)

	Mn	Fe	Ni	Co	Pb	Zn	Cu	Al
HAc	3.0	14	0.2	0	5.5	30	44	16
A/R	88	43	51	0.7	58	25	34	13
HCl	7.8	40	44	91	33	44	21	52
Res	0.9	2.9	4.7	8.0	3.2	0.5	0.8	19

Table 2.3: Average partition of elements between different phases of buried sediments from the East Pacific Rise fracture zone at 9°S. (All data are expressed as percentages of the total amount present. Number of samples analysed = 70.)

	Mn	Fe	Ni	Co	Pb	Zn	Cu	Al
HAc	4.9	5.0	1.9	0	6.6	19	25	11
A/R	82	33	48	3.0	39	22	32	12
HCl	12	59	45	83	48	58	42	55
Res	0.8	2.7	5.5	14	6.8	0.5	0.7	22

HAc: Acetic acid leach.
A/R: Acid-reducing agent leach only (i.e. A/R agent leach-HAc leach).
HCl: Hydrochloric acid leach only (i.e. HCl leach-A/R agent leach).
Res: HCl-insoluble residue (Bulk-HCl leach).

top down to the base of all the cores studied here (see Figures 2.51, 2.52). A similar relationship has also been found between the hydroxylamine HCl-soluble Fe and the depth of the sediments (see Figures 2.53, 2.54). In contrast, the percentage of Fe associated with the HCl-soluble fraction increases steadily with increasing depth in the cores (see Figures 2.55, 2.56). Although the vertical variations of Fe present in the various fractions are similar in the upper (0-40 cm) and again in the lower (40 cm - base) part of the cores, it has been observed that from 0 to about 40 cm depth the proportional changes of Fe are more sharp than between 40 cm and the base.

2.5.2 Manganese

Manganese in the surface sediments has been found, on average, almost exclusively ($\sim$ 88%) in the acid-reducible fraction, indicating the strong association of this element with the ferromanganese oxide minerals. Relatively minor amounts of Mn ($\sim$ 8%) have been found in the HCl-soluble fraction, while it appears to be sparingly soluble ($\sim$3%) in acetic acid. Only a very small amount of Mn ($\sim$1%) is associated with the HCl-insoluble residue.

The general partitioning of Mn in the subsurface sediments is similar to that in the surface sediments (on average most of the Mn being associated with the hydroxylamine HCl-soluble fraction), but there are some changes in the proportional distribution of this element among the various phases down the core.

In general, the proportion of Mn associated with the acetic acid-soluble fraction increases steadily from the surface of the

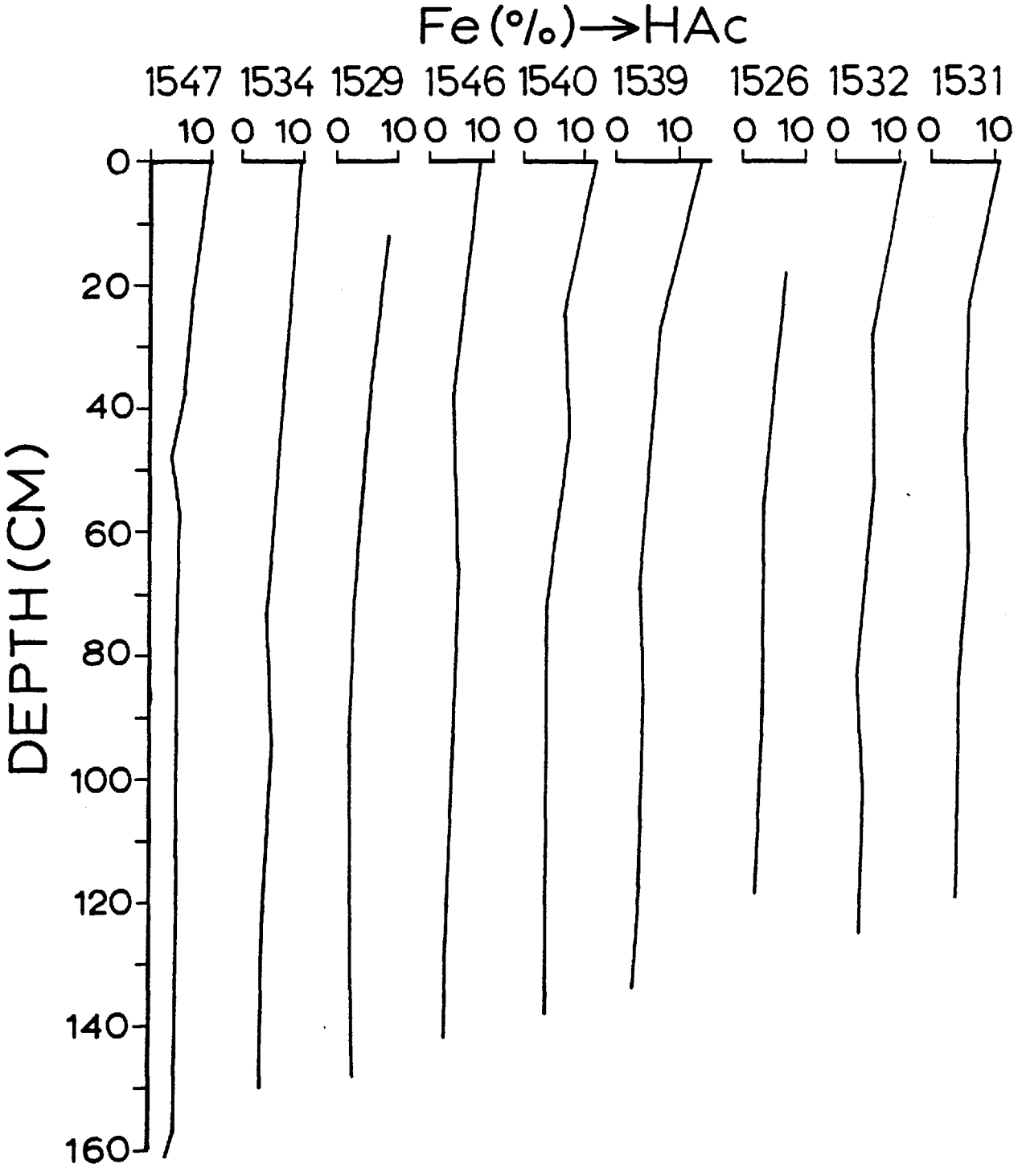

Figure 2.51: The distribution of the acetic acid-soluble Fe in fracture zone sediment cores, expressed as a percentage of the total Fe concentration.

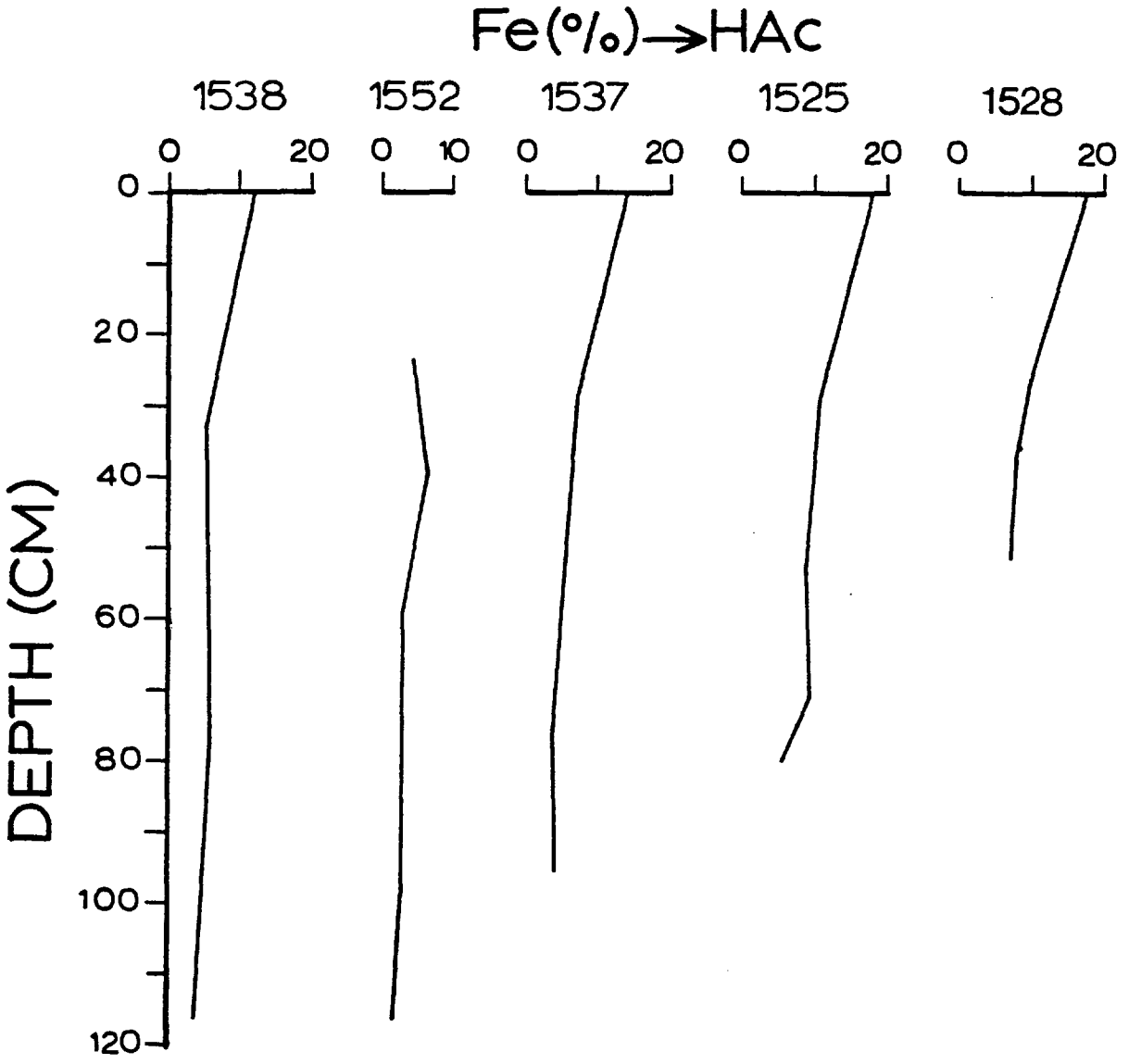

Figure 2.52: The distribution of the acetic acid-soluble Fe in fracture zone sediment cores expressed as a percentage of the total Fe concentration.

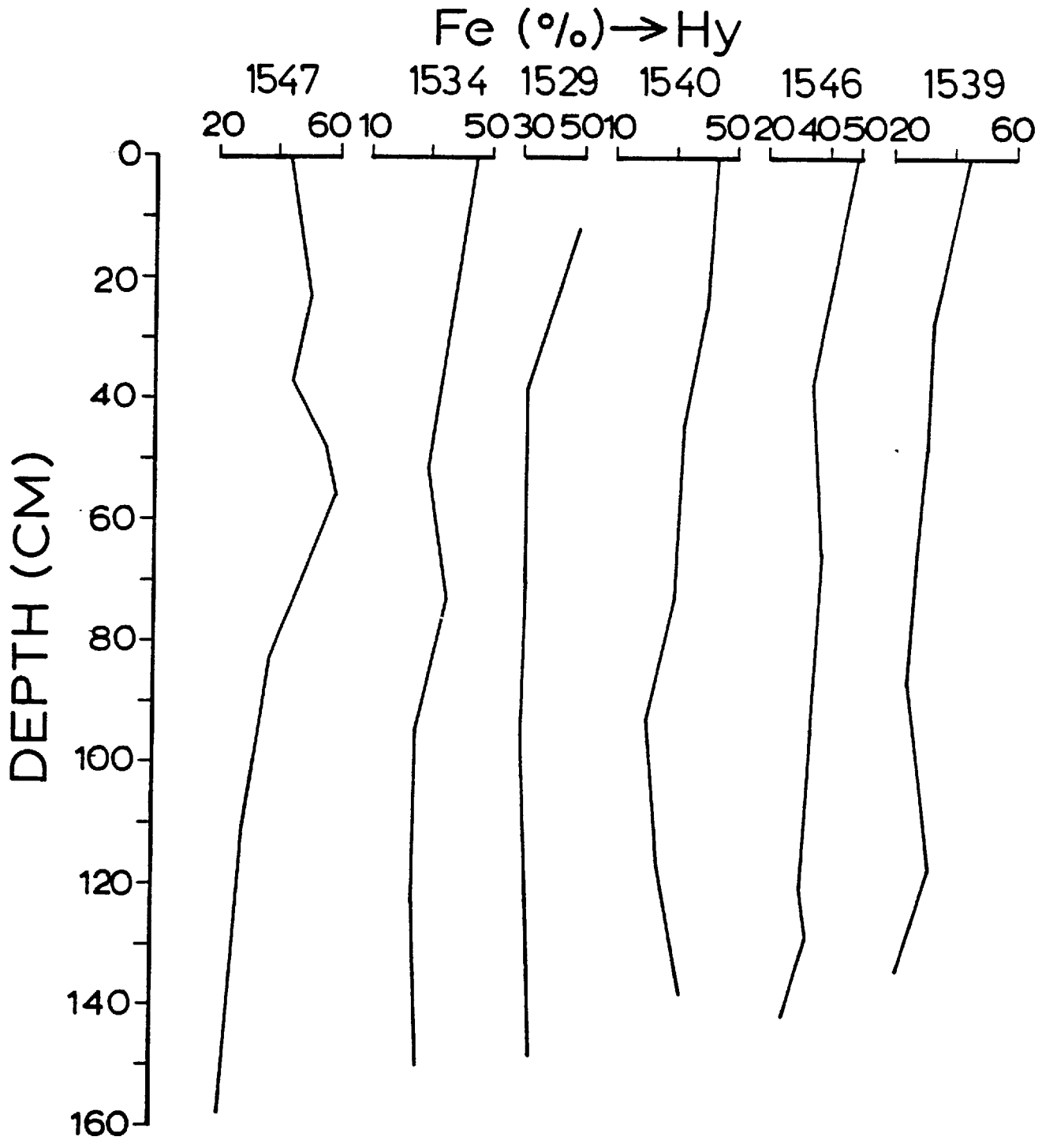

Figure 2.53: The distribution of the hydroxylamine HCl-soluble Fe in fracture zone sediment cores expressed as a percentage of the total Fe concentrations.

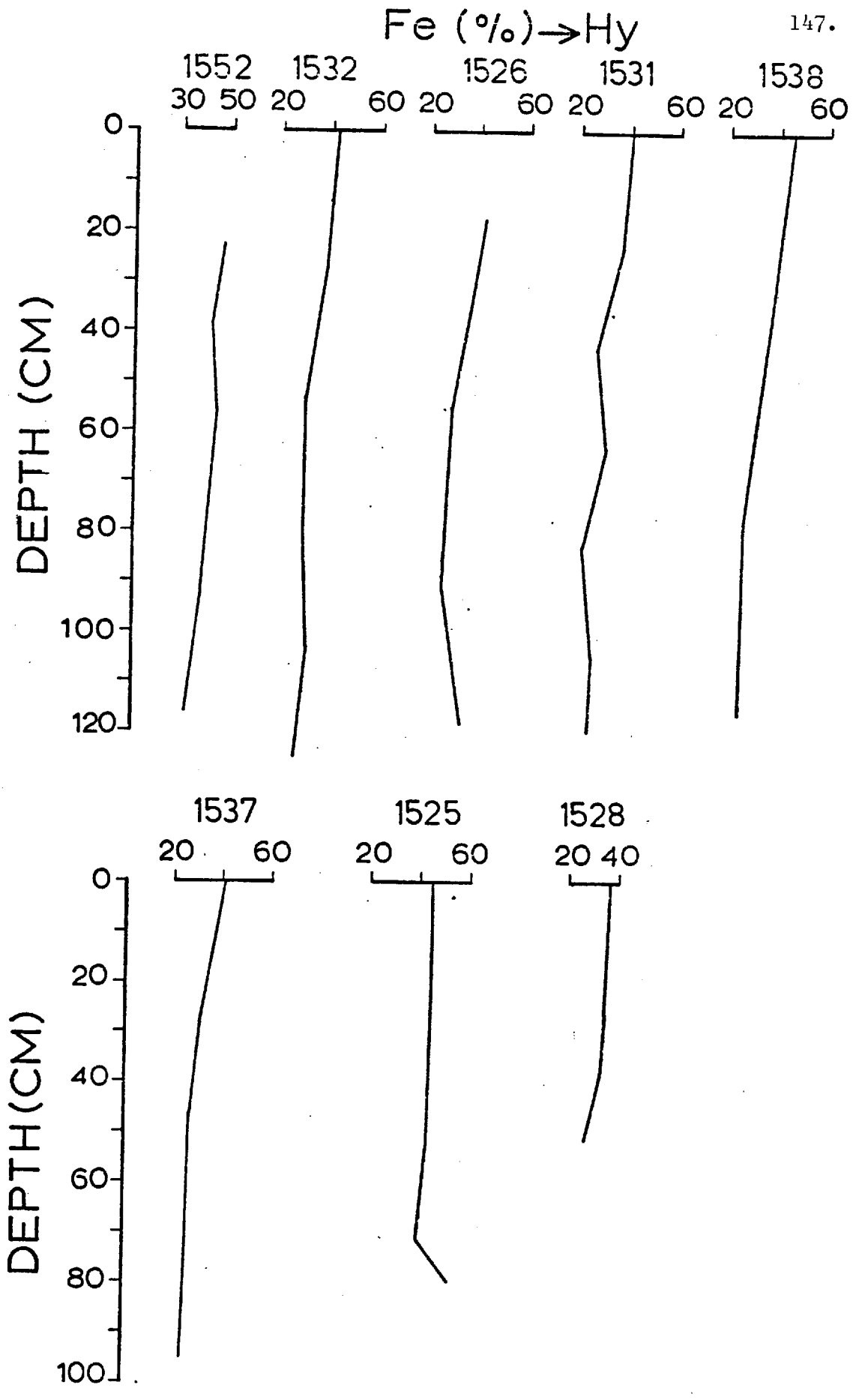

Figure 2.54: The distribution of the hydroxylamine HCl-soluble Fe in fracture zone sediment cores, expressed as a percentage of the total Fe concentration.

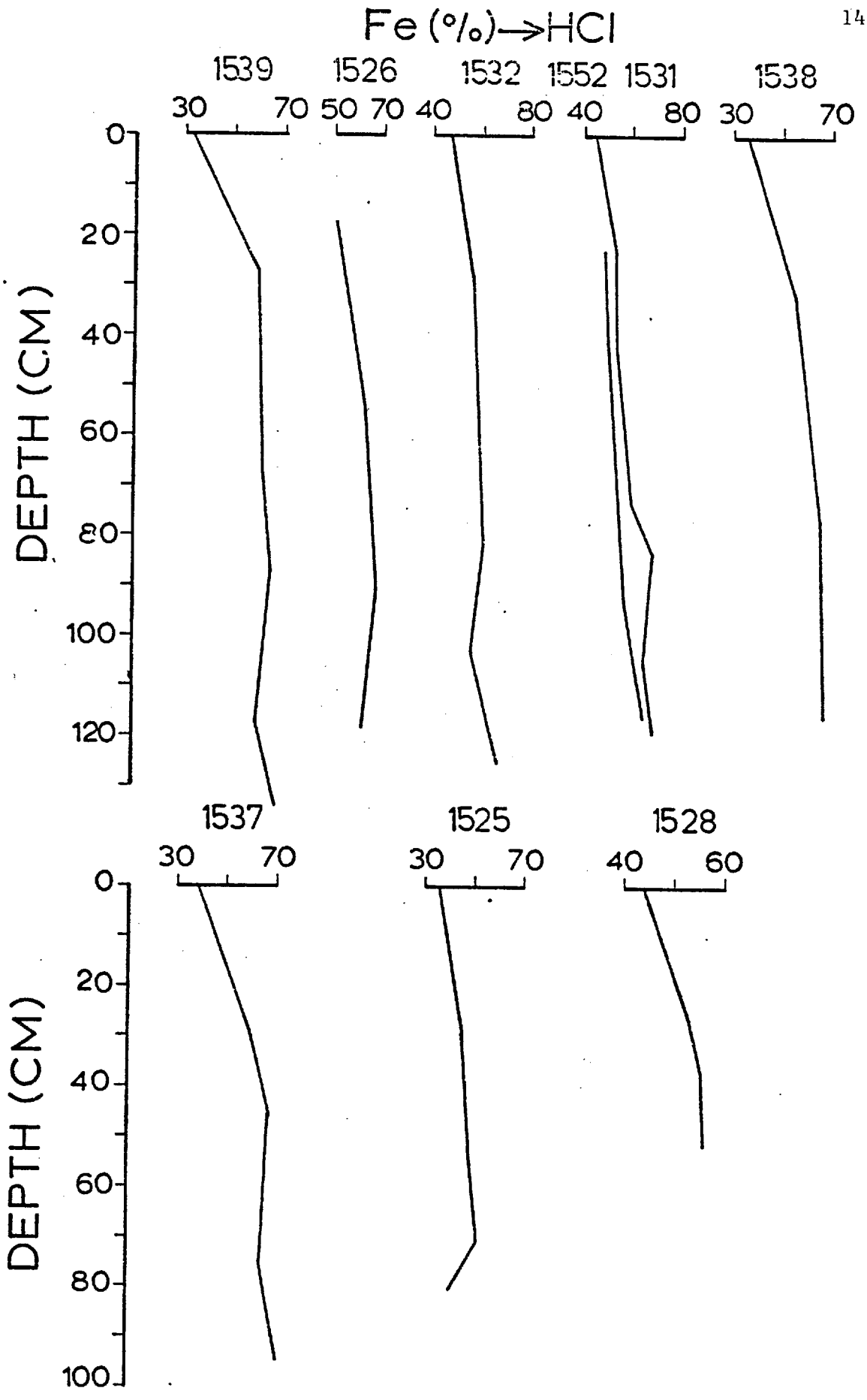

Figure 2.55: The distribution of the HCl-soluble Fe in fracture zone sediment cores expressed as a percentage of the total Fe concentration.

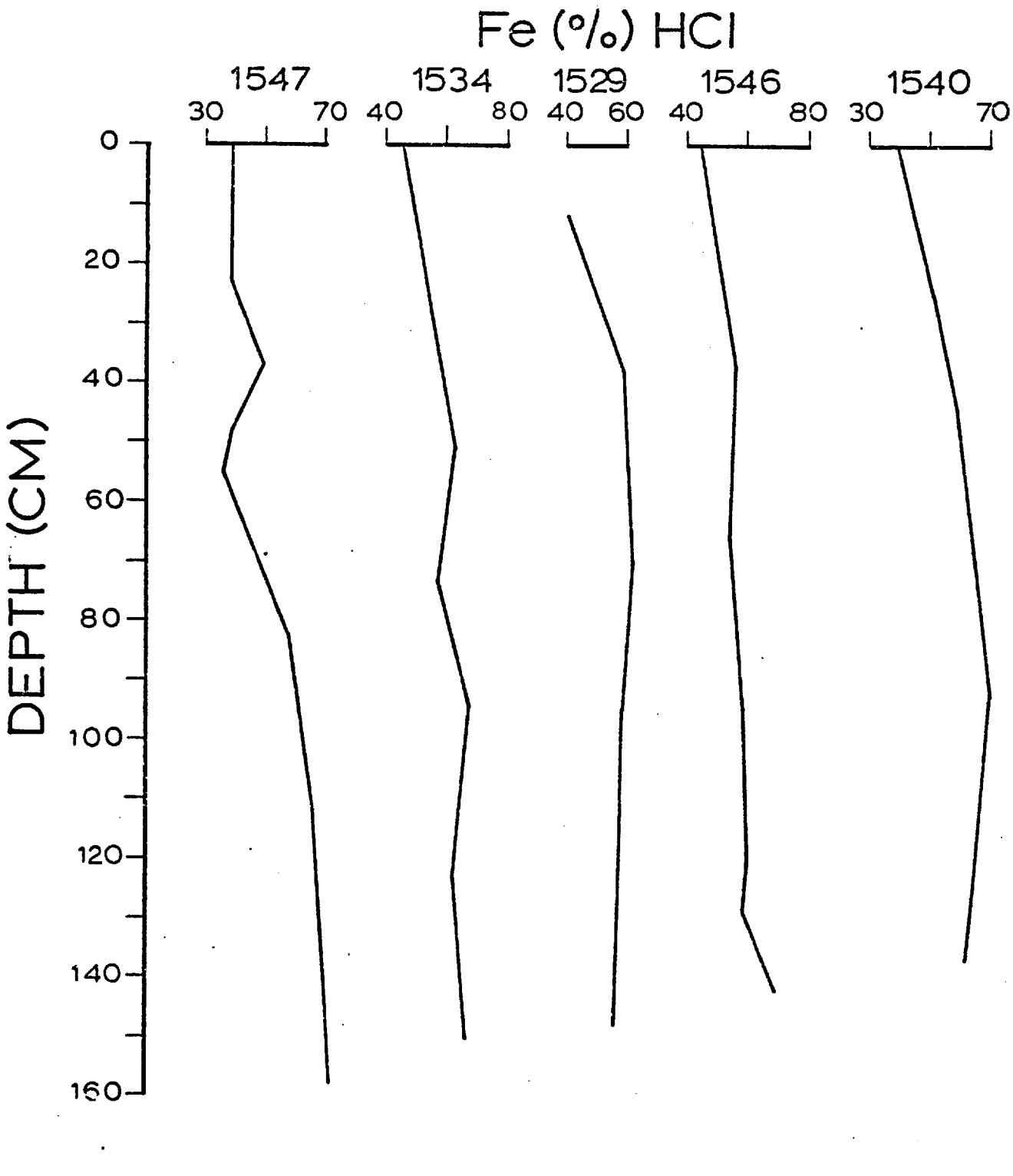

Figure 2.56: The distribution of the HCl-soluble Fe in fracture zone sediment cores expressed as a percentage of the total Fe concentration.

Table 2.4: Comparison of the average partitioning of Fe in surface and buried sediments from the fracture zone with other sediments. All data expressed as percentages of the total Fe concentrations.

	Acetic acid leach	Acid-reducing agent leach	Hydrochloric acid leach	Residue
1	14	43	40	3
2	5	33	59	3
3	3	5	79	13
4	3	10	75	12
5	3	6	66	25
6		31	68	1
7		45	54	1
8		45	54	1
9		31	68	1
10		26	73	1

1. This study: all surface sediments.
2. This study: all buried sediments.
3. Horowitz (1974): Iceland-area surface sediments.
4. Horowitz (1974): Reykjanes Ridge crest surface sediments.
5. Horowitz and Cronan (1976): Atlantic basal sediments.
6. Chester et al (1976): Quaternary calcareous clays.
7. Chester et al (1976): Pliocene (?)/Miocene (?) clays.
8. Chester et al (1976): Middle Eocene zeolitic clays.
9. Chester et al (1976): Upper Cretaceous zeolitic clays.
10. Chester et al (1976): Cretaceous (?) zeolitic clays.

sediments down to a depth of about 40 cm. In samples from this depth down to the base of the cores there are no significant differences in the concentration of the acetic acid-soluble Mn (see Figures 2.57, 2.58). In most of the cores it remains constant throughout the rest of the sediment. However, the vertical distribution of the acetic acid-soluble Mn is different in the cores SH 1546 and SH 1547. In these two cores the percentage of the acetic acid-soluble Mn remains constant from the surface of the cores down to about 30 or 40 cm depth. Below 40 cm it increases regularly down to the base of the cores. At a depth of 158 cm in core SH 1547, the proportion of Mn which is soluble in acetic acid reaches a value of 50% of the total Mn, in contrast to a value of 1% at the top of the core.

From the top of the cores down to about 40 cm depth, the percentage of Mn which is present in the hydroxylamine HCl-soluble fraction falls gradually. From 40 cm down to the base of most of the cores it tends to remain constant (see Figures 2.59, 2.60). In cores SH 1534, SH 1546 and SH 1547 the percentage of Mn found in the acid-reducible fraction continues to decline at depths below 40 cm, which is in contrast to the rest of the cores. The most marked decrease of the acid-reducible Mn with depth in the sediments is found in the core SH 1547, where in the top sediment sample 90% of the total Mn is located in the hydroxylamine HCl-soluble fraction, whereas at the depth of 158 cm this fraction contains only 25% of the total Mn.

In a number of cores (SH 1529, SH 1531, SH 1532, SH 1534 and SH 1546) the percentage of Mn present in the HCl-soluble fraction increases slightly with increasing depth from the surface sediments down to a depth of about 40 cm (see Figures 2.61, 2.62). However,

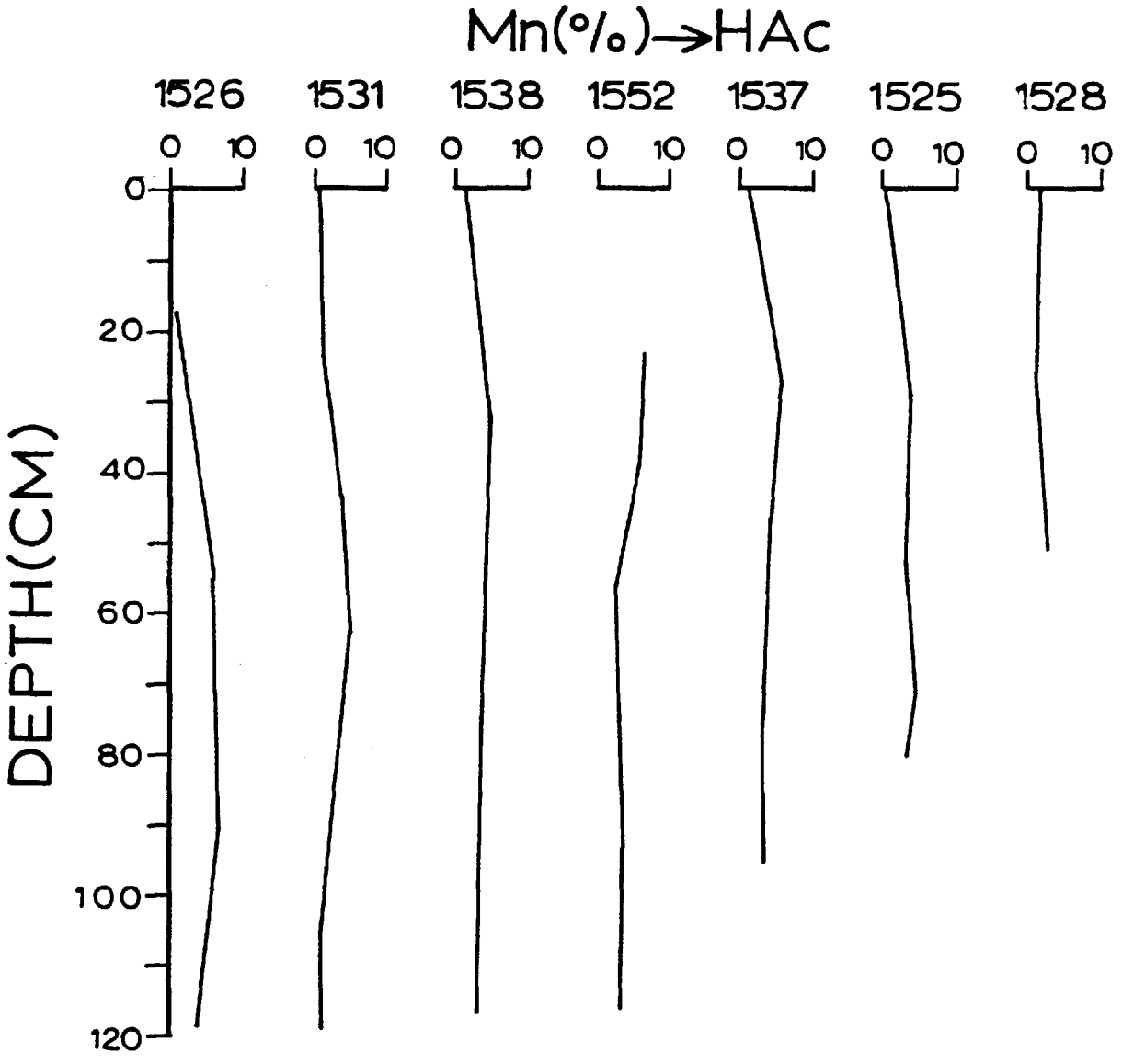

Figure 2.57: The distribution of the acetic acid-soluble Mn in fracture zone sediment cores expressed as a percentage of the total Mn concentration.

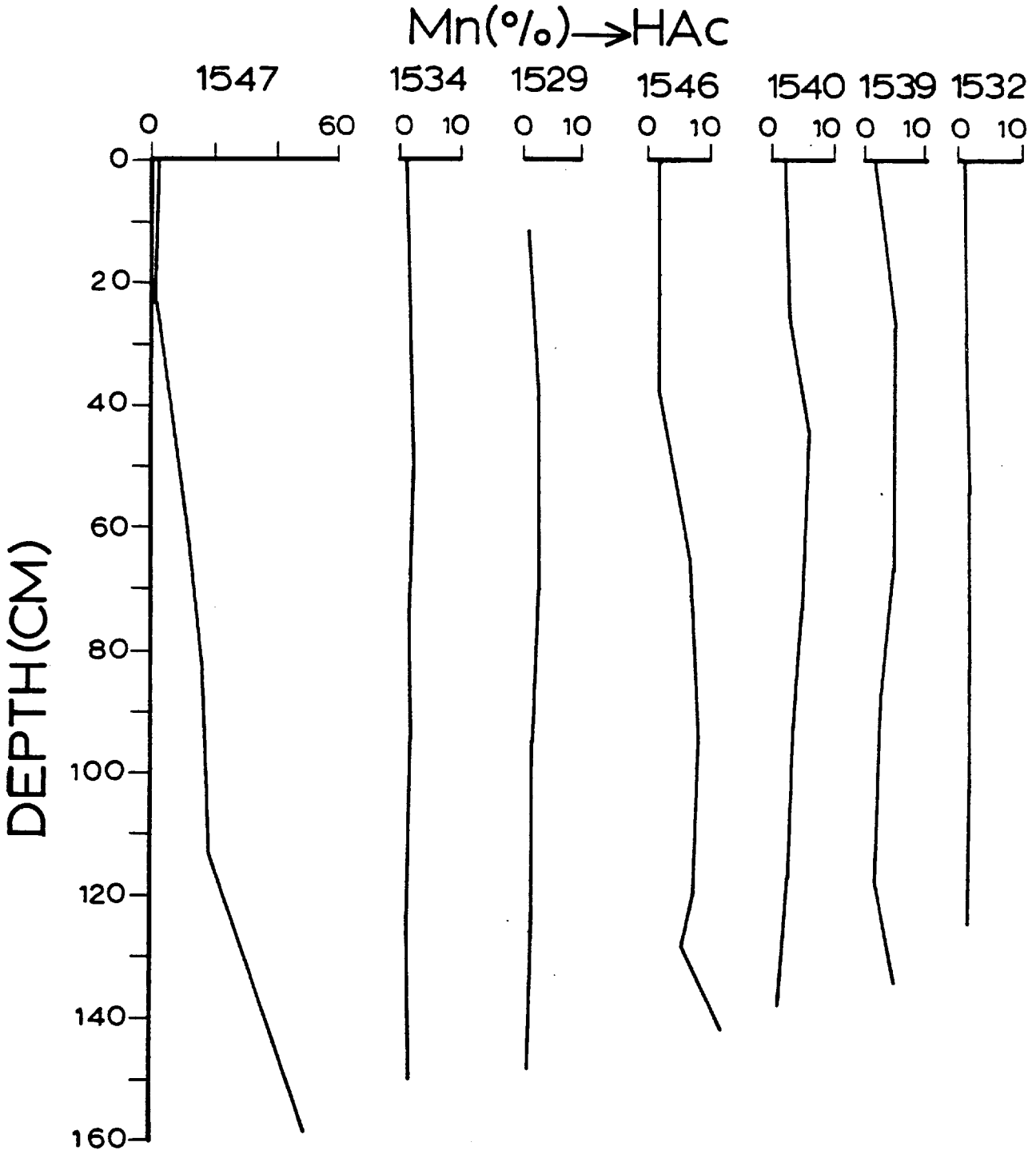

Figure 2.58: The distribution of the acetic acid-soluble Mn in fracture zone sediment cores expressed as a percentage of the total Mn concentration.

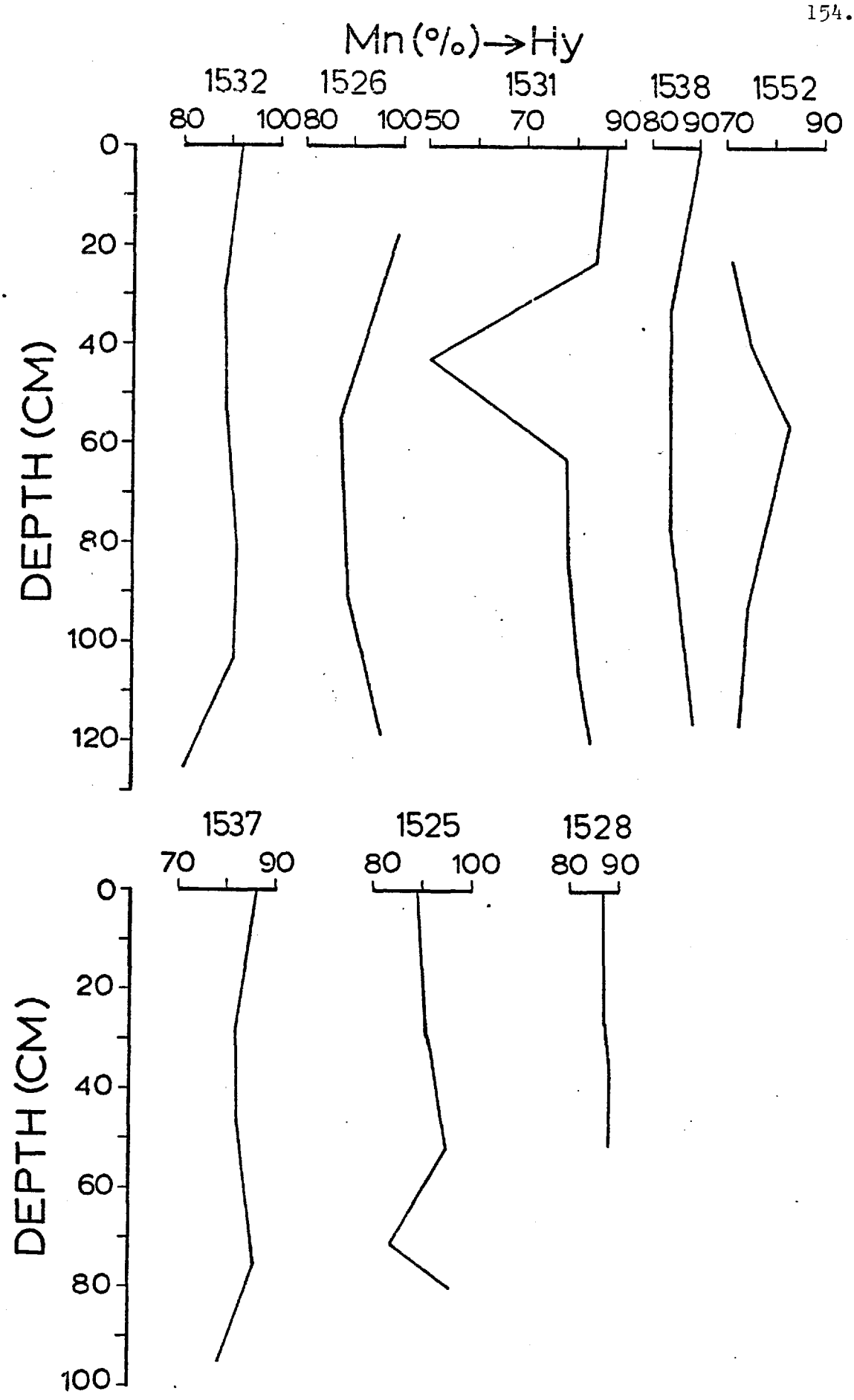

Figure 2.59: The distribution of the hydroxylamine HCl-soluble Mn in fracture zone sediment cores expressed as a percentage of the total Mn concentration.

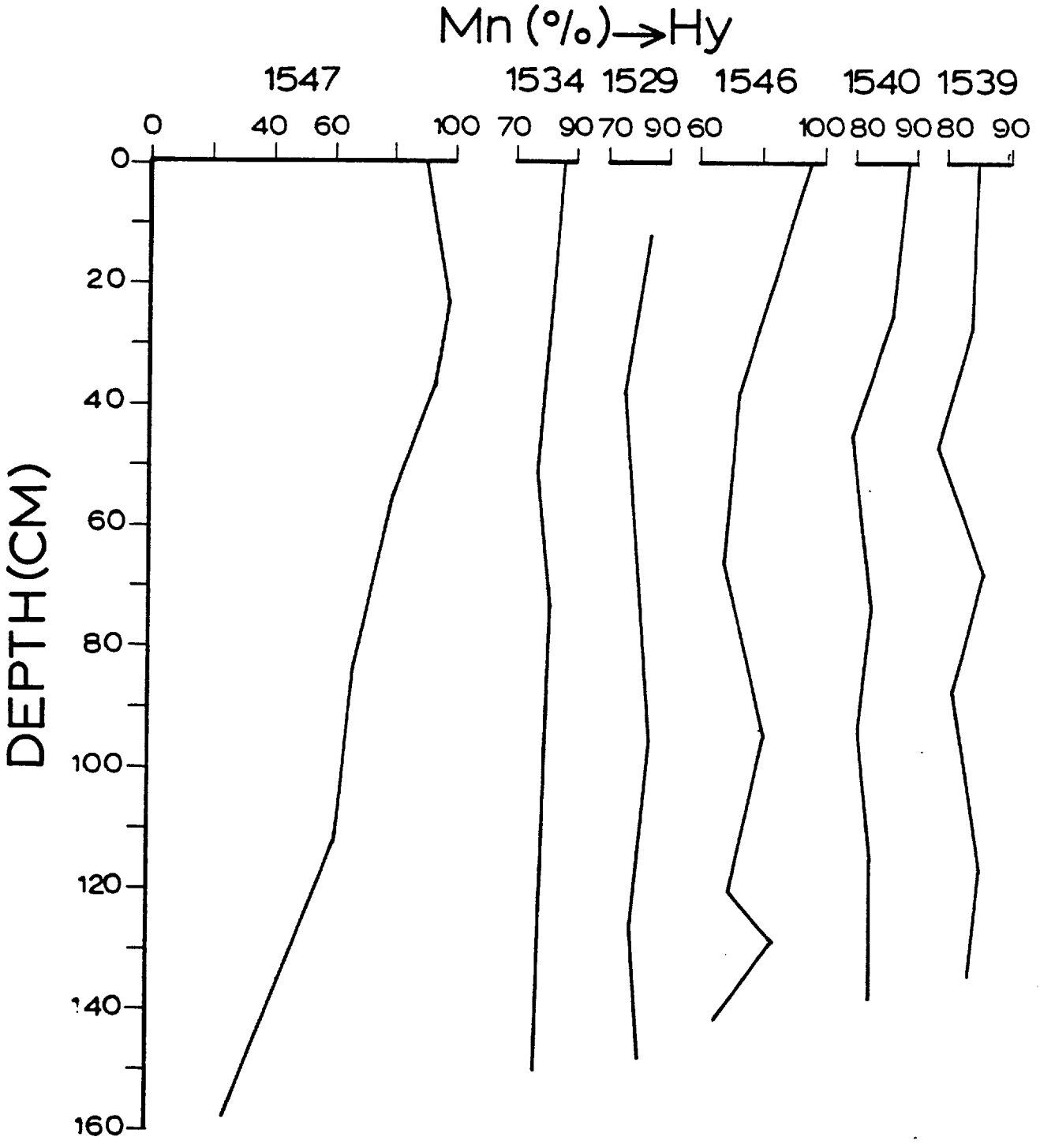

Figure 2.60: The distribution of the hydroxylamine HCl-soluble Mn in fracture zone sediment cores expressed as a percentage of the total Mn concentration.

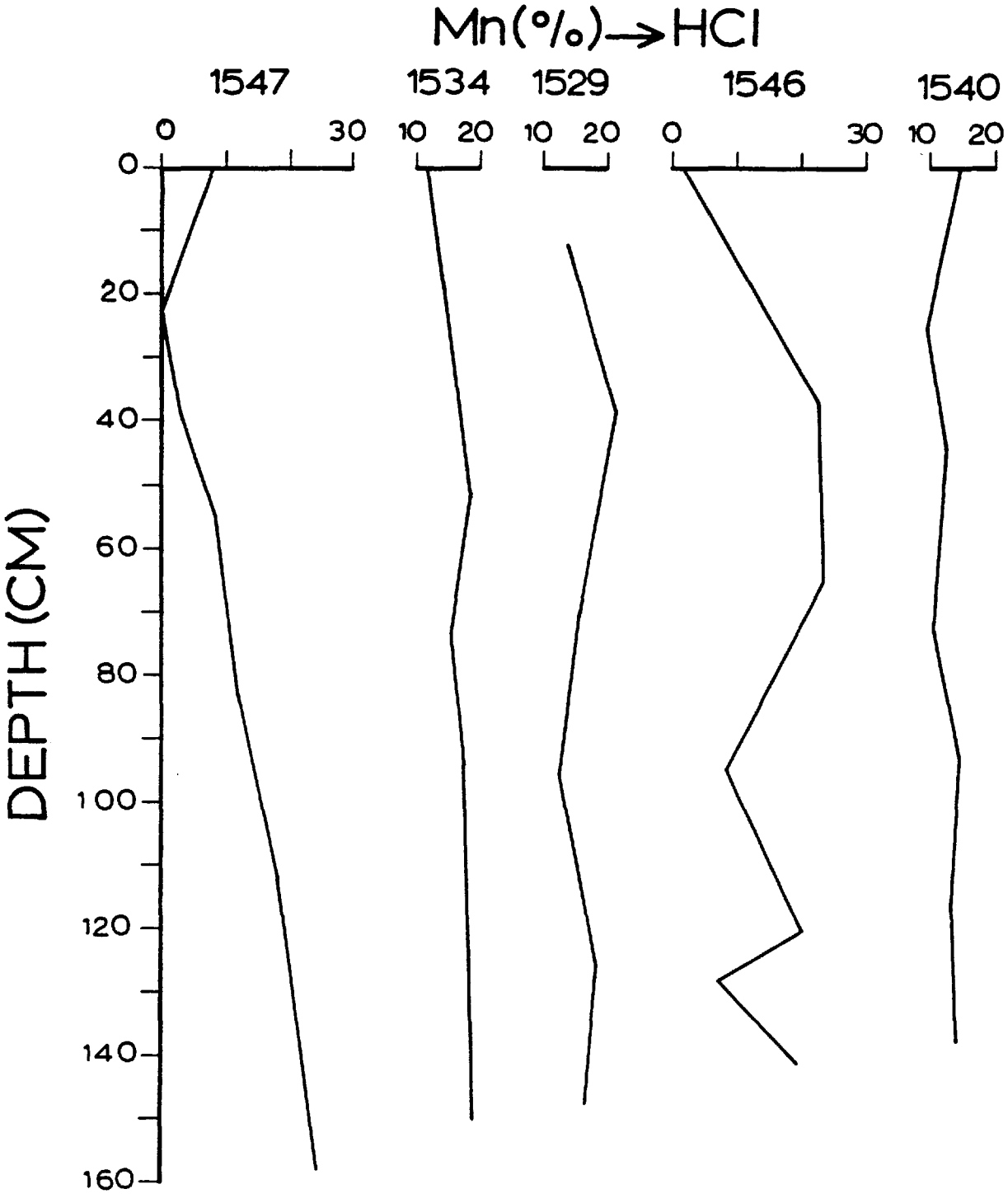

Figure 2.61: The distribution of the HCl-soluble Mn in fracture zone sediment cores expressed as a percentage of the total Mn concentration.

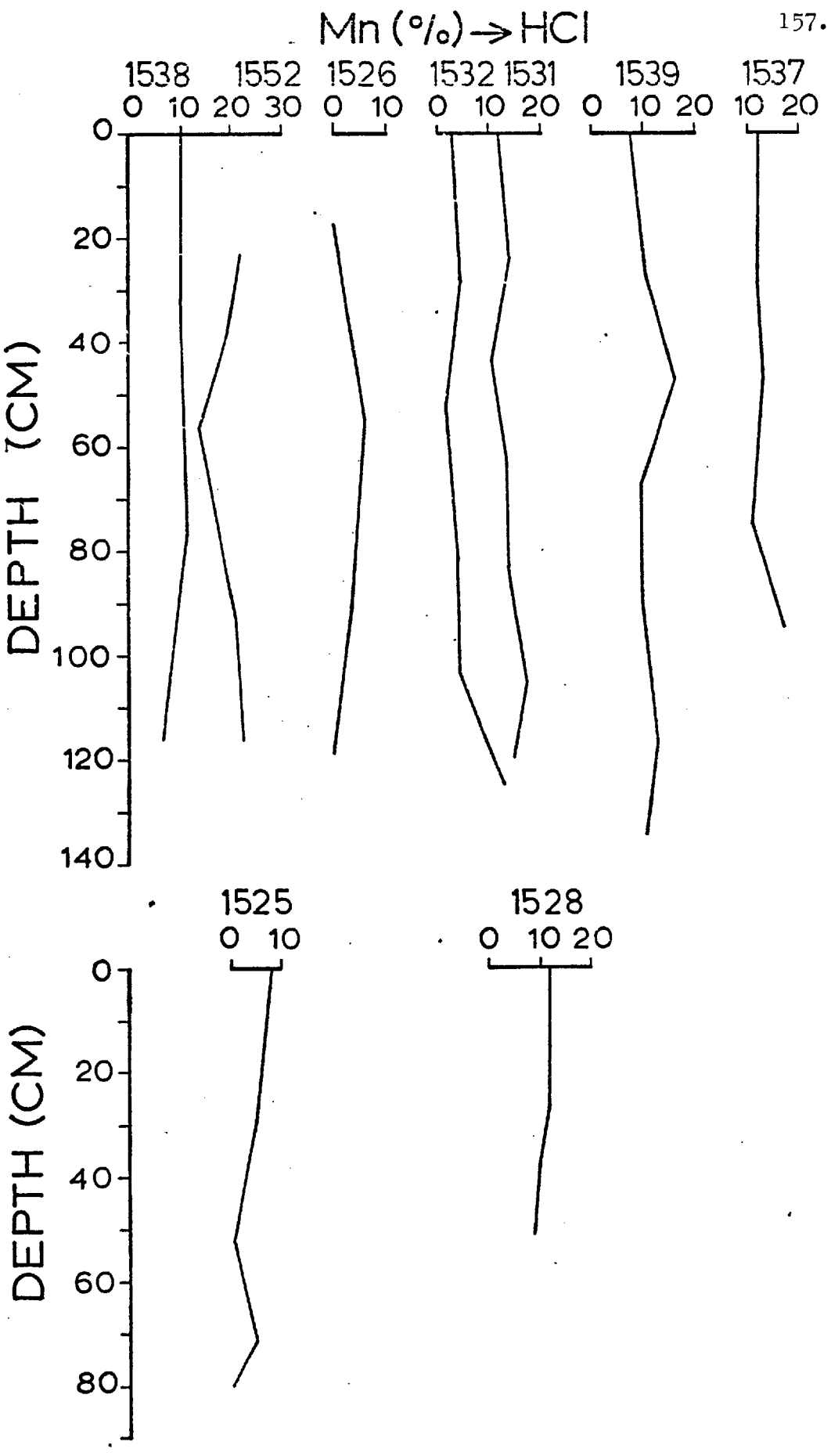

Figure 2.62: The distribution of the HCl-soluble Mn in fracture zone sediment cores expressed as a percentage of the total Mn concentration.

an inverse relationship between the HCl-soluble Mn and the depth of the sample was found for the upper part (0-30 cm) of cores SH 1525, SH 1540 and SH 1547, while this percentage remains constant from the top throughout most of the length of the cores SH 1528, SH 1537 and SH 1538. In almost all the sediment cores examined here, the percentage of Mn which is soluble in HCl varies below 40 cm depth without having any clear tendency to increase or decrease. There are significant differences in the vertical variations of the HCl-soluble Mn in core SH 1547 when compared with the distribution in the other cores. At 20-158 cm of this core there is a positive linear correlation between the percentage of Mn soluble in HCl and the depth of the sediment. It is noticeable that at about 20 cm depth, no Mn is found in the HCl-soluble fraction, while at 158 cm this fraction contains about 25% of the total Mn.

The distribution of Mn between the ferromanganese oxide minerals, the Fe-oxides and the aluminosilicates in the surface and buried sediments is similar to that reported for the Reykjanes Ridge crest sediments (Horowitz, 1974), the Atlantic basal sediments (Horowitz and Cronan, 1976), the East Pacific Rise basal metalliferous sediments (Cronan, 1976a) and all the sediments described by Chester et al (1976) from the Bermuda Rise D.S.D.P. core (see Table 2.5). In all these sediments more Mn was found associated with the ferromanganese oxide minerals than with the phases soluble in HCl. By contrast, the partition of Mn between these two phases is different from that in the Iceland-area surface sediments, where most of the total Mn is concentrated in the HCl-soluble fraction.

Table 2.5: Comparison of the average partitioning of Mn in surface and buried sediments from the fracture zone with other sediments. All data expressed as percentages of the total Mn concentrations.

	Acetic acid leach	Acid-reducing agent leach	Hydrochloric acid leach	Residue
1	3	88	8	1
2	5	82	12	1
3	2	10	51	37
4	6	40	31	23
5	14	57	23	6
6		76	23	1
7		97	2	1
8		95	4	1
9		84	14	2

1. This study: all surface sediments.
2. This study: all buried sediments.
3. Horowitz (1974): Iceland-area surface sediments.
4. Horowitz (1974): Reykjanes Ridge crest surface sediments.
5. Horowitz and Cronan (1976): Atlantic basal sediments.
6. Chester et al (1976): Quaternary calcareous clays.
7. Chester et al (1976): Middle Eocene zeolitic clays.
8. Chester et al (1976): Upper Cretaceous zeolitic clays.
9. Chester et al (1976): Cretaceous (?) zeolitic clays.

The Mn contribution made by the acetic acid-soluble fraction in the surface sediments is similar to that in the Iceland-Area surface sediments (Horowitz, 1974), but it is much lower than the contribution made by the same fraction reported for the Reykjanes Ridge crest sediments (Horowitz, 1974) and the Atlantic basal sediments (Horowitz and Cronan, 1976). These differences become less clearly defined in the buried sediments because the acetic acid-soluble fraction contains more Mn.

2.5.3 Nickel

Nickel in the surface sediments is associated with both the hydroxylamine HCl and the HCl-soluble fractions, having higher concentrations in the former than in the latter. On average, about 51% of the total Ni is concentrated in the acid-reducible fraction, indicating the strong association of this element with ferromanganese oxides, while about 44% is associated with the HCl-soluble fraction. Minor amounts of Ni have been found in the HCl-insoluble residue ($\sim$5%), whilst it is present only in traces in the acetic acid-soluble fraction.

In the subsurface sediments on average the amount of Ni soluble in the acid-reducing agent solution becomes lower ($\sim$ 48%) whereas more Ni is concentrated in the HCl-soluble fraction ($\sim$45%). The contributions to the total amount of Ni made by the acetic acid-soluble fraction and the HCl-insoluble residue become higher in the buried sediments ($\sim$2% in the former and 5% in the latter).

In general, there is an abrupt decrease of the percentage of Ni soluble in the acid-reducing agent solution from 0 to 50 cm depth (see Figures 2.63, 2.64 and 2.65). At greater depths, the proportion of Ni associated with the acid-reducible fraction varies within a large range. However, there is a tendency for this to be reduced with increasing depth in the cores. As in the case of Mn the vertical partitioning variations of Ni are more pronounced in core SH 1547. At about 20 cm depth, 66% of the total Ni is soluble in the hydroxylamine HCl solution, whereas at 158 cm depth the acid-reducible fraction contains only 8% of the total Ni.

The proportion of Ni which is soluble in HCl increases sharply from the surface of the sediments to about 50 cm depth (see Figures 2.66, 2.67 and 2.68). From 50 cm to about 90 cm depth it either remains constant (SH 1540, SH 1532, SH 1537) or it increases slightly to show a maximum between 70 and 90 cm (SH 1531, SH 1526, SH 1538). From 90 cm to 120 cm, in many cores (SH 1546, SH 1526, SH 1532, SH 1538, SH 1531) the HCl-soluble Ni is slightly reduced, to reach at the base values similar to those found at 50 cm depth.

The partition of Ni between the acid-reducible and the HCl-soluble fraction in the surface and buried sediments is similar to that of the Reykjanes Ridge crest sediments (Horowitz, 1974), the Atlantic basal sediments (Horowitz and Cronan, 1976), the Middle Eocene zeolitic clays from Bermuda Rise (Chester et al, 1976) (see Table 2.6), and the East Pacific Rise basal metalliferous sediments (Cronan, 1976a), where more Ni is concentrated in the acid-reducible than in the HCl-soluble fraction. However, there are some differences in the proportional distribution of the Ni between these two fractions. For

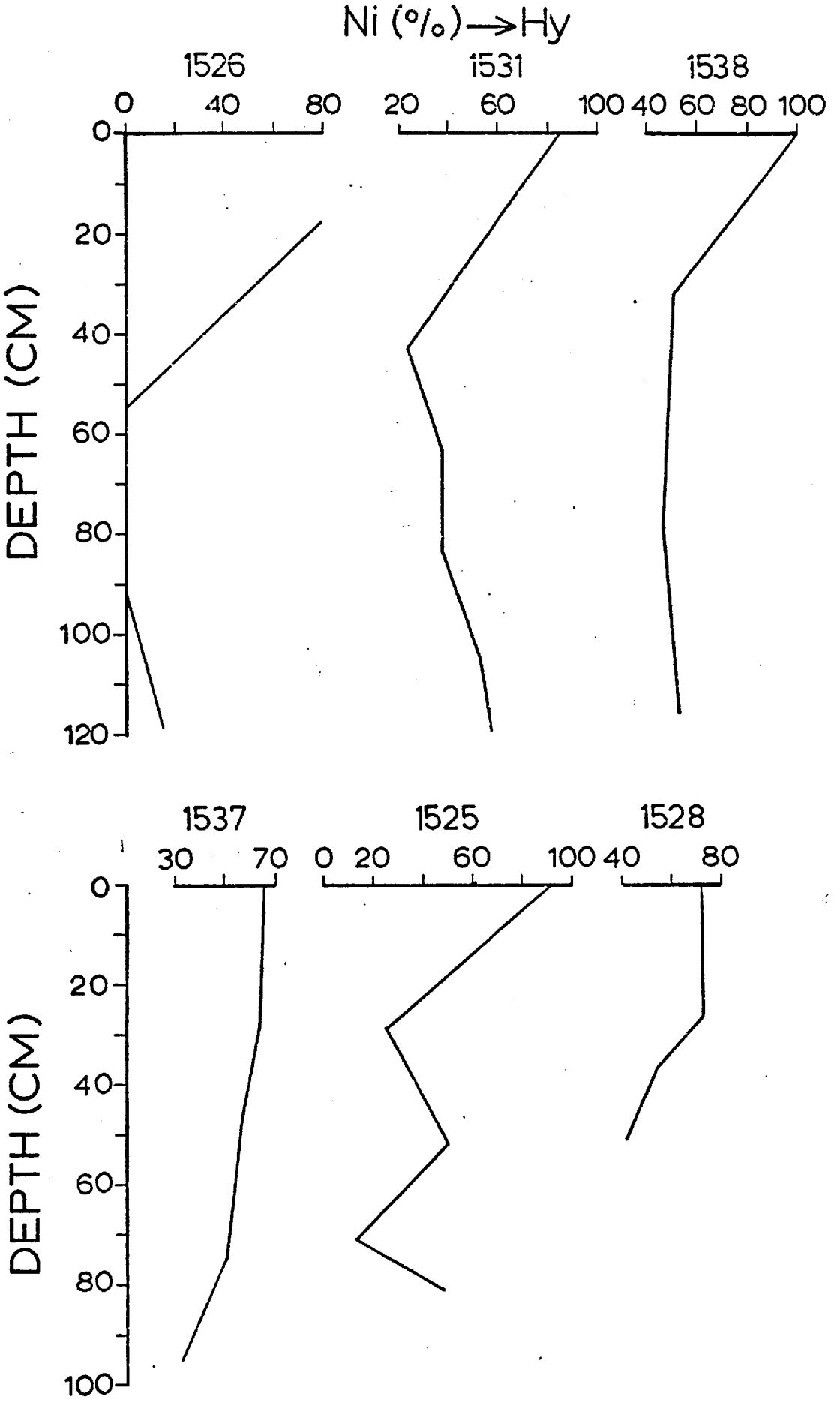

Figure 2.63: The distribution of the hydroxylamine HCl-soluble Ni in fracture zone sediment cores expressed as a percentage of the total Ni concentration.

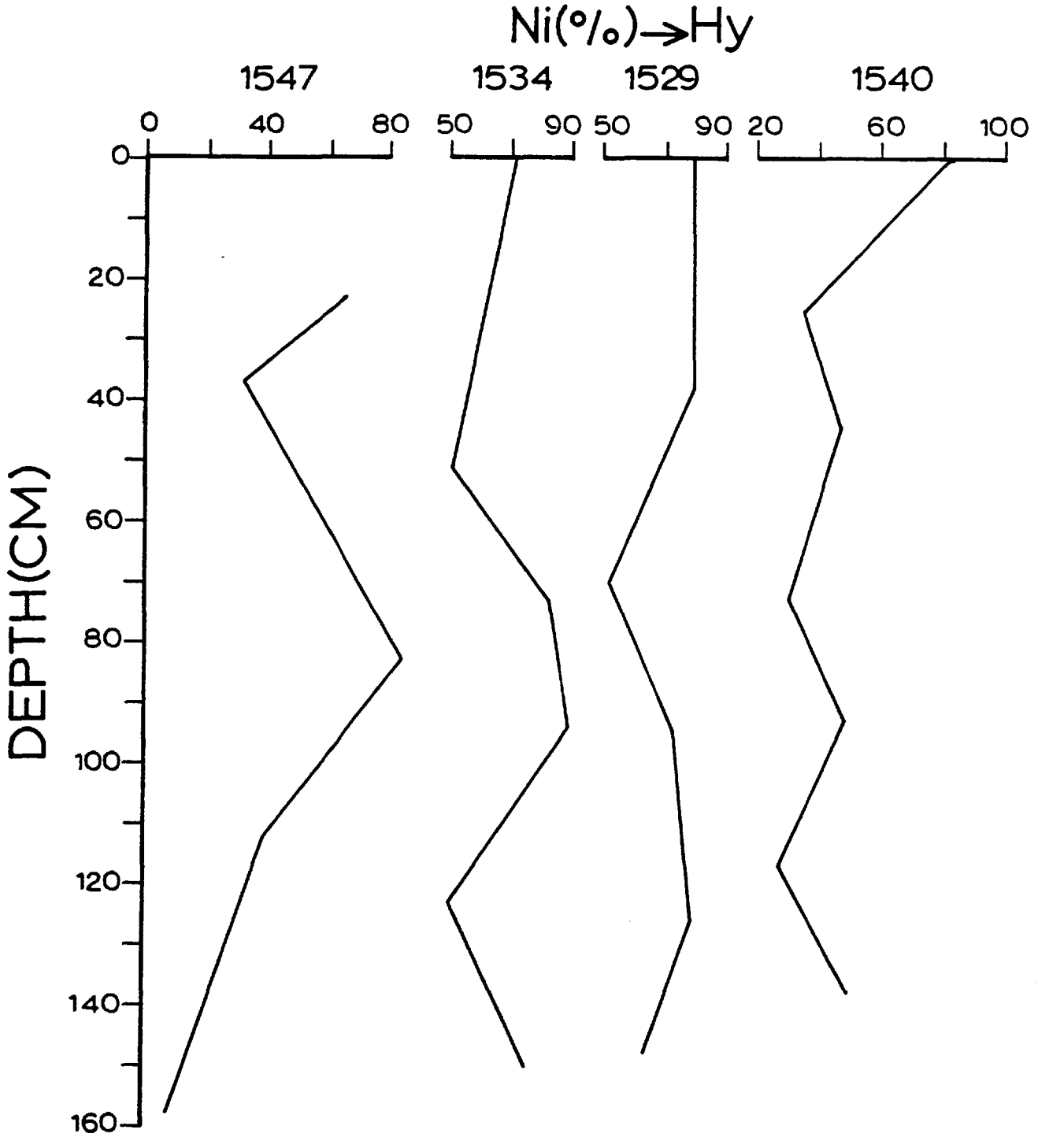

Figure 2.64: The distribution of the hydroxylamine HCl-soluble Ni in fracture zone sediment cores expressed as a percentage of the total Ni concentration.

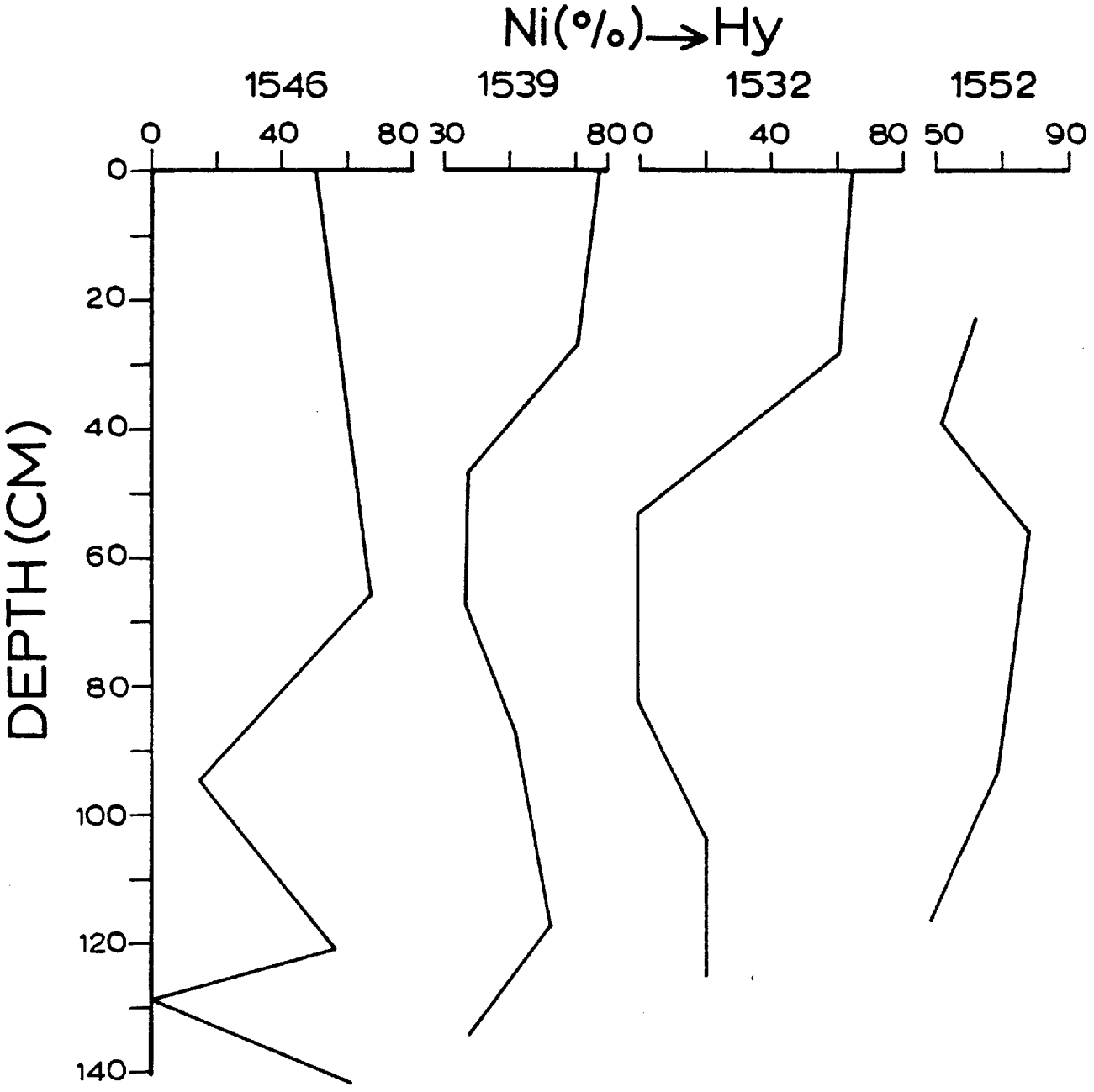

Figure 2.65: The distribution of the hydroxylamine HCl-soluble Ni in fracture zone sediment cores expressed as a percentage of the total Ni concentration.

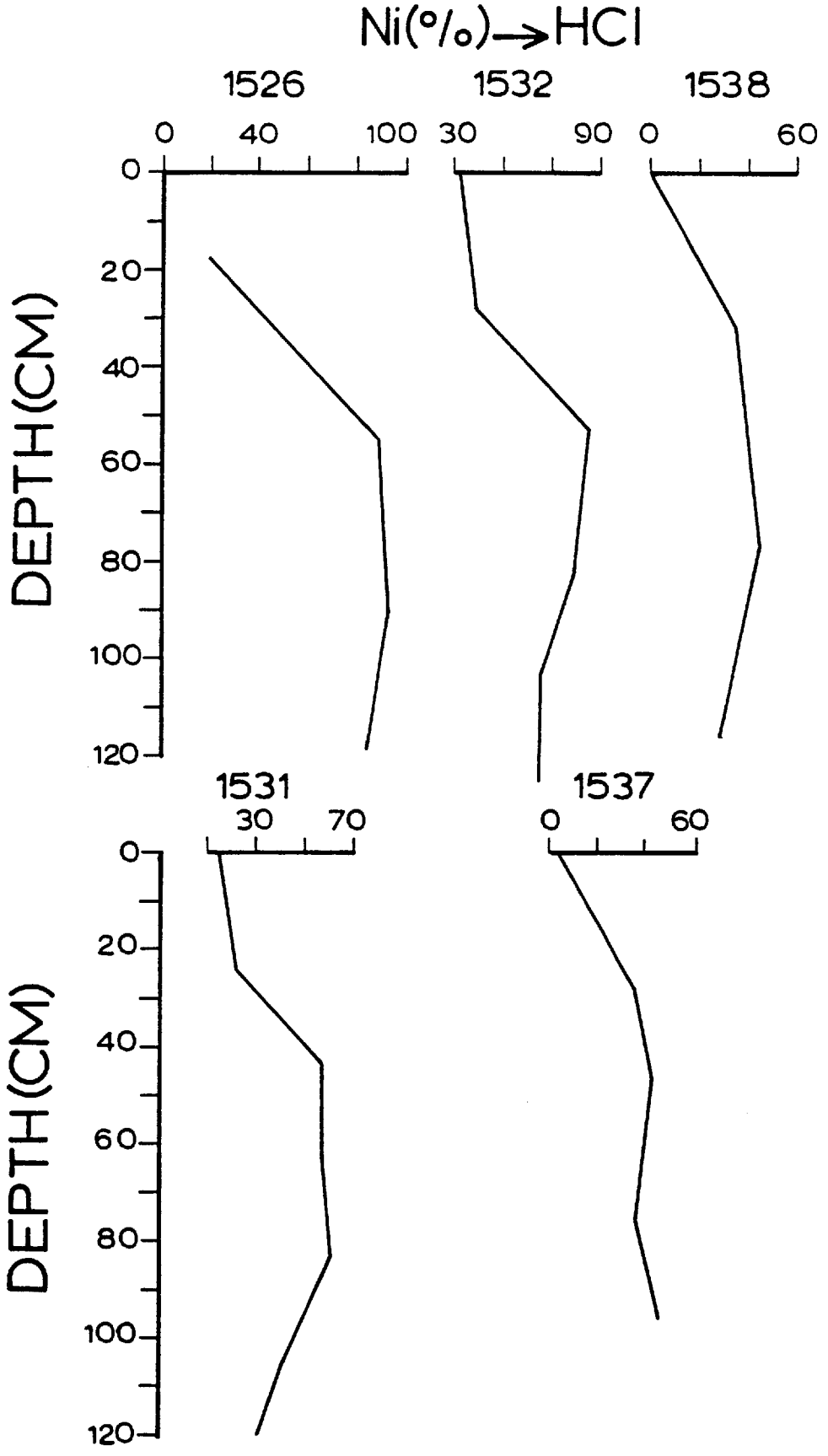

Figure 2.66: The distribution of the HCl-soluble Ni in fracture zone sediment cores expressed as a percentage of the total Ni concentration.

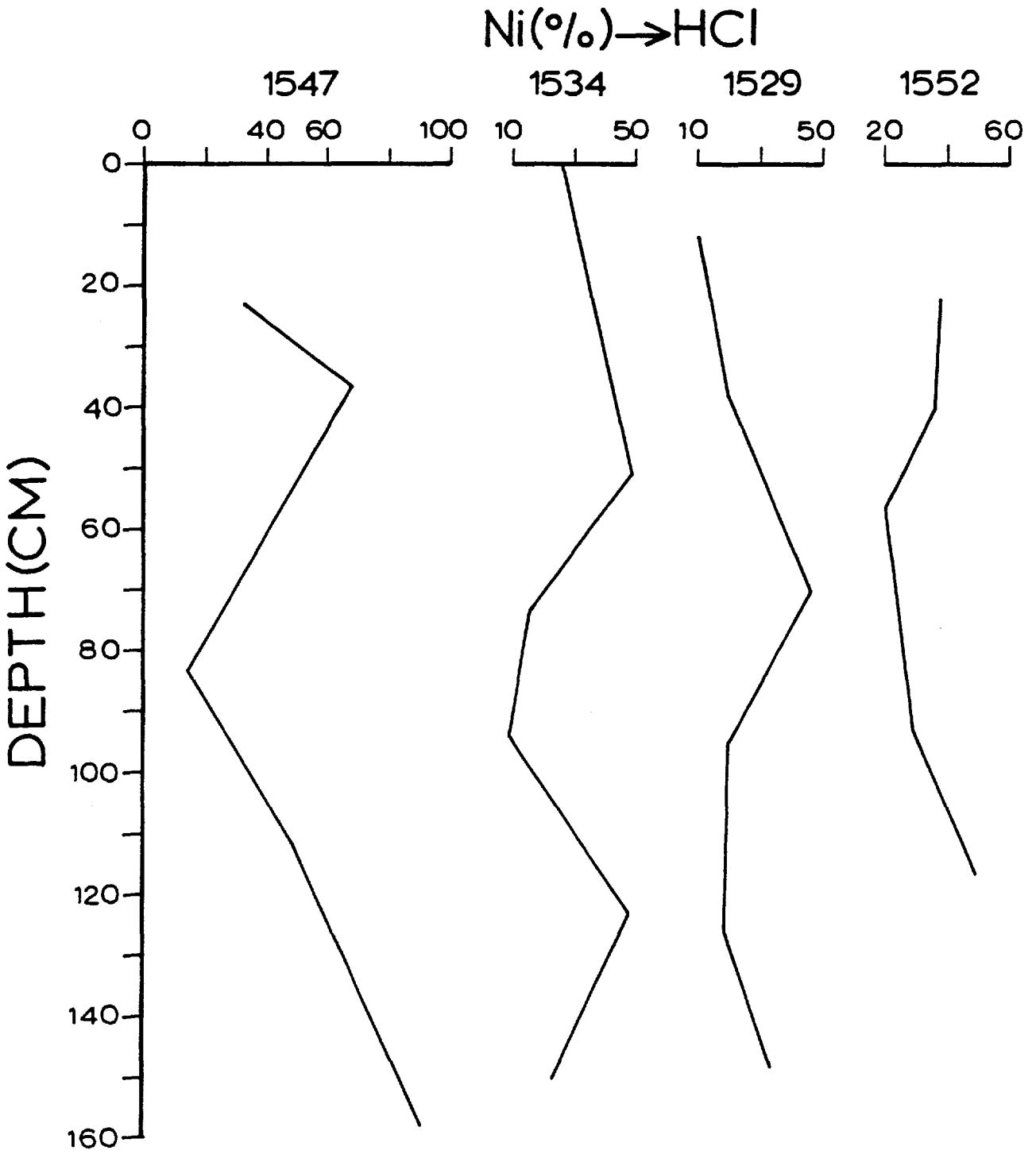

Figure 2.67: The distribution of the HCl-soluble Ni in fracture zone sediment cores expressed as a percentage of the total Ni concentration.

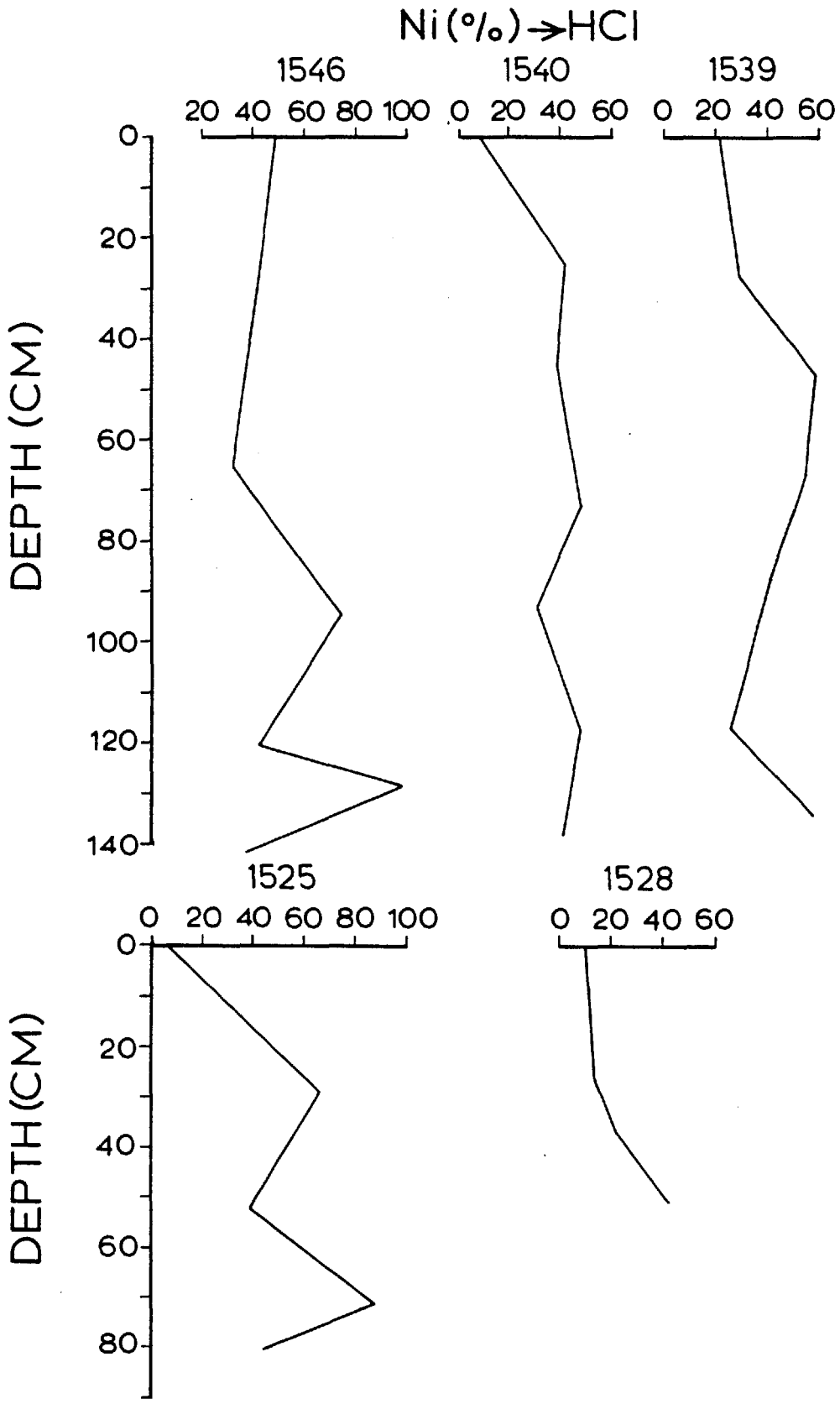

Figure 2.68: The distribution of the HCl-soluble Ni in fracture zone sediment cores expressed as a percentage of the total Ni concentration.

Table 2.6: Comparison of the average partitioning of Ni in surface and buried sediments from the fracture zone with other sediments. All data expressed as percentages of the total Ni concentrations.

	Acetic acid leach	Acid-reducing agent leach	Hydrochloric acid leach	Residue
1	traces	51	44	5
2	2	48	45	5
3	10	11	51	28
4	11	44	26	19
5	13	41	34	12
6		0	86	14
7		34	60	6
8		66	29	5
9		39	56	5
10		0	85	15

1. This study: all surface sediments.
2. This study: all buried sediments.
3. Horowitz (1974): Iceland-Area surface sediments.
4. Horowitz (1974): Reykjanes Ridge crest sediments.
5. Horowitz and Cronan (1976): Atlantic basal sediments.
6. Chester et al (1976): Quaternary calcareous clays.
7. Chester et al (1976): Pliocene (?)/Miocene (?) clays.
8. Chester et al (1976): Middle Eocene zeolitic clays.
9. Chester et al (1976): Upper Cretaceous zeolitic clays.
10. Chester et al (1976): Cretaceous (?) zeolitic clays.

instance, in the East Pacific Rise basal metalliferous sediments, over 90% of the total Ni was found in the hydroxylamine HCl-soluble fraction, whereas in the buried sediments of the fracture zone only 48% of the total Ni is associated with the acid-reducible fraction. By contrast, this partition differs from that in the Iceland-Area surface sediments (Horowitz, 1974), the Quaternary calcareous clays, the Pliocene (?)/Miocene (?) clays, and the Upper Cretaceous and the Cretaceous zeolitic clays from the Bermuda Rise D.S.D.P. core (Chester et al, 1976). In these sediments more Ni was found in the HCl-soluble fraction than in the acid-reducible fraction. Especially in the Quaternary calcareous clays and in the Cretaceous (?) zeolitic clays from the Bermuda Rise no Ni was found associated with the hydroxylamine HCl-soluble fraction.

Further comparisons of the partition of Ni among the other phases of the fracture zone sediments with its partition in the sediments from other areas showed considerable differences. The percentage of Ni in the HCl-insoluble residue is very low in comparison with the Ni contribution made by the HCl-insoluble residue of the following sediments:

1. The Iceland-Area surface sediments (Horowitz, 1974).

2. The Reykjanes Ridge crest sediments (Horowitz, 1974).

3. The Atlantic basal sediments (Horowitz and Cronan, 1976).

4. The Quaternary calcareous clays from the Bermuda Rise (Chester et al, 1976).

5. The Cretaceous zeolitic clays from the Bermuda Rise (Chester et al, 1976).

However, the percentage of Ni in the HCl-insoluble residue of the surface and buried sediments is equal to the percentage Ni contribution made by the HCl-insoluble residue of the Middle Eocene and Upper Cretaceous zeolitic clays from the Bermuda Rise (Chester et al, 1976). Nickel in the surface sediments occurs only in traces in the acetic acid-soluble fraction and ~ 2% in the subsurface sediments. The Ni contribution of the acetic acid-soluble fraction in the Iceland-Area surface sediments and the Reykjanes Ridge crest sediments (Horowitz, 1974) and the Atlantic basal sediments (Horowitz and Cronan, 1976) is much higher; in the latter sediments it reaches 13% of the total amount of Ni present.

2.5.4 Cobalt

In the surface sediments 91% of the total Co is associated, on average, with the HCl-soluble fraction. A significant amount of Co (~8%) has been found in the HCl-insoluble detrital residue. No Co has been found in the acetic acid-soluble fraction, while a very small amount (~ 1.0%) was liberated in the acid-reducing agent solution.

In contrast to the surface sediments, on average, less Co has been found in the HCl-soluble fraction of the buried sediments (~83%), whereas the contribution of the acid-reducible fraction and the HCl-insoluble residue become higher (~3% and 14%, respectively). As in the surface sediments Co is not affected chemically by the acetic acid solution.

The high concentrations of Co in the HCl-soluble fraction of the surface and buried sediments would suggest that this element is

associated either with the Fe-oxides or is located in the lattice structures of the clay minerals. Since no correlation between Co and Fe has been observed when the total concentrations of Co were plotted against the total concentrations of Fe, it is suggested that Co is most likely to be located in the lattice of clay minerals rather than associated with the Fe-oxides.

The geochemical behaviour of Co in the surface and buried sediments from the fracture zone studied here differs from that reported for Middle Eocene, Upper Cretaceous and Cretaceous zeolitic clays from the Bermuda Rise (Chester et al, 1976) (see Table 2.7), as well as from that in East Pacific Rise basal metalliferous sediments (Cronan, 1976a) where Co is strongly associated with the ferromanganese oxide phases. The distribution of Co is also different from that in the Quaternary calcareous clays and the Pliocene (?)/Miocene (?)clays from Bermuda Rise (Chester et al, 1976). In the latter, Co is equally distributed between the HCl-soluble fraction and the detrital residue. No Co was found in the acetic acid and the acid-reducible fractions.

2.5.5 Lead

A considerable amount of Pb has been found in the acetic acid-soluble fraction of many surface and subsurface sediment samples taken from the following cores: SH 1525, SH 1526, SH 1528, SH 1520, SH 1521, SH 1530, SH 1540, SH 1532, SH 1546, SH 1543, SH 1551, SH 1545. From this, it could be suggested that Pb is associated with $CaCO_3$, which comprises more than 70% of these sediments.

Table 2.7: Comparison of the average partitioning of Co in surface and buried sediments from the fracture zone with other sediments. All data expressed as percentages of the total Co concentrations.

	Acetic acid leach	Acid-reducing agent leach	Hydrochloric acid leach	Residue
1	0	1	91	8
2	0	3	83	14
3		10	40	50
4		0	50	50
5		83	11	6
6		74	23	3
7		55	20	25

1. This study: all surface sediments.
2. This study: all buried sediments.
3. Chester et al (1976): Quaternary calcareous clays.
4. Chester et al (1976): Pliocene (?)/Miocene (?) clays.
5. Chester et al (1976): Middle Eocene zeolitic clays.
6. Chester et al (1976): Upper Cretaceous zeolitic clays.
7. Chester et al (1976): Cretaceous zeolitic clays.

The distribution of Pb among the components of the surface sediments is similar to that reported for Quaternary calcareous clays, Pliocene (?)/Miocene (?) clays, Middle Eocene and Upper Cretaceous zeolitic clays from the Bermuda Rise D.S.D.P. core (Chester et al, 1976) (see Table 2.8), and for the East Pacific Rise basal metalliferous sediments (Cronan, 1976a). By contrast, it is different from the distribution of Pb in the Iceland-Area surface sediments and the Reykjanes Ridge crest surface sediments (Horowitz, 1974), and the Atlantic basal sediments (Horowitz and Cronan, 1976), where most of the Pb is associated with the HCl-soluble fraction. Conversely, the partitioning of Pb in the subsurface sediments is similar to its distribution among the phases in the Iceland-Area surface sediments and the Reykjanes Ridge crest surface sediments (Horowitz, 1974), and the Atlantic basal sediments (Horowitz and Cronan, 1976). However, it differs from that in all the sediments described by Chester et al (1976) from the Bermuda Rise D.S.D.P. core and the East Pacific Rise basal metalliferous sediments (Cronan, 1976a). The amount of Pb in the HCl-insoluble residue, expressed as a proportion of the total sediment Pb, in the fracture zone sediments and especially in the surface sediments is less than in all the other areas sampled.

2.5.6 Zinc

On average, less than half of the total Zn ($\sim$44%) in the surface sediments is associated with the Fe-oxides and the clay minerals which are soluble in HCl. A significant amount of Zn ($\sim$30%) has been found in the fraction soluble in acetic acid, which indicates that Zn is associated with carbonates or is present on the mineral

Table 2.8: Comparison of the average partitioning of Pb in surface and buried sediments from the fracture zone with other sediments. All data expressed as percentages of the total Pb concentrations.

	Acetic acid leach	Acid-reducing agent leach	Hydrochloric acid leach	Residue
1	6	58	33	3
2	7	39	48	6
3	9	8	57	26
4	7	25	47	21
5	13	26	32	29
6		51	40	9
7		77	8	15
8		68	14	18
9		66	26	8
10		30	58	12

1. This study: all surface sediments.
2. This study: all buried sediments.
3. Horowitz (1974): Iceland-Area surface sediments.
4. Horowitz (1974): Reykjanes Ridge crest surface sediments.
5. Horowitz and Cronan (1976): Atlantic basal sediments.
6. Chester et al (1976): Quaternary calcareous clays.
7. Chester et al (1976): Pliocene (?)/Miocene (?) clays.
8. Chester et al (1976): Middle Eocene zeolitic clays.
9. Chester et al (1976): Upper Cretaceous zeolitic clays.
10. Chester et al (1976): Cretaceous zeolitic clays.

surfaces of the sediments. A smaller portion of Zn (~25%) is associated with the ferromanganese oxide-minerals which are soluble in the acid-reducing agent solution whilst only ~1% is present in the HCl-insoluble residue.

In comparison with the surface sediments, there are some differences in the distribution of Zn among the chemically separated fractions of the subsurface sediments. On average, more than half of the total Zn (~58%) is concentrated in the HCl-soluble fraction, while the proportions associated with the fractions soluble in the acetic acid and the acid-reducing agent solution are lower than in the surface sediments (~19% in acetic acid and ~22% in the hydroxylamine HCl). In contrast to the surface sediments, in the buried sediments more Zn is concentrated in the fraction soluble in the acid-reducing agent solution than in the acetic acid.

In almost all the cores examined here, the percentage of Zn which is released in the acetic acid solution decreases gradually from the top down to the base of the cores, thus showing a strong negative correlation with depth (see Figures 2.69, 2.70). This reduction is more sharp in the upper part of the cores (0-40 cm). Similarly, the variations of the hydroxylamine HCl-soluble Zn show a negative correlation between the percentage of Zn which is present in the acid-reducible fraction and the depth of the samples (see Figures 2.71 and 2.72). This correlation is strong and comparatively linear in the upper 40 cm of the cores, whereas in the lower part of the sediments (below 40 cm) it is not very clear. Generally, there is a strong positive correlation between the percentage of Zn which is soluble in HCl and the depth of the sediment samples, in the top 40 cm of the cores (see Figures 2.73, 2.74 and 2.75). Below 50 cm, the

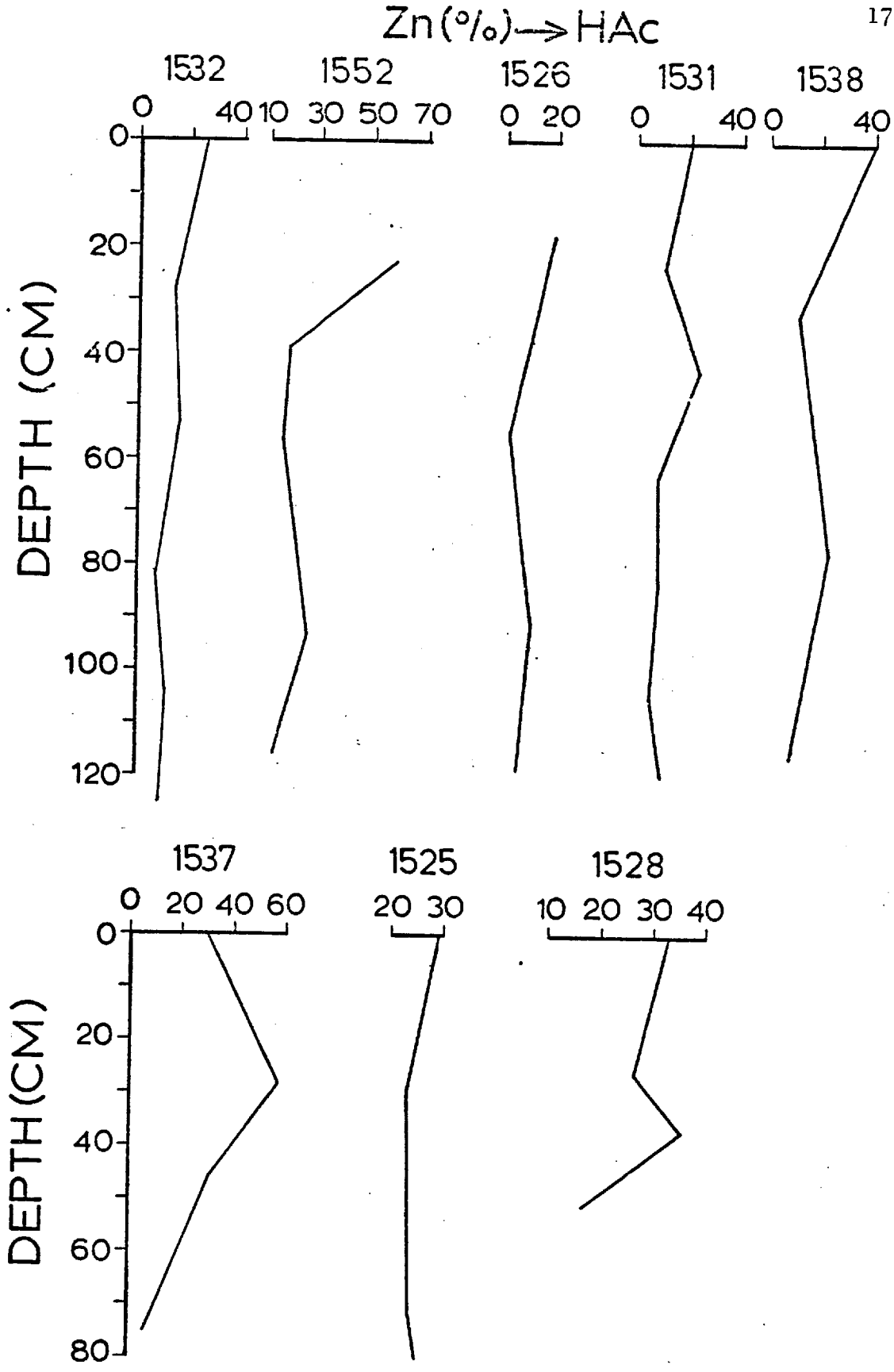

Figure 2.69: The distribution of the acetic acid-soluble Zn in fracture zone sediment cores expressed as a percentage of the total Zn concentration.

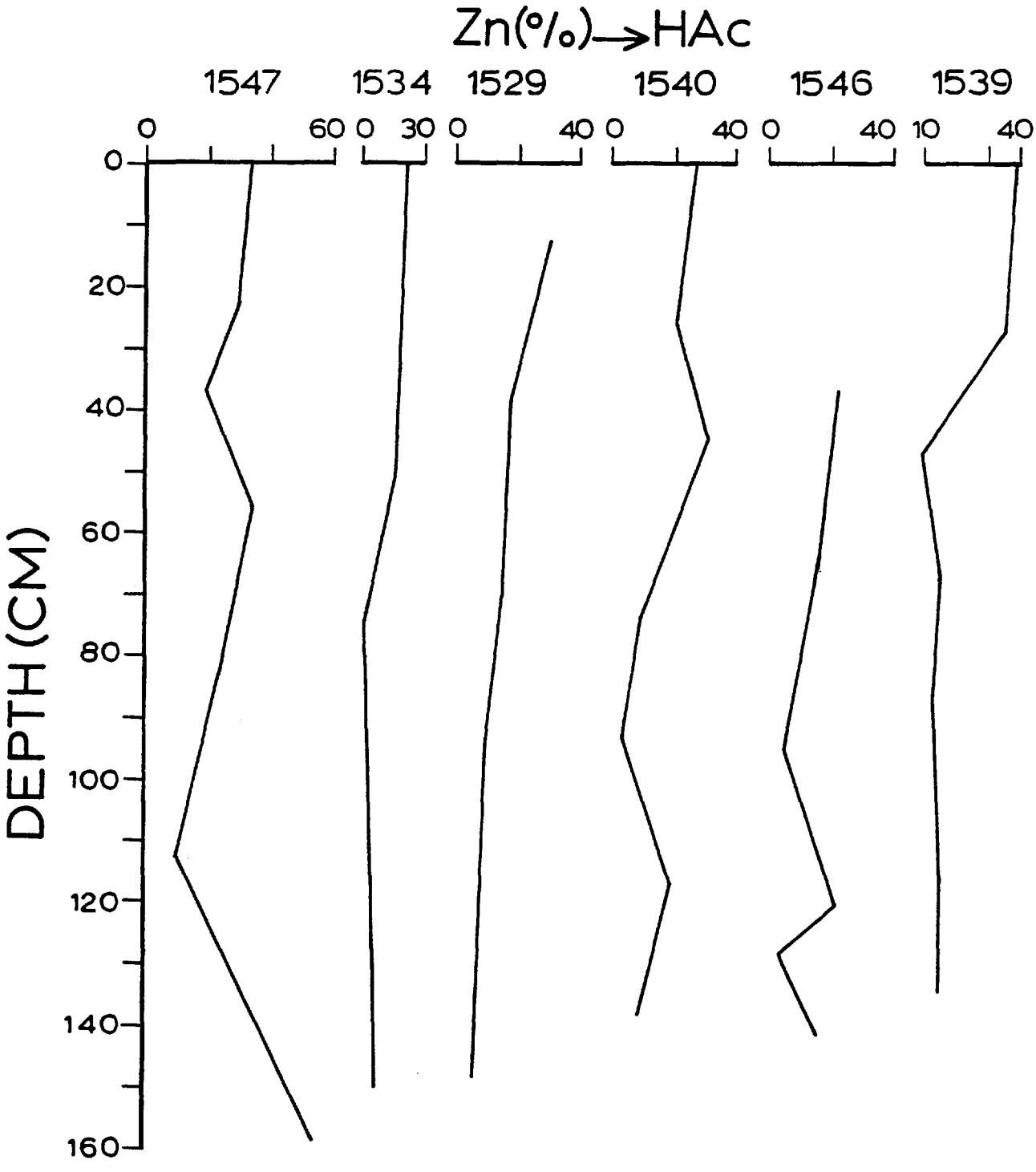

Figure 2.70: The distribution of the acetic acid-soluble Zn in fracture zone sediment cores expressed as a percentage of the total Zn concentration.

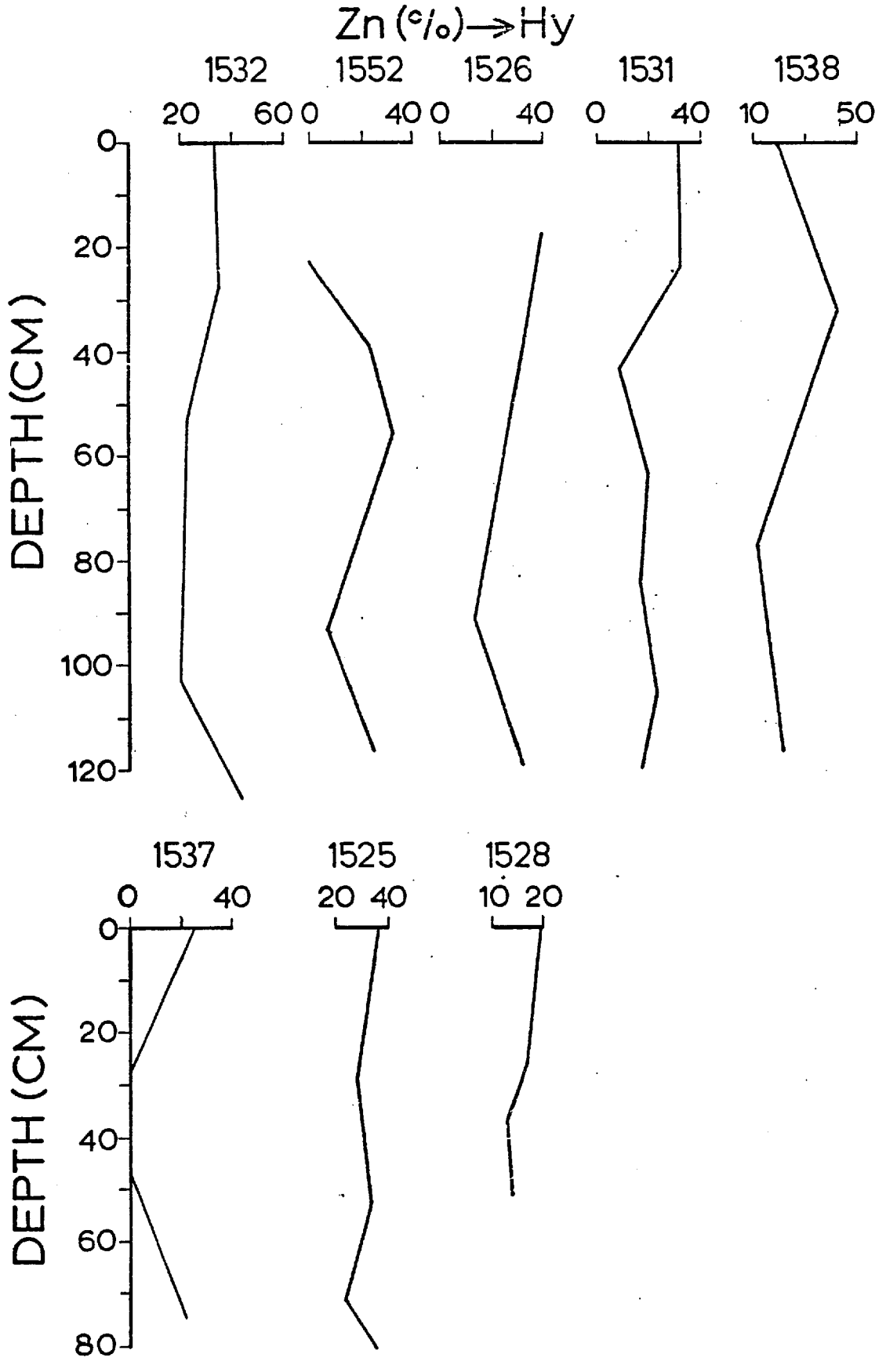

Figure 2.71: The distribution of the hydroxylamine HCl-soluble Zn in fracture zone sediment cores, expressed as a percentage of the total Zn concentration.

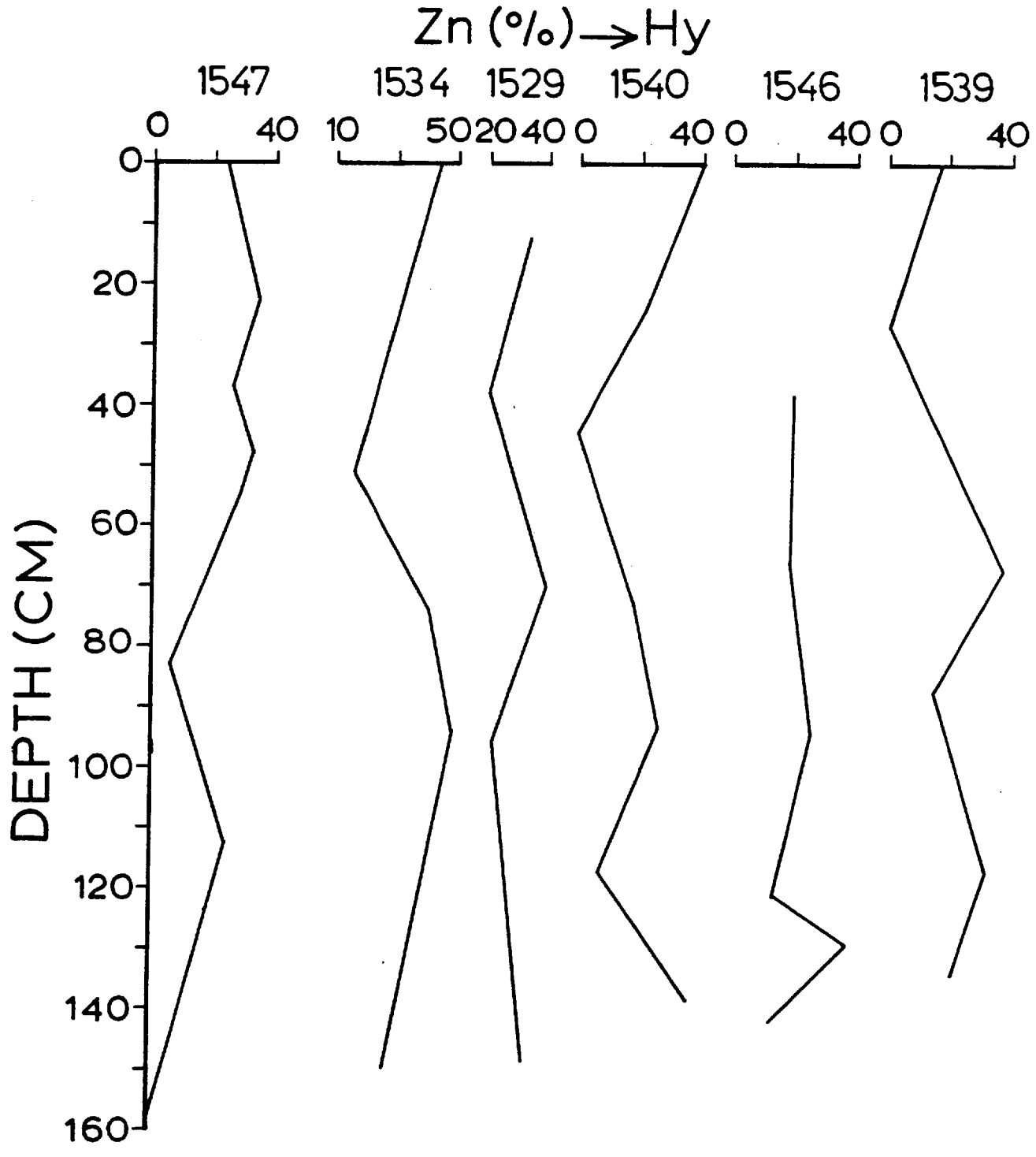

Figure 2.72: The distribution of the hydroxylamine HCl-soluble Zn in fracture zone sediment cores, expressed as a percentage of the total Zn concentrations.

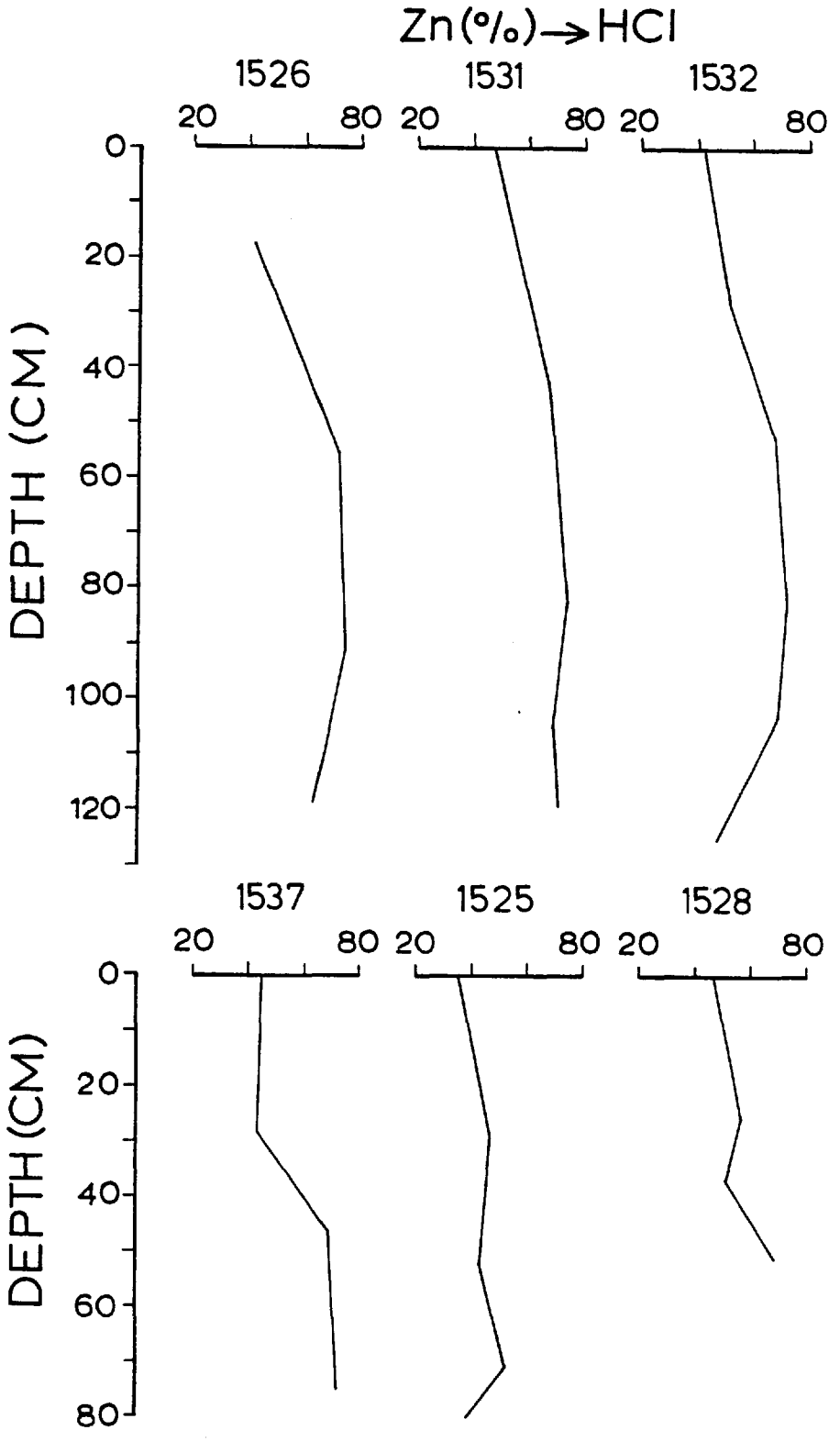

Figure 2.73: The distribution of the HCl-soluble Zn in fracture zone sediment cores expressed as a percentage of the total Zn concentration.

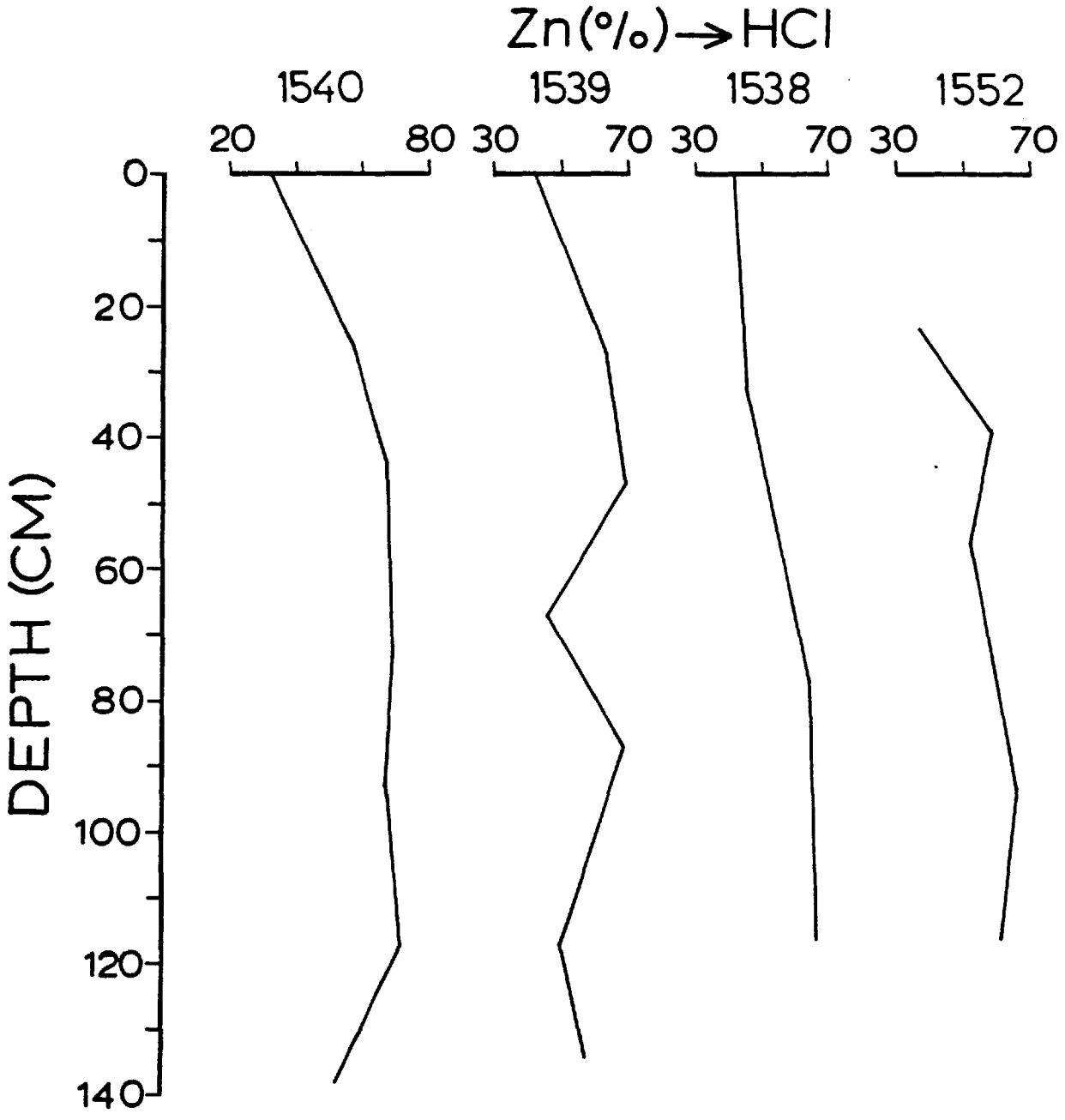

Figure 2.74: The distribution of the HCl-soluble Zn in fracture zone sediment cores expressed as a percentage of the total Zn concentration.

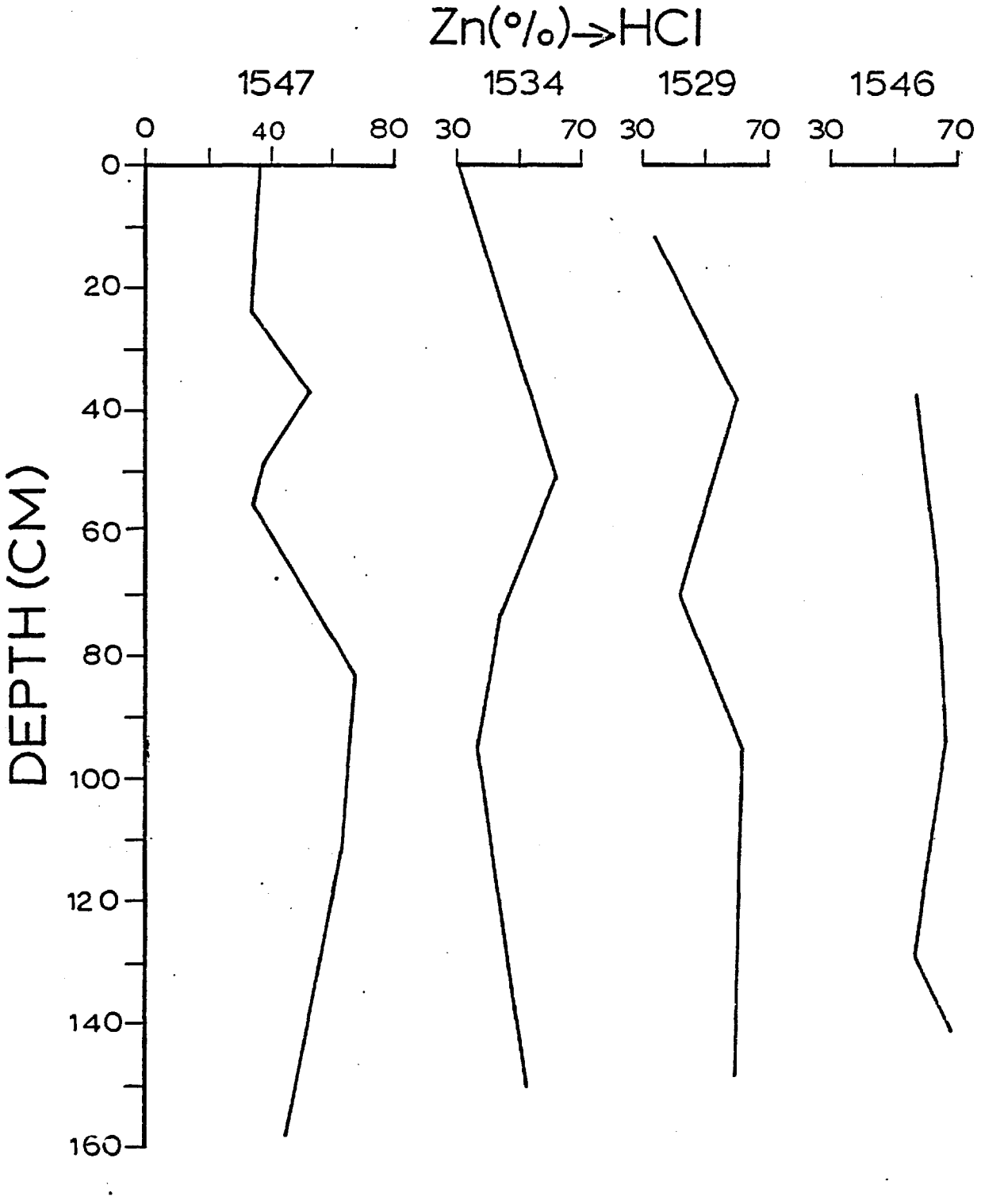

Figure 2.75: The distribution of the HCl-soluble Zn in fracture zone sediment cores expressed as a percentage of the total Zn concentration.

proportion of Zn present in the HCl-soluble fraction either remains constant throughout the rest of the sediments in many cores (SH 1526, SH 1532, SH 1525, SH 1537, SH 1529, SH 1540, SH 1539), or it continues to increase slightly down to about 90 cm (SH 1538, SH 1546, SH 1552, SH 1531). The core SH 1547 exhibits a rather peculiar vertical variation of the HCl-soluble Zn. From 0 to 30 cm it decreases, between 25 and 80 cm varies from 34 to 68% of the total amount, showing a tendency to increase with depth, and from 80 cm down to 158 it is reduced steadily.

The distribution of Zn between the acid-reducible and the HCl-soluble fraction in the surface and buried sediments from the fracture zone is similar to its distribution in other sediments such as the Iceland-Area surface sediments, the Reykjanes Ridge crest sediments (Horowitz, 1974), the Atlantic basal sediments (Horowitz and Cronan, 1976), the East Pacific Rise basal metalliferous sediments (Cronan, 1976a), and the Bermuda Rise sediments. An exception in the case of the latter sediments is the Upper Cretaceous zeolitic clays, where Zn is associated with the fraction soluble in the acid-reducing agent solution rather than in the HCl (see Table 2.9). However, there are some differences in the distribution of Zn between the other fractions. The acetic-acid soluble fraction of the surface and buried sediments from the fracture zone contains much more Zn than that found in the same fraction of the Iceland-Area surface sediments, the Reykjanes Ridge crest sediments (Horowitz, 1974), and the Atlantic basal sediments (Horowitz and Cronan, 1976).

Table 2.9: Comparison of the average partitioning of Zn in surface and buried sediments from the fracture zone with other sediments. All data expressed as percentages of the total Zn concentration.

	Acetic acid leach	Acid-reducing agent leach	Hydrochloric acid leach	Residue
1	30	25	44	1
2	19	22	58	1
3	6	7	56	31
4	6	13	60	21
5	5	20	49	26
6		26	66	8
7		39	55	6
8		36	60	4
9		55	42	3
10		14	67	19

1. This study: all surface sediments.
2. This study: all buried sediments.
3. Horowitz (1974): Iceland-Area surface sediments.
4. Horowitz (1974): Reykjanes Ridge crest surface sediments.
5. Horowitz and Cronan (1976): Atlantic basal sediments.
6. Chester et al (1976): Quaternary calcareous clays.
7. Chester et al (1976): Pliocene (?)/Miocene (?) clays.
8. Chester et al (1976): Middle Eocene zeolitic clays.
9. Chester et al (1976): Upper Cretaceous zeolitic clays.
10. Chester et al (1976): Cretaceous zeolitic clays.

2.5.7 Copper

On average, the largest portion of the total Cu in the surface sediments (~44%) is leached by the acetic acid solution. This suggests that this element is associated with carbonates or is adsorbed onto mineral surfaces. About 34% of Cu is concentrated in the hydroxylamine HCl-soluble fraction, while about 21% was found soluble in HCl. Only a small amount of Cu (~1%) is associated with the HCl-insoluble residue.

Considerable differences in the average partition chemistry of Cu have been observed between the surface and the buried sediments. In comparison with the surface sediments, less Cu is associated with the acetic acid (~25%) and the hydroxylamine HCl (~32%)-soluble fractions of the buried sediments, whereas the proportion of Cu dissolved in HCl is higher (~42%).

The vertical percentage variations of Cu present in the three separated fractions are rather similar to those found for Zn and Fe. In almost all the cores examined there is a continuous reduction of the proportion of Cu which is soluble in acetic acid from the top down to the base of the cores (see Figures 2.76, 2.77). In general, the proportion of the acid-reducible Cu decreases from 0 down to about 50 cm (see Figures 2.78, 2.79), while below this depth some differences among the individual cores were found. The cores can be classified into two groups: in the cores of the first group (SH 1531, SH 1533, SH 1538, SH 1539 and SH 1540) the percentage of the acid-reducible Cu remains constant below 50 cm, while in the cores of the second group (SH 1525, SH 1529, SH 1534 and SH 1546) it continues to decrease down most of the length of the cores. As in the case of Fe, a

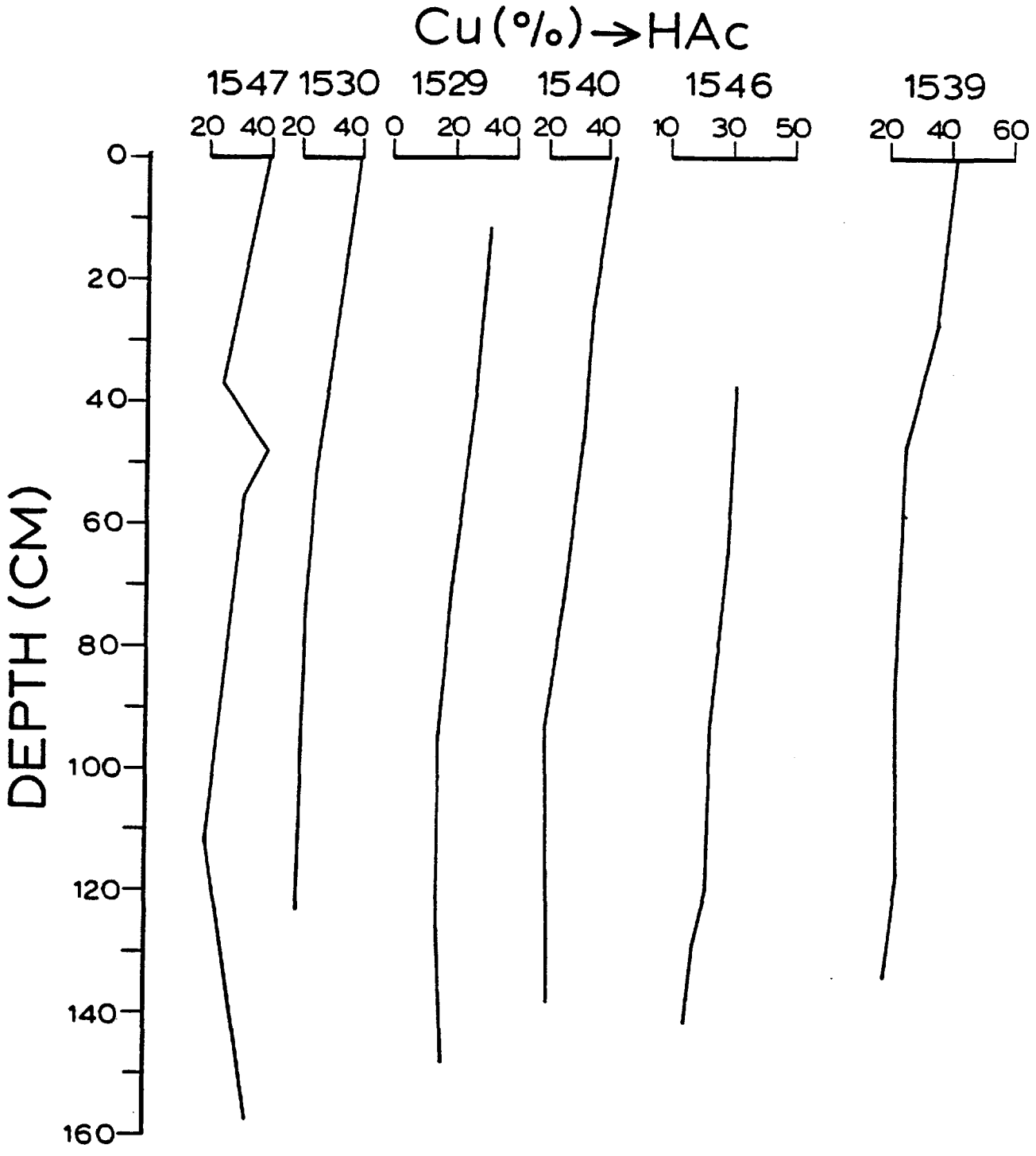

Figure 2.76: The distribution of the acetic acid-soluble Cu in fracture zone sediment cores expressed as a percentage of the total Cu concentration.

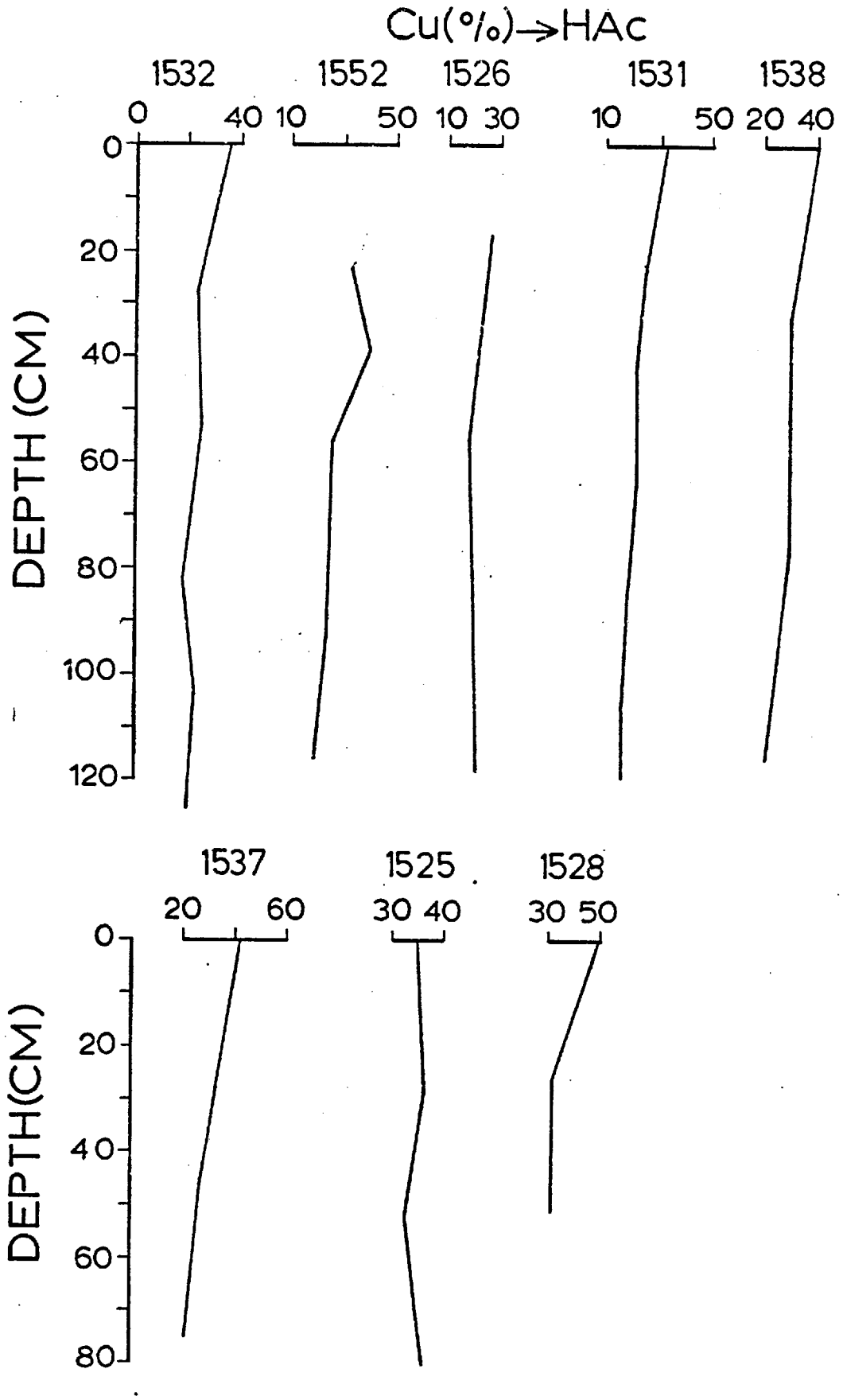

Figure 2.77: The distribution of the acetic acid-soluble Cu in fracture zone sediment cores expressed as a percentage of the total Cu concentration.

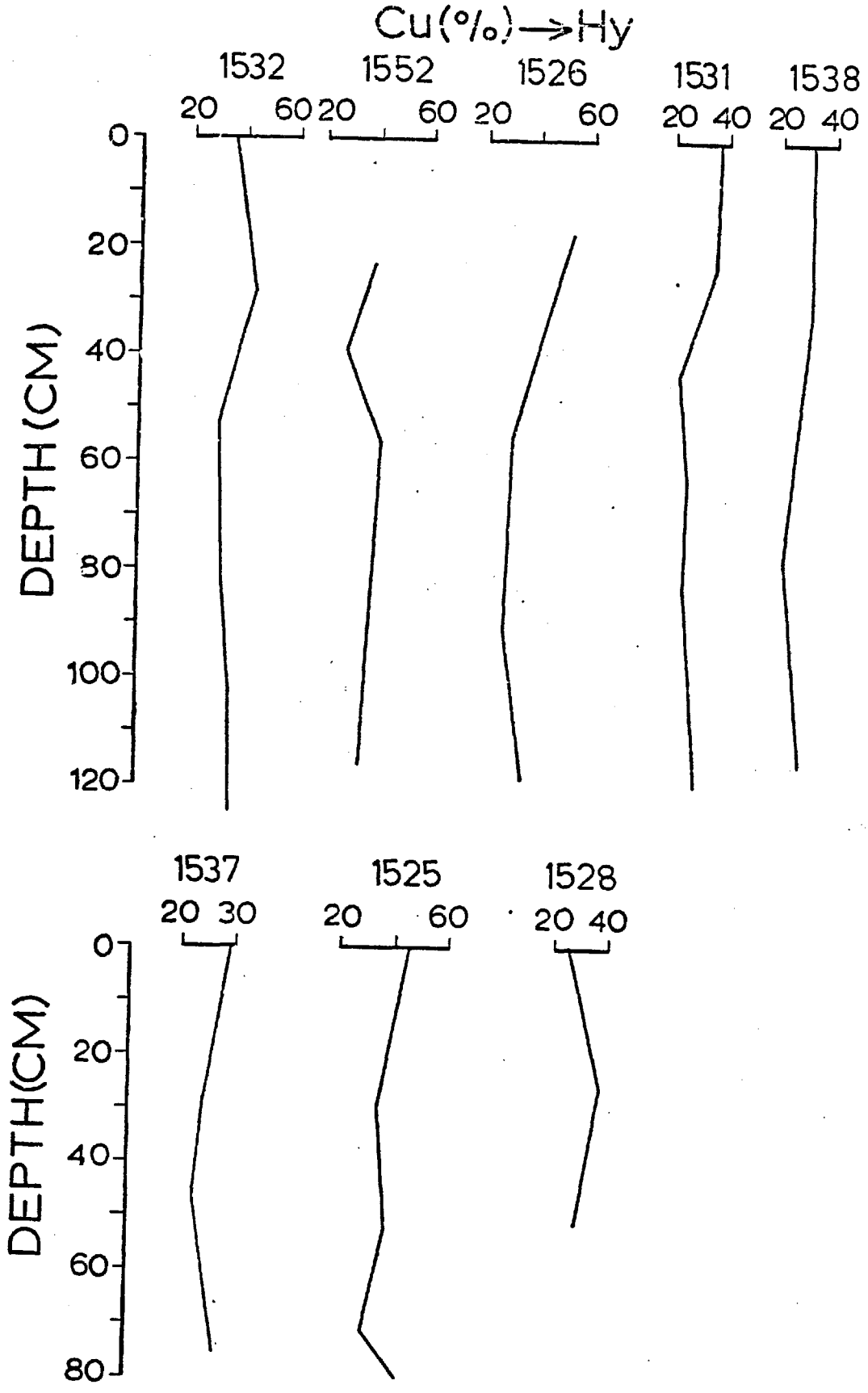

Figure 2.78: The distribution of the hydroxylamine HCl-soluble Cu in fracture zone sediment cores expressed as a percentage of the total Cu concentration.

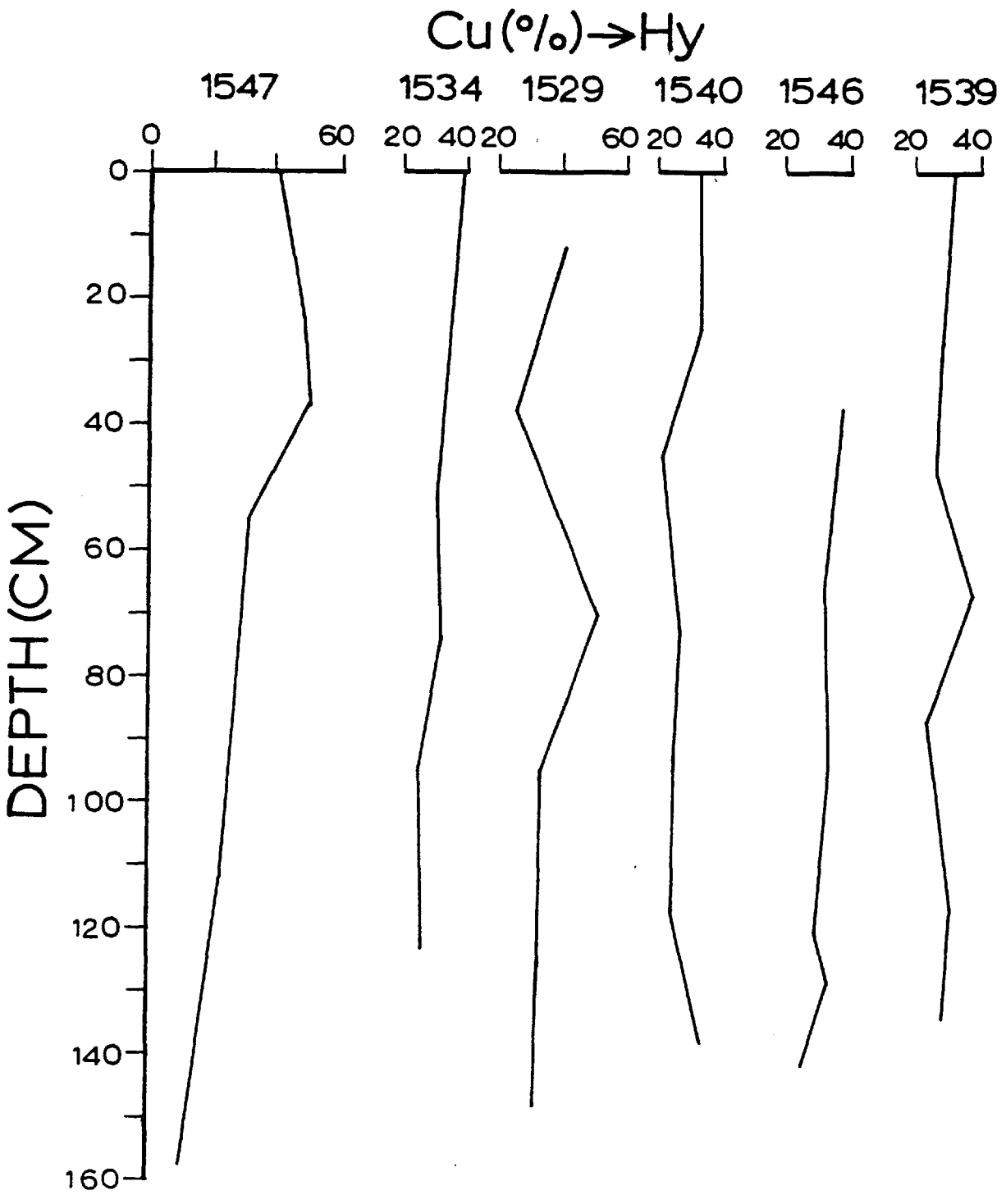

Figure 2.79: The distribution of the hydroxylamine HCl-soluble Cu in fracture zone sediment cores expressed as a percentage of the total Cu concentration.

continuous increase of the proportion of Cu which is soluble in HCl from the top down to the bottom of almost all the cores was found (see Figures 2.80, 2.81 and 2.82).

The average geochemical partition data of Cu in the surface sediments are similar to those reported for most Bermuda Rise sediments (Chester et al, 1976) (see Table 2.10). However, they are different from those found in the Iceland-Area surface sediments, Reykjanes Ridge crest sediments (Horowitz, 1974), the Atlantic basal sediments (Horowitz and Cronan, 1976) and the East Pacific Rise basal metalliferous sediments (Cronan, 1976a). In these sediments, Cu is more concentrated in the HCl-soluble fraction than in any of the other fractions. This geochemical behaviour of Cu has been found in the buried sediments of the present study.

2.5.8 Aluminium

In the surface sediments aluminium is strongly associated, on average, with the HCl-soluble fraction (about 52% of the total amount), which suggests that this element occurs in Fe-oxides and/or aluminosilicates. Because no obvious correlation between Al and Fe has been found, Al is probably largely associated with the clay minerals rather than the Fe-oxides of the sediments. A significant amount of Al is present in the HCl-insoluble detrital phases ($\sim$19%) indicating that Al is located in the lattice structure of the more resistant aluminosilicates. Aluminium is also affected by the acetic acid and the acid-reducing agent solution. Of the total Al, about 16% was found to be leached by the former and about 13% by the latter solution.

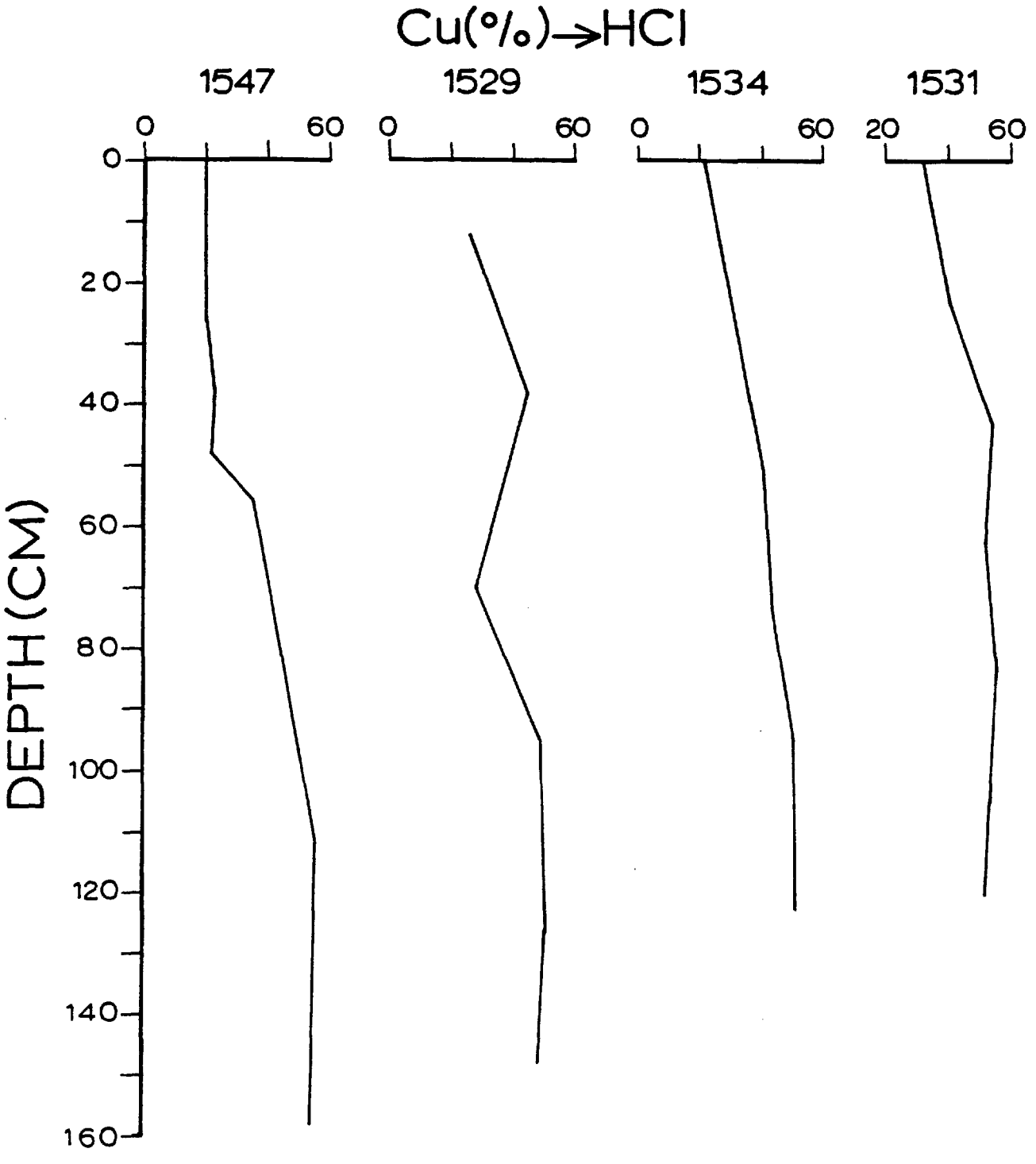

Figure 2.80: The distribution of the HCl-soluble Cu in fracture zone sediment cores expressed as a percentage of the total Cu concentration.

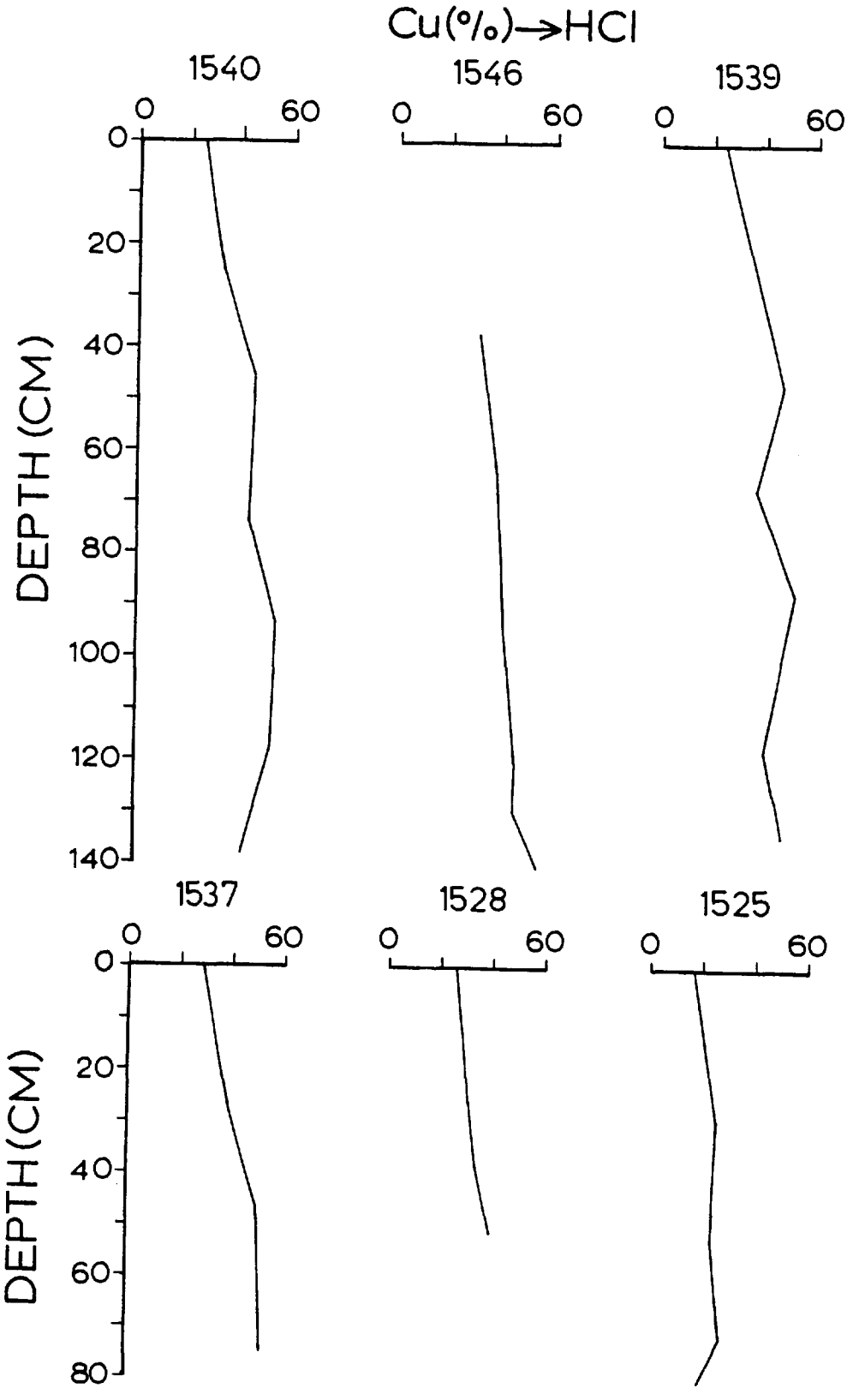

Figure 2.81: The distribution of the HCl-soluble Cu in fracture zone sediment cores expressed as a percentage of the total Cu concentration.

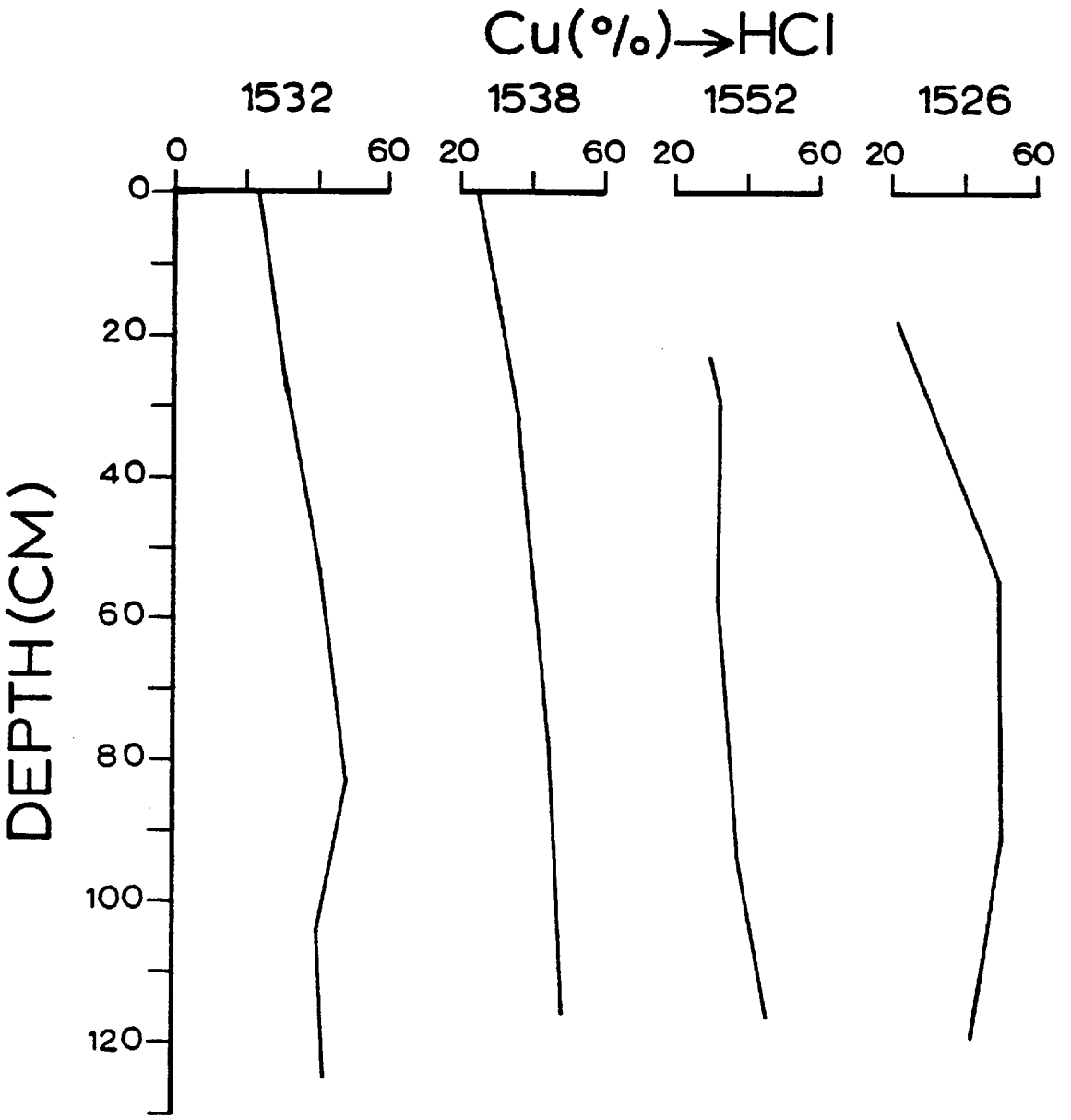

Figure 2.82: The distribution of the HCl-soluble Cu in fracture zone sediment cores expressed as a percentage of the total Cu concentration.

Table 2.10: Comparison of the average partitioning of Cu in surface and buried sediments from the fracture zone with other sediments. All data expressed as percentages of the total Cu concentrations.

	Acetic acid leach	Acid-reducing agent leach	Hydrochloric acid leach	Residue
1	44	34	21	1
2	25	32	42	1
3	7	9	60	24
4	6	33	42	19
5	6	18	56	20
6		56	22	22
7		52	35	13
8		89	10	1
9		80	18	2
10		9	78	13

1. This study: all surface sediments.
2. This study: all buried sediments.
3. Horowitz (1974): Iceland-Area surface sediments.
4. Horowitz (1974): Reykjanes Ridge crest surface sediments.
5. Horowitz and Cronan (1976): Atlantic basal sediments.
6. Chester et al (1976): Quaternary calcareous clays.
7. Chester et al (1976): Pliocene (?)/Miocene (?) clays.
8. Chester et al (1976): Middle Eocene zeolitic clays.
9. Chester et al (1976): Upper Cretaceous zeolitic clays.
10. Chester et al (1976): Cretaceous (?) zeolitic clays.

In the buried sediments the HCl extraction treatment removed more Al (~55% of the total amount) than any other fraction. The amount extracted is higher than the Al content of this fraction in the surface sediments. The contribution of the Al contained in the HCl-insoluble residue to the total sediment Al is higher in the subsurface (~ 22%) than in the surface sediments. This suggests the presence of more resistant minerals, and therefore probably a greater amount of crystalline clay minerals, in the buried sediments. In contrast, the amounts of Al removed after leaching of the buried sediments with acetic acid and acid-reducing agent solutions are lower than those removed from the surface sediments; these amounts are approximately equal.

In both the surface and the subsurface sediments, the percentage of Al associated with the HCl-insoluble residue is much lower than that associated with the same fraction of the Iceland-Area and the Reykjanes Ridge crest surface sediments (Horowitz, 1974), the Atlantic basal sediments (Horowitz and Cronan, 1976) (see Table 2.11), and the East Pacific Rise basal metalliferous sediments (Cronan, 1976a). The fracture zone surface sediments contain more Al in their HCl-soluble fraction than the Atlantic basal sediments and less than the Iceland-Area, the Reykjanes Ridge crest surface sediments and the East Pacific Rise basal metalliferous sediments. In contrast to the surface sediments, the aluminium contribution made by the HCl-soluble fraction of the buried sediments is higher than that of the Iceland-Area surface sediments, the Atlantic basal sediments and the East Pacific Rise basal metalliferous sediments. The percentage of Al found in the HCl-soluble fraction of the buried sediments is lower than that in the same fraction of the Reykjanes Ridge crest sediments. The amounts of Al

Table 2.11: Comparison of the average partitioning of Al in surface and buried sediments from the fracture zone with other sediments. All data expressed as percentages of the total Al concentrations.

	Acetic acid leach	Acid-reducing agent leach	Hydrochloric acid leach	Residue
1	16	13	52	19
2	11	12	55	22
3	2	3	48	47
4	2	3	67	28
5	2	6	38	52
6			50	45

1. This study: all surface sediments.
2. This study: all buried sediments.
3. Horowitz (1974): Iceland-Area surface sediments.
4. Horowitz (1974): Reykjanes Ridge crest surface sediments.
5. Horowitz and Cronan (1976): Atlantic basal sediments.
6. Cronan (1976): East Pacific Rise basal metalliferous sediments.

soluble in the acetic acid and the acid-reducing agent solutions are much higher in the fracture zone sediments (surface and buried) than the Iceland-Area and the Reykjanes Ridge crest sediments (Horowitz, 1974), and the Atlantic basal sediments (Horowitz and Cronan, 1976).

It is worthy of note that generally there is a gradual increase of the hydroxylamine HCl-insoluble residue with depth in the cores (see Figures 2.83, 2.84 and 2.85), which suggests a corresponding increase of the proportion of more resistant phases.

To summarize, the following partition geochemical variations have been found to be associated with burial:

1. The proportions of Fe, Zn and Cu which are associated with the acetic acid-soluble fraction decrease steadily with increasing depth from the top down to the base of almost all the fracture zone cores examined here.

2. The percentage of the acetic acid soluble Mn increases from 0 down to 40 cm depth, which is contrary to the case of Fe, Zn and Cu. Below this depth it remains constant throughout the sediments.

3. In the upper 40 cm of the sediments, the percentage of Fe, Mn, Ni, Cu and Zn which is found in the acid-reducible fraction

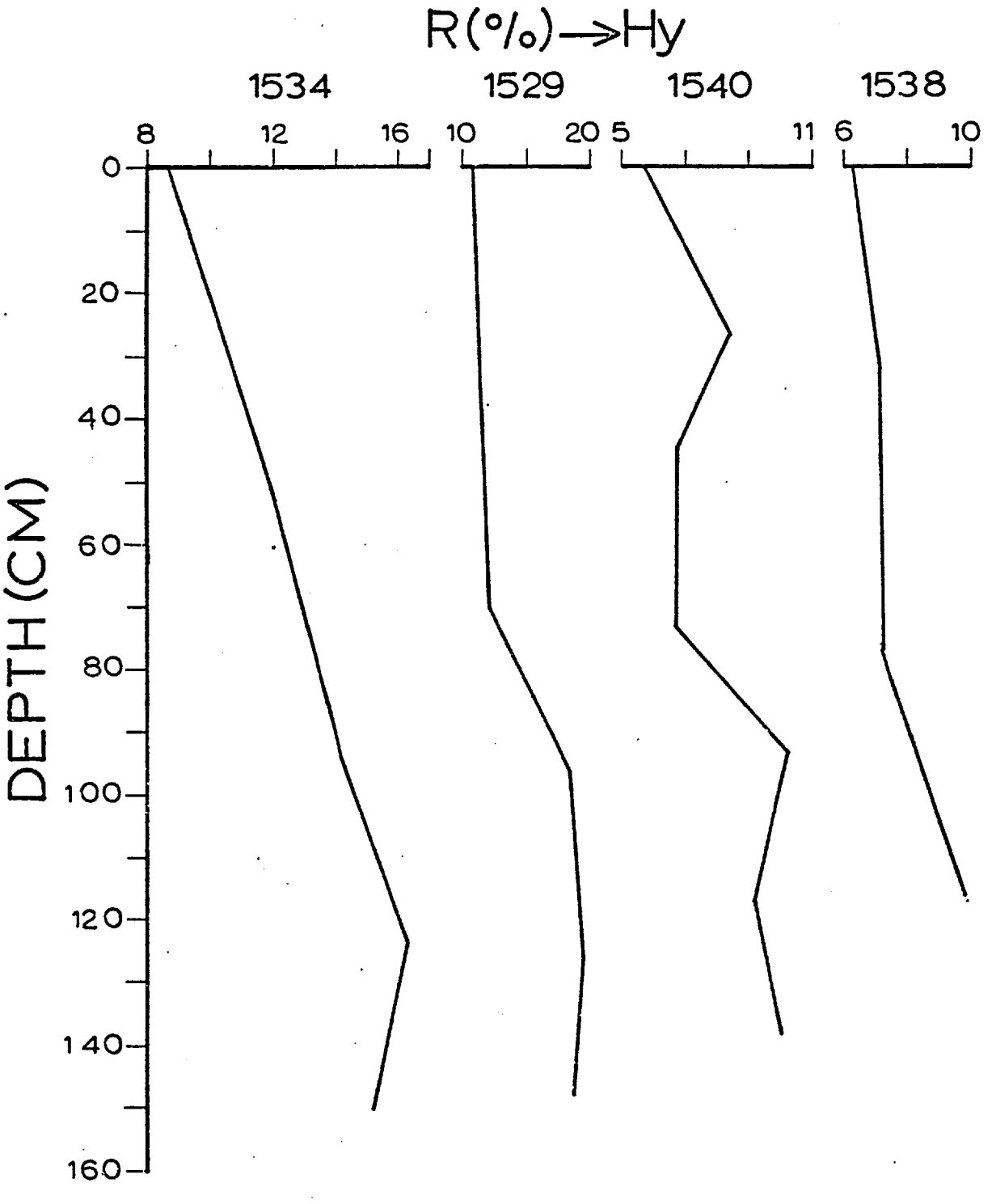

Figure 2.83: The distribution of the hydroxylamine HCl-insoluble residue in fracture zone sediment cores.

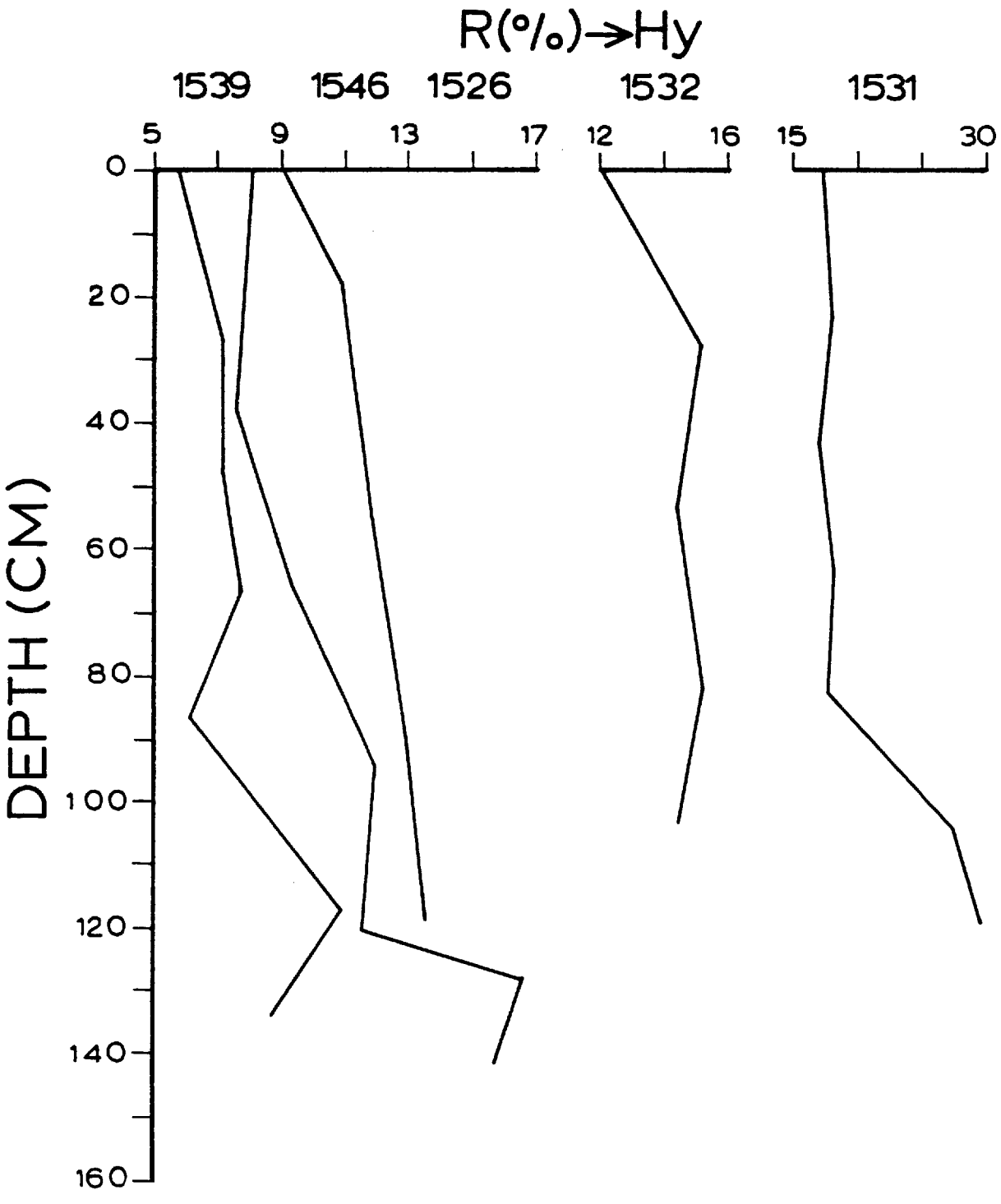

Figure 2.84: The distribution of the hydroxylamine HCl-insoluble residue in fracture zone sediment cores.

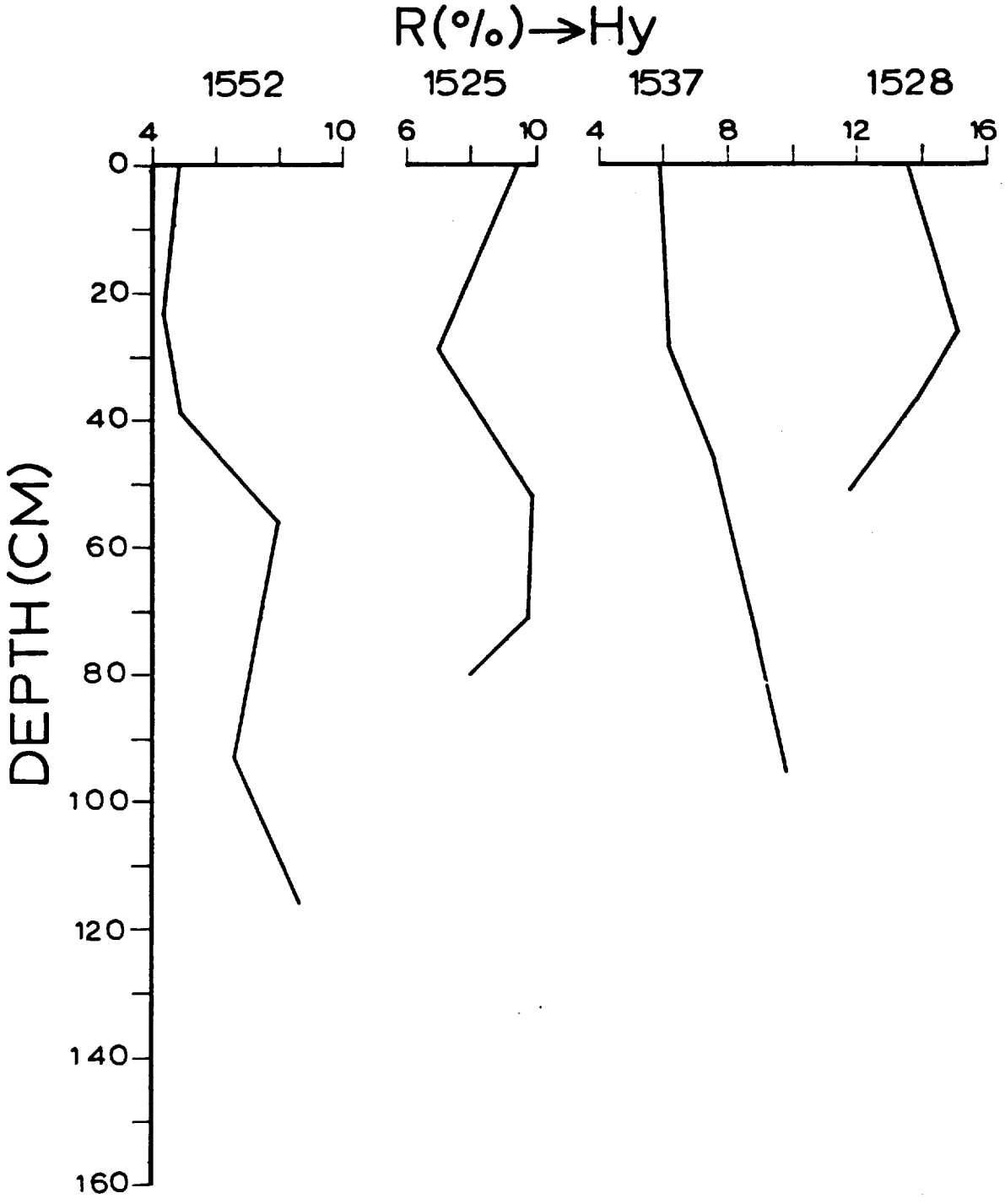

Figure 2.85: The distribution of the hydroxylamine HCl-insoluble residue in fracture zone sediment cores.

varies with depth of burial in a manner similar to the variations of Fe, Zn and Cu in the acetic acid-soluble fraction.

4. The HCl-soluble fraction is steadily enriched in Fe, Mn, Ni, Zn and Cu with depth.

5. There is a gradual increase of the hydroxylamine HCl-insoluble residue with increasing depth in the cores.

2.6 EFFECT OF DEPTH OF WATER IN THE DISTRIBUTION OF METALS AMONG PHASES

2.6.1 Introduction

One of the main aims of the present study is to investigate the role of calcium carbonate dissolution in the distribution of metals among the various phases of the sediments. The cores examined were taken from a variety of water depths (2300 m - 3800 m) and the samples have presented an opportunity to examine the possibility that metals taken up from the sea water by calcareous organisms can be transferred to other phases after the dissolution of $CaCO_3$ at greater depths. To examine this possibility the selective partition geochemical data of the surface sediments are evaluated in relation to the water depth of the stations.

2.6.2 Dissolution of $CaCO_3$ in the Sea Water

Since the earliest oceanographic investigations (Murray and Renard, 1891) it has been recognised that the distribution of carbonate sediments on the ocean floor is related to water depth. Sediments from oceanic areas such as the rises or guyots and sea mounts, have a high calcium carbonate content, most of which is biogenic in origin, arising from pelagic organisms. By contrast, less calcium carbonate occurs in the sediments from abyssal deeps.

Variability of carbonate content and its relationship with water depth is found to reflect the dissolution of $CaCO_3$ with increasing depth. Moreover, a sharp transition exists between a recognised horizon

of high calcium carbonate content and that of deeper waters depleted in calcite. A characteristic depth exists below which no carbonate sediments occur. The rate of supply of calcitic material is another important factor in the distribution of marine carbonate sediments. The water depth at which dissolution and supply rates of carbonates are equal is called the calcium carbonate compensation depth (CCD). This critical depth is established as a major oceanographic parameter and has been the subject of detailed palaeontological and chemical study. Observed CCD values vary in the world oceans, ranging from 3500 m to about 5500 m. It is understood that in the high productivity areas such as the equatorial Pacific the rate of supply of calcareous organisms is increased in comparison with other oceanic areas.

In order to study the effect of dissolution on the distribution of carbonate marine sediments, Peterson (1966) attempted direct measurement of the rates of dissolution at various depths. He exposed calcite spheres, cut from optical calcite, in sea water in the Pacific ($18^{o}49'N$, $168^{o}31'W$, 1100 km south of Honolulu) at intervals of 70 m down to a depth of 5000 m. After four months the complete profile of samples was recovered and the loss due to dissolution was determined gravimetrically for each sample. It was found that in the upper water column the spheres showed no weight loss; at greater depths a consistent but rather small loss of weight was observed. Below 3700 m depth the calcite spheres showed an abrupt increase in their loss of weight. This was explained as the result of a sharp increase in the rate of dissolution of calcium carbonate below this depth.

A similar attempt has been made by Berger (1967) who used samples of foraminiferal sediment taken from the East Pacific Rise.

He used three series of samples, one of which was washed in buffered, hot, demineralised water and the other two were boiled in buffered solution of 10% hydrogen peroxide. The purpose of the first washing was to remove any small particles fixed on the foraminiferal tests which could have been removed by water currents rather than by solution. The hydrogen peroxide removed any trace of organic material so that a study could be made of the effect of dissolution in the absence of any protecting coating. The samples were placed at various depths over a complete vertical profile (over 5000 m) in the central Pacific.

After four months, all the series of samples were recovered and the loss of weight by solution during that period was calculated. It was found that the loss of weight of all the series of samples increased with increasing depth in the water column; the weight loss of the hydrogen peroxide-treated samples being higher than that of the untreated samples. Specimens from 3000 m down to 5000 m showed a significant difference in weight loss. The specimen tests used in this experiment were originally recovered from sediments at a depth of 3190 m (EPR $22^{\circ}07'S$, $115^{\circ}10'W$). The sharp increase in weight loss observed at depths greater than 3000 m was explained by the reaction of the samples to displacement below the depth of origin. A marked increase in weight loss observed at 5000 m was attributed to the undersaturation of the sea water with respect to calcium carbonate.

The depth of the rapid increase of the rate of dissolution of $CaCO_3$, or the depth below which the effects of the calcite dissolution become easily recognised (disappearance of species of forams and coccoliths from the assemblages of calcareous microfossils) was termed

"lysocline" (Berger, 1968; Berger, 1971). Although the existence of the lysocline is universally accepted, its origin is still an open question (Morse and Berner, 1972; Ben Yaakov et al, 1974; Berner, 1974; Edmond, 1974).

Benthonic activity as well as physical oceanographic parameters such as the changes in the rate of bottom water flow have been considered to be important factors in the existence of the lysocline (Menard, 1964; Berger, 1970; Edmond, 1974). Attempts have also been made by Morse and Berner (1972), Ben Yaakov et al (1974) and by other workers to explain the existence of the lysocline in terms of thermodynamics.

2.6.3 Results

To study the possible effect of the depth of water on the distribution of the elements among the different phases of the surface sediments, the proportion of the elements in each fraction was plotted against depth of water. Any attempt to use the buried sediments in examining the possible effect of the dissolution of $CaCO_3$ on the partitioning of the elements would result in misleading conclusions due to the post-depositional changes of the chemical diagenesis, and therefore these sediments have not been used in this regard.

2.6.3a Manganese

A negative correlation between the acetic acid-soluble Mn and the depth of water was found (see Figure 2.86). By contrast, there is a positive correlation between the hydroxylamine HCl-soluble Mn and the depth of water (see Figure 2.87).

2.6.3b Iron

The proportional variations of the acetic acid-soluble and the acid-reducible Fe with depth are similar to those of Mn (see Figures 2.88 and 2.89).

2.6.3c Nickel

The proportion of Ni which is present in the acid-reducible fraction increases, whereas that soluble in HCl decreases with increasing depth of water (see Figures 2.90 and 2.91).

2.6.3d Zinc

There is a strong positive correlation between the hydroxylamine HCl-soluble Zn and the depth of water (see Figure 2.92), while a possible negative correlation between the HCl-soluble Zn and the depth of water is not very clear (see Figure 2.93).

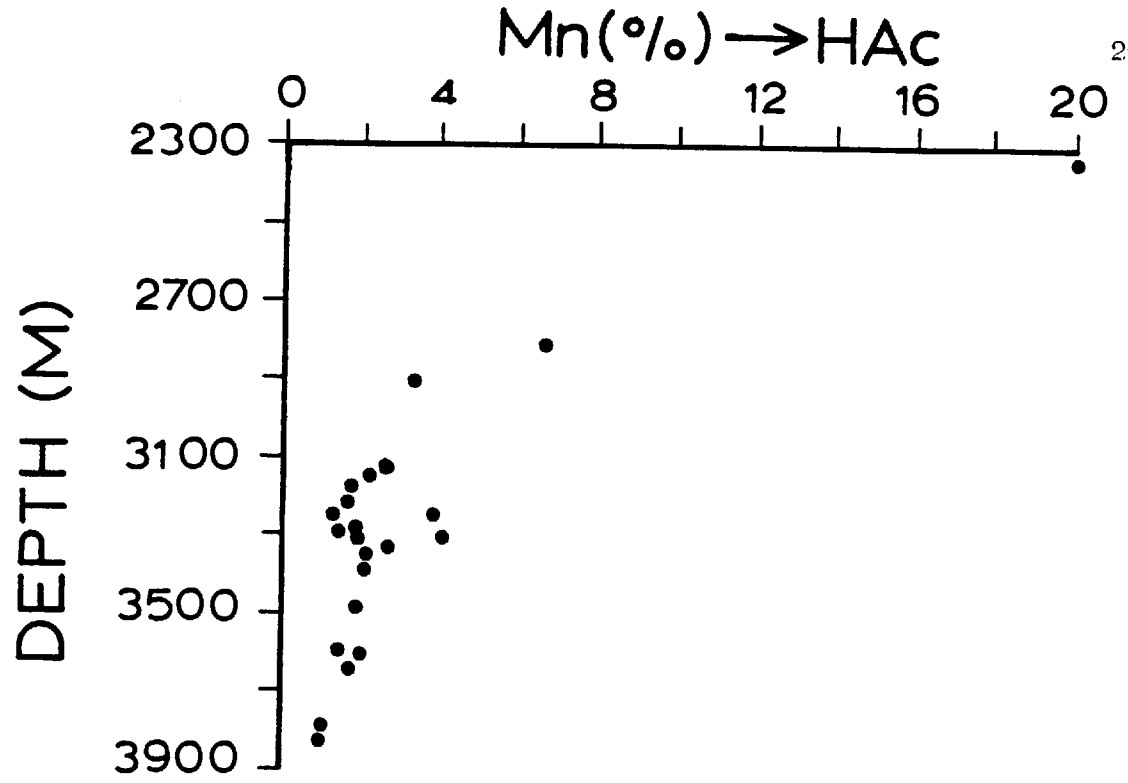

Figure 2.86: Scatter plot showing the negative correlation between the acetic acid-soluble Mn (expressed as a percentage of the total Mn concentration) in the surface sediments, and the water depth.

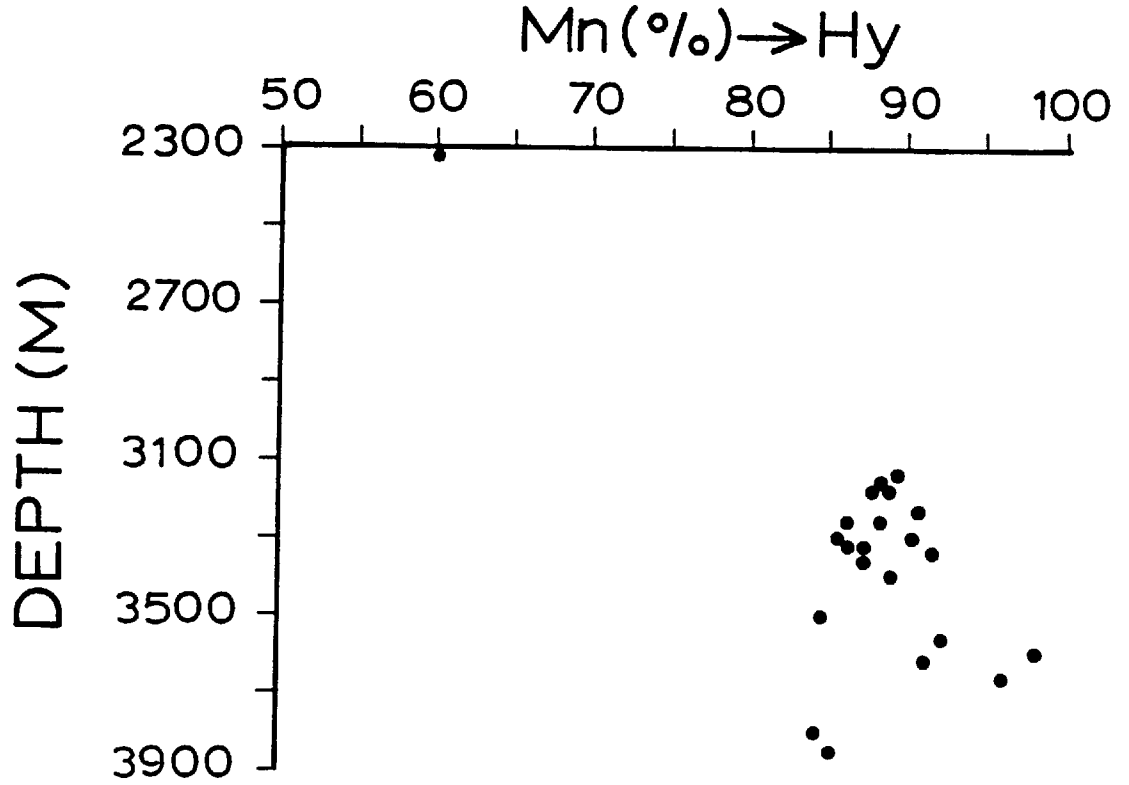

Figure 2.87: Scatter plot showing the positive correlation between the hydroxylamine HCl-soluble Mn (expressed as a percentage of the total Mn concentration) in the surface sediments, and the water depth.

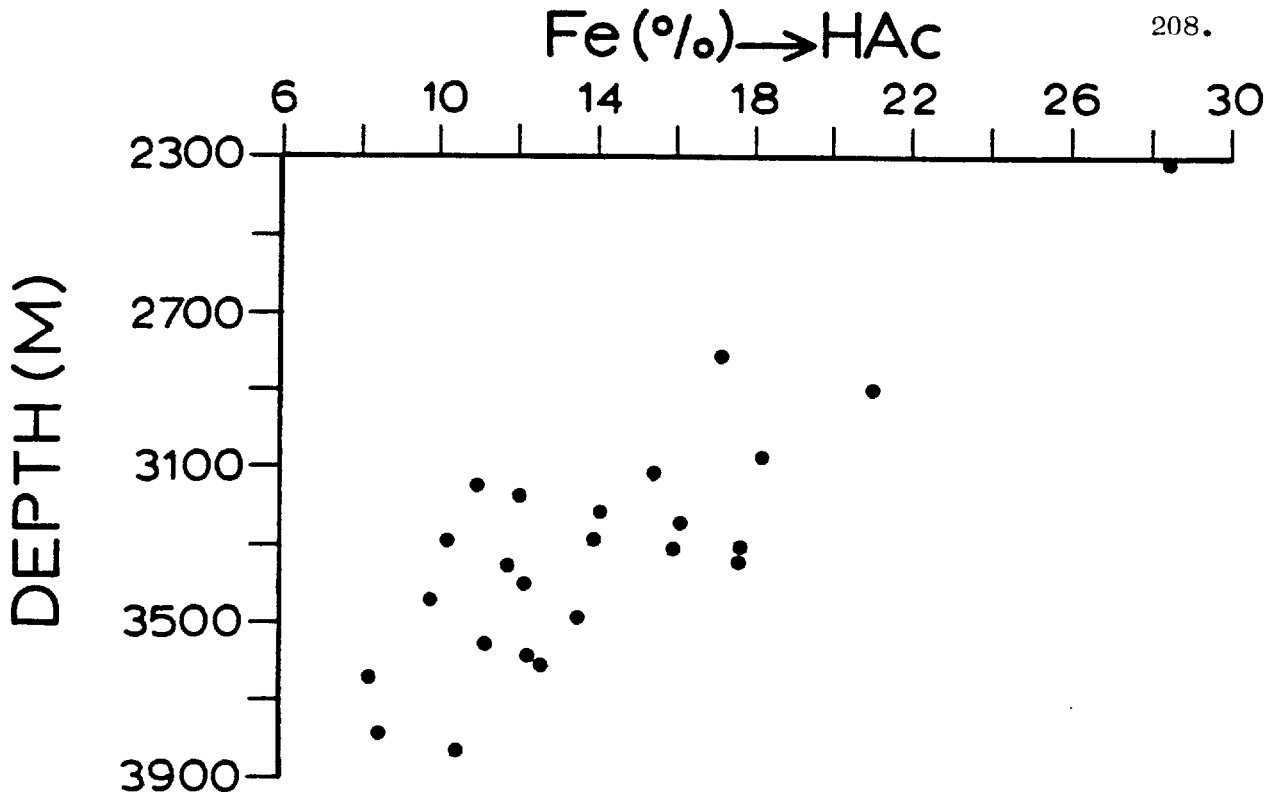

Figure 2.88: Scatter plot showing the negative correlation between the acetic acid-soluble Fe (expressed as a percentage of the total Fe concentration) in the surface sediments, and the water depth.

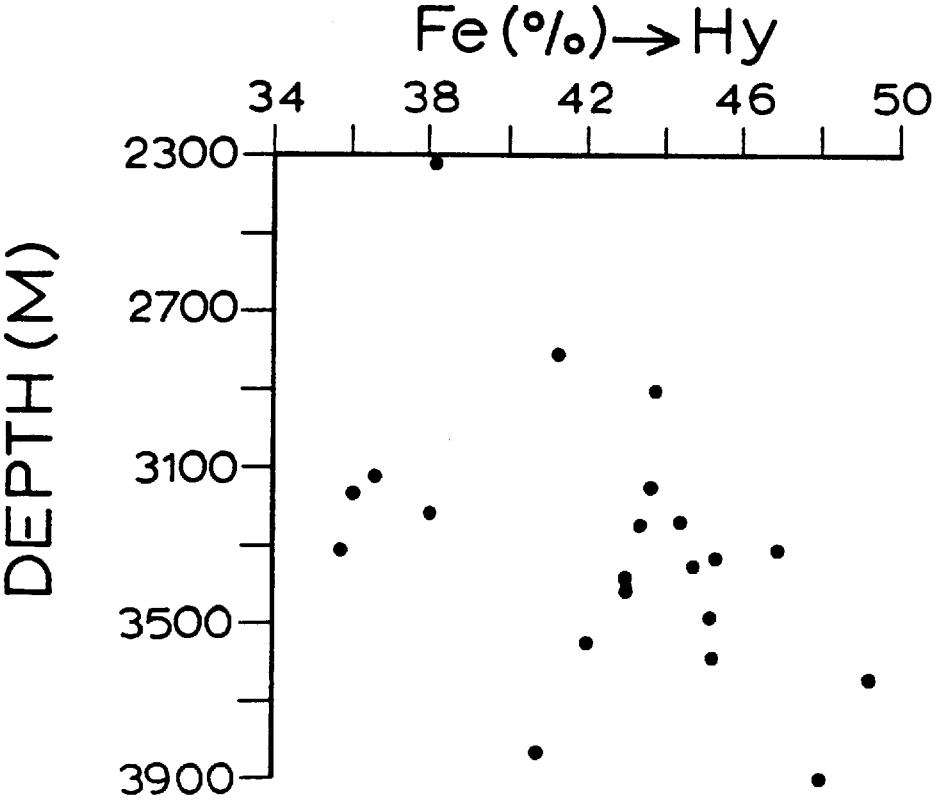

Figure 2.89: Scatter plot showing the positive correlation between the hydroxylamine HCl-soluble Fe (expressed as a percentage of the total Fe concentration) in the surface sediments, and the water depth.

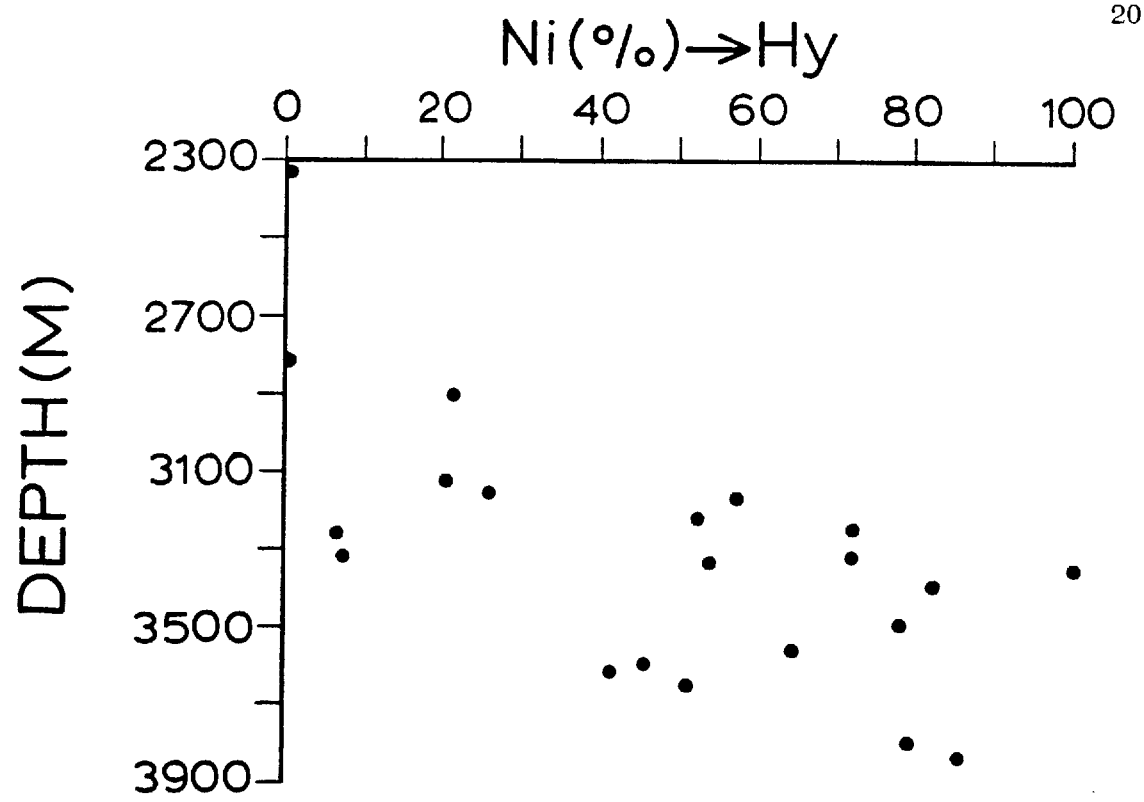

Figure 2.90: Scatter plot showing the positive correlation between the hydroxylamine HCl-soluble Ni (expressed as a percentage of the total Ni concentration) in the surface sediments, and the water depth.

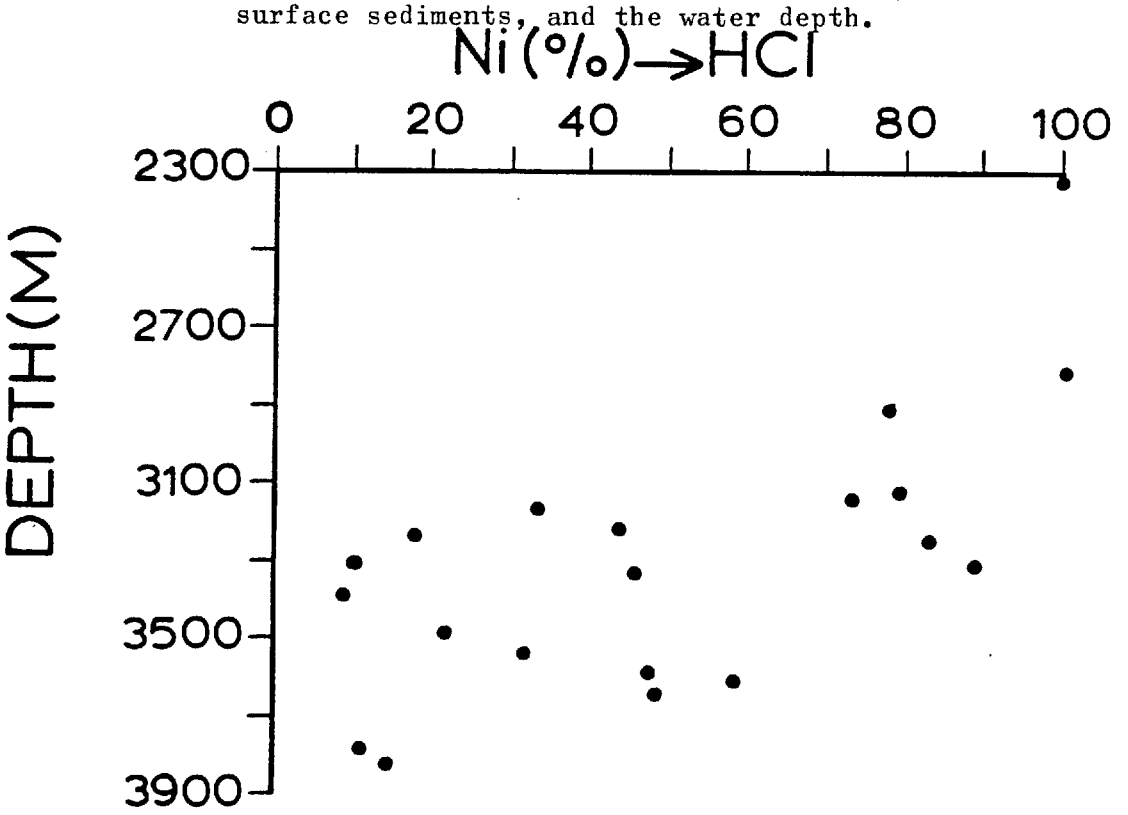

Figure 2.91: Scatter plot showing the negative correlation between the HCl-soluble Ni (expressed as a percentage of the total Ni concentration) in the surface sediments, and the water depth.

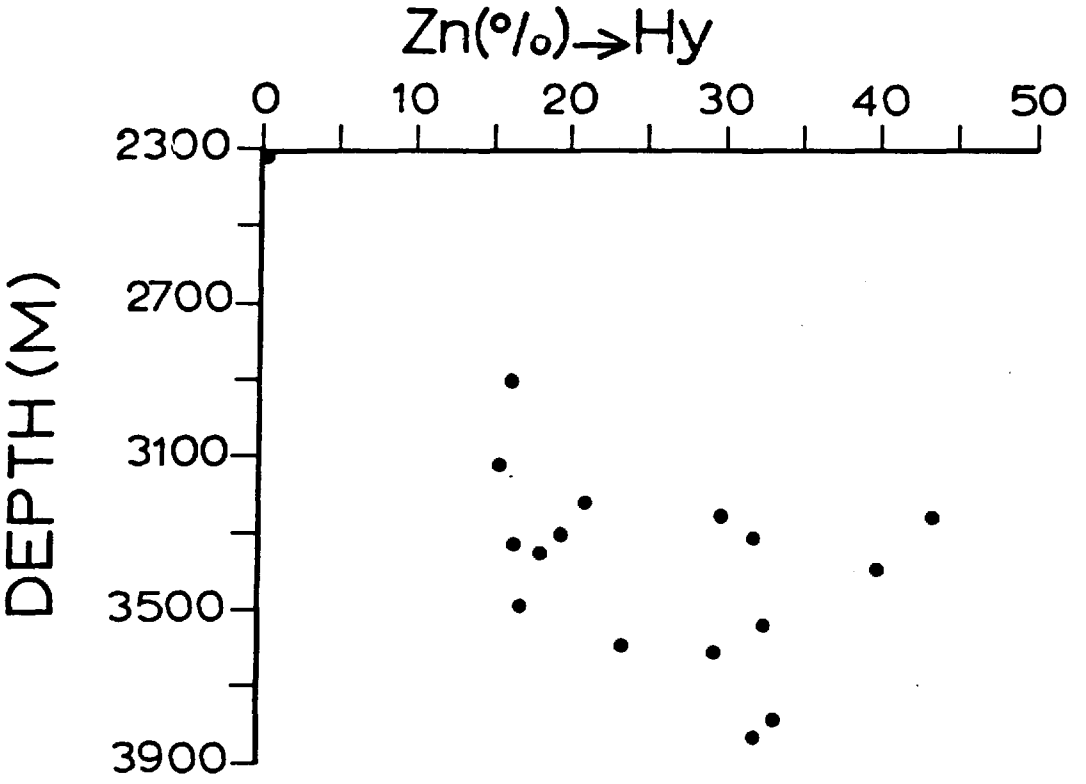

Figure 2.92: Scatter plot showing the positive correlation between the hydroxylamine HCl-soluble Zn (expressed as a percentage of the total Zn concentration) in the surface sediments, and the water depth.

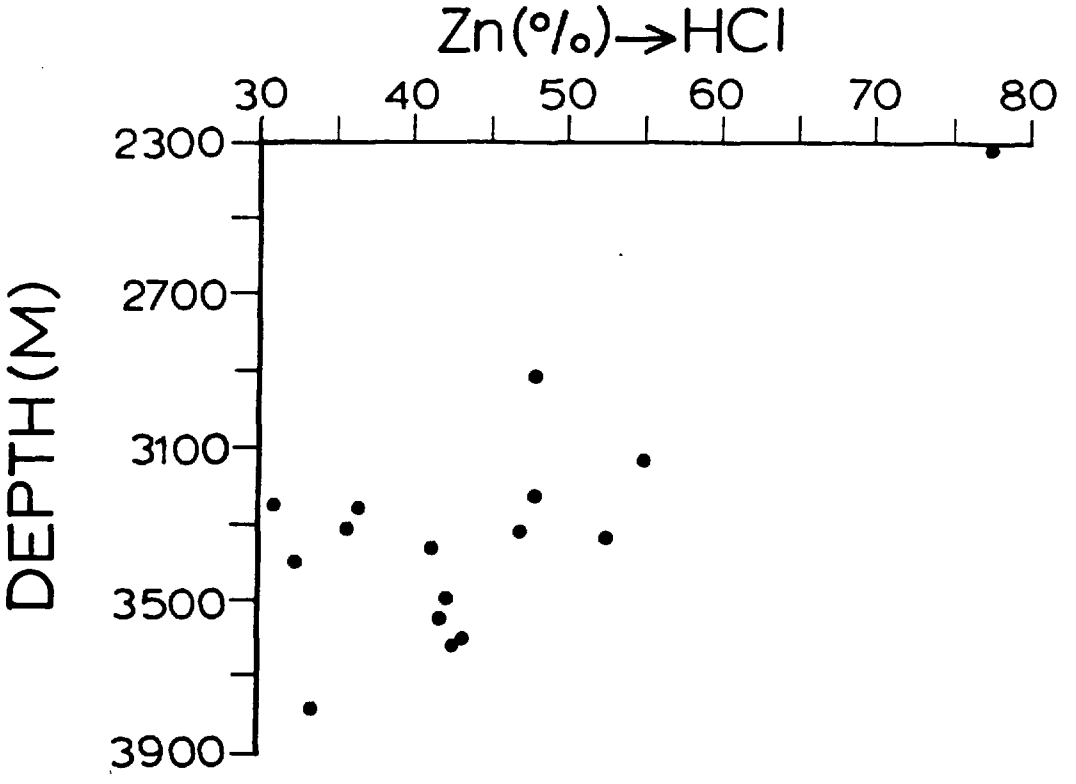

Figure 2.93: Scatter plot showing the negative correlation between the HCl-soluble Cu (expressed as a percentage of the total Cu concentration) in the surface sediments, and the water depth.

2.6.3e Copper

The effect of the water depth on the distribution of Cu between the chemically separated fractions exhibits a different pattern from that of Ni and Zn. The major difference lies in the negative correlation between the proportion of Ni and Zn present in the HCl-soluble fraction and the depth of water, which does not exist in the case of Cu. In contrast, a rather strong positive correlation between the HCl-soluble Cu and the depth of water was found (see Figure 2.94). Moreover, the positive correlation between the percentage of Cu found in the hydroxylamine HCl-soluble fraction and the water depth is markedly lower than that of Ni and Zn. The acetic acid-soluble Cu, like that of Fe and Mn, decreases steadily with increasing depth of water (see Figures 2.95 and 2.96).

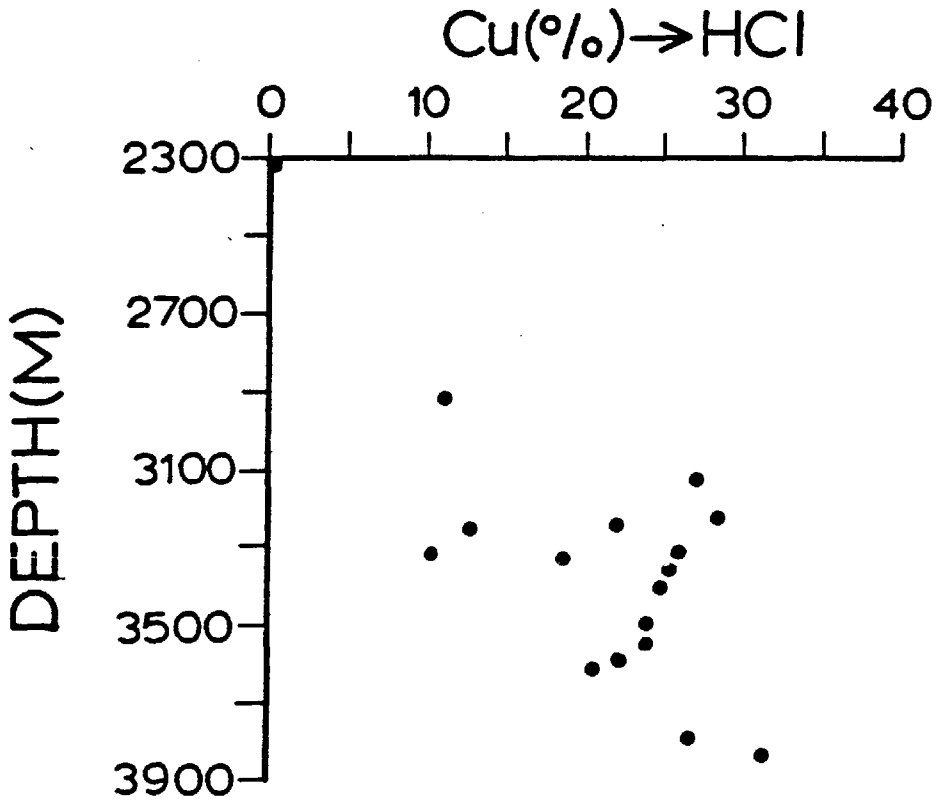

Figure 2.94: Scatter plot showing the positive correlation between the HCl-soluble Cu (expressed as a percentage of the total Cu concentration) in the surface sediments, and the water depth.

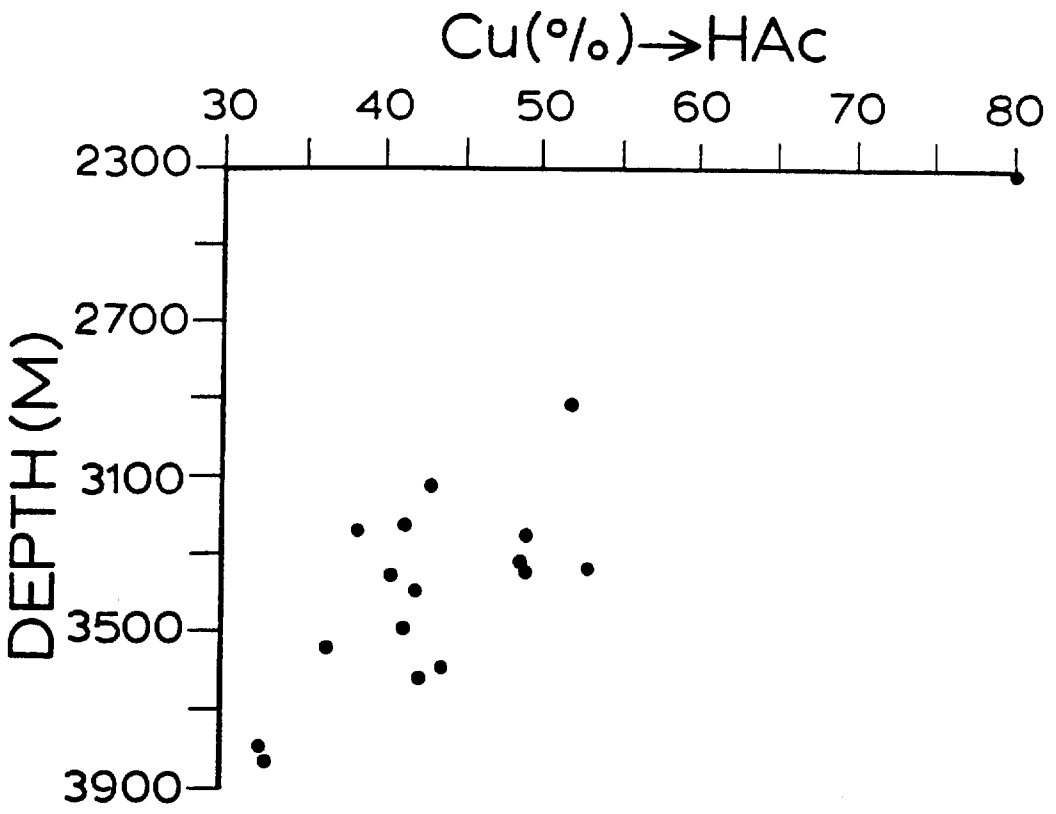

Figure 2.95: Scatter plot showing the negative correlation between the acetic acid-soluble Cu (expressed as a percentage of the total Cu concentration) in the surface sediments, and the water depth.

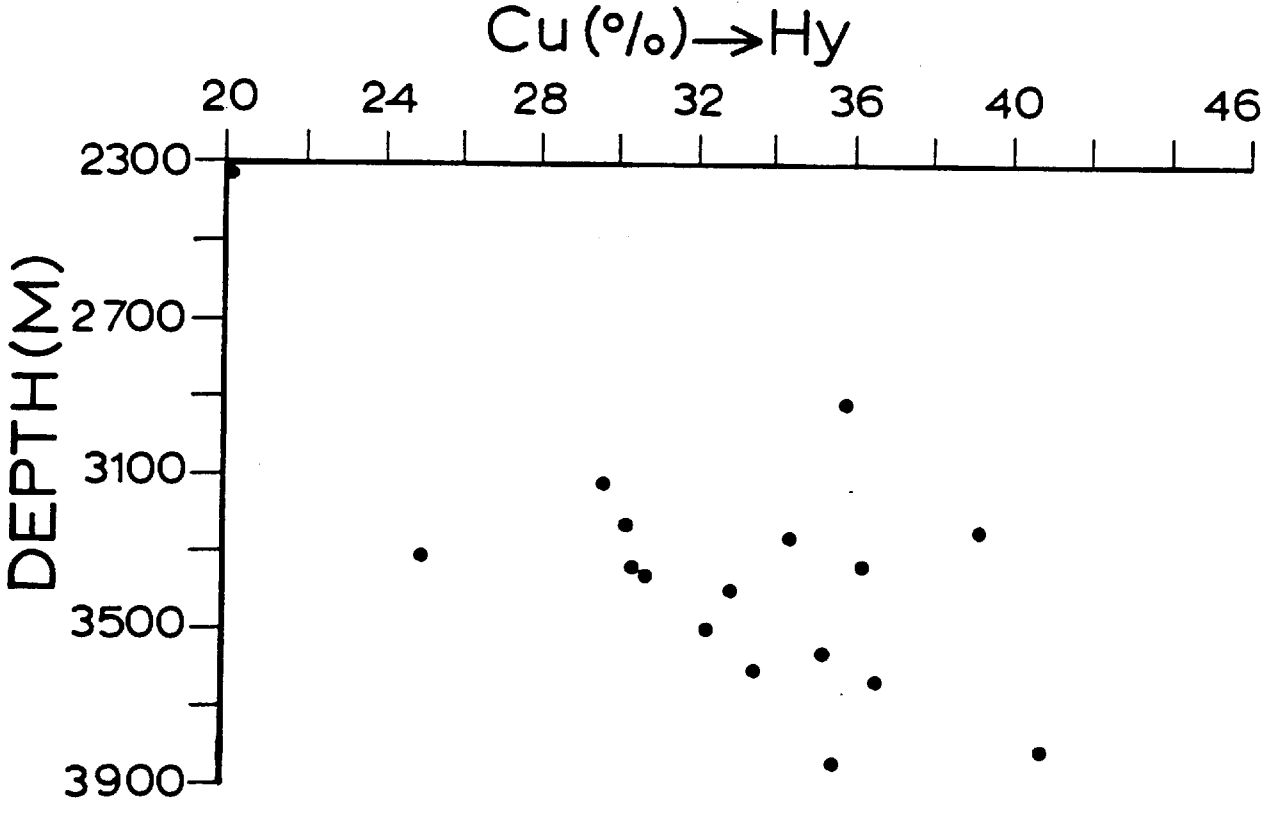

Figure 2.96: Scatter plot showing the positive correlation between the hydroxylamine HCl-soluble Cu (expressed as a percentage of the total Cu concentration) in the surface sediments, and the water depth.

2.7 DISCUSSION

2.7.1 Diagenetic Transformation of Phases

The geochemical partition data from the present study indicate the association of certain metals with various phases in the EPR fracture zone sediments. These associations reflect the mode of incorporation of the metals into the sediments.

Most of the phases occurring in EPR metalliferous sediments are authigenic. Previous mineralogical studies on such sediments have shown that carbonate minerals, goethite, Fe-rich montmorillonite, and ferromanganese oxides such as psilomelane, todorokite, and birnessite are the dominant phases present. Iron also occurs in the form of colloidal $Fe(OH)_3$ (Dasch et al, 1971; Dymond et al, 1973; Sayles and Bischoff, 1973).

The results of the partition geochemistry indicate that Fe in the surface sediments is more concentrated in the hydroxylamine HCl-soluble fraction than in the HCl-soluble fraction. Conversely, in the buried sediments the proportion of Fe soluble in HCl is greater than that soluble in hydroxylamine HCl. This partition pattern is of interest because it suggests diagenetic transformation of phases within the buried sediments.

Two processes are envisaged as being responsible for the different partitioning of Fe in the surface and buried sediments:

1) Post-depositional formation of goethite.

2) Post-depositional formation of Fe-rich smectites.

Apart from the ferromanganese oxides, Fe in the surface sediments could be precipitated in the form of colloidal Fe hydroxides which are soluble in the hydroxylamine HCl solution. These colloidal Fe aquates could be transformed later by covering with sediments to goethite, which is soluble in HCl but not in the acid-reducing agent solution. In addition, Fe-hydroxides can react, after their burial, with the SiO_2 present in the interstitial water of the sediments to produce Fe-rich smectites (Heath and Dymond, 1977). These two processes are supported by the following chemical changes:

1) The gradual decrease of Fe with depth in the acid-reducible fraction.

2) The regular increase of Fe with depth in the HCl-soluble fraction.

3) The gradual increase of the hydroxylamine HCl-insoluble residue with depth (see Figures 2.83, 2.84 and 2.85).

The second process suggested here is in good agreement with that suggested by Bischoff and Sayles (1972), who demonstrated that in some of the cores which they studied from the East Pacific Rise and the Bauer Deep, the intensity of the montmorillonite X-ray pattern appeared to increase with depth, suggesting that increasing amounts of amorphous SiO_2 had crystallized to montmorillonite in deeper sediments.

Since more Mn is found in the HCl-soluble fraction of the buried sediments than those at the surface, and less is found in the hydroxylamine HCl-soluble material of the buried than the surface

sediments, some post-depositional transformations of the Mn-phases must also occur; e.g. amorphous MnO_2 in the surface sediments may be transformed after burial to other manganese-bearing minerals. However, such transformations of Mn-phases, although possible, particularly in the upper part of the sediment cores, do not take place to such a large extent as in the case of the Fe-phases. This is supported by the less marked differences in the partition of Mn in the surface and buried sediments.

On the basis of the vertical partition geochemical patterns, the buried fracture zone sediments can be classified into upper (0-40 cm) and lower (below 40 cm) sediments. The effect of burial on the distribution of elements among the main chemical phases is clearer in the upper sediments than in the lower sediments.

A number of factors may be responsible for the increase in the percentage of Mn associated with the acetic acid-soluble fraction, with burial in the upper 40 cm of the sediments. The acetic acid solution dissolves the carbonate material and releases the ions which are adsorbed onto the surface of clay minerals. Thus, the amount of Mn which is available in the sea water during the deposition of the sediments, the amount of carbonate material present in the sediments, and the proportion of clay minerals, are some of the parameters which must be taken into account in the discussion of this matter. Since no increase in the total concentration of Mn with depth in the sediments was found, the change in the proportion of Mn associated with the acetic acid-soluble fraction with depth could not be assigned to any changes of the amount of Mn primarily being incorporated into the sediments. Most of the post-depositional chemical reactions which

cause chemical diagenesis of the sediments occur in the upper part of the sediment column. It is, therefore, suggested that the present partitioning change is due to a post-depositional process rather than to primary chemical variations.

The following diagenetic processes are suggested as possibly being responsible for the increase of Mn with depth in the acetic acid-soluble fraction:

1) Dissolution of ferromanganese oxides by oxidation of organic material, and enrichment of the pore waters in Mn.

2) Mn-coating on foraminiferal tests.

3) Formation of manganese carbonates.

The increase of the acetic acid-soluble Mn with depth may reflect its increase in the interstitial waters. Manganese precipitates from the sea water in the form of MnO_2. This phase does not easily dissolve in the upper few cms of the sediments, where oxidizing conditions occur. Therefore, the interstitial waters of the upper few cms of the sediments will be low in Mn. In contrast, in the deeper sediments MnO_2 is reduced by organic matter liberating Mn^{2+} in the interstitial waters. This diagenetic process is supported here by the decrease of the acid-reducible Mn with depth (see Figures 2.59 and 2.60), which suggests its parallel increase in the interstitial waters. Wekfield (personal communication) determined the distribution of Mn in pore waters from some East Pacific Rise sediment cores and he found an increase in the concentration of Mn with depth. Similarly, Addy et al (1976) reported an increase of Mn with depth in the

interstitial waters of a North Atlantic sediment core, and a corresponding decrease of the amount of Mn present in the acid-reducible fraction of the sediments.

Microscopic work on many sediment samples strongly suggests that the foraminiferal tests accommodate a large amount of Mn in the form of coatings. Direct observations using a binocular microscope of foraminiferal tests isolated and washed in deionised water showed that in many sediment samples black stains are present on the tests of most of the forams. It appears that there is some relationship between these black stains and the proportion of Mn which is soluble in acetic acid. The more heavily stained the tests of forams are, the higher the percentage of Mn which is soluble in acetic acid. Since most of this Mn originates probably from the resolution of MnO_2 after its burial, the present data support a post-depositional shift of Mn from the ferromanganese oxides onto the carbonate phases. In other words, a portion of the acetic acid-soluble Mn originally reached the ocean floor in the form of ferromanganese oxides and it was transferred by dissolution and reprecipitation onto the carbonate material. Perhaps some isostructural replacement of Ca by Mn throughout the foram test has also occurred. Post-depositional reactions leading to direct association of Mn with foraminiferal tests have been reported elsewhere (Emiliani, 1955; El Wkeel and Riley, 1961; Copeland, 1964). Emiliani (1955) reported heavy surface staining on foram tests, the analysis of which revealed up to 3% MnO. However, he noted that some foraminiferal tests with considerable concentrations of Mn showed no visible discolouration.

Another alternative which could explain the increase of the acetic acid-soluble Mn with depth is the formation of manganese carbonates. When the pore waters contain high concentrations of carbonate ions in the presence of Mn^{2+}, manganese carbonates may be formed (Lynn and Bonatti, 1965; Calvert and Price, 1970). The decrease of the acid-reducible Mn with depth would suggest an increase of Mn^{2+} and $CO_3^{=}$ in the interstitial waters due to the oxidation of organic carbon by reduction of MnO_2, possibly according to the following reaction:

$$H_2O + CH_2O + 2MnO_2 \longrightarrow 2Mn^{2+} + HCO_3^{-} + 3OH.$$

(Li et al, 1969; Addy et al, 1976). Subsequently, Mn^{2+} may react with $CO_3^{=}$ to form manganese carbonates. Therefore, there is evidence to suggest that conditions existing in the present sediments might lead to the formation of manganese carbonates.

X-ray diffraction patterns of selected sediment samples having high proportions of Mn in the acetic acid-soluble fraction showed that four calcite peaks had anomalously high intensities. One of these (2.84 Å) may be reinforced partly by the presence of a few percent of rhodochrosite. However, this possibility could not be confirmed as the next strongest $MnCO_3$ lines are not detected, probably due to the low concentration of rhodochrosite. Another possible reason for the other anomalous intensities is the effect of random Mn in the calcite lattice.

Calvert and Price (1970) reported the co-occurrence of oxide and carbonate manganese phases from Loch Fyne, Scotland. They postulated that manganese carbonates were produced diagenetically.

High concentrations of Mn^{2+} and carbonate ions in the interstitial waters of the sediments were considered to participate actively in the formation of manganese carbonates. The high concentrations of Mn^{2+} in the pore waters were attributed to the dissolution of MnO_2 after burial. Li et al (1969) showed that the pore waters of sediments from the Arctic basin were saturated with respect to $MnCO_3$ at a certain depth. They demonstrated that inorganic CO_2 and Mn^{2+} displayed a parallel increase with depth in the interstitial waters, reaching their highest concentrations at about the same depth. The increase of the dissolved Mn in the pore waters was assigned to the oxidation of organic carbon by reduction of MnO_2.

It is of interest to note that the acetic acid-soluble Fe, Zn and Cu decrease steadily with depth in the sediments, in contrast to the case of Mn. From 0 down to about 40 cm the decrease of these elements in the acetic acid-soluble fraction is more sharp, while below that depth it becomes more smooth. If most of the Fe, Zn and Cu which is liberated into the acetic acid solution was held in the tests of the carbonate microfossils, their decrease with depth would be explained if the $CaCO_3$ content was reduced with depth. However, no such trend was found in the vertical variations of the $CaCO_3$ content of the sediments. Therefore, it seems most likely that the decrease of Fe, Zn and Cu with depth in the acetic acid-soluble fraction reflects the corresponding depletion of these elements in the interstitial waters or loosely sorbed onto mineral phases. Iron is extracted during the process of formation of Fe-rich smectites, as has been discussed before, while Zn and Cu are incorporated in the structure of the newly-formed mineral. This is consistent with the

increase of the amount of these metals which is soluble in HCl with depth in the sediments. Since the dissolution of ferromanganese oxides with depth releases a fair amount of Cu and Zn in the pore waters, it is concluded that the diagenetic process occurring leads to the shift of these elements from the ferromanganese oxides to the Fe-rich smectites or the Fe-oxides. The interstitial waters of the sediments act as an intermediate aqueous medium through which their transfer from one phase to another takes place.

2.7.2 Role of $CaCO_3$ Dissolution in Supplying Metals to Other Phases

The distribution of $CaCO_3$ in the sediments examined in this study shows a clear relationship between the carbonate content and the water depth. As the water depth increases, the amount of $CaCO_3$ present in the sediments diminishes correspondingly. The scatter diagram of $CaCO_3$ content in the surface sediments expressed as a function of water depth shows this relationship (see Figure 2.97). These data are consistent with the direct measurements of the rates of calcite dissolution made by Peterson (1966) and Berger (1967) at various depths in the oceans. Moreover, there is fundamental agreement with the large scale distribution maps of calcite in the Pacific (Bezrakov, 1969, 1970; Bramlette, 1961).

A negative correlation between the acetic acid-soluble Mn, Fe and Cu and the depth of water was found (see Figures 2.86, 2.88 and 2.95). It is known that 25% acetic acid dissolves not only the carbonates but also releases adsorbed ions from the surface of clay

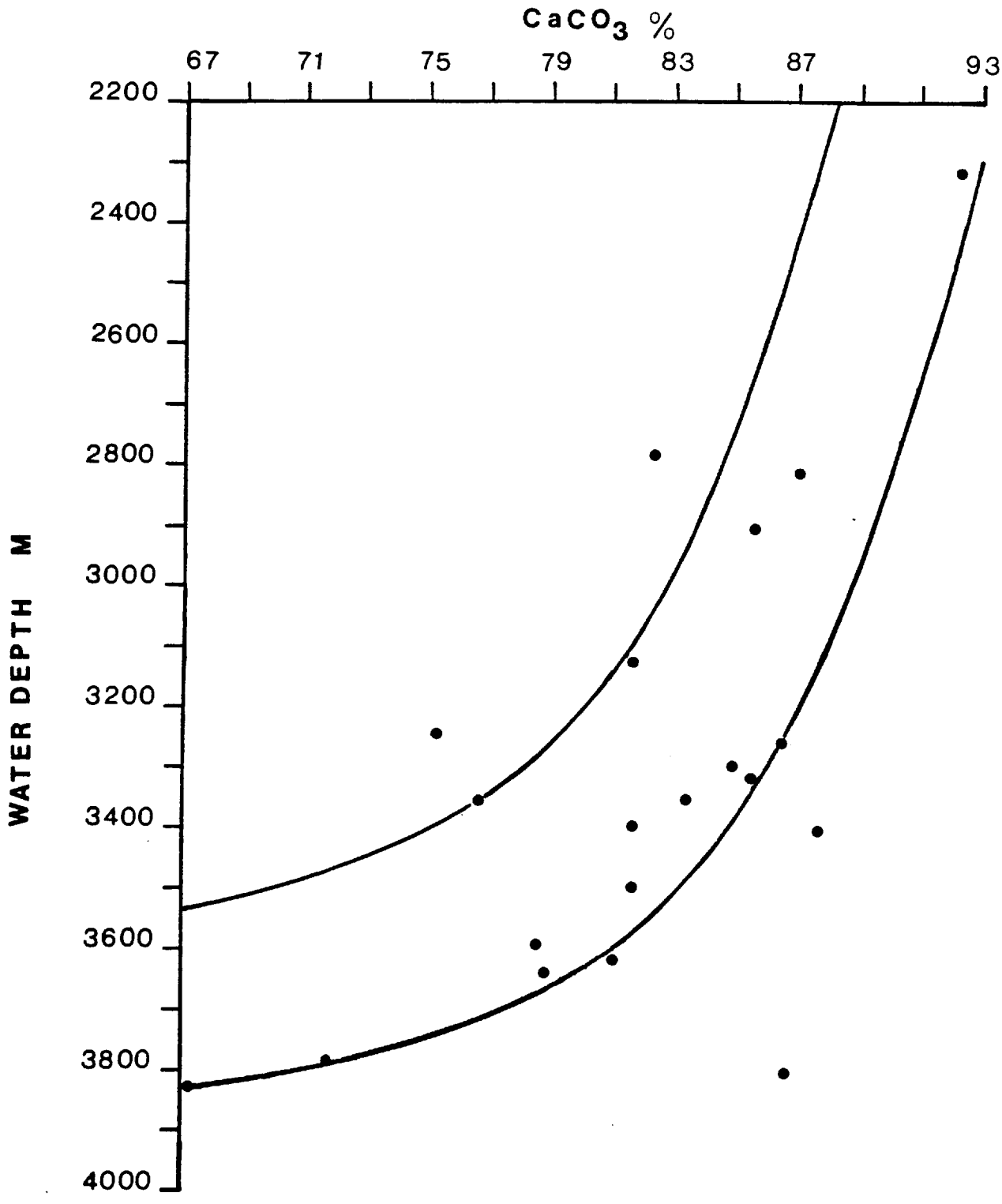

Figure 2.97: Scatter plot showing the negative correlation between the $CaCO_3$ content in the surface sediments, and the water depth.

minerals. However, in this case the acetic acid-soluble fraction of the surface sediments represents mainly the carbonate material because most of the sediments examined here consists of calcareous microfossils. Moreover, as has been discussed above, the proportion of clay minerals (Fe-rich smectites) is very small in the surface sediment samples. By contrast, Fe-rich smectites abundance increases with depth, being formed as a result of chemical diagenesis of the sediments. Therefore, in the surface sediments only a very small proportion of the acetic acid-soluble elements would not be related to the carbonate material. It is concluded that the decrease in the proportion of Fe, Mn and Cu associated with the acetic acid-soluble fraction with water depth is due to the dissolution of $CaCO_3$. As the water depth increases a higher proportion of $CaCO_3$ is dissolved and thus a higher proportion of Fe, Mn and Cu associated with the carbonates is released in the solution. Conversely, a smaller proportion of these elements remains in the carbonate microfossils.

The increase of the percentage of Mn and Fe associated with the hydroxylamine HCl-soluble fraction with depth of water suggests that environmental conditions favour the formation of ferromanganese oxides in the deeper rather than in the shallower sediments. This implies either greater amount of Mn and Fe being available in the deeper waters or more pronounced oxidising conditions. A considerable number of sediment samples examined here was taken from the fracture zone basins. The geochemical data of section 1 support ponding of metals in these basins. It is, therefore, concluded that the first possibility exists here. Moreover, the ferromanganese oxide phases in deeper areas may increase by the addition of similar phases being

formed elsewhere (vent areas) and transported to their present position. In conclusion, the source of a portion of the "excess" Mn and Fe in the deeper sediments is probably the calcareous material. After dissolution, Fe and Mn may be released into the bottom waters in the divalent state. Their later oxidation leads to the precipitation of ferromanganese oxides. Copper concentrations in the acetic acid-soluble fraction were found to vary sympathetically with Fe and Mn in a proportional decrease with depth, indicating that at least a portion of Cu originates from the dissolution of $CaCO_3$. Turekian and Imbrie (1966) reported a strong positive correlation between Cu and $CaCO_3$ for Atlantic surface sediments. They noted that although Cu is not in the lattice structure of the carbonates, it is preserved with the calcium carbonate fraction.

To summarize, the geochemical partition data support the concept that, due to the dissolution of $CaCO_3$ in deeper waters, a gradual shift of Fe, Mn and Cu from the carbonates into the ferromanganese oxide phase probably occurs with increasing depth of water.

2.8 CONCLUSIONS

1) The average partition geochemical data of the buried sediments are different from those of the surface sediments. On average, the HCl-soluble Mn, Fe, Ni, Pb, Zn, Cu and Al is greater in the buried than in the surface sediments. By contrast, the proportion of these elements which is soluble in the acid-reducing agent solution is smaller in the buried sediments.

2) The percentage of the acetic acid-soluble Mn increases from 0 down to 40 cm depth. Below this depth it remains constant throughout the sediments. Post-depositional reactions leading to the shift of Mn from the ferromanganese oxide phases to the carbonates may be responsible for this partition trend. The following diagenetic processes may participate:

   (a) Dissolution of ferromanganese oxides by oxidation of organic material and enrichment of pore waters in Mn.

   (b) Mn-coating on foraminiferal tests.

   (c) Formation of manganese carbonates.

3) The proportion of Fe, Zn and Cu which is associated with the acetic acid-soluble fraction decreases steadily with increasing depth from the top down to the base of almost all the fracture zone cores examined here. This is a result of the depletion of these metals in the interstitial waters due to formation of goethite and/or Fe-smectites in the structure of which they are incorporated.

4) In the upper 40 cm of the sediments, the percentage of Fe, Mn, Ni, Cu and Zn which is found in the acid-reducible fraction decreases with depth of burial. This is a reflection of the dissolution of ferromanganese oxides by oxidation of organic carbon.

5) There is a strong positive correlation between the HCl-soluble Fe, Mn, Ni, Zn and Cu and the depth within cores.

6) There is a gradual increase of the hydroxylamine HCl-insoluble residue with depth in the sediments, which suggests a corresponding increase of the proportion of more resistant phases.

7) Based on conclusions 4), 5) and 6) it is suggested that some diagenetic transformations of phases occur. The following post-depositional reactions may take place:

$Fe(OH)_3$ (amorphous) $\xrightarrow{\text{diagenesis}}$ FeOOH (goethite)

$Fe(OH)_3 + SiO_2 \xrightarrow{\text{diagenesis}}$ Fe-rich smectites

MnO_2 (amorphous) $\xrightarrow{\text{diagenesis}}$ other Mn-minerals

8) The distribution of $CaCO_3$ in the surface sediments is consistent with the direct measurements of the rates of calcite dissolution made by other workers. There is a negative correlation between the concentrations of $CaCO_3$ and the depth of water. At a certain depth the decrease of $CaCO_3$ becomes more abrupt.

9) Examination of the partition chemical results of the surface sediments in the fracture zone indicates some marked variations with depth of water. Definite trends support the

concept that the dissolution of $CaCO_3$ in the deep ocean waters is reflected in the partition chemistry of the sediments. A high negative correlation between the acetic acid-soluble Fe, Mn and Cu and the depth of water was found, which is related to the dissolution of $CaCO_3$.

10) There is a tendency for the hydroxylamine HCl-soluble Fe and Mn to increase with increasing depth of water. A portion of Fe and Mn associated with the ferromanganese oxides may originate from the dissolution of $CaCO_3$.

SECTION 3

GEOCHEMISTRY OF HYDROTHERMAL DEPOSITS
FROM THE GALAPAGOS SPREADING CENTER

3.1 INTRODUCTION

The Galapagos spreading center forms part of the global mid-oceanic ridge system. It extends between the triple junction formed by the boundaries of the Pacific plate, Cocos plate and Nazca plate ($2^{o}N$ $102^{o}W$), and the Panama fracture zone ($82^{o}W$). It is spreading at a half rate of 35 mm/yr (Klitgord and Mudie, 1974) and heat flow and bottom water temperature measurements show an increase of these parameters in this area (Sclater et al, 1974; Detrick et al, 1974).

As a result of the separation of the earth's crust a number of vents are formed along the axis of spreading which allow the circulation of sea water in the basaltic rocks. It mixes with hydrothermally derived fluids which have leached the crust, and the mixture transports metals to the sea floor (Corliss, 1971; Corliss et al, in press). The rapid precipitation of the hydrothermal solutions gives rise to certain types of metalliferous deposits. Mn-oxide crusts, Fe-oxides and Fe-nontronites are the main phases present in the Galapagos deposits (Moore and Vogt, 1976; Corliss et al, 1978).

Although the source and the mechanism of transportation of the metals present in the mid-ocean ridge deposits appear to be relatively uniform (Seyfried and Bischoff, 1977), their concentrations differ from one ridge to another (Horowitz, 1970; Cronan, 1972). Another considerable difference lies in the number of phases which are formed from the precipitation of the metals. For example, the Red Sea metal deposits consist of several hydrothermal phases (sulfides, aluminosilicates, Fe-oxides, Mn-oxides; Bignell et al, 1976), whereas in most of the other mid-ocean ridge deposits only one hydrothermal phase is present (Fe-Mn-oxides).

In this study some hydrothermal deposits drilled by DSDP Leg 54 across a seafloor mound field 22 km south of the Galapagos spreading center (see Figure 3.1) are investigated as follows:

1) The bulk chemical composition of the deposits has been determined and it is compared with other hydrothermal deposits.

2) The profiles of the vertical distribution of the metals are studied.

3) The hydrothermal phases present have been separated chemically and the proportional distribution of metals in each one is determined.

4) An attempt has been made to deduce the process of formation of the deposits.

3.2 PREVIOUS INVESTIGATIONS

Ménard et al (1964) reported the existence of an east-west striking fracture zone west of the Galapagos Islands, and Acharya (1965) determined the locations of a number of seismically active epicenters near these islands. Heron and Heitzler (1967) located a band of magnetic anomalies north of the main group of the islands. It was found that the topography in the region of the magnetic anomalies was characterized by the absence of sediments and roughness. Sediments were found mainly to the north and to the south of the area. It was also revealed that a magnetic symmetry occurred which consisted of positive magnetic anomalies, which decreased in number and wavelength on

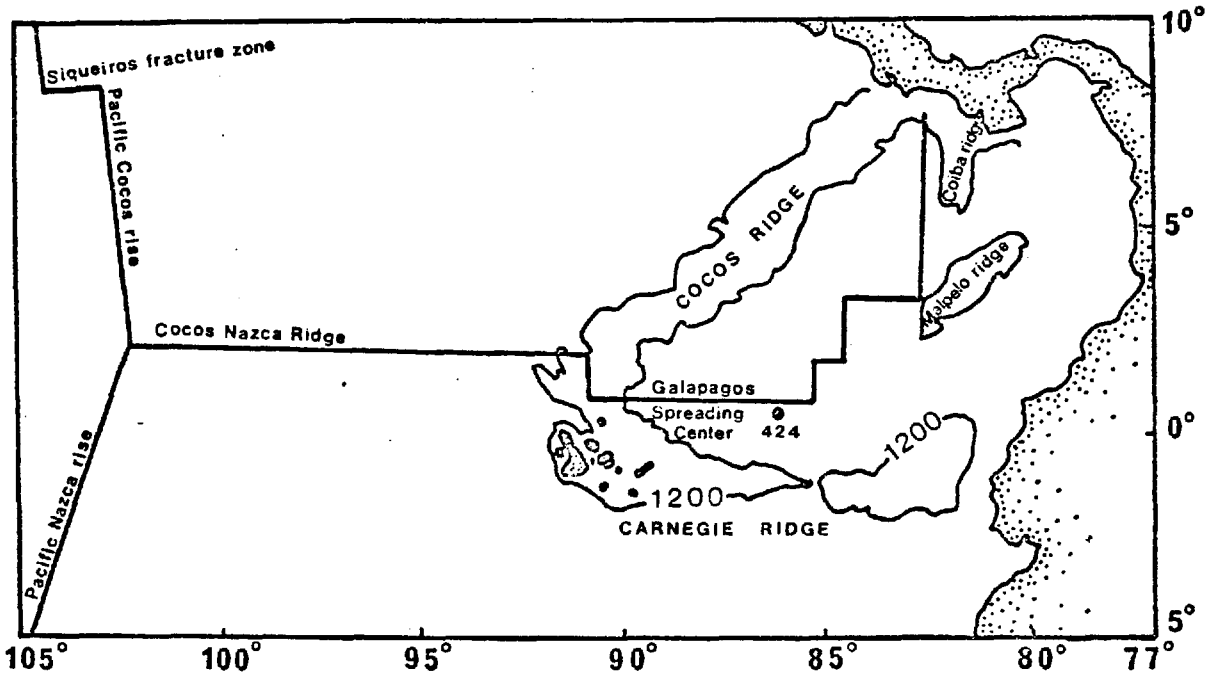

Figure 3.1: General bathymetric map of the Eastern Pacific Ocean showing the DSDP site 424 (Leg 54) from the Galapagos spreading center.

both sides of a negative anomaly. Based on the topography and the magnetic data, the authors suggested that spreading along the axis of the magnetic symmetry should occur.

In 1969, a detailed near bottom survey over the Galapagos spreading center at 86°W was conducted by a scientific group from the Scripps Institution of Oceanography aboard the R/V Thomas Washington, during which the presence of magnetic anomalies was confirmed, the rate of spreading was determined, and much further information about the topography, the heat flow, the bottom water temperatures, etc. was collected. In 1970, the research vessel Argo revisited the area and completed the previous expedition with more accurate measurements. The results of these investigations revealed that volcanic activity was occurring within 2 km from the spreading center, which was characterized by a lack of sediments. A small median valley was located, the rate of spreading being found to vary along the axis of the center and at 86°W it was 33 mm/yr (half rate). The bathymetric relief of the area was lineate parallel to the spreading center, and several scarps occurred which phased the center of spreading. It was also found that there was an increase in the thickness of the sediments away from the center, a characteristic which is typical of spreading centers. The upper sediments were siliceous-calcareous oozes which characterize the shallow equatorial region (Klitgord and Mudie, 1974). A minimum in the heat flow, located on the northern flank of the Galapagos spreading center, was explained by Sclater et al (1974) in terms of hydrothermal circulation of ocean bottom water. They suggested that either the oceanic crust has a permanent permeability, or certain chemical reactions occurred to close and open the cracks of the rocks. Measurements of bottom-water temperatures showed anomalies in the

lower 10 m of the water column which were attributed to the hydrothermal activity (Detrick et al, 1974). It was concluded that the heat flux over the Galapagos spreading center caused renewal of the bottom sea water in the Panama basin.

In 1972, a new survey of the Galapagos spreading center was undertaken by scientists from the Scripps Institution of Oceanography, during which chains of mounds oriented parallel to the spreading axis were discovered. It was suggested that they were formed from hydrothermal fluids which flow out from fissures of the basaltic rocks (Klitgord and Mudie, 1974). The shape and the structure of the mounds were described in 1976, when the area was revisited during the Pleiades expedition of the same institution. It was revealed that most of the mounds were conical in shape and covered with Mn-crusts, associated with Fe-oxides and Fe-rich smectites (Lonsdale, 1977). The geochemical study of dredged Mn-crusts confirmed their hydrothermal origin (Moore and Vogt, 1976). It was shown that they were formed rapidly and were similar to those reported from the Mid-Atlantic Ridge by Scott et al (1974). Their Fe/Mn ratios as well as their transition metal concentrations were very low, whereas they were characterized by high Mn concentrations. Analyses of collected water samples showed that there was a considerable flux of Mn into the bottom water above the mounds. The highest concentration of total dissolved Mn was found in samples taken from less than 5 m above the sea floor (Klinkhammer et al, 1977).

More recently, a series of dives in the submersible"Alvin" to the Galapagos spreading center, carried out by scientists from the Oregon State University in 1977, gave a wealth of new information

about the physiography and the ecology of the region. It was the first direct visual observation of the hydrothermal field (Corliss et al, in press). Active hydrothermal vents were located and the hydrothermal fluids were sampled. It was noticed that all vent areas were near the axial ridge in pillow lavas, and the mixing of cold and warm water caused shimmering over the vents. A white-milky precipitate, formed in the water above the vents, was identified as elemental sulfur, while the rocks were covered with a thin Mn-oxide coating. The maximum temperature of the fluids differed from one vent area to another, ranging between 7° and $17^{\circ}C$. The composition and the temperature of the fluids was considered to be the result of two mixing processes. The first was subsurface mixing of ascending hydrothermal fluids and descending cold water, and the second was surface mixing of the fluids with ambient bottom water. Linear positive relationships between Si and temperature, Si and Ba, Mn and Ba were found. The concentrations of H_2S differed from one vent area to another, ranging from 20μmol/l to 160μmol/l. The fluids were depleted in Ni, Cu and Cd.

The hydrothermal mounds were located and described visually by the Alvin scientific party. They were within the area of high heat flow, between 18 and 25 km from the spreading axis. Their height varied from less than a meter to over 20 m, the small mounds having gentle slopes while the larger ones had steeper slopes. It was seen that black Mn-oxides were overlying orange Fe-oxides, which in turn were overlying green Fe-nontronites.

The chemistry of the hydrothermal mounds showed that Fe and Mn were strongly fractionated. Fe was found almost exclusively in the

Fe-nontronite or the Fe-oxides while Mn formed separate phases consisting of todorokite and birnessite (Corliss et al, 1978). It was shown that the concentrations of Ca, Ni and Zn were independent of the relative abundance of todorokite and birnessite in the Mn-phases and it was suggested that Mn^{2+} was substituted by Ni^{2+}, Cu^{2+} and Zn^{2+} in both minerals.

3.3 LITHOLOGY - STRATIGRAPHY

The general lithology of the sediments drilled by DSDP Leg 54 in the Galapagos spreading center area is summarized in Figure 3.2. The following material was recovered from this area:

1) hydrothermal deposits,
2) foraminifer-nanofossil ooze,
3) siliceous nanofossil ooze,
4) siliceous ash-rich layers.

The hydrothermal deposits were subdivided into three subunits:

(a) green hydrothermal mud,
(b) Fe-Mn material intermixed with green hydrothermal mud,
(c) Fe-Mn concretions.

The hole 424, the geochemistry of which is studied here, was drilled on a mound-like feature and its dominant lithology is alternations of hydrothermal deposits with carbonate sediments (Hekinian et al, 1978). The top of the core down to 13.8 m consists of hydrothermal sediment, made up essentially of green Fe-rich clays intermixed with Fe-Mn concretions. At 13.8-14.2 m, a thin layer of

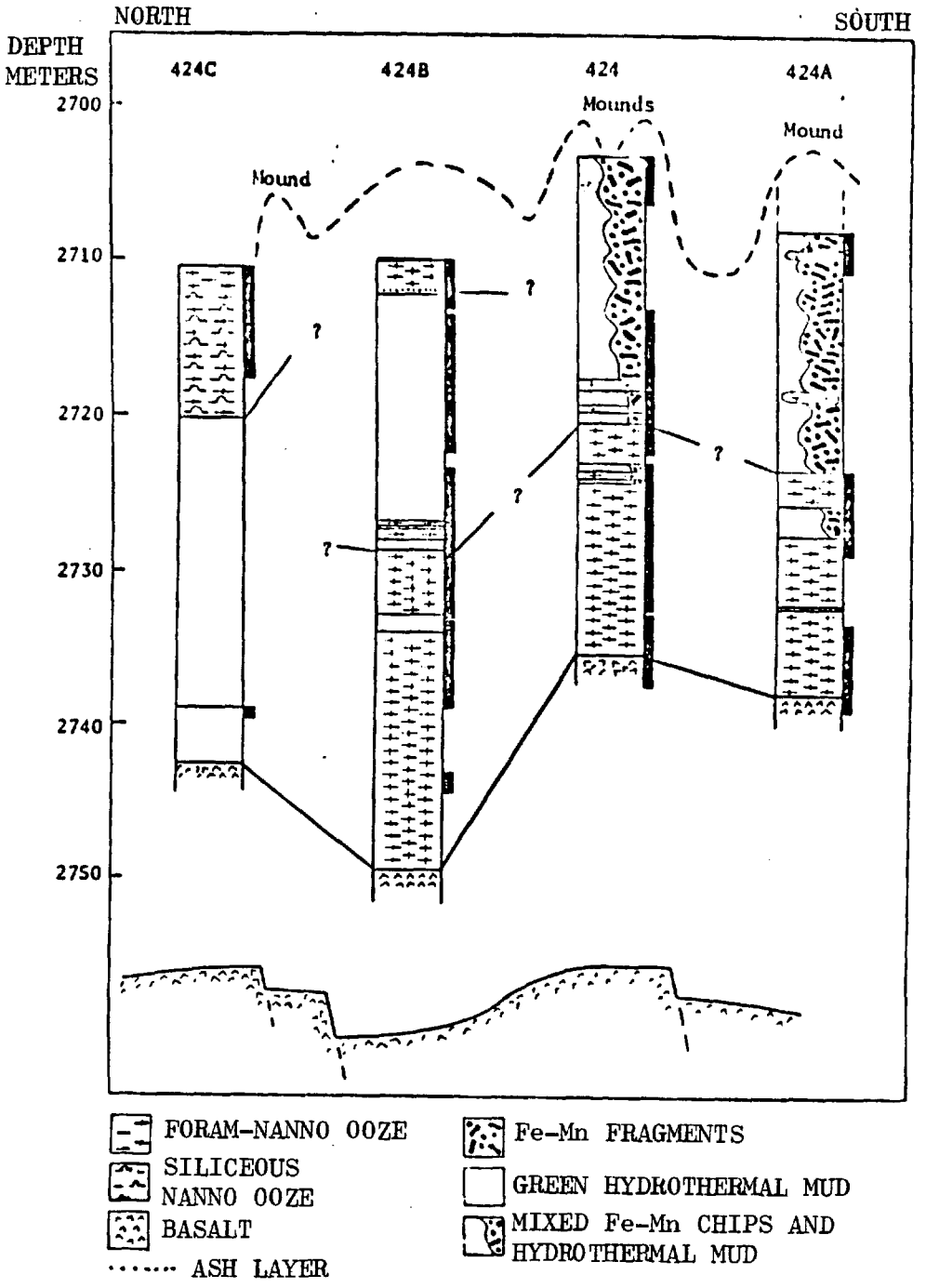

Figure 3.2: Lithologic columns for the holes drilled in the Galapagos spreading center area (adapted from Hekinian et al, 1978).

foraminifer-nanofossil ooze occurs, in which Mn nodules are present. Hydrothermal sediments similar to those found in the upper part of the sediment sequence form the core at 14.2-15.1 m and 15.5-16.2 m with foraminifer-nanofossil ooze between them. Between 16.2 and 19.0 m there is a stratum of carbonate sediments which is followed by another horizon of green hydrothermal material (19.0-19.5 m). From 19.5 m down to the bottom of the sediment column the core is composed of foraminiferal-nanofossil ooze.

On the basis of the presence of radiolaria, which are abundant and well-preserved in a large part of the core, the age of the basal sediments was determined to be not greater than 1.2 m.y. (Amphiropalum ypsilon zone). The younger sediments are Collosphaera tuberosa zone, but the lower boundary of this zone was not determined due to barren sediments.

3.4 CHEMISTRY OF THE DEPOSITS

3.4.1 Bulk Chemical Composition

Chemical analyses of 19 samples from various depths of the Hole 424 were carried out following the methods which are described in Appendix B, and the results are given in Table 3.1. All analyses are also given on a carbonate-free basis in Table 3.2.

The chemical composition of the deposits shows that certain sediment horizons occur which are markedly ferruginous, whereas in other layers the concentration of Fe is lower and in some cases it is

Table 3.1: Chemical composition of sediments from the Galapagos spreading center (Leg 54, Hole 424).

	Sample Number	Depth m	Ca %	$CaCO_3$ %	Mn %	Fe %	Ni ppm	Co ppm	Pb ppm	Zn ppm	Cu ppm	Mg %	Al %	SiO_2 %
1	6	Top	1.02	0.01	33.00	7.25	81	16	48	126	39	1.65	0.15	13.84
2	15	1.20	0.33	0.01	3.80	22.00	17	22	150	35	14	2.20	0.09	42.72
3	39	1.94	0.17	0.01	0.35	22.50	7	12	80	39	8	2.30	0.06	45.99
4	48	9.87	0.18	0.01	0.078	22.00	12	22	95	28	9	2.50	0.03	45.22
5	51	10.97	0.19	0.01	0.077	22.00	7	27	80	29	11	2.65	0.05	47.32
6	38	11.38	0.15	0.01	0.054	22.00	17	22	50	30	12	2.70	0.07	46.56
7	2	12.21	0.17	0.01	0.063	22.50	12	22	50	27	10	2.47	0.05	46.32
8	25	12.91	0.17	0.01	0.067	22.00	17	22	50	33	12	2.40	0.07	45.06
9	28	13.72	0.21	0.01	0.090	21.00	27	22	50	54	24	2.70	0.43	47.00
10	19	13.91	17.25	40.98	0.185	7.75	60	16	21	171	74	1.62	1.29	21.39
11	18	14.40	0.22	0.01	0.105	22.00	17	22	50	38	20	2.50	0.17	44.67
12	1	15.22	15.50	36.53	0.190	8.00	52	19	29	138	82	2.02	1.36	24.94
13	32	15.75	4.02	7.34	0.100	16.50	37	20	42	87	58	2.67	1.07	41.32
14	47	17.41	18.50	44.16	0.255	6.70	193	34	23	233	105	2.07	2.40	23.84
15	12	19.10	0.52	0.01	10.75	18.45	16	17	294	57	13	2.15	0.05	38.08
16	54	19.36	0.29	0.01	0.080	21.00	27	22	49	35	14	2.75	0.21	43.95
17	35	21.30	20.75	49.89	0.205	4.75	95	14	19	210	95	3.85	2.10	20.76
18	7	30.69	11.50	26.35	1.180	6.60	192	36	52	238	238	2.27	2.75	26.28
19	14	36.90	30.75	75.32	0.510	1.27	52	11	19	81	57	0.82	1.30	9.64

Table 3.2: Chemical composition of sediments from the Galapagos spreading center (Leg 54, Hole 424), expressed on a carbonate-free basis.

	Sample Number	Depth m	Ca %	$CaCO_3$ %	Mn %	Fe %	Ni ppm	Co ppm	Pb ppm	Zn ppm	Cu ppm	Mg %	Al %	SiO_2 %	Fe/Mn
1	6	Top	1.02	0.01	33.00	7.25	81	16	48	126	39	1.65	0.15	13.84	0.22
2	15	1.20	0.33	0.01	3.80	22.00	17	22	150	35	14	2.20	0.09	42.72	5.79
3	39	1.94	0.17	0.01	0.35	22.50	7	12	80	39	8	2.30	0.06	45.99	64.29
4	48	9.87	0.18	0.01	0.078	22.00	12	22	95	28	9	2.50	0.03	45.22	282.05
5	51	10.97	0.19	0.01	0.077	22.00	7	27	80	29	11	2.65	0.05	47.32	285.71
6	38	11.38	0.15	0.01	0.054	22.00	17	22	50	30	12	2.70	0.07	46.56	407.41
7	2	12.21	0.17	0.01	0.063	22.50	12	22	50	27	9	2.47	0.05	46.32	357.14
8	25	12.91	0.17	0.01	0.067	22.00	17	22	50	33	12	2.40	0.07	45.06	328.36
9	28	13.72	0.21	0.01	0.090	21.00	27	22	50	54	24	2.70	0.43	47.00	233.33
10	19	13.91	17.25	40.98	0.314	13.13	101	27	35	289	125	2.77	2.19	36.19	41.82
11	18	14.40	0.22	0.01	0.105	22.00	17	22	50	38	20	2.50	0.17	44.67	209.52
12	1	15.22	15.50	36.53	0.300	12.61	82	30	46	218	129	3.17	2.14	39.28	42.03
13	32	15.75	4.02	7.34	0.108	17.81	40	22	45	94	63	2.89	1.16	44.57	164.91
14	47	17.41	18.50	44.16	0.457	12.00	346	60	41	418	189	3.72	4.30	42.65	26.26
15	12	19.10	0.52	0.01	10.75	18.45	16	17	294	57	13	2.15	0.05	38.08	1.72
16	54	19.36	0.29	0.01	0.080	21.00	27	22	49	35	14	2.75	0.21	43.95	262.50
17	35	21.30	20.75	49.89	0.409	9.48	190	29	37	418	189	7.65	4.19	41.35	23.18
18	7	30.69	11.50	26.35	1.603	8.96	261	49	71	323	324	3.10	3.74	35.66	5.59
19	14	36.90	30.75	75.32	2.068	5.17	210	44	75	329	233	3.34	5.27	39.03	2.50
Average of nine ferruginous samples			0.19	0.01	0.107	21.90	16	22	62	35	13	2.55	0.13	45.79	

similar to that in normal pelagic clays. The Mn-crusts at the top of the sediment sequence contain very little Fe, while its concentrations in the underlain green hydrothermal deposits range between 21 and 22.5% by weight. From 19.5 m down to the basement, where carbonate sediments occur, the concentrations of Fe tend to decrease and at the basement they reach values which are comparable to those of normal pelagic sediments. It is observed that at the top of each of the distinct ferruginous horizons a thin ferromanganese layer occurs, whereas at greater depths the whole horizon is exceedingly depleted in Mn (see Figure 3.3). In the upper ferruginous horizon the top sediment sample contains 3.8% Mn, while in the top sediment sample of the fourth Fe-rich horizon Mn reaches the value of 10.75% by weight.

Between 13.8 and 14.2 m and at 15.1-15.5 m where carbonate sediments enriched in Fe occur, the concentrations of Mn are higher than in the green hydrothermal clays; however, they are still below the average background values in Pacific pelagic clays. In contrast, Mn in the foraminifer-nanofossil ooze present below the lower ferruginous horizon increases, and at the basement it reaches a fourfold enrichment when compared with normal pelagic sediments.

The trace element geochemical data of the highly ferruginous horizons show that these sediments are extremely depleted in trace metals such as Ni, Co, Zn and Cu, when compared with the average composition of the Pacific surface pelagic clays. In the upper Fe-rich clays (0-13.8 m) the concentrations of these metals do not show any significant variation with increasing depth; in contrast, there is a tendency for their concentrations to increase with depth in the carbonate sediments (Figure 3.4). The maximum concentrations of Ni,

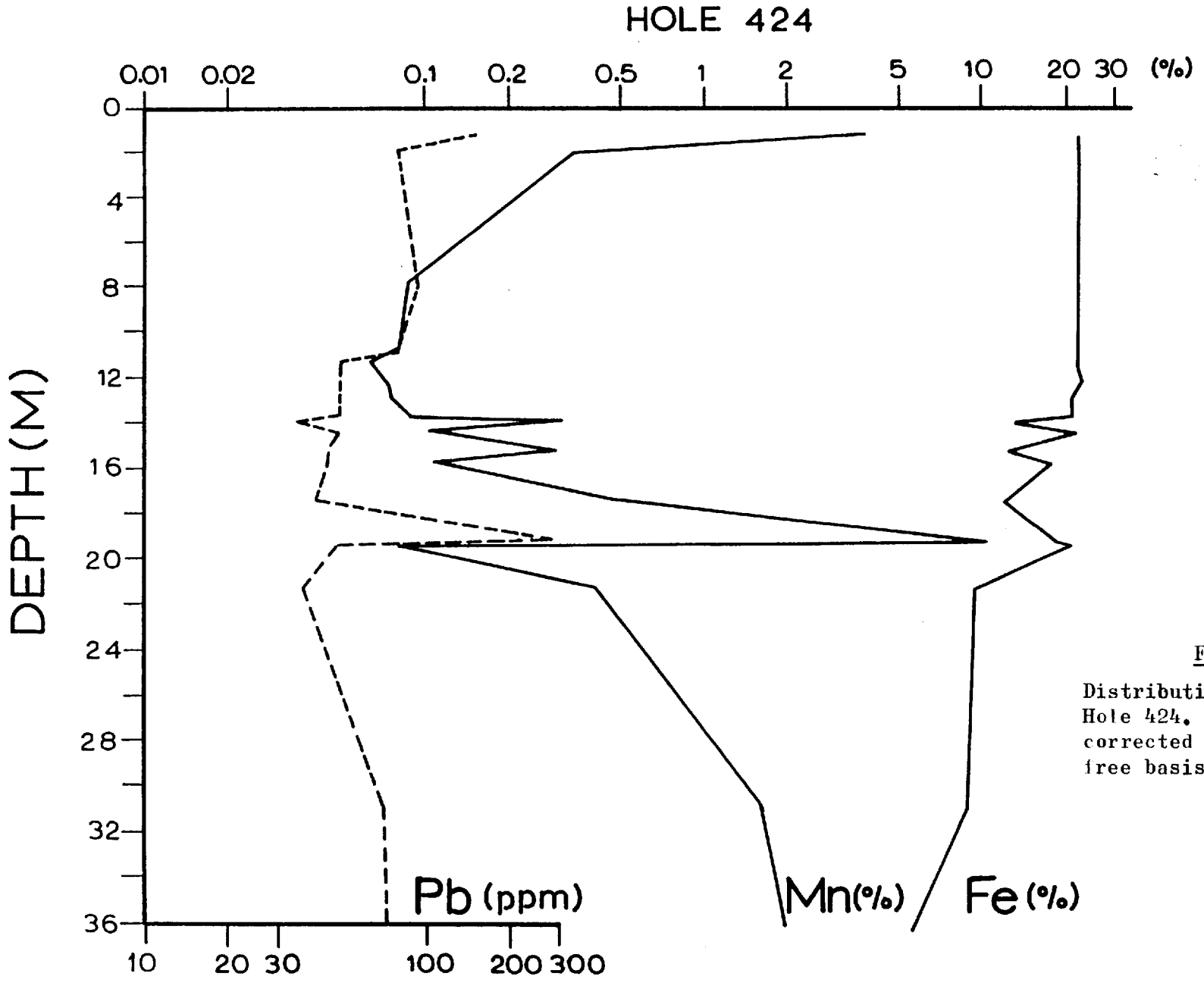

Figure 3.3

Distribution of Pb, Mn and Fe in Hole 424. Concentrations are corrected to a calcium carbonate free basis.

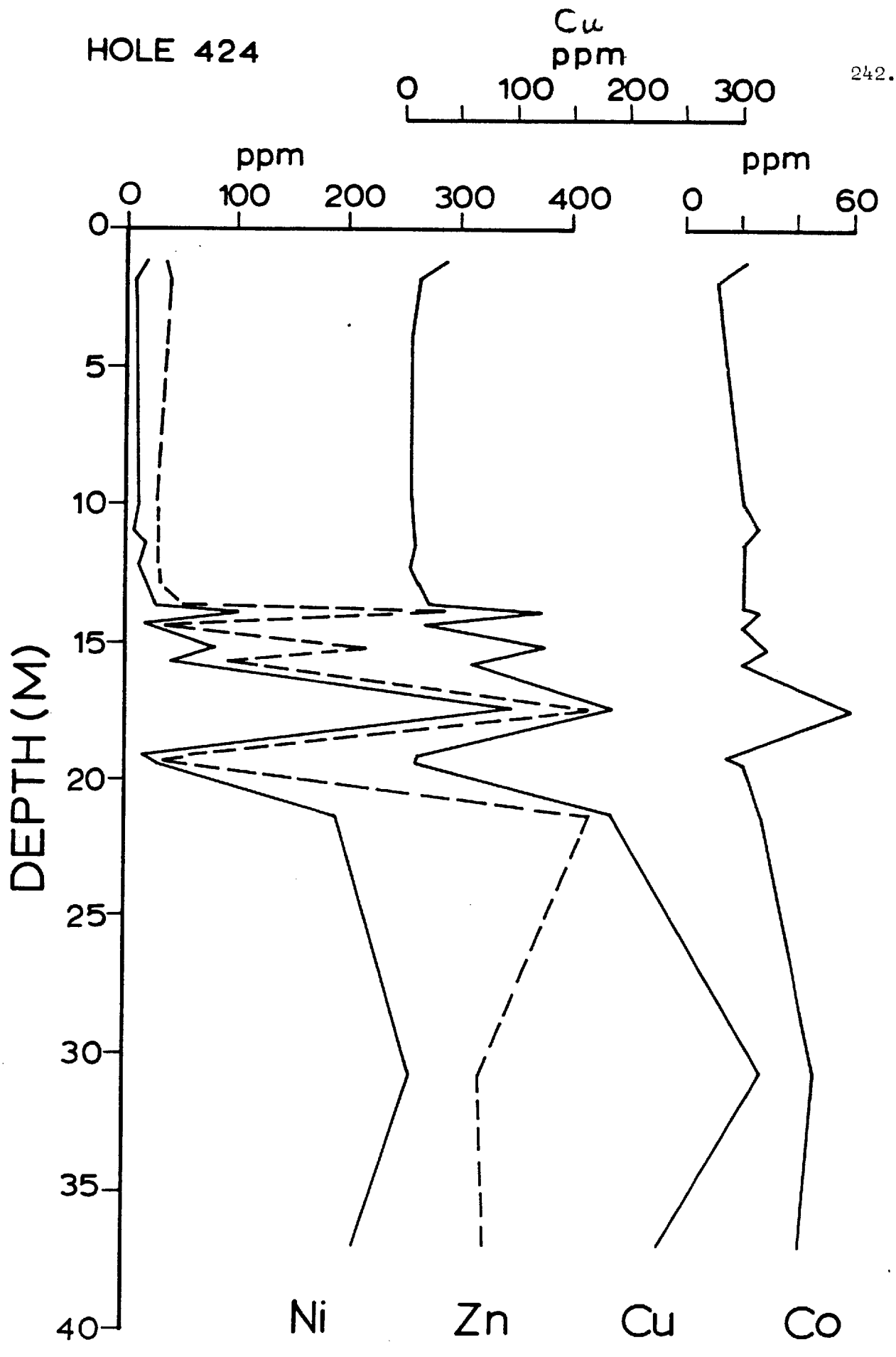

Figure 3.4: Distribution of Ni, Zn, Cu and Co in Hole 424. Concentrations are corrected to a calcium carbonate free basis.

Co and Zn occur at 17.4 m (346, 60, 418 ppm, respectively), while Cu shows its highest concentration at 30.69 m (324 ppm). In both cases these depths fall within the foraminifer-nanofossil ooze layers. The vertical variations of Ni, Co, Cu and Zn are positively correlated with each other.

In contrast to the other trace metals, Pb does not show any depletion in the Fe-rich sediments, its concentrations being similar to the average concentration of Pb in normal pelagic clays. Furthermore, the vertical variations of Pb produce a different pattern from that produced from the vertical distribution of Ni, Co, Cu and Zn. Figure 3.3 shows that a decrease in the concentrations of Pb with increasing depth within the upper ferruginous horizon occurs which continues in the carbonate sediments below. The two characteristic peaks in the concentration of Pb which have been found at the depths of 1.20 and 19.10 m are associated with the ferro-manganese layers occurring at the top of the ferruginous horizons. Comparison of the vertical distribution of Pb between 0 and 17.4 m with its distribution between 17.4 and 36.9 m shows that within these two sections of the core, similar variations of Pb occur. At the top of both sections the sediments are remarkably enriched in Pb, whereas a rather sharp fall in its concentration with increasing depth was found.

The Fe-rich sediments are characterized by very low Al content, while in the other sediments the concentration of Al increases in parallel to the variations of $CaCO_3$. Silica is strongly enriched in the Galapagos sediments, the concentrations of SiO_2 ranging between 39.03% and 47.32% on a C.F.B. There is a tendency for the concentration of SiO_2 to decrease with increasing depth in the core 424, while a

positive linear correlation between Si and Fe concentrations was found (Figure 3.5a). Thus, it would appear that Si and Fe have similar distributions in the sediments examined here.

Comparison of the average composition of nine green clay samples from various depths of the core 424 with the average composition of Pacific surface pelagic clays (Cronan, 1969) indicates significant differences. The green hydrothermal clays are remarkably enriched in Fe and they are significantly depleted in Mn and trace metals such as Ni, Co, Zn and Cu. The only similarity between the present ferruginous sediments and the normal pelagic clays is that in both groups of sediments Pb has similar average concentrations.

Further comparison of the average composition of the Galapagos ferruginous sediments with the average composition of metalliferous sediments from active mid-ocean ridges and other oceanic areas associated with volcanic activity shows some similarities as well as significant differences. In most cases these sediments are enriched in Fe when compared with the normal deep sea sediments; however, the concentrations of Fe vary from one area to another within a large range. In the present sediments the concentration of Fe is greater than that of the surface sediments described by Bostrom and Peterson (1969) from the crest of the East Pacific Rise (EPR) and those from the EPR fracture zone at $9^{o}S$ (the present study). Moreover, the concentrations of Fe in the Galapagos Fe-rich clays is higher than that of the ferruginous sediments from the median valley Mid-Atlantic Ridge (MAR) (Cronan, 1972), the EPR basal metalliferous sediments (Cronan, 1976a), the Fe-rich basal sediments from the Indian Ocean, site 245, D.S.D.P. (Warner and Gieskes, 1974), and the Bauer Deep

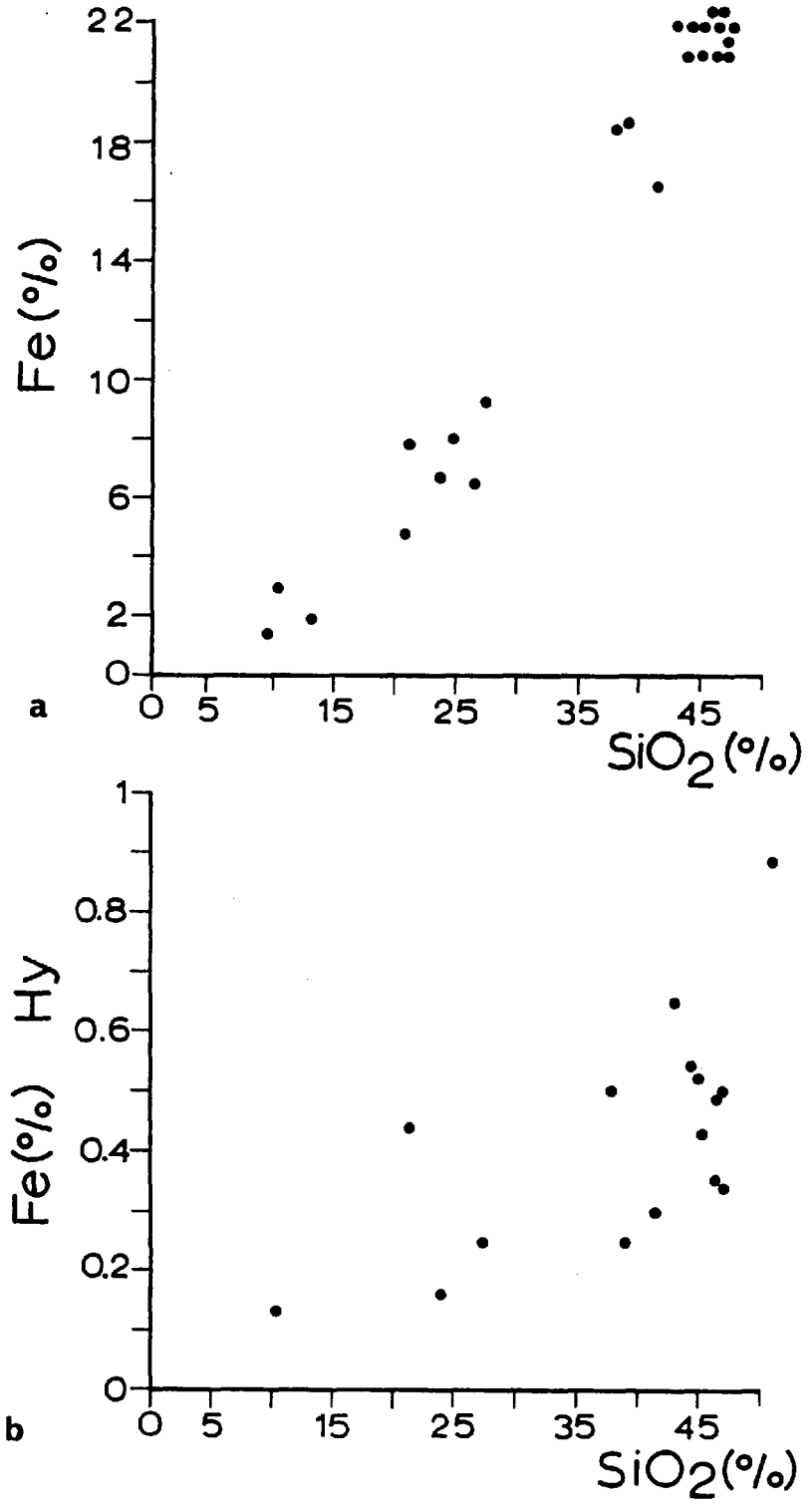

Figure 3.5: (a) Scatter plot of SiO_2 content versus Fe. Concentrations are corrected to a calcium carbonate free basis.

(b) Scatter plot of SiO_2 content, corrected to a calcium carbonate free basis, versus hydroxylamine HCl - soluble Fe expressed as a percentage of the total Fe concentration.

metalliferous sediments (Sayles and Bischoff, 1973; Sayles et al, 1975). In contrast, it is lower than that in the D.S.D.P., sites 37, 38 and 39 metalliferous sediments from N.E. Pacific (Dymond et al, 1973), the D.S.D.P., site 183, basal ferromanganoan sediments from N.W. Pacific (Natland, 1973), and the Santorini Fe-deposits (Bonatti et al, 1972b; Smith and Cronan, 1975).

The Galapagos ferruginous sediments, like other metalliferous sediments associated with submarine volcanic activity and especially those at the mid-ocean ridges, are depleted in Al. However, the Al content of the present sediments is much lower than that in the EPR sediments (Bostrom et al, 1969; the present study).

The most remarkable difference between the sediments examined here and the Fe-rich sediments from the mid-ocean ridges and other submarine volcanic areas, is that no enrichment in trace metals was found here. In addition, very low concentrations of Mn are found in the Galapagos Fe-rich clays, whereas in most of the Fe-rich sediments described from other oceanic areas such as the EPR (Bostrom and Peterson, 1969), the Bauer Deep (Sayles and Bischoff, 1973; Sayles et al, 1975), and the various sites of D.S.D.P. (Natland, 1973; Warner and Gieskes, 1973; Dymond et al, 1973; Cronan, 1976) Mn is remarkably enriched.

However, the average chemical composition of the Galapagos green hydrothermal material shows similarities with those of the clay-rich sediments described from the Gulf of Aden (Cann et al, 1977) and from the transform fault A in the Famous area (Hoffert et al, 1978a). Also, the depletion of Mn in Fe-deposits is known from the Red Sea (Bignell et al, 1976), the MAR (Cronan, 1972), the Santorini (Bonatti

et al, 1972b), and the Amph D2, a Pacific seamount (Bonatti and Joensuu, 1966) (see Table 3.3).

3.4.2 Results and Discussion of the Partition Studies

In the investigation of the distribution of Ca, Mn, Fe, Ni, Co, Pb, Zn, Cu and Al among the components of the Galapagos sediments, partition analysis has been carried out on ten samples from various depths of Hole 424. The partitioning data are given in Table 3.4, while Table 3.5 shows the average partitioning of elements in each type of sediment (Fe-rich clays, carbonate sediments, Mn-rich sediments). Details concerning the selective chemical attacks performed for the partition analysis are included in Appendix C (see also Section 2).

3.4.2a Manganese

Manganese is partitioned differently in the three groups of sediments.

In the Fe-rich clays, Mn is more concentrated in the HCl-soluble fraction (34%) than in any other fraction. This geochemical behaviour of Mn is rather unusual in comparison with its distribution in other metalliferous sediments studied so far (Cronan, 1976; this study). It may suggest that in this case Mn is held in the lattice structure of the Fe-rich clays (Horowitz, 1974). Horder (1979) reported that 36% of the total Mn was soluble in HCl leach in metal rich clays from D.S.D.P. sites 216 and 254. However, he noted that where the absolute values of Mn were higher it was almost exclusively

Table 3.3: Average analyses of DSDP, Site 424, ferruginous samples compared to other deposits.

	Ca %	Mn %	Fe %	Ni ppm	Co ppm	Pb ppm	Zn ppm	Cu ppm	Mg %	Al %	Si %
1	0.19	0.107	21.90	16	22	62	35	13	2.55	0.13	21.4
2		6.00	18.00	430	105		380	730		0.50	6.1
3	31.62	3.74	13.42	366	84	112	307	644		0.90	10.12
4		0.61	12.67							5.56	
5	1.47	6.06	20.07	460	82	100	470	790	2.08	2.73	10.84
6		3.20	11.00				250	200			
7		3.71	13.49	1000	200			980	2.33	2.34	21.0
8		6.66	23.60	630	86		600	1070		2.39	7.11
9		4.16	23.80	257	44	38	2	1550			
10	0.66	0.20	27.00	<5	<5			9	0.83	0.30	6.5
11	5.50	0.22	21.50	0	25	510	5200	2800			
12	0.55	<0.1	22.75	6	12		2	0	1.80	0.33	22.12
13	0.43	0.0774	26.51	10	2		6	46	1.76	0.11	21.27

1. This study: average of 9 ferruginous green clay samples from the DSDP, Site 424.
2. Bostrom and Peterson, 1969: East Pacific Rise crest surface sediments.
3. This study: East Pacific Rise surface sediments from the fracture zone at $9^{o}S$.
4. Cronan, 1972: average of four ferruginous sediment samples from the Mid-Atlantic Ridge near $45^{o}N$.
5. Cronan, 1976: East Pacific Rise basal metalliferous sediments.
6. Warner and Gieskes, 1974: Fe-rich basal sediments from the Indian Ocean, Site 245, DSDP.
7. Sayles and Bischoff, 1973: average composition of eight samples from the Bauer Deep.
8. Dymond et al, 1973: metalliferous sediments from N.E. Pacific, DSDP, Sites 37, 38 and 39.
9. Natland, 1973: DSDP, Site 183, basal ferromanganoan sediments from N.W. Pacific.
10. Bonatti et al, 1972b: iron deposits from Santorini.
11. Bignell et al, 1976: green smectite from the Atlantis II Deep.
12. Cann et al, 1977: green hydrothermal clay-rich material from the Gulf of Aden.
13. Hoffert et al, 1978: green hydrothermal clay-rich material from the Famous Area (MAR).

Table 3.4: Chemical Results from the partition studies of selected D.S.D.P. Leg 54, Hole 424, sediments.

Sample Number Depth (m)		Ca (%) a	Ca (%) b	Mn (%) a	Mn (%) b	Fe (%) a	Fe (%) b	Ni (ppm) a	Ni (ppm) b	Co (ppm) a	Co (ppm) b	Pb (ppm) a	Pb (ppm) b	Zn (ppm) a	Zn (ppm) b	Cu (ppm) a	Cu (ppm) b	Al (%) a	Al (%) b
424-1-1, (1.20)	119-121	0.33		3.80		22.00		17		22		149		35		14		0.09	
	HAc	0.14	42.42	0.11	2.89	0.65	2.95	6	35.29	9	40.91	9	6.04	3	8.57	0	0.00	0.01	11.11
	A/R	0.19	57.58	3.28	86.32	0.65	2.95	11	64.71	3	13.64	73	48.99	8	22.86	4	28.57	0.01	11.11
	HCl	0.00	0.00	0.00	0.00	20.31	92.32	0	0.00	10	45.45	22	14.77	8	22.86	0	0.00	0.04	44.45
	Res	0.00	0.00	0.41	10.79	0.39	1.78	0	0.00	0	0.00	45	30.20	16	45.71	10	71.43	0.03	33.33
424-2-1, (9.87)	36-38	0.18		0.08		22.00		12		22		95		28		9		0.03	
	HAc	0.07	38.89	0.02	25 00	0.10	0.46	0	0.00	0	0.00	0	0.00	1	3.57	0	0.00	0.01	33.33
	A/R	0.11	61.11	0.03	37.50	0.43	1.95	8	66.67	0	0.00	72	75.79	2	7.14	4	44.44	0.00	0.00
	HCl	0.00	0.00	0.03	37.50	20.37	92.59	4	33.33	4	18.18	0	0.00	6	21.43	0	0.00	0.00	0.00
	Res	0.00	0.00	0.00	0.00	1.10	5.00	0	0.00	18	81.82	23	24.21	19	67.86	5	55.56	0.02	66.67
424-2-2, (11.38)	37-39	0.15		0.05		22.00		17		22		50		30		12		0.07	
	HAc	0.08	53.33	0.02	40.00	0.18	0.82	0	0.00	1	4.55	0	0.00	0	0.00	1	8.33	0.01	14.29
	A/R	0.04	26.67	0.01	20.00	0.49	2.23	8	47.06	1	4.55	36	72.00	1	3.33	5	41.67	0.01	14.29
	HCl	0.00	0.00	0.02	40.00	21.05	95.68	5	29.41	2	9.09	0	0.00	14	46.67	0	0.00	0.04	57.13
	Res	0.03	20.00	0.00	0.00	0.28	1.27	4	23.53	18	81.81	14	28.00	15	50.00	6	50.00	0.01	14.29
424-2-3, (12.91)	40-42	0.17		0.07		22.00		17		22		50		33		12		0.07	
	HAc	0.10	58.82	0.02	28.57	0.17	0.77	0	0.00	1	4.55	0	0.00	0	0.00	1	8.33	0.01	14.29
	A/R	0.03	17.65	0.01	14.29	0.52	2.37	8	47.06	6	27.27	33	66.00	2	6.06	6	50.00	0.00	0.00
	HCl	0.01	5.88	0.03	42.86	21.31	96.86	5	29.41	0	0.00	6	12.00	18	54.55	0	0.00	0.04	57.14
	Res	0.03	17.65	0.01	14.28	0.00	0.00	4	23.53	15	68.18	11	22.00	13	39.39	5	41.67	0.02	28.57

Table 3.4: Continued.

Sample Number Depth (m)		Ca (%) a	Ca b	Mn (%) a	Mn b	Fe (%) a	Fe b	Ni (ppm) a	Ni b	Co (ppm) a	Co b	Pb (ppm) a	Pb b	Zn (ppm) a	Zn b	Cu (ppm) a	Cu b	Al (%) a	Al b
424-2-3,	121-123	0.21		0.09		21.00		27		22		50		54		24		0.43	
(13.72)	HAc	0.12	57.14	0.04	44.44	0.26	1.24	0	0.00	0	0.00	0	0.00	5	9.26	4	16.66	0.01	2.33
	A/R	0.03	14.29	0.01	11.12	0.50	2.38	18	66.67	0	0.00	23	46.00	3	5.56	10	41.67	0.03	6.98
	HCl	0.00	0.00	0.04	44.44	20.24	96.38	9	33.33	4	18.18	0	0.00	32	59.26	10	41.67	0.29	67.44
	Res	0.06	28.57	0.00	0.00	0.00	0.00	0	0.00	18	81.82	27	54.00	14	25.92	0	0.00	0.10	23.25
424-2-3,	140-142	17.25		0.18		7.75		60		16		21		171		74		1.29	
(13.91)	HAc	15.00	86.96	0.01	5.55	0.05	0.64	0	0.00	0	0.00	0	0.00	2	1.17	7	9.46	0.08	6.20
	A/R	0.00	0.00	0.03	16.67	0.44	5.68	0	0.00	3	18.75	14	66.67	9	5.26	9	12.16	0.11	8.53
	HCl	0.00	0.00	0.03	16.67	2.28	29.42	19	31.67	0	81.25	0	0.00	31	18.13	38	51.35	1.10	85.27
	Res	2.25	13.04	0.11	61.11	4.98	64.26	41	68.33	13	0.00	7	33.33	129	75.44	20	27.03	0.00	0.00
424-2-4,	39-41	0.22		0.11		22.00		17		22		50		38		20		0.17	
(14.40)	HAc	0.13	59.09	0.05	45.46	0.20	0.91	0	0.00	0	0.00	0	0.00	0	0.00	4	20.00	0.01	5.88
	A/R	0.04	18.18	0.01	9.09	0.54	2.45	3	17.65	0	0.00	43	86.00	3	7.89	6	30.00	0.01	5.88
	HCl	0.00	0.00	0.04	36.36	21.26	96.64	14	82.35	0	0.00	0	0.00	22	57.90	10	50.00	0.11	64.71
	Res	0.05	22.73	0.01	9.09	0.00	0.00	0	0.00	22	10.00	7	14.00	13	34.21	0	0.00	0.04	23.53
424-2-5,	24-26	4.02		0.10		16.50		37		20		42		87		58		1.07	
(15.75)	HAc	3.97	98.76	0.03	30.00	0.24	1.45	7	18.92	5	25.00	5	11.90	2	2.30	8	13.79	0.02	1.87
	A/R	0.05	1.24	0.01	10.00	0.30	1.82	13	35.14	6	30.00	4	9.52	5	5.75	14	24.14	0.03	2.80
	HCl	0.00	0.00	0.06	60.00	14.53	88.06	16	43.24	9	45.00	17	40.48	52	59.77	17	29.31	0.65	60.75
	Res	0.00	0.00	0.00	0.00	1.43	8.67	1	2.70	0	0.00	16	38.10	28	32.18	19	32.76	0.37	34.58

Table 3.4: Continued.

Sample Number Depth (m)		Ca (%) a	Ca b	Mn (%) a	Mn b	Fe (%) a	Fe b	Ni (ppm) a	Ni b	Co (ppm) a	Co b	Pb (ppm) a	Pb b	Zn (ppm) a	Zn b	Cu (ppm) a	Cu b	Al (%) a	Al b
424-2-6, (17.41)	40-42	18.50		0.26		6.70		193		34		23		233		105		2.40	
	HAc	17.12	92.54	0.14	53.85	0.19	2.84	16	8.29	0	0.00	5	21.74	20	8.58	24	22.86	0.09	3.75
	A/R	0.14	0.76	0.00	0.00	0.16	2.39	20	10.36	0	0.00	0	0.00	16	6.87	19	18.09	0.06	2.50
	HCl	0.00	0.00	0.10	38.46	4.95	73.88	157	81.35	34	100.0	18	78.26	178	76.40	40	38.10	1.32	55.00
	Res	1.24	6.70	0.02	7.69	1.40	20.89	0	0.00	0	0.00	0	0.00	19	8.15	22	20.95	0.93	38.75
424-3-1, (19.10)	9-11	0.52		10.75		18.45		16		17		294		57		13		0.05	
	HAc	0.34	65.29	0.24	2.23	0.14	0.76	0	0.00	0	0.00	0	0.00	1	1.76	1	7.69	0.01	20.00
	A/R	0.10	19.23	9.62	89.49	0.51	2.76	13	81.25	2	11.76	279	94.90	5	8.77	6	46.15	0.00	0.00
	HCl	0.01	1.92	0.53	4.93	17.16	93.01	0	0.00	2	11.76	0	0.00	12	21.05	0	0.00	0.02	40.00
	Res	0.07	13.46	0.36	3.35	0.64	3.47	3	18.75	13	76.48	15	5.10	39	68.42	6	46.15	0.02	40.00

Column 'a' presents the chemical concentrations.
Column 'b' presents the percentage of element removed by each attack.

The results opposite the sample number are the bulk chemical concentrations in the sample.

HAc: Acetic acid leach.
A/R: Acid-reducing agent leach only (i.e. A/R agent leach-HAc leach).
HCl: Hydrochloric acid leach only (i.e. HCl leach-A/R agent leach).
Res: HCl-insoluble residue (Bulk-HCl leach).

Table 3.5: Summary of the partition studies. The results are expressed as percentages of bulk composition.

		Ca	Mn	Fe	Ni	Co	Pb	Zn	Cu	Al
Fe-rich clays	A	51.62	31.06	1.19	5.88	8.33	1.01	3.57	8.88	13.54
	B	32.58	29.72	2.39	51.64	7.58	65.80	8.81	39.39	6.38
	C	0.98	33.52	95.08	34.64	15.15	4.46	43.78	15.27	48.48
	D	14.83	5.69	0.21	7.84	68.93	28.74	43.85	36.44	31.61
Carbonate sediments	A	95.65	41.93	1.42	13.61	12.50	16.82	5.44	18.33	2.81
	B	1.00	5.00	2.11	22.75	15.00	4.76	6.31	21.12	2.65
	C	0.00	49.23	80.97	62.30	72.50	59.37	68.09	33.71	57.88
	D	3.35	3.85	14.78	1.35	0.00	19.05	20.17	26.86	36.67
Mn-rich sediments	A	65.39	2.23	0.76	0.00	0.00	0.00	1.76	7.69	20.00
	B	19.23	89.49	2.76	81.25	11.76	94.90	8.77	46.15	0.00
	C	1.92	4.93	93.01	0.00	11.76	0.00	21.05	0.00	40.00
	D	13.46	3.35	3.47	18.75	76.48	5.10	68.42	46.15	40.00

A: Acetic acid leach (HAc).

B: Acid-reducing agent leach only (i.e. A/R agent leach-HAc leach).

C: HCl leach only (i.e. HCl leach-A/R agent leach).

D: HCl-insoluble residue (Bulk-HCl leach).

present in the acid-reducible fraction, indicating its association with the Fe-Mn oxide aggregates. A similar partition pattern is found here, as is shown below. The majority of the remainder Mn (31%) is found to be soluble in acetic acid, which may reflect its removal from adsorbed sites on the surface of the clays. A considerable amount of Mn (30%) is associated with Fe-Mn oxides which are soluble in the acid-reducing agent solution, while only 5% remains in the HCl-insoluble residue.

Although the majority of Mn in the carbonate sediments is also found in the HCl-soluble fraction (49%), the amount of Mn which is present in the acetic acid-soluble fraction (42%) is much higher than in the case of the Fe-rich clays. This may be due to the breakdown of Mn coatings on carbonate microfossils. Moreover, the proportion of Mn which is associated with the hydroxylamine HCl-soluble fraction in the carbonates (5%) is much lower than that found in the Fe-rich clays, thus indicating the lower proportion of Fe-Mn oxide aggregates present in these sediments. No significant differences have been found between the HCl-insoluble Mn in the carbonates and the Fe-rich clays.

The partition geochemistry of the Mn-rich sediments is in agreement with previous results from similar material (Cronan, 1976a; this study). About 90% of Mn is concentrated in the acid-reducing agent solution with little Mn present in the remaining chemical fractions. This indicates that Mn here is almost entirely in the form of ferromanganese oxide minerals.

There has been a change in the distribution of Mn between the chemically separated fractions with increasing depth down the length of the core. In the upper part of the sediments most of the

Mn is associated with the hydroxylamine HCl-soluble fraction, whereas at greater depths it is more concentrated in the HCl-soluble fraction. Figure 3.6 shows an increase in the proportion of Mn being dissolved in HCl and a parallel decrease of that found in the acid-reducing agent solution with depth in the core. This would suggest transfer of Mn from the Fe-Mn oxides to the Fe-rich clays or to the Fe-oxides with burial, or it could just reflect the relative abundance of oxides and silicates with depth. There is also a tendency for the acetic-acid soluble Mn to increase with depth in the core (Figure 3.7).

3.4.2b Iron

The partition of Fe is remarkably constant throughout the sediment column and generally similar in all types of sediment. It is chiefly in the HCl-soluble fraction (see Table 3.5), most probably as Fe-rich clays and Fe-oxides, while it is present only in minor amounts in the remaining fractions. However, it is noted that in the carbonate sediments a considerable amount of Fe is found in the HCl-insoluble residue, thus indicating its association with detrital minerals.

3.4.2c Nickel

In the Fe-rich clays Ni is associated with both the hydroxylamine HCl-soluble and the HCl-insoluble fractions, having higher concentrations in the former than in the latter. About 52% of the total Ni is concentrated in the acid-reducible fraction, indicating

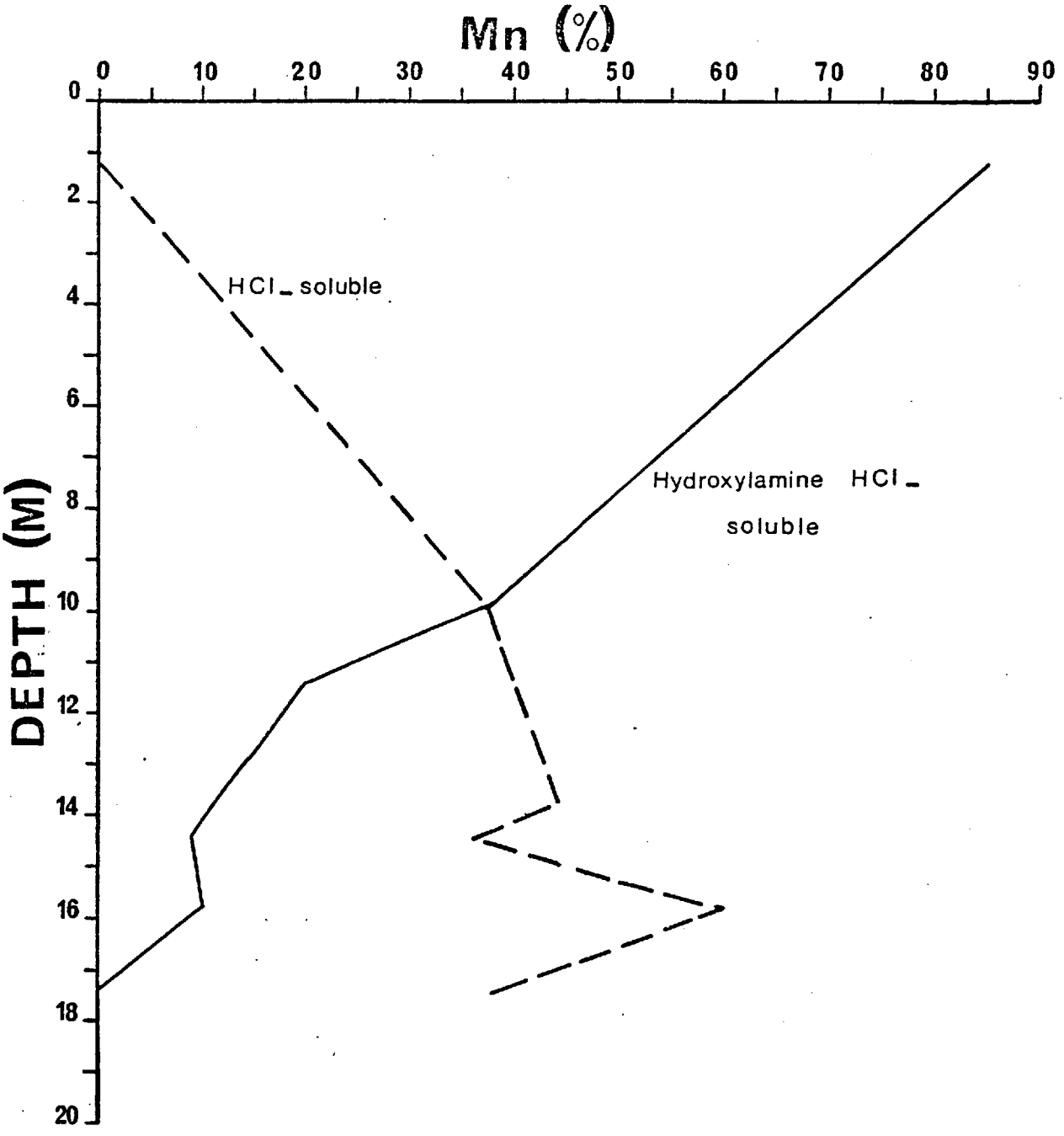

Figure 3.6: Distribution of the hydroxylamine HCl and the HCl-soluble Mn in the hole 424 expressed as a percentage of the total Mn concentration.

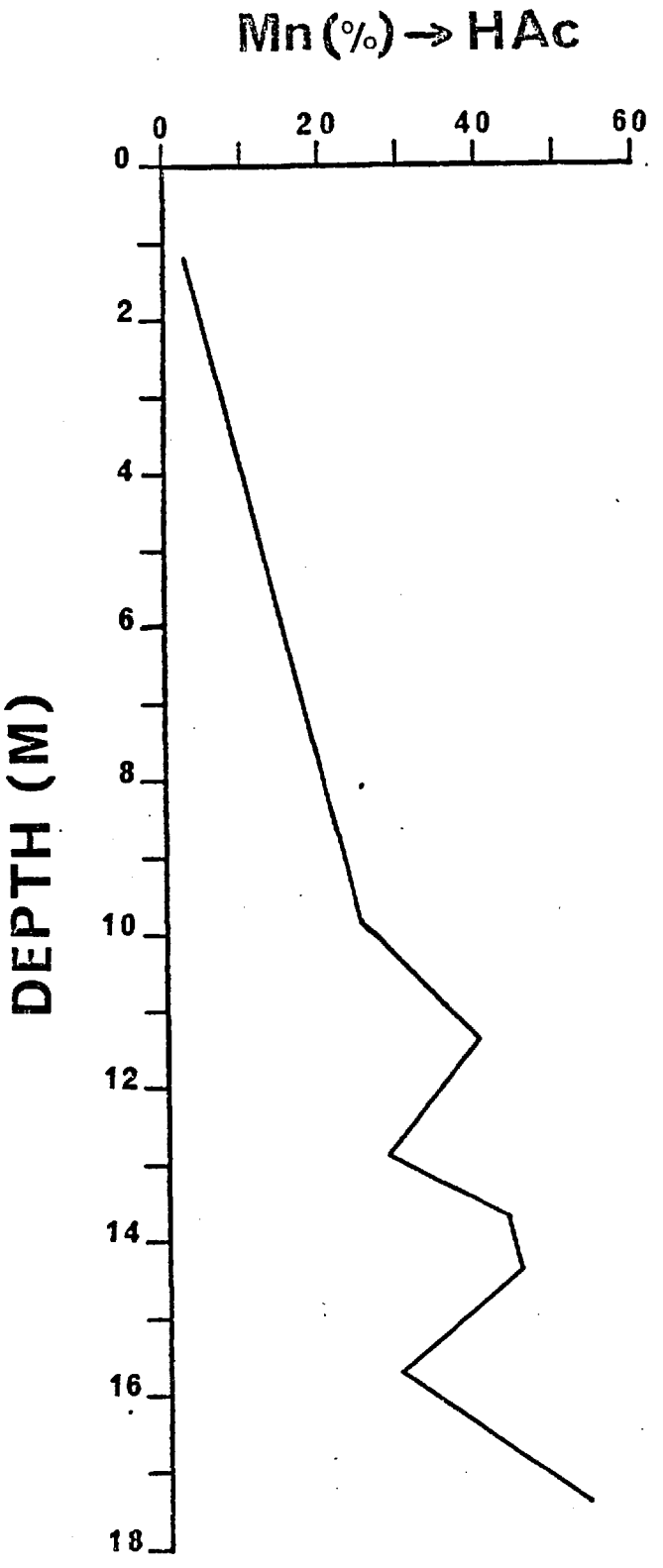

Figure 3.7: Distribution of the acetic acid soluble Mn in hole 424, expressed as a percentage of the total Mn concentration.

the strong association of this element with the Fe-Mn oxides, while about 35% is associated with the HCl-soluble fraction, being located in Fe-rich clays and the Fe-oxides. The remaining Ni is almost equally distributed between the acetic acid-soluble fraction and the HCl-insoluble residue.

In the carbonate sediments the amount of Ni which is soluble in the acid reducing agent solution is lower (23%), whereas more Ni is concentrated in the HCl-soluble fraction (62%). Thus, it is likely that Ni in the carbonate sediments is preferentially held in the Fe-oxides and the aluminosilicates rather than in the Fe-Mn oxides. In addition, the amount of Ni found soluble in the acetic acid (14%) is much greater in the carbonates. This is probably due to the adsorption of Ni on the Mn coatings present on the tests of forams (see partition of Mn in these sediments).

In the Mn-rich sediments the partition of Ni is rather similar to that found in the Fe-rich clays. About 81% of the Ni is found to be soluble in the hydroxylamine HCl-soluble fraction, showing its strong association with Fe-Mn oxides, while the remaining Ni (19%) is present in the HCl-insoluble residue, most probably held in the lattice of detrital minerals.

Generally it appears that the vertical distribution of Ni between phases varies with depth in a manner similar to that of Mn. Figure 3.8 shows an increase in the proportion of Ni being dissolved in HCl and a decrease of that located in the acid-reducible fraction with increasing depth. This might suggest transfer of Ni from the ferromanganese oxides to the Fe-oxides and the aluminosilicates with burial.

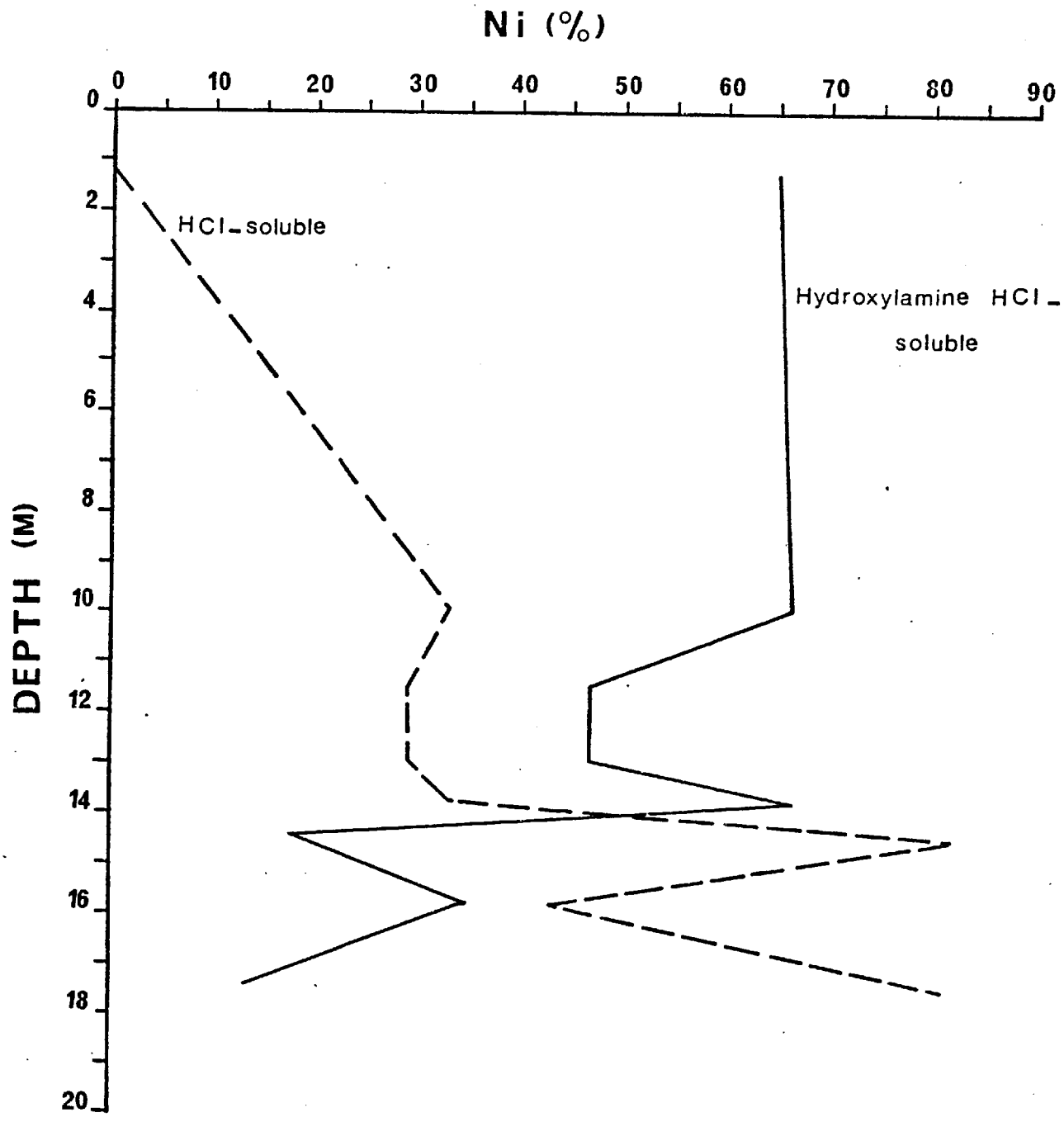

Figure 3.8: Distribution of the hydroxylamine HCl and the HCl-soluble Ni in hole 424 expressed as a percentage of the total Ni concentration.

3.4.2d Cobalt

Since Co in the Fe-rich clays is more enriched (69%) in the HCl-insoluble residue than in either of the other fractions, it is suggested that this element is mainly located in the structure of the more resistant silicates and aluminosilicates. The contribution of the rest of the chemical fractions to the total Co in the sediments decreases in the following order: HCl-soluble fraction (15%), acid-reducing soluble fraction (8%) = acetic acid soluble fraction (8%).

In contrast to the Fe-rich clays, in the carbonate sediments the majority of Co (73%) is found to be soluble in HCl, while no Co is present in the HCl-insoluble residue. The remaining Co is almost equally distributed between the acetic acid and the hydroxylamine HCl-soluble fractions.

As in the case of the Fe-rich clays, Co in the Mn-rich sediments is more concentrated in the HCl-insoluble residue (76%), while the remainder is equally distributed between the acid-reducible and the HCl-soluble fraction. The strong association of Co with the HCl-insoluble fraction in the Fe-rich clays and in the Mn-rich sediments indicates the presence of basaltic detrital minerals in these sediments. This partition pattern is in contrast to the case of the EPR at 9^{o}S fracture zone sediments, where most of the Co was found to be soluble in HCl.

3.4.2e Lead

Most of the Pb in the Fe-rich clays is associated with the Fe-Mn oxides, being soluble in the hydroxylamine HCl solution (66%). Most of the remaining Pb is essentially partitioned between the HCl-

soluble and insoluble fraction. More Pb occurs in the latter (28%) than in the former (5%) fraction. Only a very small amount of Pb is found in the acetic acid-soluble fraction.

The large contribution of the HCl-insoluble fraction to the total Pb in the Fe-rich clays may reflect the presence of basaltic detrital minerals in the sediments. The association of Pb with alteration of tholeitic basalts has been reported from elsewhere (Piper, 1973; Bertine, 1974).

In the carbonate sediments the largest portion of Pb (59%) is associated with the Fe-oxides and the aluminosilicates, being soluble in HCl. About 19% of it is in the HCl-insoluble residue, while 17% is associated with the acetic acid-soluble fraction. The association of Pb with the acetic acid-soluble fraction in carbonate sediments has been reported from elsewhere (Horowitz, 1974; Horder, 1979; this study).

In the Mn-rich sediments, Pb is almost all associated with Fe-Mn oxides, being soluble in the hydroxylamine HCl agent solution (95%). The remainder is present in the HCl-insoluble detrital residue.

3.4.2f Zinc

In the Fe-rich clays Zn is mainly distributed between the fraction soluble in HCl (44%) and the HCl-insoluble residue (44%), which indicates the strong association of this element with the Fe-rich clays, the Fe-oxides and the more resistant silicates and aluminosilicates. The Fe-Mn oxides contain a small amount of Zn (~ 9% is found in the acid-reducible fraction), while the least proportion of Zn is associated with the acetic acid-soluble fraction (3%).

In the carbonate sediments the majority of Zn (68%) is associated with the Fe-oxides and the alumino-silicates, being soluble in HCl. About 20% of the Zn is held in the lattice structure of detrital minerals (HCl-insoluble residue), while the remainder, 12%, is equally distributed between the acid-reducible and the acetic acid-soluble fractions.

In the Mn-rich sediments Zn is most concentrated in the HCl-insoluble residue (69%), indicating its strong association with the detrital material. The HCl-soluble fraction contains less Zn (21%), in contrast to the case of the Fe-rich clays and the carbonate sediments. However, the contribution of the acid-reducible fraction to the total Zn in the Mn-rich sediments is similar to that in the Fe-rich clays (9%).

Considerable variations in the vertical partition geochemistry of Zn are exhibited. The principal changes are in the distribution of Zn between the fractions which are soluble or insoluble in HCl. Generally, the contribution of the HCl-soluble fraction to Zn in the sediments increases with increasing depth in the core (see Figure 3.9). Certain variations in the Zn associated with the acid-reducible fraction also occur. These variations enable the core to be divided into two sediment units. In the upper sediment unit (0-10 m) a decrease in the proportion of Zn associated with the acid-reducible fraction occurs with increasing depth, whereas in the lower sediment unit this proportion remains constant.

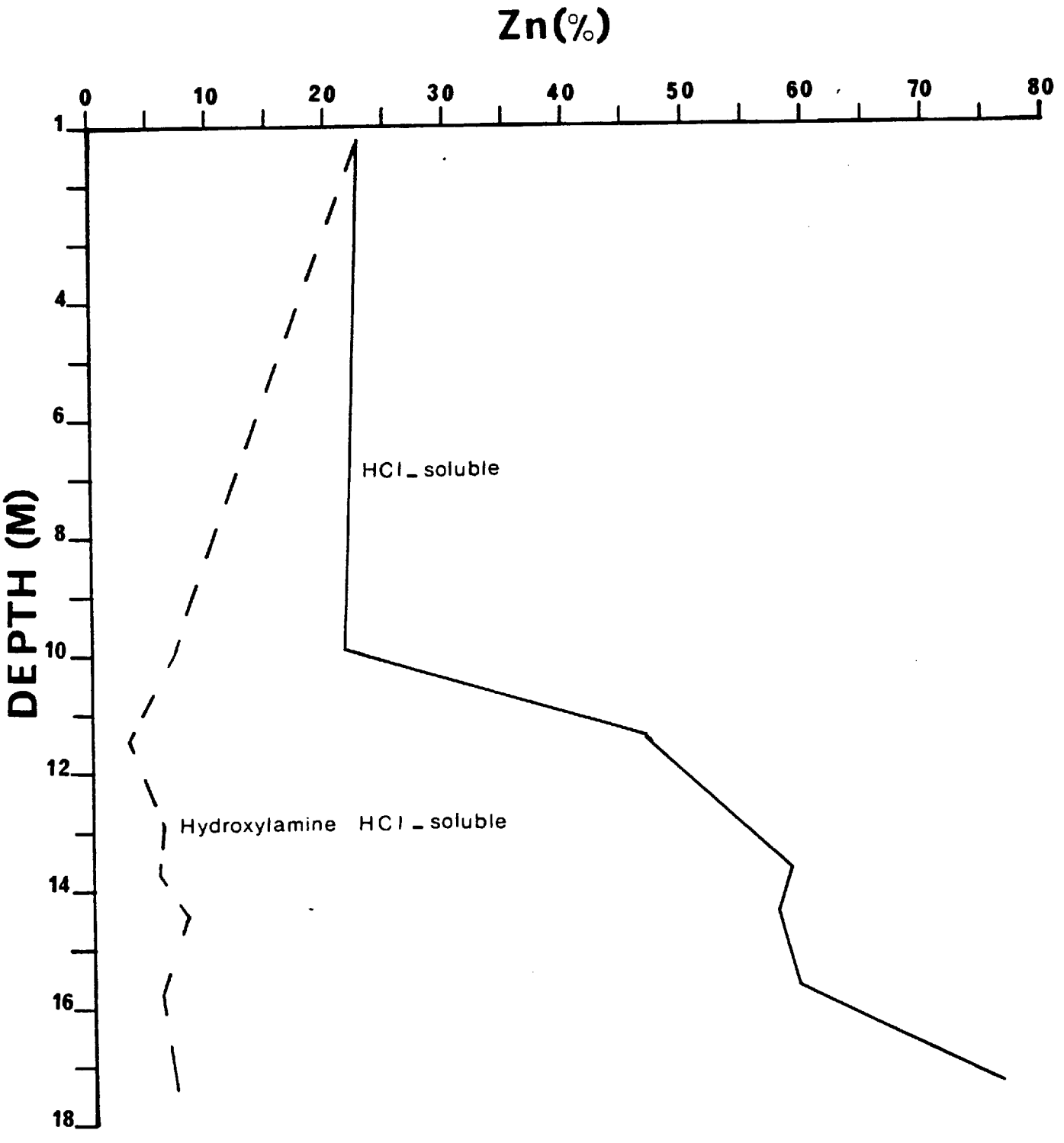

Figure 3.9: Distribution of the hydroxylamine HCl and the HCl-soluble Zn in hole 424 expressed as a percentage of the total Zn concentration.

3.4.2g Copper

In the Fe-rich clays about equal percentages of Cu are concentrated in the HCl-insoluble residue (37%) and the acid-reducible fraction (39%), indicating its strong association with the Fe-Mn oxides and the more resistant silicates and aluminosilicates. However, a considerable amount of Cu (15%) is located in the Fe-rich clays and the Fe-oxides, as it is soluble in HCl. About 9% of Cu is present in the acetic acid-soluble fraction.

Considerable differences in the partition chemistry of Cu have been observed between the Fe-rich clays and the carbonate sediments. In the latter the HCl-soluble Cu is higher than in any other fraction (34%). Moreover, the acetic acid-soluble Cu is greater in the carbonates than in the Fe-rich clays.

In the Mn-rich sediments, Cu is essentially distributed between the hydroxylamine HCl-soluble fraction and the HCl-insoluble residue.

In the upper part of the sediments (from 0 down to about 13 m) the proportion of Cu associated with the hydroxylamine HCl-soluble fraction increases while the HCl-insoluble detrital residue is constantly depleted in Cu with increasing depth. No Cu is found to be soluble in the acetic acid or in the HCl in these sediments. At about 13 m the geochemical behaviour of Cu in regard to its partition between phases changes dramatically. The acetic acid and the HCl-soluble sediment is progressively enriched in Cu with increasing depth, while a decrease in the proportion of Cu associated with the acid-reducible material occurs (see Table 3.4).

3.4.2b Aluminium

The partition of Al in the Fe-rich clays and in the carbonate sediments is rather similar. In both cases the majority of Al is concentrated in the HCl-soluble fraction with a considerable amount of it in the HCl-insoluble residue. Minor amounts of Al are found to be soluble in the acetic acid and in the hydroxylamine HCl agent solution.

In the Mn-rich sediments equal amounts of Al are present in the HCl-soluble fraction and in the HCl-insoluble residue (40%). The remainder Al (20%) is concentrated in the acetic acid-soluble fraction.

There are some variations in the partitioning of Al between the hydroxylamine HCl-soluble fraction and the HCl-insoluble residue down the length of the core. From 0 down to 10 m depth the acid-reducible Al decreases, while that remaining insoluble in the HCl increases with depth. From 10 m down to 17 m there is a tendency for the hydroxylamine HCl-soluble Al to increase, while that present in the HCl-insoluble residue decreases with depth (see Figure 3.10).

3.4.3 Summary and Conclusions of the Partition Studies

1) There are considerable differences in the partition patterns between the Fe-rich clays, the carbonate sediments, and the Mn-rich sediments.

2) In the Fe-rich clays most of the Mn, Fe and Al are associated with the HCl-soluble fraction, while the majority of Ni, Pb and Cu are located in the hydroxylamine HCl-soluble

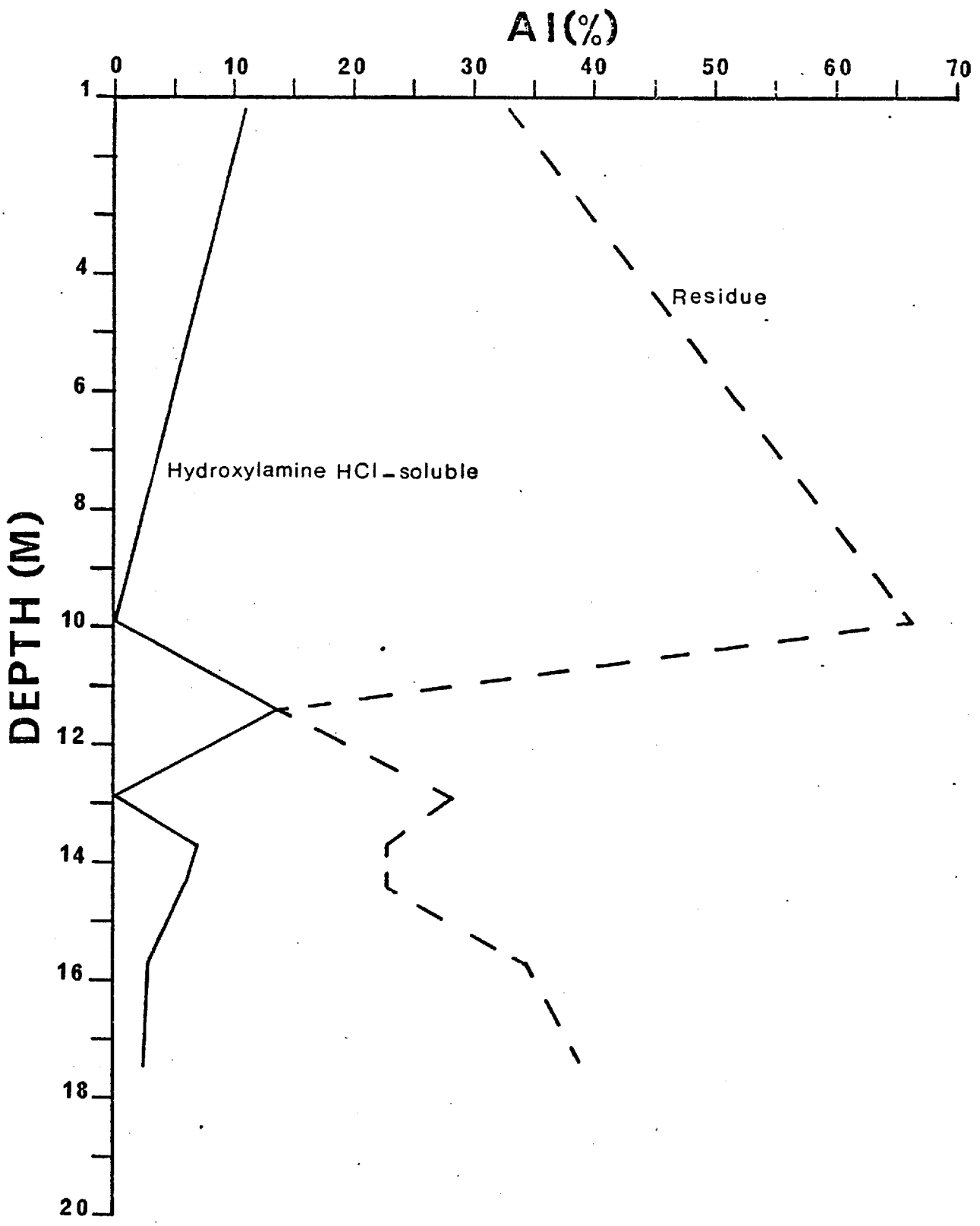

Figure 3.10: Distribution of the hydroxylamine HCl-soluble Al and that remaining in the HCl-insoluble residue in hole 424 expressed as a percentage of the total Al concentration.

fraction. Cobalt is more concentrated in the HCl-insoluble residue, while Zn is equally distributed between the HCl-soluble fraction and the HCl-insoluble residue. The presence of significant amounts of Co, Pb, Zn, Cu and Al in the HCl-insoluble residue of the Fe-rich clays would suggest the incorporation of large quantities of basaltic detrital material in these sediments. Since there is no carbonate material in these sediments, the high proportion of Mn associated with the acetic acid-soluble fraction may reflect its removal from adsorbed sites on the surface of the Fe-rich clays.

3) Except for Ca, the majority of all other elements (Mn, Fe, Ni, Co, Pb, Zn, Cu and Al) in the carbonate sediments is associated with the HCl-soluble fraction. This may reflect the process of normal pelagic sedimentation, where these elements are incorporated in the clayey fraction of the sediments. However, the high concentrations of Mn, Pb and Cu in the acetic acid-soluble fraction indicate the removal of these elements from biogenic calcium carbonate (microfossils) or from coatings on carbonate material. The low proportion of Fe, Mn and trace metals in the acid-reducible fraction of the carbonate sediments may reflect the low quantities of Fe-Mn oxides present in these sediments, possibly because of their reducing nature.

4) The Mn-rich sediments show partition patterns different from those of Fe-rich clays and the carbonate sediments. However, the general partition patterns of the Mn-rich sediments are more similar to those observed for the Fe-rich clays than for the carbonates. This is due to the presence of Fe-rich clayey

material in these sediments. In the Mn-rich sediments Mn, Ni and Pb are associated with the acid-reducible fraction, Fe is more concentrated in the HCl-soluble fraction, while Co and Zn are predominantly in the HCl-insoluble residue. Copper is equally distributed between the acid-reducible fraction and the HCl-insoluble residue. Aluminium is equally distributed between the HCl-soluble and the HCl-insoluble fraction. The high proportion of Mn associated with the hydroxylamine HCl-soluble fraction indicates the presence of high quantities of Fe-Mn oxides in the sediments.

5) The general decrease of the hydroxylamine HCl-soluble Mn and Ni with depth in the core and the parallel increase of these elements in the HCl-soluble fraction might suggest post-depositional transfer of Mn and Ni from the Fe-Mn oxides to the Fe-oxides and the Fe-rich clays, or it could just reflect the relative abundance of oxides and silicates with depth.

6) The acetic acid-soluble Mn increases with increasing depth in the core.

3.5 GENERAL DISCUSSION

It is notable that the concentrations of Ni, Co, Zn and Cu are extremely low in the Galapagos sediments, particularly in the distinct ferruginous horizons. Two possible explanations are envisaged for the depletion of these metals in the hydrothermal deposits:

1) The hydrothermal solutions which are responsible for their formation are depleted in these metals.

2) The rapid precipitation of the major phases (Fe-rich clays, Fe-oxides) does not allow scavenging of the metals from sea water.

Cronan (1976b) suggested that oxidizing sea water may penetrate and circulate within the fractures and fissures of the upper part of the oceanic crust, this leading to a mixing with hydrothermal solutions which may cause precipitation of metal sulfides. This suggestion is supported by the direct observations and measurements made by the scientific party aboard the submersible 'Alvin' while they were investigating the hydrothermal regions within the Galapagos Rift (Ballard, 1977; Corliss et al, unpub. ms.). It was observed that hot water which was rich in H_2S was coming out from a number of vents within the area examined; Mn and other elements were precipitating out of the hot water, forming a brown stain on the lava surface. The presence of H_2S, taken up by bacteria, provided the basis of a food chain which supported a dense biological community around the cracks. Its source was attributed to the convection of the sea water sulfate to hydrogen sulfide, after the subsurface mixing of the sea water with the hydrothermal fluids.

It seems likely that the H_2S formed reacts with the metals dissolved in the ascending hydrothermal fluids to form insoluble metal sulfides, possibly according to the following reactions:

$$H_2S + Zn \longrightarrow ZnS + H_2$$

$$H_2S + Cu \longrightarrow CuS + H_2$$

$$2H_2S + Fe \longrightarrow FeS_2 + 2H_2$$

Unlike Ni, Co, Zn and Cu, not all Fe precipitates in this form. Provided that the circulation of sea water occurs within the upper part of the newly formed crust within fissures and cracks, the basement faults of the DSDP site 424 are the most probable sites for the deposition of metal sulfides. Fe-oxides may also precipitate within the basement faults, above the metal sulfides and close to the sediment-basalt boundary, where more oxidizing conditions occur (Cronan, 1976b).

Thus the hydrothermal solutions which flow out from the basement faults during a subsequent period first pass over the precipitates of metal sulfides, and secondly over the Fe-oxides, which may play an active role in determining the final composition of the hydrothermal solutions, before they reach the ocean floor (Moore and Vogt, 1976). The precipitates of metal sulfides and Fe-oxides may act as "filters" of metals absorbing Ni, Co, Zn and Cu from the passing hydrothermal solutions (Krauskopf, 1956), so that when they reach the sea water they are markedly depleted in these metals.

Although this hypothesis explains why the Galapagos Fe-rich sediments are not enriched in trace metals, it is not able to explain why the concentrations of trace metals in these sediments are lower than the average concentrations which occur in normal pelagic sediments.

It is known that "scavenging" of metals from sea water by suspended material and their transference to the sea-floor is an important process in the incorporation of trace metals in deep-sea sediments (Goldberg, 1954). Precipitates such as MnO_2, and Fe-hydroxides which exist in the ocean waters, are efficient scavengers of trace metals, so that they participate along with other processes in the removal of trace elements from the sea water and transferring them to the sediments.

Chemical studies of manganese nodules and ferruginous pelagic clays provided evidence of the scavenging action of Fe and Mn hydroxides. Goldberg (1954) found a positive linear correlation between Mn and Ni in Mn-nodules and Fe-rich pelagic clays, which indicates that Ni has been incorporated into the nodules and reached the sediments by its adsorption onto MnO_2. That Co has been similarly scavenged by Fe-hydroxides is illustrated by a linear relationship with the Fe content in Mn nodules.

The following factors are important in controlling the amount of trace elements being adsorbed onto dispersed phases in sea water:

1) The amounts of trace elements which are dissolved in the sea water: as the amount of the trace elements in solution increases, the degree of scavenging becomes greater.

2) The total surface area of the scavengers: the increase of the amount of the dispersed material results in the increase of the scavenging.

3) The time during which the precipitates remain in suspension in the sea water, before they reach the ocean floor: the longer the scavengers remain in the sea water, the higher is the amount of the adsorbed trace elements.

It seems reasonable that all these factors control the concentration of Ni, Co, Zn and Cu in the sediments studied here. Because the concentrations of Ni, Co, Zn and Cu in these sediments are much lower than the concentrations found in normal pelagic sediments (Cronan, 1969), which are deposited slowly from normal sea water, it is concluded that the formation of these sediments took place under

different physico-chemical conditions from those occurring during normal pelagic sedimentation.

The factor which is probably most important in explaining the extremely low concentrations of trace metals in the Galapagos Fe-rich sediments is their rate of deposition. It is suggested that the rate of deposition of the major phases is very high and the time of their residence in the sea water is so short that the scavenging is very limited. This explanation is consistent with the trace element veil theory proposed by Wedepohl (1960), in which it has been assumed that the "excess" trace elements in deep sea sediments reach their present position by a homogeneous removal from sea water. Any geographical variation in their concentrations has been attributed to the variations of the rate of sedimentation. It is also in full agreement with Chester et al (1976), who found a negative linear correlation between the concentrations of Ni, Zn and Cu, which were not bound to crystal lattices, and the sedimentation rates of the host Bermuda Rise sediments.

Therefore, it is concluded that a combination of two factors determines the composition of the present sediments; the rapid precipitation of the Fe-rich sediments along with the depletion of the hydrothermal solutions in trace metals.

An attempt has been made in the present study to investigate the form in which Si is present in the Galapagos sediments, and to determine the possible form in which it precipitated from the hydrothermal solutions. The selective chemical analyses indicate that Fe is associated chiefly with the HCl-soluble fraction ($\sim$86%). This, along with the fact that there is a positive linear correlation

between the Fe which is soluble in HCl and the total SiO_2 (Figure 3.11) leads to the conclusion that the majority of Fe and Si in the sediments examined are present in the form of an Fe-rich clay mineral.

Comparison of the Fe-Mn-Si ternary diagram for the Galapagos sediments of site 424 with a similar diagram given by Corliss et al (1978) for Galapagos mound samples, shows that the ferruginous sediments of the DSDP site 424 fall into the field of nontronite (Figure 3.12). Therefore, it was assumed that most of the Fe and Si present in the sediments studied is in the form of this mineral. This was subsequently confirmed by X-ray diffraction. It has been formed either by direct precipitation from the hydrothermal solutions which contain large amounts of Fe and Si, or diagenetically from the reaction between Fe-hydroxides and SiO_2 after their precipitation from the hydrothermal solutions as two separated phases. Which of these two processes takes place is not always easy to determine.

To examine the possibility of diagenetic formation of an Fe-rich clay mineral, after the precipitation of Fe and Si from the hydrothermal solutions, the following reaction should be considered.

$$\text{Fe-hydroxides} + SiO_2 \xrightarrow{\text{diagenesis}} \text{Fe-rich clay mineral}$$

If this reaction takes place in the Galapagos sediments, then the proportion of Fe present in the sediments in the form of Fe-hydroxides should decrease, whereas that associated with the Fe-rich clays should increase with time. This can be tested by examining variations in the distribution of Fe between the acid-reducible fraction and the fraction soluble in HCl, because the Fe which is present in the form of Fe-hydroxides is partly soluble in the acid-reducing agent solution, while

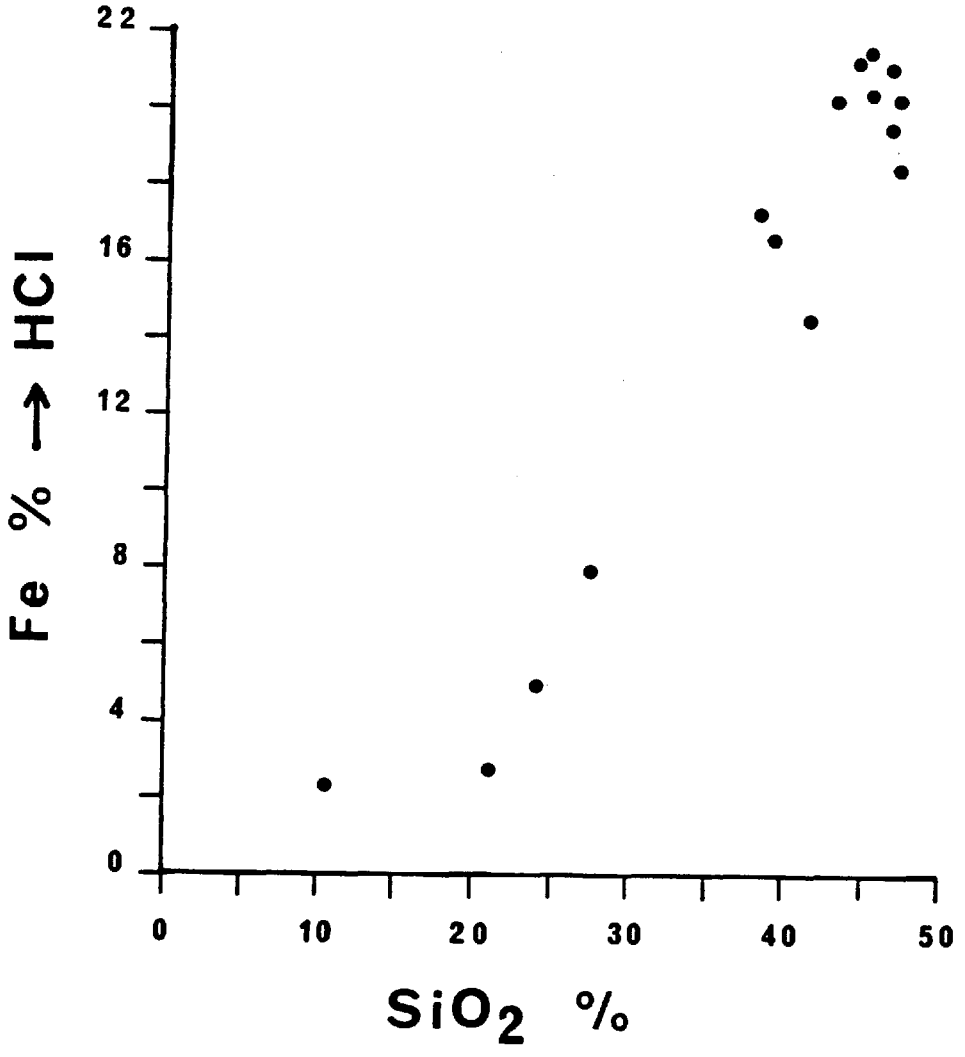

Figure 3.11: Scatter plot of SiO_2 content, corrected to a calcium carbonate free basis, versus HCl-soluble Fe expressed as a percentage of the total Fe concentration.

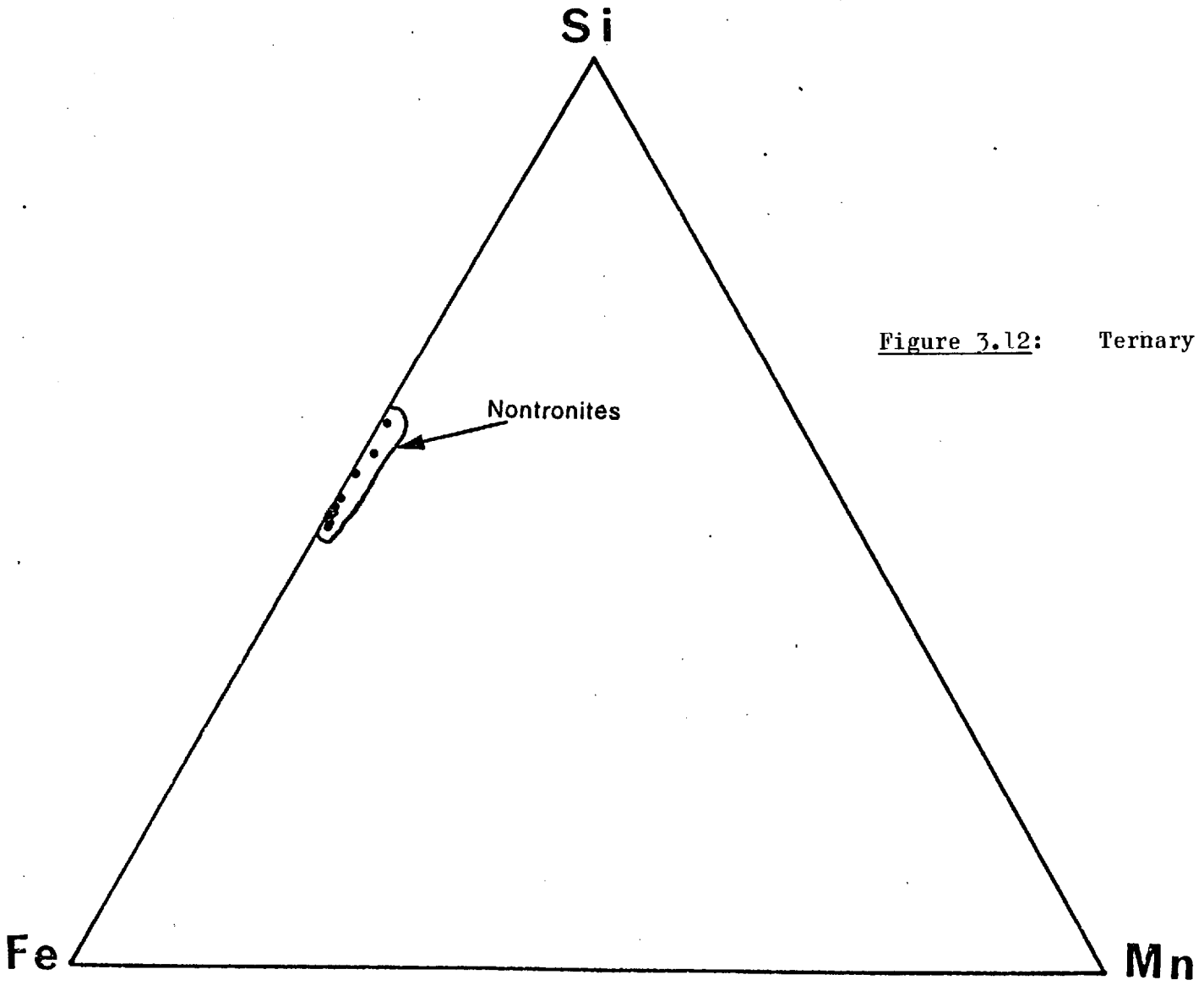

Figure 3.12: Ternary diagram of Fe-Mn-Si.

that located on the clay minerals is dissolved only in HCl. There is no tendency for the Fe associated with the HCl-soluble fraction to increase with increasing depth in the core. In addition, the proportion of Fe which is soluble in the hydroxylamine HCl solution is constant down the length of the core.

Thus, it is concluded that no transformations of one Fe phase to another occurs in the present sediments. Therefore, there is no evidence of the diagenetic formation of Fe-rich clay minerals from reaction between SiO_2 and Fe-hydroxides after their precipitation from the hydrothermal solutions. It is, therefore, reasonable to suggest that the Fe-rich clays found in the Galapagos sediments precipitate directly from the hydrothermal solutions, after becoming mixed with sea water.

The fact that the Mn-crusts present at the top of the sediments contain very little Fe, while the underlain Fe-rich deposits are depleted in Mn, indicates that a fractionation between Fe and Mn occurs in the sediments. The experimental conditions for the direct precipitation of nontronite from hot solutions containing Fe and Si require a reducing environment (Harder, 1976). Therefore during the precipitation of the Fe-rich nontronites (reducing conditions) Mn remains in solution, and as it takes a relatively long time to precipitate (Seyfried and Bischoff, 1977) it has the potential for migrating away from its hydrothermal source. The vertical distribution of Mn in the core 424 (Figure 3.3) indicates that it remains in the sea water after the precipitation of Fe, so that it precipitates later at the top of the Fe-deposits, although some may escape from the area by dispersion through sea water.

The Fe/Mn ratios vary vertically in the core, showing an increase with increasing depth from the surface sediments down to 11.38 m, while at greater depths there is an alternation of layers with high Fe/Mn ratios with others having low Fe/Mn ratios. The importance of the vertical variations of the Fe/Mn ratios is that they provide evidence of hydrothermal solutions being discharged periodically onto the ocean floor. The layers with high Fe/Mn ratios represent sediments deposited during the time when discharge of hydrothermal solutions starts, whereas those having lower Fe/Mn ratios are sediments which have been formed from the residual solutions of the hydrothermal activity. This is consistent with the observations on the Santorini hydrothermal deposits made by Smith and Cronan (1975), where the sediments from the inner exhalative zone (close to the fumarolic outlets) are characterized by high Fe/Mn ratios in contrast to the outer exhalative zone (away from the fumarolic center), where the Fe/Mn ratios are low. Fluctuations in the Fe/Mn ratios are also reported from sediments near Stromboli (Bonatti et al, 1972b), which suggests a similar process of sedimentation. Similarly, there is a marked fractionation of Mn from Fe in the Red Sea hydrothermal deposits, where a pattern including geochemical zones was found around the Atlantis II deep (Bignell et al, 1976). The precipitation of Fe before Mn formed an inner geochemical halo, while Mn formed an outer halo extending 10 km from the deep.

Therefore, there is evidence to conclude that the geochemical conditions which occur during the precipitation of the Galapagos deposits are similar to those found in the Red Sea and the Santorini hydrothermal areas. The phenomenon of the fractionation of Mn from Fe,

as well as the relative position of the Fe and Mn deposits, would suggest that the same chemical process is taking place in these three areas. The only difference is that in the Galapagos deposits the results of this process are exhibited vertically, whereas in the Santorini and the Red Sea surface sediments they are exhibited horizontally.

3.6 SUMMARY AND CONCLUSIONS

1) Fe-rich hydrothermal sediments form distinct horizons of considerable thickness in the DSDP, site 424 deposits. There is a positive linear relationship between Fe and Si, and the HCl-soluble Fe and Si. The majority of Fe is present in the form of an Fe-rich clay mineral, probably nontronite.

2) There has been a fractionation between Mn and Fe, the Mn being deposited at the top of the sediment column, in the form of Mn-oxide crusts, which contain very little Fe.

3) The Fe-rich hydrothermal sediments are extremely depleted in Al, Mn and trace metals such as Ni, Co, Zn and Cu. The concentrations of Pb are close to the average concentration in Pacific surface pelagic clays.

4) The strong depletion of the ferruginous clays in trace metals can be attributed to their absence from the hydrothermal solutions and to the rapid precipitation of the clays so that scavenging is limited. The depletion of Ni, Co, Zn and Cu in the hydrothermal solutions is due to the earlier precipitation of these elements in the form of metal sulfides within the basaltic vents.

5) The average chemical composition of the Galapagos hydrothermal clays shows similarities with those of the clay-rich sediments described from the Gulf of Aden and from the Famous area.

6) There is no evidence of diagenetic formation of the Fe-rich clays because there is no tendency for the Fe associated with the HCl-soluble fraction to increase with increasing depth in the core. The proportion of Fe which is soluble in the hydroxylamine HCl solution is constant down the length of the core.

7) It is suggested that the Fe-rich clays precipitate directly from the hydrothermal solutions under reducing conditions.

8) The vertical variations of the Fe/Mn ratios show that there is an alternation of layers with high Fe/Mn ratios with others having low Fe/Mn ratios. This implies periodical discharge and fractionation of the hydrothermal solutions onto the ocean floor.

9) The chemical composition and the mode of emplacement of the Galapagos deposits suggest that the chemical process which is responsible for their formation is similar to that taking place in the Santorini and the Red Sea hydrothermal areas. However, in the Galapagos deposits the results of this process are exhibited vertically, whereas in the Santorini and the Red Sea sediments are exhibited horizontally.

10) There are considerable differences in the partition patterns between the Fe-rich clays, the carbonate sediments and the Mn-rich sediments.

11) There is an increase in the proportion of Mn and Ni being dissolved in HCl and a parallel decrease of these elements in the hydroxylamine HCl-soluble fraction with depth in the core.

12) There is a tendency for the acetic acid-soluble Mn to increase with depth in the core.

SECTION 4

GEOCHEMICAL INVESTIGATIONS ON METALLIFEROUS SEDIMENTS FROM THE BAUER DEEP

4.1 INTRODUCTION

Bauer Deep sediments are enriched in a number of metals such as Ni, Cu and Mn above their normal values in pelagic clays. Because of their great extent (larger than the United Kingdom) they have been spoken of as a large low-grade ore body (Heath et al, 1972) which, because of their fine-grained and unconsolidated state, might be pumped to the surface in the same manner as Red Sea brines and metalliferous sediments. There has been some controversy between the 'Oregon State School' (Heath and Dymond, 1977) who considered the metals in Bauer Deep sediments to have been derived from the East Pacific Rise crest and transported to the Bauer Deep by currents, and the 'Hawaii Institute of Geophysics School' (McMurtry and Burnett, 1975) who consider the metal enrichments to be of local volcanic origin.

In this work, a study of the chemistry of five sediment cores from the Bauer Deep was undertaken. The locations of the cores are shown in Figure 4.1. Bulk and partition analyses on a considerable number of sediment samples were carried out. All the results have been evaluated in relation to water depth and the process of formation of Fe-rich smectites was investigated.

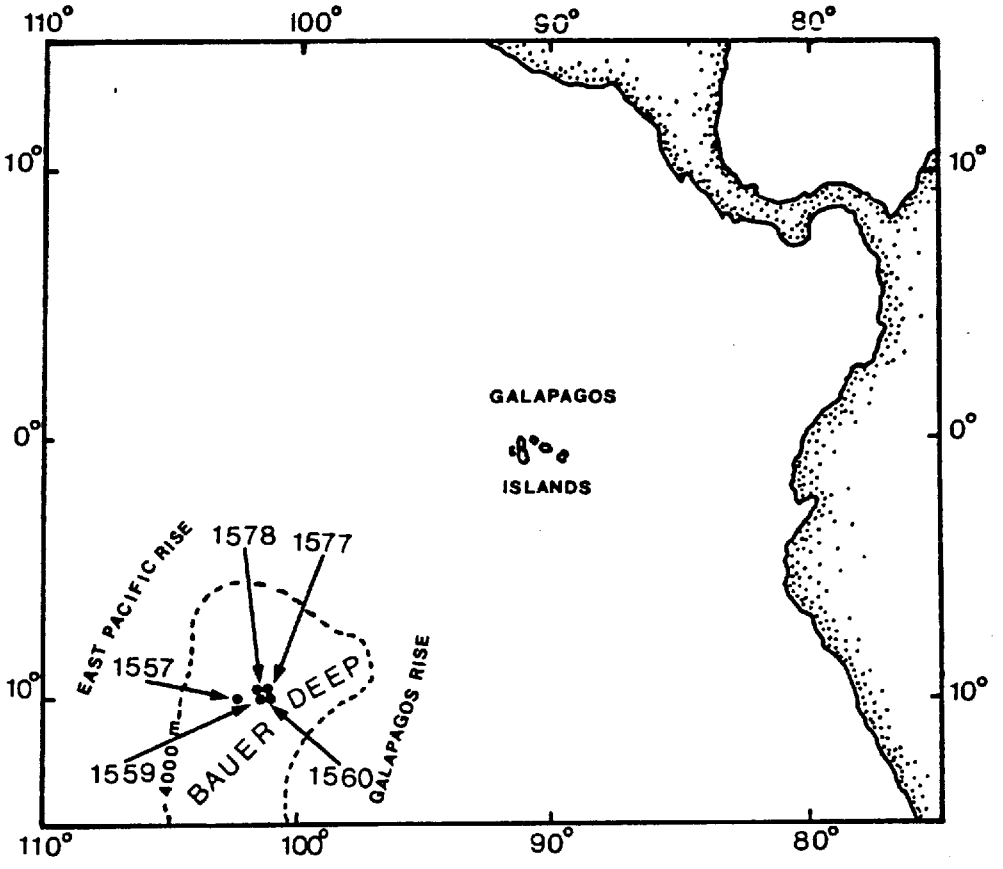

Figure 4.1: Map showing the location of Bauer Deep cores studied.

4.2 PREVIOUS GEOCHEMICAL STUDIES ON METALLIFEROUS SEDIMENTS FROM THE BAUER DEEP

In a comparative chemical, mineralogical and isotopic study of metalliferous sediments from near the basement of the S.E. Pacific, the East Pacific Rise and the Bauer Deep, Dymond et al (1973) indicated that these sediments had a common origin. However, they found significant differences in chemical composition between the sediments from the Bauer Deep, the Rise crest and the D.S.D.P. sites. Compared with the EPR and the DSDP sediments, the Bauer Deep sediments were characterized by less marked Fe and Mn enrichments, while their Si and Ni enrichments were higher. This was attributed to the dilution of Fe and Mn by the presence of an Fe-rich montmorillonite, which was identified in lower concentrations in the East Pacific Rise and the DSDP samples. The same mineral was considered to be responsible for the increased Si content in the Bauer Deep sediments, while the higher concentrations of Ni were explained as the result of these sediments containing a greater proportion of ferro-manganese micronodules. The authors concluded that the sediments from the Bauer Deep were the most chemically and mineralogically extreme of the three groups studied and that this was a reflection of the processes accompanying transport of the elements from the East Pacific Rise crest to the Bauer Deep.

Sayles and Bischoff (1973) investigated a considerable number of sediment cores from the Bauer Deep in order to establish their general mineralogical and chemical composition and they found that 90% of the non-carbonate mineral fraction was made up of smectites with micronodules comprising about 10% of the sediment.

Minor amounts of quartz and felspars were also found to be present, while phillipsite was rare or absent. It was shown that the distribution of metalliferous deposits within the Deep was largely governed by water depth. The surface layer of the cores taken from below 4200 m depth consisted almost exclusively of ferromanganoan sediment and all sediments recovered from above 4000 m depth were entirely of calcareous material. The surface sediment of the cores obtained at about 4100 m depth was calcareous, grading into carbonate-free metal-rich sediment deeper in the cores. Compared to normal pelagic clays the Bauer Deep sediments were found to be enriched in certain elements such as Fe, Mn, Ni, Cu, Zn, Co, Pb and Ba. The authors excluded the possibility that the smectites had a detrital origin and they postulated that it had formed diagenetically in the upper 20 cm of the sediments.

However, in a later study Sayles et al (1975) suggested that there was no evidence of a diagenetic origin for the Fe-rich montmorillonite in the Bauer Deep sediments. Since there was no continental source for this mineral (Griffin et al, 1968) they concluded that it must have formed authigenically throughout the entire area. A hydrothermal source was rejected, based on mineralogical differences from known hydrothermal smectites. The dilution effect of SiO_2 on the Fe content was shown by a strong negative correlation between Fe and Si.

McMurtry (1975) investigated the mineralogy and geochemistry of sediments across the Nazca plate at $12^{o}S$ and he noted the presence of metalliferous sediments between $90^{o}W$ and $105^{o}W$ which were characterized by an abundance of phillipsite and barite and a depletion of quartz and mica. In contrast to the mineralogical data of Sayles and Bischoff (1973), McMurtry (1975) reported that montmorillonite comprised

less than 10% of the non-carbonate fraction of the Bauer Deep sediments. Since phillipsite has been found to associate with volcanic products its occurrence was considered as an indication of the presence of local volcanism. Consequently the association of barite with phillipsite and calcite was explained as the result of its volcanic and biological origin. Other minerals such as goethite, apatite, kaolinite and chlorite were also identified in the bulk samples of the metalliferous sediments. It was shown that there has been size fractionation for some minerals. For instance, phillipsite was most abundant in the $>2\,\mu m$ fraction, while goethite and montmorillonite were most abundant in the $<2\,\mu m$ fraction. A rough estimate of the proportion of amorphous material present in the sediments showed that a mixture of biogenic and metalliferous sediments was characterized by moderate (40% to 80%) amounts of amorphous material. By contrast, low carbonate metalliferous sediments contained a high proportion (>80%) of amorphous material. Based on high Fe and Mn to Al_2O_3 ratios and on high Mn accumulation rates, the author concluded that the Bauer Deep metal-rich sediments were derived locally from a hydrothermal source.

Dymond et al (1976) have presented data showing the vertical variation in the chemical composition of metalliferous sediments from D.S.D.P. site 319. They demonstrated that the upper 20 m of the sediments are similar in composition to surface Bauer Deep sediments, while the basal sediments strongly resembled East Pacific Rise sediments. The elements Ca, Zn, Mn and Fe are strongly correlated with each other and they have their highest concentrations in the basal sediments. In contrast, the upper sediments (0-20 m) are more enriched in Ni, Co, Ba and La relative to Fe and Mn. The authors

suggested that the clear distinction between the chemical composition of near-basement and near-surface sediments was a result of differing sources for the elements and of different conditions during their deposition. Based on geophysical data, which suggest that site 319 was near the crest of the Galapagos Rise between 16 and 13 m.y. ago (a period during which the lower 40 m of the sediments were deposited) these authors concluded that the basal sediments originated from a hydrothermal process accompanying mid-ocean ridge volcanism. In contrast, the surface sediments (0-20 m) were deposited after the site had moved from the Galapagos Rise into the Bauer Deep. Thus, it was considered that this type of sediment was formed by direct precipitation of phases from sea water or from transportation of hydrothermal phases from the East Pacific Rise. Although hydrothermal activity from the East Pacific Rise was not considered to be responsible for the differences in composition of near-surface and basal sediments, it was demonstrated that the formation of the East Pacific Rise was reflected in the sediments. It was found that the sample which represented an age of 8 m.y. had metal accumulations higher than the samples above and below. According to the geophysical data, the initiation of spreading at the East Pacific Rise began 8 m.y. ago. In addition, at the time when the East Pacific Rise began to form, site 319 was closer to the East Pacific Rise (300 km) than to the Galapagos spreading center (600 km). It was therefore argued that the increase of metal accumulation rates in the sample represented by 8 m.y. age was a reflection of the East Pacific Rise volcanism but the concordance of the ages of the basement basalts and the overlying sediments indicated that the basalts were emplaced on the Galapagos Rise. In

conclusion, the authors rejected the possibility suggested by Anderson and Halunnen (1974) and McMurtry (1975) that a local hydrothermal source has generated the Bauer Deep metalliferous sediments.

More recently, Heath and Dymond (1977) proposed a diagenetic model for the origin of Bauer Deep smectites based on deep water circulation patterns. It was suggested that the water crossing eastwards over the East Pacific Rise carried hydrothermally-derived fine-grained Fe-hydroxides and that these hydroxides sorbed other elements both from sea water and from hydrothermal solutions. East and south of the East Pacific Rise these waters met,biogenically depositing Si which could react with the Fe-hydroxides to produce Fe-rich smectites. The feasibility of this reaction was supported by a systematic loss of Fe-hydroxides to Fe-rich smectites from the East Pacific Rise to the Northern Central Basin.

4.3 TOPOGRAPHY AND STRUCTURE OF THE BAUER BASIN

The Bauer Basin extends as a topographical depression between about 100° and 108°W latitude and 5° and 20°S longitude. It is bounded to the east by the Galapagos Rise and to the west by the East Pacific Rise. This includes an area in excess of 150,000 km^2. The bathymetric map given by Mammerickx et al (1975) shows that the bottom topography of the Bauer Basin is generally rough, the water depth ranging from 3800 m to 4500 m.

The data obtained from leg 34 of the Deep Sea Drilling Project offered an opportunity to study the structure and the geologic history at least of the southern Bauer Basin. Hole 319 was drilled in a basin about 8 km wide at 13°00.8'S. Around this area other basins existed which were bounded by faults with vertical displacements of 200-500 meters. Sea mounts up to 2000 meters in height were also present. The basaltic basement was mantled by 110 m of sediments. Four sediment units were distinguished in the sediment column . The uppermost unit consisted of a 4 meter carbonate-free sediment of late Miocene to Quaternary age. It was almost exclusively Fe-rich brown clay. However, $CaCO_3$ increased towards the base of the unit. Additionally, phillipsite and ferruginous particles were present. Iron-bearing calcareous brown clay and clayey nanno ooze of 24.5 meters thickness comprised the second unit. While the number of Fe-particles decreases with depth, the percentage of $CaCO_3$ increased with depth in this unit. The third sediment unit was nanno ooze, 47.5 m thick, of middle Miocene age, and the remaining 34 meters comprising the fourth unit consisted of Fe-bearing nanno ooze, also of

middle Miocene age. The basement surface of the site 319 appeared to be irregular. There was a 13 meter difference in basement depth at holes 319 and 319A.

The geologic history of the southern Bauer Deep is described in the D.S.D.P. site 319 report as follows: Northwest-trending topographical features of volcanic origin were first formed. Subsequently block faulting along the same trend took place, which was followed by the middle Miocene sedimentation of nannofossil ooze above the calcite compensation depth (CCD). A subsidence of the seafloor probably followed so that the deposition of the late Miocene to Quaternary metalliferous clays occurred below the calcite compensation depth (CCD).

4.4 LITHOLOGICAL AND CHEMICAL DESCRIPTION OF THE CORES

For the lithological description of the cores the Olausson classification system was followed, which is described in detail in Appendix A. The Munsell color system was also used. The number code showing the color of the sediment is on the right of the core log (see Table A1).

In the chemical logs the data for Mn, Fe, Ni, Co, Pb, Zn, Cu, Al and SiO_2 are presented on a carbonate-free basis (C.F.B.).

The following signs were used in the lithological description of the cores:

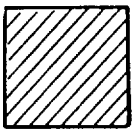

Marl Ooze

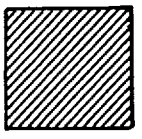

Chalk Ooze

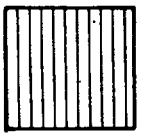

Red Clay

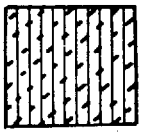

Calcareous Red Clay

4.4.1 Core SH 1557 (see Figures 4.2 and 4.3)

4.4.1a Lithology

Down to about 20 cm the core consists of dark reddish-brown calcareous clay (5YR 2/2). At 20-110 cm the core is composed of clay of the same colour. At about 110 cm the core becomes very dark-brown clay (10YR 2/2) which continues down to the base of the core.

Reddish-brown mottles (5YR 4/4) of very fine clay are present at the top of the core as well as between 10 and 20 cm. Similar material is also found in the form of microlayers between 13 and 13.5 and between 14 and 14.5 cm. A large reddish-brown mottle is also present at 109 cm.

4.4.1b Chemistry

The core is enriched in $CaCO_3$ in the top 25 cms. At 25 cm the sediments become deficient in $CaCO_3$, the concentration of which remains low down to the base of the core.

The concentrations of Mn, Fe, Ni, Co and Cu follow the same pattern when plotted versus depth. They diminish gradually with depth in the carbonate section of the core (0-25 cm). At 25-110 cm the concentrations of these elements show no significant variations, while from 110 cm down to the bottom of the core they increase with increasing depth. At 119 cm Co and Cu exhibit a strong maximum, while the highest concentrations of Mn, Fe and Ni are shown at the base of the core.

The vertical distribution of Pb is rather irregular throughout the core and shows no relationship with depth.

Figure 4.2: CORE SH 1557. Lithological and chemical description (see p. 290).

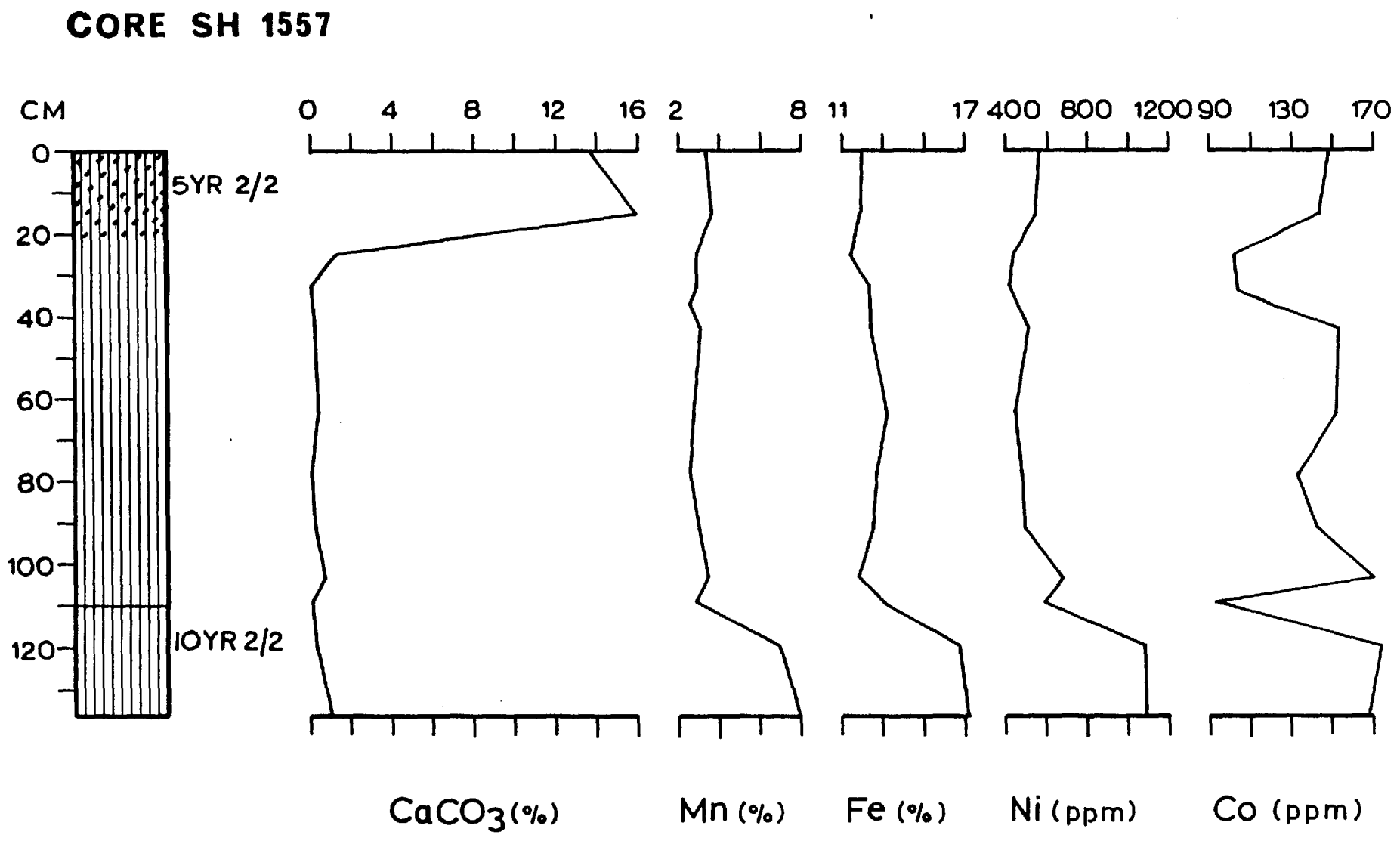

Figure 4.3: CORE SH 1557. Lithological and chemical description (see P. 290).

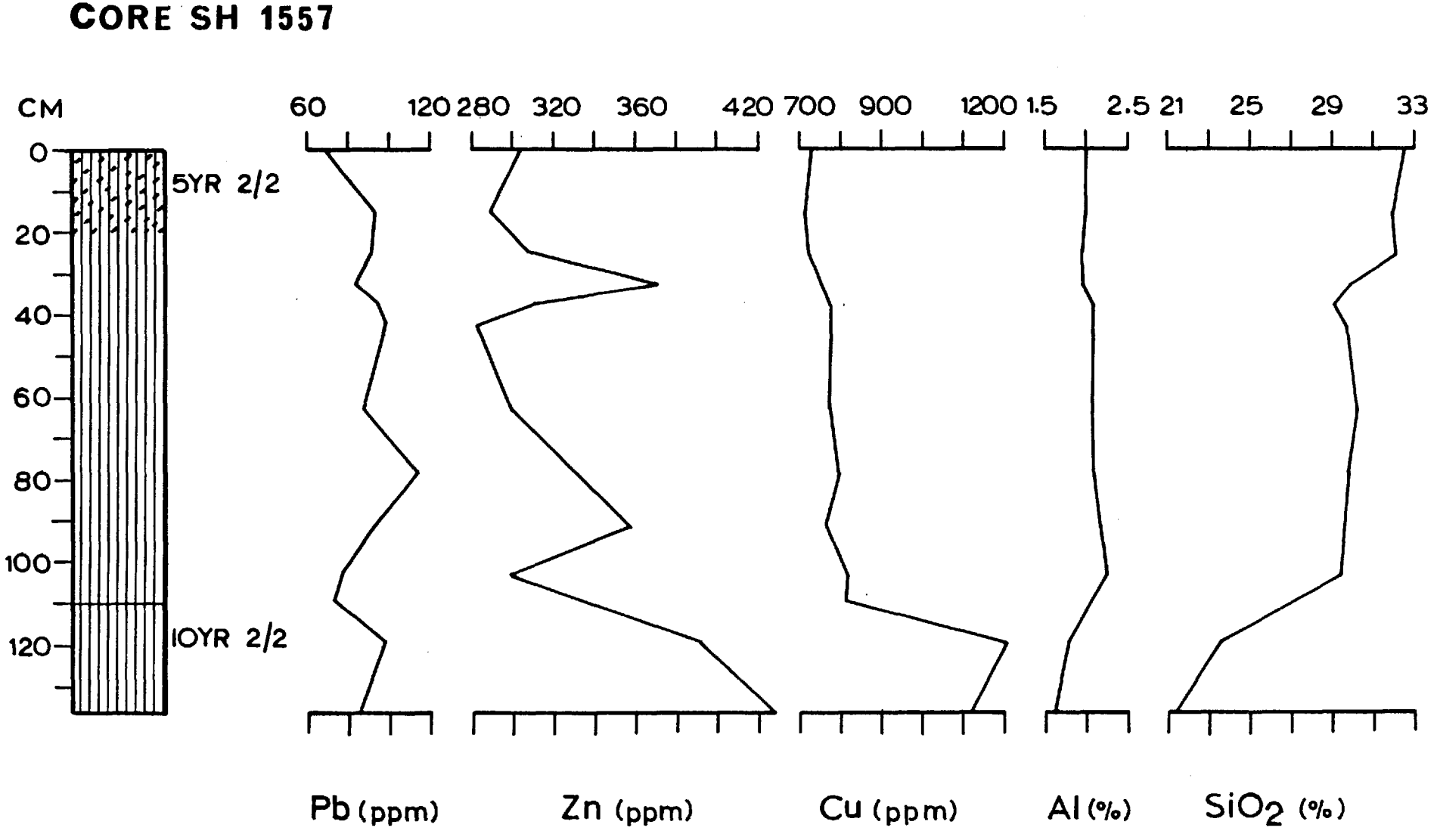

Down to 110 cm Zn appears to have irregular distribution with three minima at 15, 42 and 103 cm, and two peaks at 32 and 91 cm. From 103 cm, Zn begins to increase gradually with depth to reach its highest concentration at the base of the core.

Down to 103 cm, Al is uniformly distributed, its concentration being rather constant. Below this depth it diminishes gradually down to the bottom of the core, where it reaches its lowest concentration.

The content of SiO_2 decreases slightly with depth, having a first minimum at 37 cm; below 103 cm the reduction in SiO_2 concentration becomes more marked, thus the lowest concentration of this component is expressed in the samples which were analysed from the base of the core. There appears to be a positive correlation between the Al and the SiO_2 contents of the lower part of the core (103-136 cm).

It is noteworthy that the maxima in the concentrations of Co and Cu at 119 cm and of Fe, Mn, Ni and Zn at the base of the core, together with the minima of Al and SiO_2 at 136 cm, are all associated with the very darkly-coloured horizon at the base of the core.

4.4.2 Core SH 1559 (see Figures 4.4 and 4.5)

4.4.2a Lithology

The whole core is composed of very dark brown (10YR 2/2) ferruginous clay. At 29 and 37 m a rather peculiar mottle is present. It consists of an outer reddish-brown (5YR 5/4) ring and an inner

Figure 4.4: CORE SH 1559. Lithological and chemical description (see p. 290).

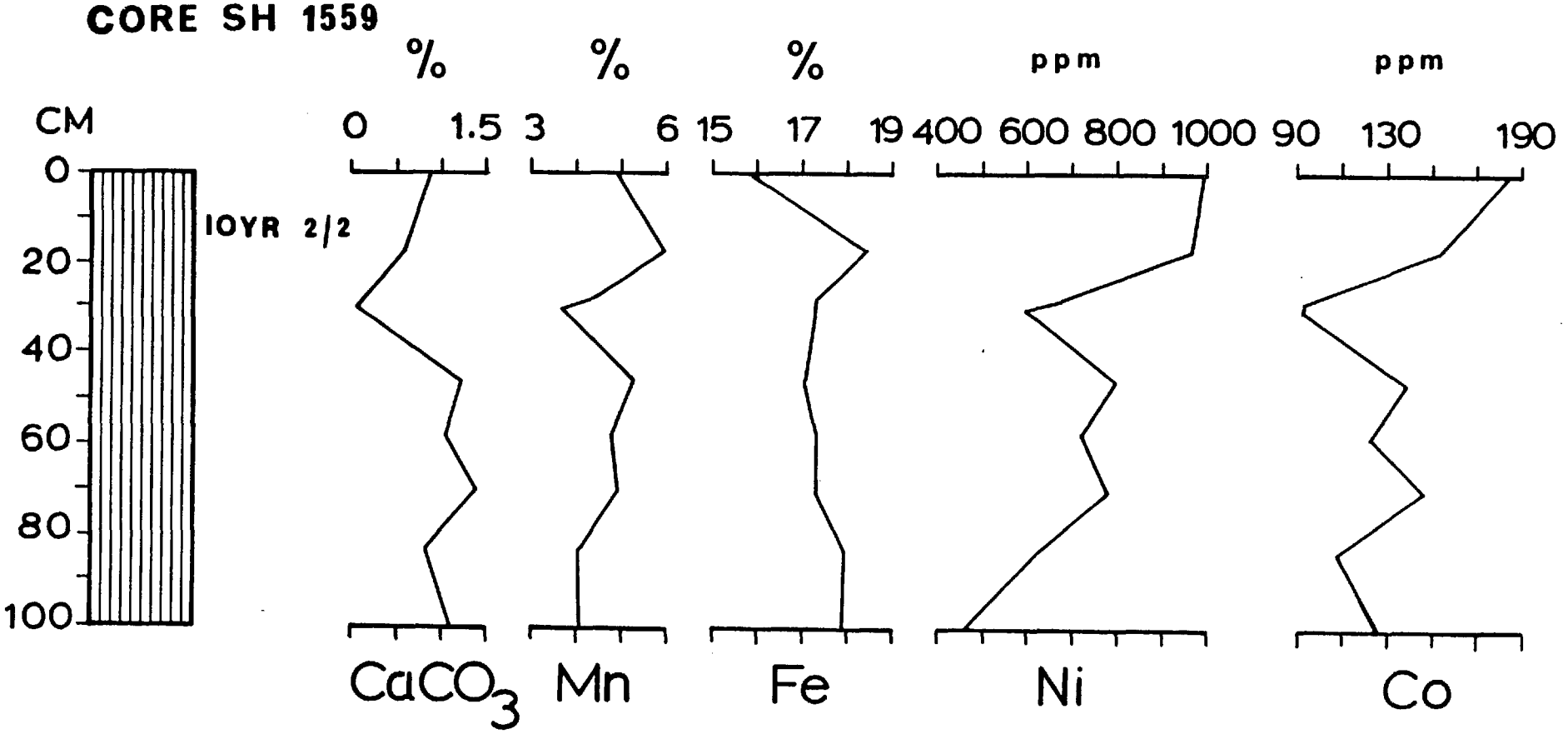

Figure 4.5: CORE SH 1559. Lithological and chemical description (see p. 290).

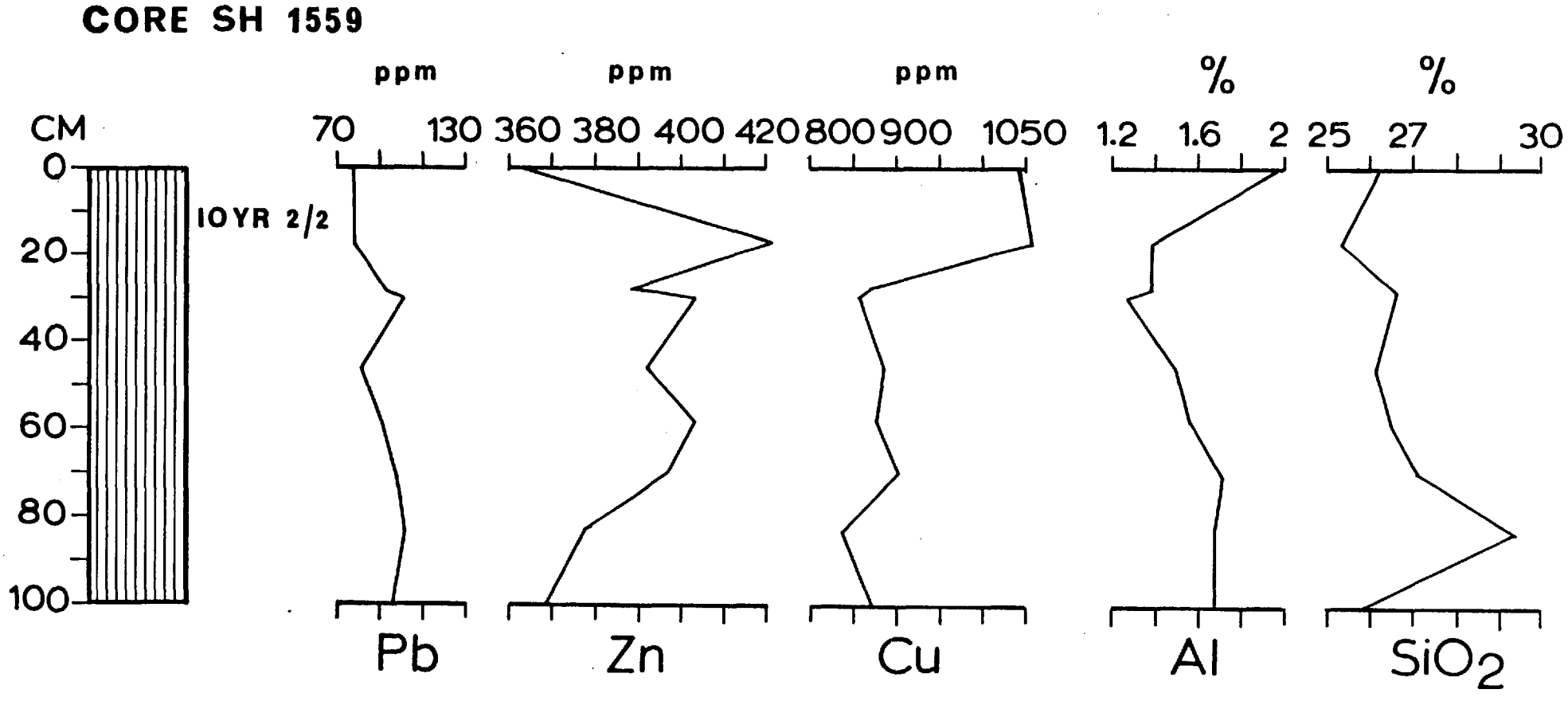

very dark brown core of very fine clay. Very fine reddish-brown (5YR 5/4) clay also forms mottles at 30, 36, 63 and 94 cm.

4.4.2b Chemistry

The content of $CaCO_3$ is generally low. Except for a sharp depression at 30 cm, there are only minor fluctuations in the concentration of $CaCO_3$ down the length of the core. The abundance pattern of Mn in the core is similar to that of $CaCO_3$. However, at 17 cm, Mn exhibits a maximum which is not present in the distribution pattern of $CaCO_3$. At 17 cm, Fe, like Mn, shows its highest concentration, whereas in the rest of the core there is no relationship between Fe and Mn. Below 20 cm the abundance of Fe is almost constant at 17-18% on a carbonate-free basis, whereas Mn shows an abrupt minimum at 30 cm.

The concentrations of Ni and Co display similar patterns. They are both enriched in the surface layer and diminish in concentration with depth down to 30 cm. Below, and down to 70 cm depth, the concentrations of Ni and Co tend to increase, thus displaying a minimum at 30 cm similar to that of $CaCO_3$ and Mn. In the lower section of the core (70-100 cm) the concentrations of Ni and Co decrease with increasing depth.

The concentrations of Pb show little variation down the length of the core, but two weak maxima at 30 and 83 cm are apparent. In the surface sediments Zn exhibits its lowest concentration, while at 17 cm there is an abrupt increase to a very strong maximum (the highest concentration of Zn in the core). Below this depth, the concentration of Zn decreases with increasing depth to reach, at the base of the core, values similar to those found at the top of the core.

Copper, like Ni and Co, but in contrast to the case of Zn, is enriched in the surface sediments. However, the abundance pattern of Cu shows a weak maximum at 17 cm, below which the concentrations of Cu fall drastically down to 30 cm where a first minimum is shown. Below this depth the concentrations of Cu vary little down to the base of the core. However, a second depression occurs at 83 cm, thus indicating the tendency for the concentrations of Cu to decrease towards the bottom of the core.

The curve of Al content shows an abrupt depression at 30 cm which coincides with the minimum of $CaCO_3$, Mn, Ni, Co and Cu. Otherwise the distribution of Al is rather irregular. Except for a very sharp peak at 83 cm, the content of SiO_2 varies at 25-27% on a carbonate-free basis throughout the sediment core.

4.4.3 Core SH 1560 (see Figure 4.6)

4.4.3a Lithology

A number of Mn-nodules, ranging in diameter from a few mm to 1 cm, were found at the top of the core. The top 5 cm of the core consist of very dark brown (10YR 2/2) marl ooze. At 5-16 cm the colour of the ooze becomes dark yellowish-brown (10YR 5/4). From 16 cm down to 66 cm the core is composed of yellowish-brown (10YR 5/4) marl ooze with transitions to chalk ooze of the same colour at 36 and 60 cm. At 66-73 cm there is light yellowish-brown (10YR 6/4) chalk ooze. Very dark brown (10YR 2/2) clayey mottles are present at 7 and 13 cm.

Figure 4.6: CORE SH 1560. Lithological and chemical description (see p. 290).

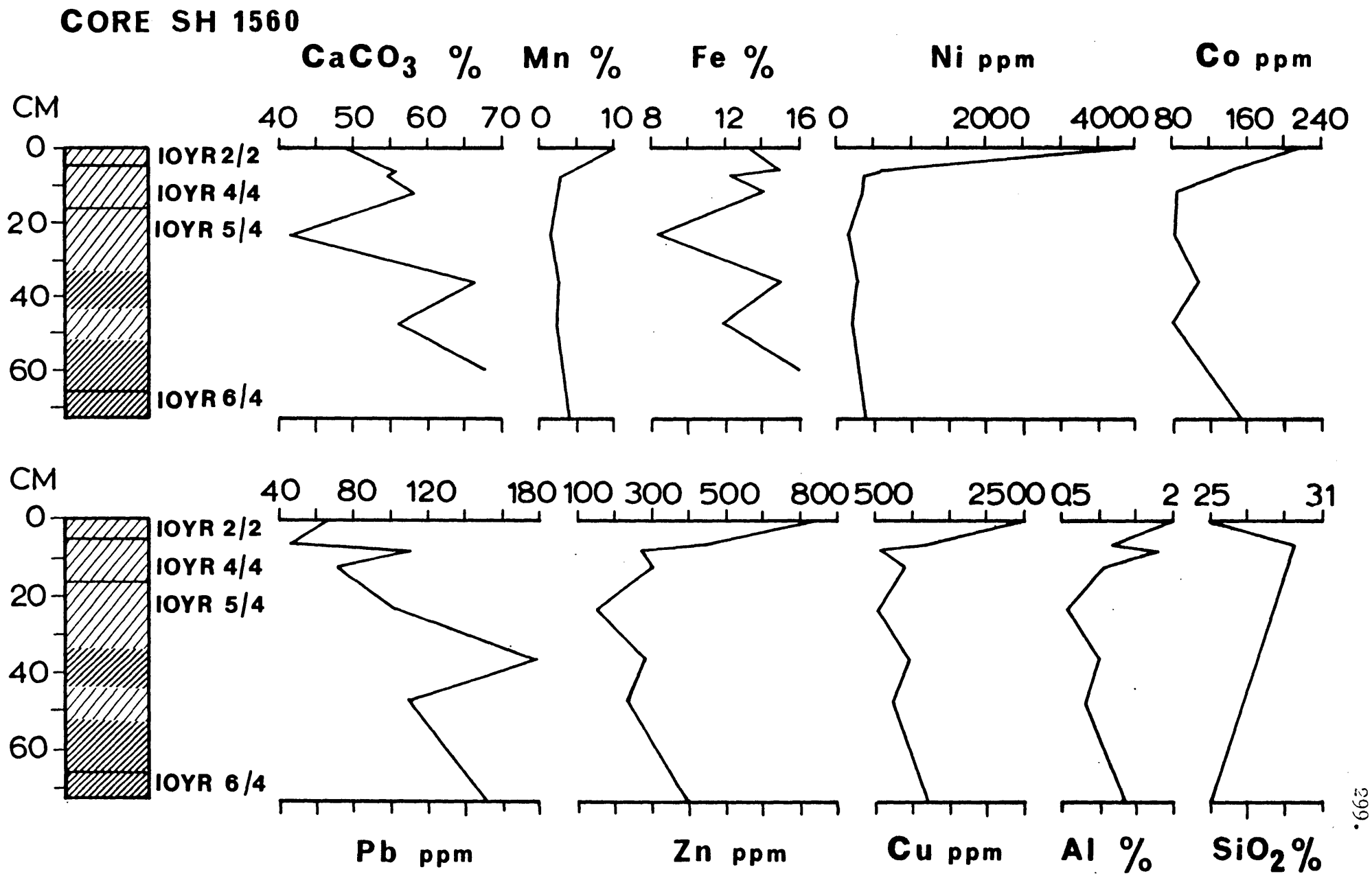

4.4.3b Chemistry

The content of $CaCO_3$ is relatively high throughout this core but forms a depression at 23 cm. Apart from two maxima, one at 36 and the other at 60 cm, there is a general tendency for the $CaCO_3$ content to increase with depth in the core. The increase of the $CaCO_3$ content with depth in the core is correlative with the gradual change in the colour of the sediments from dark to pale following the sequence:

very dark brown ⟶ dark yellowish-brown ⟶
yellowish-brown ⟶ light yellowish-brown.

Manganese, Ni, Co, Zn and Cu follow each other in their distribution within the buried sediments. There is an abrupt decrease in their concentrations from the top sample to 7 cm, while from 7 cm down to 23 cm their decrease becomes less sharp. Below 23 cm the concentrations of Mn and Ni vary within a very narrow range having a tendency to increase slightly towards the base of the core. In contrast, the variations of Co, Zn and Cu are much wider and their increase in the lower section of the core is more pronounced.

A strong positive relationship appears to exist between Fe and $CaCO_3$ since the two constituents follow the same pattern in their vertical distribution. Lead also displays a similar distribution pattern below 23 cm, but there is some inverse correspondence between Pb and $CaCO_3$ in the upper 23 cm of the core.

Except for a weak peak at 7 cm the vertical distribution of Al is similar to that of Zn and Cu.

Due to the small number of samples analysed for Si from this core the distribution of Si versus depth is not very clear. However, it is observed that the top sample contains less Si when compared with the Si content of the sample taken at 6 cm. Furthermore, the lower concentration of Si at 36 cm would suggest a probable decrease of this content at greater depths in the core.

4.4.4 Core SH 1577 (see Figures 4.7 and 4.8)

4.4.4a Lithology

At the top of the core down to 10 cm there is very dark brown (10YR 2/2) marl ooze. At 10-16 cm dark yellowish-brown (10YR 3/4) marl ooze occurs. Below 16 cm and down to 30 cm there is an alternation of microlayers of calcareous clay and marl ooze. At 16-19 and 21-25 cm there is a very dark brown (10YR 2/2) calcareous clay, while at 19-21 and 25-30 cm marl ooze occurs. Below 30 cm down to 80 cm a stratum of very dark brown (10YR 2/2) clay follows, which changes to calcareous clay of the same colour at 80-95 cm. The core at 95-120 cm is composed of light yellowish-brown (10YR 6/4) chalk ooze with many very dark brown (10YR 2/2) mottles disseminated throughout the sediment. Dark yellowish-brown (10YR 3/4) marl ooze forms the core at 120-132 cm. Below, calcareous clay of very dark brown colour follows, and persists down to 152 cm. Between 152 and 170 cm there is marl ooze changing at 157 cm from yellowish-brown to dark yellowish-brown. A stratum of yellowish-brown (10YR 5/4) chalk ooze forms the core at 170-178 cm. Dark yellowish-brown (10YR 4/4) marl ooze follows, the colour of which changes at 185 cm to very dark brown (10YR 2/2). The basal 7 cm of the core (190-197) consists of calcareous clay of the same colour.

Figure 4.7: CORE SH 1577. Lithological and chemical description (see p. 290).

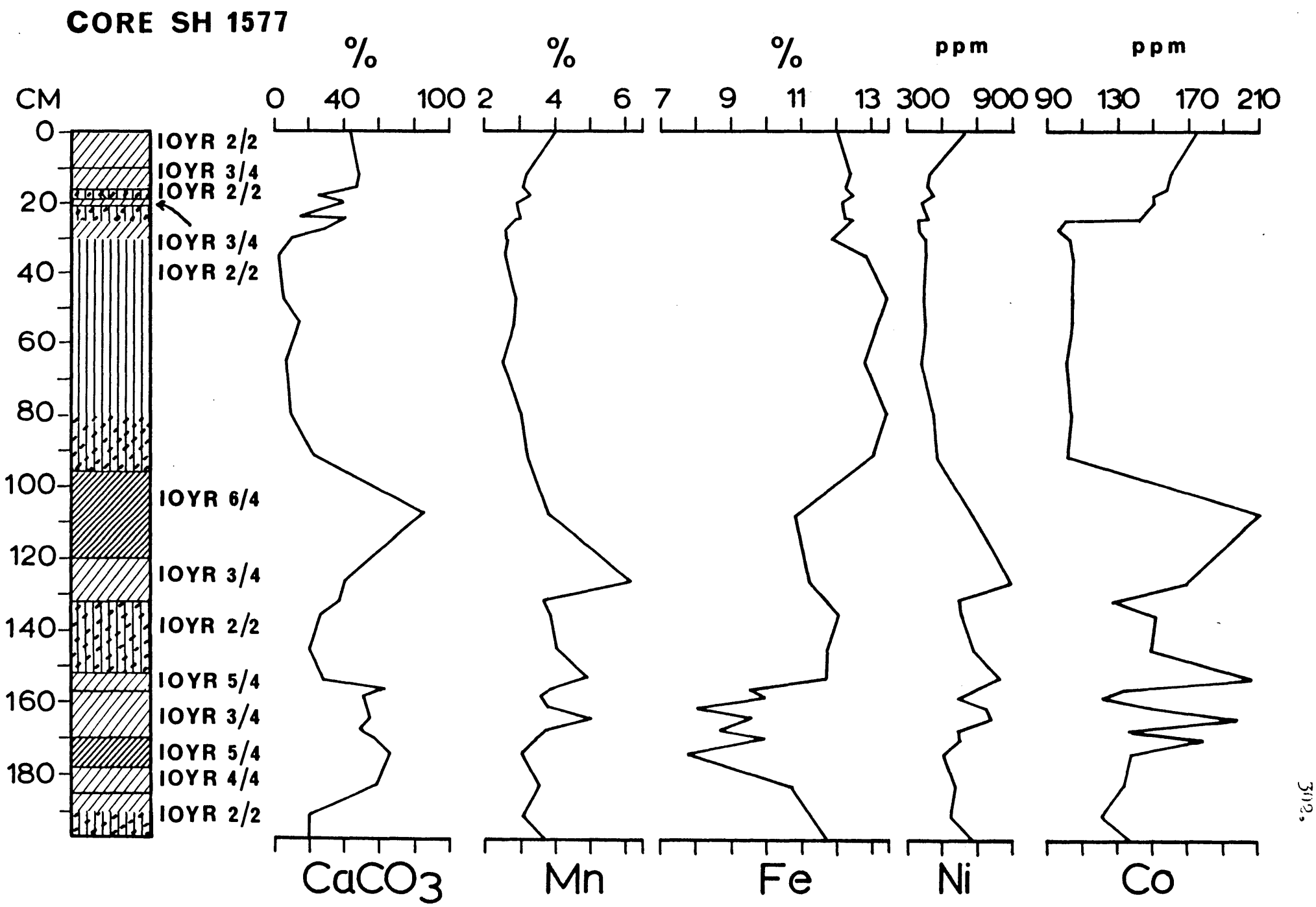

Figure 4.8: CORE SH 1577. Lithological and chemical description (see p. 290).

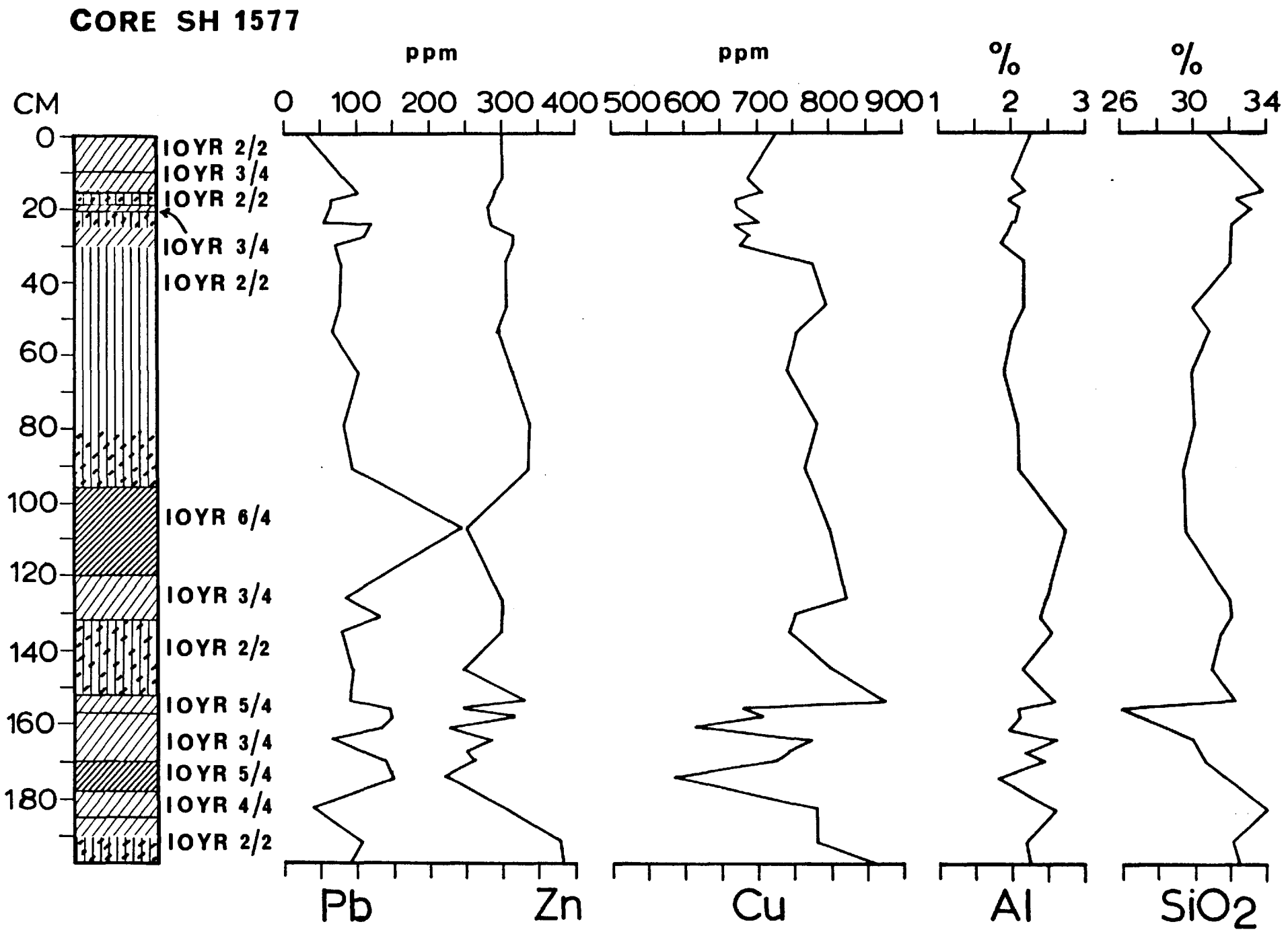

4.4.4b Chemistry

The upper 15 cm of the core are enriched in $CaCO_3$. Below, down to 30 cm, the $CaCO_3$ content decreases with depth to remain low at 30-80 cm. From 80 cm down to the base of the core the $CaCO_3$ content shows a rather irregular distribution with a number of maxima and minima which are reflected in the lithological description of the core. The highest content of $CaCO_3$ is seen at 107 cm where it reaches the value of 92%.

The abundance patterns for Mn, Ni and Co are similar. Their concentrations decrease gradually with increasing depth down to 30 cm, while they are almost constant between 30 and 80 cm. Then a gradual increase in the concentrations of these elements with increasing depth follows, so that Mn and Ni reach their highest values at 126 cm and Co at 107 cm. Below, down to the bottom of the core, the concentrations of Mn, Ni and Co vary considerably, displaying maxima at 152 and 164 cm.

The distribution of Fe differs from that of Mn, Ni and Co. From the top of the core down to 80 cm the concentrations of Fe increase gradually with increasing depth, showing two weak peaks at 47 and 79 cm. Below, down to 174 cm there is a gradual decrease of the Fe content with depth. In the lower section of the core (174-197 cm) an abrupt increase in the concentration of Fe occurs, which displays a sharp minimum at 174 cm.

Lead follows $CaCO_3$ in its distribution, indicating that the concentrations of Pb are closely related to the presence of $CaCO_3$ in the sediments. The distribution of Cu is partly similar to that of

Mn and partly to that of Fe. Down to 30 cm the content of Cu diminishes in a manner similar to that of Mn. From 30 to 154 cm it tends to increase so that at 154 cm it reaches its highest value, exhibiting a sharp peak. From 154 cm down to the base of the core Cu varies between 570 and 850 ppm, following closely the variations of Fe, with a sharp peak at 164 cm and two minima at 161 and 174 cm.

The abundance pattern of Zn shows little variation in the upper 90 cm. From 90 cm to 174 cm the concentrations of Zn tend to decrease with increasing depth, displaying a number of minima, one of which (at 107 cm) coincides with a sharp maximum in the concentrations of $CaCO_3$ and Pb. From 174 cm down to the base of the core Zn, like Fe and Cu, shows an abrupt increase. In general, it is observed that below 90 cm the Zn content is closely related to the concentrations of Fe in the sediments.

In the top 30 cm of the core the Al content decreases steadily with increasing depth, showing some relationship with Mn, Ni, Co and Cu. Below, and down to the bottom of the core, only very minor fluctuations of the Al content are observed. It is noted that in the lower section of the core (140-197 cm) the abundance variations of Al follow those of Fe and Cu. In the upper 20 cm of the core a slight increase of the SiO_2 content occurs, while between 20 and 110 cm it decreases systematically with depth. Below, down to the base of the core, the content of SiO_2 increases with increasing depth. However, at 156 cm the curve of SiO_2 shows an abrupt depression which coincides with a maximum in the concentrations of Zn and Cu. It appears that in the upper (0-20 cm) and in the lower (170-197 cm) part of the core, there is a positive relationship between SiO_2 and Fe, whereas in the remaining section of the core (20-170 cm) there is some inverse correspondence between these two elements.

4.4.5 Core SH 1578 (see Figures 4.9 and 4.10)

4.4.5a Lithology

The top 20 cm of the core consists of calcareous red clay, while the remainder is composed of red clay only.

4.4.5b Chemistry

The content of $CaCO_3$ in the upper 20 cm of the core is low, ranging between 10 and 16%. From 20 cm to 170 cm $CaCO_3$ is almost completely absent from the sediments. At 170-190 cm it increases to reach the value of 8%.

When plotted versus depth the concentrations of Mn, Fe, Ni, Co and Cu display rather similar patterns. All elements are enriched in the surface sediments and exhibit three minima at about 10, 48 and 97 cm. However, certain differences in their vertical distribution exist. Instead of the minimum occurring at 97 cm in the distribution of Fe, it is at 82 cm. Except for the minima noted, which are very weak in the case of Mn and Fe, the concentrations of these two elements are constant down the length of the core. In contrast Ni and Co vary within a large range, displaying abrupt changes in their distributions with two sharp maxima at 20 and 63 cm. In general, the abundance patterns of Zn and Cu in the core resemble those of Ni and Co. However, at 74 cm there is a sharp maximum in the distribution of Zn and Cu which is absent from the abundance patterns of Ni and Co. The distribution of Pb is rather irregular, with little fluctuations down the length of the core.

Figure 4.9: CORE SH 1578. Lithological and chemical description (see p. 290).

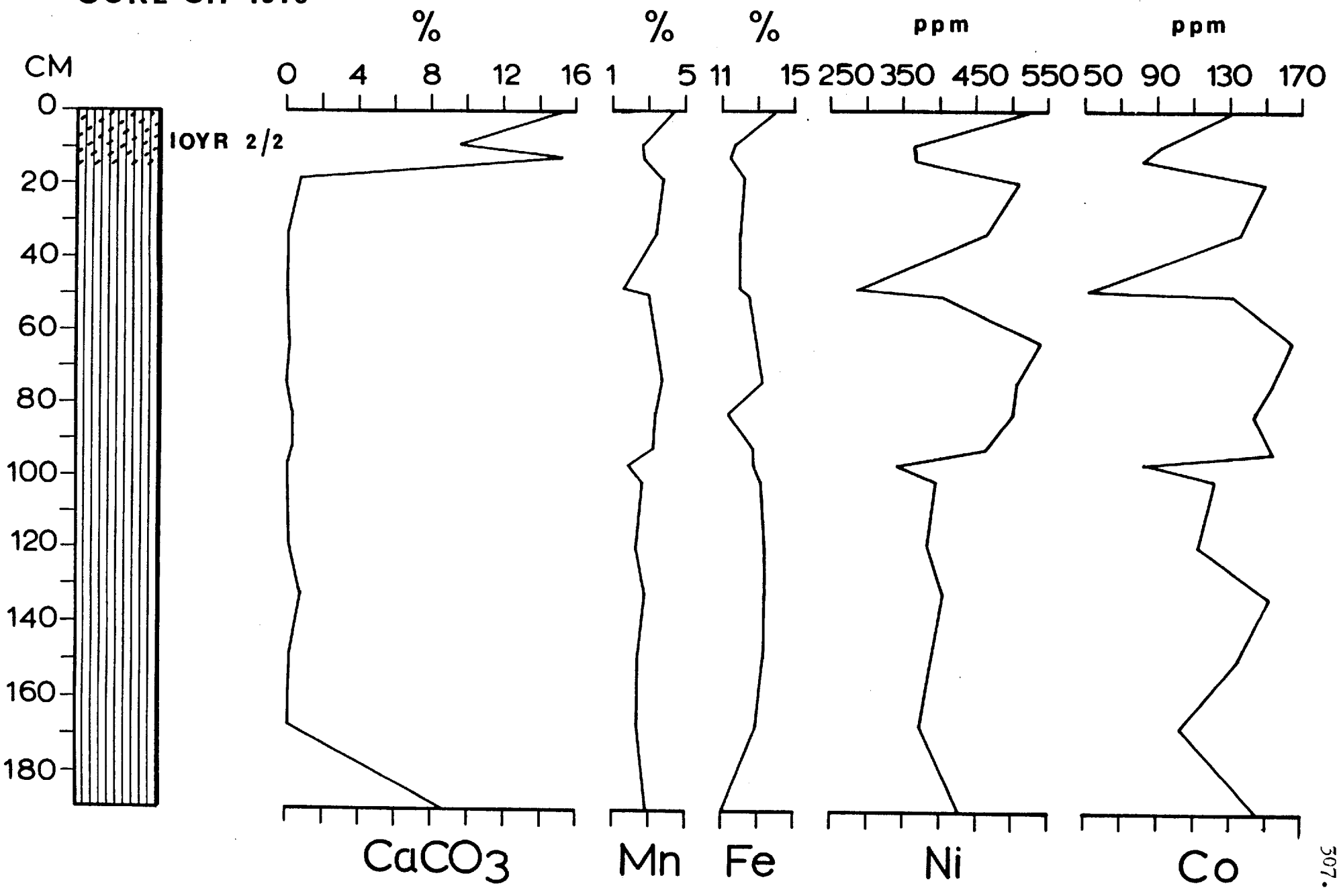

Figure 4.10: CORE SH 1578. Lithological and chemical description (see p. 290).

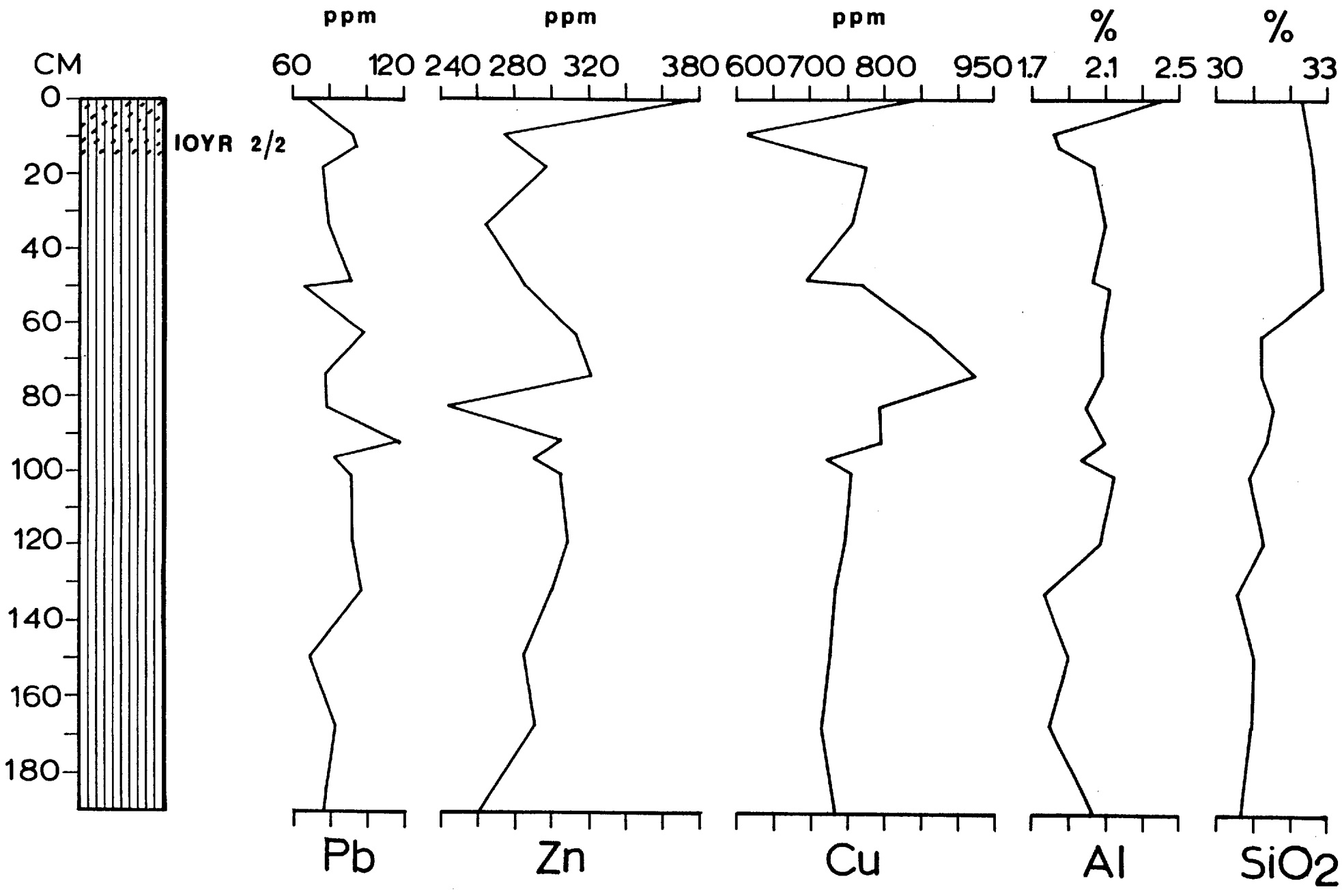

At the top of the core Al shows its highest content, while at 10 cm it exhibits a minimum similar to that of Zn and Cu. Below 10 cm very little variation in the concentrations of Al occurs; however, there is a tendency for it to be diminished towards the bottom of the core. The content of SiO_2 is higher in the upper 50 cm of the core, whereas at greater depths it decreases gradually, thus showing some relationship with Al.

It is noticeable that the minimum shown in the distribution of Mn, Fe, Ni, Co, Zn, Cu and Al at 10-13 cm coincides with a maximum of the $CaCO_3$ content. However, at the top of the core, where $CaCO_3$ displays its highest content, Mn, Fe, Zn and Al also have their highest values. Moreover, Ni, Co and Cu are relatively enriched in the surface, when compared with the buried, sediments.

4.5 GEOCHEMICAL PARTITION PATTERNS

In the investigation of the distribution of Ca, Fe, Mn, Ni, Co, Pb, Zn, Cu and Al among the components of the Bauer Deep sediments, partition analyses have been carried out on samples from all the stations. The partitioning data for all the sediment samples are tabulated in Table 4.1, while Tables 4.2 and 4.3 show the average partitioning of elements in each core and in all cores, respectively. Details concerning the selective chemical attacks performed for the partition analysis are included in Appendix C.

Because there are no significant differences between the average partitioning data for each core and all averages, the latter were used to describe the distribution of elements between phases.

4.5.1 Iron

Iron is more concentrated in the HCl-soluble fraction ($\sim$ 60%) than in any of the other fractions, suggesting its possible association with the Fe-rich montmorillonites. Almost all the remainder Fe ($\sim$ 37%) was found to be soluble in the acid-reducing agent solution, showing that it forms ferromanganese oxide minerals. Less than 2% of the total Fe is soluble in acetic acid, whilst about 1% remains in the HCl-insoluble residue.

In general, the proportion of Fe which is soluble in acetic acid remains constant throughout the sediment cores (see Figure 4.11). However, cores SH 1577 and SH 1560 show a slight decrease of the acetic acid-soluble Fe from the top sediments down to a depth of about 10 cm.

Table 4.1: Partition of elements between different phases of Bauer Deep sediments (as percentages of the total amount present).

CORE SH 1557																						
Sample No. (Interval sampled, cm)		Ca		Mn		Fe		Ni		Co		Pb		Zn		Cu		Al	
		a (%)	b	a (%)	b	a (%)	b	a (ppm)	b	a (ppm)	b	a (ppm)	b	a (ppm)	b	a (ppm)	b	a (%)	b
232 (0-10)	A	6.56		2.91		10.36		491		127				262		629		1.73	
	B	5.50	83.84	0.01	0.34	0.27	2.61	22	4.48	4	3.15			22	8.40	71	11.29	0.11	6.36
	C	1.06	16.16	2.73	93.81	4.95	47.78	383	78.01	95	74.80			136	51.91	344	54.69	0.36	20.81
	D	0.00	0.00	0.17	5.85	5.14	49.61	66	13.44	2	1.58			104	39.69	214	34.02	0.92	53.18
	E	0.00	0.00	0.00	0.00	0.00	0.00	20	4.07	26	20.47			0	0.00	0	0.00	0.34	19.65
233 (10-20)	A	7.41		3.06		10.08		461		121		77		243		600		1.68	
	B	6.45	87.04	0.01	0.33	0.23	2.28	14	3.04	3	2.48	0	0.00	18	7.41	73	12.17	0.10	5.95
	C	0.95	12.82	2.85	93.14	4.80	47.62	366	79.39	103	85.12	70	90.91	133	54.73	338	56.33	0.33	19.64
	D	0.01	0.14	0.15	4.90	4.49	44.54	51	11.06	0	0.00	7	9.09	92	37.86	189	31.50	0.90	53.57
	E	0.00	0.00	0.05	1.63	0.56	5.56	30	6.51	15	12.40	0	0.00	0	0.00	0	0.00	0.35	20.84
237 (40-45)	A	1.23				12.40				153		97		281		776		2.07	
	B	0.77	62.60			0.23	1.85			9	5.88	0	0.00	23	8.19	71	9.15	0.16	7.73
	C	0.32	26.02			6.22	50.16			116	75.82	81	83.51	200	71.17	513	66.11	0.28	13.53
	D	0.01	0.81			5.52	44.52			0	0.00	16	16.49	58	20.64	121	15.59	1.06	51.21
	E	0.13	10.57			0.43	3.47			28	18.30	0	0.00	0	0.00	71	9.15	0.57	27.53

Table 4.1: Continued

CORE SH 1557																				
Sample No. (Interval sampled, cm)		Ca		Mn		Fe		Ni		Co		Pb		Zn		Cu		Al	
		a (%)	b	a (%)	b	a (%)	b	a (ppm)	b	a (ppm)	b	a (ppm)	b	a (ppm)	b	a (ppm)	b	a (%)	b
238 (60-66)	A	1.32		2.83		13.16		452		151				298		769		2.05	
	B	0.80	60.60	0.01	0.35	0.21	1.60	26	5.75	6	3.97			23	7.72	58	7.54	0.15	7.32
	C	0.24	18.18	2.61	92.23	5.83	44.30	317	70.13	113	74.84			146	48.99	406	32.80	0.43	20.98
	D	0.11	8.34	0.21	7.42	7.12	54.10	97	21.46	0	0.00			129	43.29	305	39.66	1.01	49.27
	E	0.17	12.88	0.00	0.00	0.00	0.00	12	2.66	32	21.19			0	0.00	0	0.00	0.46	22.43
241 (100-106)	A	1.45		3.48		11.89		670		169		76		295		811		2.22	
	B	0.87	60.00	0.02	0.57	0.10	0.84	23	3.43	6	3.55	0	0.00	22	7.46	61	7.52	0.14	6.31
	C	0.26	17.93	3.19	91.67	4.44	37.34	497	74.18	142	84.02	75	98.68	131	44.40	431	53.15	0.40	18.02
	D	0.06	4.14	0.27	7.76	7.35	61.82	126	18.81	0	0.00	1	1.32	142	48.14	298	36.74	1.15	51.80
	E	0.26	17.93	0.00	0.00	0.00	0.00	24	3.58	21	12.43	0	0.00	0	0.00	21	2.59	0.53	23.87
243 (116-122)	A	1.28		6.89		16.73		1077		172		97		389		1199		1.67	
	B	0.92	71.88	0.12	1.74	0.08	0.48	41	3.81	6	3.49	0	0.00	43	11.05	113	9.42	0.08	4.79
	C	0.12	9.38	6.20	89.99	5.25	31.38	993	92.20	138	80.23	75	77.32	278	71.47	735	61.30	0.27	16.17
	D	0.10	7.81	0.57	8.27	10.58	63.24	43	3.99	0	0.00	22	22.68	68	17.48	322	26.86	1.04	62.27
	E	0.14	10.93	0.00	0.00	0.82	4.90	0	0.00	28	16.28	0	0.00	0	0.00	29	2.42	0.28	16.77

Table 4.1: Continued.

CORE SH 1559																				
Sample No. (Interval sampled, cm)		Ca (%)		Mn (%)		Fe (%)		Ni (ppm)		Co (ppm)		Pb (ppm)		Zn (ppm)		Cu (ppm)		Al (%)	
		a	b	a	b	a	b	a	b	a	b	a	b	a	b	a	b	a	b
245 (0-10)	A	1.48		4.94		15.70		981		182		77		361		1035		1.97	
	B	0.08	5.41	0.02	0.41	0.11	0.70	33	3.36	8	4.40	0	0.00	26	7.20	64	6.18	0.12	6.09
	C	1.06	71.62	4.57	92.51	5.62	35.80	803	81.86	146	80.22	75	97.40	192	53.19	537	51.89	0.40	20.30
	D	0.14	9.46	0.22	4.45	9.97	63.50	145	14.78	0	0.00	2	2.60	143	39.61	434	41.93	1.06	53.81
	E	0.20	13.51	0.13	2.63	0.00	0.00	0	0.00	28	15.38	0	0.00	0	0.00	0	0.00	0.39	19.80
246 (14-20)	A	1.38		5.91		18.31		958		152		77		419		1052		1.38	
	B	0.82	59.42	0.02	0.34	0.08	0.44	38	3.97	6	3.95	0	0.00	35	8.35	61	5.80	0.08	5.80
	C	0.56	40.58	5.30	89.68	5.74	31.35	853	89.04	93	61.18	77	100.00	209	49.88	554	52.66	0.23	16.67
	D	0.00	0.00	0.29	4.91	11.99	65.48	61	6.37	0	0.00	0	0.00	175	41.77	437	41.54	0.88	63.77
	E	0.00	0.00	0.30	5.07	0.50	2.73	6	0.62	53	34.87	0	0.00	0	0.00	0	0.00	0.19	13.76
252 (42-50)	A	1.62		5.19		16.86		787		137		81		388		876		1.47	
	B	0.97	59.88	0.01	0.19	0.04	0.24	28	3.56	6	4.38	0	0.00	31	7.99	43	4.91	0.06	4.08
	C	0.26	16.05	4.83	93.07	4.60	27.28	660	83.86	98	71.53	81	100.00	172	44.33	390	44.52	0.18	12.25
	D	0.14	8.64	0.27	5.20	12.22	72.48	99	12.58	6	4.38	0	0.00	185	47.68	443	50.57	0.84	57.14
	E	0.25	15.43	0.08	1.54	0.00	0.00	0	0.00	27	19.71	0	0.00	0	0.00	0	0.00	0.39	26.53
255 (67-73)	A	1.68		4.86		17.14		766		143		97		392		890		1.68	
	B	1.02	60.71	0.01	0.20	0.03	0.18	33	4.31	8	5.59	0	0.00	22	5.61	39	4.38	0.06	3.57
	C	0.32	19.05	4.56	93.83	5.60	32.67	658	85.90	101	70.63	78	80.41	189	48.21	416	46.74	0.23	13.69
	D	0.19	11.31	0.19	3.91	11.13	64.94	75	9.79	0	0.00	17	17.53	181	46.18	419	47.08	1.09	64.88
	E	0.15	8.93	0.10	2.06	0.38	2.21	0	0.00	34	23.78	2	2.06	0	0.00	16	1.80	0.30	17.86
258 (95-100)	A	1.58		4.00		17.66		482		121		96		366		857		1.66	
	B	0.97	61.39	0.01	0.25	0.05	0.28	26	5.39	6	4.96	0	0.00	18	4.92	28	3.27	0.07	4.22
	C	0.27	17.09	3.82	95.50	5.17	29.28	408	84.65	89	73.55	95	98.96	171	46.72	319	37.22	0.19	11.45
	D	0.04	2.53	0.17	4.25	12.44	70.44	48	9.96	0	0.00	1	1.04	177	48.36	510	59.51	0.97	58.43
	E	0.30	18.99	0.00	0.00	0.00	0.00	0	0.00	26	21.49	0	0.00	0	0.00	0	0.00	0.43	25.90

Table 4.1: Continued.

CORE SH 1560																				
Sample No. (Interval sampled, cm)		Ca		Mn		Fe		Ni		Co		Pb		Zn		Cu		Al	
		a (%)	b	a (%)	b	a (%)	b	a (ppm)	b	a (ppm)	b	a (ppm)	b	a (ppm)	b	a (ppm)	b	a (%)	b
260 (0-4)	A	20.40		5.15		5.73		1915		112		34		377		1239		1.04	
	B	16.98	83.24	0.01	0.20	0.21	3.66	38	1.98	0	0.00	0	0.00	55	14.54	146	11.78	0.07	6.73
	C	2.25	11.03	4.82	93.59	3.19	55.67	1852	96.71	97	86.61	34	100.00	260	68.97	1013	81.76	0.22	21.15
	D	0.10	0.49	0.22	4.27	2.33	40.67	25	1.31	0	0.00	0	0.00	60	15.91	80	6.46	0.50	48.08
	E	1.07	5.24	0.10	1.94	0.00	0.00	0	0.00	15	3.39	0	0.00	2	0.53	0	0.00	0.25	24.04
261 (4-8)	A	23.09		1.77		6.58		264		59		20		194		505		0.52	
	B	21.35	92.46	0.01	0.56	0.04	0.61	9	3.41	0	0.00	0	0.00	14	7.22	36	7.13	0.02	3.85
	C	0.00	0.00	1.73	97.74	1.16	17.63	214	81.06	31	52.54	20	100.00	90	46.39	198	39.21	0.03	5.77
	D	0.96	4.16	0.01	0.57	5.38	81.76	41	15.53	0	0.00	0	0.00	90	46.39	271	53.66	0.33	63.46
	E	0.78	3.38	0.02	1.13	0.00	0.00	0	0.00	28	47.46	0	0.00	0	0.00	0	0.00	0.14	26.92
266 (33-39)	A	27.15		0.89		5.04		94		37		60		96		322		0.34	
	B	24.92	91.78	0.01	1.12	0.02	0.40	0	0.00	0	0.00	0	0.00	5	5.21	32	9.94	0.01	2.94
	C	2.09	7.70	0.88	98.88	0.77	15.28	56	59.58	6	16.22	18	30.00	26	27.08	70	21.74	0.01	2.94
	D	0.14	0.52	0.00	0.00	4.25	84.32	32	34.04	0	0.00	14	23.33	65	67.71	220	68.32	0.22	64.71
	E	0.00	0.00	0.00	0.00	0.00	0.00	6	6.38	31	83.78	28	46.67	0	0.00	0	0.00	0.10	29.41

Table 4.1: Continued.

CORE SH 1577																						
Sample Number (Interval sampled, cm)		Ca		Mn		Fe		Ni		Co		Pb		Zn		Cu		Al	
		a (%)	b	a (%)	b	a (%)	b	a (ppm)	b	a (ppm)	b	a (ppm)	b	a (ppm)	b	a (ppm)	b	a (%)	b
289 (0-8)	A	18.27		2.27		6.82		360		99				169		410		1.28	
	B	16.37	89.60	0.01	0.44	0.23	3.37	9	2.50	0	0.00			19	11.24	78	19.02	0.08	6.25
	C	1.50	8.21	2.12	93.39	3.64	53.37	293	81.39	69	69.70			102	60.36	220	53.66	0.23	17.97
	D	0.00	0.00	0.14	6.17	2.95	43.26	40	11.11	0	0.00			48	28.40	112	27.32	0.48	37.50
	E	0.40	2.19	0.00	0.00	0.00	0.00	18	5.00	30	30.30			0	0.00	0	0.00	0.49	38.28
290 (10-14)	A	20.29		1.64		6.38		224		82				154		352		1.06	
	B	18.36	90.49	0.01	0.61	0.12	1.88	2	0.89	0	0.00			10	6.49	45	12.79	0.06	5.66
	C	1.00	4.93	1.53	93.29	2.86	44.83	183	81.70	48	58.54			74	48.05	189	53.69	0.18	16.98
	D	0.00	0.00	0.07	4.27	3.40	53.29	36	16.07	6	7.32			70	45.46	118	33.52	0.41	38.68
	E	0.93	4.58	0.03	1.83	0.00	0.00	3	1.34	28	34.14			0	0.00	0	0.00	0.41	38.68
298 (31-39)	A	2.69		2.49		12.34		400		142				294		745		2.09	
	B	1.81	67.29	0.01	0.40	0.18	1.46	19	4.75	6	4.23			16	5.44	45	6.04	0.12	5.74
	C	0.62	23.05	2.37	95.18	4.97	40.28	283	70.75	101	71.13			137	46.60	360	48.32	0.42	20.10
	D	0.14	5.20	0.11	4.42	7.19	58.26	94	23.50	1	0.70			141	47.96	319	42.82	1.02	48.80
	E	0.12	4.46	0.00	0.00	0.00	0.00	4	1.00	34	23.94			0	0.00	21	2.82	0.53	25.36
300 (50-58)	A	6.87		2.41		11.24		351		126		58		251		646		1.72	
	B	5.46	79.48	0.01	0.41	0.13	1.16	12	3.42	6	4.76	0	0.00	11	4.38	44	6.81	0.08	4.65
	C	0.84	12.23	2.22	92.12	4.38	38.97	254	72.36	93	73.81	48	82.76	122	48.61	341	52.79	0.36	20.93
	D	0.16	2.33	0.13	5.40	6.73	59.87	75	21.37	1	0.79	10	17.24	118	47.01	261	40.40	0.85	49.42
	E	0.41	5.96	0.05	2.07	0.00	0.00	10	2.85	26	20.64	0	0.00	0	0.00	0	0.00	0.43	25.00

Table 4.1: Continued.

CORE SH 1577																				
Sample Number (Interval sampled, cm)		Ca		Mn		Fe		Ni		Co		Pb		Zn		Cu		Al	
		a (%)	b	a (%)	b	a (%)	b	a (ppm)	b	a (ppm)	b	a (ppm)	b	a (ppm)	b	a (ppm)	b	a (%)	b
304 (104-110)	A	34.39		0.59		1.67		105		32		38		38		123		0.42	
	B	30.98	90.08	0.01	1.69	0.03	1.80	0	0.00	0	0.00	0	0.00	5	13.16	27	21.95	0.03	7.14
	C	3.41	9.92	0.49	83.05	0.68	40.72	79	75.24	7	21.88	19	50.00	16	42.11	64	52.03	0.07	16.67
	D	0.00	0.00	0.08	13.56	0.88	52.69	18	17.14	0	0.00	5	13.16	17	44.73	32	26.02	0.18	42.86
	E	0.00	0.00	0.01	1.70	0.08	4.79	8	7.62	25	78.12	14	36.84	0	0.00	0	0.00	0.14	33.33
307 (132-138)	A	11.73		2.83		8.80		451		111		59		218		544		1.86	
	B	10.70	91.22	0.01	0.35	0.09	1.02	11	2.44	0	0.00	0	0.00	11	5.05	51	9.38	0.08	4.30
	C	1.03	8.78	2.58	91.17	3.19	36.25	366	81.15	88	79.28	57	96.61	100	45.87	294	54.04	0.27	14.52
	D	0.00	0.00	0.11	3.89	5.08	57.73	57	12.64	3	2.70	2	3.39	107	49.08	199	36.58	0.76	40.86
	E	0.00	0.00	0.13	4.59	0.44	5.00	17	3.77	20	18.02	0	0.00	0	0.00	0	0.00	0.75	40.32
317 (180-185)	A	24.19		1.45		4.45		239		55				126		323		1.06	
	B	22.13	91.48	0.04	2.76	0.06	1.35	0	0.00	0	0.00			8	6.35	46	14.24	0.06	5.66
	C	2.06	8.52	1.29	88.97	1.42	31.91	165	69.04	37	67.27			44	34.92	135	41.80	0.12	11.32
	D	0.00	0.00	0.09	6.20	2.97	66.74	74	30.96	0	0.00			72	57.14	89	27.55	0.51	48.11
	E	0.00	0.00	0.03	2.07	0.00	0.00	0	0.00	18	32.73			2	1.59	53	16.41	0.37	34.91
319 (189-193)	A	9.03		2.45		9.03		437		96		86		302		624		1.77	
	B	8.21	90.92	0.06	2.45	0.10	1.11	16	3.66	1	1.04	0	0.00	13	4.30	62	9.94	0.09	5.09
	C	0.82	9.08	2.32	94.69	2.82	31.23	275	62.93	95	98.96	67	77.91	99	32.78	282	45.19	0.26	14.69
	D	0.00	0.00	0.07	2.86	5.73	63.46	141	32.27	0	0.00	10	11.63	139	46.03	271	43.43	0.83	46.89
	E	0.00	0.00	0.00	0.00	0.38	4.20	5	1.14	0	0.00	9	10.46	51	16.89	9	1.44	0.59	33.33

Table 4.1: Continued.

CORE SH 1578																		
Sample Number (Interval sampled, cm)		Ca		Mn		Fe		Ni		Co		Zn		Cu		Al		
		a (%)	b	a (%)	b	a (%)	b	a (ppm)	b	a (ppm)	b	a (ppm)	b	a (ppm)	b	a (%)	b	
273 (15-22)	A	1.45		3.76		12.14		505		149		294		770		2.02		
	B	0.90	62.07	0.01	0.27	0.26	2.14	26	5.15	6	4.03	26	8.84	78	10.13	0.15	7.43	
	C	0.20	13.79	3.53	93.88	6.17	50.82	389	77.03	119	79.86	169	57.48	449	58.31	0.43	21.29	
	D	0.10	6.90	0.22	5.85	5.71	47.04	86	17.03	0	0.00	99	33.68	243	31.56	0.82	40.59	
	E	0.25	17.24	0.00	0.00	0.00	0.00	4	0.79	24	16.11	0	0.00	0	0.00	0.62	30.69	
274 (30-37)	A	1.20		3.39		12.08		463		135		265		757		2.10		
	B	0.77	64.17	0.02	0.59	0.29	2.40	26	5.62	9	6.67	28	10.57	83	10.96	0.16	7.62	
	C	0.23	19.17	3.10	91.45	6.43	53.23	344	74.30	106	78.52	152	57.36	444	58.65	0.49	23.33	
	D	0.07	5.83	0.27	7.96	5.36	44.37	71	15.33	0	0.00	85	32.07	222	29.33	0.94	44.76	
	E	0.13	10.83	0.00	0.00	0.00	0.00	22	4.75	20	14.81	0	0.00	8	1.06	0.51	24.29	
276 (48-52)	A	1.16		2.90		12.45		400		131				771		2.12		
	B	0.70	60.34	0.02	0.69	0.25	2.01	21	5.25	4	3.06			66	8.56	0.17	8,02	
	C	0.24	20.69	2.66	91.72	5.42	43.53	284	71.00	96	73.28			410	53.18	0.41	19.34	
	D	0.05	4.31	0.16	5.52	6.48	52.05	95	23.75	1	0.76			295	38.26	0.80	37.73	
	E	0.17	14.66	0.06	2.07	0.30	2.41	0	0.00	30	22.90			0	0.00	0.74	34.91	
277 (60-66)	A	1.19		3.47		12.89		539		164		313		861		2.08		
	B	1.00	84.03	0.02	0.58	0.23	1.78	23	4.27	6	3.66	25	7.99	81	9.41	0.16	7.69	
	C	0.00	0.00	2.98	85.88	5.11	39.65	369	68.46	110	67.07	130	41.53	397	46.11	0.35	16.83	
	D	0.04	3.36	0.47	13.54	7.40	57.41	137	25.42	16	9.76	158	50.48	375	43.55	0.88	42.31	
	E	0.15	12.61	0.00	0.00	0.15	1.16	10	1.85	32	19.51	0	0.00	8	0.93	0.69	33.17	

Table 4.1: Continued.

CORE SH 1578																		
Sample Number (Interval sampled, cm.)		Ca		Mn		Fe		Ni		Co		Zn		Cu		Al		
		a (%)	b	a (%)	b	a (%)	b	a (ppm)	b	a (ppm)	b	a (ppm)	b	a (ppm)	b	a (%)	b	
278 (70-78)	A			3.75		13.21		507		154		321		926				
	B			0.02	0.53	2.13	16.12	12	2.37	0	0.00	0	0.00	72	7.78			
	C			3.40	90.67	4.28	32.40	371	73.17	127	82.47	181	56.39	464	50.11			
	D			0.32	8.53	6.80	51.48	124	24.46	0	0.00	140	43.61	390	42.11			
	E			0.01	0.27	0.00	0.00	0	0.00	27	17.53	0	0.00	0	0.00			
285 (129-135)	A	1.46		2.82		13.33		402		150		297		728		1.75		
	B	0.72	49.32	0.07	2.48	0.23	1.73	29	7.22	9	6.00	22	7.41	59	8.10	0.14	8.00	
	C	0.32	21.92	2.41	85.46	4.94	37.06	246	61.19	111	74.00	132	44.44	337	46.29	0.35	20.00	
	D	0.00	0.00	0.28	9.93	8.16	61.22	115	28.61	12	8.00	143	48.15	332	45.61	0.90	51.43	
	E	0.42	28.77	0.06	2.13	0.00	0.00	12	2.99	18	12.00	0	0.00	0	0.00	0.36	20.57	
286 (146-152)	A	1.20		2.40		13.28		373		135				727		1.90		
	B	0.70	58.33	0.07	2.92	0.25	1.88	24	6.43	9	6.67			56	7.70	0.15	7.89	
	C	0.20	16.67	2.17	90.42	4.94	37.20	212	56.84	97	71.85			332	45.67	0.35	18.42	
	D	0.14	11.67	0.16	6.66	8.09	60.92	131	35.12	0	0.00			339	46.63	0.88	46.32	
	E	0.16	13.33	0.00	0.00	0.00	0.00	6	1.61	29	21.48			0	0.00	0.52	27.37	

A: Bulk composition.
B: Acetic acid leach (HAc).
C: Acid-reducing agent leach only (i.e. A/R agent leach - HAc leach).
D: Hydrochloric acid leach only (i.e. HCl leach - A/R agent leach).
E: HCl-insoluble residue (Bulk - HCl leach).

Table 4.2: Average partition of elements between different phases of Bauer Deep sediments (as percentages of the total amount present).

Station No.		Ca	Mn	Fe	Ni	Co	Pb	Zn	Cu	Al
SH 1557	A	71	0.7	1.6	4.1	3.8	0	8.4	9.5	6.4
	B	17	92	43	79	79	88	57	57	18
(6 samples)	C	3.5	6.8	53	14	0.3	12	35	31	54
	D	8.7	0.4	2.3	3.4	17	0	0	2.4	22
SH 1559	A	49	0.3	0.4	4.1	4.7	0	6.8	4.9	4.8
	B	33	93	31	85	71	95	48	47	15
(5 samples)	C	6.4	4.5	67	11	0.9	4.2	45	48	60
	D	11	2.3	1.0	0.1	23	0.4	0	0.4	21
SH 1560	A	89	0.6	1.6	1.8	0	0	9.0	9.6	4.5
	B	6.3	97	30	79	52	77	47	48	10
(3 samples)	C	1.7	1.6	69	17	0	7.8	43	43	59
	D	2.9	1.0	0	2.1	48	16	0.2	0	27
SH 1577	A	86	1.1	1.6	2.2	1.3	0	7.0	13	5.6
	B	11	91	40	74	68	77	45	50	17
(8 samples)	C	0.9	5.9	57	21	1.4	11	46	35	44
	D	2.2	1.5	1.8	2.8	30	11.8	2.3	2.6	34
SH 1578	A	63	1.2	4.0	5.2	4.3		7.2	8.9	7.8
	B	15	90	42	69	75		50	51	20
(7 samples	C	5.4	8.3	54	24	2.7		43	40	44
	D	16	0.6	0.5	1.7	18		0	0.3	29

A: Acetic acid leach (HAc).
B: Acid-reducing agent leach only (i.e. A/R agent leach - HAc leach).
C: Hydrochloric acid leach only (i.e. HCl leach - A/R agent leach).
D: HCl-insoluble residue (Bulk - HCl leach).

Table 4.3: Average partition of elements between different phases of all Bauer Deep sediment samples (as percentages of the total amount present).

	Ca	Mn	Fe	Ni	Co	Pb	Zn	Cu	Al
A	72	0.8	1.9	3.5	2.8	0	7.7	9.1	5.8
B	16	93	37	77	69	84	50	51	16
C	3.6	5.4	60	17	1.1	8.9	42	39	52
D	8.3	1.2	1.1	2.0	27	7.0	0.5	1.1	26

A: Acetic acid leach (HAc).

B: Acid-reducing agent leach only (i.e. A/R agent leach - HAc leach).

C: Hydrochloric acid leach only (i.e. HCl leach - A/R agent leach).

D: HCl-insoluble residue (Bulk - HAc leach).

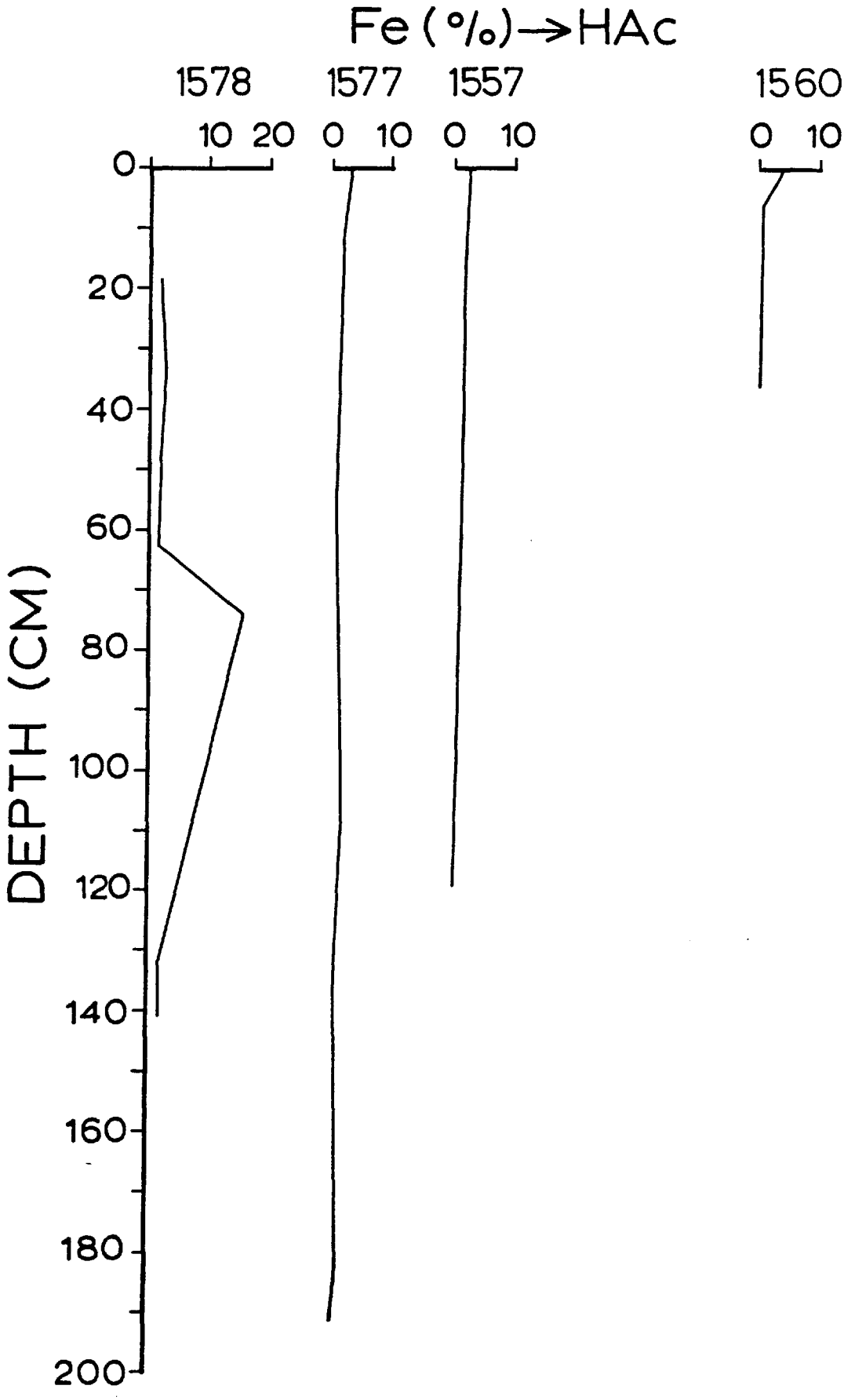

Figure 4.11: Distribution of the acetic acid-soluble Fe in Bauer Deep sediment cores expressed as a percentage of the total Fe concentration.

From the top of the cores SH 1577, SH 1559 and SH 1560 down to about 40 cm depth the percentage of Fe which is soluble in the acid-reducing agent solution falls gradually, while in the cores SH 1578 and SH 1557 it remains fairly constant (see Figure 4.12). Below 40 cm in the cores SH 1577, SH 1557 and SH 1559 the hydroxylamine HCl-soluble Fe varies, having the tendency to decrease with depth. In core SH 1578 a systematic decrease of the acid-reducible Fe was found from 40 cm down to about 70 cm, whilst below this depth it remains constant.

In the upper 40 cm of the cores SH 1577, SH 1559, SH 1560 and SH 1578 the percentage of Fe associated with the HCl-soluble fraction is found to increase steadily with increasing depth (see Figure 4.13). Below 40 cm it shows no clear relationship with depth. However, the vertical variations of the HCl-soluble Fe in the core SH 1557 display a different pattern. Down to 40 cm there is a gradual decrease of the HCl-soluble Fe with depth. Below, down to the bottom of the core, the percentage of Fe associated with the HCl-soluble fraction increases steadily.

4.5.2 Manganese

Manganese has been found almost exclusively ($\sim 93\%$) in the hydroxylamine HCl-soluble fraction, indicating the strong association of this element with the ferromanganese oxide minerals. Relatively minor amounts of Mn ($\sim 5\%$) have been found in the HCl-soluble fraction, while it appears to be sparingly soluble ($\sim 0.8\%$) in acetic acid. Only a very small amount of Mn ($\sim 1\%$) remains in the HCl-insoluble residue.

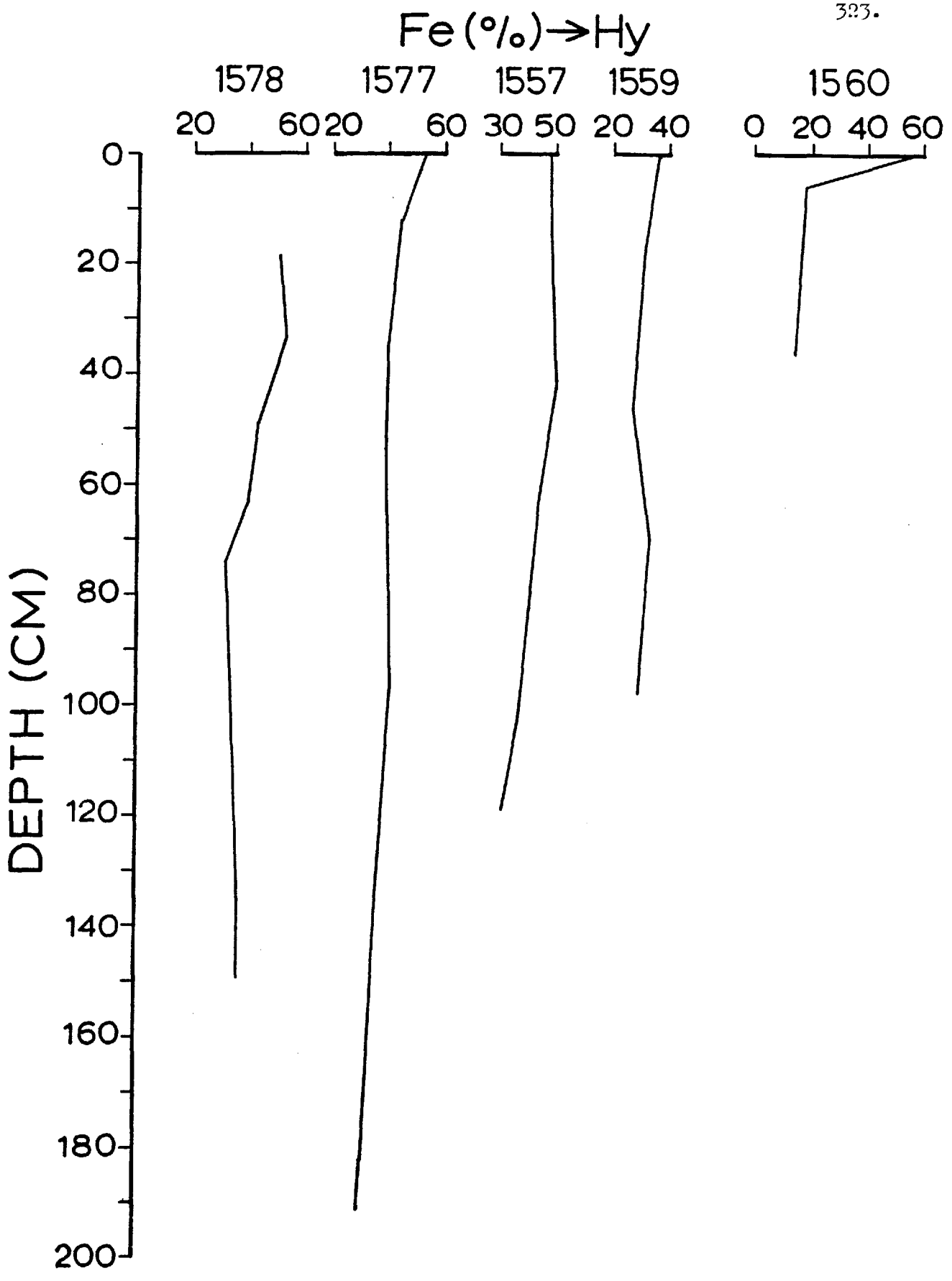

Figure 4.12: Distribution of the hydroxylamine HCl-soluble Fe in Bauer Deep sediment cores expressed as a percentage of the total Fe concentration.

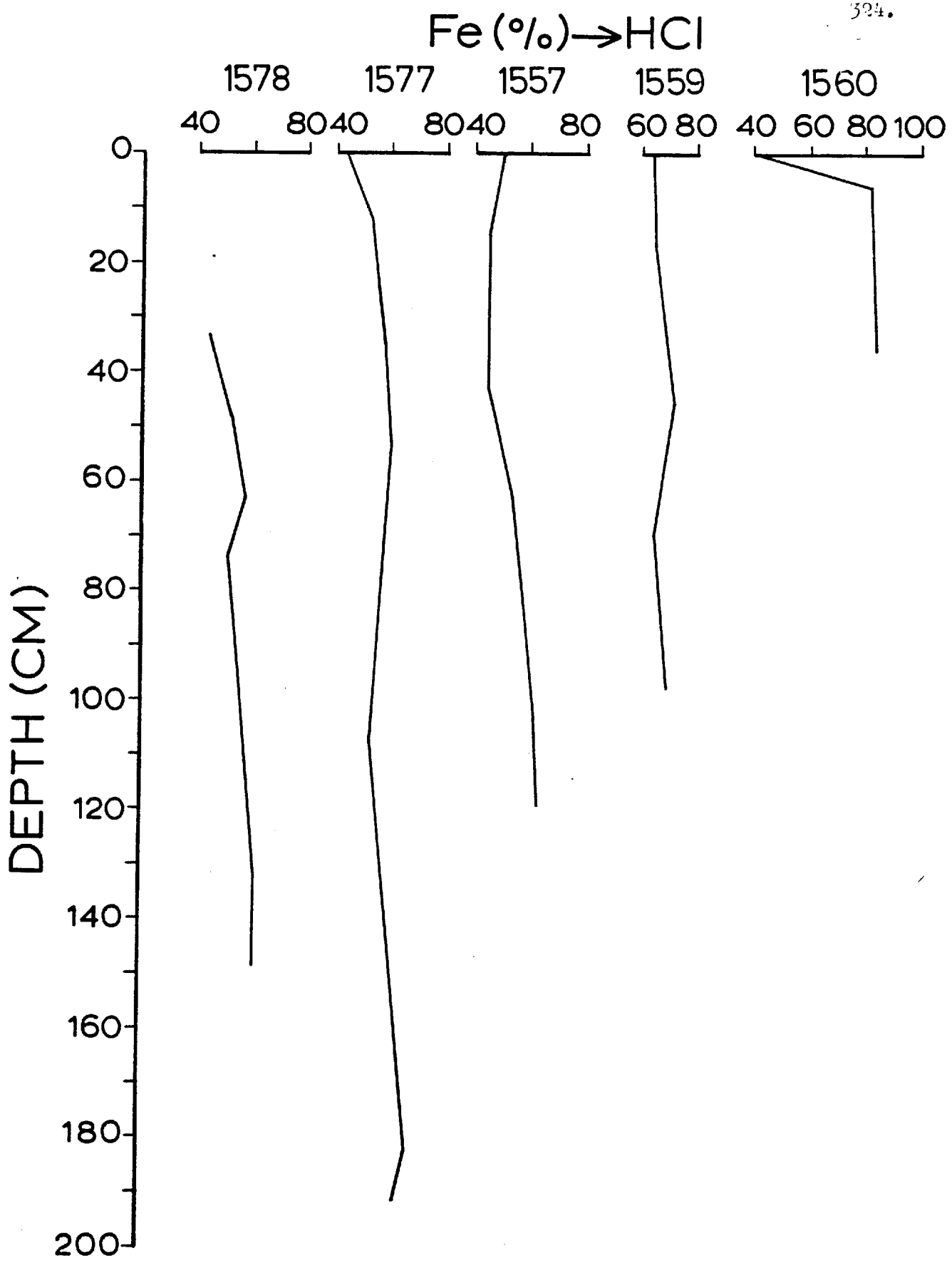

Figure 4.13: Distribution of the HCl-soluble Fe in Bauer Deep sediment cores expressed as a percentage of the total Fe concentration.

The percentage of Mn which is released in the acetic acid solution remains constant throughout all the cores examined here (see Figure 4.14).

Down to 110 cm in the cores SH 1577, SH 1578 and SH 1557 the percentage of Mn which is present in the hydroxylamine HCl-soluble fraction diminishes with depth. In the core SH 1559 this percentage decreases from 0 to 20 cm, while below this depth it remains constant (see Figure 4.15).

The vertical fluctuations of the percentage of Mn associated with the HCl-soluble fraction show no clear relationship with depth (see Figure 4.16).

4.5.3 Nickel

The majority of the Ni is associated with the fraction soluble in the hydroxylamine HCl reagent solution ($\sim$ 77%), which indicates its association with the ferromanganese oxides. Most of the remaining Ni ($\sim$ 17%) is present in the Fe-rich montmorillonite phase, being soluble in HCl. Minor amounts of Ni ($\sim$ 4%) have been found in the acetic acid soluble fraction, while only 2% remains in the HCl-insoluble residue.

In general, the vertical variations in the percentage of Ni associated with the acetic acid-soluble fraction show no clear relationship with depth in the cores. However, in the cores SH 1557 and SH 1577 there is a slight reduction of this proportion from 0 to 15 cm depth (see Figure 4.17).

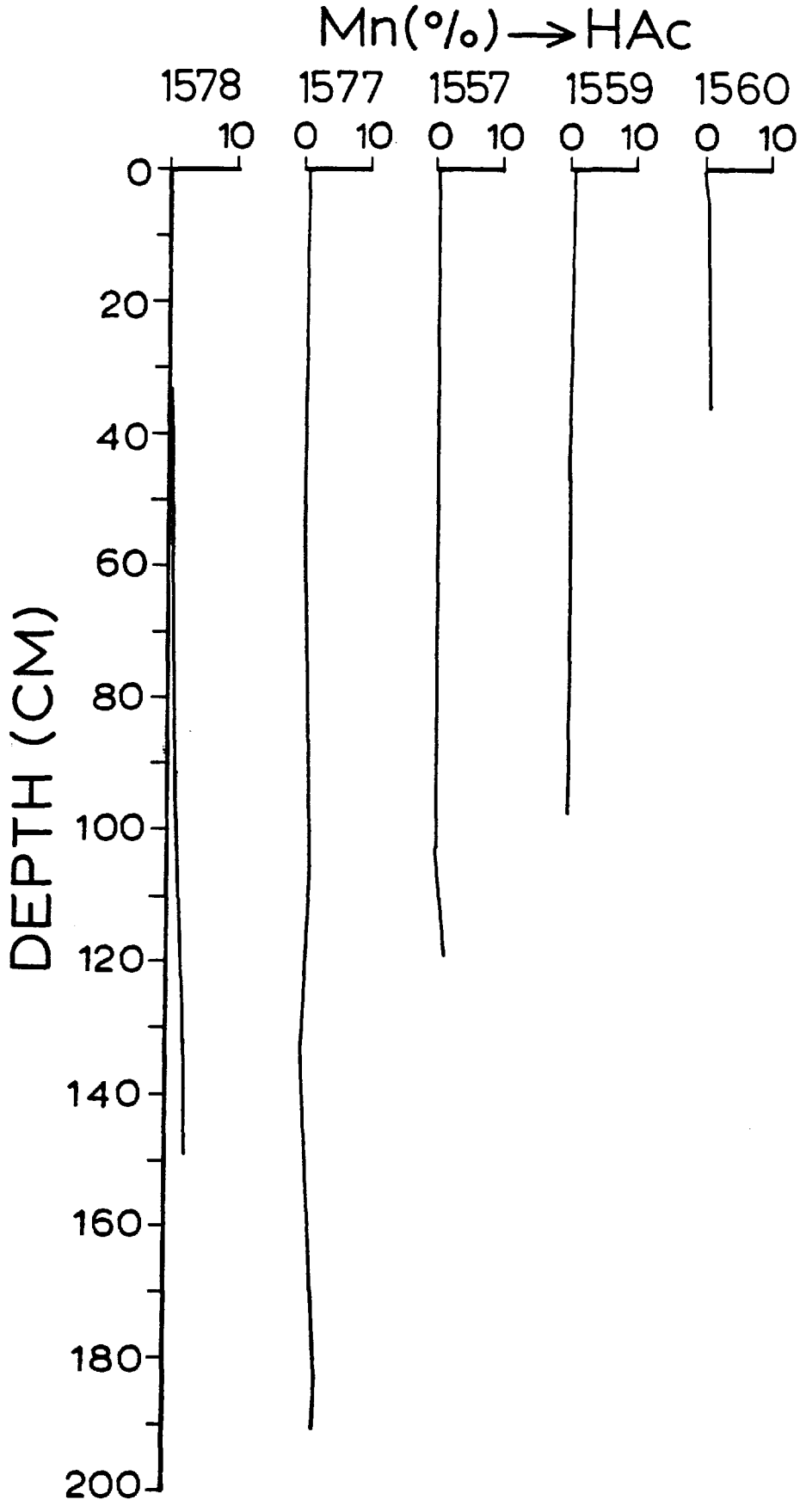

Figure 4.14: Distribution of the acetic acid-soluble Mn in Bauer Deep sediment cores expressed as a percentage of the total Mn concentration.

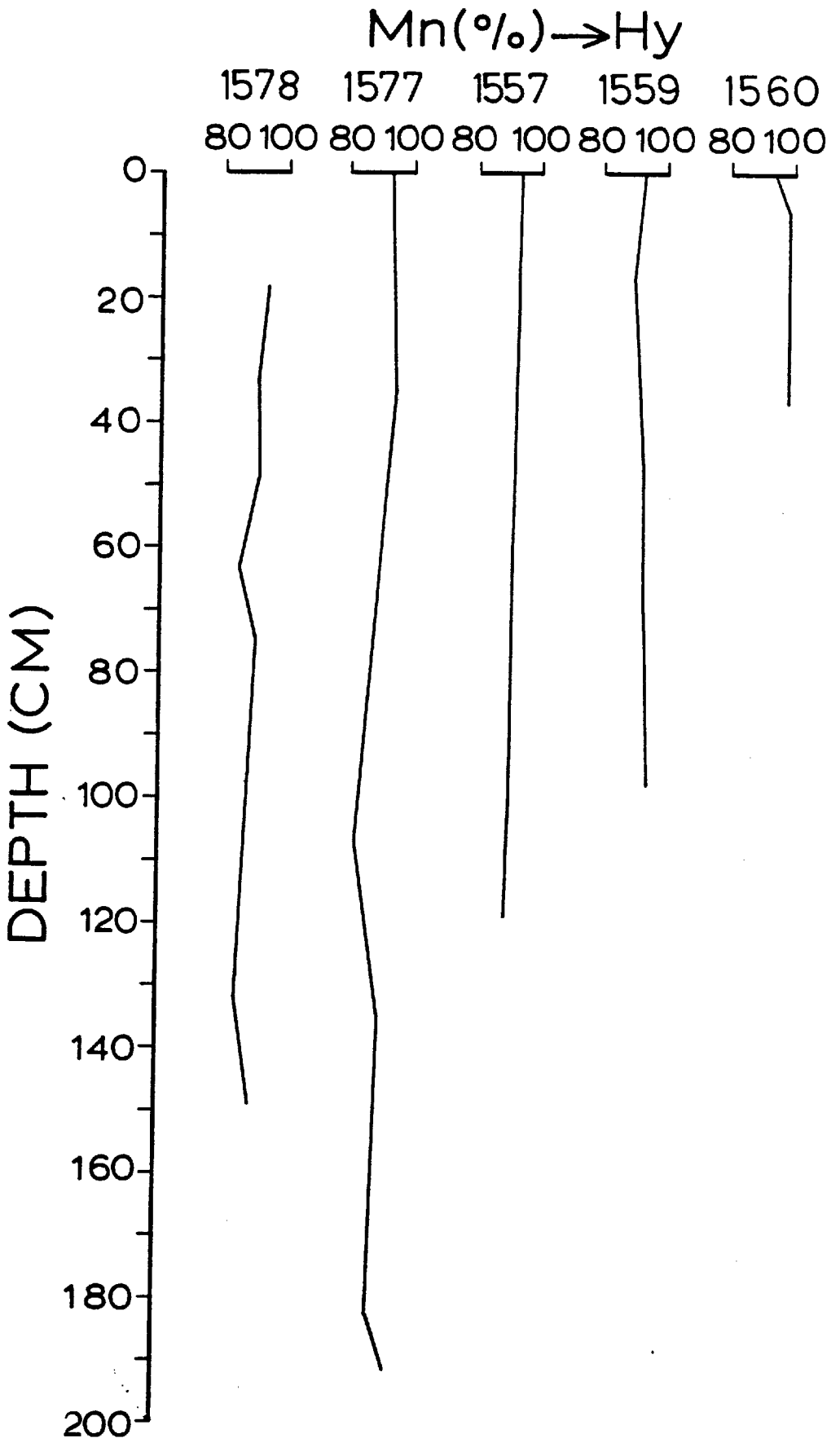

Figure 4.15: Distribution of the hydroxylamine HCl-soluble Mn in Bauer Deep sediment cores expressed as a percentage of the total Mn concentration.

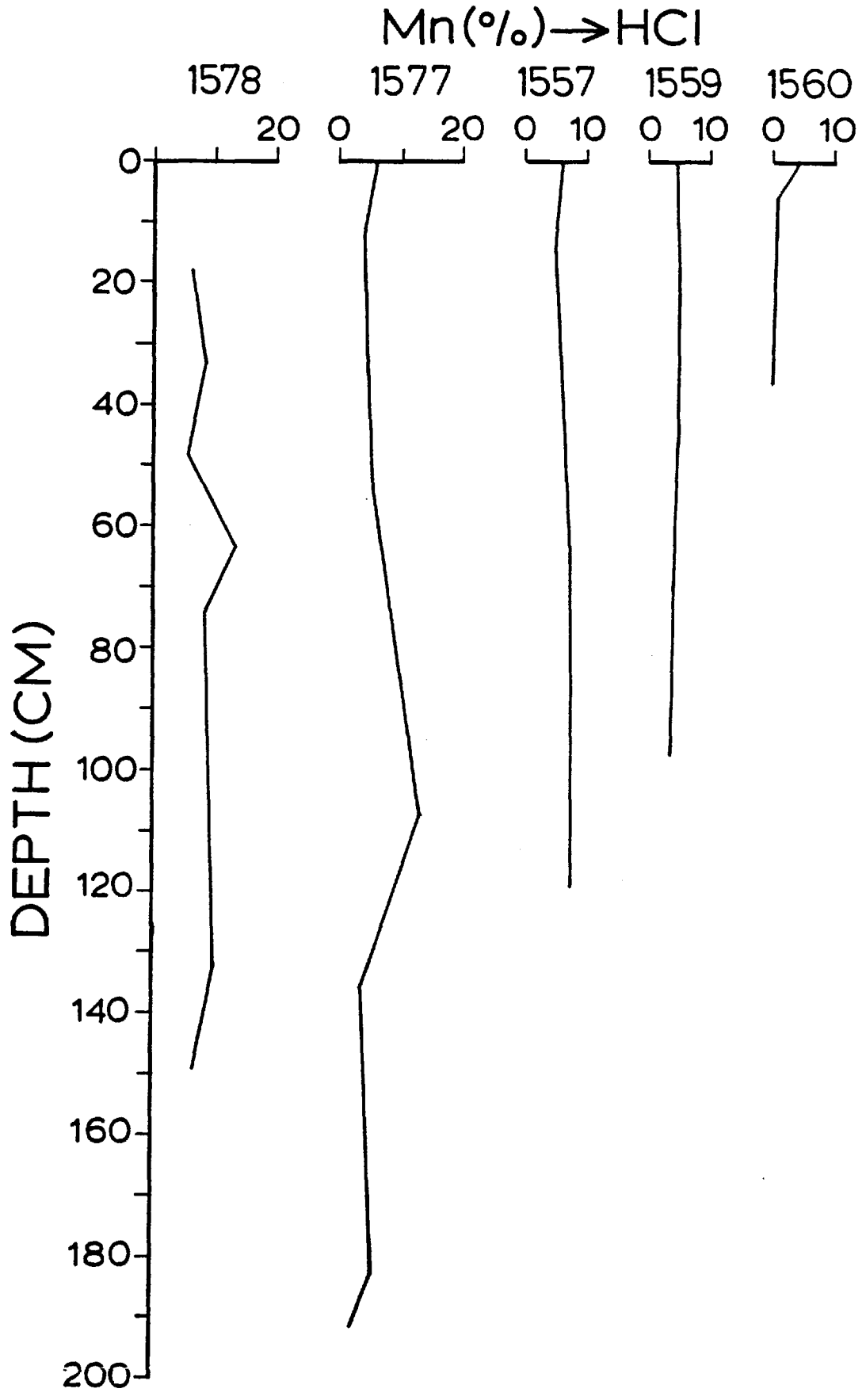

Figure 4.16: Distribution of the HCl-soluble Mn in Bauer Deep sediment cores expressed as a percentage of the total Mn concentration.

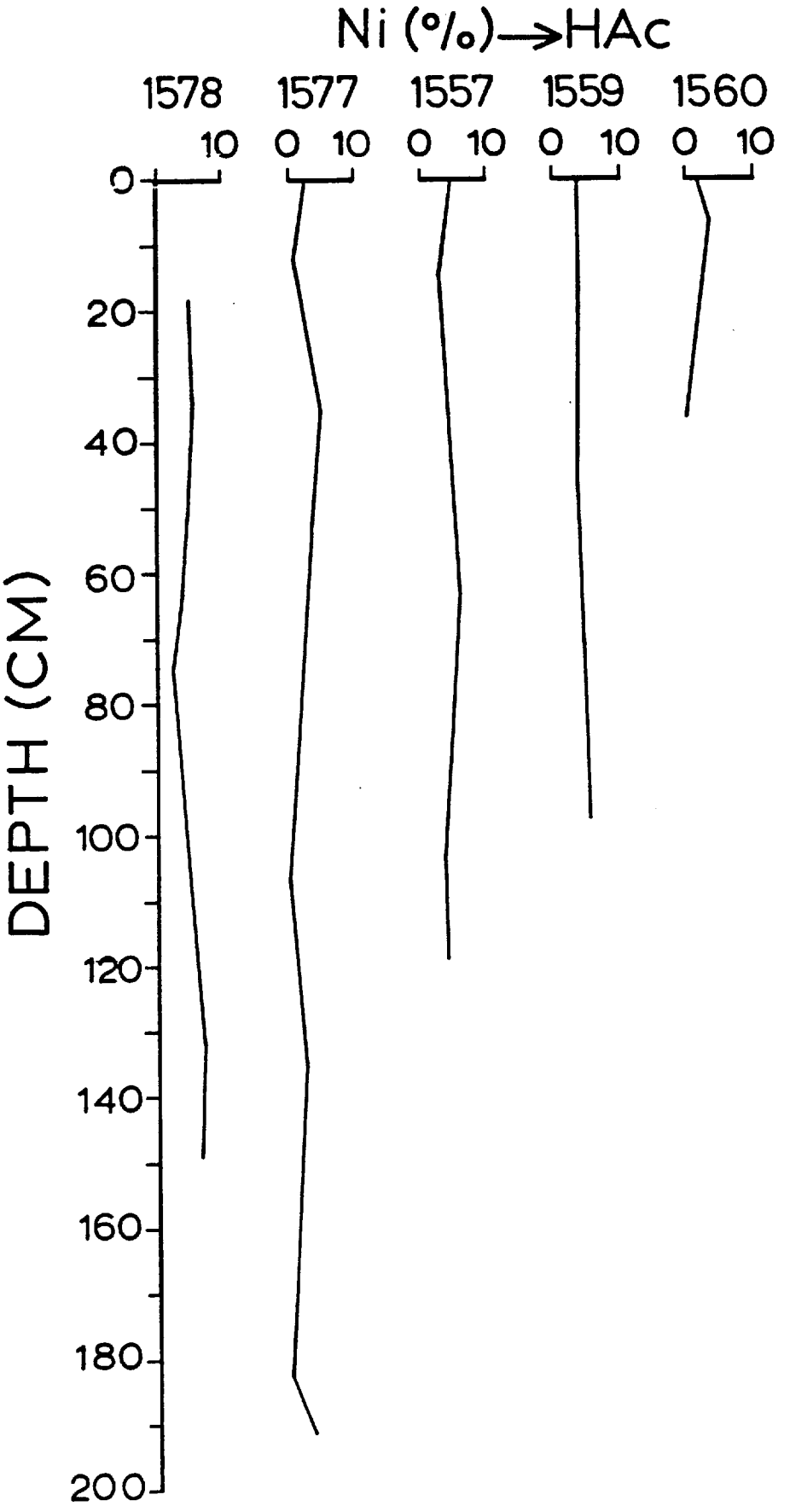

Figure 4.17: Distribution of the acetic acid-soluble Ni in Bauer Deep sediment cores expressed as a percentage of the total Ni concentration.

In the cores SH 1577, SH 1578, SH 1557 and SH 1560 the percentage of Ni which is present in the acid-reducible fraction diminishes gradually from the top down to about 40 cm, thus showing a negative correlation with depth. This reduction is sharper in core SH 1560, while in the core SH 1578 it continues to the greater depth of 150 cm. Core SH 1559 displays a slight increase of the hydroxylamine HCl-soluble Ni from 0 to about 20 cm, whilst below this depth it remains constant (see Figure 4.18).

The variations in the proportion of Ni soluble in HCl differ from one core to another. Core SH 1577 shows an increase of the HCl-soluble Ni from 0 to 35 cm, while below 35 cm there is no relationship between the percentage extracted and the depth. By contrast, in core SH 1578 there is a tendency for the percentage of Ni which is soluble in HCl to increase with increasing depth toward the lower part of the core (40-150 cm). Core SH 1560 exhibits an increase of the HCl-soluble Ni from 0 to 10 cm while in cores SH 1557 and SH 1559 this proportion shows no significant variations with depth (see Figure 4.19).

4.5.4 Cobalt

Cobalt, like nickel, is strongly associated with ferromanganese oxide phases. About 69% of the total Co is soluble in the hydroxylamine HCl reagent solution. In contrast to the case of Ni, the majority of the remainder Co ($\sim$ 27%) occurs in the lattice structure of the detrital material, as it is associated with the HCl-insoluble residue. About 3% being dissolved in acetic acid is related to the carbonates or mineral surfaces. Only 1% of the total Co is found in the HCl-soluble fraction, thus showing the minor relationship of this element with the Fe-rich phases (Fe-smectites).

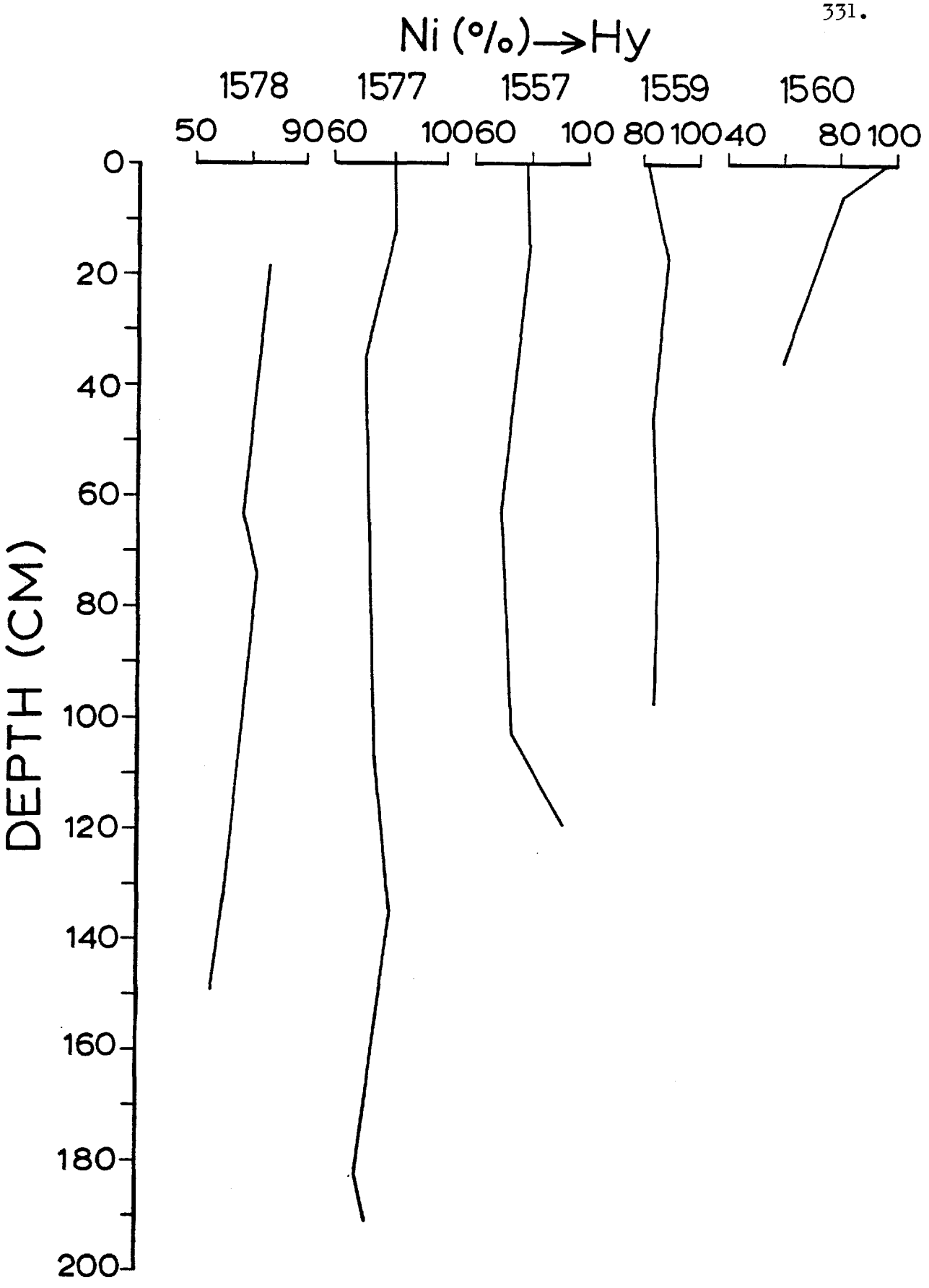

Figure 4.18: Distribution of the hydroxylamine HCl-soluble Ni in Bauer Deep sediment cores expressed as a percentage of the total Ni concentration.

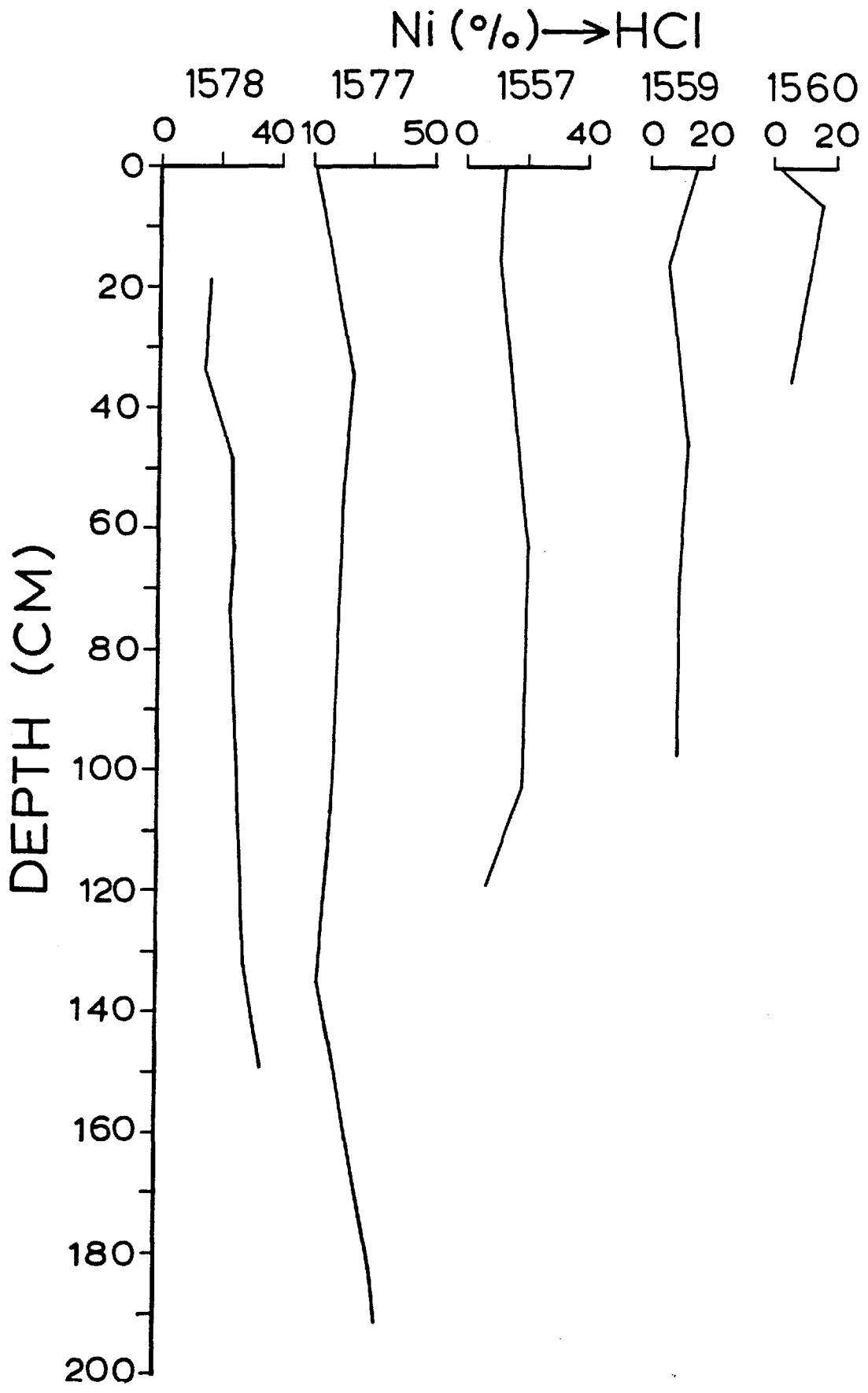

Figure 4.19: Distribution of the HCl-soluble Ni in Bauer Deep sediment cores expressed as a percentage of the total Ni concentration.

4.5.5 Lead

The geochemical partition data for Pb indicate that the majority of this element, like Ni and Co, is present in the acid-reducible fraction, which again suggests its strong association with the ferromanganese oxide phases. Pb is completely absent from the acetic acid-soluble fraction, while the HCl-soluble and insoluble fractions contribute little to the total Pb content of the sediments (see Table 4.3).

4.5.6 Zinc

Zinc is associated with both the ferromanganese oxide minerals and the Fe-rich montmorillonites, having higher concentrations in the former than in the latter. About 50% of the total Zn is concentrated in the acid-reducible fraction, while 42% is present in the fraction soluble in HCl. The acetic-acid soluble material contributes about 8% to the total Zn in the sediment. However, this proportion is rather high when compared with other marine sediments (see Section 2 of this thesis). This indicates that a considerable amount of Zn is adsorbed onto the surface of the Fe-rich montmorillonite which comprises the main phase of the sediments (the $CaCO_3$ content is generally low).

When plotted versus depth in cores SH 1577 and SH 1560, the percentage of Zn associated with the acetic-acid-soluble fraction displays similar patterns. This percentage gradually decreases with depth in the upper 40 cm of the sediment (see Figure 4.20). A similar pattern is also evident in the vertical variations of the hydroxylamine

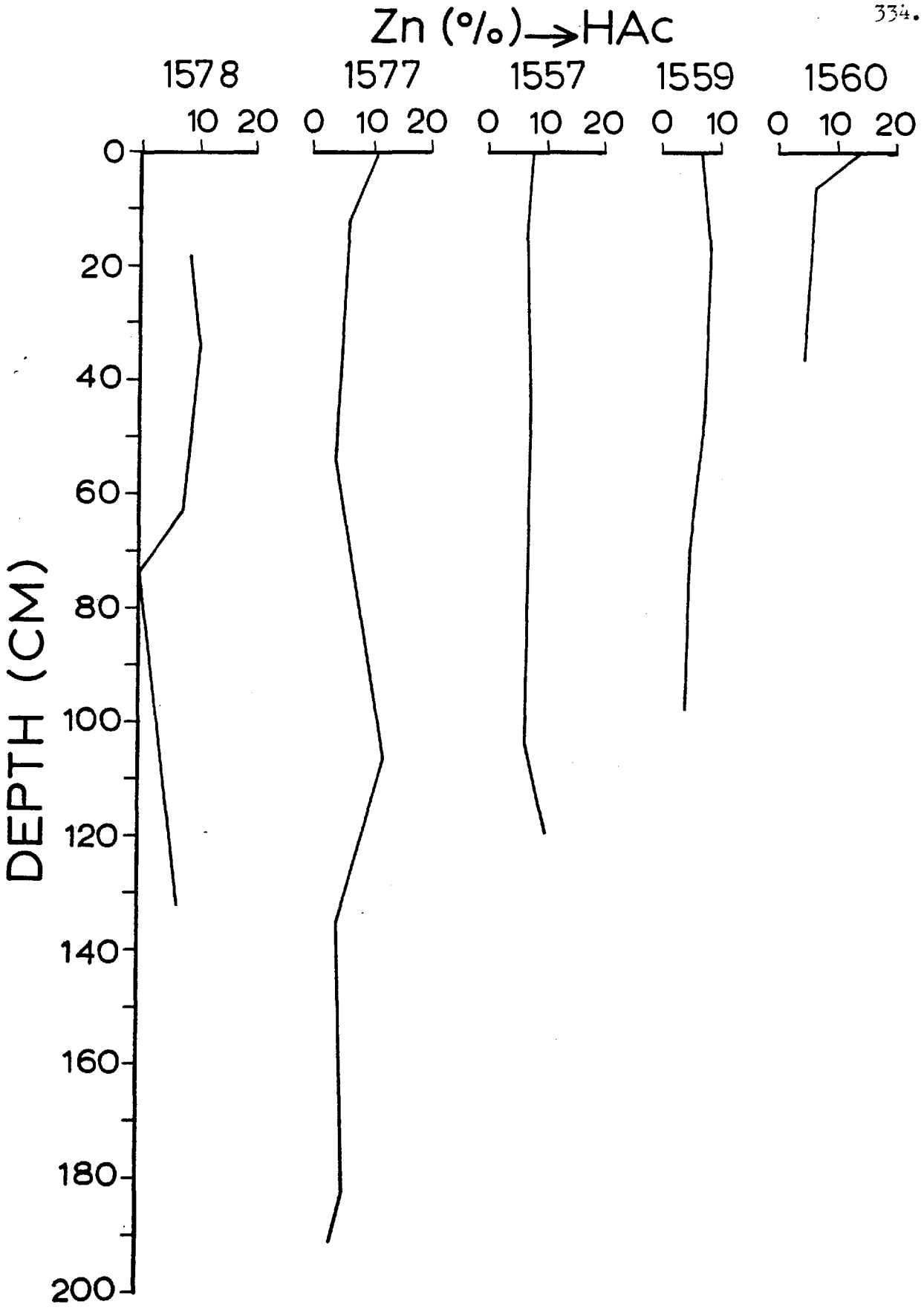

Figure 4.20: Distribution of the acetic acid-soluble Zn in Bauer Deep sediment cores expressed as a percentage of the total Zn concentration.

HCl-soluble Zn in cores SH 1577, SH 1560 and SH 1559 (see Figure 4.21). The percentage of Zn present in the acid-reducible fraction, like that soluble in acetic acid, diminishes gradually with increasing depth from 0 down to about 40 cm. This reduction is sharper in core SH 1560, where a value of 24% is exhibited at 36 cm depth, which is in contrast to the surface sediments where the acid-reducible fraction contributes 70% of the total Zn. Furthermore, the HCl-soluble Zn in the cores SH 1577, SH 1559 and SH 1560 increases steadily with increasing depth in the upper 40 cm. The variations of the partitioning data for Zn do not produce any discernible pattern in the remaining cores (SH 1557 and SH 1578) (see Figure 4.22).

4.5.7 Copper

On average, copper is essentially distributed between the ferromanganese oxide and the Fe-rich montmorillonite phases. Approximately 51% of the Cu is associated with the ferromanganese oxides in the hydroxylamine HCl-soluble fraction and ~39% is located in the Fe-rich montmorillonites being soluble in HCl.

Almost all the remainder Cu ($\sim 9\%$) is liberated in the acetic acid solution. Since the Bauer Deep sediments are very poor in $CaCO_3$ this portion of Cu is located on the surface of the Fe-rich montmorillonites.

There does not seem to be a significant amount of Cu in the HCl-insoluble residue, thus suggesting that the lattice structure of detrital material accommodates very little of this element.

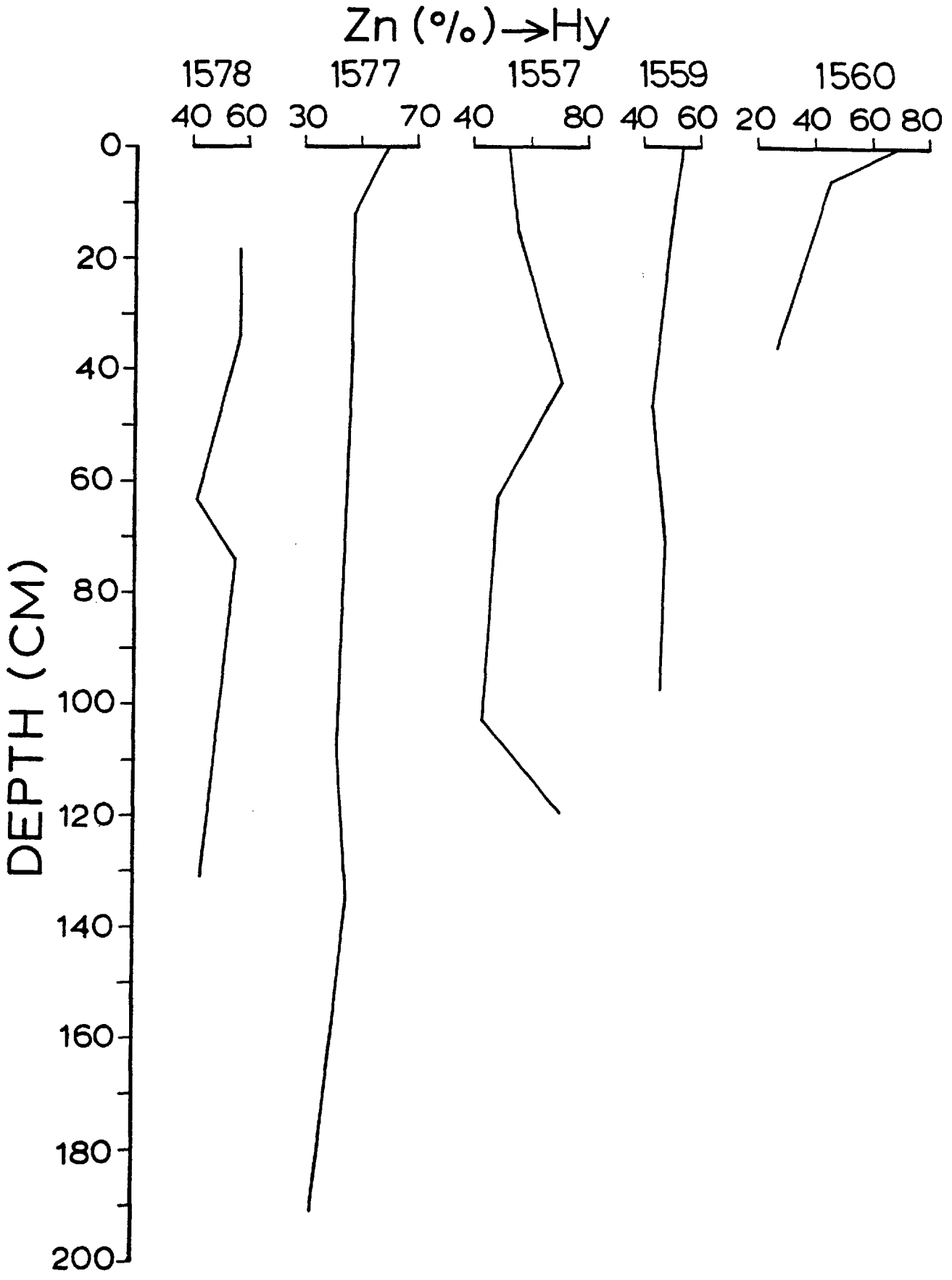

Figure 4.21: Distribution of the hydroxylamine HCl-soluble Zn in Bauer Deep sediment cores expressed as a percentage of the total Zn concentration.

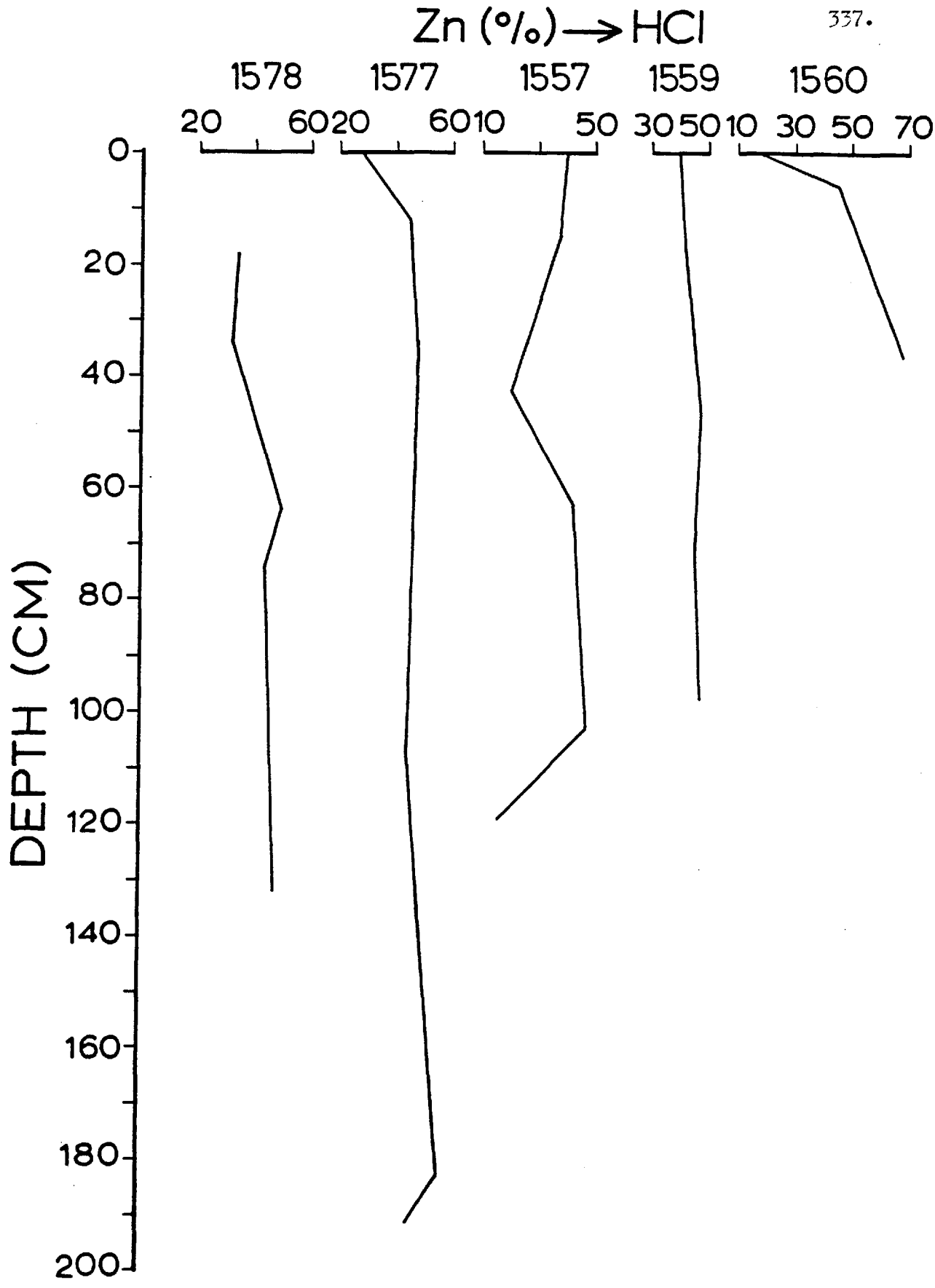

Figure 4.22: Distribution of the HCl-soluble Zn in Bauer Deep sediment cores expressed as a percentage of the total Zn concentration.

The variations of the partitioning data for Cu versus depth are similar in cores SH 1577, SH 1578, SH 1559 and SH 1560. In general, there is a continuous reduction in the proportion of Cu which is soluble in both the acetic acid and that present in the hydroxylamine HCl-soluble fraction from the top of the cores down to about 40 cm (see Figures 4.23 and 4.24). In contrast, Cu, like Fe, increases gradually with depth in the HCl-soluble fraction (see Figure 4.25). In the core SH 1560 the decrease of the percentage of Cu associated with the hydroxylamine HCl-soluble fraction and the increase of that soluble in HCl are very sharp.

It appears that below 40 cm, there are no significant variations in the proportional distribution of Cu among the various fractions of the sediments. However, in core SH 1559 the proportion of Cu present in the hydroxylamine HCl-soluble fraction continues to decrease.

4.5.8 Aluminium

Approximately 52% of the Al forms Fe-rich montmorillonites being dissolved in HCl. Almost 26% is present in the HCl-insoluble detrital phases indicating the considerable contribution of the lattice structure of the more resistant aluminosilicates. A significant amount of Al (~16%) is located in ferromanganese oxide minerals, being soluble in the hydroxylamine HCl reagent solution. It is also present in the acetic acid-soluble fraction (6% of the total amount).

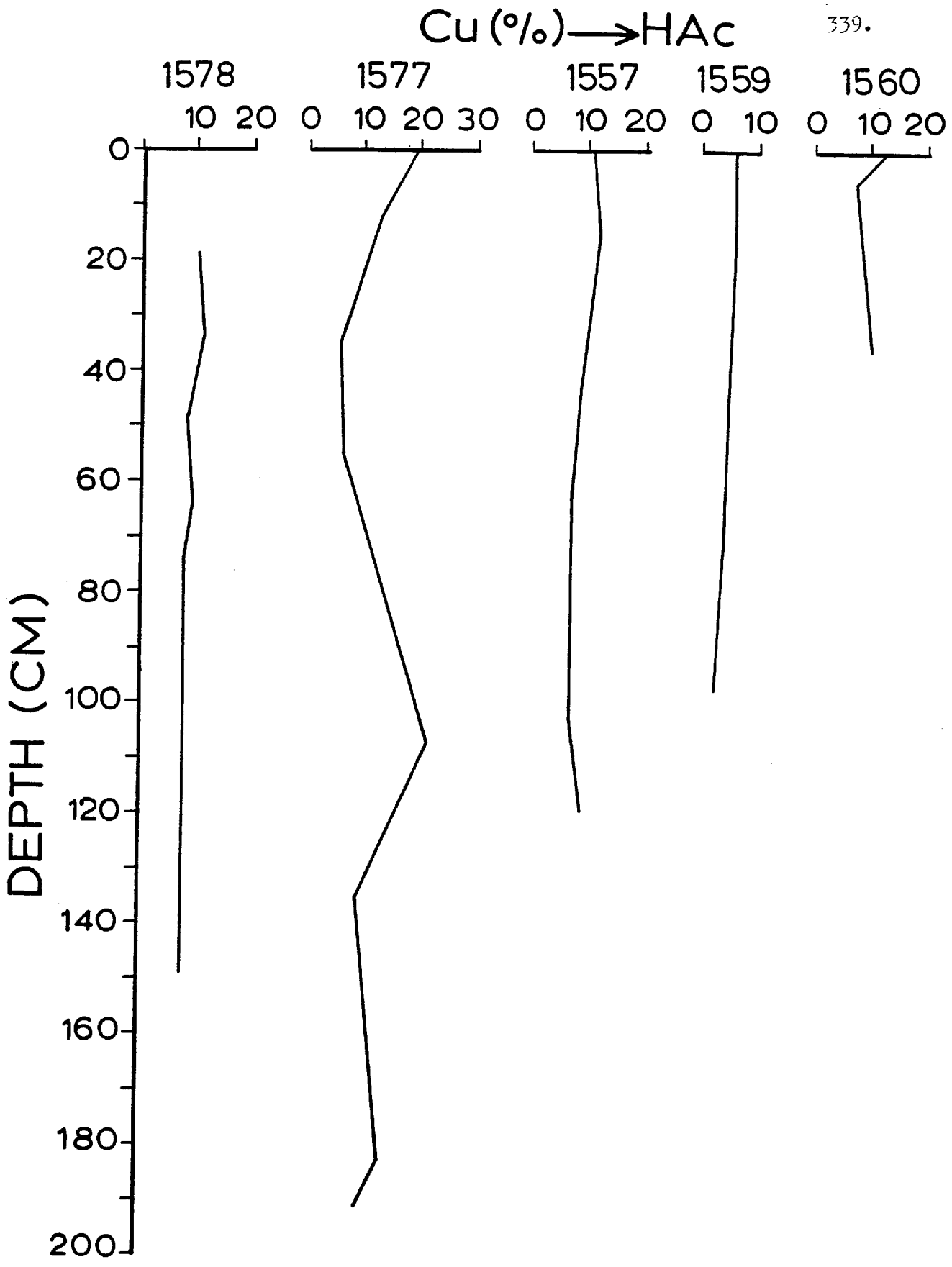

Figure 4.23: Distribution of the acetic acid-soluble Cu in Bauer Deep sediment cores expressed as a percentage of the total Cu concentration.

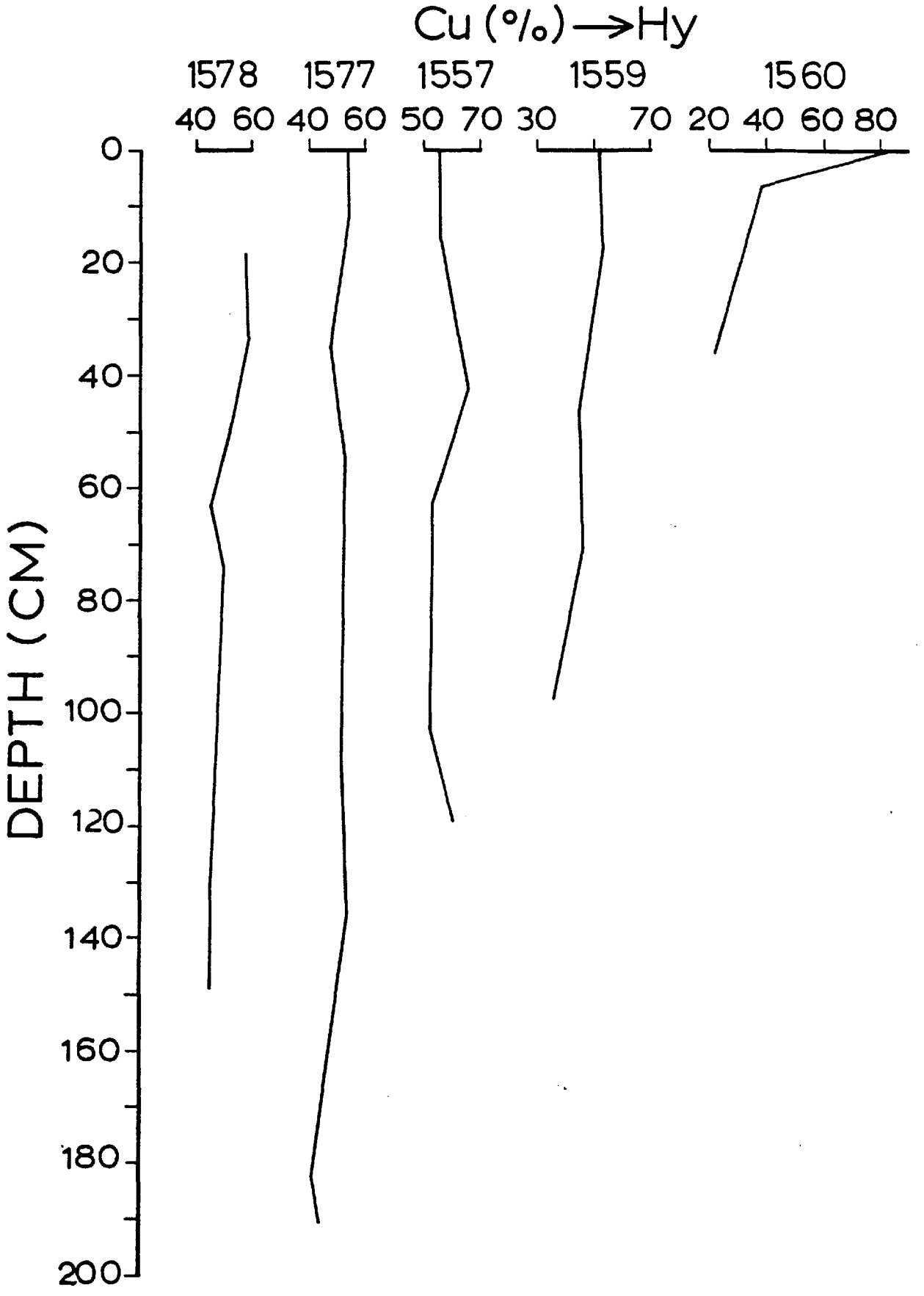

Figure 4.24: Distribution of the hydroxylamine HCl-soluble Cu in Bauer Deep sediment cores expressed as a percentage of the total Cu concentration.

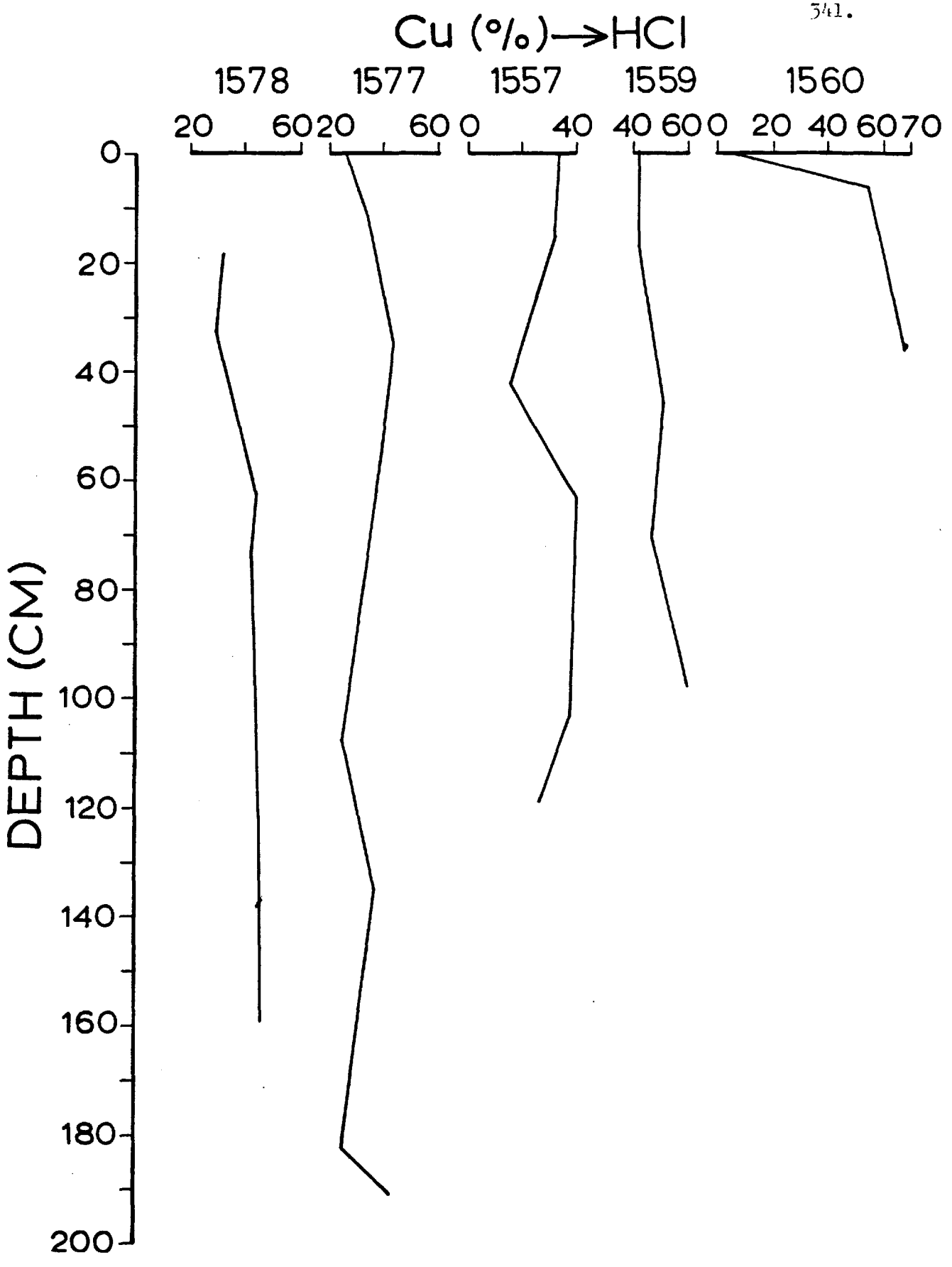

Figure 4.25: Distribution of the HCl-soluble Cu in Bauer Deep sediment cores expressed as a percentage of the total Cu concentration.

The vertical partitioning variations of Al are similar to those found for Fe, thus showing the association of these two elements in the Fe-rich montmorillonite structure. As in the case of Fe, the proportion of Al which is present in the hydroxylamine HCl-soluble fraction diminishes with depth in the upper part of the sediment cores SH 1577, SH 1559 and SH 1560 (see Figure 4.27). By contrast, there is an increase of the HCl-soluble Al with depth in the upper sediments (see Figure 4.28). At greater depths, both the hydroxylamine HCl and the HCl-soluble fractions do not show variations in their contribution of Al to the total sediment. Similarly, the percentage of Al which is released in the acetic acid solution remains constant down the length of the cores (see Figure 4.26).

4.5.9 Calcium

Most of the Ca is concentrated in the acetic acid-soluble fraction (~72%), which reflects the presence of Ca mainly in the $CaCO_3$ of the sediments. A significant amount of Ca is found to be soluble in the hydroxylamine HCl reagent solution (~16%) occurring in the ferromanganese oxide minerals. Minor amounts are found in the HCl-soluble and insoluble fractions, located in the structure of the Fe-rich montmorillonites (see Table 4.3).

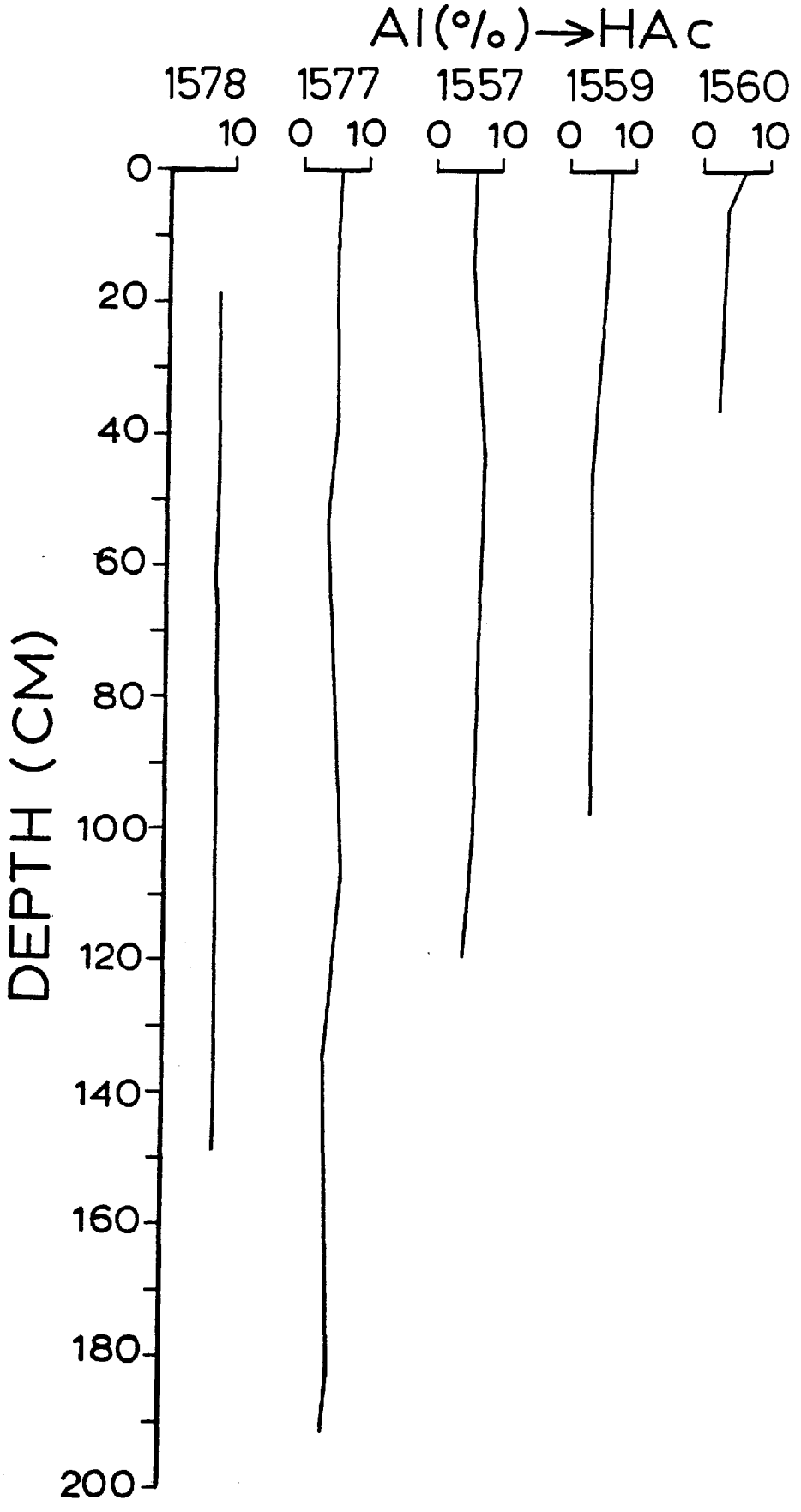

Figure 4.26: Distribution of the acetic acid-soluble Al in Bauer Deep sediment cores expressed as a percentage of the total Al concentration.

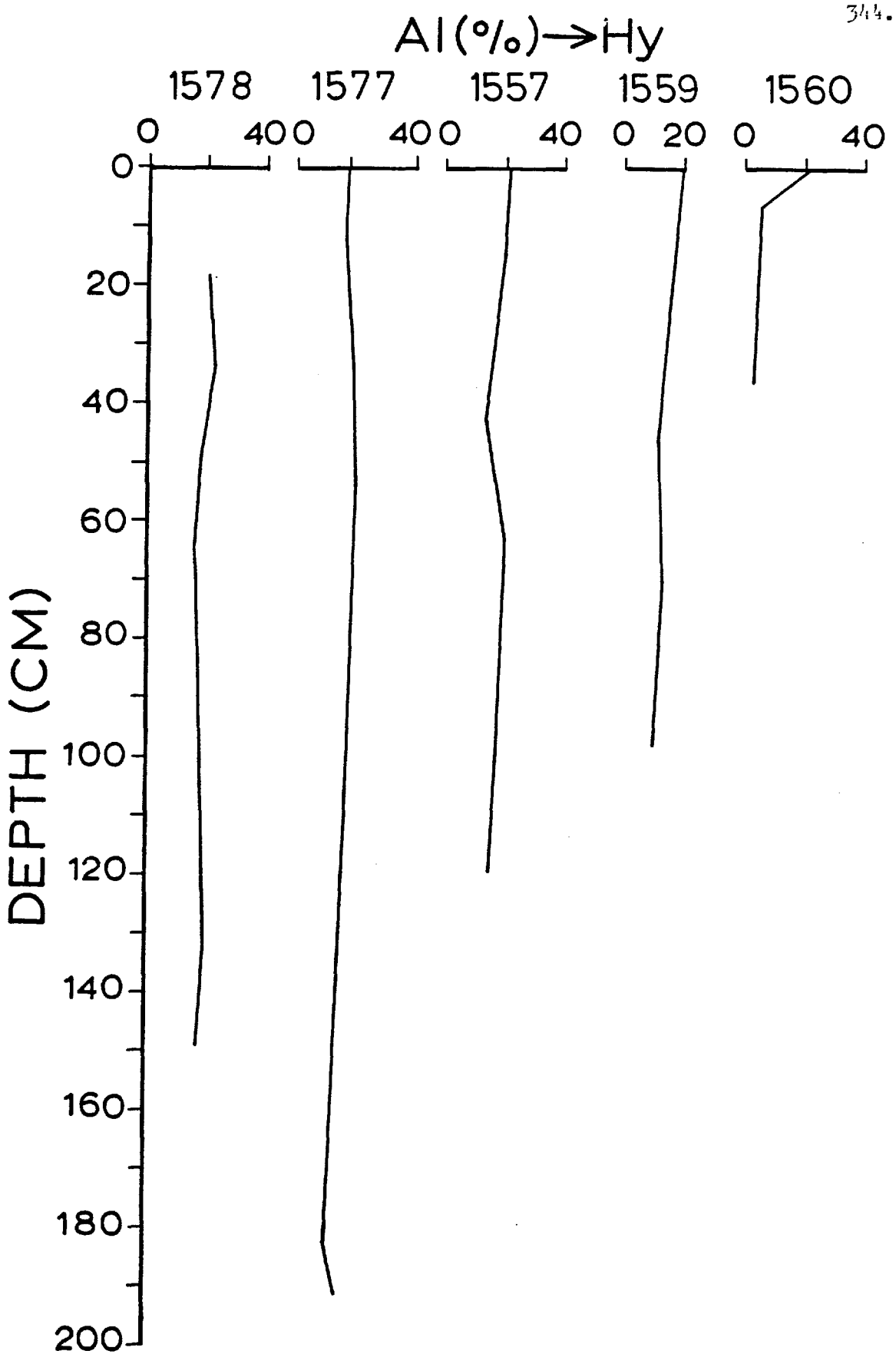

Figure 4.27: Distribution of the hydroxylamine HCl-soluble Al in Bauer Deep sediment cores expressed as a percentage of the total Al concentration.

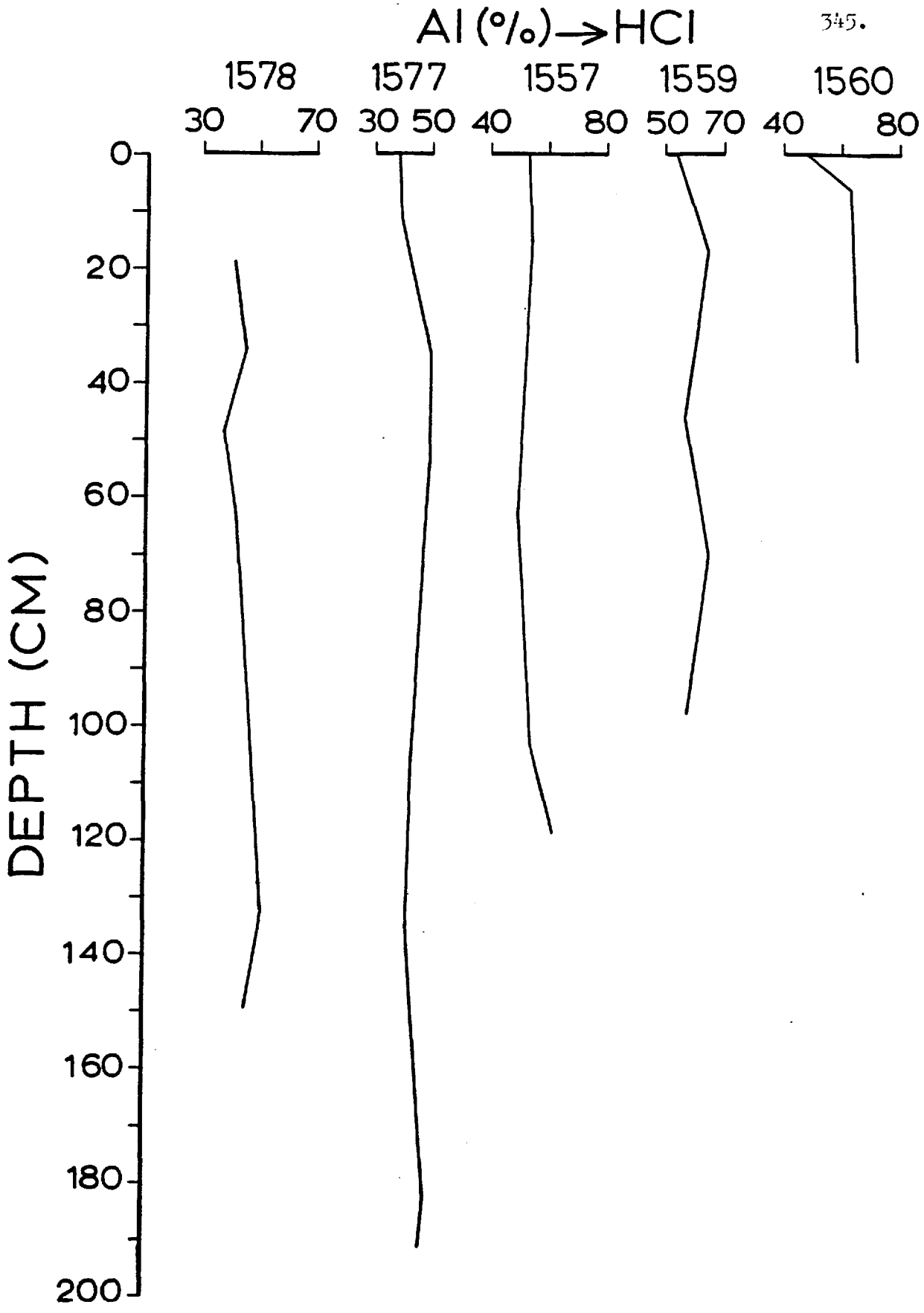

Figure 4.28: Distribution of the HCl-soluble Al in Bauer Deep sediment cores expressed as a percentage of the total Al concentration.

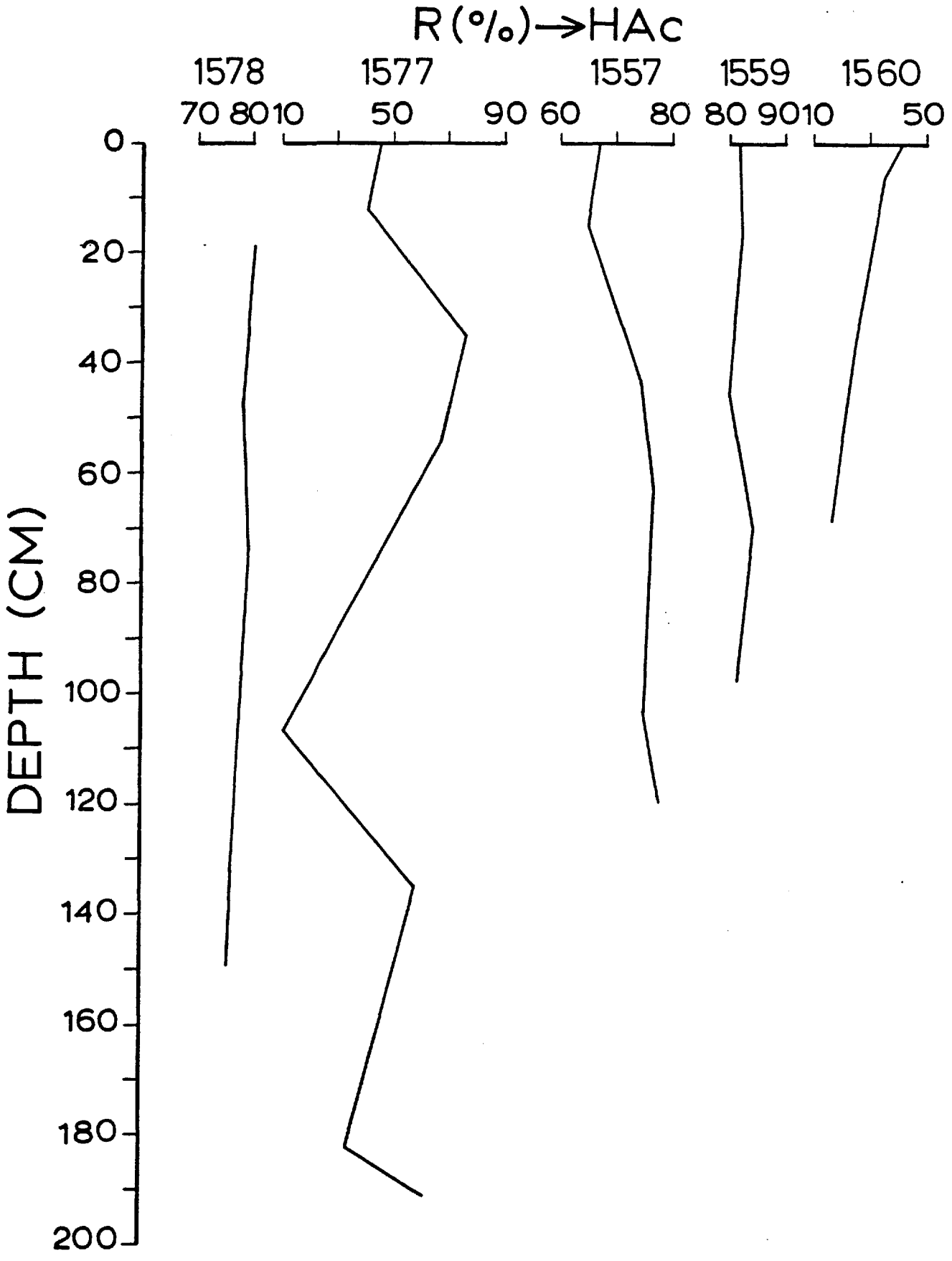

Figure 4.29: Distribution of the acetic acid-insoluble residue in Bauer Deep sediment cores.

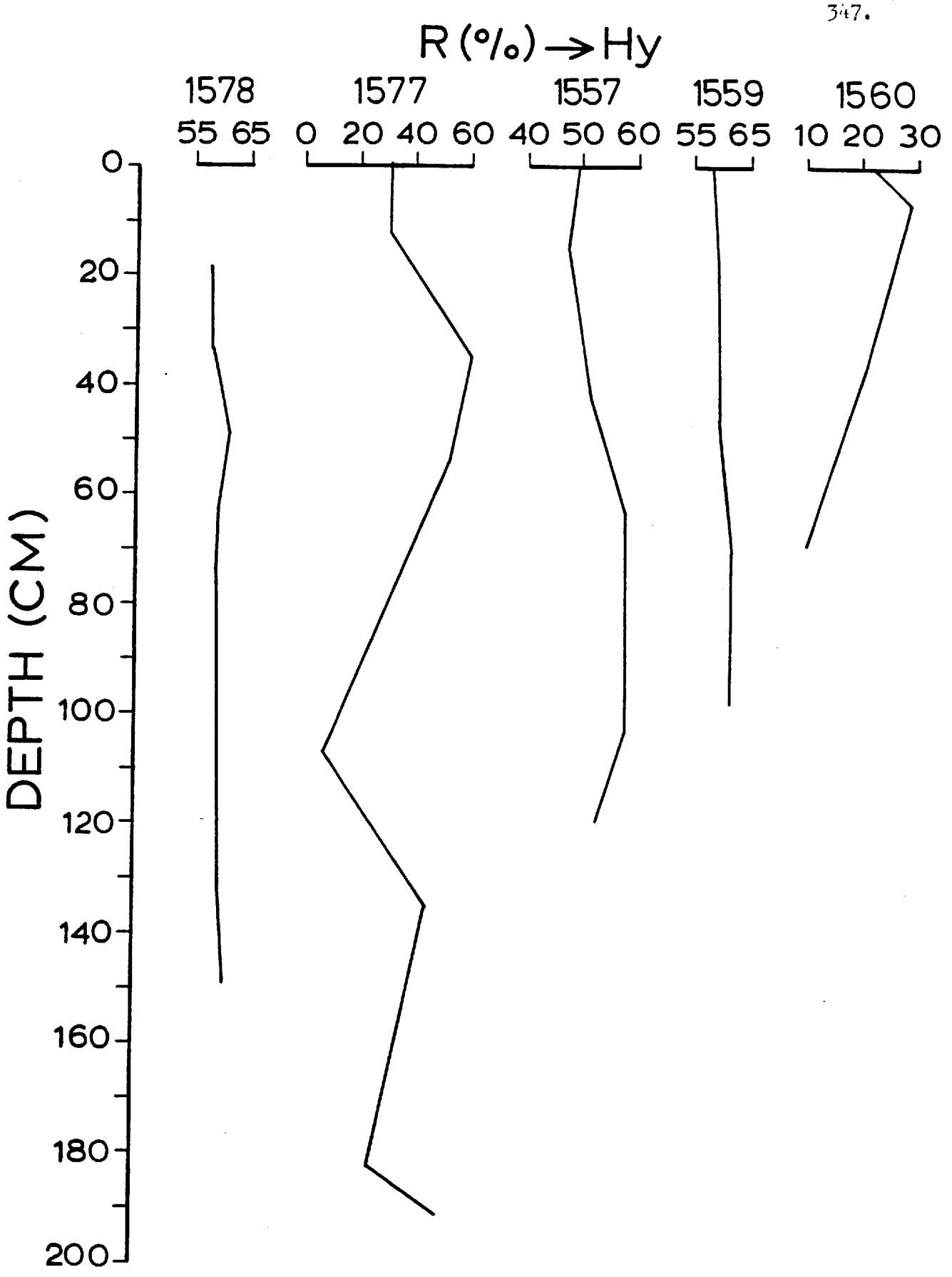

Figure 4.30: Distribution of the hydroxylamine HCl-insoluble residue in Bauer Deep sediment cores.

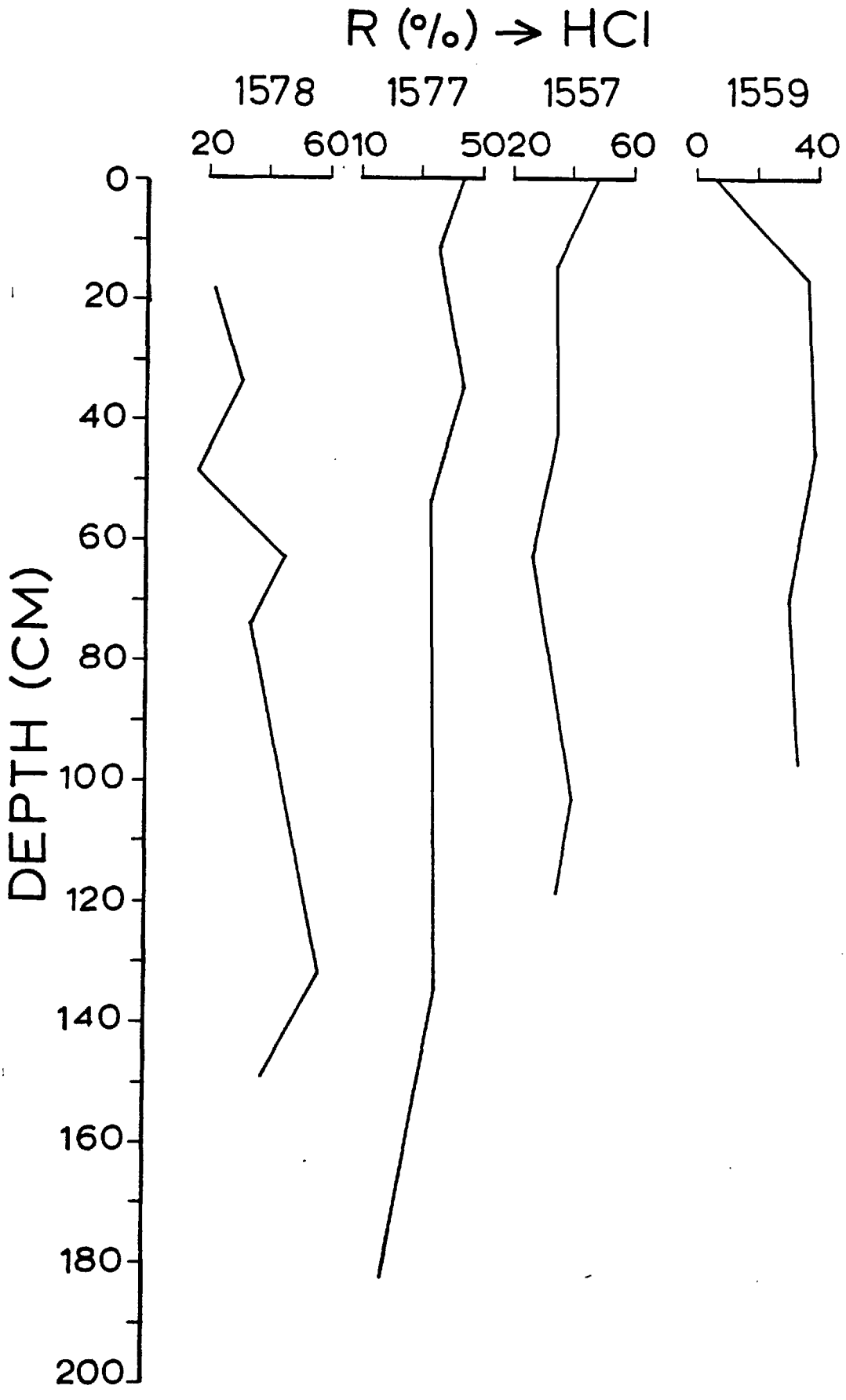

Figure 4.31: Distribution of the HCl-insoluble residue in Bauer Deep sediment cores.

4.6 GENERAL CHEMISTRY OF THE SEDIMENTS AND CHEMICAL INTER-RELATIONSHIPS

As described, the sediments have been analysed for Ca, Mn, Fe, Ni, Co, Pb, Zn, Cu, Al and Si by atomic absorption spectroscopy according to the procedures described in Appendix B. The results have been described core by core and are given on a carbonate-free basis (C.F.B.) in Table 4.4.

A summary of the bulk chemical composition of the Bauer Deep sediments is shown in Table 4.5. The average composition of the surface and that of the buried sediments is presented in this table, along with the composition of metalliferous sediments from this basin and other areas determined by other workers. The average composition of Pacific surface pelagic clays is also included for comparison.

In general, the Bauer Deep sediments show an enrichment in Fe (to over 2 times), Mn (to over 9 times), Cu (to over 5 times), Ni (to over 4 times), Zn, and Co, and a depletion in Al and Si relative to their average concentrations in Pacific pelagic clays (see Table 4.5). Certain differences are found between the average composition of the surface and that of buried sediments. Manganese, Ni, Cu and Zn are more enriched in the surface than in the buried sediments. The concentrations of Pb in the surface sediments are similar to its average content in Pacific pelagic clays, whereas there is a twofold enrichment of Pb in the buried sediments. Moreover, the content of Al is somewhat higher in the surface than in the buried sediments. The average concentrations of Fe, Co and Si are similar in the two groups of sediment samples.

The average composition of the Bauer Deep sediments presented in this study resembles the average composition of Bauer Deep samples given by Sayles and Bischoff (1973). However, the concentrations

Table 4.4: Chemical composition of Bauer Deep sediments expressed on a carbonate-free basis.

Station Number	Sample Number	Interval sampled, (cm)	$CaCO_3$ (%)	Ca (%)	Mn (%)	Fe (%)	Ni (ppm)	Co (ppm)	Pb (ppm)	Zn (ppm)	Cu (ppm)	Al (%)	SiO_2 (%)
SH 1557	232	0-10	13.79	6.56	3.38	12.01	570	148	68	304	730	2.00	32.49
	233	10-20	15.95	7.41	3.64	11.99	549	144	92	289	714	2.00	32.00
	234	20-30	1.30	1.65	2.95	11.41	449	102	91	307	726	1.97	32.13
	235	30-35	0.01	1.09	2.98	12.33	435	104	83	370	753	1.99	29.99
	236	35-40	0.13	1.19	2.63	12.43	474	124	93	310	773	2.09	29.15
	237	40-45	0.23	1.23	3.06	12.43	517	153	97	282	778	2.07	29.69
	238	60-66	0.45	1.32	2.84	13.22	454	152	87	299	772	2.06	30.28
	239	75-81	0.13	1.19	2.63	12.73	484	133	113	330	793	2.09	29.84
	240	88-94	0.34	1.27	3.04	12.57	488	142	92	356	764	2.16	29.59
	241	100-106	0.79	1.45	3.51	11.99	676	170	76	298	817	2.24	29.45
	242	109 (mottle)	0.14	1.19	2.89	13.14	595	94	73	331	814	2.09	
	243	116-122	0.35	1.28	6.91	16.79	1080	173	97	391	1204	1.68	23.57
	244	129-136	0.98	1.53	7.85	17.15	1087	169	88	420	1132	1.64	21.87
Average buried sediments:			1.73	1.82	3.74	13.18	607	138	90	332	837	2.01	28.87

Table 4.4: Continued.

Station Number	Sample Number	Interval sampled, (cm)	$CaCO_3$ (%)	Ca (%)	Mn (%)	Fe (%)	Ni (ppm)	Co (ppm)	Pb (ppm)	Zn (ppm)	Cu (ppm)	Al (%)	SiO_2 (%)
SH 1559	245	0-10	0.87	1.48	4.98	15.84	990	184	78	364	1044	1.99	26.22
	246	14-20	0.61	1.38	5.94	18.42	964	153	78	421	1058	1.39	25.30
	247	28 (mottle)	0.01	1.12	3.64	16.80	585	91	132	409	809	1.43	
	248	30 (mottle)	0.08	1.17	3.62	17.30	593	92	101	403	858	1.27	
	249	26-30	0.11	1.18	4.35	17.30	679	93	92	388	868	1.38	26.64
	252	42-50	1.21	1.62	5.26	17.06	797	138	82	392	886	1.49	26.14
	253	54-62	1.04	1.55	4.79	17.39	720	121	91	403	877	1.56	26.48
	255	67-73	1.39	1.68	4.92	17.38	777	145	98	397	903	1.71	27.12
	256	80-86	0.84	1.47	4.06	17.91	620	108	102	378	839	1.68	29.36
	258	95-100	1.07	1.56	4.04	17.85	487	123	97	370	866	1.68	26.29
Average buried sediments:			0.71	1.41	4.51	17.49	691	118	97	396	885	1.51	26.76
SH 1560	260	0-4	49.01	20.40	10.10	11.24	3756	219	66	739	2429	2.04	25.08
	261	4-8	55.85	23.09	4.01	14.91	598	133	45	440	1145	1.18	29.49
	262	7-8 (mottle)	54.46	22.55	3.01	12.27	376	126	111	270	589	1.77	
	264	9-15	58.03	23.95	2.85	14.51	340	86	71	301	935	1.07	
	265	20-26	41.68	17.52	1.49	8.35	154	82	102	156	525	0.57	
	266	33-39	66.17	27.15	2.64	14.91	278	108	178	283	953	1.00	27.52
	267	44-50	56.08	23.18	2.35	11.88	204	80	109	235	733	0.81	
	268	57-62	67.76	27.78	3.08	16.00	298	116	129	310	962	1.08	
Average buried sediments:			57.15	23.60	2.78	13.26	321	104	106	285	835	1.07	28.51

Table 4.4: Continued.

Station Number	Sample Number	Interval sampled, (cm)	$CaCO_3$ (%)	Ca (%)	Mn (%)	Fe (%)	Ni (ppm)	Co (ppm)	Pb (ppm)	Zn (ppm)	Cu (ppm)	Al (%)	SiO_2 (%)
	289	0-8	43.59	18.27	4.03	12.08	638	175	33	300	727	2.28	30.81
	290	10-14	48.70	20.29	3.20	12.43	436	160	84	301	687	2.07	33.06
	291	14-17	47.44	19.79	3.12	12.30	426	158	102	291	707	2.20	33.81
	292	17-19	25.84	11.30	3.31	12.45	453	151	67	287	671	1.99	32.48
	293	19-21	39.50	16.67	2.92	12.15	382	151	67	282	673	2.11	33.21
	294	21-27	15.11	7.08	3.01	12.28	425	143	56	285	704	2.09	32.16
	295	24-25 (mottle)	41.77	17.56	2.90	12.44	379	101	122	286	672	2.04	
	296	27-28 (mottle)	29.62	12.79	2.66	12.16	377	97	113	316	692	1.96	
	297	29-31	10.40	5.23	2.64	11.89	409	116	72	315	679	1.87	
	298	31-39	3.94	2.69	2.59	12.85	417	147	79	306	775	2.18	32.06
	299	44-50	5.77	3.41	2.89	13.43	404	145	77	305	794	2.17	29.97
	300	50-58	14.59	6.87	2.82	13.17	411	147	67	294	756	2.01	30.79
	301	62-68	6.47	3.68	2.52	12.80	391	114	103	312	742	1.89	29.84
	302	76-82	9.65	4.93	3.06	13.43	460	138	83	339	783	2.07	30.01
	303	88-94	22.27	9.90	3.21	13.05	478	120	96	335	764	2.08	29.40
	304	104-110	84.60	34.39	3.83	10.85	679	211	246	250	798	2.74	29.55
	305	123-129	40.81	17.18	6.14	11.28	905	169	84	299	822	2.49	31.95
	306	130-132	38.97	16.46	3.65	11.74	608	128	132	300	753	2.38	32.08
	307	132-138	26.93	11.73	3.88	12.04	617	152	80	298	744	2.54	31.48
	308	142-148	20.59	9.24	4.04	11.76	679	149	95	245	804	2.26	31.09
	309	152-155	58.20	24.02	4.93	11.73	838	206	90	331	878	2.58	32.22
	310	155-157	62.10	25.55	3.89	9.59	700	135	145	248	682	2.07	26.04
	311	157-159	51.41	21.35	3.60	9.99	591	121	147	315	707	2.10	27.08
	312	159-163	52.80	21.89	3.80	8.01	751	149	134	231	619	1.98	
	313	163-165	54.85	22.70	5.03	9.62	785	199	68	284	775	2.62	29.97
	314	165-169	48.82	20.33	3.78	8.70	601	137	105	250	745	2.16	
	315	169-170	57.43	23.72	3.48	9.98	610	177	139	262	727	2.44	30.61
	316	172-176	66.31	27.21	3.09	7.79	510	138	150	221	584	1.82	
	317	180-185	58.63	24.19	3.51	10.76	577	133	41	304	781	2.57	34.06
	319	189-193	20.06	9.03	3.07	11.29	546	120	108	378	781	2.21	32.15
	320	193-197	19.89	8.96	3.60	11.68	640	134	97	383	840	2.24	32.46
SH 1577													
Average of buried sediments:			36.12	15.34	3.47	11.45	550	362	254	295	738	2.20	31.15

Table 4.4: Continued.

Station Number	Sample Number	Interval sampled, (cm)	$CaCO_3$ (%)	Ca (%)	Mn (%)	Fe (%)	Ni (ppm)	Co (ppm)	Pb (ppm)	Zn (ppm)	Cu (ppm)	Al (%)	SiO_2 (%)
SH 1578	270	0-7	15.85	7.37	4.55	14.36	533	131	68	381	861	2.45	32.31
	271	9-10	9.64	4.93	2.67	11.77	365	92	92	274	617	1.82	
	272	12.5-13.5	15.26	7.14	2.77	11.54	357	82	94	283	666	1.85	
	273	15-22	0.78	1.45	3.79	12.24	509	150	76	297	776	2.04	32.63
	274	30-37	0.15	1.20	3.40	12.09	464	135	79	265	758	2.10	32.74
	275	48-49	0.01	0.97	1.55	12.02	288	53	91	283	696	2.03	
	276	48-52	0.05	1.16	2.90	12.46	400	131	66	285	771	2.12	32.87
	277	60-66	0.13	1.19	3.47	12.90	540	164	98	313	862	2.08	31.22
	278	70-78	0.01	0.99	3.75	13.21	507	154	78	321	926	2.07	31.21
	279	78-87	0.38	1.29	3.43	11.44	501	144	78	244	795	1.99	31.54
	280	89-95	0.38	1.29	3.29	12.75	462	154	118	304	795	2.09	31.37
	281	96-97	0.01	1.08	1.97	12.78	341	83	82	291	725	1.97	
	282	98-104	0.06	1.17	2.72	13.22	396	121	91	304	756	2.14	30.91
	283	116-122	0.11	1.18	2.37	13.41	382	113	92	308	747	1.97	31.29
	285	129-135	0.81	1.46	2.84	13.44	406	152	96	300	734	1.77	30.57
	286	146-152	0.15	1.20	2.40	13.30		135	69	285	728	1.90	31.00
	287	164-170	0.13	1.19	2.39	12.93	375	104	83	291	714	1.79	30.99
	288	182-188	6.76	3.80	2.72	11.39	419	136	77	267	729	1.98	30.75
Average buried sediments:			2.05	1.92	2.85	12.52	420	124	86	289	753	1.98	31.47

Table 4.5: Average chemical composition of Bauer Deep sediments compared to other deposits. (The results are expressed on a carbonate-free basis.)

	Mn %	Fe %	Ni ppm	Co ppm	Pb ppm	Zn ppm	Cu ppm	Al %	Si %
1	5.41	13.11	1297	171	63	418	1158	2.15	13.73
2	3.47	13.58	518	169	127	319	810	1.75	13.72
3	4.44	13.35	908	170	95	369	984	1.95	13.73
4	3.71	13.49	1000	200			980	2.34	21.00
5	6.91	16.73	1400	270			980	3.06	13.77
6	5.74	15.83	1066			413	1171	3.24	17.43
7	6.00	18.00	430	105		380	730	0.50	6.10
8	3.00	10.50	675	230		290	960	4.63	14.00
9	6.06	20.07	460	82	100	470	790	2.73	10.84
10	2.74	7.44	300	41	70	180	310	0.36	2.84
11	6.66	23.60	630	86		600	1070	2.39	7.11
12	0.48	5.07	211	101	68		323	9.20	23.00

1. This study: all surface sediments.
2. This study: all buried sediments.
3. This study: all Bauer Deep sediments.
4. Sayles and Bischoff (1973): Bauer Deep sediments.
5. McMurtry (1975): Bauer Deep sediments.
6. Heath and Dymond (1977): Bauer Deep sediments.
7. Boström and Peterson (1969): East Pacific Rise crest sediments.
8. Boström and Peterson (1969): East Pacific Rise flank sediments.
9. Cronan (1976a): basal non-carbonate sediments from the eastern Pacific.
10. Cronan (1976a): basal carbonate sediments from the eastern Pacific.
11. Dymond et al (1973): D.S.D.P. sediments from sites 37, 38 and 39.
12. Cronan (1969): Pacific pelagic clays.

of Si and Al presented here are lower than those reported by these authors. In contrast, the average composition of the Bauer Deep sediments obtained in this study shows lower concentrations of metals when compared with those presented by McMurtry (1975) and Heath and Dymond (1977). However, the concentrations of Cu and Si presented here are similar to those of McMurtry (1975). The relatively higher concentrations of metals reported by Heath and Dymond (1977) for the Bauer Deep sediments are due to the fact that these authors not only made corrections for $CaCO_3$, but also corrected their analyses for salt, the values of which range between 4 and 19%.

Comparison of the average composition of the Bauer Deep sediments with the average composition of East Pacific Rise surface and basal D.S.D.P. sediments indicates significant differences. The Fe and Mn values obtained during this study are lower than those reported for crestal East Pacific Rise and basal non-carbonate sediments, whereas they are higher than those found in surface sediments from the flanks of the East Pacific Rise and in carbonate basal D.S.D.P. sediments (Boström and Peterson, 1969; Dymond et al, 1973; Cronan, 1976a). The Bauer Deep sediments contain much more Si than the sediments from the above regions. Moreover, Ni and Cu show greater enrichment in the Bauer Deep sediments than in any of the other areas. The enrichment of Cu (to over 1.68 times) in the present sediments is lower than that found in the sediments from the flanks of the East Pacific Rise (to over 2.27 times, Boström and Peterson, 1969), while no enrichment of this element occurs in the crestal or the basal East Pacific Rise sediments. Pb is slightly enriched (by a factor of 1.4) in the Bauer Deep sediments, thus having similar concentrations to those of the non-carbonate basal metalliferous sediments (Cronan, 1976a). The Bauer Deep sediments are characterized by lower concentrations of Zn

compared to the sediments from D.S.D.P., 37, 38, 39 and the East Pacific Rise basal non-carbonate sediments, but the concentration of this element is higher than that found in the surface sediments from the flanks of the East Pacific Rise and in the basal carbonate metalliferous sediments. However, the concentrations of Zn in the sediments studied here resemble those of the surface sediments from the crest of East Pacific Rise (Dymond et al, 1973; Boström and Peterson, 1969; Cronan, 1976a). Except for the sediments from the crest of the East Pacific Rise and the basal carbonate sediments from the S.E. Pacific, the Al content in the present sediments is lower than in any of the other oceanic areas which are compared here.

As has been mentioned above, one of the most significant differences between the chemical composition of the Bauer Deep and the East Pacific sediments is the higher content of Si in the former which dilutes the other elements, especially Fe and Mn. The diluting effect of Si on the Fe content is demonstrated by Figure 4.32, where a negative correlation between these two elements is shown.

Since 50% HCl dissolves almost all the Fe present in deep-sea sediments (Cronan, 1976a), a negative correlation found between the percentage of Fe soluble in HCl and the total content of SiO_2 (see Figure 4.34) demonstrates the same diluting effect of Si as shown by the bulk analyses described above. In contrast, there is a positive correlation between the percentage of Fe present in the hydroxylamine HCl-soluble fraction and the total content of SiO_2 (Figure 4.33), which indicates a positive relationship between the Fe associated with the ferromanganese oxide phases and Si.

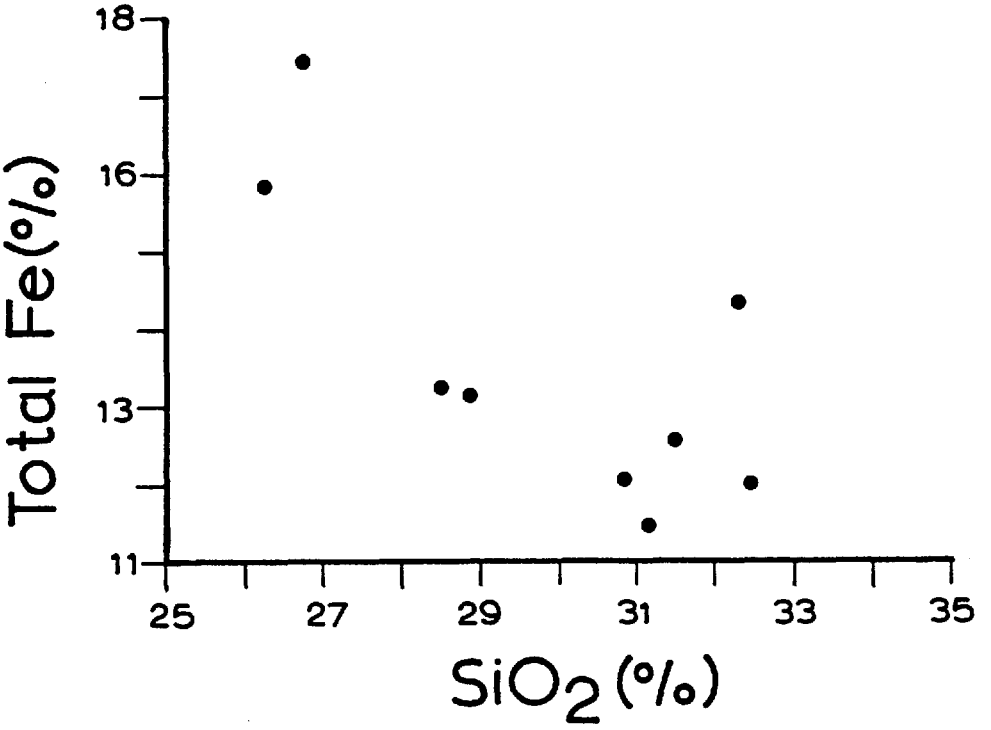

Figure 4.32: Scatter plot showing the negative correlation between Fe and SiO_2 in Bauer Deep sediments. Concentrations are corrected to a calcium carbonate-free basis.

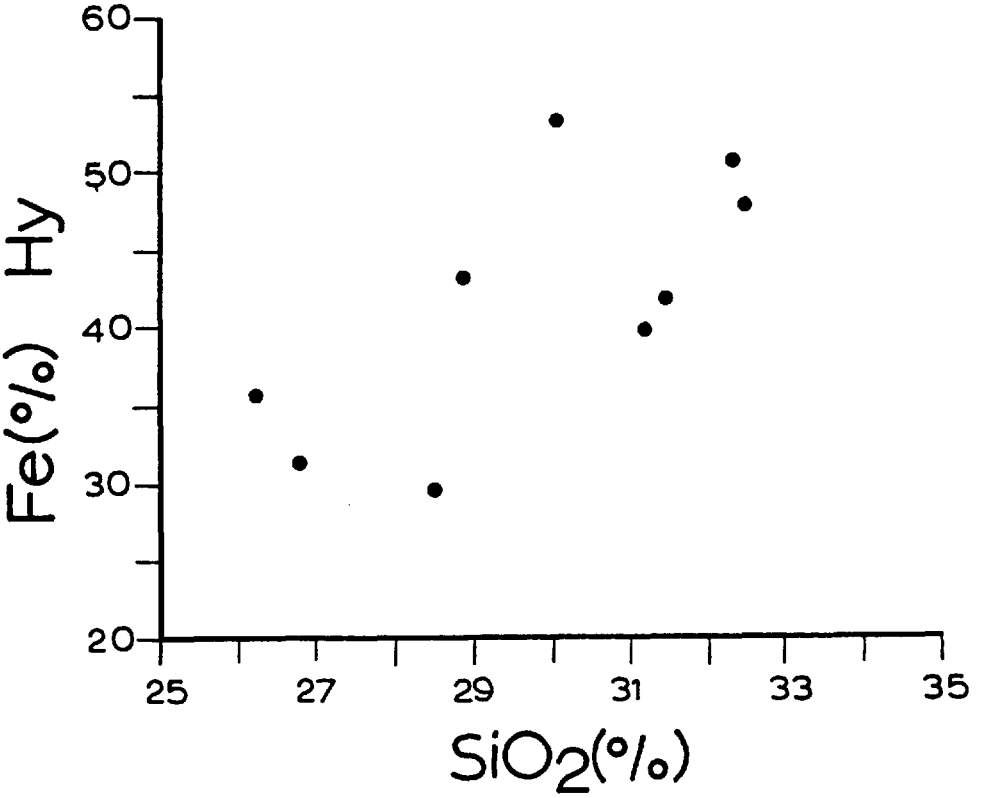

Figure 4.33: Scatter plot showing the positive correlation between the hydroxylamine HCl-soluble Fe (expressed as a percentage of the total Fe concentration), and the SiO_2 content (C.F.B.) in Bauer Deep sediments.

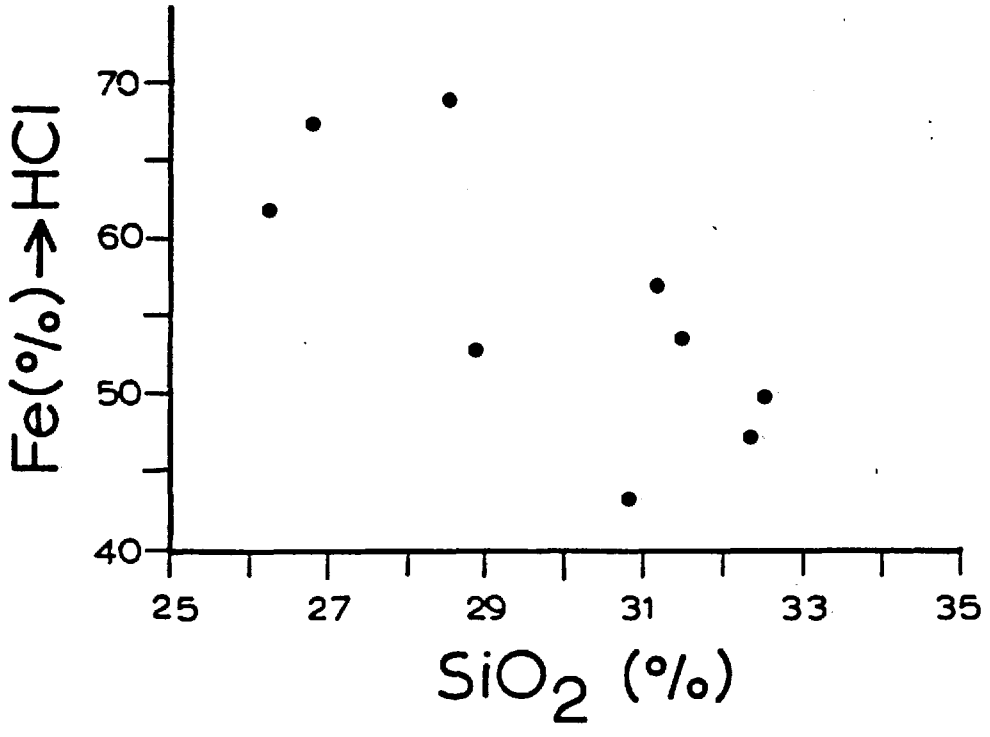

Figure 4.34: Scatter plot showing the negative correlation between the HCl-soluble Fe (expressed as a percentage of the total Fe concentration), and the SiO_2 content (C.F.B.) in Bauer Deep sediments.

The fact that the partitioning of elements between phases varied from one core to another, as described, leads to the conclusion that local factors may influence the incorporation of the elements into the various phases.

To examine the possible existence of regional trends in concentration of elements or other geochemical parameters within the Bauer Deep, the factor "depth of water" is evaluated in relation to the bulk and partition chemistry of the sediments. For this purpose the total concentrations of the elements in the surface samples, as well as their percentages associated with each fraction, were plotted against the depth of water. Since post-depositional transformation of phases may occur within the sediment column, no buried sediments were used in this exercise.

This exercise revealed that the distribution of elements in the surface sediments is strongly influenced by the depth of water. It is observed that the total contents of $CaCO_3$ and Co in the surface sediments decrease with increasing water depth (see Figures 4.35 and 4.36). In contrast, Fe and Mn tend to increase with increasing depth of water (see Figures 4.37 and 4.38). A consistent decrease of the proportion of Fe, Ni and Zn present in the hydroxylamine HCl-soluble fraction with depth of water occurs (see Figures 4.39b, 4.40 and 4.42). Conversely, the percentage of Fe, Ni and Zn associated with the HCl-soluble fraction increases with water depth (see Figures 4.39a, 4.41 and 4.43), indicating the transition of these elements to a more stable phase.

Figures 4.44a and b illustrate that there is a gradual increase of the proportion of sediment remaining insoluble in acetic acid and in the acid-reducing agent solution with depth of water. In contrast,

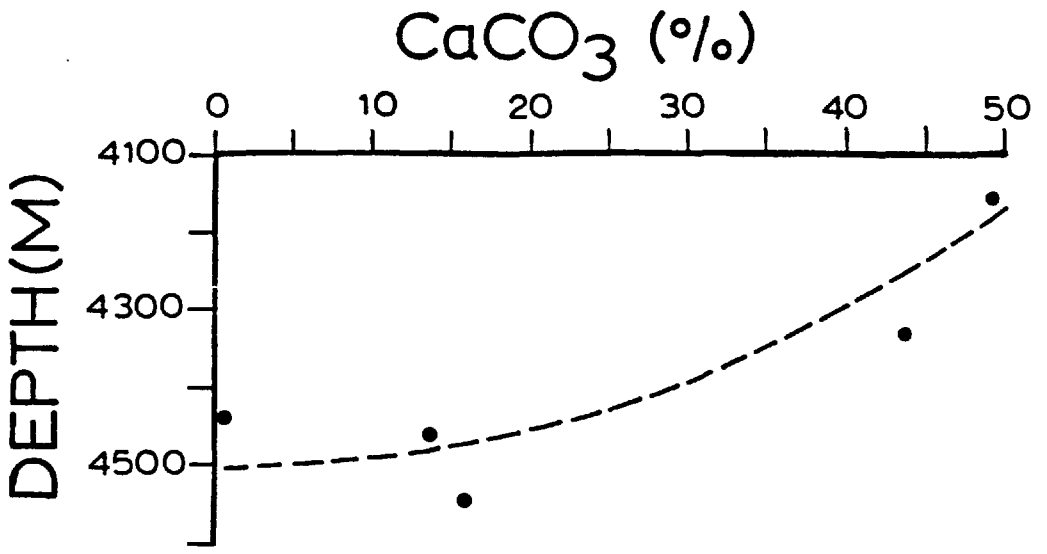

Figure 4.35: Scatter plot showing the decrease of $CaCO_3$ content with water depth in Bauer Deep surface sediments.

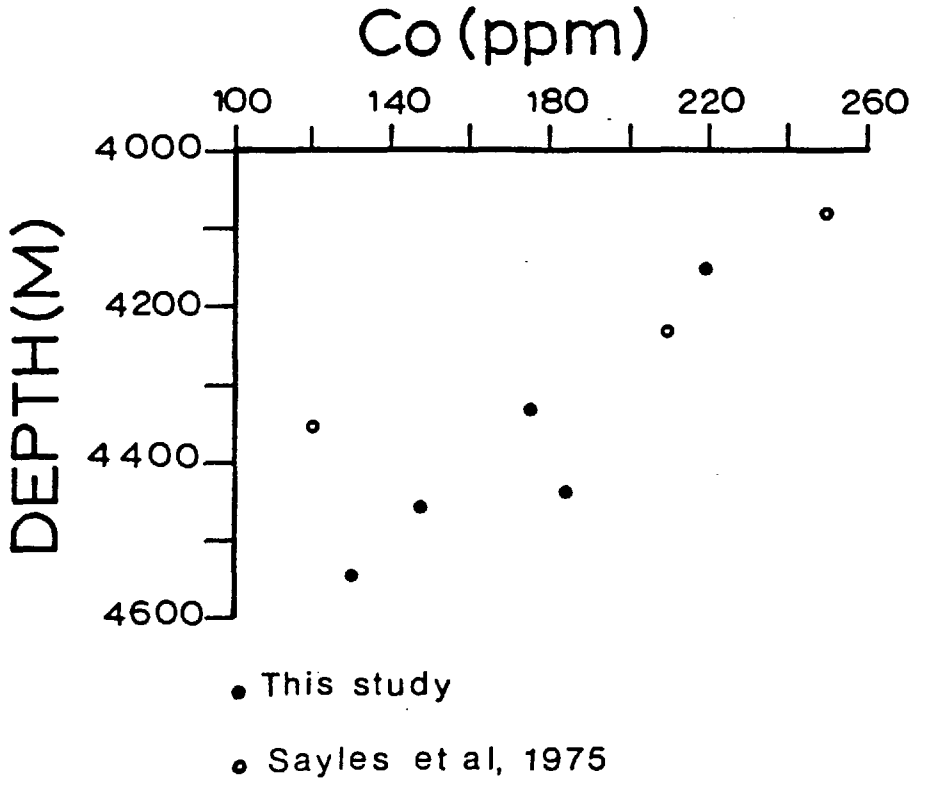

Figure 4.36: Scatter plot showing the negative correlation between the carbonate-free concentrations of Co in Bauer Deep surface sediments and the water depth.

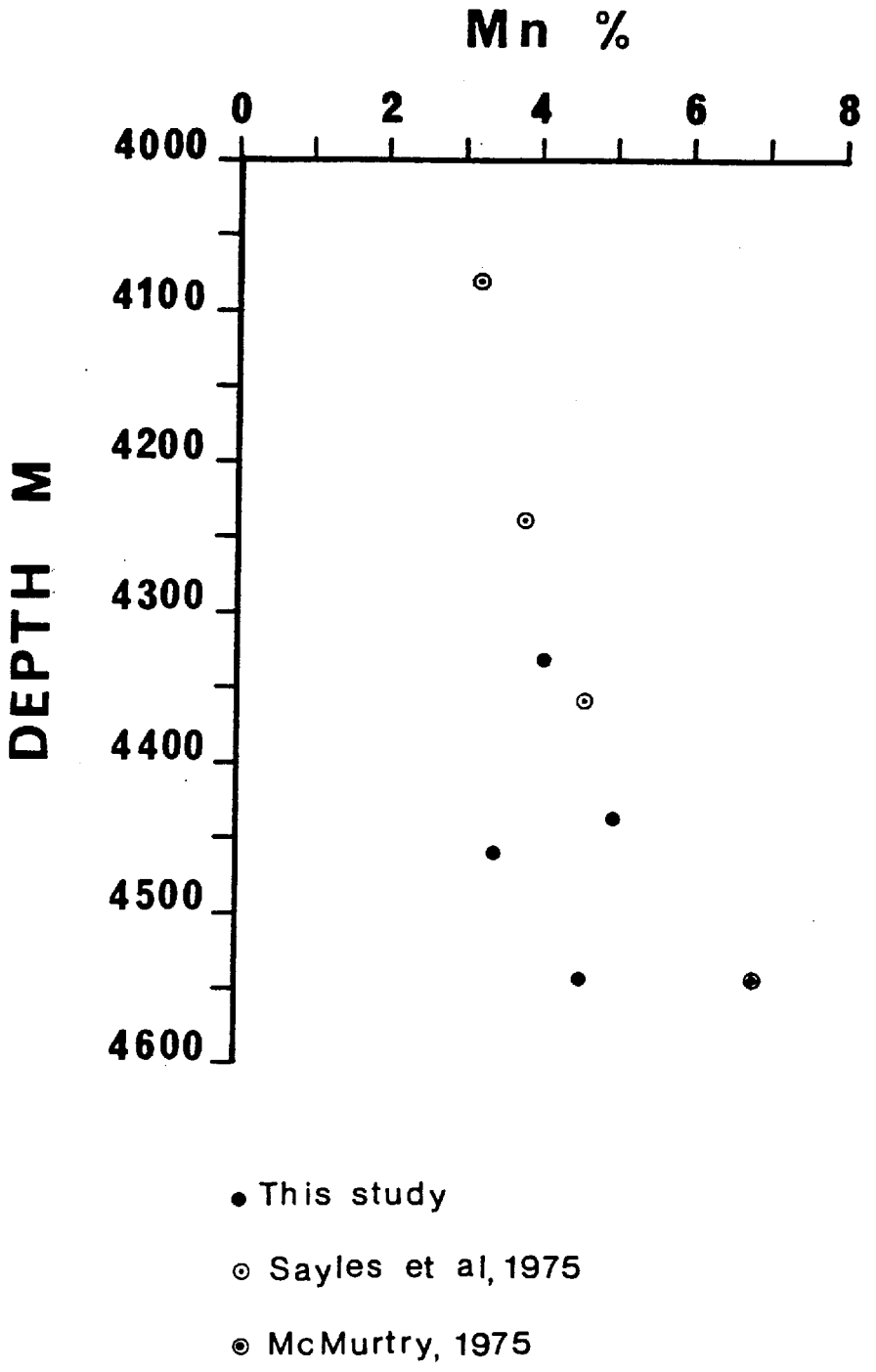

Figure 4.37: Scatter plot showing the positive correlation between the carbonate-free concentrations of Mn in Bauer Deep surface sediments and the water depth.

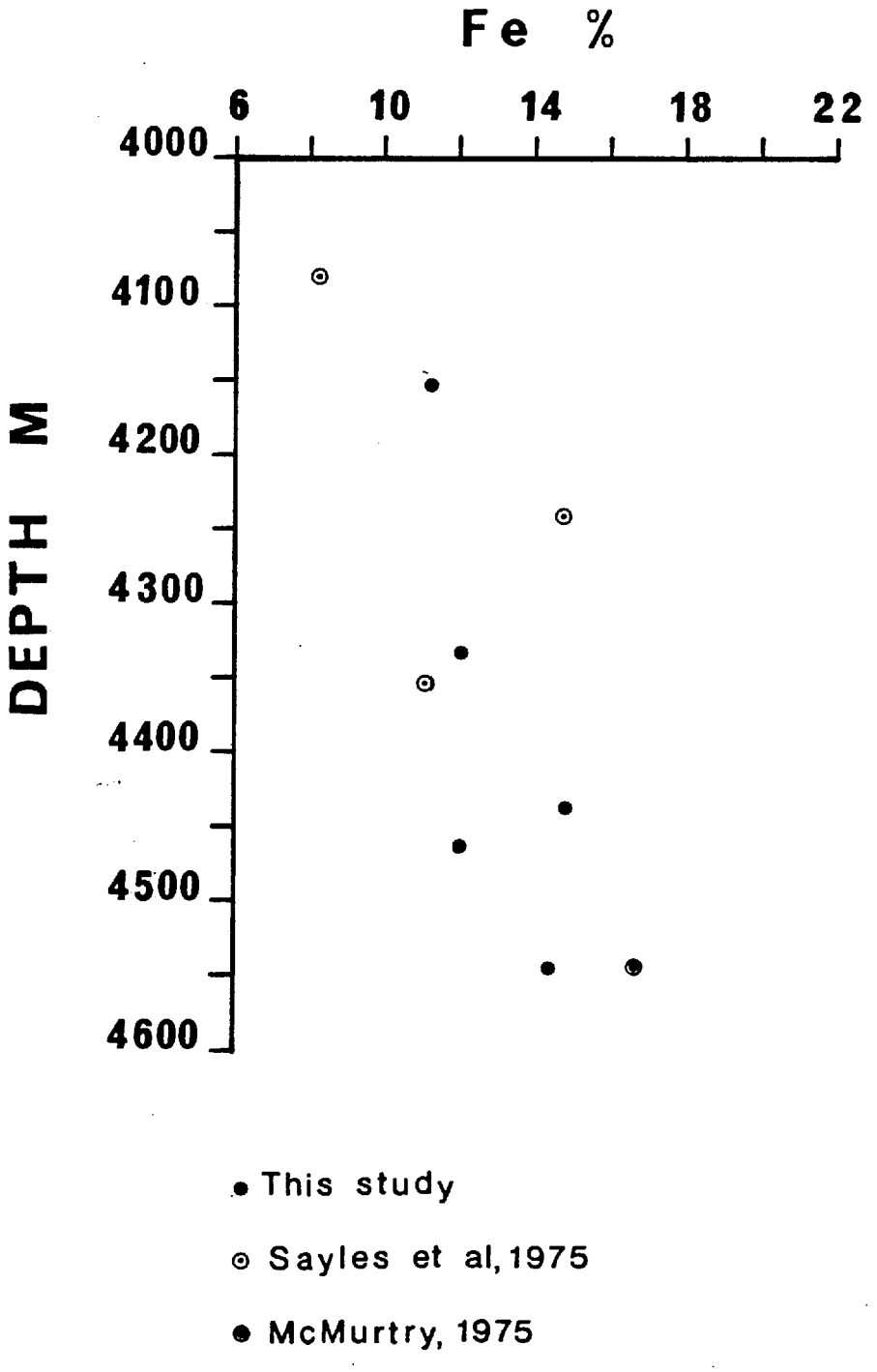

Figure 4.38: Scatter plot showing the positive correlation between the carbonate-free concentrations of Fe in Bauer Deep surface sediments and the water depth.

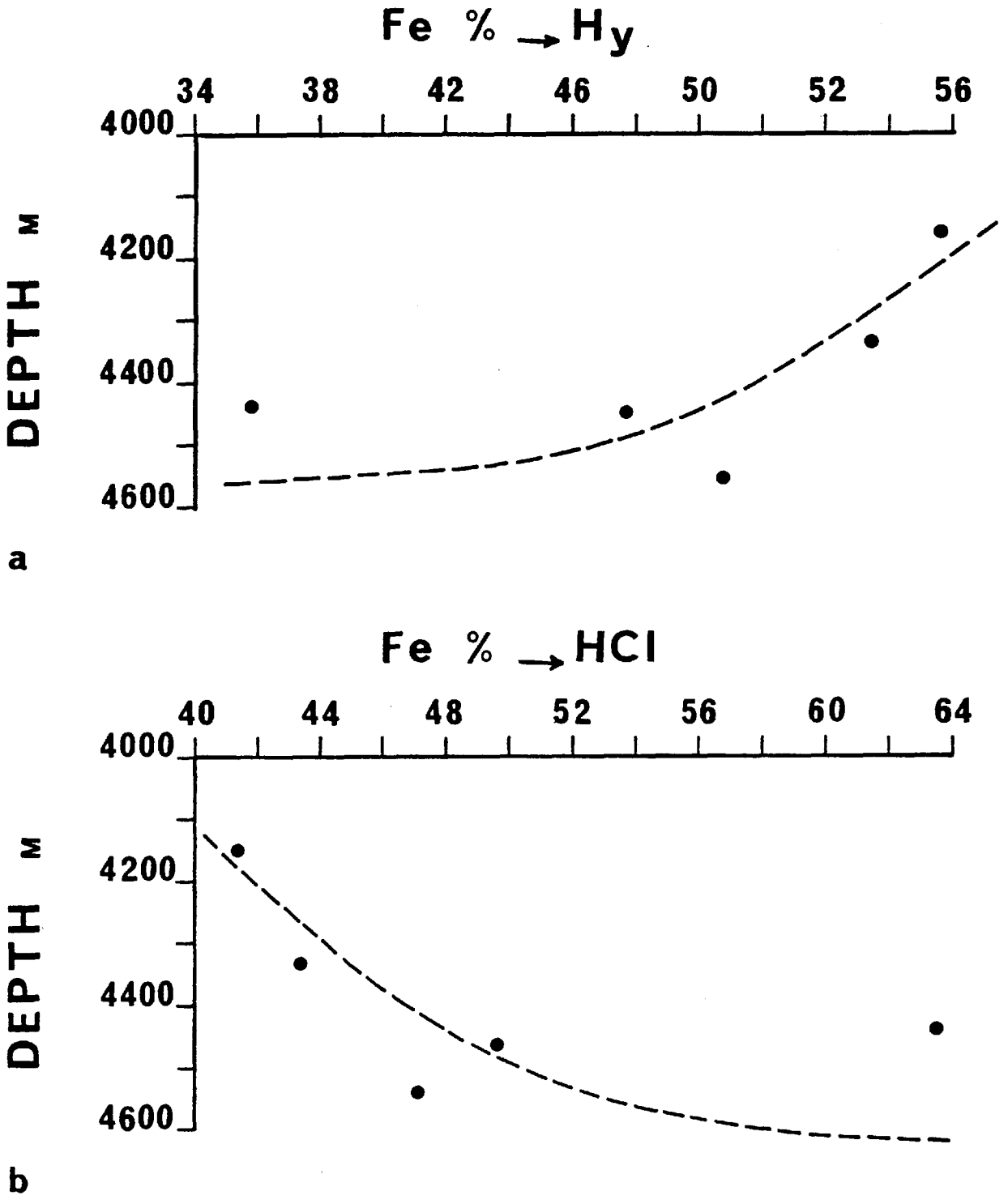

Figure 4.39 (a) Scatter plot showing the negative correlation between the acid-reducible Fe (expressed as a percentage of the total amount present) in the surface sediments, and the water depth.

(b) Scatter plot showing the positive correlation between the HCl-soluble Fe (expressed as a percentage of the total amount present) in the surface sediments, and the water depth.

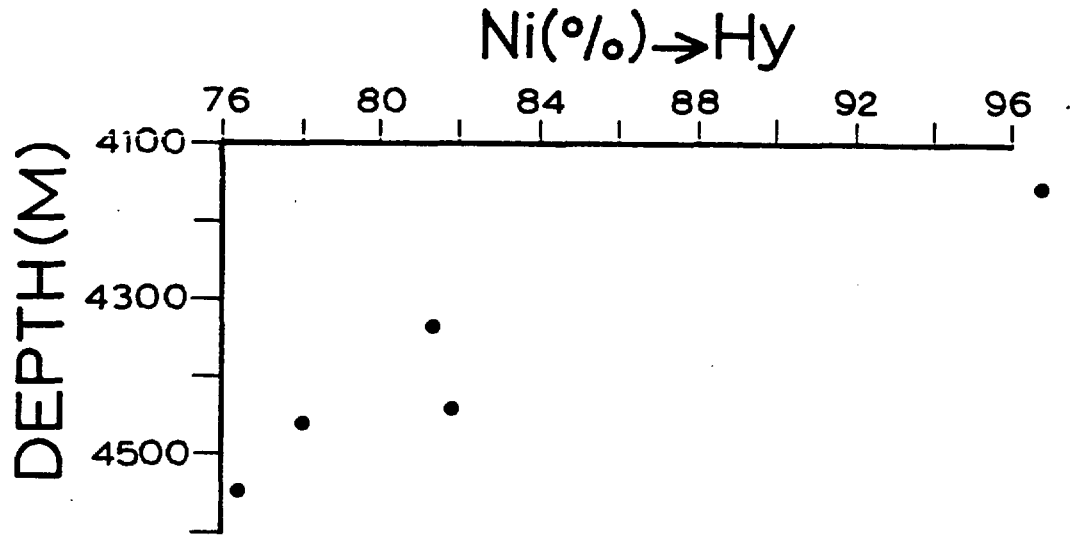

Figure 4.40: Scatter plot showing the negative correlation between the hydroxylamine HCl-soluble Ni (expressed as a percentage of the total Ni concentration) in Bauer Deep surface sediments, and the water depth.

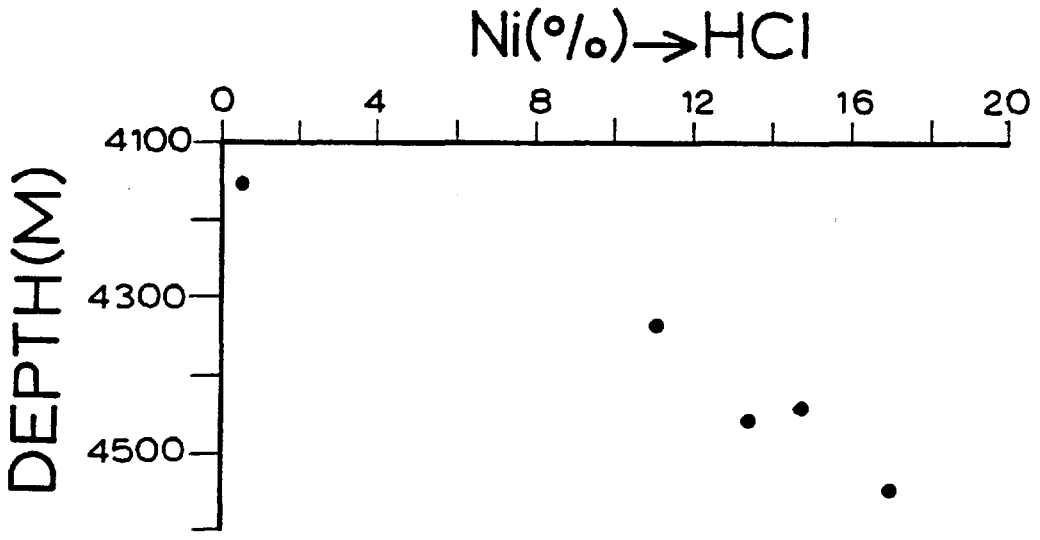

Figure 4.41: Scatter plot showing the positive correlation between the HCl-soluble Ni (expressed as a percentage of the total Ni concentration) in Bauer Deep surface sediments, and the water depth.

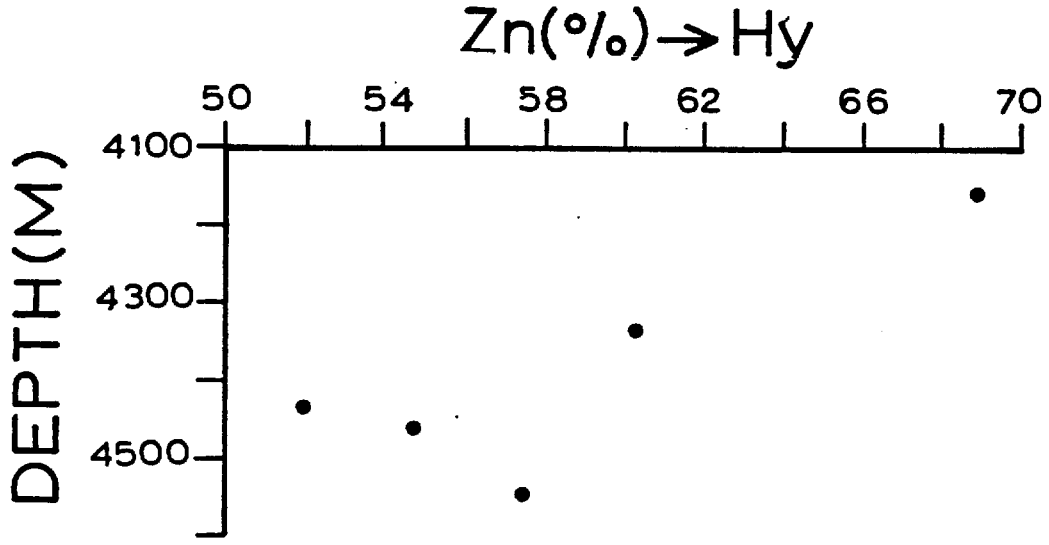

Figure 4.42: Scatter plot showing the negative correlation between the hydroxylamine HCl-soluble Zn (expressed as a percentage of the total Zn concentration) in Bauer Deep surface sediments, and the water depth.

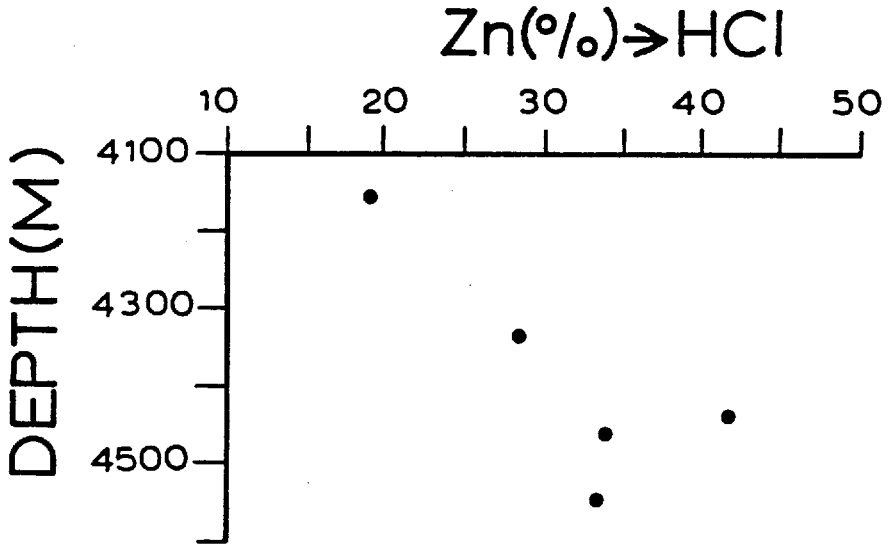

Figure 4.43: Scatter plot showing the positive correlation between the HCl-soluble Zn (expressed as a percentage of the total Zn concentration) in Bauer Deep surface sediments, and the water depth.

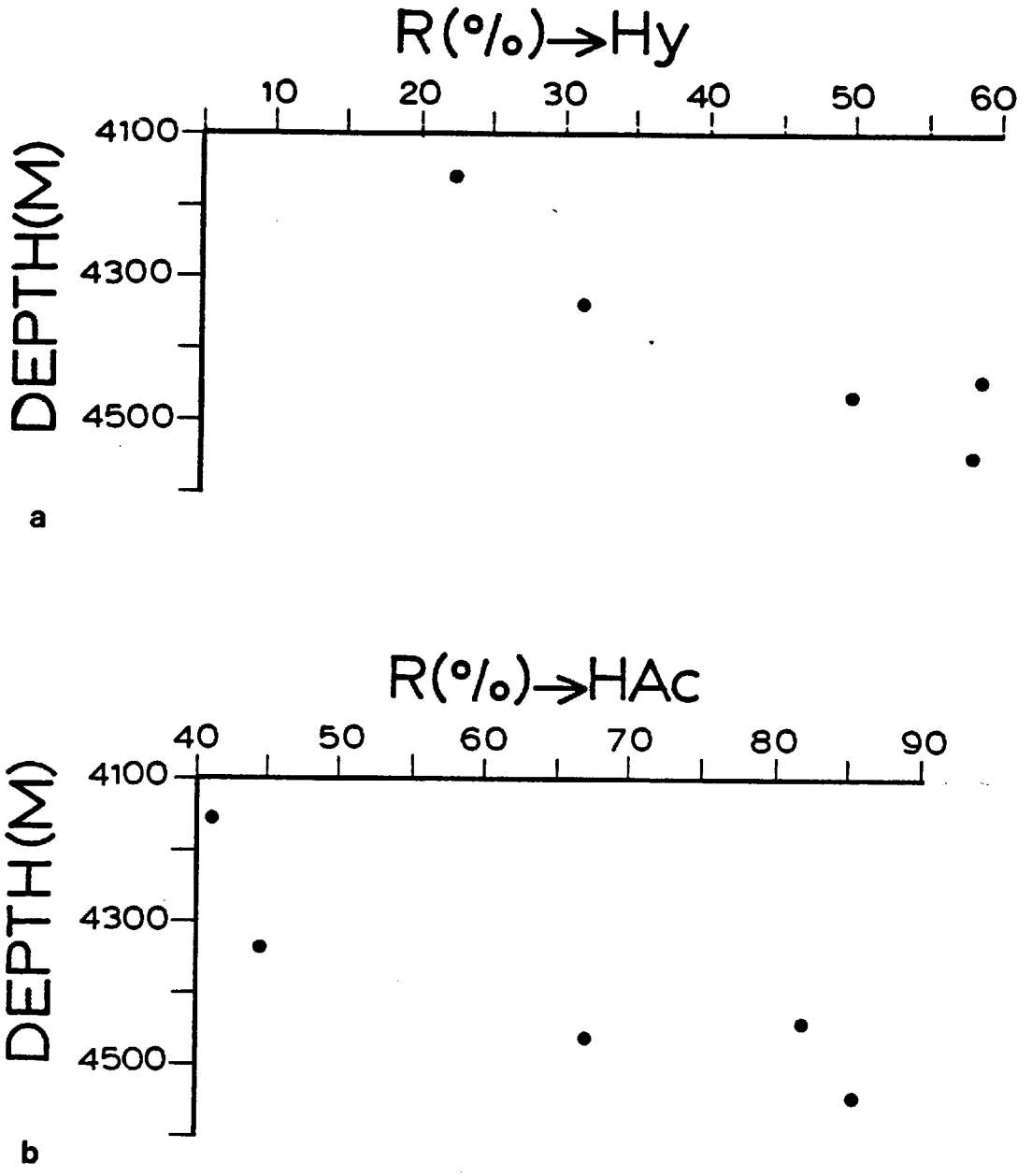

Figure 4.44: (a) Scatter plot showing the positive correlation between the hydroxylamine HCl-insoluble residue and the water depth in Bauer Deep surface sediments.

(b) Scatter plot showing the positive correlation between the acetic acid-insoluble residue and the water depth in the same sediments.

it is observed that the HCl-insoluble residue in the surface samples decreases with increasing water depth (see Figure 4.45).

Assuming that any silica in excess of 3 times the level of alumina is biogenous (Boström et al, 1973) the following equation was used in determining the biogenic silica in Bauer Deep surface sediments:

$$SiO_2 \text{ (biogenic)} = SiO_2 \text{ (bulk)} - 3Al_2O_3$$

(see Table 4.6). It can be seen from Figure 4.46 that it increases with increasing water depth.

The relationship between Fe and Mn is not constant throughout the entire area studied. In the sediments from stations SH 1557, SH 1559 and SH 1578 there is a positive correlation between Fe and Mn (see Figure 4.47), while at stations SH 1560 and SH 1577 the concentrations of Mn remain constant as the concentrations of Fe increase (see Figure 4.48).

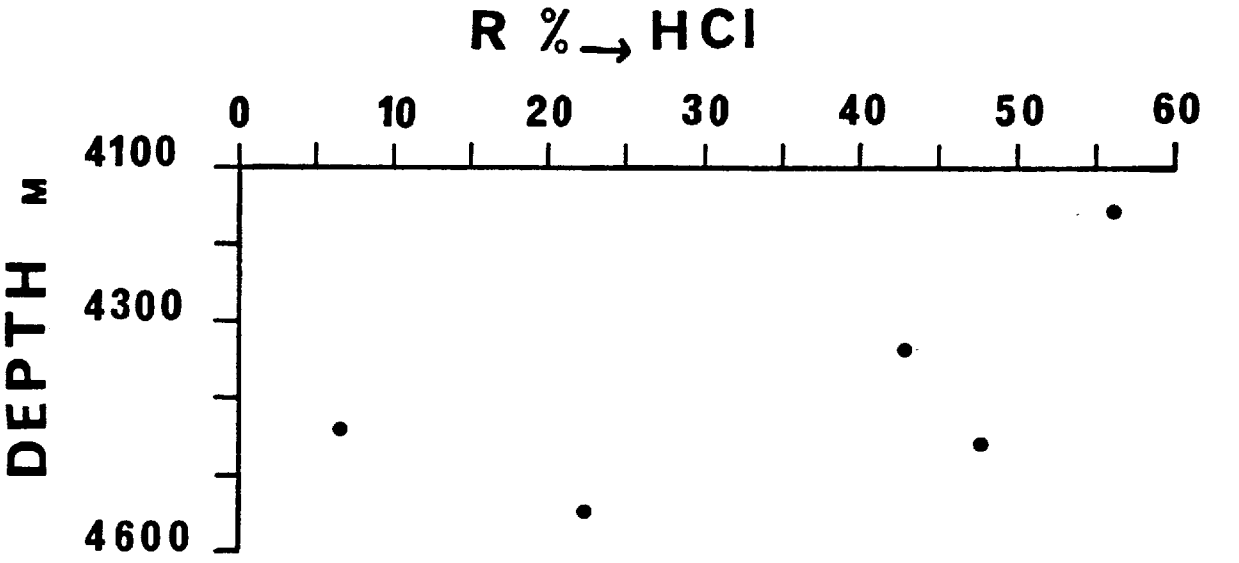

Figure 4.45: Scatter plot showing the decrease of the HCl-insoluble residue in Bauer Deep surface sediments with water depth.

Table 4.6: Results of the analyses for total SiO_2, total Al_2O_3 and biogenic SiO_2 in Bauer Deep surface sediments.

Station No.	Water Depth (m)	SiO_2 (%) C.F.B.	Al_2O_3 (%) C.F.B.	SiO_2 (bulk) - $3Al_2O_3$
1560	4156	25.08	3.85	13.53
1577	4333	30.81	4.31	17.88
1559	4438	26.22	3.76	14.94
1557	4461	32.49	3.78	21.15
1578	4546	32.31	4.63	18.42

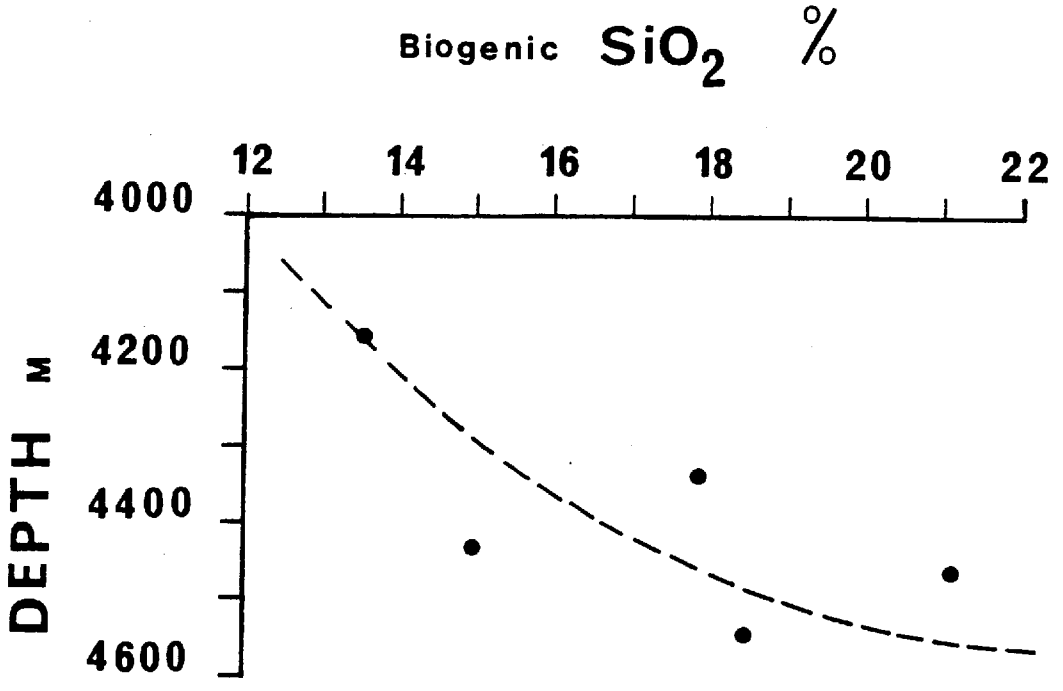

Figure 4.46: Scatter plot showing the positive correlation between the biogenic silica present in Bauer Deep surface sediments and the water depth.

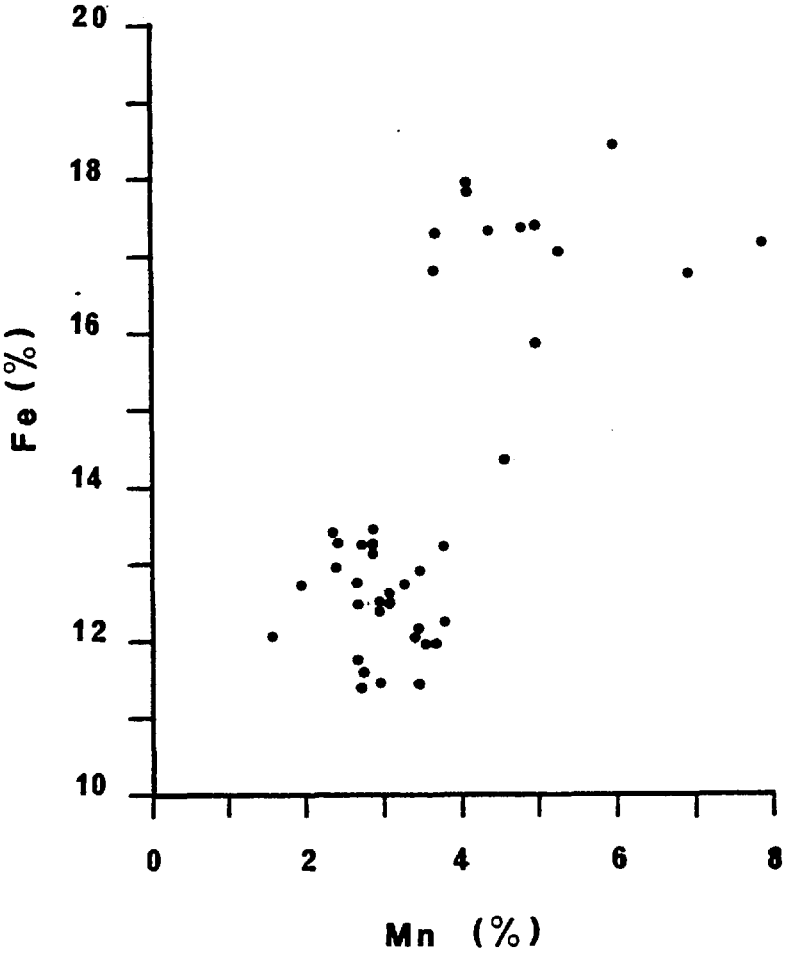

Figure 4.47: Scatter plot showing the relationship between Fe and Mn in sediments from cores SH 1557, SH 1559 and SH 1578. Concentrations are corrected to a calcium carbonate-free basis.

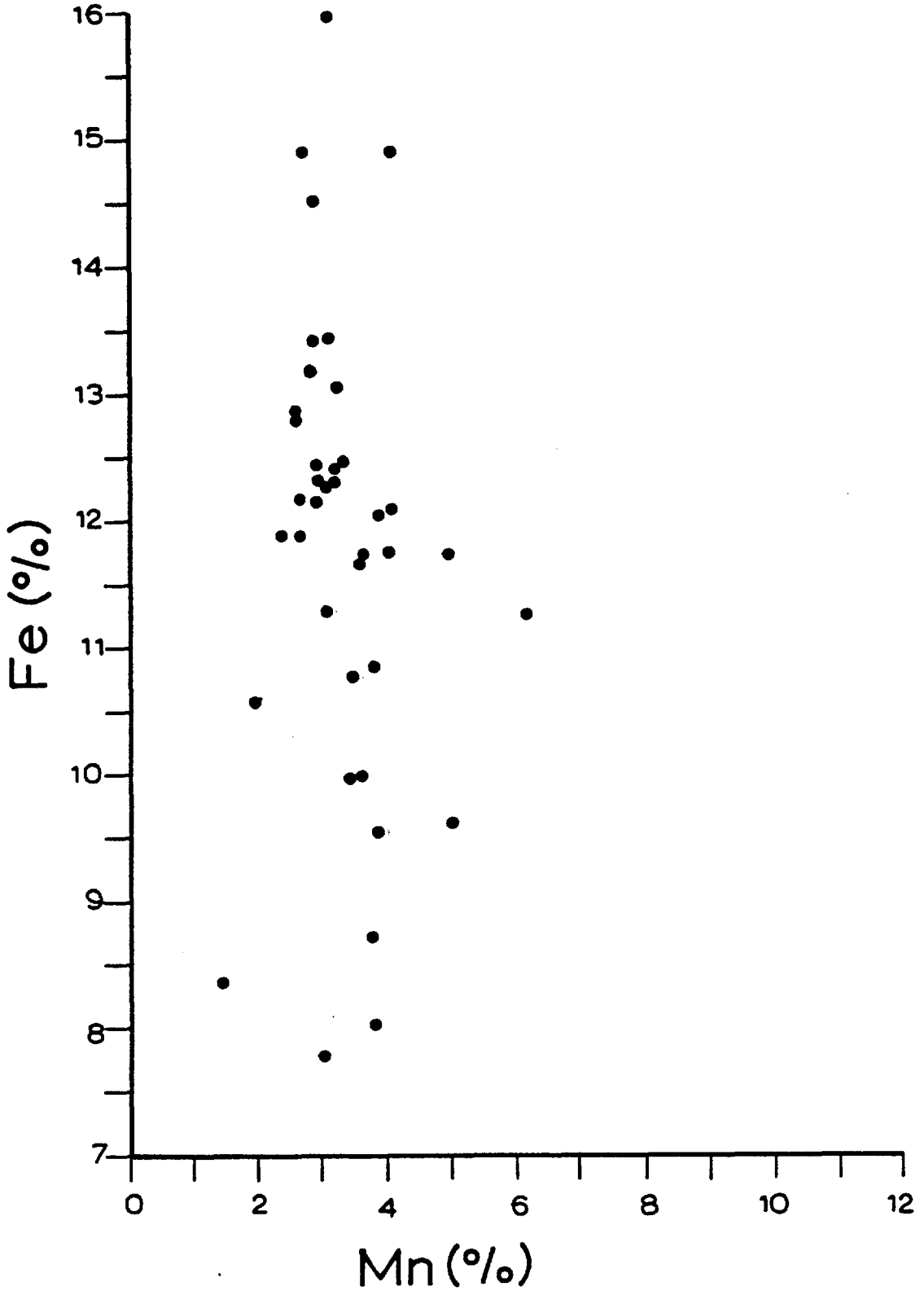

Figure 4.48: Scatter plot showing the relationship between Fe and Mn in sediments from the cores SH 1577 and SH 1560. Concentrations are corrected to a calcium carbonate-free basis.

4.7 DISCUSSION

Although the Bauer Deep sediments have been the subject of considerable investigation recently (Sayles and Bischoff, 1973; Dymond et al, 1973; Sayles et al, 1975; McMurtry and Burnett, 1975; Heath and Dymond, 1977; Dymond and Eklund, 1978), most of the workers considered the area as a whole, without investigating possible trends within the Deep. The geochemical data obtained in this study are of interest in that they present evidence that certain variations occur in the behaviour of elements within the Bauer Deep. In this discussion it is demonstrated that the environmental conditions which prevail during the incorporation of the elements into the various phases or during their transfer from one phase to another are not uniform throughout the entire Deep. Local factors, such as the depth of water, the content of $CaCO_3$ and SiO_2, biological productivity, sea bottom currents, etc. may modify the general character of the sediments. This might be expected in view of the areal extent, the rough bottom topography, and the large range of water depths in the Bauer Deep. The present discussion is also a further contribution to the solution of the existing problem of the source of the metals present in the Bauer Deep sediments.

The Bauer Deep sediments are dominated by Fe-rich smectites with moderate to abundant barite, and moderate δ-MnO_2 and phillipsite. Trace amounts of quartz and plagioclase are also present, while goethite is rare (Heath and Dymond, 1977).

A number of mechanisms have been proposed for the formation of authigenic smectites in the deep sea:

1) Direct precipitation of smectites from hydrothermal solutions (nontronite in the Red Sea, Bischoff (1972); nontronite in the Galapagos spreading center, Section 3 of this thesis).

2) Precipitation of authigenic smectites from solutions at low temperatures into fissures of basalt at mid-ocean ridges (Seyfried et al, 1976).

3) Formation of smectites by alteration of basaltic fragments and volcanic glass (Scheidegger and Stakes, 1977; Vallier and Kidd, 1977; Hein and Scholl, 1978).

4) Formation of smectites by low temperature reaction between Fe-oxyhydroxide and silica (Heath and Dymond, 1977; Hein et al, 1979).

The data from the present study are consistent with a diagenetic origin of the Bauer Deep Fe-rich smectites, as will be discussed now, which involves the fourth mechanism.

Previous investigations had shown that the chemical composition and the pH of the pore waters of Bauer Deep sediments were typical of pelagic pore solutions and very similar to the overlying bottom sea water (Bischoff and Sayles, 1972). There was also a positive correlation between the proportion of Fe leached and that remaining insoluble in the acid-reducing agent solution, in the Bauer Deep sediments (Sayles et al, 1975). Based on the above observations these authors concluded that no chemical reactions occurred in the sediments which could justify diagenetic formation of Fe-rich smectites. Thus, they suggested that the Fe-montmorillonites had sedimented from the overlying water column, rejecting an "in situ" origin for their

formation. Similarly, Kendrick (1974) suggested that the poorly crystalline smectites present both in the Bauer Deep and on the East Pacific Rise were of authigenic origin. He found no changes in the crystal size of the smectites with time and he concluded that this phase was formed simultaneously with the precipitation of Fe-hydroxides, and that there was no further crystallization of it with time.

In contrast to these reports the decrease of the acid-reducible Fe with depth in the sediments and the corresponding increase of that soluble in HCl, found in this study, would suggest the occurrence of chemical reactions which result in the transfer of Fe to a more stable phase. Transformation of Fe-Mn-hydroxides to Fe-rich smectites may take place by reaction between Fe and biogenic Si.

The presence of Al, Fe and Mg hydroxides in the sediments and dissolved Si in the interstitial waters are important factors for the above reaction to occur. Laboratory experiments have shown that poorly crystalline smectites can be synthesized from the precipitation of amorphous Al, Fe and Mg hydroxides which may scavenge Si (Harder, 1972). Johnson (1976) reported an increase of dissolved Si with depth in the interstitial waters of siliceous sediments from the eastern tropical Pacific and a corresponding decrease of siliceous microfossils in the sediments. Similar decrease of the relative abundance of siliceous microfossils with depth was also reported from elsewhere in the Pacific (Riedel and Funnel, 1964), from the Atlantic (Schrader, 1971), and the Mediterranean (Chamley and Millot, 1972). In all cases this was attributed to their post-burial dissolution. It was shown that a portion of Si released from dissolving siliceous microfossils present in the sediments may escape by diffusion into the overlying sea water

(Fanning and Schink, 1969), while a portion should be incorporated back into some solid phase of the sediments (Johnson, 1976). Electron microscope studies of siliceous sediments from the eastern tropical Pacific showed the genetic relationship of clay minerals with the dissolution of biogenic opal. Clay aggregates were found to be approximately the same size as radiolaria and appeared to be casts of radiolaria, suggesting that they formed in their interior before their dissolution. X-ray diffraction studies of the sediments containing the clay aggregates showed the presence of smectites, the abundance of which increased with depth (Johnson, 1976).

Other metals such as Ni and Zn, associated with Fe-hydroxides or the Fe-Mn oxide phases, are also transferred, at least partly, to the newly formed phase (Fe-rich smectites). This is evinced by the general increase of these metals in the HCl-soluble fraction (see Figures 4.19 and 4.22) and their parallel decrease in the acid-reducible fraction with depth in the sediments (see Figures 4.18 and 4.21).

Since Mn, originallly associated with ferromanganese oxides, is not accepted in the smectite structure it recrystallizes as very pure todorokite micronodules (Eklund, 1974; Lyle et al, 1977). However, the enrichment of Mn in the surface sediments and its abrupt decrease with increasing depth at certain stations suggests that at least a portion of Mn is diagenetically remobilised and diffused upward to reprecipitate in the surface sediments.

The vertical distribution patterns obtained from the distribution of elements between the acid-reducible and the HCl-soluble fractions in the cores SH 1577 and SH 1560 indicate that the diagenetic

process described above is more pronounced at these two stations. It is also of interest to note that these stations are distinguished from the remainder by the following features:

1. The most significant characteristic is that there is a remarkable enrichment of Mn in the surface sediments, the concentration of which decreases rapidly with increasing depth down to about 30 cm.

2. A number of Mn-nodules were found at station SH 1560.

3. In the sediments from these stations the vertical distribution patterns of Fe and Mn are dissimilar, whereas there is a strong positive correlation between these two elements at the remaining stations.

4. The content of $CaCO_3$ is rather high ($> 40\%$) in the upper part of the sediment cores.

5. At station SH 1560 Fe, and to a lesser extent Pb, follow $CaCO_3$ in their vertical distribution.

6. The depth of water here is shallower (above 4350 m) than at the other stations.

The distribution of Mn, Ni, Co, Cu and Fe in these cores allows a rough determination of the environmental conditions prevailing in the sediments at these stations. The decrease of the concentrations of Mn, Ni, Co and Cu with depth down to 30 cm, in contrast to the case of Fe which remains constant in this part of the core, suggests possible post-depositional redistribution of these elements. This implies their liberation in the interstitial waters of the subsurface sediments.

Their dissolution is dependent upon the redox potential (Eh) and the pH conditions. Bonatti et al (1971) gave the following values of Eh at which the various elements become soluble in the interstitial waters (pH 8):

Element:	Ni	Co	Mn	Cu	Fe
Eh (volts):	+0.8	+0.6	+0.5	+0.1	-0.2

When reducing conditions prevail in the interstitial waters of the buried sediments the elements with the higher redox potential would tend to go into solution. The fact that Cu is remarkably enriched in the surface layer of the cores SH 1577 and SH 1560, but not Fe, suggests that Cu in the subsurface sediments goes in the interstitial waters while Fe remains in the solid phase. Therefore, it is concluded that the Eh below the surface layer is less than +0.1 but greater than -0.2 volts (considering that pH is $\sim$8).

The relationship between Fe and Mn is a significant parameter which is often used to study the evolution of a chemical system existing in an oceanic area where the precipitation of metalliferous sediments occurs. When mixing of hydrothermal solutions with oxygenated sea water occurs, Fe may be fractionated from Mn by its early precipitation close to the hydrothermal source. In contrast, Mn has a longer residence time in solution, thus being precipitated later and occasionally away from the source (Krauskopf, 1957; Stumm and Morgan, 1970; Bignell et al, 1976; Seyfried and Bischoff, 1977). The variations of Fe/Mn ratios in the submarine hydrothermal deposits from Santorini, Stromboli, Mid-Atlantic Ridge, Red Sea and Galapagos spreading center (Smith and Cronan, 1975; Bonatti et al, 1972b;

Cronan, 1972; Section 3 of this thesis) demonstrate this phenomenon. No such fractionation has been found so far in the East Pacific Rise and the Bauer Deep metalliferous sediments (Heath and Dymond, 1977). It was reported that Fe and Mn distributions correlate well in the sediments across the Nazca plate at 12°S (McMurtry, 1975).

The present geochemical study reveals that the relationship between Fe and Mn in the Bauer Deep sediments is not constant throughout the entire area. Figure 4.47 shows the relationship between Fe and Mn in the cores SH 1578, SH 1557 and SH 1559, while Figure 4.48 illustrates the relationship between the same elements in the cores SH 1577 and SH 1560. It is seen that in the first group there is a positive correlation between Fe and Mn, whereas in the latter the concentrations of Mn remain constant as the concentrations of Fe increase. In this respect sediments at stations SH 1577 and SH 1560 differ from the other sediments. As has been mentioned above, there is no evidence of post-depositional redistribution of Fe in the cores SH 1577 and SH 1560 in contrast to the case of Mn, which is remarkably enriched in the upper layer due to its upward migration. Thus, the relationship between Fe and Mn in these two cores does not represent their initial distribution in the sediments. At least in part, it is a reflection of the mobilization and redistribution of one of the two elements (Mn).

It could be suggested that the diagenetic mobilization of Mn is greater in sediments from shallower waters where the content of $CaCO_3$ is rather high ($> 40\%$). This may be due to the generally larger grain size of these sediments allowing greater circulation of pore fluid and resulting in a greater degree of diffusion.

Detailed examination of the partitioning of elements as a function of water depth leads to the suggestion that the abundance of Fe-rich smectites increases with increasing water depth. This is supported by the increase of the percentage of Fe associated with the HCl-soluble fraction with increasing water depth (see Figure 4.39b) and the corresponding decrease of that leached by the acid-reducing reagent solution (see Figure 4.39a). Moreover, the hydroxylamine HCl-insoluble residue increases with increasing water depth, suggesting the proportional increase of a more resistant phase (i.e. Fe-smectites). It is, therefore, suggested that the formation of Fe-rich smectites in the Bauer Deep sediments may be influenced by the depth of water.

As has been discussed above, the mechanism of formation of the Fe-rich smectites present in the sediments studied is that involving combination of Fe-Mn-hydroxides and biogenic Si. It appears that as the depth of water increases, this reaction is promoted. The following factors are envisaged to contribute in the promotion of this reaction at greater water depths:

1. The relative abundance of siliceous microfossils in the sediments: as the depth of water increases, the proportion of siliceous microfossils increases because radiolaria and diatoms tend to avoid topographic highs and accumulate in lows (Berger, 1976). In the present sediments this is illustrated by Figure 4.46, which shows a positive correlation between biogenic Si and water depth. Thus, at greater depths the proportion of siliceous microfossils which may participate in the reaction examined is greater.

2. Dissolution of $CaCO_3$ in the sediments: the dissolution of calcareous microfossils at greater depths may also play an active role in the formation of Fe-smectites. It provides high alkalinity in the environment (Kastner, 1977), which is due to the following reactions:

$$CaCO_3 \xrightarrow{\text{dissolution}} CaO + CO_2 \nearrow$$
$$CaO + H_2O \longrightarrow Ca(OH)_2,$$

which lead to the formation of calcium hydroxide ($Ca(OH)_2$). Since silica is soluble in an alkaline environment, the dissolution of $CaCO_3$ may promote the dissolution of siliceous microfossils, which results in the enrichment of dissolved Si in the bottom sea water. At the same time the dissolution of siliceous organisms may lead to the enrichment of Fe, Al, and probably Mg, in the sediments. The dilutant effect of SiO_2 on Fe can be seen in the negative correlation found between these two constituents (see Figure 4.32).

It is, therefore, suggested that as the depth of water increases Fe, Al, Mg and Si become more active to react for the production of Fe-rich smectites. According to laboratory experiments (Harder, 1972), the reaction should start with scavenging of dissolved Si by the Al, Mg and Fe hydroxides. The involvement of siliceous organisms in the mechanism of formation of Fe-smectites was shown by direct observations of such microorganisms in the process of dissolution associated with smectites from the eastern tropical Pacific (Johnson, 1976) and the Tiki basin (Hoffert et al, 1978b).

The partitioning of Ni and Zn is also influenced by the depth of water. While the concentrations of these metals associated with the acid-reducible fraction diminish, those soluble in HCl increase with water depth (see Figures 4.40, 4.41, 4.42 and 4.43). This may be a result of the gradual shift of Ni and Zn from the ferromanganese oxides to the Fe-rich smectites with increasing water depth, or it could just reflect the relative abundance of these two phases. In contrast, Mn does not show any clear relationship with water depth in its distribution between the acid-reducible and the HCl-soluble fraction. This is probably due to the fact that this element is not accepted by the smectite structure (Eklund, 1974).

To summarize, the following processes are involved in the scheme proposed here for the genesis of Fe-rich smectites in the Bauer Deep sediments: precipitation of amorphous Fe, Al, Mg hydroxides $\longrightarrow$ dissolution of $CaCO_3$ $\longrightarrow$ dissolution of biogenic SiO_2 $\longrightarrow$ increase of dissolved Si in the sea water and enrichment of Fe, Al and Mg in the sediments $\longrightarrow$ scavenging of Si by Fe, Al and Mg hydroxides $\longrightarrow$ production of Fe-rich smectites.

The local conditions required for the above scheme to be completed are as follows:

1) Low detrital input,

2) Low rates of sedimentation,

3) Great depth of water.

Hoffert et al (1978b), working on the distribution of metals in sediments from the Tiki Basin, found that in zones where the sediments were rich in $CaCO_3$ ($>70\%$) the concentrations of Fe and Mn

increased as the content of CaO decreased. In sediments with $CaCO_3$ content ranging between 30 and 70% the concentrations of Fe and Mn remained constant when the content of $CaCO_3$ diminished. The sediments containing less than 30% $CaCO_3$ were characterized by the presence of high contents of Fe-smectites and micronodules. It was also found that the correlation between Fe and Mn was higher in the sediments rich in carbonates with oxyhydroxides than in metalliferous sediments rich in Fe-smectites and micronodules.

The following similarities are recognized between the Bauer Deep and the Tiki Basin:

1) Association of Fe-smectites with Mn-nodules.

2) Variations of the Fe/Mn ratios with $CaCO_3$ content. Lower Fe/Mn ratios are found in carbonate sediments.

3) Dependence of the concentration of Fe and Mn upon the depth of water and the content of $CaCO_3$.

4) Low input of detrital material.

5) Dependence of the presence of Fe-smectites upon the depth of water.

The importance of the common features recognized for the basins lies in their geographical position. Since the Bauer Deep occurs on the eastern and the Tiki Basin on the western flank of the East Pacific Rise, some correlation should exist between the sediments present in the two basins and the hydrothermally-derived sediments found on the crest of the Rise. The common chemical

behaviour of the elements in the two basins would suggest symmetrical transportation of hydrothermally derived phases, east and west of the East Pacific Rise, to the basins. Mixing of these phases with biological material results in their transportation to new phases, so that their original hydrothermal character is significantly changed. This conclusion corroborates the data of Heath and Dymond (1977), who found a symmetrical increase in oxalate-insoluble Fe from East Pacific Rise to northern Rise to Bauer Deep. Since in both basins the transformations take place under similar environmental conditions (low detrital input, dissolution of biogenic silica), the final products are the same (Fe-rich smectites and Mn-micronodules).

4.8 SUMMARY AND CONCLUSIONS

1. The geochemical behaviour of elements is not uniform for the whole Bauer Deep. Certain variations occur which are dependent upon the depth of water and upon local environmental conditions.

2. There is a negative correlation between Fe and Si in the Bauer Deep sediments which shows the dilutant effect of Si on Fe.

3. The chemical conditions in the subsurface sediments at stations SH 1577 and SH 1560 allow remobilization of Mn, Ni, Co and Cu. Since no remobilization of Fe occurs in these sediments the Eh should be less than +0.1 but greater than -0.2 volts.

4. The Fe/Mn ratios in the Bauer Deep sediments are not constant, but they vary within a large range. Sediments with high content of $CaCO_3$ are characterized by low Fe/Mn ratios.

5. The partitioning data suggest that the Fe-rich smectites present in the Bauer Deep sediments studied here are of diagenetic origin. They may form by reaction between Fe-Mn-hydroxides and biogenic silica. Silica released into the interstitial waters or into the bottom sea water by the dissolution of siliceous microfossils is being used probably by adsorption on the surface of the hydroxides. Harder (1978) showed that reducing conditions aid in the synthesis of smectites from reaction between hydroxides and silica.

Remobilization of Mn and other elements found in the subsurface sediments studied suggests that such conditions may occur here. Post-burial dissolution of siliceous microfossils in Pacific sediments was shown by various workers (Riedel and Funnel, 1964; Johnson, 1976). Thus, the Bauer Deep subsurface sediments offer a more favourable environment for the formation of Fe-rich smectites. This is evinced here by the general increase of the Fe soluble in HCl with depth in the sediments and its corresponding decrease in the acid-reducible fraction. However, Fe-rich smectites may form also in the surface sediments since a portion of the dissolved silica escapes by diffusion into the bottom sea water (Fanning and Schink, 1969). Nickel and Zn are transferred from the ferromanganese oxides to the Fe-rich smectites during the transformation of the former to the latter.

6. The formation of Fe-rich smectites from the reaction between Fe-hydroxides and silica is influenced by the depth of water. This reaction is promoted at greater depths and may be directly linked to the dissolution of $CaCO_3$. The tendency of radiolaria and diatoms to accumulate in lows (Berger, 1976) may increase the proportion of biogenic silica being available for the reaction with the Fe-hydroxides. The alkalinization of the environment caused by the dissolution of calcareous organisms at greater depths may promote the dissolution of siliceous microfossils, which in turn leads to the enrichment of dissolved Si in bottom sea water and to the enrichment of Fe, Al and Mg in the sediments.

7. The common geochemical features found for the Bauer Deep and the Tiki Basin sediments suggest similar environmental conditions in the two basins. Their geographical position could also support some association of the metals found in the sediments of the basins with the East Pacific Rise hydrothermal activity.

BIBLIOGRAPHY

ACHARYA, H.K. (1965) Seismicity of the Galapagos Islands and vicinity. Bull. Seis. Soc. Amer., 55, pp. 609-617.

ADDY, S.K., PRESLEY, B.J. and EWING, M. (1976) Distribution of manganese, iron and other trace elements in a core from the northwest Atlantic. J. Sedim. Petrol., 46, pp. 813-818.

ANDERSON, R.N. and HALUNEN, A.J. (1974) Implications of heat flow for metallogenesis in the Bauer Deep. Nature, 251, pp. 473-475.

ASTON, S.R., CHESTER, R., GRIFFITHS, A. and RILEY, J.P. (1972a) Distribution of cadmium in North Atlantic deep sea sediments. Nature, 239, p. 393.

ASTON, S.R., BRUTY, D., CHESTER, R. and RILEY, J.P. (1972b) Distribution of mercury in North Atlantic deep sea sediments. Nature (Phys, Sci.), 237, p. 125.

BALLARD, R.D. (1978) Notes on a major oceanographic find. Oceanus, 20, (3), pp. 35-44.

BENDER, M., BROECKER, W., GORNITZ, V., MIDDEL, U., KAY, R., BISCAYE, P. AND SHINE-SOON-SUN (1971) Geochemistry of three cores from the East Pacific Rise. Eart. Planet. Sci. Letters, 12, pp. 425-433.

BEN YAAKOV, S., RUTH, E. and KAPLAN, I.R. (1974) Calcium carbonate saturation in northeastern Pacific: in situ determination and geochemical implications. Deep-Sea Res., 21, pp. 229-243.

BERGER, W.H. (1967) Foraminiferal ooze: Solution at depths. Science, 156, pp. 383-385.

_____ (1968) Planktonic foraminifera: Selective solution and paleoclimatic interpretation. Deep-Sea Res., 15, pp. 31-43.

_____ (1970) Planktonic foraminifera: Selective solution and the lysocline. Mar. Geol., 8, pp. 111-138.

_____ (1971) Sedimentation of planktonic foraminifera. Mar. Geol., 11, pp. 325-358.

_____ (1976) Biogenous deep sea sediments: Production, preservation and interpretation. In: Chemical Oceanography, Vol. 5, (Riley, J.P. and Chester, R., Eds.), Academic Press, London, New York and San Francisco, pp. 265-388.

BERNER, R.A. and WILDE, P. (1972) Dissolution kinetics of calcium carbonate in seawater: I. Saturation state parameters for kinetic calculations. Am. J. Sci., 272, pp. 826-839.

BERNER, R.A. (1974) Physical chemistry of carbonates in the oceans. In: W.W. Hay (Editor), Studies on Paleo-Oceanography. Soc. Econ. Paleontol. Mineral., Spec. Publ., 20, pp. 37-43.

BERTINE, K.K. (1974) Origin of Lau Basin Sediments. Geochim.Cosmochim.Acta, 38, pp. 629-640.

BEZRUKOV, P.L. (1969) Microflora and Microfauna in the recent sediments of the Pacific Ocean. The Pacific Ocean, 8, I. Akad. Nauk, Moscow.

BEZRUKOV, P.L. (1970) Sedimentation in the Pacific Ocean. The Pacific Ocean, 6, 2 pts., Izdat, Nauk, Moscow.

BIGNELL, R.D., CRONAN, D.S. and TOOMS, J.W. (1976) Metal dispersion in the Red Sea as an aid to marine geochemical exploration. Trans. Inst. Min. Metall. (B), 85, pp. B274-B278.

BISCHOFF, J.L. and SAYLES, F.L. (1972) Pore fluids of recent marine sediments - III. Pelagic sediments, Galapagos Islands to East Pacific Rise. J. Sed. Petrol., 42, pp. 711-724.

BISCHOFF, J.L. (1972) A ferroan nontronite from the Red Sea geothermal system. Clays and Clay Minerals, 20, pp. 217-223.

BONATTI, E. and JOENSUU, O. (1966) Deep sea iron deposit from the South Pacific. Science, 154, pp. 643-645.

BONATTI, E., FISHER, D.E., JOENSUU, O. and RYDELL, H.S. (1971) Postdepositional mobility of some transition elements, phosphorus, uranium and thorium in deep sea sediments. Geochim. Cosmochim. Acta, 35, pp. 189-201.

BONATTI, E., KRAEMER, T. and RYDELL, H. (1972a) Classification and genesis of submarine iron-manganese deposits. In Papers from a Conference on Ferromanganese deposits on the ocean floor, D.R. Horn (Ed.), pp. 149-166, IDOE/NSF, Washington.

BONATTI, E., HONNOREZ, J., JOENSUU, O. and RYDELL, H.S. (1972b) Submarine iron deposits from the Mediterranean Sea. In: Stanley, D.J. (Ed.), Symposium on the Sedimentation in the Mediterranean Sea: VIII International Sediment. Congress, Heidelberg, pp. 701-710.

BONATTI, E., KOLLA, V., MOORE, W.S. and STERN, C. (1979) Metallogenesis in marginal basins: Fe-rich basal deposits from the Philippine Sea. Mar. Geol., 32, pp. 21-37.

BOSTRÖM, K. and PETERSON, M.N.A. (1966) Precipitations from hydrothermal exhalations on the East Pacific Rise. Econ. Geol., 61, pp. 1258-1265.

BOSTRÖM, K. (1967) The problem of excess manganese in pelagic sediments. In: Researches in geochemistry, 2, pp. 421-452, Abelson, P.H. (Ed.), J. Wiley and Sons, New York.

BOSTRÖM, K., PETERSON, M.N.A., JOENSUU, O. and FISHER, D.E. (1969) Aluminium-poor ferromanganoan sediments on active ocean ridges. J. Geophys. Res., 74, pp. 3261-3270.

BOSTRÖM, K. and PETERSON, M.N.A. (1969) The origin of aluminium-poor ferromanganoan sediments in areas of high heat flow on the East Pacific Rise. Mar. Geol., 7, pp. 427-447.

BOSTRÖM, K., JOENSUU, O., VALDES, S. and RIERA, M. (1972a) Geochemical history of South Atlantic Ocean sediments since Late Cretaceous. Mar. Geol., 12, pp. 85-122.

BOSTRÖM, K., FARQUHARSON, B. and EYL, W. (1972b) Submarine hot springs as a source of active ridge sediments. Chem. Geol., 10, pp. 189-203.

BOSTRÖM, K., KRAEMER, T. and GARTNER, S. (1973) Provenance and accumulation rates of opaline silica, Al, Ti, Fe, Mn, Cu, Ni and Co in Pacific pelagic sediments. Chem. Geol., 11, pp. 123-148.

BRAMLETTE, M.N. (1961) Pelagic sediments. In: Sears, M. (Ed.), Oceanography, Washington, D.C., Am. Assoc. Adv. Sci. Pub., pp. 345-366.

BRUTY, D., CHESTER, R., ROYLE, L. and ELDERFIELD, H. (1972) Distribution of Zn in North Atlantic deep sea sediments. Nature (Phys. Sci.), 237, pp. 86-87.

CALVERT, S.E. and PRICE, N.B. (1970) Composition of manganese nodules and manganese carbonates from Loch Fyne, Scotland. Contr. Mineral. and Petrol., 29, pp. 215-233.

CANN, J.R., WINTER, C.K. and PRITCHARD, R.G. (1977) A hydrothermal deposit from the floor of the Gulf of Aden. Mineral. Mag., 41, pp. 193-199.

CHAMLEY, H. and MILLOT, G. (1972) Néoformation de montmorillonite à partir de diatomées et de cendres dans les sédiments marins de Santonin (Mediterranée orientale). Acad. Sci. Comptes Rendus, S.D., 274, pp. 1132-1134.

CHESTER, R. and HUGHES, M.J. (1966) The distribution of manganese, iron and nickel in a North Pacific deep-sea clay core. Deep-Sea Res., 13, pp. 627-634.

CHESTER, R. and HUGHES, M.J. (1967) A chemical technique for the separation of ferro-manganese minerals, carbonate minerals and adsorbed trace elements from pelagic sediments. Chem. Geol., 2, pp. 249-262.

CHESTER, R. and HUGHES, M.J. (1969) The trace element geochemistry of a North Pacific pelagic clay core, Deep-Sea Res., 16, pp. 639-654.

CHESTER, R. and MESSIHA-HANNA, R. (1970) Trace element partition patterns in North Atlantic deep sea sediments. Geochim. Cosmochim. Acta, 34, pp. 1121-1128.

CHESTER, R., ASTON, S.R. and BRUTY, D. (1976) The trace element partition geochemistry in an ancient deep-sea sediment core from the Bermuda Rise. Mar. Geol., 21, pp. 271-288.

COOK, H. (1971) Iron and manganese-rich sediments overlying oceanic basalt sediment, Equatorial Pacific, Leg 9, D.S.D.P. Geol. Soc. Am., Abs. with Program., 3, pp. 530-531.

COPELAND, R.A. (1970) Trace element distribution in sediments of the Mid-Atlantic Ridge. Ph.D. Thesis, Massachusetts Inst. of Tecb.

CORLISS, J.B. (1971) The origin of metal-bearing submarine hydrothermal solutions. J. Geophys. Res., 76, pp. 8128-8138.

CORLISS, J.B., LYLE, M., DYMOND, J. and CRANE, K. (1978) The chemistry of hydrothermal mounds near the Galapagos Rift. Earth Planet. Sci. Letters, 40, pp. 12-24.

CORLISS, J.R., DYMOND, J., GORDON, L.I., EDMOND, J.M. von HERZEN, R.P., BALLARD, R.D., GREEN, K., WILLIAMS, D., BAINBRIDGE, A., CRANE, K. and van ANDEL, T.H. (1979) Submarine thermal springs on the Galapagos Rift. (Unpublished manuscript.)

CRONAN, D.S. (1969) Average abundances of Mn, Fe, Ni, Co, Cu, Pb, Mo, V, Cr, Ti and P in Pacific pelagic clays. Geochim. Cosmochim. Acta, 33, pp. 1562-1565.

CRONAN, D.S. (1972) The Mid-Atlantic Ridge near 45°N., XVII - Al, As, Hg and Mn in ferruginous sediments from the median valley. Can.J. Earth Sci., 9, pp. 319-323.

CRONAN, D.S. , VAN ANDEL, T.J., HEATH, G., DINKLEMAN, M., BENNET, R., BUKRY, D., CHARLESTON, S., KANAPS, A., RODOLFO, K. and YEATS, R. (1972) Iron-rich basal sediments from the eastern equatorial Pacific: Leg XVI, D.S.D.P. Science, 175, pp. 61-63.

CRONAN, D.S. and GARRETT, D. (1973) The distribution of elements in metalliferous Pacific sediments collected during the D.S.D.P. Nature (Phys. Sci.), 242, pp. 88-89.

CRONAN, D.S. (1974) Authigenic minerals in deep-sea sediments. In: The Sea, 5 (Ed. E. Goldberg), John Wiley and Sons Inc., New York, pp. 491-525.

CRONAN, D.S., DAMIANI, V.V., KINSMAN, D.J.J. (1974) Sediments from the Gulf of Aden and western Indian Ocean. In: Initial Reports of the D.S.D.P., 24, pp. 1047-1110, Fisher, R.L. et al (Eds.), U.S. Govt. Print. Office, Washington D.C.

CRONAN, D.S. (1976a) Basal metalliferous sediments from the eastern Pacific. Bull. Geol. Soc. Am., 87, pp. 928-934.

CRONAN, D.S. (1976b) Implications of metal dispersion from submarine hydrothermal systems for mineral exploration on mid-ocean ridges and in island arcs. Nature, 262, pp. 567-569.

DASCH, E.J., DYMOND, J.R. and HEATH, G.R. (1971) Isotopic analysis of metalliferous sediments from the East Pacific Rise. Earth. Planet. Sci. Letters, 13, pp. 175-180.

DETRICK, R.S., WILLIAMS, D.L., MUDIE, J.D. and SCLATER, J.G. (1974) The Galapagos Spreading Center: bottom-water temperatures and the significance of geothermal heating. Geophys., J.R. Astr. Soc., 38, pp. 627-636.

DYMOND, J., CORLISS, J.B., HEATH, G.R., FIELD, C.W., DASCH, E.J. and VEEH, H.H. (1973) Origin of metalliferous sediments from the Pacific Ocean. Bull. Geol. Soc. Am., 84, pp. 3355-3372.

DYMOND, J., CORLISS, J.B. and STILLINGER, R. (1976) Chemical composition and metal accumulation rates of metalliferous sediments from Sites 319, 320 and 321. In. Initial Reports of the D.S.D.P., 34, pp. 575-588. Yeats, R.S., Hart, S.R. et al (Eds.), U.S. Govt. Print. Office, Washington D.C.

DYMOND, J. and EKLUND, W. (1978) A microprobe study of metalliferous sediment components. Earth and Planet. Sci. Letters, 40 pp. 243-251.

EDMOND, J.M. (1974) On the dissolution of carbonate and silicate in the deep ocean. Deep-Sea Res., 21, pp. 455-480.

EKLUND, W.A. (1974) A microprobe study of metalliferous sediment components. M.Sc. Thesis, Corvallis, Oregon State University, pp. 77f.

ELDERFIELD, H. (1976) Hydrogenous material in marine sediments; excluding manganese nodules. In: Chemical Oceanography, Vol. 5, (Riley, J.P. and Chester, R., Eds.), Academic Press, London, New York and San Francisco, pp. 137-215.

EL WAKEEL, S.K. and RILEY, J.P. (1961) Chemical and mineralogical studies of deep-sea sediments. Geochim. Cosmochim. Acta, 25, pp. 110-146.

EMILIANI, C. (1955) Mineralogical and chemical composition of the tests of certain pelagic foraminifera. Micropaleont., 1(4), pp. 377-380.

FANNING, K.A. and SCHINK, D.R. (1969) Interaction of marine sediments with dissolved silica. Limmol. Oceanog., 14, pp. 59-68.

FISHER, D.E. and BOSTRÖM, K. (1969) Uranium-rich sediments on the East Pacific Rise. Nature, 224, pp. 64-65.

FLEET, A.J. and KEMPE, D.R.C. (1974) Preliminary geochemical studies of sediments from D.S.D.P., Leg 26, Southern Indian Ocean. In: Initial Reports of the D.S.D.P., 26, pp. 541-551, Davies, T.A., Luyendyk, B.P. et al (Eds.), U.S. Govt. Print. Office, Washington D.C.

GOLDBERG, E.D. (1954) Marine chemistry. I: Chemical scavengers of the sea. J. Geol., 62, pp. 249-265.

GOLDBERG, E.D. and ARRHENIUS, G. (1958) Chemistry of pelagic Pacific sediments. Geochim. Cosmochim. Acta, 13, pp. 153-212.

GRIFFIN, J.J., WINDOM, H. and GOLDBERG, E.D. (1968) The distribution of clay minerals in the world oceans. Deep-Sea Res., 15, pp. 433-459.

HARDER, H. (1972) The role of magnesium in the formation of smectite minerals. Chem. Geol., 10, pp. 31-39.

HARDER, H. (1976) Nontronite synthesis at low temperatures. Chem. Geol., 18, pp. 169-180.

_____ (1978) Synthesis of iron layer silicate minerals under natural conditions. Clays and Clay Minerals, 26, pp. 65-72.

HART, R.A. (1973) A model for chemical exchange in the basalt-sea water system of oceanic layer II: Can. J. Earth Sci., pp. 799-816.

HEATH, G.R., DYMOND, J. and VEEH, H.H. (1972) Metalliferous sediments from the southeastern Pacific: The IDOE Nazca Plate project. (Unpublished manuscript.)

HEATH, G.R. and DYMOND, J. (1977) Genesis and transformation of metalliferous sediments from the East Pacific Rise, Bauer Deep and Central Basin, North-West Nazca Plate. Bull. Geol. Soc. Am., 88, pp. 723-733.

HEIN, J.R. and SCHOLL, D.W. (1978) Diagenesis and distribution of late Cenozoic volcanic sediment in the southern Bering Sea. Geol. Soc. Am. Bull., 89, pp. 197-210.

HEIN, J.R., YEH, H.W. and ALEXANDER, E. (1979) Origin of iron-rich montmorillonite from the manganese nodule belt of the north equatorial Pacific. Clays and Clay Minerals, 27, pp. 185-194.

HEKINIAN, R., ROSENDAHL, B.R., CRONAN, D.S., DMITRIEV, V., FODOR, R.V., GOLL, R.M., HOFFERT, M., HUMPHRIES, S.E., MATTEY, D.P., NATLAND, J., PETERSEN, N., ROGGENTHEN, W., SCHRADER, E.L., SRIVASTAVA, R.K. and WARREN, M. (1978) Hydrothermal deposits and associated basement rocks from the Galapagos spreading center. Oceanol. Acta, 1 (4), pp. 473-482.

HERRON, E.M., and HEIRTZLER, J.R. (1967) Sea-floor spreading near the Galapagos. Science, 158, pp. 775-780.

HIRST, D.M. and NICHOLLS, G.D. (1958) Techniques in sedimentary geochemistry. 1. Separation of the detrital and non-detrital fractions of limestones. J. Sedim. Petrol., 28, pp. 461-468.

HOFFERT, M., PERSEIL, A., HEKINIAN, R., CHOUKROUNE, P., NEEDHAM, H.D., FRANCHETEAU, J. and LE PICHON, X. (1978a) Hydrothermal deposits sampled by diving saucer in transform fault 'A' near 37°N on the Mid-Atlantic Ridge, Famous area. Oceanol. Acta, 1, pp. 73-86.

HOFFERT, M., KARPOFF, A.M. and SCHAAF, A. (1978b) La couverture sédimentaire du bassin Tiki (Pacifique Sud-est): Passage de vases carbonatées à des sédiments métallifères. (Unpublished manuscript.)

HORDER, M.F. (1979) Geochemical investigations of deep sea sediments from the Indian Ocean. Unpubl. Ph.D. Thesis, University of London.

HOROWITZ, A. (1970) The distribution of Pb, Ag, Sn, Ti, Zn in sediments on active ocean ridges. Mar. Geol., 9, pp. 241-259.

HOROWITZ, A. (1974) Geochemical investigations of sediments associated with the Mid-Atlantic Ridge, Unpubl. Ph.D. Thesis, University of London.

HOROWITZ, A. and CRONAN, D.S. (1976) The geochemistry of basal sediments from the north Atlantic Ocean. Mar. Geol., 20, pp. 205-228.

JOHNSON, T.C. (1976) Biogenic opal preservation in pelagic sediments of a small area in the eastern tropical Pacific. Geol. Soc. Am. Bull., 87, pp. 1273-1282.

KASTNER, M., KEENE, J.B. and GIESKES, J.M. (1977) Diagenesis of siliceous oozes - I. Chemical controls on the rate of opal-A to opal-CT transformation - an experimental study. Geochim. Cosmichim. Acta, 41, pp. 1041-1059.

KENDRICK, J.W. (1974) Trace element studies of metalliferous sediments in cores from the East Pacific Rise and Bauer Deep, 10°S. M.Sc. Thesis, Corvallis, Oregon State University, 117, p.

KLINKHAMMER, G., BENDER, M. and WEISS, R.F. (1977) Hydrothermal manganese in the Galapagos Rift. Nature, 269, pp. 319-320.

KLITGORD, K.D. and MUDIE, J.D. (1974) The Galapagos spreading center: A near-bottom geophysical survey. Geophys. J.R. Astr. Soc., 38, pp. 563-568.

KRAUSKOPF, K.B. (1956) Factors controlling the concentrations of thirteen rare metals in sea water. Geochim. Cosmochim. Acta., 9, pp. 1-32.

_____ (1957) Separation of manganese from iron in sedimentary processes. Geochim. Cosmochim. Acta, 12, pp. 61-84.

KU, T.L., BROECKER, W.S. and ORDYKE, N. (1968) Comparison of sedimentation rates measured by paleomagnetic and ionium methods of age determination. Earth Planet. Sci. Letters, 4, pp. 1-16.

LAEVASTU, T. and MELLIS, O. (1955) Extraterrestrial material in deep-sea deposits. Trans. Am. Geophys. Un., 36, pp. 385-389.

LANDERGREN, S. (1964) On the geochemistry of deep sea sediments. Rep. Swed. Deep-Sea Expedition, 10(5), pp. 57-154.

LI, Y-H., BISCHOFF, J. and MATHIEU, G. (1969) The migration of manganese in the Arctic Basin sediment. Earth Planet. Sci. Letters, 7, pp. 265-270.

LONSDALE, P. (1976) Abyssal circulation of the southeastern Pacific and some geological implications. J. Geophys. Res., 77, pp. 7196-7202.

_____ (1977) Deep-tow observations at the mounds abyssal hydrothermal field, Galapagos Rift. Earth Planet. Sci. Letters, 36, pp. 92-110.

LYLE, M., DYMOND, J. and HEATH, G.R. (1977) Copper-nickel enriched ferromanganese nodules and associated crusts from the Bauer Basin, northwest Nazca Plate. Earth Planet. Sci. Letters, 35, pp. 55-64.

LYNN, D.C. and BONATTI, E. (1965) Mobility of manganese in diagenesis of deep sea sediments. Mar. Geol, 3, pp. 457-474.

MAMMERICKX, J., ANDERSON, R.N., MENARD, H.W. and SMITH, S.M. (1975) Morphology and tectonic evolution of the east central Pacific. Geol. Soc. Am. Bull., 86, pp. 111-118.

MARCHIG, V. and VALLIER, T.L. (1974) Geochemical studies of sediments and interstitial water, Sites 248 and 249, Leg 25, Deep Sea Drilling Project. In: Initial Reports of the D.S.D.P., 25, pp. 405-415, Simpson, E.S.W., et al (Eds.), U.S. Govt. Print. Office, Washington, D.C.

McMURTRY, G.M. (1975) Geochemical investigations of sediments across the Nazca Plate at 12°S. M.Sc. Thesis, University of Hawaii.

McMURTRY, G.M. and BURNETT, W.C. (1975) Hydrothermal metallogenesis in the Bauer Deep of the south-eastern Pacific. Nature, 254, pp. 42-44.

MENARD, H.W., CHASE, T.E. and SMITH, S.M. (1964) Galapagos Rise in the southeastern Pacific. Deep-Sea Res., 11, pp. 233-242.

MENARD, H.W. (1964) Marine Geology of the Pacific. McGraw-Hill, New York, 271 pp.

MOORE, W.S. and VOGT, P.R. (1976) Hydrothermal manganese crusts from two sites near the Galapagos spreading axis. Earth Planet. Sci. Letters, 29, pp. 349-356.

MORSE, J.W. and BERNER, R.A. (1972) Dissolution kinetics of calcium carbonate in sea water. II. A kinetic origin for the lysocline. Am. J. Sci., 272, pp. 840-881.

MURRAY, J. and RENARD, A.F. (1891) Deep-Sea deposits, Report on the Challengerexpedition 1873-76. Thomson, C.W. and Murray, J. (Eds.), H.M.S.O., 525 pp.

NATLAND, J.H. (1973) Basal ferromanganoan sediments at D.S.D.P. Site 183, Aleutian abyssal plain, and Site 192, Meiji guyot, northwest Pacific, Leg 19. In: Creager, J.S., Scholl, D.W. et al (1973) Initial Reports of the Deep Sea Drilling Project, 19, U.S. Govt. Print. Office, Washington D.C., pp. 629-636.

OLAUSSON, E. (1960) Descriptions of sediment cores from the central and western Pacific with adjacent Indonesian region. Rep. Swed. Deep-Sea Exped., 1947-1948, 6 (5), pp. 161-214.

PETERSON, M.N.A. (1966) Calcite: rates of dissolution in a vertical profile in the central Pacific. Science, 154, pp. 1542-1544.

PIMM, A.C. (1974) Mineralization and trace element variation in deep-sea pelagic sediments of the Wharton Basin, Indian Ocean. In: Initial Reports of the D.S.D.P., 22, pp. 469-476, von der Borch, C.C. et al (Eds.), U.S. Govt. Print. Office, Washington D.C.

PIPER, D.Z. (1973) Origin of metalliferous sediments from the East Pacific Rise. Earth Planet. Sci. Letters, 19, pp. 75-82.

PIPER, D.Z. and GRAEF, P.A. (1974) Gold and rare-earth elements in sediments from the East Pacific Rise. Mar. Geol., 17, pp. 287-297.

RIEDEL, W.R. and FUNNELL, B.M. (1964) Tertiary sediment cores and microfossils from the Pacific Ocean floor. Geol. Soc. London Quart. Journal, 120, pp. 305-368.

RYDELL, H., KRAEMER, T., BOSTRÖM, K. and JOENSUU, O. (1974) Postdepositional injections of uranium-rich solutions into East Pacific Rise sediments. Mar. Geol., 17, pp. 151-164.

SAYLES, F.L. and BISCHOFF, J.L. (1973) Ferromanganoan sediments in the equatorial East Pacific. Earth Planet. Sci. Letters, 19, pp. 330-336.

SAYLES, F.L., KU, T.L. and BOWKER, P.C. (1975) Chemistry of ferromanganoan sediments of the Bauer Deep. Bull. Geol. Soc. Am., 86, pp. 1423-1431.

SCHEIDEGGER, K.F. and STAKES, D.S. (1977) Mineralogy, chemistry and crystallization sequence of clay minerals in altered tholeitic basalts from the Peru Trench. Earth Planet. Sci. Letters, 36, pp. 413-422.

SCHRADER, H.J. (1971) Ursache und Ergebnis von Auflosung von Kieselskeletten in den oberen Sedimentbereichen am Beispiel zweier Kern-Profile vor Marokko und Portugal. In: Farinacci, A. (Ed.), Plankton. Conf. 2nd, Proc., Rome, 1970, pp. 1149-1155.

SCLATER, J.G., von HERZEN, R.P., WILLIAMS, D.L., ANDERSON, R.N. and KLITGORD, K. (1974) The Galapagos spreading centre: heat-flow on the north flanks. Geophys. J.R. Astr. Soc., 38, pp. 609-626.

SCOTT, M.R., SCOTT, R.B., RONA, P.A., BUTLER, L.W. and NALWALK, A.J. (1974) Rapidly accumulating manganese deposit from the median valley of the Mid-Atlantic Ridge. Geophys. Res. Letters, 1, pp. 355-358.

SEYFRIED, W.E., SHANKS, W.C. and BISCHOFF, J.L. (1976) Alternation and vein formation in Site 321 basalts. Initial Reports of the Deep Sea Drilling Project, 34, pp. 385-392.

SEYFRIED, W.E. and BISCHOFF, J.L. (1977) Hydrothermal transport of heavy metals by sea water: the role of sea water/basalt ratio. Earth Planet. Sci. Letters, 34, pp. 71-77.

SMITH, P.A. and CRONAN, D.S. (1975) The dispersion of metals associated with an active submarine exhalative deposit. 3rd Oceanology International, Brighton, England, pp. 111-114.

STUMM, W. and MORGAN, J.J. (1970) Aquatic chemistry. New York, Wiley Interscience, 583 pp.

TUREKIAN, K.K. and IMBRIE, J. (1966) The distribution of trace elements in deep-sea sediments of the Atlantic Ocean. Earth Planet. Sci. Letters, 1, pp. 161-168.

TUREKIAN, K.K. and BERTINE, K. (1971) Deposition of Mo and U along the major ocean ridge systems. Nature, London, 229, pp. 250-251.

VALLIER, T.L. and KIDD, R.B. (1977) Volcanic sediments in the Indian Ocean. In: Indian Ocean Geology and Biostratigraphy, J.R. Heirtzler, H.M. Bolli, T.A. Davies, J.B. Saunders and J.G. Sclater (Eds.), Am. Geophys. Un., Washington D.C., pp. 87-118.

VEEH, H.H. and BOSTRÖM, K. (1971) Anomalous $^{234}U/^{238}U$ on the East Pacific Rise. Earth Planet. Sci. Letters, 10, pp. 372-374.

VON DER BORCH, C.C. and REX, R.W. (1970) Amorphous iron oxide precipitates in sediments cored during Leg V, Deep Sea Drilling Project. In: Initial Reports of the D.S.D.P., 5, pp. 541-544. McManus, D.A. et al (Eds.), U.S. Govt. Print. Office, Washington D.C.

VON DER BORCH, NESTERHOFF, W.D. and GALEHOUSE, J.S. (1971) Iron-rich sediments cored during Leg 8 of the Deep Sea Drilling Project. In: Initial Reports of the D.S.D.P., 8, pp. 829-836, Tracey, J.I., Jr. (Ed.), U.S. Govt, Print. Pffice, Washington D.C.

WARNER, T.P. and GIESKES, J.M. (1974) Iron-rich basal sediments from the Indian Ocean: Site 245, Deep Sea Drilling Project. In: Initial Reports of the D.S.D.P., 25, pp. 395-404, Simpson, E.S.W. et al (Eds.), U.S. Govt. Print. Office, Washington D.C.

WEDEPOHL, K.H. (1960) Spurenanalytische Untersuchungen an Tiefseetonen aus den Atlantik. Geochim. Cosmochim. Acta, 18, pp. 200-231.

APPENDICES

APPENDIX A

SAMPLE COLLECTION AND DESCRIPTION OF THE CORES

The material used in the investigation of the fracture zone at 9°S and the Bauer Deep was supplied to the author in the form of sediment cores. These were collected by Dr. D.S. Cronan during the spring of 1976 aboard the British research vessel RRS Shackleton.

When the cores arrived at the laboratory they were stored horizontally in a deep-freezer. This was done to prevent possible movement of pore waters from one end to the other, particularly in the case of the Bauer Deep sediments, where a large amount of water was included in the cores. Before splitting the cores, they were taken out of the freezer for several hours and they were allowed to semithaw. Splitting was carried out by cutting through the plastic linear with a specially designed core-cutter (see Plate A1), then passing a cheese-wire through the sediment, and finally splitting the core using a palette knife. When the cores had thawn out completely, they were visually described and color-coded, using the Munsell color code system (see Table A1), and sampled. Generally, samples were taken at changes of the lithological character of the sediment. Visual estimation of the grain size distribution, the calcium carbonate content and the color were taken into account in order to decide the location of each sample in the core. In the case of a long homogeneous core, samples were taken every 20 cms.

The Galapagos D.S.D.P. samples were supplied to the author in a wet state in plastic tubes. Therefore, no core-splitting was involved in the preparation of this material.

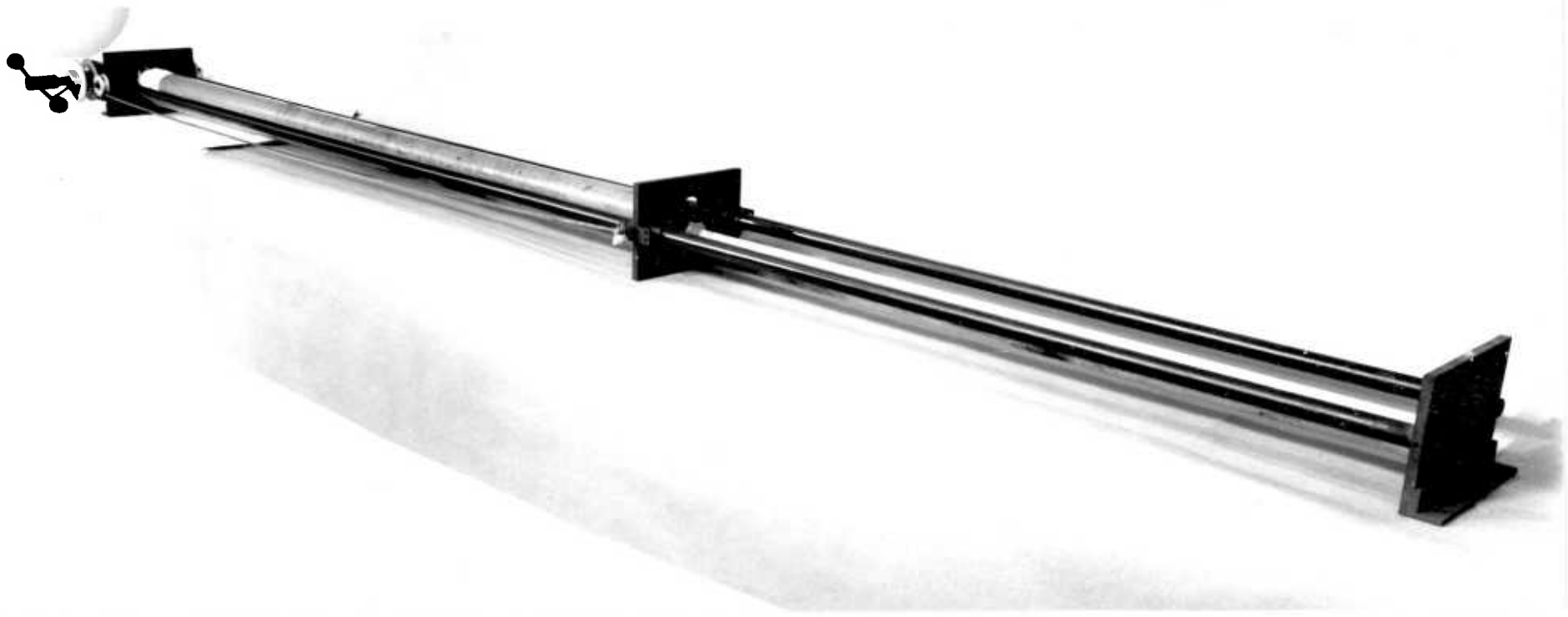

Plate A1: Core-cutter used for splitting of the cores.

Table A1: Part of the Munsell color code system which was used in the description of the cores.

10YR	
8/4, 7/3, 7/4	Very pale brown
6/4	Light yellowish brown
5/3	Brown
5/4	Yellowish brown
4/3	Brown-dark brown
4/4, 3/4	Dark yellowish-brown
3/3	Dark brown
2/2	Very dark brown
5YR	
2/2	Dark reddish-brown

All sediment samples were dried using a Chemical Laboratory Instruments Ltd. Model S.B.4 Freeze Drier. When dry, the samples were ground to a fine powder, using an agate mortar and pestle and stored in plastic vials. The final lithological description of the cores was made after the analysis of the sediments and the nomenculture and the classification system suggested by Olausson (1960) was followed. This is summarized here:

I. PELAGIC DEPOSITS

A. Oozes:

1. $CaCO_3 > 30\%$:

a. Skeletal remains of pelagic forams or pteropods lower than 30%:

aa. $CaCO_3$ = 30-60% .... marl ooze.

bb. $CaCO_3 > 60\%$ ..... chalk ooze.

b. Skeletal remains of pelagic forams or pteropods higher than 30%:

aa. $CaCO_3$ = 30-60% .... foraminiferal (pteropod) marl ooze.

bb. $CaCO_3 > 60\%$ ..... foraminiferal (pteropod) chalk ooze.

2. $CaCO_3 < 30\%$ Skeletal remains of siliceous organisms > 30%:

a. diatom ooze.

b. radiolarian ooze.

B. Red Clay. $CaCO_3 < 30\%$ and the amount of siliceous skeletal remains $< 30\%$. The sediments are dominated by pelite. The red clay is considered as calcareous if $CaCO_3$ = 10-30%.

II. TERRIGENOUS DEPOSITS

A. Organic muds: $CaCO_3$ or skeletal remains of siliceous organisms $> 30\%$.

1. $CaCO_3 > 30\%$:

a. Skeletal remains of pelagic forams or pteropods $< 30\%$:

aa. $CaCO_3$ = 30-60% .... marl mud or sand.

bb. $CaCO_3 > 60\%$ ..... chalk mud or sand.

b. Skeletal remains of pelagic forams or pteropods $> 30\%$:

aa. $CaCO_3$ = 30-60% .... foraminiferal (pteropod) marl mud.

bb. $CaCO_3 > 60\%$ ..... foraminiferal (pteropod) chalk mud.

2. $CaCO_3 < 30\%$: The amount of siliceous skeletal remains $> 30\%$:

a. diatom mud.

b. radiolarian mud.

B. Inorganic muds.: Skeletal remains of siliceous organisms $< 30\%$. $CaCO_3 < 30\%$.

1. Clayey muds. The average diameters < 5 micron.

   Black (blue, green, gray, etc.) mud.

2. Silty or sandy muds or sands. The average diameters > 5 micron.

   Black (blue, green, red, gray, etc.) silty mud.

   Black (blue, green, red, gray, etc.) sandy mud.

   Black (blue, green, red, gray, etc.) silty sand.

APPENDIX B

BULK CHEMICAL ANALYSIS AND DATA HANDLING

B1. Determination of Ca, Mn, Fe, Ni, Co, Pb, Zn, Cu, Ba and Al

Chemical analysis for Ca, Mn, Fe, Ni, Co, Pb, Zn, Cu, Ba and Al was carried out on a Perkin-Elmer 403 atomic absorption spectrograph. The samples were first digested using a combined HF-$HClO_4$-HNO_3 digestion. This method had a procedure as follows: 0.25 g of sample was weighed out into clean, dry P.T.F.E. beakers and 8 ml of HF, 3 ml of $HClO_4$, and 3 ml of HNO_3 were added. The samples were then strongly fumed for 20 mins at 200°C to ensure boiling point of $HClO_4$ reached, in order to prevent precipitation of CaF_2. They were then cooled and an additional 1-2 mls of HF was added. The beakers were then warmed for 12 hours, or until near dryness was achieved. They were then removed from the heat and allowed to cool, after which an additional 2 ml of $HClO_4$ was added. The beakers were then returned to the hot-plate and fumed to dryness but not baked. Finally, the beaker was washed with 5 M HCl and brought up to volume, so that the final solution was approximately 1 M in HCl.

All samples were analysed in duplicate and some in triplicate. Each series of analytical determinations usually consisted of about 60 samples, of which approximately 20% consisted of blanks, standards and duplicates.

B1.a Correction procedure for calcium interference:

A major problem of analysis of carbonate material by atomic absorption spectrophotometry is the Ca interference in the measurement of several metals, especially where these are present at low levels. In this study, Ca interference has been recorded for Ni, Co, Pb, Zn, Cu and Ba. This was considerably high in the case of the fracture zone sediments, which contained high concentrations of Ca as $CaCO_3$. For this reason, the following procedure was adopted in order to determine the true concentrations of the above elements in the sediments: after analysing all samples for Ca, Ca standard solutions in 1M HCl were made, covering the whole range of concentrations of the measured Ca. Then the standards were measured on the spectrophotometer, using the lamps of Ni, Co, Pb, Zn, Cu and Ba. Since none of these metals was added in the standard solutions, the readings obtained were the result of Ca interference. A graph was drawn for each element, plotting its readings against the Ca concentrations which produced these readings. Knowing the Ca concentration of each sample, the graphs were then used to determine the interference correction factor for each element, which was then subtracted from the total values. The results represented the true concentrations of the elements in the samples. Figures B1 and B2 show typical graphs of Ca interference corrections.

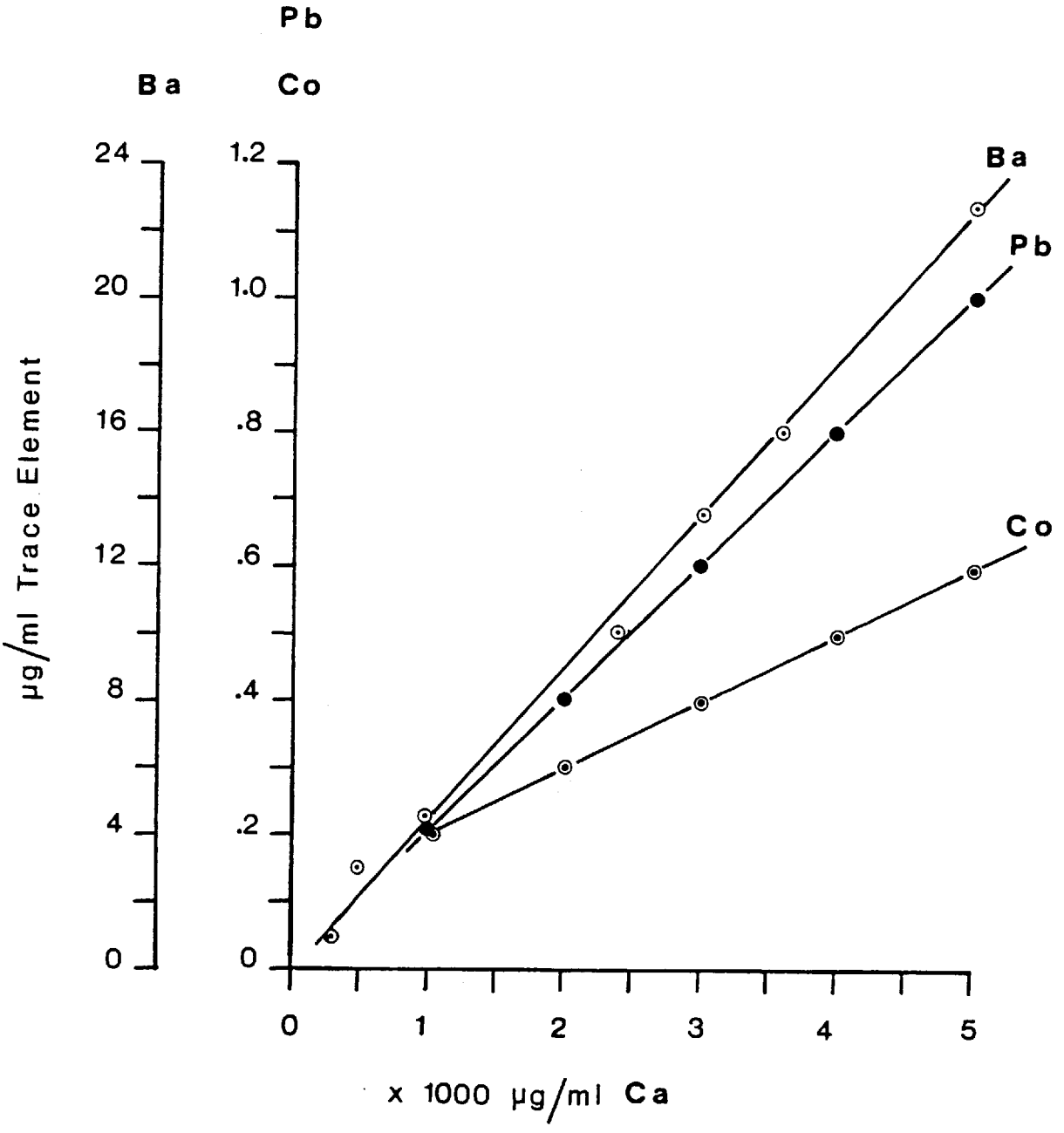

Figure B1: Graphs of calcium interference corrections.

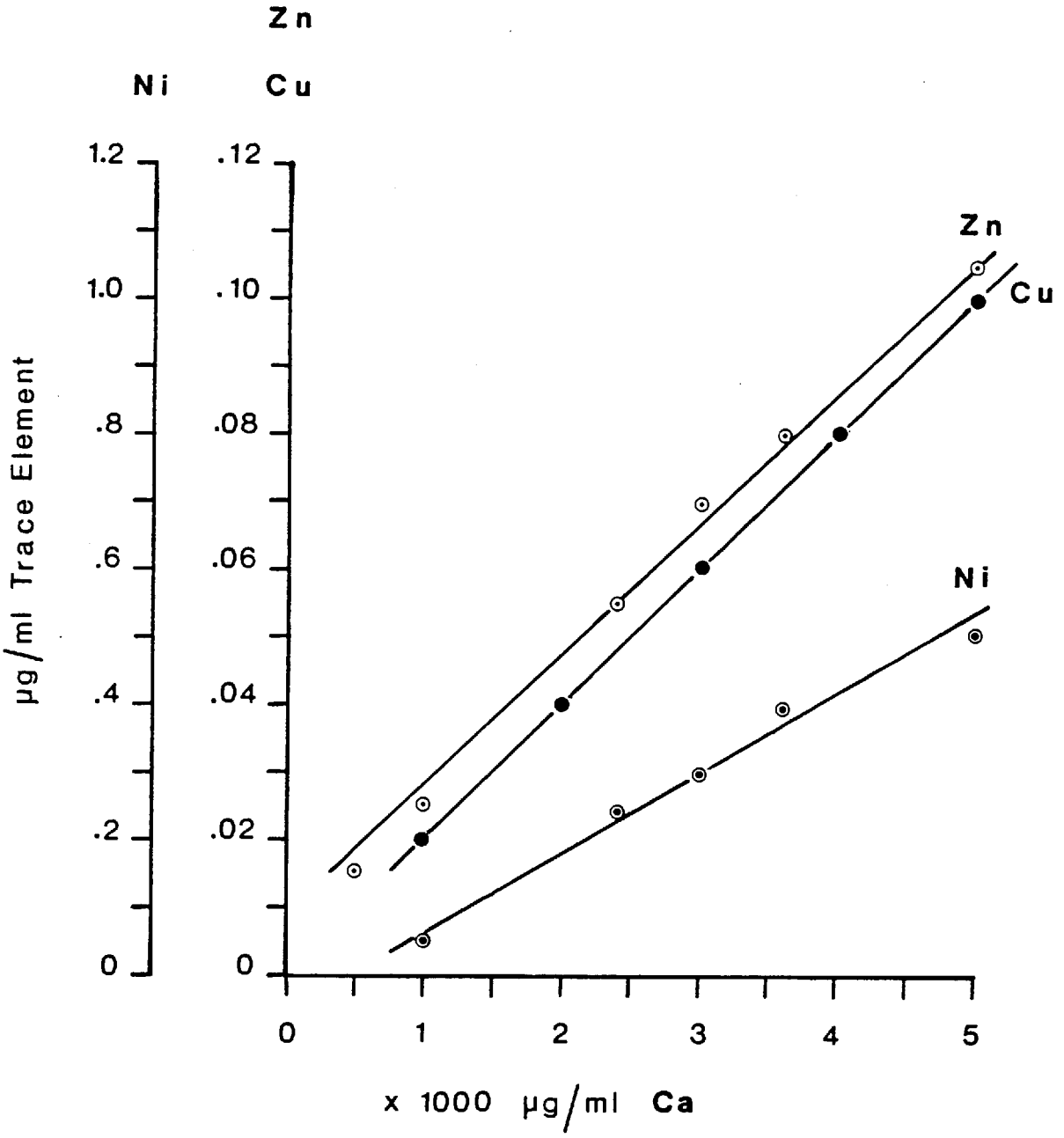

Figure B2: Graphs of calcium interference corrections.

B2. Determination of Silica (SiO_2)

The analysis for Si was carried out on a Perkin-Elmer 403 atomic absorption spectrograph. The samples were first digested using a combined HCl-HF-HBO_3 digestion. In this method 0.25 g (in the case of siliceous sediments 0.15 g) of sample was weighed out accurately into clean, dry polypropylene bottles and 5 ml of concentrated HCl and 5 ml of HF were added. The bottles were sealed and placed in the oven at 95°C. After one hour the oven was switched off and allowed to cool. The caps of the bottles were then unscrewed and the pressure was released every five minutes. The bottles were then removed from the oven and 4 g of boric acid was added. They were then shaken until nearly all the boric acid was dissolved. The mixture was then diluted to approximately 50 ml with D.I.W. in the same polypropylene bottles. They were then sealed and put back in the oven at 90-100°C for one-half hour. The mixture was allowed to cool and transferred to 50 ml volumetric flasks.

B3. Data Handling

In recent years, the chemical analyses of marine sediments have usually been given on a treated basis. The justification for this has been that it represents a more accurate picture of the geochemistry.

Boström et al (1969) recommended normalization of chemical data in marine sediments to Al+Fe+Mn, while Boström et al (1972)

introduced normalization to 4Al+Fe+Mn+Ti+P. More recently Piper (1973) suggested normalizing to Al_2O_3. The rationale behind these normalizations assumes both a constant and slow sedimentation rate (Boström et al, 1972; Piper, 1973).

A more common treatment of chemical data in marine sediments is their recalculation to a carbonate-free basis. The use of this method assumes that the carbonate fraction of the sediments does not contain proportions of these trace metals which one is analysing for. It should also be noted that small errors in the determination of $CaCO_3$ content may cause large differences in the correction factors employed. However, considering the presence of high concentrations of $CaCO_3$ in most of the sediments studied here and its diluting effect on the trace metals, the chemical data were corrected to a carbonate-free basis. Moreover, this treatment made the comparison of the present data with previously published data possible, because most of them have been reported in this form.

The $CaCO_3$ concentration of all sediment samples was calculated from the spectrochemically determined Ca values using the method of Dymond et al (1976). The equation used is:

$$\text{Wt \% } CaCO_3 = \frac{Ca_T - 0.41S - Ca_{NC}}{Ca_C - Ca_{NC}}$$

where: Ca_T = wt % of Ca in total sample, determined by AAS;

Ca_{NC} = wt % of Ca in non-CO_3 fraction;

Ca_C = wt % of Ca in $CaCO_3$ which is 40.04%;

S = wt fraction of salt in the sample;

0.41 = constant to allow for the wt % of Ca in the salt fraction of the sample, which Dymond et al (1976) report as 1.14% for sea salts.

The Ca content of the non-carbonate fraction (Ca_{NC}) of Nazca plate sediments was found to be 0.73 $\pm$ 0.12 (Dymond et al, 1976). This value was used in the present study because all the sediments examined here were from the Nazca plate and its use would thus facilitate meaningful comparisons.

In order to check the results obtained from the above method, the $CaCO_3$ content of a considerable number of samples was determined using a Collins Calcimeter. In this method the amount of CO_2 liberated when 0.2 gms of sample reacted with 5 ml 25% HCl was measured. The equation for the reaction is:

$$CaCO_3 + 2HCl = CaCl_2 + H_2O + CO_2$$

The measured CO_2 was used in the following formula to calculate the $CaCO_3$ content:

$$\text{wt \% } CaCO_3 = C \times \frac{44.0}{C_S} \times A \times W \times T \times P \times V$$

where:

- C = cc of CO_2 evolved;
- C_S = cc of CO_2 obtained from Analar $CaCO_3$ for a particular sample batch;
- A = correction factor for atomic weight of CO_2, 100.08/44.08 in $CaCO_3$;
- W = correction for difference in sample weight, W = 0.20/sample weight;
- T = correction factor for variation in room temperature, T = (r.t. initial)/(r.t. at measurement);
- P = correction for variations in barometric pressure, P = (P initial)/(P at measurement);
- V = correction for volume of reaction vessel, $V = V_o/V_A$; V_o = 100 cc, V_A = actual volume.

Comparison of the results obtained from this method with those obtained from Dymond et al's (1976) method showed 1:1 agreement (see Fig. B3).

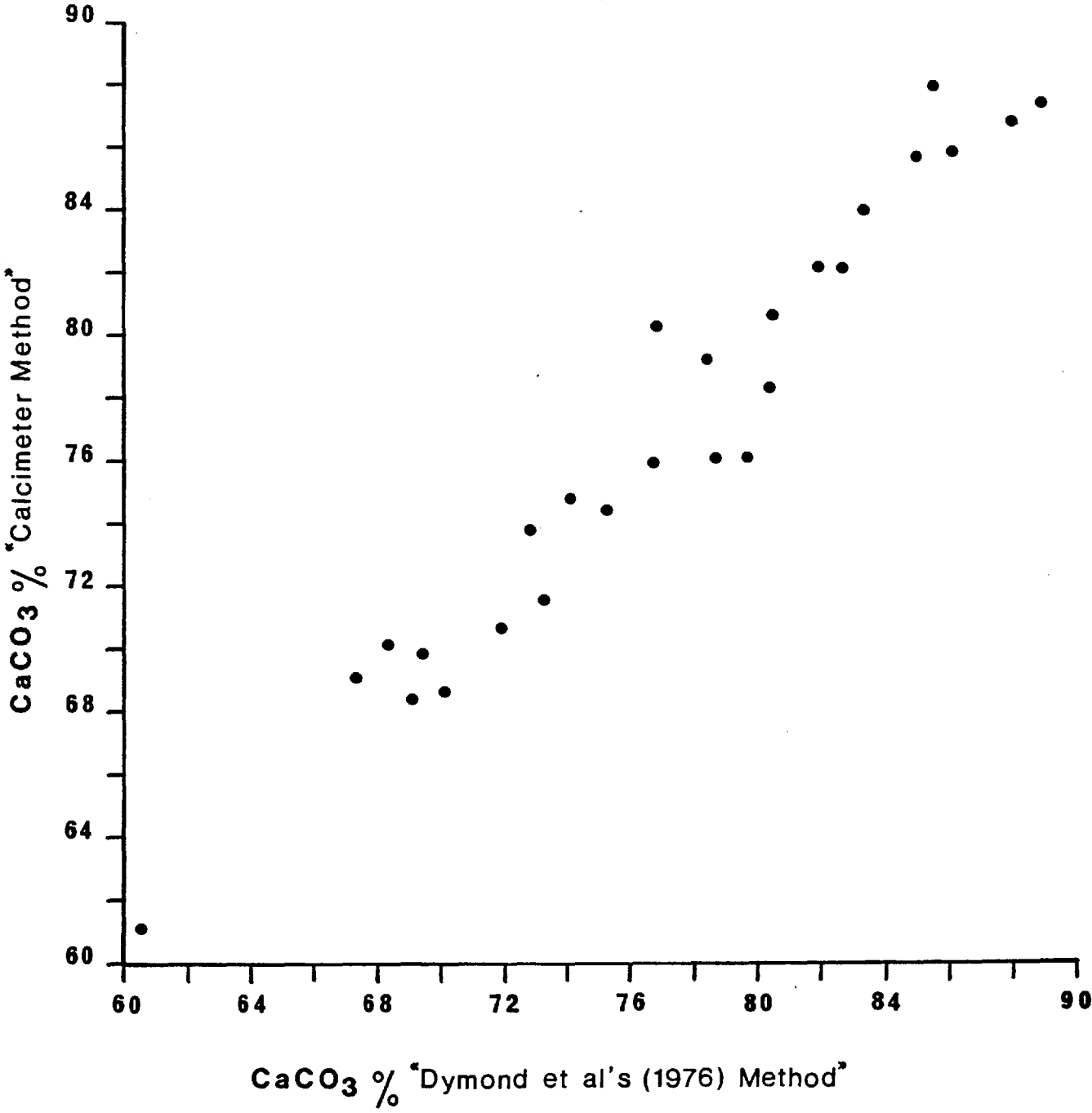

Figure B3: Comparison of $CaCO_3$ content determined by Dymond et al's method with that measured by calcimeter.

B4. Precision and Accuracy

The precision and accuracy of the results are given in Table B1 and were based on the replicate analysis of internal standards. These were a red clay sample, an internal carbonate sample and the USGS international standards: NBS-1b, AGV-1, PCC-1 and DTS-1.

Table B1: Precision and Accuracy of the bulk chemical analyses.
All data expressed on a carbonate-free basis.

No. of Analyses	Standard		Ca %	Mn %	Fe %	Ni ppm	Co ppm	Pb ppm	Zn ppm	Cu ppm	Ba %	Al %	SiO_2 %
7	RED CLAY	Reported	1.47	0.45	5.60	120	N.D	33	130	100	0.045	9.48	
		Found	1.38	0.44	5.65	124	N.D	45	138	110	0.07	9.43	
		Accuracy %	6.52	2.27	0.88	3.22		26.66	5.80	9.09	35.71	0.05	
10	NBS-1b (USGS) ARG. LIMESTONE	Reported	36.40	1.58	5.00							5.7	
		Found	36.42	1.57	5.30							6.11	
		Accuracy %	0.05	0.64	5.66							6.71	
24	INTERNAL		32.72	1.35	9.59	103	104		236	393	11736	1.02	
		Found	33.71	1.38	9.80	101	81		224	414	11588	0.98	
		Accuracy %	2.93	2.17	2.14	1.98	28.39		536	5.07	1.28	4.08	
4	AGV-1 (USGS)	Reported											59.00
		Found											58.72
		Accuracy %											0.48
4	PCC-1 (USGS)	Reported											41.90
		Found											41.04
		Accuracy %											2.09
4	DTS-1 (USGS)	Reported											40.50
		Found											39.15
		Accuracy %											3.45
REPLICATE SAMPLE PRECISION			1%	3%	4%	8%	17%	20%	4%	3%	10%	4%	2%

APPENDIX C

CHEMICAL PARTITION TECHNIQUES

C1. Acetic Acid Leach

In this technique, 1 gm of sample was weighed out accurately into 100 ml, stoppered, 'Quickfit' conical flasks and 10 ml of 25% (V/V) acetic acid were added. The samples were then mechanically shaken for four hours and allowed to settle. They were then vacuum-filtered through previously weighed-out millipore filter papers. The filtrates and washings were collected in 100 ml conical flasks and the acetic acid was destroyed by evaporating the solutions and by addition of concentrated HNO_3, which was evaporated off. The samples were then leached with 1 M HCl and were made up in 25 ml graduated flasks to give 1 M HCl solution.

C2. Acid-Reducing Agent Leach

1 gm of sample was weighed out accurately into 100 ml, stoppered 'Quickfit' conical flasks and 50 mls mixed acid-reducing agent were added. The samples were allowed to stand for four hours with occasional agitation. They were then vacuum-filtered through previously weighed-out millipore filter papers. The filtrates and washings were collected in 100 ml conical flasks and the excess acid-reducing agent was evaporated and destroyed by excess concentrated HNO_3 effervescence; more HNO_3 was added until the solutions were a clear yellow colour.

C3. Hydrochloric Acid Leach

In this method 0.5 g of sample was weighed out accurately into a 100 ml beaker and 5 mls of 50% V/V HCl was added. The beakers were covered with a watch glass, the samples were heated until just boiling and refluxed for three hours until the solutions were a clear yellowish-orange colour. The samples were then vacuum-filtered through previously weighed-out millipore filter papers. The filtrates were made up in 25 ml graduated flasks together with washings, to give 1 M HCl solution.

APPENDIX D

LOCATION OF THE CORES STUDIED

Table D1: Location of Cores Studied from the East Pacific Rise fracture zone at 9°S.

	Core No.	Depth fathoms	Depth meters	Latitude S	Longitude W
1	SH 1519	1506	2812	8°54.723'	107°59.67'
2	SH 1520	1240	2313	8°54.542'	108°0.689'
3	SH 1521	1684	3147	8°52.308'	108°4.483'
4	SH 1525	1650	3083	8°53.89'	108°15.66'
5	SH 1526	1740	3252	8°55.3'	108°20.05'
6	SH 1528	1770	3310	8°58.8'	108°33.4'
7	SH 1529	2028	3798	9°7.692'	108°42.251'
8	SH 1530	1922	3597	9°08.096'	108°37.630'
9	SH 1531	2046	3832	9°5.224'	108°55.44'
10	SH 1532	1896	3547	8°57.425'	109°8.379'
11	SH 1533	1494	2789	8°52.454'	109°14.927'
12	SH 1534	1736	3245	8°54.573'	109°09.366'
13	SH 1535	1672	3124	9°5.266'	108°46.31'
14	SH 1536	1778	3352	9°12.709'	108°24.148'
15	SH 1537	1759	3285	9°9.147'	108°13.807'
16	SH 1538	1802	3356	9°8.016'	108°11.315'
17	SH 1539	1868	3492	9°07.901'	108°08.456'
18	SH 1540	1858	3398	9°11.019'	108°8.378'
19	SH 1541	1760	3290	9°10.004'	108°2.361'
20	SH 1543	1740	3252	9°07.730'	107°57.369'
21	SH 1544	1782	3332	9°10.19'	108°2.685'
22	SH 1545	1932	3616	9°13.025'	108°10.787'
23	SH 1546	1946	3642	9°7.569'	108°35.532'
24	SH 1547	1760	3290	9°4.941'	108°24.533'
25	SH 1548	1560	2902	9°08.8'	108°22.3'
26	SH 1550	1820	3404	9°9.506'	107°49.107'
27	SH 1551	1776	3317	9°13.8'	107°40.1'
28	SH 1552	2032	3802	9°14.118'	107°27.599'
29	SH 1553	1700	3177	8°51.881'	108°02.145'
30	SH 1555	1724	3222	8°55.0'	108°5'
31	SH 1556	1700	3177	8°55.7'	108°10.8'

Table D2: Location of Cores studied from the Bauer Deep

	Core Number	Depth		Latitude	Longitude
		Fathoms	Meters	S	W
1	SH 1557	2376	4461	$10^{\circ}1.908'$	$102^{\circ}7.862'$
2	SH 1559	2364	4438	$10^{\circ}04.639'$	$101^{\circ}39.669'$
3	SH 1560	2216	4156	$10^{\circ}4.149'$	$101^{\circ}24.619'$
4	SH 1577	2308	4333	$9^{\circ}59.1'$	$101^{\circ}31'$
5	SH 1578	2421	4546	$9^{\circ}59.68'$	$101^{\circ}49.30'$

Table E1: Bulk Chemical Composition of sediments from the East Pacific Rise fracture zone at 9°S expressed on a carbonate-free basis.

Station No.	Sample No.	Interval sampled cm.	$CaCO_3$ (%)	Ca (%)	Mn (%)	Fe (%)	Ni (ppm)	Co (ppm)	Pb (ppm)	Zn (ppm)	Cu (ppm)	Al (%)	Ba (%)	SiO_2 (%)
SH 1541	1	Top	84.91	34.52	2.39	8.15	232	73	166	225	411	0.66	1.72	20.41
	2	14-16	83.36	33.91	2.70	9.98	240	60	84	234	422	0.72	1.44	
	3	40-42	82.63	33.62	1.61	8.46	161	75	127	184	363	0.81	1.73	
	4	60-62	86.44	35.12	1.33	8.33	147	133	81	177	339	0.88	2.21	
	5	80-82	81.03	32.99	1.42	8.75	153	116	84	190	395	0.84	1.85	
	6	100-102	83.01	33.77	1.41	8.53	200	124	129	200	406	1.00	1.88	
	7	124-126	78.70	32.08	1.97	9.67	178	70	113	211	404	0.89	1.22	
	8	139-143	81.91	33.34	1.22	8.02	127	116	116	171	287	0.77	1.66	
	9	163-167	82.49	33.57	1.14	8.97	126	114	80	194	366	0.86	1.94	
	Average		82.72	33.66	1.69	8.76	174	98	109	198	377	0.83	1.74	
SH 1535	10	Top	82.39	33.53	3.18	9.99	290	34	114	267	494	0.68	1.59	25.16
	11	26-31	79.18	32.26	2.83	9.46	255	72	82	202	427	0.67	1.39	
	12	46-50	88.09	35.77	1.01	8.23	202	84	143	202	285	1.18	2.43	
	13	66-70	85.44	34.73	1.72	9.13	117	76	124	206	350	0.76	1.99	
	14	86-90	87.84	35.67	1.48	8.72	156	82	164	206	337	0.82	2.71	
	15	106-110	87.23	35.43	1.25	8.93	157	78	86	196	376	1.10	2.51	
	16	138-142	83.45	33.94	1.27	8.34	211	115	121	181	338	1.09	2.05	
	17	162-166	67.06	27.50	1.06	4.43	58	30	36	109	209	0.61	1.34	
	Average		82.59	33.60	1.73	8.40	181	71	109	196	352	0.86	2.00	

Station No.	Sample No.	Interval sampled cm.	$CaCO_3$ (%)	Ca (%)	Mn (%)	Fe (%)	Ni (ppm)	Co (ppm)	Pb (ppm)	Zn (ppm)	Cu (ppm)	Al (%)	Ba (%)	SiO_2 (%)
SH 1536	24	Top	83.43	33.94	2.60	9.60	199	115	133	266	513	0.72	1.99	15.33
	25	23-28	86.32	35.07	1.47	9.68	137	107	134	226	374	1.33	3.03	
	26	35-39	84.55	34.38	0.40	10.50	137	116	119	197	289	1.22	2.39	
	27	49-53	84.58	34.39	1.83	9.65	213	74	159	217	477	1.08	2.29	
	28	70-75	84.81	34.48	1.84	9.74	182	79	83	215	425	1.54	2.63	
	Average		84.74	34.45	1.63	9.83	174	98	126	224	416	1.18	2.47	
SH 1551	33	Top	85.54	34.77	1.66	5.60	263	76	118	173	325	0.55	1.45	13.83
	34	25-30	87.61	35.58	1.99	6.19	214	168	109	157	329	0.77	1.81	
	35	50-55	86.21	35.03	1.53	5.59	233	174	189	153	306	0.73	1.72	
	36	75-80	85.65	34.81	1.49	6.77	190	125	110	173	332	0.87	1.81	
	37	100-105	84.21	34.24	1.55	8.49	210	155	80	203	441	0.89	1.65	
	38	125-130	85.17	34.62	1.84	7.40	190	112	98	207	419	0.74	1.47	
	39	150-155	84.21	34.24	1.19	6.26	191	86	107	160	278	0.72	1.31	
	40	170-175	85.00	34.55	0.82	6.54	171	118	135	168	338	0.85	1.45	
	Average		85.45	34.73	1.51	6.61	208	127	118	174	346	0.77	1.58	
SH 1552	41	Top	86.69	35.22	1.88	6.54	293	128	120	210	458	0.98	1.65	19.38
	42	20-26	88.81	36.05	1.25	5.99	214	143	197	170	357	1.25	2.14	20.91
	43	36-42	87.50	35.54	1.28	6.08	304	176	264	176	344	1.12	2.08	21.44
	44	53-59	84.23	34.25	2.22	8.88	247	152	140	241	571	1.59	2.09	26.57
	45	90-95	86.07	34.97	1.72	7.47	266	129	258	194	424	1.29	1.94	22.76
	46	113-118	83.00	33.77	1.82	9.82	212	106	159	224	588	1.24	1.71	22.18
	Average		86.05	34.97	1.70	7.46	256	139	190	203	457	1.25	1.94	22.21

Station No.	Sample No.	Interval sampled cm.	$CaCO_3$ (%)	Ca (%)	Mn (%)	Fe (%)	Ni (ppm)	Co (ppm)	Pb (ppm)	Zn (ppm)	Cu (ppm)	Al (%)	Ba (%)	SiO_2 (%)
SH 1548	47	Top	85.60	34.79	2.08	7.92	257	118	132	215	368	1.04	1.04	17.99
	48	36-41	81.00	32.98	2.52	9.54	207	98	118	211	362	1.17	0.72	
	49	44-49	78.19	31.88	2.96	12.50	172	102	116	226	391	2.11	0.76	
	50	70-75	83.96	34.15	1.77	9.10	161	130	126	171	325	1.54	1.12	
	51	93-99	81.82	33.30	1.28	7.65	125	109	104	142	222	2.46	1.04	
	Average		82.11	33.42	2.12	9.34	184	111	119	193	334	1.66	0.94	
SH 1531	52	Top	67.08	27.51	2.98	11.54	228	94	106	255	529	2.10	1.06	27.73
	53	20-27	68.36	28.01	1.99	10.56	190	101	123	180	357	2.91	0.92	31.01
	54	40-46	69.40	28.42	1.57	9.97	163	72	108	180	356	2.65	0.95	28.04
	55	60-66	69.14	28.32	1.20	9.82	149	71	91	178	369	2.07	0.84	30.36
	56	80-86	71.97	29.43	1.03	9.99	121	107	93	189	375	2.93	0.93	32.61
	57	102-108	60.54	24.94	1.72	11.15	152	81	117	213	456	3.52	0.96	33.12
	58	117-122	56.80	23.47	1.55	11.39	194	81	93	213	498	3.36	0.63	33.73
	Average		66.18	27.16	1.72	10.63	171	87	104	201	420	2.79	0.90	30.94
SH 1532	59	Top	70.60	28.89	3.71	13.27	269	102	116	299	616	1.50	0.75	21.87
	60	25-32	69.04	28.28	2.94	13.21	216	103	110	229	452	1.94	0.90	24.32
	61	50-56	72.22	29.53	1.66	10.66	155	101	112	191	338	2.42	1.01	25.88
	62	79-85	72.28	29.55	1.70	11.83	166	105	155	209	390	2.13	0.94	27.24
	63	100-106	74.31	30.35	1.67	11.25	163	105	117	210	397	2.22	1.13	28.53
	64	122-129	67.25	27.58	1.62	11.15	171	95	110	211	452	2.81	0.89	31.97
	Average		70.95	29.03	2.22	11.90	190	102	120	225	441	2.18	0.94	26.64

Station No.	Sample No.	Interval sampled cm.	$CaCO_3$ (%)	Ca (%)	Mn (%)	Fe (%)	Ni (ppm)	Co (ppm)	Pb (ppm)	Zn (ppm)	Cu (ppm)	Al (%)	Ba (%)	SiO_2 (%)
SH 1525	65	Top	72.82	29.77	4.49	13.54	533	107	132	331	728	0.40	0.84	20.31
	66	25-32	78.70	32.07	3.57	12.16	263	122	136	300	624	0.61	1.27	20.80
	67	49-55	72.37	29.59	5.79	13.79	355	101	130	322	684	0.47	0.87	20.85
	68	68-74	74.27	30.34	3.15	12.24	210	101	109	257	501	0.70	0.82	21.22
	69	77-82	76.71	31.30	5.50	12.41	361	112	125	253	480	0.77	1.12	20.82
	Average		74.97	30.61	4.50	12.83	344	109	126	293	603	0.59	0.98	20.80
SH 1539	70	Top	81.76	33.28	2.91	10.91	280			258	543	0.77	1.21	18.09
	71	24-30	85.50	34.75	1.31	9.03	166			193	386	1.72	1.59	26.55
	72	44-50	85.99	34.94	1.36	10.35	228			214	443	1.00	1.21	25.98
	73	64-70	80.83	32.91	1.10	8.97	151			167	365	0.99	1.25	20.55
	74	84-90	84.70	34.44	2.03	14.77	222			281	680	1.57	1.96	31.11
	75	114-120	82.85	33.71	2.80	15.39	227			297	735	1.52	1.46	29.56
	76	131-137	77.71	31.69	0.85	8.21	103			166	314	0.88	1.08	19.38
	Average		82.76	33.67	1.77	11.09	197			225	495	1.21	1.39	24.46
SH 1537	77	Top	84.18	34.58	3.22	13.15	341			278	601	0.76	1.07	20.29
	78	24-31	85.43	34.72	1.17	8.17	172			158	336	1.30	1.37	22.51
	79	42-49	79.56	32.42	1.13	7.14	137			142	303	0.68	1.22	19.03
	80	71-78	84.56	34.38	1.81	12.89	227			233	525	1.36	1.62	27.33
	81	92-98	82.22	33.46	1.63	11.25	231			214	512	1.29	1.24	27.17
	Average		83.19	33.91	1.79	10.52	222			205	455	1.08	1.30	23.27

Station No.	Sample No.	Interval sampled cm.	$CaCO_3$ (%)	Ca (%)	Mn (%)	Fe (%)	Ni (ppm)	Co (ppm)	Pb (ppm)	Zn (ppm)	Cu (ppm)	Al (%)	Ba (%)	SiO_2 (%)
SH 1540	82	Top	81.68	33.25	2.51	9.77	251			218	480	0.66	1.47	18.01
	83	22-29	87.90	35.69	2.48	11.65	273			231	496	1.49	1.82	26.69
	84	39-41	83.37	33.91	0.42	6.37	150			156	331	1.08	1.38	
	85	43.5-45.5	87.66	35.60	1.22	9.56	186			203	470	1.46	2.19	29.25
	86	51-52	83.93	34.13	0.56	7.90	93			180	373	0.81	1.80	
	87	66-67	85.75	34.85	0.49	10.81	133			196	477	1.05	1.68	
	88	70-76	84.46	34.34	1.16	8.24	161			174	373	0.90	1.54	21.49
	89	91-94	84.02	34.17	1.63	13.33	250			257	563	1.44	1.75	28.79
	90	103-105.5	81.19	33.06	2.87	11.80	266			239	649	1.12	1.49	24.99
	91	115-119	80.59	32.82	1.49	10.25	216			206	495	1.03	1.34	22.72
	92	136-140	78.40	31.96	2.13	11.06	171			227	537	0.83	1.44	22.87
	93	148-149	73.37	29.98	0.79	8.86	128			154	285	2.22	1.01	
	Average		82.69	33.65	1.48	9.97	190			203	461	1.17	1.58	24.35
SH 1538	94	Top	76.68	31.28	2.06	8.32	163	26	99	274	566	0.51	1.29	15.69
	95	28-35												
	96	40-43	82.31	33.60	0.28	7.63	79	40	11	158	317	0.96	1.41	
	97	56-63	83.29	34.72	1.44	8.92	144	36	78	174	347	0.96	1.50	24.00
	98	73-80												
	99	93-101	81.90	33.46	1.77	10.88	193	33	11	221	519	1.22	1.49	22.04
	100	112-119	82.36	34.41	1.64	12.81	193	34	68	232	544	1.47	1.19	26.81
	101	129-136	83.48	34.64	2.18	11.99	206	36	79	218	545	1.51	1.15	20.82
	102	143-150	78.80	32.04	2.50	11.46	307	5	19	212	500	0.90	0.75	17.12
	103	165-172	83.93	34.78	1.18	11.14	149	31	131	174	373	1.12	1.37	23.34
	Average		81.59	33.62	1.63	10.39	179	30	62	208	464	1.08	1.27	21.40

Station No.	Sample No.	Interval sampled cm.	$CaCO_3$ (%)	Ca (%)	Mn (%)	Fe (%)	Ni (ppm)	Co (ppm)	Pb (ppm)	Zn (ppm)	Cu (ppm)	Al (%)	Ba (%)	SiO_2 (%)
SH 1526	104	Top	78.20	31.88	3.03	11.65	248	41	78	284	564	0.69	0.69	21.74
	105	16.5-18.5	69.80	28.58	7.25	14.00	371	40	83	341	722	0.50	0.56	19.74
	106	30-32	73.20	29.92	2.54	13.84	131	41	78	295	653	0.60	0.68	
	107	32-36	76.65	31.27	2.83	11.65	133	38	60	253	471	0.81	0.56	20.39
	108	52-57	77.51	31.61	1.42	11.20	124	36	76	209	409	0.89	0.71	26.46
	109	88-93	77.35	31.55	1.28	13.33	159	40	124	234	472	1.10	0.97	25.96
	110	117.5-119.5	70.12	28.71	2.64	12.15	134	40	80	224	485	1.00	0.57	22.56
	Average		74.69	30.50	3.00	12.55	186	39	83	263	539	0.80	0.68	22.81
SH 1534	111	Top	75.29	30.74	3.04	11.45	320	40	77	259	514	1.05	0.69	17.08
	112	21-26	74.63	30.48	2.80	11.90	257	39	63	225	441	1.26	0.63	19.39
	113	48-53	76.75	31.31	1.59	10.71	168	39	77	202	343	1.71	0.82	23.61
	114	70-75	76.27	31.12	1.90	11.97	126	38	80	215	405	1.43	0.76	26.09
	115	91-97	74.56	30.45	1.57	11.71	118	39	75	208	406	1.69	0.90	27.04
	116	120-126	74.03	30.24	1.85	13.44	150	39	77	239	520	1.66	0.89	29.11
	117	148-151	75.08	30.65	1.85	11.84	116	36	76	221	502	2.41	0.88	26.81
	Average		75.23	30.71	2.09	11.86	179	39	75	224	447	1.60	0.80	24.16

Station No.	Sample No.	Interval sampled cm.	$CaCO_3$ (%)	Ca (%)	Mn (%)	Fe (%)	Ni (ppm)	Co (ppm)	Pb (ppm)	Zn (ppm)	Cu (ppm)	Al (%)	Ba (%)	SiO_2 (%)
SH 1547	118	Top	81.64	33.23	3.54	13.73	321	44	87	321	632	0.93	0.87	24.07
	119	22-24	73.80	30.15	9.12	12.10	378	38	80	313	603	0.61	0.73	16.53
	120	34-39	77.44	31.58	3.15	11.75	124	80	71	244	465	0.80	0.62	18.57
	121	46-49	78.72	32.08	6.77	11.18	305	52	80	216	437	1.03	0.85	22.09
	122	54-57	76.19	31.09	1.97	7.43	105	38	63	143	265	0.84	0.84	17.43
	123	81-86	77.93	31.77	1.86	7.29	122	50	18	154	308	1.04	0.86	22.29
	124	110-113	74.73	30.52	1.86	10.21	158	40	59	174	360	0.71	0.67	30.75
	125	137-140	79.67	32.46	1.92	11.51	152	34	49	192	438	0.98	0.84	29.51
	126	155-160	82.41	33.54	1.36	8.87	148	34	85	188	352	1.02	0.85	26.61
	127	160-161	80.11	32.63	2.41	9.95	141	90	85	241	402	1.16	1.06	
	Average		78.26	31.91	3.40	10.40	195	50	68	219	426	0.91	0.82	23.09
SH 1529	128		71.98	29.44	3.21	12.10	282	39	71	264	575	1.14	0.79	18.31
	129	35-41	80.42	32.75	1.89	12.00	128	36	26	220	449	2.04	1.07	29.88
	130	67-73	76.25	31.11	1.35	10.40	126	38	72	189	383	1.64	0.84	25.85
	131	92-97	73.51	30.04	1.81	13.48	215	38	76	230	502	2.53	1.13	34.47
	132	123-128	69.94	28.63	1.60	12.54	133	70	77	226	532	2.46	0.93	31.87
	133	145-150	67.78	27.78	2.36	13.31	158	37	74	248	556	1.40	0.43	29.67
	Average		73.31	29.96	2.04	12.31	174	43	66	230	500	1.87	0.87	28.34

Station No.	Sample No.	Interval sampled cm.	$CaCO_3$ (%)	Ca (%)	Mn (%)	Fe (%)	Ni (ppm)	Co (ppm)	Pb (ppm)	Zn (ppm)	Cu (ppm)	Al (%)	Ba (%)	SiO_2 (%)
SH 1530	134	Top	78.62	32.05	3.04	11.65	267	37	75	257	543	0.84	0.84	18.76
	135	15-20	75.54	30.84	2.90	11.08	241	37	57	225	466	0.86	0.78	
	136	22-25	76.55	31.23	3.28	12.07	273	38	60	226	486	1.24	0.90	
	137	30-33	80.15	32.65	1.91	9.42	141	65	60	176	368	1.46	1.16	
	138	64-69	79.21	32.28	1.49	9.96	106	38	58	183	361	1.15	0.91	
	139	74-79	81.84	33.31	1.10	9.53	116	33	55	204	396	1.27	1.05	
	140	102-107	78.83	32.13	1.65	11.67	132	38	57	217	491	1.75	1.04	
	141	117-122	72.48	29.63	2.47	10.50	145	36	58	193	422	1.13	0.65	
	142	131-135	78.89	32.15	1.28	9.14	133	38	76	189	427	1.75	0.99	
	Average		78.01	31.81	2.12	10.56	173	40	62	208	429	1.27	0.92	
SH 1545	143	Top	81.01	32.98	2.53	9.16	253	121	153	232	458	0.63	1.00	18.85
	144	18-23	81.11	33.02	2.06	8.05	196	90	139	182	358	0.83	1.13	
	145	50-54	81.28	33.09	1.18	7.59	96	123	101	166	337	0.85	0.96	
	146	80-85	81.39	33.13	1.93	11.12	177	124	167	247	548	1.29	1.61	
	147	108-113	76.74	31.31	2.02	9.89	146	103	86	202	451	0.77	0.82	
	148	122-128	78.41	31.96	0.97	8.06	88	176	130	171	306	0.79	0.97	
	Average		79.99	32.58	1.78	8.98	159	123	129	200	410	0.86	1.08	

Station No.	Sample No.	Interval sampled cm.	$CaCO_3$ (%)	Ca (%)	Mn (%)	Fe (%)	Ni (ppm)	Co (ppm)	Pb (ppm)	Zn (ppm)	Cu (ppm)	Al (%)	Ba (%)	SiO_2 (%)
SH 1544	149	Top	86.03	34.96	2.65	9.31	265	115	107	258	494	0.72	1.07	19.90
	150	16-21	81.35	33.12	2.31	8.41	172	91	145	209	391	0.59	0.59	
	151	31-34	82.93	33.74	1.35	6.68	100	117	152	158	293	0.82	1.00	
	152	70-74	84.70	34.44	1.05	7.45	111	203	203	157	288	0.78	1.31	
	153	112-117	72.39	29.60	1.01	10.47	120	109	80	217	474	1.01	0.83	
	155	151-155	78.29	31.92	1.75	8.38	157	111	92	189	355	0.74	0.78	
	156	168-173	79.01	32.20	0.91	7.72	91	91	91	167	272	0.62	0.76	
	Average		80.67	32.85	1.58	8.35	145	120	124	194	367	0.75	0.91	
SH 1546	157	Top	78.86	32.14	2.70	10.17	222	128	90	241	497	0.80	0.66	18.50
	158	18-23	76.17	31.08	2.69	9.95	185	105	126	193	403	0.88	0.63	
	159	35-40	80.38	32.74	3.92	8.66	204	122	97	178	362	1.22	0.92	18.71
	160	63-68	80.11	32.63	2.11	8.55	141	121	146	181	347	1.11	0.90	25.09
	161	92-97	76.43	31.19	1.91	10.31	161	85	85	178	352	1.15	0.76	23.67
	162	120-121	78.38	31.95	3.38	10.78	222	134	93	204	435	1.43	1.02	30.16
	163	127-130	69.48	28.45	2.62	11.21	161	111	69	190	380	1.34	0.82	25.10
	164	139-144	73.84	30.17	1.53	10.32	153	99	42	191	440	1.68	0.80	29.59
	Average		76.71	31.29	2.61	9.99	181	113	94	195	402	1.20	0.81	24.40

Station No.	Sample No.	Interval Sampled cm.	$CaCO_3$ (%)	Ca (%)	Mn (%)	Fe (%)	Ni (ppm)	Co (ppm)	Pb (ppm)	Zn (ppm)	Cu (ppm)	Al (%)	Ba (%)	SiO_2 (%)
SH 1535	174	Top	81.78	33.29	2.09	8.84	263	126	154	209	406	1.48	0.77	20.53
	175	12-17	78.85	32.14	2.17	9.17	156	113	132	199	397	1.70	0.61	
	176	37-43	80.42	32.75	1.23	8.22	117	92	143	169	306	2.35	0.61	
	177	73-79	79.07	32.22	1.19	10.56	143	91	153	172	377	4.68	0.57	
	178	104	74.33	30.36	2.53	11.84	203	43	101	210	460	2.77	0.39	
	179	102-106	78.74	32.09	1.55	8.84	136	89	132	174	315	3.29	0.28	
	180	128-134	81.91	33.34	0.72	7.35	127	72	105	149	221	3.10	0.39	
	181	164-170	73.89	30.18	0.65	8.73	119	38	84	153	237	5.17	0.54	
	Average		78.62	32.05	1.52	9.19	158	83	126	179	340	3.07	0.52	
SH 1543	182	Top	86.59	35.18	1.94	7.38	231	149	209	224	410	0.67	0.97	14.39
	183	34-40	87.04	35.36	1.31	6.71	123	162	216	193	324	1.00	1.47	
	184	64-70	86.29	35.06	1.39	7.73	153	153	124	204	372	0.73	1.24	
	185	100-106	82.84	33.70	6.76	13.93	157	157	251	192	390	0.82	1.28	
	186	125-131	85.20	34.63	1.55	8.78	149	209	277	223	453	0.95	1.28	
	187	145-148	80.30	32.70	1.93	9.04	198	122	102	223	467	0.76	0.76	
	188	169-174	84.60	34.40	1.17	10.52	130	32	97	240	474	0.91	1.23	
	Average		84.69	34.43	2.29	9.16	163	141	182	214	413	0.83	1.18	

Station No.	Sample No.	Interval sampled cm.	$CaCO_3$ (%)	Ca (%)	Mn (%)	Fe (%)	Ni (ppm)	Co (ppm)	Pb (ppm)	Zn (ppm)	Cu (ppm)	Al (%)	Ba (%)	SiO_2 (%)
SH 1550	189	Top	87.74	35.63	2.53	8.32	277	147	212	245	465	0.65	1.14	20.23
	190	20-24	85.62	34.80	2.16	8.07	216	146	174	209	396	0.76	1.18	
	191	39-41	80.45	32.76	0.10	2.66	92	97	148	107	169	0.36	0.72	
	192	59-65	84.47	34.34	1.22	6.37	142	71	103	167	296	0.58	1.09	
	193	80-86	84.83	34.49	1.85	9.62	178	145	204	224	448	1.19	1.85	
	194	116-122	79.57	32.42	1.71	8.66	113	88	132	206	421	0.64	0.83	
	195	161-167	82.37	33.52	0.68	5.90	85	102	108	147	261	0.74	1.02	
	Average		83.58	33.99	1.46	7.09	158	114	154	186	351	0.70	1.12	
SH 1528	210	Top	76.37	31.16	2.20	10.28	212	55	97	216	423	3.72	0.47	31.15
	211	23-29	70.49	28.85	2.37	10.78	241	44	81	203	386	2.51	0.44	27.89
	212	34-40	72.01	29.45	1.82	9.90	179	57	75	161	332	2.07	0.71	25.94
	213	44-46	66.78	27.39	2.26	11.11	96	45	78	181	379	1.54	0.51	
	214	48-54	76.90	31.37	1.47	9.18	152	39	87	156	312	2.38	0.87	26.10
	215	78-84	76.95	31.39	1.17	9.07	74	43	87	169	334	0.95	0.61	
	216	103-108	79.28	32.31	1.98	11.05	130	39	87	203	396	0.97	0.72	21.38
	217	132-137	81.25	33.08	1.07	8.27	128	53	107	176	331	1.01	0.96	
	218	160-164	81.12	33.03	0.95	7.42	138	26	74	164	328	0.85	0.85	
	Average		75.68	30.89	1.70	9.67	150	45	86	181	358	1.78	0.68	26.49